STATE OF LOUISIANA
COASTAL PROTECTION AND RESTORATION AUTHORITY

MID-BARATARIA SEDIMENT DIVERSION (MBSD) PROJECT
STATE PROJECT No. BA-0153
LaGOV NO. 4400020885

NUMERICAL MODELING FOR THE 90% PHASE OF ENGINEERING AND DESIGN

for

Prepared By:
AECOM Technical Services
8555 United Plaza Boulevard
Suite 300
Baton Rouge, LA 70809

June 3, 2022

Rev	Date	Description
0	7/6/2021	60% Draft Submittal
1	6/3/2022	90% Draft Submittal

ftn Associates Ltd.
water resources / environmental consultants

DRAFT

MID-BARATARIA SEDIMENT DIVERSION (BA-0153) NUMERICAL HYDRAULIC MODELING FOR THE 90% PHASE ENGINEERING AND DESIGN

JUNE 3, 2022

DRAFT

MID-BARATARIA SEDIMENT DIVERSION
(BA-0153)
NUMERICAL HYDRAULIC MODELING FOR THE 90% PHASE ENGINEERING AND DESIGN

Prepared for

AECOM Technical Services
7389 Florida Blvd., Ste 300
Baton Rouge, LA 70806

Prepared by

FTN Associates, Ltd.
7648 Picardy Ave, Ste 100
Baton Rouge, LA 70808

FTN No. R05540-1566-008

June 3, 2022

TABLE OF CONTENTS

TABLE OF CONTENTS (CONTINUED)

TABLE OF CONTENTS (CONTINUED)

TABLE OF CONTENTS (CONTINUED)

TABLE OF CONTENTS (CONTINUED)

TABLE OF CONTENTS (CONTINUED)

LIST OF APPENDICES

LIST OF TABLES

LIST OF TABLES (CONTINUED)

LIST OF FIGURES

LIST OF FIGURES (CONTINUED)

LIST OF FIGURES (CONTINUED)

LIST OF FIGURES (CONTINUED)

LIST OF FIGURES (CONTINUED)

LIST OF FIGURES (CONTINUED)

LIST OF FIGURES (CONTINUED)

LIST OF FIGURES (CONTINUED)

LIST OF FIGURES (CONTINUED)

LIST OF FIGURES (CONTINUED)

LIST OF FIGURES (CONTINUED)

LIST OF FIGURES (CONTINUED)

LIST OF FIGURES (CONTINUED)

1.0 INTRODUCTION

1.1 General

The Mid-Barataria Sediment Diversion (MBSD) Project (the Project) is a cornerstone project of the Louisiana Coastal Master Plan (CMP, 2017) developed by the Louisiana Coastal Protection and Restoration Authority (CPRA). The project proposes to divert sediment-laden Mississippi River (MR) water through a controlled opening on the right descending bank or the west bank of the river. The location was decided to be at River Mile (RM) 60.7 Above Head of Passes (AHP) in the previous planning studies by the CPRA and The Water Institute of the Gulf (WI). A similar project, called the Mid-Breton Sediment Diversion (MBrSD) is also planned upstream of MBSD at RM 68 on the east bank of the river.

The report documents the numerical hydraulic modeling performed to support the currently advanced 90% Phase Engineering and Design (E&D) of the MBSD project. Before arriving at the current design, several design alternatives were evaluated and screened in the 15% and 30% and 60% Phase E&D which have been documented in previous reports. The current 90% report retains the analysis done for the final design as of 60% and also includes additional modeling reflecting changes from 60% to 90% design. Two additional chapters, Chapter 10 and 11 have also been added since 60% phase and documents basin side diversion effects and operational modeling of the diversion respectively.

Chapters 2 through 11 and Appendix B1 describe the work performed by FTN Associates, Ltd (FTN) as the lead numerical modeling member of the AECOM Design Team for the Project. Additional hydraulic analyses and numerical modeling performed by AECOM is included as appendices B2, B3, and B4.

1.2 Numerical Modeling Goals

The overall goal of the numerical modeling is to develop the design of an Intake Structure that can divert a maximum flow of 75,000 cfs flow when the Mississippi River reaches 1,000,0000 cfs at USGS Gage 07374525 on the MR at Belle Chasse, Louisiana with as high Sediment Water Ratio (SWR) and Cumulative Sediment Water Ratio (CSWR) as achievable.

A complex three-dimensional (3D) flow field with the entrained river sediment is expected in the near-field region of the structure. The purpose of the numerical modeling was to assist the Design Team (DT) in selecting an invert for the structure and the type of structure from a choice of constructible designs (e.g., an Open Cut, U-Frame, U Frame with interior walls, Submerged Culvert) based on the sediment capture efficiency and energy loss. The numerical modeling also estimates river-side and basin-side effects of diversion operations.

1.3 MBSD System Components and Key Hydraulic Processes

For the purposes of hydraulic modeling the proposed MBSD project is viewed as a system made up of five major components. They are, the Mississippi River, the three structural components, namely, the headworks, the conveyance channel, the outfall transition feature, and the receiving basin. Each of the three structural components support one or more functions and together they help accomplish the project goals. The river component provides the sediment-laden water and in the process responds to the presence of the diversion influencing water levels, velocity and sediment aggradation/ degradation. On the other end, the receiving basin component receives the water and sediment resulting in land building, distributary channel developments, water level, velocity and salinity changes. Note that the comprehensive evaluation of salinity changes in the receiving basin is beyond the scope of this engineering work and only a a few limited scenarios, that concern the base flow period diversion operations and those that may not have been covered elsewhere before, is presented later in Chapter 11. For a detailed analysis of salinity effects in the basin the reader is referred to the environmental impacts study conducted by CPRA separately.

The design of each component is driven by specific hydraulic processes that will be modeled. The system components, functions and hydraulic processes are shown in Figure 1.1. The general hydraulic characteristics of each component are described briefly in the following sub-sections.

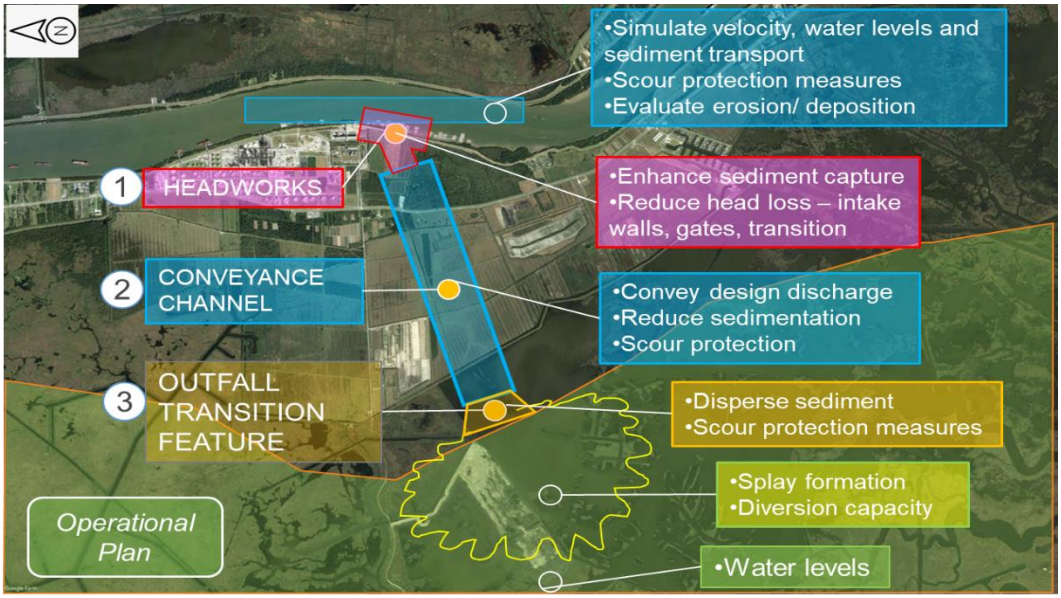

Figure 1.1. The components, functions and hydraulic processes of the Mid-Barataria Sediment Diversion Project.

1.3.1 Mississippi River

The Mississippi River carries sediment-laden flows south to the Gulf of Mexico (GoM). At the project location, the depth of the river is approximately 120 feet and a sand bar (knows as the Alliance sand bar) exists from a depth of about 50 feet to about 110 ft at the Right Descending Bank (RDB). The river bed towards the Left Descending Bank (LDB) and at the thalweg is a mixed bedrock alluvial relict substratum composed of highly resistant bed of oxidized clay from Pliestoscene fluvio-glacial deposits that forms a firm bed over which sand dunes can pass (Nittrouer et al., 2011). There are USACE-constructed revetments on both banks of the river mostly within 50 ft depth. The top width of the river is approximately 2,000 feet. At this location, the river flow can range from 150,000 cfs to 1,250,000 cfs during typical annual flood events. The transported sediment consists of clay, silt and sand particles. The dominant hydraulic processes in the vicinity of the diversion are primary longitudinal velocities and weak transverse secondary currents due to the upstream river bend. Most of the annual sediment load moves through this river section as suspended load over the sand bar accompanied by bed load transport moving as dunes along the deeper portions of the sandbar. The presence of the diversion is likely to have both near-field and far-field morphological effects in the river with both erosion and deposition

possible. The three-dimensional turbulent velocity fields generated at the diversion intake are of interest for the design of an efficient diversion intake in relation to the hydraulics, sediment capture, design of armoring and to assess potential effects on navigation.

The MBSD diversion intake as-designed in the 90% E&D phase is constructed at an invert of -25 ft, NAVD888, located on the Alliance sand bar near RM 60.7. The river bed on the sand bar is typically composed of fine to medium sand having a median diameter (d_{50}) of 225 μ, a 10th percentile grain diameter of 176 μ and a 90th percentile grain diameter of 303 μ (Ramirez et al., 2013). The diversion is expected to be supplied by both locally sourced sand (>176 μ) and wash load. The wash load includes both non-cohesive and cohesive sediment in suspension, composed of very fine to fine sand (<176 μ) sources from upstream along with silt (2 μ -32 μ) and clay (<2 μ) (Allison, 2011). With a Rouse number (a ratio between the sediment fall velocity and the product of the von Kármán constant and the shear velocity) of less than one, most of the sediment is in suspension on the sandbar, during diversion operations (at greater than 450,000 cfs MR flow).

1.3.2 The Headworks

The headworks consists of the rip-rapped intake open structure in the river, followed by the concrete U-Frame with bulk-head gates and a rip-rapped gradual flared transition to the conveyance channel. The gate bays will open to the conveyance channel via a transition channel segment. The existing railroad will cross the rectangular bays.

The key hydraulic processes modeled in the river are the 3D velocity distribution, transport of sediment, potential erosion and deposition, shear stress variation and significance to the navigation. In the intake the important processes are the turbulence losses, sediment suspension, vorticity and any sediment deposition.

The gated diversion opening is approximately 220 feet wide. The gated structure is located on the protected side of the MRL. The structure is designed to capture as much sediment as possible at the design flow of 75,000 cfs and to obtain as high a SWR as achievable. Numerical models show that during operation, a complex three-dimensional velocity and turbulence field associated with sediment transport is generated at the structure entrance. A transition section, most likely trapezoidal in section, is required between the downstream side of

the gated structure and the conveyance channel which has a bottom width of about 250 feet and 1:7 channel side slopes. The important hydraulic considerations for the transition section are the reduction of contraction/expansion losses and reducing the potential for sediment deposition.

1.3.3 Conveyance Channel

The discharge and sediment from the gated structure enters the Conveyance Channel (CC) which transports it into the Barataria Basin. This channel has a trapezoidal cross-section with 100-ft wide side berms, a bottom width of about 250 feet and side slopes of about 1:7 (V:H). The length of the channel from the diversion gates to the outfall at the basin-side is approximately 2 miles. The channel invert is at -25 ft, NAVD88. The maximum design flow capacity is 75,000 cfs. About halfway along its length, the Highway 23 bridge crosses the proposed channel.

The key hydraulic processes modeled are the transport of sediment, potential deposition of sediment along the channel and uphill through the Outfall Transition Feature to the basin-side, which has a prevailing mud bottom grade elevation at about -4 ft, NAVD88. The energy loss by friction in the channel is the most important factor in maintaining 75,000 cfs design capacity.

The diversion is likely to be fully open between the months when the Mississippi River (MR) flow is predominantly above 450,000 cfs, with partial closure only when MR flow around 1,000,000 cfs and above. The gates will be partially open when MR flow is less than 450,000 cfs and this period, typically Aug-Dec is termed as base flow period. It is anticipated that a base flow or pulsed low flow will be required during river low flow periods (when the diversion is not operating for sediment delivery). This base or pulsed low flow is likely necessary to maintain water quality standards in the conveyance channel and the receiving basin. There is a possibility that sediment deposition will occur in the Conveyance channel during these base flow operations and occasional channel flushing may be required by opening the gates fully for a short period during the

1.3.4 Outfall Transition Feature

The Outfall Transition Feature (OTF) is a gradually flaring portion of the conveyance channel as it transitions from a deeper, regular trapezoidal cross-section to a shallower, wider basin Outfall. The key hydraulic processes in this region are the decelerating velocity field, formation of scour beyond the rip-rapped edge of the OTF and sediment distribution in the basin. The purpose of this feature is to achieve a gradual invert change from the conveyance channel to the basin floor so that the design flow can be achieved with minimal energy losses. The design is primarily important in the initial years of full operation during which the land beyond the OTF will evolve.

1.3.5 Barataria Basin

The discharge and sediment are released directly into the middle portion of the Barataria Basin. The basin is about 1,600 square miles with depths ranging from about 2 to 10 feet. The important hydraulic considerations in the basin are sediment dispersal and, deposition and erosion in the vicinity of the OTF and the surrounding areas. Water levels near the communities in the basins and velocities and sediment deposition in the navigation waterways are also important considerations.

1.4 Overall Modeling Approach

As described in the previous section, the nature of the hydraulics varies from the MR to the basin. The three-dimensional nature of the flow is important at the intake side while two-dimensional treatment of flow is sufficient at the basin side. Analyzing this large system entirely with a three-dimensional model would have made meeting the project schedule impossible, would have been cost-prohibitive and was determined to be unnecessary. Instead, each of the system components was modeled separately using appropriate modeling programs, while maintaining consistency in the boundary conditions. Additionally, larger domain models were developed combining the individually finalized diversion components so that the performance of the entire diversion system can be evaluated.

The modeling approach leverages work previously completed by CPRA /WI during the planning efforts including the model setup (e.g., model geometry, boundary conditions, Relative Sea Level Rise and Subsidence) and findings.

Two numerical models, FLOW-3D (FlowScience 2018) and Delft3D (Deltares 2018), were used for the analyses, to exploit their individual strengths. FLOW-3D is a fully three-dimensional non-hydrostatic Computational Fluid Dynamics (CFD) code and is used to compute the energy losses through the diversion system, detailed fluid structure interactions (e.g., flow around gates, walls, dolphins, transitions etc.) and study vertical velocity effects where important (e.g., flow over intake wing-walls). It is also used to estimate the SWR of the suspended sand using particle tracking, a completely different technique to Delft3D's scalar advection-diffusion method for sediment and therefore provides an independent insight. Delft3D solves the hydrostatic shallow water equations either in 2D or 3D mode which theoretically provides a slightly less accurate solution of the flow field in the immediate near-field of the intake but can be effectively calibrated through bottom roughness setups to yield similar horizontal velocities and energy losses as FLOW-3D through inter-model calibration. The strength of Delft3D lies in its strong suite of coupled sediment transport (both cohesive and non-cohesive) and morphology modeling including bedload transport, contribution of locally sourced sediment to suspension and is therefore able to compute areas of sediment scour and deposition. Another important aspect of Delft3D is the ability to run basin scale domains with multi-year hydrographs due to the lower computational overhead in solving the simpler hydrostatic equations without the non-hydrostatic pressure solver as in FLOW-3D. The results of both models are being augmented with a 1:65 scale undistorted live-bed physical model simulations which are documented in a separate technical report.

FLOW-3D Modeling

- Develop the MR only (without the diversion) FLOW-3D model geometry. Calibrate and validate the model using observed velocity and sediment profile data.
- Add diversion structures to the MR model and simulate the hydrodynamics and particle transport at a constant 1,000,000 cfs in the river and 75,000 cfs through the diversion structure (a steady-state simulation). Perform a hydrodynamics only model at constant 600,000 cfs MR flow and 48,000 cfs diverted flow for low flow.

- Calculate the water level, velocity and energy loss through the headworks.
- Calculate the SWR for the intake structure. Use the energy head loss available from the FLOW-3D modeling and perform Delft3D sediment transport model
- Calculate flow losses and determine discharge capacity when gates are partially closed either during base flow to limit flow to 5,000 cfs or at high flow when diversion flow can exceed 75,000 cfs without gate operations.

Delft3D Modeling

- Develop the MR only (without the diversion) Delft3D model geometry. Calibrate and validate the model using observed velocity and sediment profile data.
- Add diversion structures to the MR model and calibrate the energy losses through the structure under the same constant 1,000,000 cfs (High Flow) 600,000 cfs (Low Flow) scenarios (steady-state simulations) as FLOW-3D.
- Develop rating curves for flow through the structure using multi-year hydrograph simulations and calculate SWR and CSWR for the structure.
- Perform 50-year future modeling with structure morphology, vegetation growth and senescence associated vertical accretion and salinity modeling to evaluate basin-side and riverside effects. Sea level, subsidence and consolidation are also included in the modeling.

1.5 Scope, Assumptions and Limitations

The hydraulic modeling is focused on the Engineering & Design of the diversion system that will meet the project goals of providing 75,000 cfs flow. Several related modeling activities such as evaluation of secondary project features (e.g., diversion intake marine protection features) are not completed at this stage.

1.6 Modeling Programs

Considering the important hydraulic processes and the previous work by the WI CPRA, two multi-dimensional modeling programs were selected. The modeling programs are briefly described below.

1.6.1 FLOW-3D Modeling Program

Several CFD models exist that can be used to model the MBSD diversion. In this application, it is imperative that the model has the ability to efficiently solve for the location of the free surface as well as the turbulent three-dimensional near field hydrodynamics produced due as a result of fluid structure interaction at the intake. The FLOW-3D three-dimensional (3D) CFD platform licensed from Flow Science, USA (FLOW-3D 2018) was selected as the appropriate modeling tool for the near-field hydrodynamic and the suspended sediment transport modeling. FLOW-3D was used previously by CPRA/WI to model the flow and suspended sediment through sediment diversions during the planning phase (Meselhe et al. 2012, ARCADIS & WI 2013). It was proven to be able to capture the complex 3D flow field in the vicinity of the diversion as well as quantifying the spatial distribution of the suspended sediment on the lateral bar near the diversion. FLOW-3D was also used in the study by HDR Engineering as described in the 30% design report (HDR 2014) for alternatives screening. FLOW-3D is currently the only available commercial CFD model capable of simulating suspended sediment in free surface flows over complicated river bathymetries, irregular banks and intake structure using structured grids (Allison et al. 2017). Since FLOW-3D solves the complete 3D Reynolds-Averaged Navier-Stokes equations with turbulence closure, it is inherently non-hydrostatic and gives more accurate vertical flow profiles than models that are based on the shallow water equations. However, the model is computationally intensive, with relatively long computational times for this application. Therefore, the FLOW-3D analysis was only applied to selected steady-state flow conditions. The model was used to determine the energy loss through the system and the SWR using a discrete particle (with mas) tracking model. One limitation of FLOW-3D is that it does not include a validated and efficient model for simulating bedload transport and the erosion and deposition of sediment near the diversion. Therefore, it is not applied for morphology modeling in this modeling effort.

1.6.2 Delft3D Modeling Program

The Delft3D model (Deltares 2018), on the other hand, solves the hydrostatic shallow water equations either in a 2D or a 3D mode with sigma co-ordinates and unlike FLOW-3D is ideally suited for long term simulations over large spatial scales. The unique advantage of Delft3D is its ability to model morphology change with sediment transport (suspended and bedload) that is coupled with the hydrodynamics. Thus, Delft3D has been used widely as the most reliable model for long term morphology and sediment transport tasks by CPRA/WI during the planning phase (Meselhe et al. 2015, Meselhe et al. 2016, Gaweesh et al. 2016) and will remain as the model of choice for the present project for long term and large-scale simulation runs where the hydrostatic assumption mostly holds true. For the present modeling tasks Delft3D will be used for hydraulic and sediment design of the conveyance channel, evaluating deposition/erosion in the Mississippi river, the conveyance outfall and discharge conditions. The discharge conditions shall be furnished to CPRA/WI, in a coordinated effort, to develop long term land-building and evolution of channels in the basin side, basin-wide flooding concerns, navigation concerns and basin-wide impacts of diversion operations and climate change.

1.7 Multi-Scale Domains Used for Modeling

Several 2D and 3D numerical models of varying spatial details were developed to focus on specific hydraulic processes and aspects of the diversion in a computationally efficient manner. Table 1.1 provides the general model descriptions. The model names are based on their spatial extents which are shown in Figure 1.1. The FTNULMR model is shown in in Figure 1.4.

Each named model is either a FLOW-3D or a Delft3D model. The FLOW-3D was always used in the 3D mode while the Delft3D model was used in either a 2D or a 3D mode. To maintain consistency with the related modeling performed by the WI for CPRA, the DT obtained the projected land-building topography, Gulf of Mexico Year 50 water levels and the Seal Level Rise (SLR) trend from WI's Basin-wide model (Figure 1.3) and incorporated the same for all tasks dealing with future conditions. The WI had also developed an OMBA (Outfall Management BArataria basin) Delft3D model, the extent of which is similar to DT's FTNOMBA model.

Table 1.1. Mid-Barataria Sediment Diversion numerical models developed by the Design Team.

Model Name	Modeling Software	Spatial extent	Application
FTNMS	FLOW-3D Delft3D (2D) (Hydrodynamics Only) Delft3D (3D)	MR only FLOW-3D between RM 58.1 and 62.7 Delft3D between RM 56 and 66	• Calibrate and validate with the observed discharge, water levels and sediment concentrations in the MR
FTNMSDI	FLOW-3D Delft3D (2D) (Hydrodynamics Only) Delft3D (3D)	MR + Headworks + Conveyance Channel segment 1500 ft	• Screen intake size and alternatives including optimizations using total energy loss and SWR • Refine transition segment, estimate Zone of Influence • Provide data for navigation simulations • FLOW-3D Gate modeling for gate position analysis important for transition rip-rap design • FLOW-3D used to calculate the discharge, WL, DAV and energy grade line for use in Delft3D calibration • DELFT3D morphology model for intake sediment mound flushing analysis
FTN2COMP	Delft3D (2D) (Hydrodynamics Only) Delft3D (3D)	MR + Headworks + Conveyance Channel segment 4150 ft	• Model diversion operation scenarios • Calculate CSWR with the final selected intake, MR hydrograph runs • Calculate flow and sediment load rating curve at the end of conveyance channel • Investigate stability of sand bar with MR hydrograph runs • Investigate river deposition/erosion within ~5 mi upstream/downstream of diversion
FTN3COMP	FLOW-3D	MR + Headworks + Conveyance Channel (full) + basin portion (~3 mi from end of conveyance channel)	• FLOW-3D used to calculate the discharge, WL, DAV and energy grade line for use in Delft3D FTNOMBA diversion structure calibration • FLOW-3D modeling of OTF jet structure on non-erodible bed (no MR domain) • Turbulent flow structure analysis within scour hole (eroded bed) formed at the end of OTF armored extent (no MR domain)
FTNOMBA and FTNOMBARefined	Delft3D (2D)	MR + Headworks + Conveyance Channel (full) + Barataria basin (whole)	• Capacity estimation of the three-component MBSD design under various possible MR discharge/water level and basin side water level combinations • Develop boundary conditions for above models • Basin-side water levels and velocities • Outfall evolution modeling with and without river sediment (no MR domain) • Wind induced water level and velocities during regular diversion operations (no MR domain) • FTNOMBARefined has the same domain as FTNOMBA but 4x times (25 ft x 25 ft grid sizes in horizontal in Refined compared to 50 ft x 50 ft in FTNOMBA) higher grid refinement within 4.7 miles from the end of the conveyance channel in the outfall vicinity. Domain decompositions also improved in FTNOMBARefined to enhance load balancing among processors and to improve model run times • Salinity modeling during diversion operations, particularly channel flushing modeling
FTNGATE3Bay (Not shown in Figure 1)	FLOW-3D Delft3D (3D)	Intake U-Frame + Conveyance Channel (full)	• FLOW-3D Modeling of high velocity under-gate jet during low openings at highest MR water levels • FLOW-3D Modeling of intake transition design • Delft3D modeling of channel berm deposition • Delft3D modeling of channel deposition during base flow and channel flushing modeling
FTNULMR	Delft3D (2D)	MR from Reserve, LA (RM 140) to W Pt A La Hache (RM 48.7) +MBSD headworks +MBrSD intake +MBSD Conveyance Channel segment (4150 ft)	• Joint or single diversion induced setdown in MR particularly at Bonnet Carre • Joint or single diversion induced morphology change in MR

Table 1.1. Mid-Barataria Sediment Diversion numerical models developed by the Design Team (continued).

Model Name	Modeling Software	Spatial extent	Application
FTNOMLV-CONSOL	Delft3D (2D)	MR from RM 66 to RM 56 (for hydrodynamics only) +MBSD headworks +MBrSD intake +MBSD Conveyance Channel segment (full) +Barataria Basin (whole)	• Basin-side 50 year future modeling of morphology, vegetation accretion, sea level rise, subsidence and consolidation. • Dredging estimates and discharge capacity change in the future as a result of sea level rise and land building.
FTNOMBA-ULMR	Delft3D (2D)	MR from RM 66 to RM 56 +MBSD headworks +MBrSD intake +MBSD Conveyance Channel segment (full) +Barataria Basin (whole)	• Diversion operations modeling of tidally influenced water levels and diversion discharge variation • Base flow operations

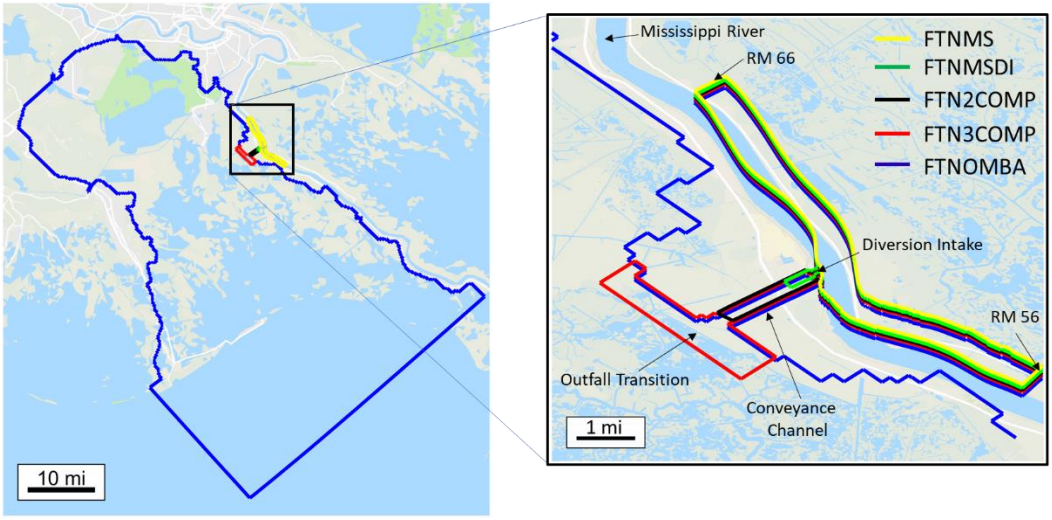

Figure 1.2. Spatial extents of numerical models developed by the Design Team for the Mid-Barataria Sediment Diversion project. Inset view is isometric to show distinction in the overlapping model boundaries.

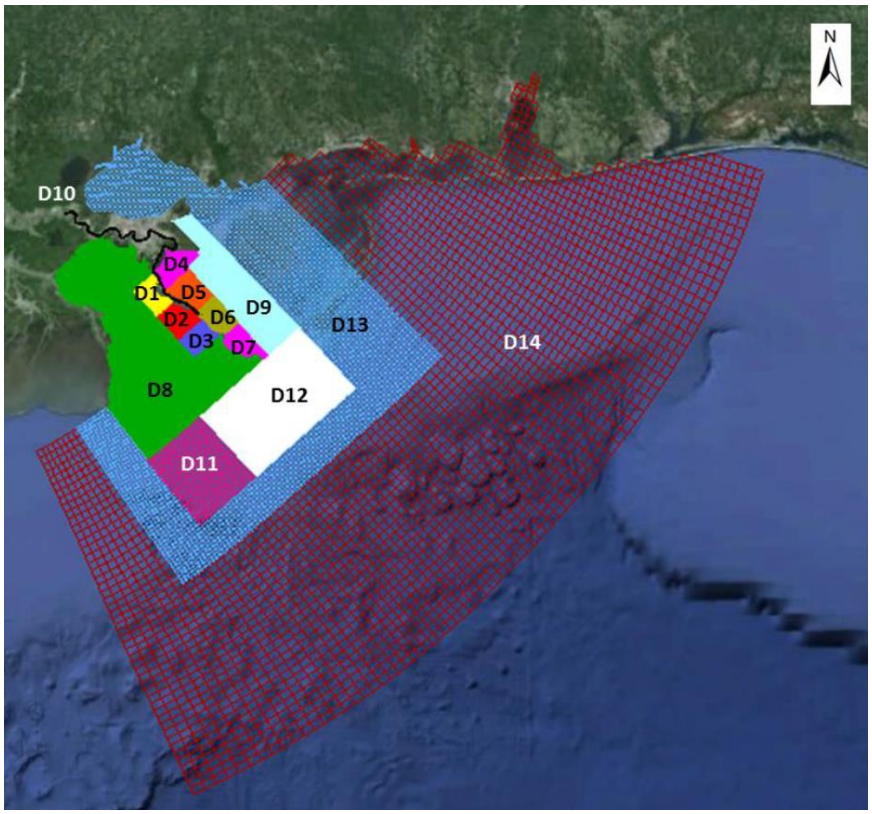

Figure 1.3. The Basin-wide Delft3D model by the Water Institute.

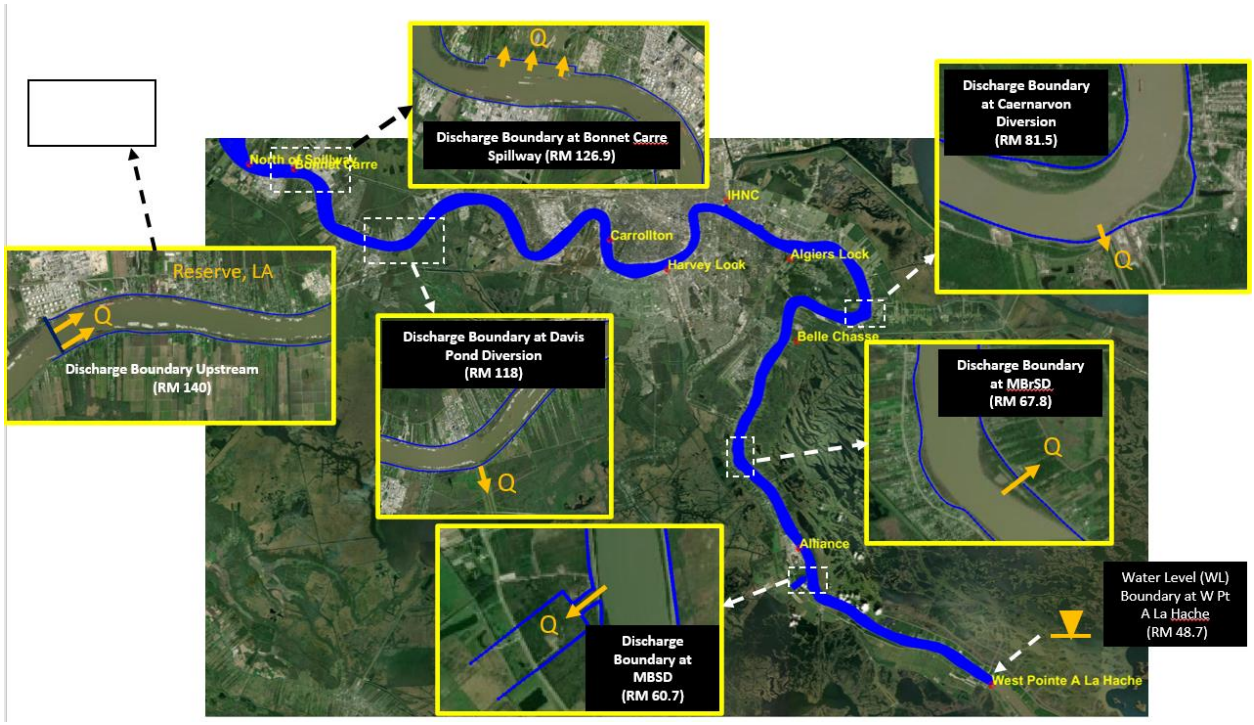

Figure 1.4. FTN Upper Lower-Mississippi-River (FTNULMR) model consisting of the MR between RM 140 to RM 48.7 and the two proposed diversions (MBSD and MBrSD) along with Davis Pond and Caernarvon.

2.0 MISSISSIPPI RIVER FLOW AND SEDIMENT DATA ANALYSIS

2.1 Introduction

This section describes the MR hydraulic and sediment monitoring data collected and used for numerical modeling. For a full description of the methods of collection, the locations and the events the reader is referred to the relevant MR field data collection reports from 2008-2011 (Allison 2011), from 2018 (Allison et al. 2018) and 2019-2020 (TBS 2019, 2020). The data analyses that were directly used for modeling and whose descriptions are not in the aforementioned reports are only presented here.

The 2020 data collection is described as an example. Similar analyses were performed for the 2018 and 2019 data sets. The locations of the 2020 Acoustic Doppler Current Profiler (ADCP) MR monitoring transects, bed grabs and isokinetic data collection are shown in Figure 2.1 and 2.2. The Phoenix bend location was additionally selected for monitoring survey in 2020 because the sediment transport modeling conducted in the 30% E&D phase indicated possible deposition along the Myrtle Grove sand bar and the ship channel that is in close proximity to this bend as a result of diversion operations. The collected data was used to inform and calibrate model results for river morphology modeling as presented in Chapter 9.

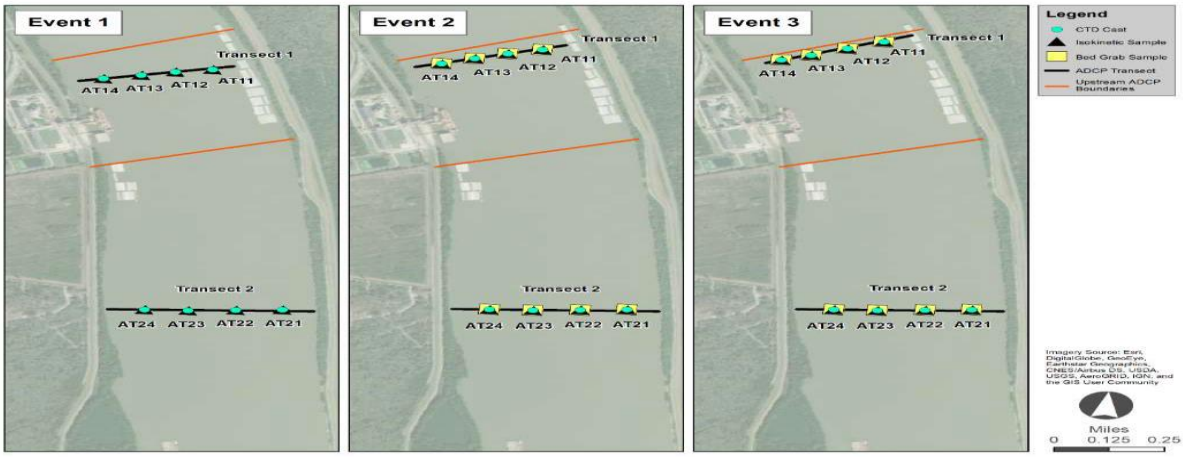

Figure 2.1. Locations of 2020 MR ADCP, bed grab and isokinetic measurement transects upstream and on the Alliance sand bar.

Figure 2.2. Locations of 2020 MR ADCP, bed grab and isokinetic measurement transects downstream near the Phoenix bend over the Myrtle Grove sand bar.

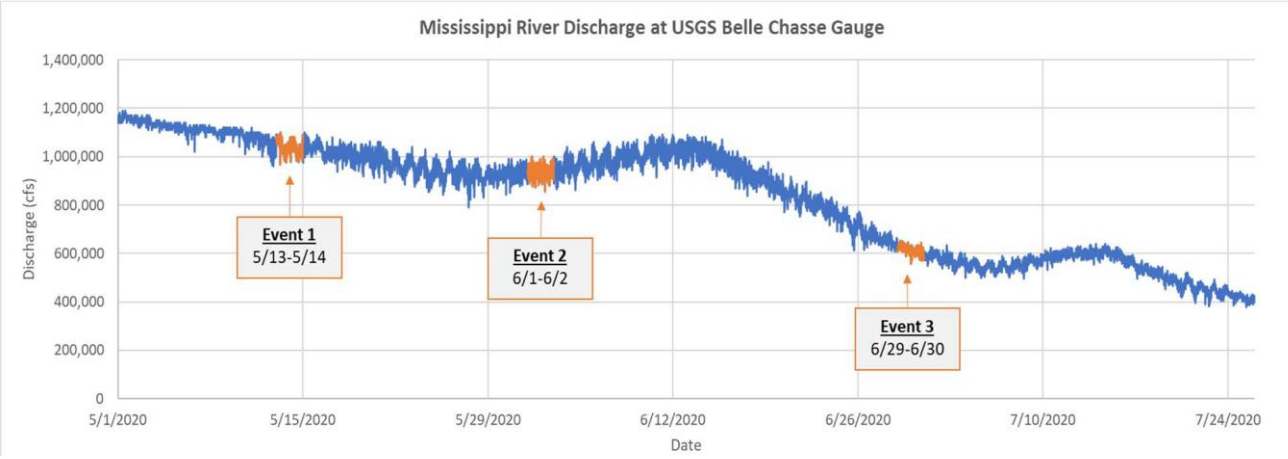

Figure 2.3. Dates of the data collection events in 2020 (Reproduced from TBS 2020).

2.2 ADCP Data Analysis

The ADCP data analysis was conducted using the USGS VMT toolbox and the WinRiver software to analyze the raw data collected from 2018-2020. The MR monitoring data collected from the earlier study period 2008-2011 was directly obtained from Allison (2011). Figure 2.3 shows the data collection events in 2020 with the MR hydrograph at Belle Chasse. For the 2018-2020 period, the following data were analyzed:

1. Cross-sectional velocity distribution at the transects as shown for example in Figure 2.4 for 2020. The net discharge flux through each ADCP 2D vertical grid was obtained by multiplying the velocity at a grid point by the cross-sectional area of the grid.
2. Cross-sectional sediment concentration derived from the isokinetic data calibrated ADCP backscatter. For more details see Allison et al. (2018) and TBS (2019 and 2020).
3. Total suspended sediment load (flux in tonnes/day) was computed by integrating the net sediment discharge flux at each cell over the entire 2D vertical transect. The sediment discharge at each cell was obtained by multiplying the discharge flux from step #1 above with the concentration from step #2 above.

Sediment loads computed in step #3 were then used for calibrating/validating net sediment flux in the sediment transport models as presented in Chapter 3.

2.3 Multibeam Data Analysis

Multibeam data (24 hour spaced snapshots) from 2018-2020 were analyzed in Allison et al., (2018) and TBS (2019 2020) to develop bedload transport flux (tonnes/day) over the Alliance sand bar. The method of Nittrouer et al. (2008) was used to compute the bedload transport. The observed bedload was used to calibrate and validate the sediment transport models as shown in Chapter 3. Additional data for bedload transport rates from 2008-2011 period was obtained from Allison (2011) and compared with model results as well.

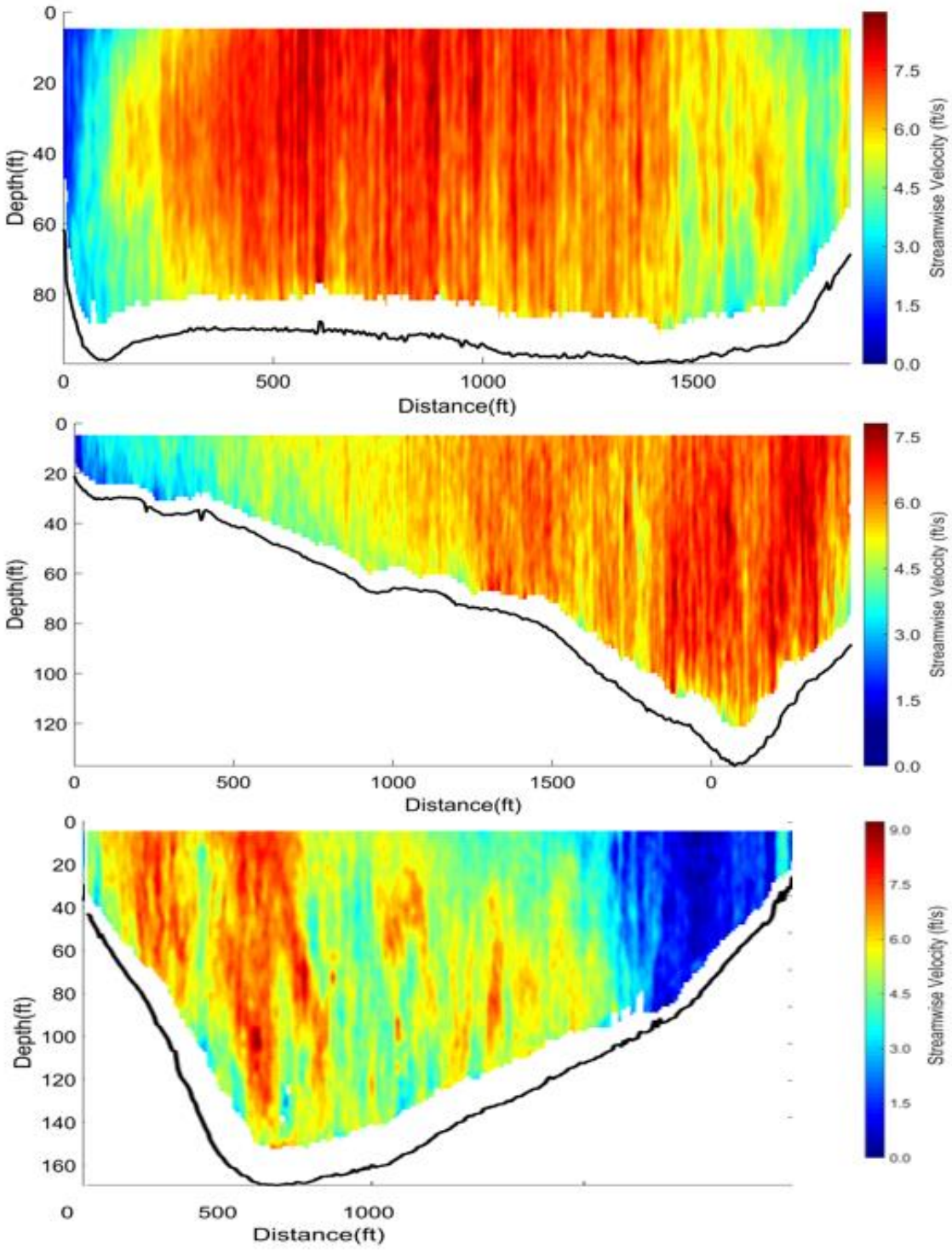

Figure 2.4. Example of ADCP data analysis of Event 1 in 2020 using USGS VMT Toolbox. Top panel shows the upstream-most Transect 1, mid-panel shows Transect 2 at the proposed MBSD location and the bottom panel shows Transect 3. All transects are shown looking upstream.

2.4 Suspended Sediment Data Analysis

Suspended sediment transport data analysis consisted of isokinetic and suspended sediment grain size distribution. The latter was available for the 2020 events only.

2.4.1 Isokinetic Data Analysis

Isokinetic data collected at discrete points along the vertical was used to calibrate and validate the modeled vertical suspended sediment concentration profiles as shown in Chapter 3. Both data sets from 2008-2011 and 2018-2020 were used even though only the 2008-2011 period is shown in the results. The isokinetic data was independently used by TBS (2019, 2020) to calibrate the backscatter-based suspended sediment concentrations explained in Section 2.2 above that was later used for development of MR suspended sediment transport flux.

2.4.2 Suspended sediment grain size distribution

A Beckman Coulter particle size distribution analysis was used to determine the d10 (10% retained), d50 (50% retained or median diameter) and d90 (90% retained) particle sizes of the sand (> 63 micron) fraction of the sediment. Even though the particle size distribution was below 63 microns for the fines was available, this was not determined to be of significant value for modeling as in field conditions almost all of the fines are in flocculated state. The Beckman Coulter method being a laboratory method does not retain the in-situ floc structure, therefore results from this method for fines can be misleading. Instead CTD/LISST data collected for in-situ median size was used to inform the model grain size for fines which indicated median floc sizes of around 20-48 micron for most of the suspended fines. In the model a single 32-micron diameter grain size is used as the representative silt fraction size and 2 micron for clay. Also due to lack of definitive scientific support in the literature for the classification of silt classes in the flocculated regime, attempts to divide the silt class further (into say fine to coarse silt) was avoided to avoid the risk of ‘over-tuning’ the model. Therefore, the focus of the isokinetic suspended sediment particle size distribution analysis for modeling was on sand, particularly to understand if the grain sizes vary spatially or from event to event and whether the model could reproduce those changes.

Figures 2.5, 2.6 and 2.7 show the vertical variation of sand d10 (green), d50 (blue) and d90 (magenta) for the 2020 Events 1,2 and 3, respectively. Note that all the events in 2020 were falling limb events unlike the 2008-2011 period data by Allison (2011) which was analyzed by Ramirez et al. (2013). Therefore, the sand size distribution analyzed here allowed for the first time to understand the falling limb size classification. Interestingly, the d50 of the near-bed suspended sand (at a distance of at least 10% of the depth above the bed), remained slightly below 170 micron (110-170 micron) for all the locations except AT24 (Event 1 Figure 2.4). This confirms Ramirez et al (2013)'s observations that the median sand size in suspension is finer than 176 micron for most of the discharge hydrograph. The AT24 location was on a region over the sand bar affected greatly by dunes of height over 6 ft and traveling near the thalweg and may have been affected by high energy turbulent bursts which were able to suspend medium to coarse sand. Comparing the observed results to the model output indicated that the model shows a median size variation of about 100-150 micron (based on flow) near the bed is able to capture the range of observed variation well.

In particular note that at the upstream Transect 1, AT11-AT14 the cross-sectional variation of the grain sizes is lower than at the Transect 2, because Transect 1 is located between two consecutive sand bars (the Alliance sand bar on which MBSD is proposed and one just upstream of the CHS terminal near the RDB) where it is at a more or less uniform depth (see Figure 2.4 top panel). The choice of the upstream transect was Slight coarsening of sand is indicated at AT12 and AT13 and based on the model of suspended sediment movement from the model appears to be due to streaming of bedload from the shallower upstream bar flowing over the deeper zone and able to remain suspended due to the turbulence in the deeper depths and short distance between the bars. The figures also show that at AT21, the transect closest to the intake of the MBSD diversion and where the sediment sizes in the MR are likely to be the most representative of the sediment sizes in the intake as well, the sand in suspension is predominantly finer (mostly very fine to fine sand in the 80–110-micron range) than that near the deeper portions of the Alliance bar (say AT 13 and At14). This is because of the lack of bedform activity in the relative low velocity zone (see Figure 2.4, mid panel at the shallow 20 to 40 ft deep zone near the right descending bank) which results in most of the sand available to the

diversion sourced from the suspended load either from local resuspension or from upstream bars. However, this interpretation does not consider the effect of the diversion on the river sediment and particularly the tendency of the diversion to be able to draw sand from the deeper inverts as will be explained in Chapter 4 later. As the results will show, some local coarsening of the suspended sand may be expected, fed by bedload and drawn towards the diversion when the diversion is operational. Model results show around 100–150-micron median grain size of the diverted sand and contains about 28% of medium sand (250 micron) by weight, mainly sourced from the bed material load.

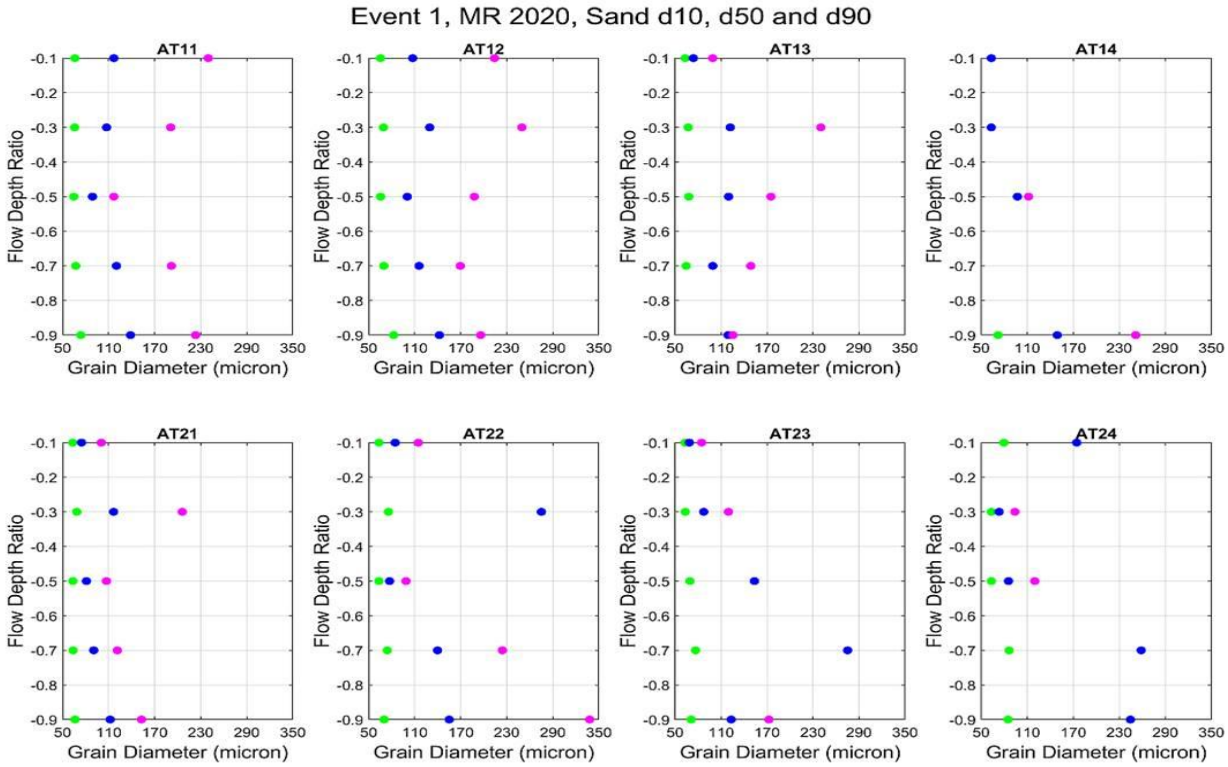

Figure 2.5. Event 1 of 2020, vertical variation of d10, d50 and d90 of sand (d50 >63 micron). Top panel shows locations along Transect 1 and bottom panel along Transect 2 as in Figure 2.1.

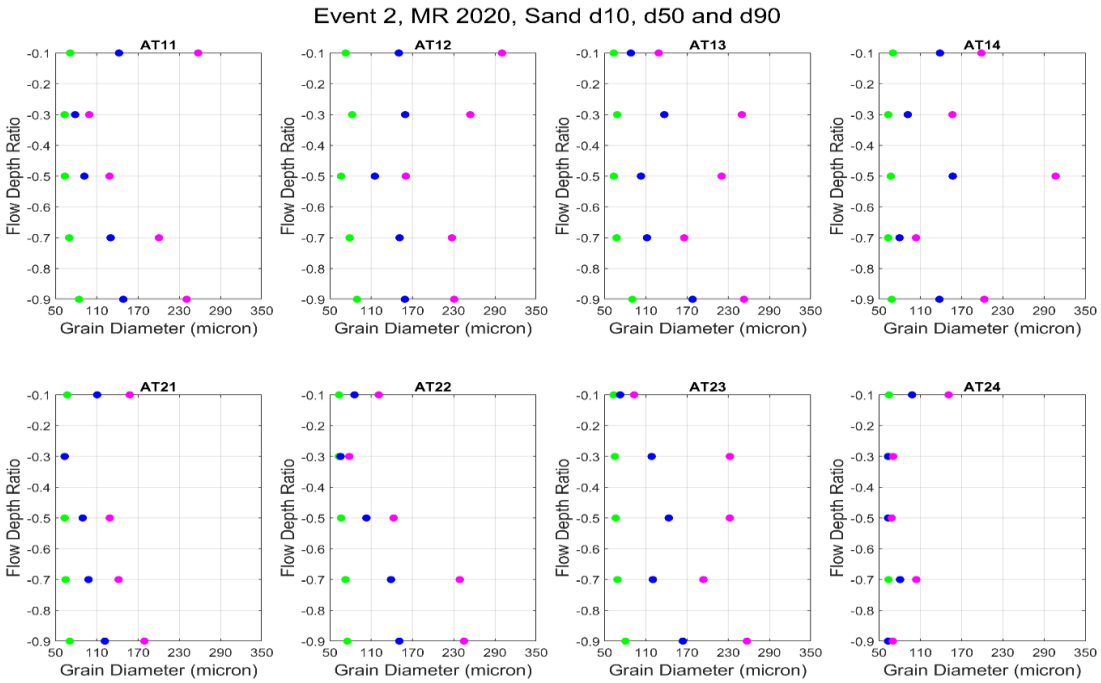

Figure 2.6. Event 2 of 2020, vertical variation of d10, d50 and d90 of sand (d50 >63 micron). Top panel shows locations along Transect 1 and bottom panel along Transect 2 as in Figure 2.1.

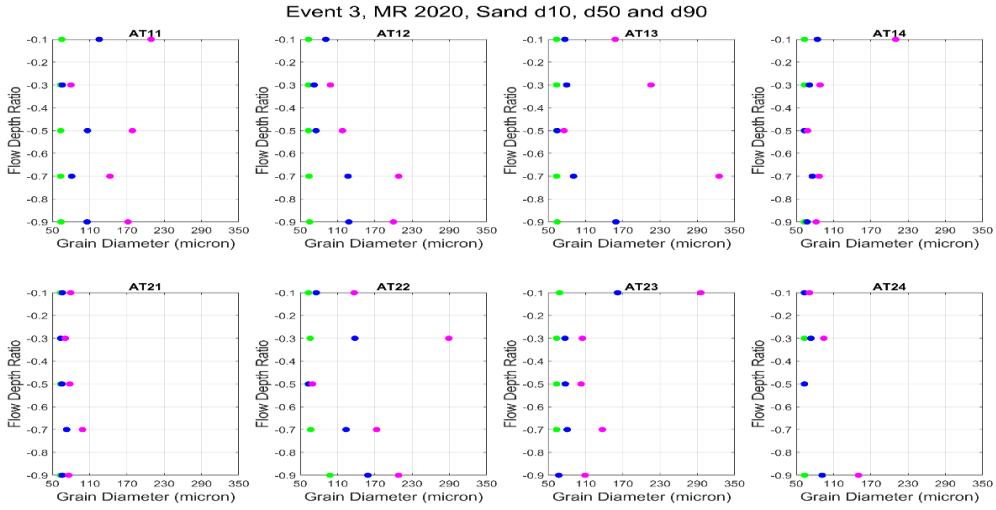

Figure 2.7. Event 23 of 2020, vertical variation of d10, d50 and d90 of sand (d50 >63 micron). Top panel shows locations along Transect 1 and bottom panel along Transect 2 as in Figure 2.1.

2.5 Historical Evolution of the Alliance South Sandbar (1964-2018)

To provide a context for understanding the results of the river morphology model (Chapter 9), long-term changes in the Alliance sandbar were examined using the historical observed records. The purpose of this analysis is to understand the general trend in the sand-bar evolution over the last 55 years (1964-2018). The USACE channel surveys data from 1964 through 2013 were used along with the 2018 multibeam data collected by Allsouth Consulting, a member of the DT. During the 2018-2020 hydrograph, the maximum intra-annual variation of bed elevation was found to be about 10-20 ft. Most of the variation was between 2-8 ft within the most active part of the bar that spans between -60 to -110 ft, NAVD88. This range of variation agrees with the dune heights of 2-3 m observed by Ramirez et al. (2013) in this region during the 2008-2011 MR surveys.

Figure 2.8 shows the evolution of the sandbar over time from 1964 to 2018. This period is particularly relevant as it shows the local response of the Alliance bar as part of the regional LMR reach response to the combined effect of the opening of the Old River Control structure in the early 1960s resulting in a backwater effect and reduced bed material supply (Mossa 1996, Biedenharn et al. 2000, Wu and Mossa 2019). It shows that there has been a distinct downstream migration of the bar (seen from the -60 ft to -90 ft, NAVD88 contours) along the right descending bank from 1964 to 1992. From 2004 onward the top part of the bar (shallower than -60 ft) appears to be shrinking in size along with a deepening of the thalweg. The cross-river distance between the -60 ft and -90 ft contours has increased considerably between 2004 to 2018 indicating flattening of the bar between the -60 to -90 ft, NAVD88 contours. The relative downstream movement of the bar and deepening of the thalweg agrees well with the general trend in this LMR reach between the BCS and Empire, LA which is currently degrading (Wang and Xu 2018). In light of these observations, the possibility of the sandbar reducing further in size due to the river dynamics alone (i.e., without the diversion) in the next 50 years cannot be entirely dismissed.

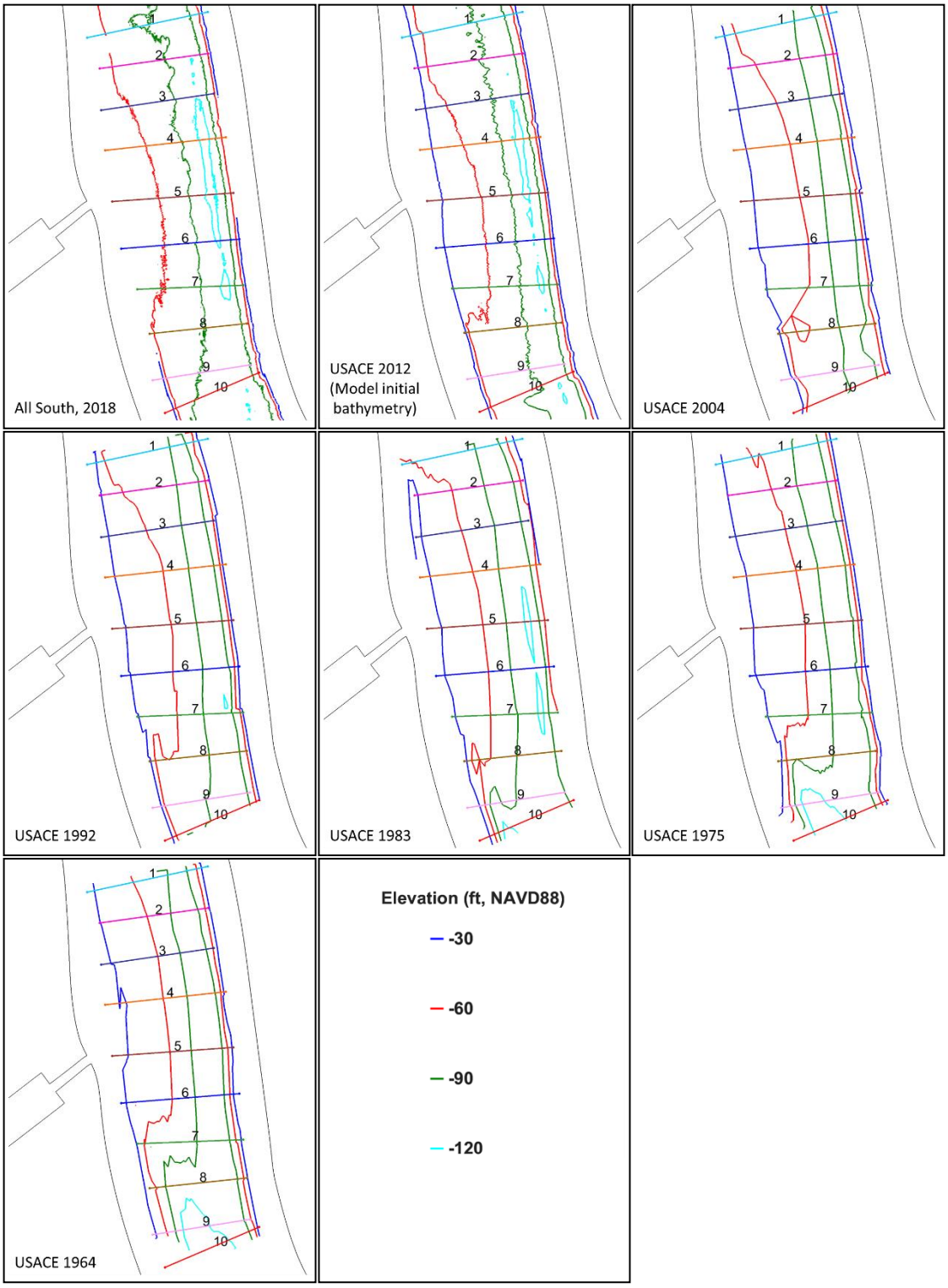

Figure 2.8. Historical evolution of the Alliance sandbar between 1964 to 2018. Cross-sectional evolution along the line transects is shown in Figure 4.2.

Figure 2.9 shows the evolution of the sandbar cross-sections along transects 2, 4, 6, 8 and 10. Transects 8 and 10 clearly show the downstream movement of the sandbar as explained before. The downstream portion of the sandbar south of transect 6 shows more variability than the upstream portion between transects 2 and 6. In general, transects 2 to 6 show an elevation variation of about 30-40 ft on the sandbar between -50 to -90 ft, NAVD88. The deepening of the thalweg is also consistent after 2004. In comparison, the cross-section zones shallower than -50 ft (protected by USACE revetments) do not show much variation (8-13 ft). A steep fall in elevation is visible for both transect 2 and transect 4 at the edge of the revetment zone in the recent 2012 and 2018 surveys.

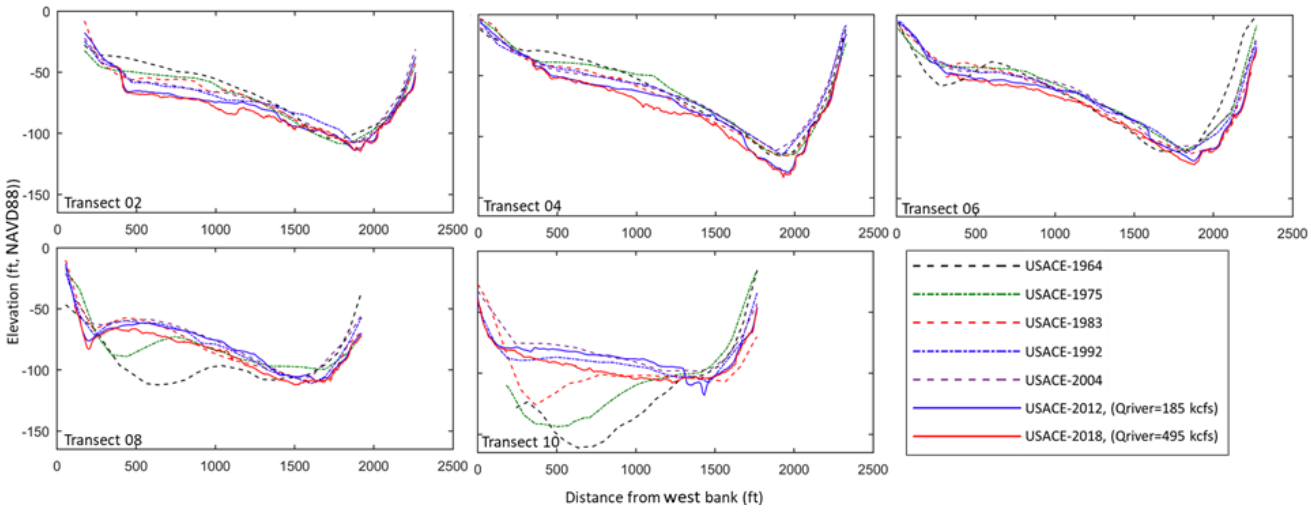

Figure 2.9. Historical evolution of the Alliance sandbar cross-section, looking upstream, over time (1964-2018). Transects locations shown in Figure 2.1.

3.0 MODEL SETUP, CALIBRATION AND VALIDATION

3.1 Introduction

This chapter describes the setup, calibration and validation of the *without-structure* FLOW-3D (fully 3D) and Delft3D (2D and 3D) MR models (FTNMS) used in this study. The setup of the *with-structure* models (FTNMSDI/FTN2Comp and FTNOMBA) and the larger FTNULMR 2D Delft3D model are also described in this section. The summary of model domains and purpose is presented in Table 1.1 and Figure 1.2.

3.2 FLOW-3D (FTNMSDI) Model

A FLOW-3D fully three-dimensional (3D) model with the diversion structure (FTNMSDI) was developed to model the intake hydrodynamics whose results are described later in Section 4.0. The model without the diversion structure (FTNMS) needed to be first calibrated and validated against observed MR hydrodynamic and sediment data for without-structure conditions to assess performance of the model in predicting the flow-field approaching the diversion and the cross-sectional distribution of sand. The riverside flow-field and the cross-sectional sand distribution are the two most important governing factors of the primary design goals, which are to minimize head loss and maximize sand SWR to the extent possible under the site-specific conditions and constraints of a constructible and economic design.

3.2.1 Model Setup

The FTNMS/FTNMSDI model bathymetry of the MR extends from RM 58.1 downstream to RM 62.7 upstream. The proposed MBSD diversion is located at RM 60.7. The DT combined the US Army Corps of Engineers (USACE) 2013 published (collected in 2012) multibeam survey data and the USACE 2017 collected and published revetment survey data into one three-dimensional geometry (XYZ) file (Figure 3.1). In addition, lidar data was used to set the levee heights. A high resolution stereolithography (.STL) file (Figures 3.3 and 3.4) with 1.4 million triangulated faces was created to represent the MR bathymetry in FLOW-3D. The STL file had a surface grid resolution of 25 m in the north and south 3.5 mi zones (Figure 3.2)

between RM 62.5-RM 66 and RM 56-RM 59.5, respectively, while the middle three miles between RM 59.5-62.5 had a 3 m resolution where the diversion intake is located.

To reduce the computational cost (computer time) while maintaining accuracy, the actual model domain in FLOW-3D was truncated compared to the corresponding Delft3D FTNMS or FTN2Comp models (which extend from RM 56 to RM 66) at the upstream and downstream extents. Sensitivity results from initial runs showed the boundaries were far enough in the FLOW-3D models to not affect diversion intake dynamics. The upstream boundary was placed at approximately RM 62.7 and the downstream boundary at approximately RM 58.1, consisting of approximately 4.6-mile-long MR domain. The diversion intake geometry was first created in Autodesk Civil 3D. Later, the Civil 3D drawing (.DWG) files were processed in Solidworks and converted into Solidworks ".STL" files for use in the numerical model. To create the model geometry with the structure, the diversion intake .STL file was merged with the river geometry to produce a single bed surface consisting of the river and the diversion intake structure.

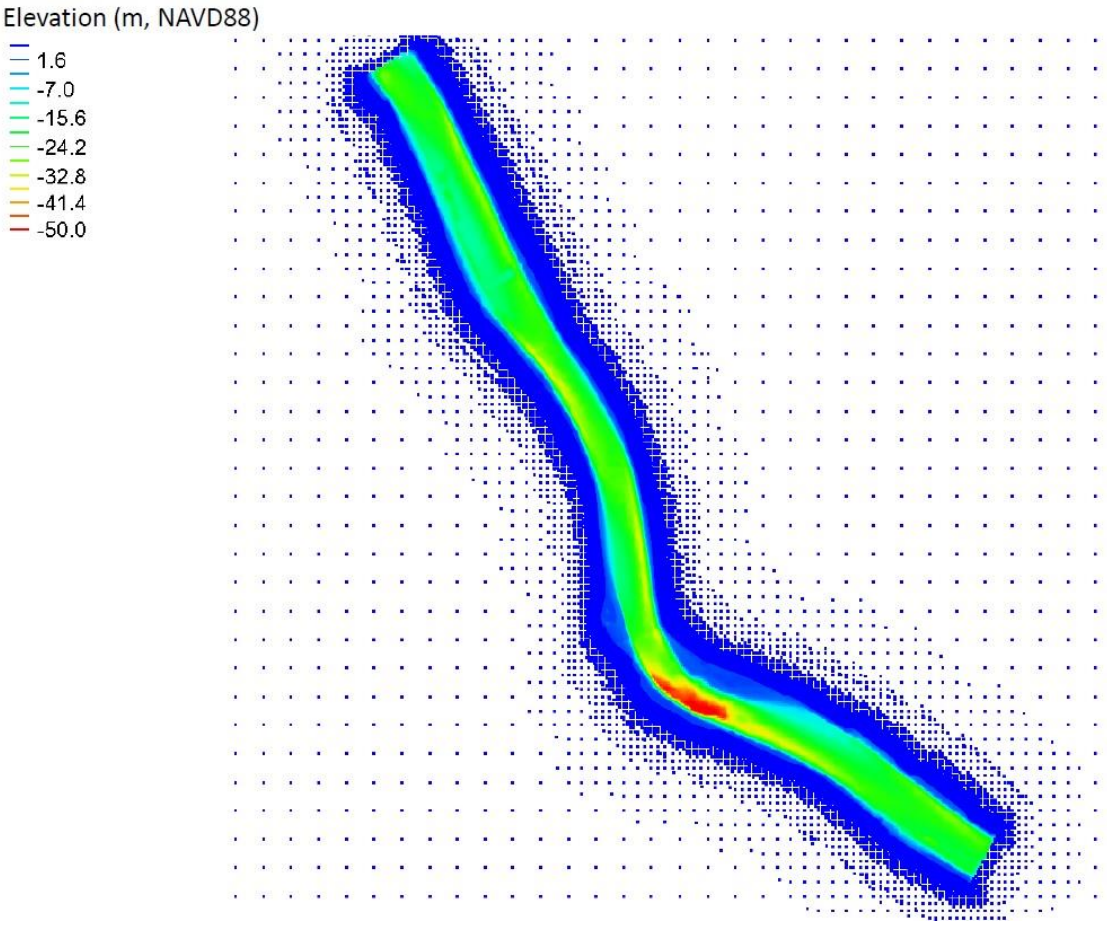

Figure 3.1. Contour plot of the river bathymetry shown using point cloud (XYZ) data.

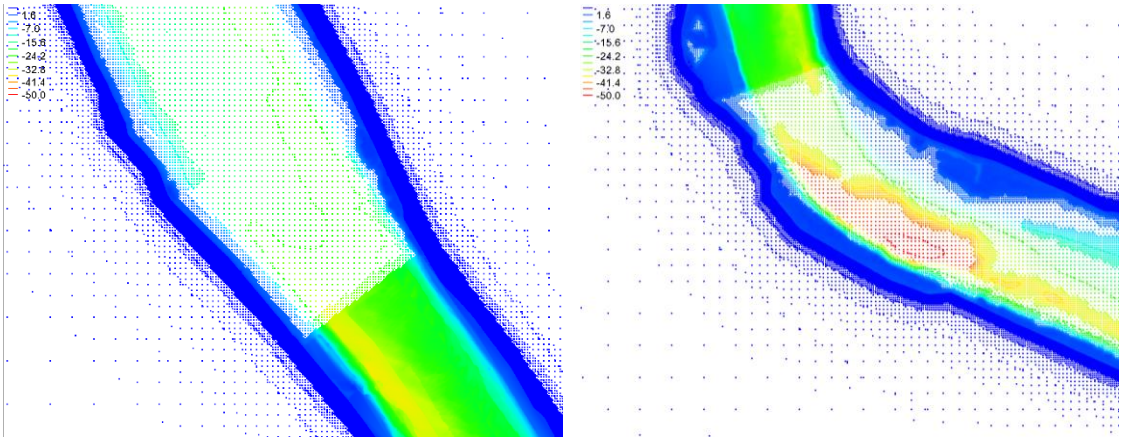

Figure 3.2. Bathymetry resolution: 25 m (82 ft) for the northern and southern 3.5-mile sections and 3 m (9.8 ft) for the middle 3-mile segment (Elevations are in meters, NAVD88).

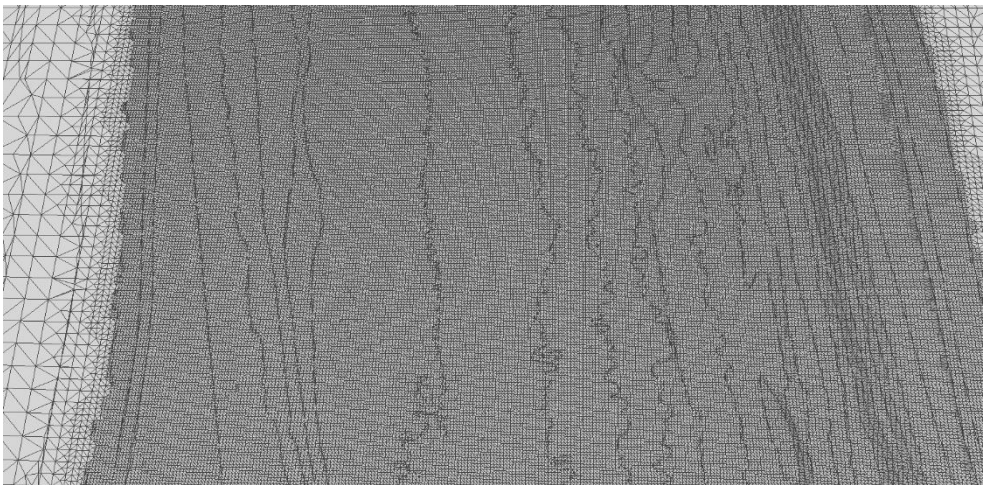

Figure 3.3. Snapshot of the middle block with 3-meter resolution face triangles in the stereolithography (.STL) file.

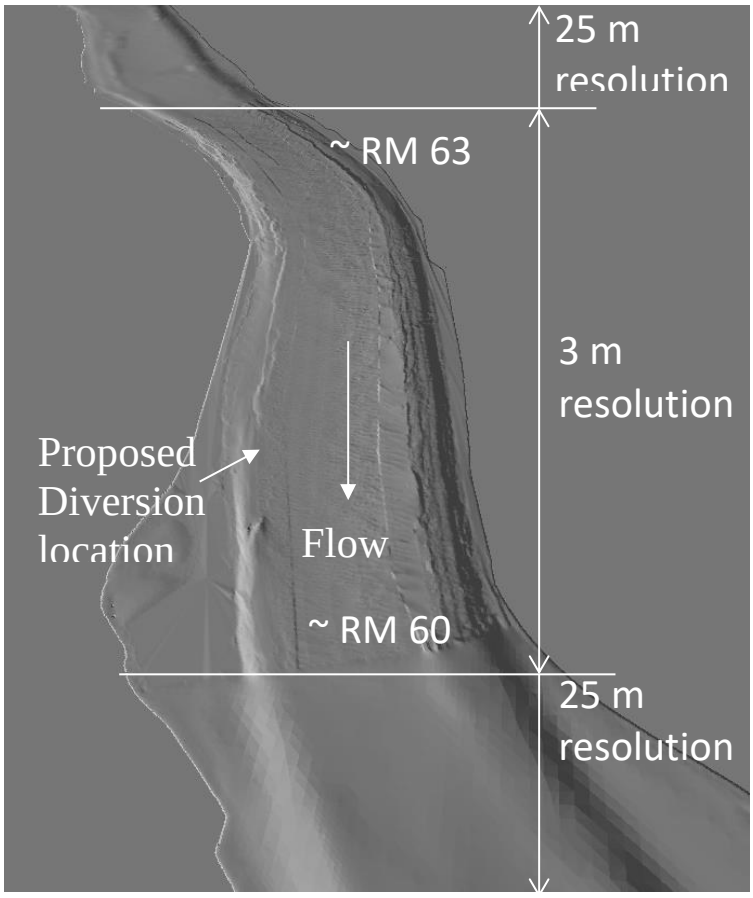

Figure 3.4. Illustration of the final river-only (FLOW-3D FTNMS) bed surface geometry.

The FLOW-3D model uses a structured hexahedral mesh. Each mesh block has six sides and grid lines must extend straight through the entire mesh. FLOW-3D allows the use of multiple mesh blocks where flow passes between adjacent mesh blocks to vary the grid resolution in specific zones of interest. The FLOW-3D mesh used for the simulations consists of three mesh blocks. The middle block includes the diversion geometry and extends 0.3 mi upstream to 0.6 mi downstream of the diversion location. As shown in Table 3.1, the mesh resolution for Block #2 varies from 1.3 m to 6 m (4.3 ft to 19.7 ft) in the horizontal plane (Δx and Δy) with coarser resolutions at the north and south ends and the highest resolution (1.3 m or 4.3 ft) near the diversion. For all mesh blocks, a similar vertical resolution linear grading was adopted with the largest mesh size of 3.5 m (11.5 ft) at -60 m (-197 ft), NAVD88 the deepest point to 0.7m (2.3 ft) at 0 m (0 ft), NAVD88 with a uniform 0.7 m (2.3 ft) mesh size at points above 0 ft, NAVD88 up to the water surface (+3m or +9.8 ft, NAVD88). The higher near surface resolution was necessary to resolve complex fluid structure interactions of the free surface.

Table 3.1. Mesh sizes for the three mesh blocks in FLOW-3D.

Block No.	Δx (m)	Δy (m)	Δz (m)
1	4.5-10.0	6.0-10.0	1.0-3.5
2	1.3-6.0	1.3-6.0	0.7-3.5
3	5-10.0	5.0-8.0	1.0-3.5

The FTNMSDI model with the intake structure as designed at the current 60% E&D phase has an invert elevation of -7.63 m (-25 ft), NAVD88. The model domain has about 5 million active cells. The active cells are defined as those that constitute the computational domain filled with water or ai. The remaining inactive cells, being blocked by the solid part of the 3D STL geometry or below the bed surface, do not enter into model calculations.

The hydrodynamic and sediment data from the April 2009 monitoring completed by Allison (Allison, 2011) in the MR was used to calibrate the FLOW-3D model. The model domain (FTNMS) for calibration includes the MR geometry only and does not contain any diversion structure. Flow at the upstream model boundary (RM 62.7) was set to 741,608 cfs (21,000 cms) based on the discharge recorded at Myrtle Grove on April 9, 2009 (Allison 2011).

Since the monitoring did not include measurement of water surface elevation at the downstream boundary (RM 58.1), it was obtained by running the steady state FTNMS 2D Delft3D model (after its own calibration/validation) as will be described in the Section 3.3 later. This FTNMS 2D Delft3D model spanning between RM 56 and RM 66 was set up and calibrated for water surface elevation and velocities for the April 9, 2009, flow conditions. The RM 58.1 water elevation of 6.2 ft (1.9 m) NAVD88 was extracted from that model and used in FLOW-3D as the downstream boundary condition.

In FLOW-3D, the channel bed roughness is defined as an absolute roughness height rather than a roughness coefficient such as Manning's *n*, a common practice in CFD models. The river bed roughness height was set to 1.97 ft (0.60 m) following a series of sensitivity runs in FLOW-3D and is consistent with prior WI modeling (Meselhe et al. 2012, Meselhe et al. 2014) and the average dune height on the sand bar of around 2 ft at medium flow (Ramirez et al. 2013). A comparison with USACE Alliance gage reading for the April 9, 2009, condition indicated a difference within 3-5% of the observed water level indicating the validity of the roughness value choice. For turbulence modeling, a widely used, RNG K-epsilon model was selected which was also used in prior WI work (Meselhe et al. 2012). The initial water elevation was set to 6.2 ft (1.9 m), NAVD88, same as the downstream water level. The FLOW-3D model reached hydrodynamic steady state after approximately 1.5 hours of model simulation time (approximately 12-18 hours CPU clock time on a 128 core Intel Xeon High Performance Computing (HPC) cluster). In this case, the steady state is defined as the model state when the temporal variation of the free surface and cross section velocities varied less than 5%. Reported hydrodynamic and sediment results are averaged over 10 mins (600 secs) following the steady state.

Sand (median diameter d50 > 63 micron) is the main particle size class of interest from SWR performance perspective. Fines (silt and clay with d50 < 63 micron) are well-distributed horizontally and vertically (Meselhe et al. 2012, Allison 2011) in the river so that SWR is about 1.0 for fines. Therefore, the design of the intake is influenced very little from fines capture point of view and is excluded from the subsequent discussions. However, the fine sediment is modeled in Delft3D and the calibration results are shown in the next section.

For simulations of sediment transport, the Lagrangian particle simulation module in FLOW-3D with mass particles was used. The modeling with mass particles allows for the individual diameter (and therefore mass) of the sand classes to be specified explicitly and includes buoyancy, inertia and drag effects. Note that this method of modeling is only applicable if the river flow has majority of the sand in suspension. Therefore, flows only above 600,000 cfs, where over about 80-98% of the sand is in suspension (Meselhe et al. 2012, Ramirez et al. 2013), over the sand bar is modeled here. Since the diversion is built over the sand bar, it is the suspended sand which is designed to be the primary source of sand sized material in the diversion. Mining the local bed material by the diversion intake flow is not desirable as this could destabilize the local bedload transport equilibrium near the intake and lead to sand bar degradation over a long term. It could also lead to lowering of the river bed elevation near the intake, thereby depriving the diversion of the near-bed but suspended sand rich sediment source.

Once the hydrodynamics reached steady state, particle transport simulations were initiated. The particles are continuously added to the simulation at a constant rate until the sediment transport reaches steady state conditions. This was determined as the time when the number of particles in the domain attained a constant value. 1.5 hours of additional model simulation time (approximately 24 hours CPU clock time on a 128 core Intel Xeon HPC cluster) was required to reach steady state for the sediment following the steady state for the hydrodynamics. The particles were released at RM 61.4, about 0.7 miles upstream of the proposed diversion location (RM 60.7). Note that this location is downstream of the actual upstream boundary at RM 62.7 and was selected based on a series of sensitivity tests. The vertical extent of the seeding plane was also calibrated. When particles were seeded over a zone extending between the water surface and 20 m below the water surface the model results matched the observed concentration profile data best. The seeding rate was set at 2,000 particles per second with 29% of the particles being 250 μ sand, 38% of the particles being 125 μ sand and 33% being 83 μ sand. This seeding rate was determined based on optimum run time consideration and such that the computed SWR was independent of the choice of this value. The percentage distribution of sand size classes was based on the data provided by WI/CPRA from BCS sediment monitoring (Meselhe et al. 2016) at high river flows.

In the Lagrangian particle tracking method, as each particle moves through the flow field, it receives a random perturbation based on the turbulent kinetic energy in the cell. Thus, two particles released from the same location do not necessarily follow the same trajectory, neither the trajectories are repeatable from run to run as the process is inherently random and guided by a unique random number generator function for each run as the process tries to mimic the natural diffusion of the particles. The diffusion coefficient for sand particles was set as 0.05 consistent with WI's modeling (Meselhe et al. 2012). Note that a particle release rate of 2,000 per second is far fewer particles than what is moving in the river. Each particle is thus a representation of a 'cloud' of a large number of particles. Therefore, a dimensionless factor ($\mathrm{Xfactor_i}$) is defined to convert the particle concentration ($\mathrm{C_i}$) to real-world sediment concentration($\mathrm{C_{pi}}$). Note that the Xfactor is only valid for conversion of particle concentration to sediment concentration at a given river transect where observed sand concentration data is available, if a different transect is chosen a separate $\mathrm{Xfactor_i}$ must be calculated with observed data corresponding to that transect site. Note that the use of variable X factors has no influence on SWR computations in the FTNMSDI (with-structure) models as SWR is a Factory ratio of particle passing rates which is proportional to the concentration ratios. The following formulae were used to convert particle concentration to sediment concentration at the Myrtle Grove diversion site:

$$C_i = C_{pi} * Xfactor_i$$

$$\alpha_i * C_{total} = \frac{ParticleRate_i * V_i * \rho}{Q} * Xfactor_i$$

Where C_i is the modeled sand concentration (kg/m^3) for the ith size class at a particular river transect corresponding to a modeled particle based concentration C_{pi} (kg/m^3) at the same location, α_i is the concentration fraction of the ith size class, C_{total} is the total sand concentration obtained from observed data (kg/m^3),
$ParticleRate_i$ is the particle pass rate per unit time though the river transect at the proposed diversion location (1/s), V_i is the volume of a single particle of the ith size class (m^3),
ρ is the density of sand (kg/m^3),
Q is the flow rate passing transect plane (m^3/s) and $Xfactor_i$ is the particle to sediment concentration conversion factor.

For calculating the Xfactor for each sand class, first the particle passing rate across the MR transect at the proposed diversion location was calculated. Then the particle-based concentration rate was calculated from the model and the Xfactor was derived from the ratio of the particle-based concentration and the actual concentration from observation. For the calibration process using the April 2009 data, the observed sand concentration in the river is 0.036 kg/m^3 and the Xfactors for 250-, 125- and 83 μ sand are 3.4 x 10^7, 2.1x 10^8 and 7.4 x 10^8, respectively.

The monitoring data collected by CPRA/WI (Allison 2011) in the MR at the Myrtle Grove location from 2009-2011 were used for model calibration and validation. The data from April 2009 were used for calibration while data from March 2011 were used for validation. The calibration and validation locations are shown on Figure 3.5. For the hydrodynamic calibration and validation, the depth-averaged velocity profile along a horizontal transect (marked in the blue/yellow line on Figure 3.5) at the diversion site and the vertical velocity profile at three selected locations (marked in the blue/yellow square on Figure 3.5) were used for comparison. For sediment calibration and validation, three following locations were selected as shown on Figure 5.1:

- MGup2 (approximately 984 ft {300 m} from the west MRL),
- MGup3 (approximately 1,804 ft {550 m} from the west MRL) and
- MGup4 (approximately 2,296 ft {700 m} from the west MRL).

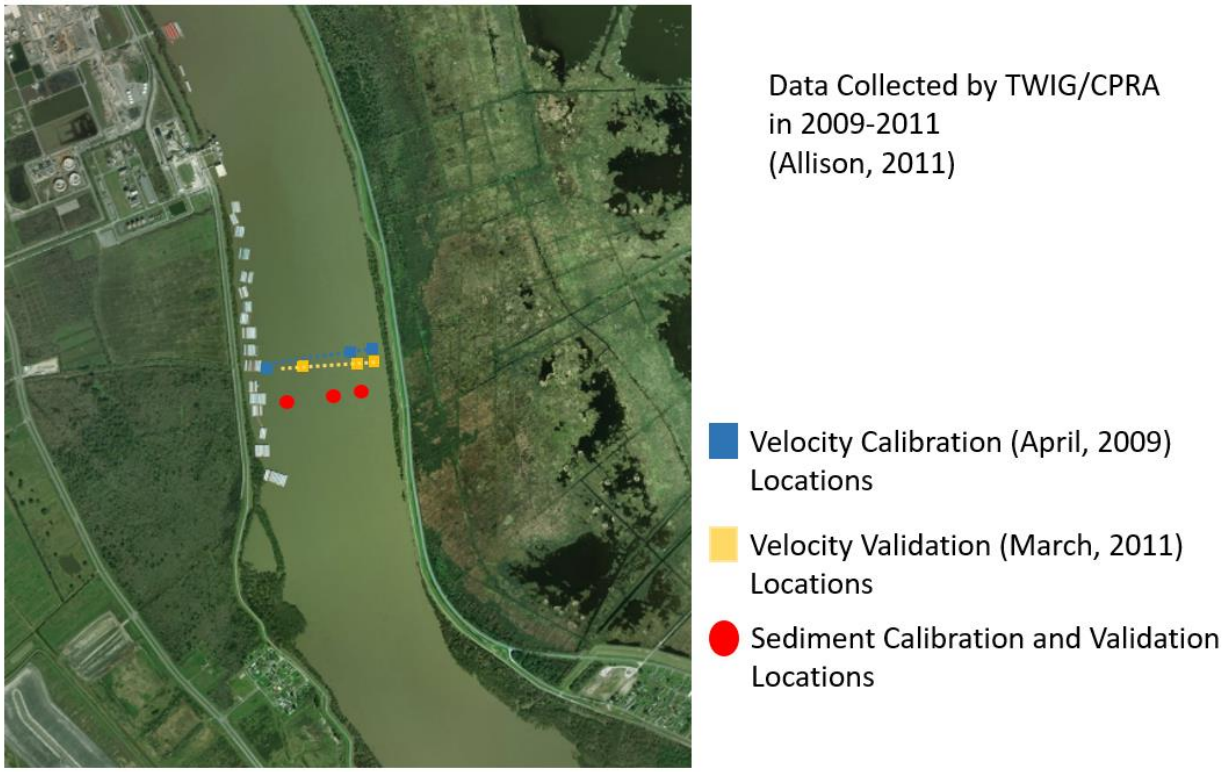

Figure 3.5. Calibration and validation locations.

The model setup for the validation run was same as the calibration except for the boundary conditions. The MR March 2011 monitoring data were used for the validation comparison. The MR upstream model boundary discharge value at RM 66 was set to 966,000 cfs based on the discharge recorded at Myrtle Grove for the March 2011 event. As was done in the calibration process, the downstream river elevation of 7.35 ft (2.24 m) NAVD88 was extracted from the FTNMSD 2D Delft3D model output to use as a downstream boundary condition. The Xfactors were calculated based on sediment concentration observed from March 2011. The observed sand concentration in the river in March 2011 is 0.081 kg/m^3 and the dimensionless Xfactors for 250-, 125- and 83- μ sand were 9.1 x 10 ^{7}, 6.0 x 10 ^{8} and 2.2 x 10 ^{9}, respectively. The particles were released at the same location and the seeding rate kept unchanged.

Similar to calibration, the validation process included comparing the depth-averaged velocities on the horizontal transect (as indicated with the yellow dotted line on Figure 3.5),

velocity magnitude vertical profiles at three selected locations (marked with yellow squares on Figure 3.5) and sediment concentration vertical profiles in the three selected locations (shown in red dots on Figure 3.5). Note the observed data for the validation event were collected at slightly different locations in the river compared to the calibration locations.

3.2.2 Results

Figure 3.6 shows the depth-averaged velocity profile (April 2009 MR discharge about 742,000 cfs) at the horizontal transect, looking upstream across the MR near the diversion site. The observed ADCP backscatter-based velocity data (Meselhe et al. 2012) is shown with the blue points while the red dashed line is the FLOW-3D simulation result. The X-axis shows the distance from the west bank (in meters) to the east bank. A comparison of observed data with simulation results shows good agreement between the two. Most of the measured velocities are within +/- 15% of the computed velocities. Note that ADCP backscatter based observed data tend to have large scatter. The west bank side model results show a slight overprediction which may be due to changes in bathymetry near the shallow bank between 2009 (the year of data samples) and 2013 (the year of model geometry topography) and also due to sheltering effect of upstream barges that may have been there during velocity monitoring. Currently, there is a barge parking area in the vicinity which is likely going to be removed in future and therefore not included in the model geometry.

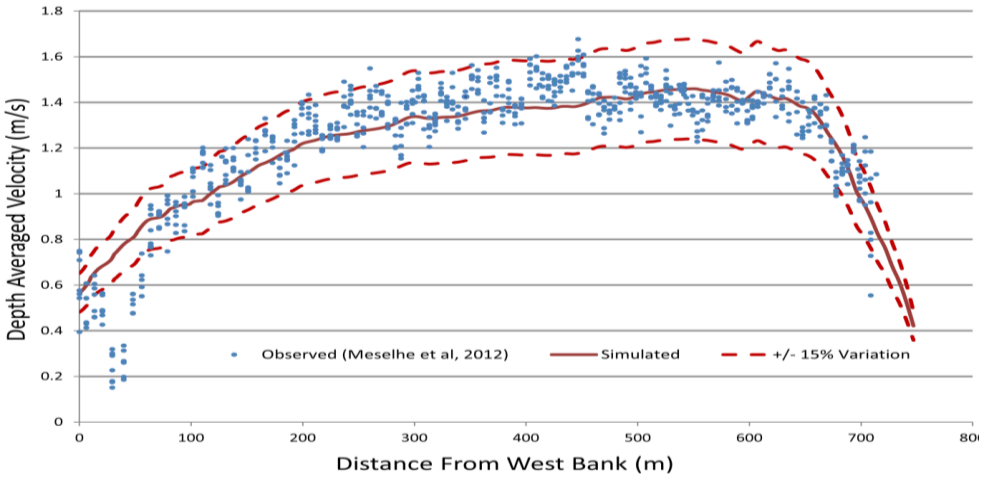

Figure 3.6. Depth-averaged velocity calibration at the proposed diversion site.

Figure 3.7 shows the vertical velocity profiles at the three locations in Figure 3.5: near the right descending bank (RDB), at the thalweg and near the left descending bank (LDB). The red error bars show the spread in the observed data and black lines show simulation results. Both are in general good agreement indicating an acceptable calibration of the model.

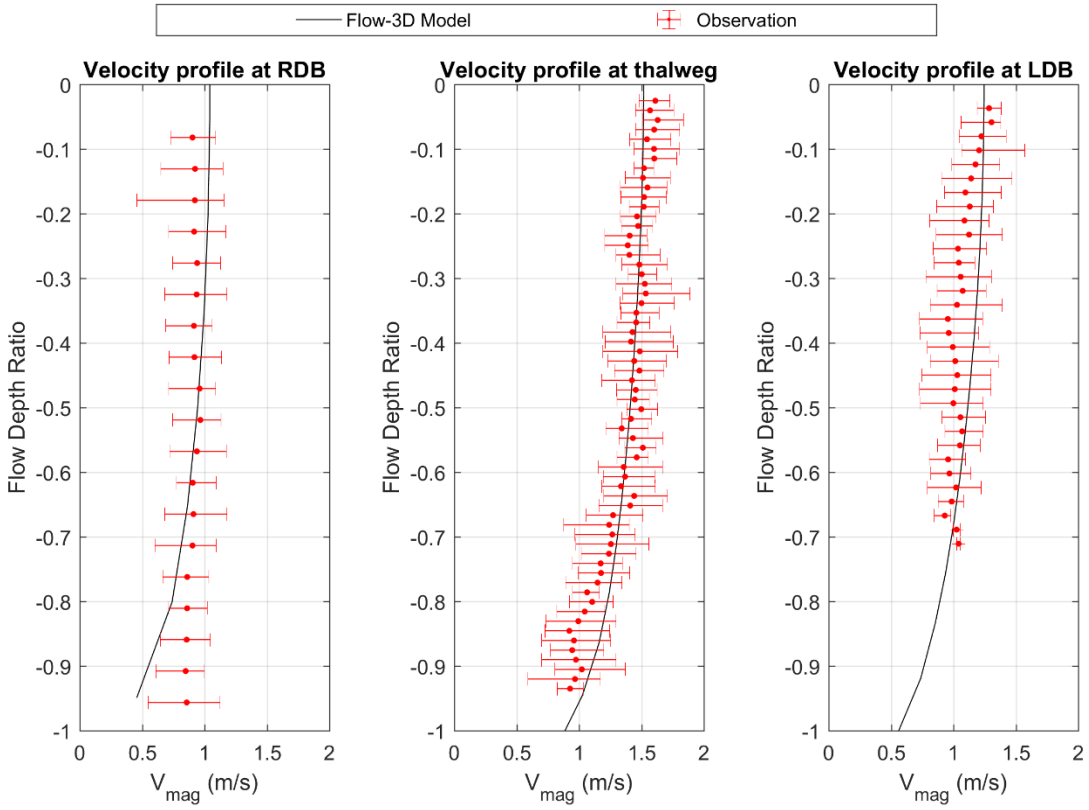

Figure 3.7. Vertical velocity calibration at the proposed diversion site.

Figure 3.8 shows the observed and predicted sediment profiles at the three selected locations shown in Figure 3.5. The profile for the west bank at MGup2 matches well with observed data. Since this location is over the sand bar near the proposed diversion location, it is important for the model to reproduce the observed sediment concentration profile at this location very well. Some underprediction of sediment is seen at the thalweg which is possibly affected by near-bed sand-rich suspensions from bedforms, not modeled here, in that area.

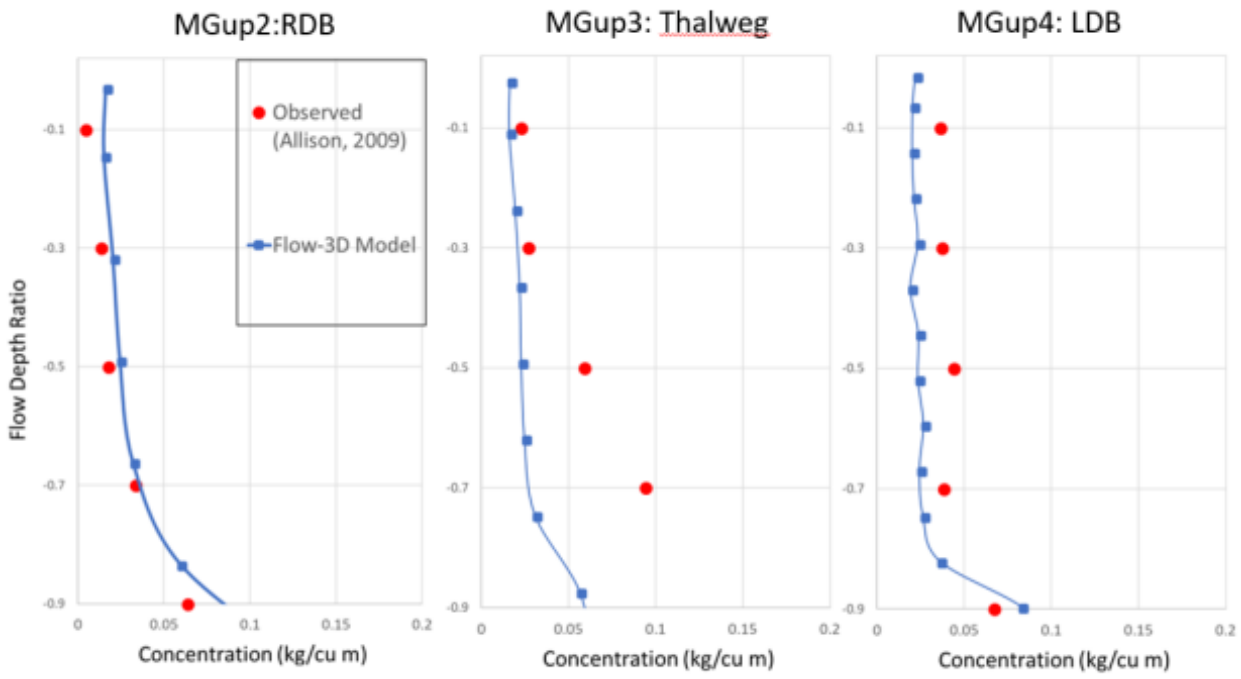

Figure 3.8. Vertical sediment profile calibration at three locations.

Figure 3.9 shows the validation of the depth-averaged velocity profile at the horizontal transect near the diversion site from the March 2011 event (MR Flow about 966,000 cfs). The X-axis shows the distance from west bank (in meters) to the east bank. The field monitoring data (Meselhe et al. 2012) is shown with blue scatter points. The red dashed line indicates the FLOW-3D modeling results and shows that most of the observed data falls within +/- 15% of the computed velocity. A comparison of the observed data with FLOW-3D simulation results shows good overall agreement between the two. A slight underprediction of velocities along the shallow portion of the west bank is possibly due to bathymetry differences or barge effects as discussed before.

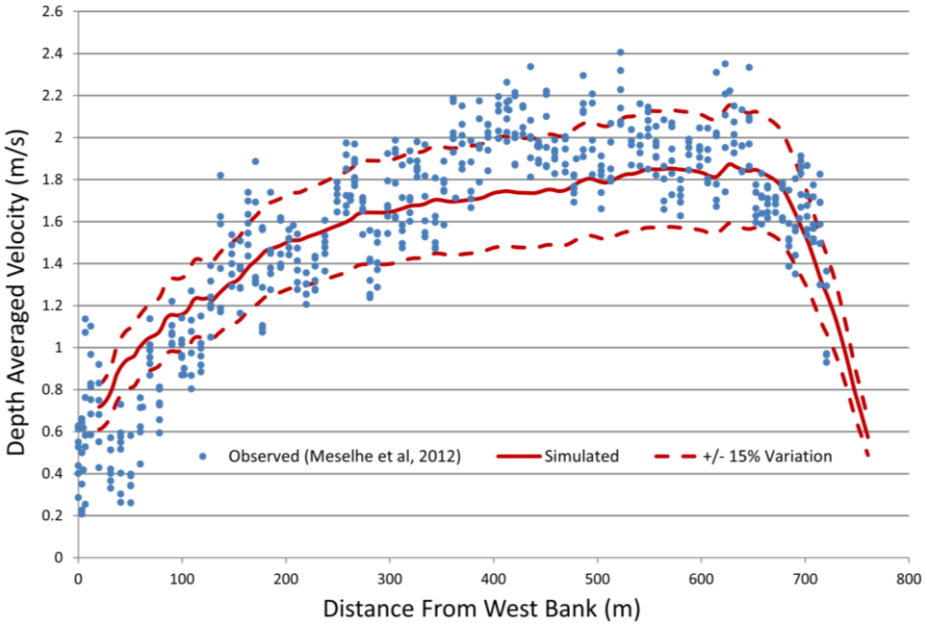

Figure 3.9. Depth-averaged velocity validation at the diversion site.

Figure 3.10 shows the vertical profiles of velocity magnitude at three selected locations: near the RDB, at the thalweg and near the LDB as shown in Figure 3.5. Red bars show the observed data spread and black lines show simulation results which are in general good agreement indicating a good validation.

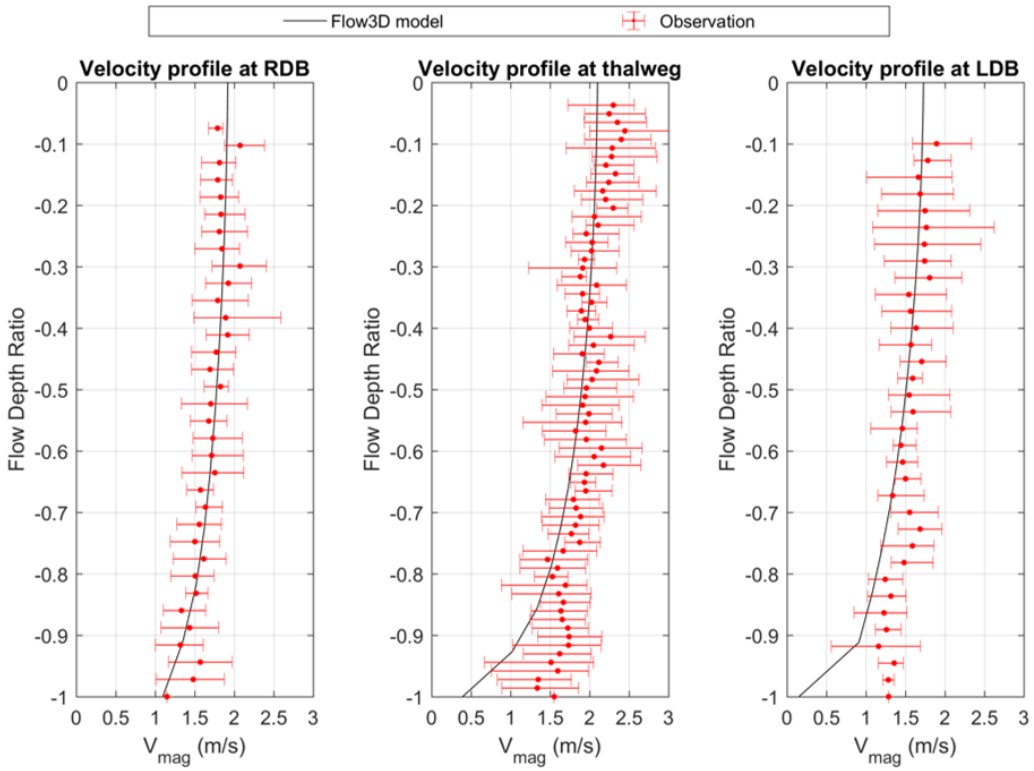

Figure 3.10. Validation of vertical profiles of velocity magnitudes at three locations.

Figure 3.11 shows observed and predicted sediment at three selected locations for the validation event. The profile for the west bank at MGUp2 matches well with the observed data. Since this location is over the sand bar near the proposed diversion location, it is important for the model to reproduce the observed sediment concentration profile. There is an underprediction of near-bed sediment over the thalweg similar to that noted in the calibration. There is a possible indirect implication of this underprediction on the subsequently reported sand SWR values from FLOW-3D even though the concentrations near the west bank (where the diversion intake will be placed) are matching well. Since the sediment load in the river is calculated as a cross-sectional sum and the average concentration in the river is used in the denominator of SWR (defined as ratio of cross-sectional uniform concentration in the intake to that in the river), it is possible that FLOW-3D sand SWR values may be somewhat overpredicted due to the fact that the predicted cross-sectional river sediment concentration may be lower than the observed in this case. Therefore, FLOW-3D predicted sand SWR values were strictly used for the comparison of

performance among different designs throughout the design process. The FLOW-3D SWR should not be taken as the indication of expected sand SWR. The Delft3D model presented in the later sections provides more realistic estimates of SWR. The Delft3D model simulates bedload transport resulting in improved estimates of cross-sectional variation in near-bed concentration.

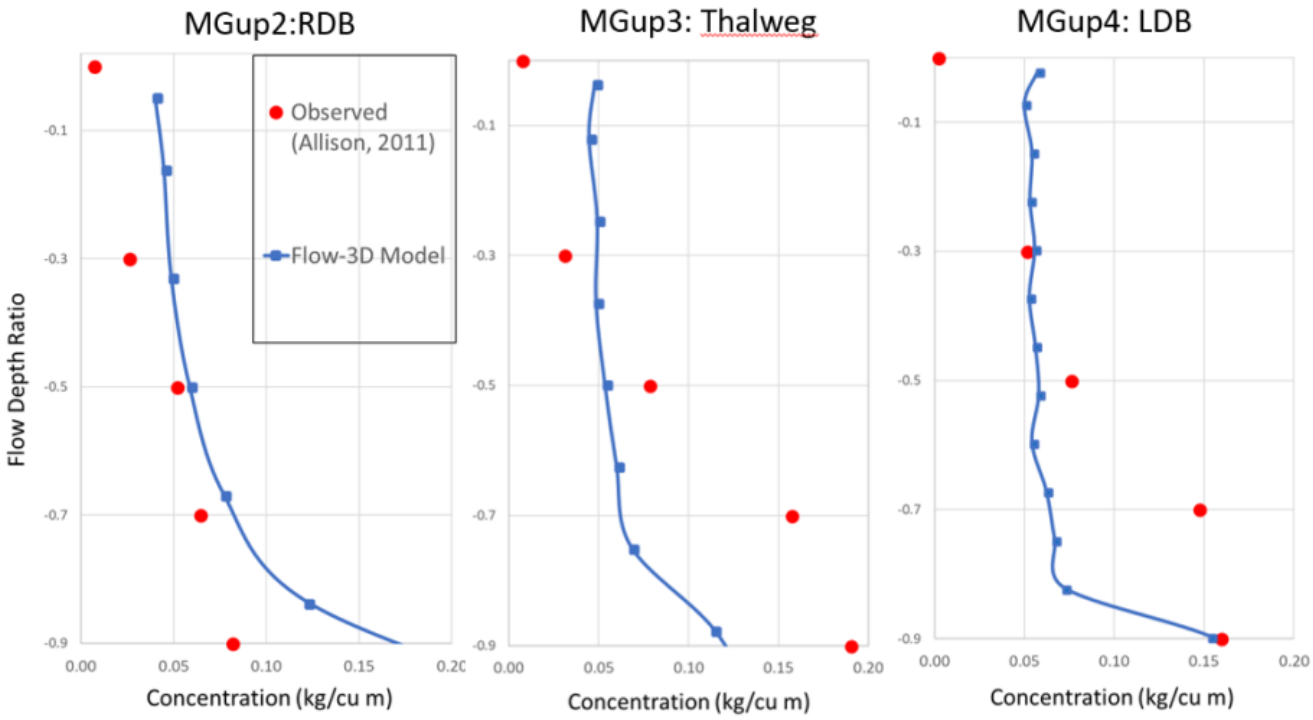

Figure 3.11. Validation of vertical profile of suspended sediment concentration at three locations.

3.3 Delft3D (FTNMSDI) Model

In addition to FLOW-3D, Delft3D 2D and 3D modeling was performed. The following section describes the setup, calibration and validation of the FTNMS Delft3D river model (without-structure) and setup of the FTNMSDI Delft3D model (with-structure).

3.3.1 Model Setup

FTN used the WI OMBA ("Outfall Model BArataria") model provided by CPRA as an initial basis for this modeling effort. The WI OMBA model extended from Belle Chasse at approximately RM 73 to RM 56. The WI OMBA model included the entire Barataria Basin (Figure 3.11). FTN created separate grids in the MR for the without- structure (river only) and with- structure investigations. These two grids will henceforth be called the FTNMS and the FTNMSDI model grids, respectively. Both grids contain the lower 10-mile stretch of the MR channel from RM 66 upstream to RM 56 downstream of the WI OMBA MR domain. The MR west bank or the RDB on which the diversion is located, was further refined in the FTN model grids to better resolve the local velocities and sediment concentrations. The smoothness of the grading of the mesh from larger cells near the boundaries to smaller cells near the diversion structure was also improved and the curvilinear mesh system better oriented within the river limits to remove or eliminate orthogonality issues. The mesh resolution of the zone near the intake was refined further to accommodate geometry details of the intake neck, transition of the intake into the conveyance channel, and the conveyance channel itself. The final structured mesh was composed of only quadrilateral elements with 19,279 elements in the FTNMS grid and 22,809 elements in the FTNMSDI grid. When run in a 3D mode, Delft3D uses the sigma (σ)-coordinate system in the vertical direction. For the models presented in this report, 10 non-uniform layers were found to be adequate to reproduce both the hydrodynamics and the sediment transport quantities in the water column. The finer layers were near the bottom to provide better resolution in the near-bed region where the velocity gradients are the highest and the coarser layers were near the open water surface.

Figure 3.12 shows the grid size distribution for the two meshes. The mesh density increases significantly near the diversion site to better resolve the complex near-field flow field caused by the presence of the diversion structure. The mesh sizes vary from 164 ft (50 m) to 16.4 ft (5 m) for the FTNMS grid and 164 ft (50 m) to 9.84 ft (3 m) for the FTNMSDI grid with the smallest grid sizes being in the river near the intake and within the intake zone. The intake and conveyance channel grids were widened in the FTN grid setups to accommodate the entire intake headworks of the diversion.

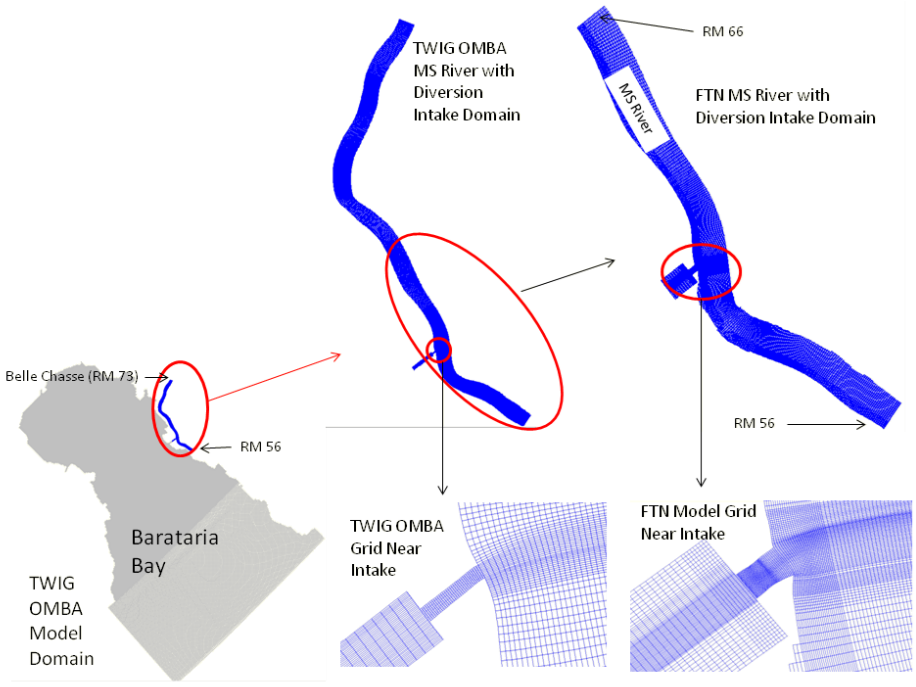

Figure 3.12. Comparison of the WI OMBA model grid with the FTNMSDI diversion intake model grid.

As in the case of the FLOW-3D model, the USACE 2013 multibeam river channel data and the USACE 2017 revetment survey data were used to create the model bathymetry (Figure 3.13) by interpolating the bathymetric data sets to the computational grid points. The horizontal (UTM Zone 15) and vertical reference coordinate systems (NAVD88) were kept the same as in the FLOW-3D model.

To implement the Open Channel intake headworks structure in Delft3D, the scatter (xyz) points created from the Solidworks stereolithography (.STL) files used in FLOW-3D were interpolated in Delft3D. Unlike in FLOW-3D, Delft3D cannot represent the detailed three-dimensional structural geometry of the interior bay walls so these were represented by thin dams.

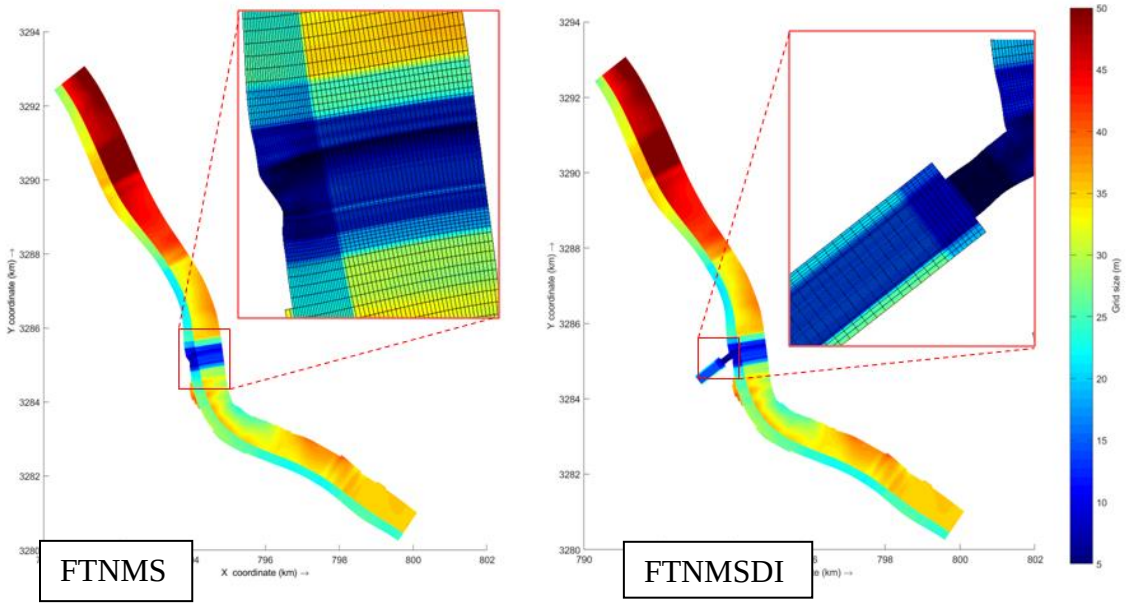

Figure 3.13. Grid resolution of the 2D Delft3D models. The highest resolution is 5 m in the river near the proposed intake structure and 3 m within the intake.

Similar to FLOW-3D for both the FTNMS and FTNMSDI Delft3D models (Figure 3.13) the upstream MR boundary at RM 66 was set as a discharge boundary and the downstream boundary at RM 56 as water elevation specified by a stage-discharge (Q-H) relation. The Q-H relation was developed from observed daily gage data at the USACE Alliance (RM 62.5), the USACE W Pt A La Hache (RM 48.7) and the USGS Belle Chasse gages from 2008-2018 (Figure 3.14). The downstream boundary location RM 56 is located in between the observed gages. Therefore, the Q-H at RM 56 was obtained by linear interpolation accounting for the relative distance between RM 56 and the other gage locations. A piecewise continuous function is used to develop the Q-H relation. For water levels below MR flow 650,000 cfs a parabolic function is used while above this flow a linear function is used. A two-function representation is adopted to capture a similar distinct trend in the observed data which is result of the change in shape of the effective flow cross-section in the river with increasing water level. Below 650,000-750,000 cfs the MR flow south of Bohemia, LA (about RM 43.5) on the left descending bank is confined to the main river channel due to the presence of the MR levees, but above this flow the MR water tends to overtop and exit through the Bohemia Spillway which was

constructed by USACE in 1926 to alleviate flooding. This diverted flow reduces the water level rise with MR discharge at the MBSD location and results in a milder (linear instead of parabolic) rise in water level for higher discharges. Being able to represent the Q-H distribution accurately and hence the water level at various discharges in the river is an important part of the diversion modeling because the diversion discharge is driven by the head difference between the river and the basin. The diversion discharge is more sensitive to the MR water level at the diversion location than the discharge in the river. Note the adoption of Q-H relation eliminates the complex tidal and wind generated water level effects on diversion discharge. This aspect is discussed further in Chapter 9 under Three-Component-Modeling. It will be analyzed further under the task of Operations Modeling in the 90% E&D phase. For hydraulic modeling supporting design (discharge capacity and sediment transport modeling) a best fit or mean MR water level at each MR discharge is considered sufficient. This approach is expected to yield a corresponding mean diversion discharge. Note that for structural design grades and water levels historical maximum and minimum are considered by the DT.

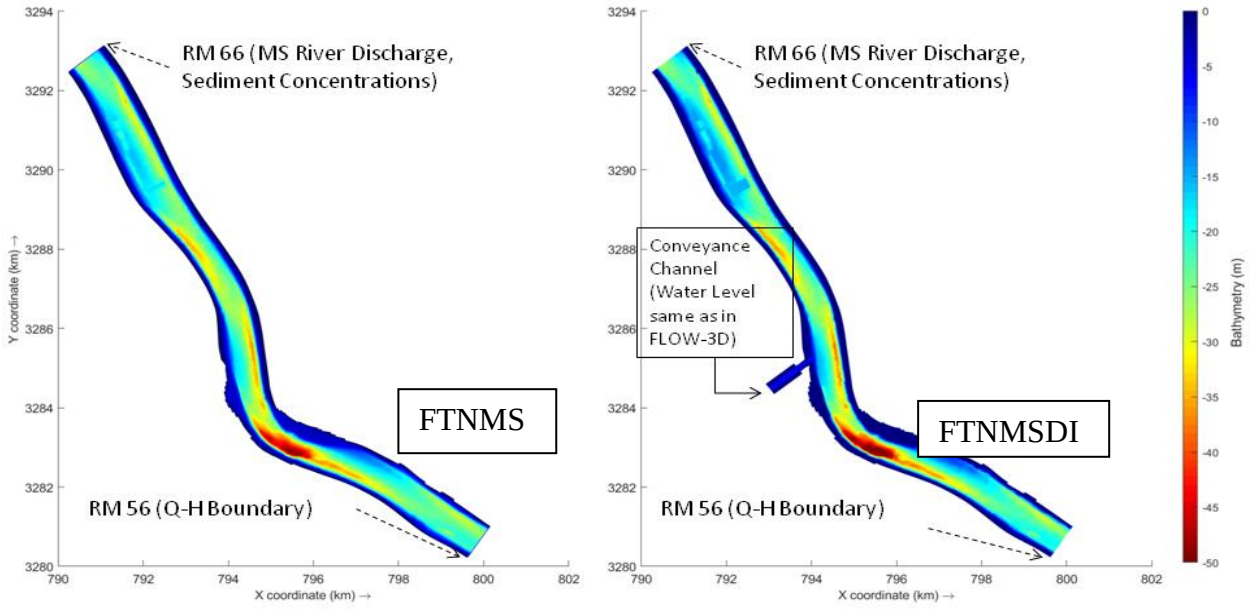

Figure 3.14. Bathymetric elevation (m, NAVD88) is shown with the boundary conditions. Horizontal datum is UTM 15N NAD83.

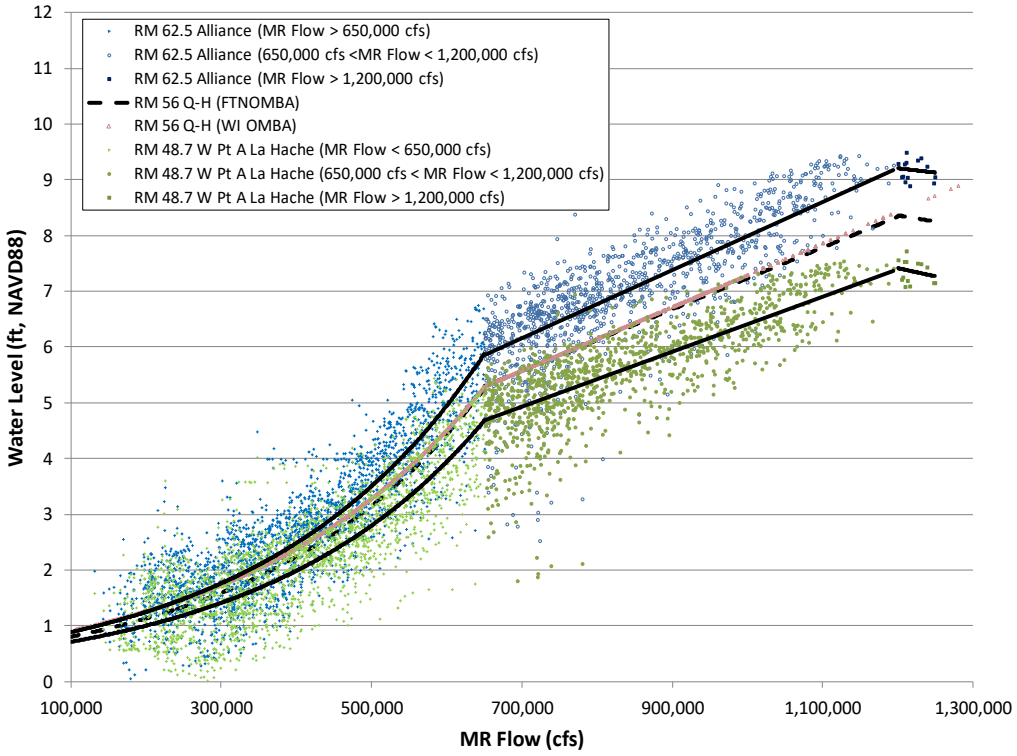

Figure 3.15. Q-H relationship for the downstream boundary condition. The maximum MR discharge is capped at 1.25M cfs based on historical data and based on allowable maximum MR flows within this reach.

For sediment modeling, the FTNMS and FTNMSDI Delft3D models considered both sand (defined as non-cohesive sediment with median grain size $d_{50} \geq 63$ μ) and fines (defined as cohesive sediment with $d_{50} < 63$ μ). Non-cohesive sediment is modeled by the Van Rijn (1993) equations while cohesive sediment erosion follows Partheniades-Krone (1965) formulation. The fines have been divided into silt and clay similar to the previous modeling efforts by the WI for the Louisiana Coastal Master Plan. The sand sizes modeled in WI's past modeling efforts have varied due to the difference in resolution, study objectives and sediment transport modeling capabilities of different models.

The WI's basin-wide model (Figure 1.3; called WI-BW model hereafter) is used for delta land-building projections by CPRA. The WI-BW model had only one uniform grain size for sand (175 μ) while WI's OMBA model had two (175 μ and 83 μ) sand grain sizes. The choice of 175 μ is due to the fact that sand sizes below 176 μ median size (or fine sand) are considered

wash-load (sediment from non-local source, possibly over several sand bars up to 10's of miles upstream of the MR) while greater than 176 μ is considered *bed material* (sourced locally from the channel bed and dynamically deposited and eroded from the sand bar at various river flows). Note that *bed material* must not be confused with *bed-load*, the latter being a descriptor of the mode of transport rather than of a source of sediment and is a function of the local bed shear stress (i.e., river flow). It may be composed of variable size distributions depending on the discharge. For example, bed load sampling at Myrtle Grove at high (≥1,000,000 cfs MR flow) shows a 90^{th} percentile distribution for 303 μ sand on the sand bar.

Together with silt and clay, fine sand is found to comprise of the majority of the suspended sand load in the MR at this location (Ramirez et al. 2013). However, to draw a complete picture of the intake sediment capture performances for a range of sediment sizes, both non-local and local sand grain sizes need to be considered to be able to derive a mix of sediment in the model bed that approximates the observed bed material distribution.

WI's FLOW-3D modeling (Meselhe et al. 2012) which represented sand as discrete suspended particles, provides a greater resolution of sand sizes comprising of four size classes, namely, 63 μ, 96 μ, 125 μ and 250 μ and offered better resolution of distinct particle behavior in flow. To remain consistent with the past Delft3D and FLOW-3D modeling efforts by the WI as well as within FTN's Delft3D and FLOW-3D models, the sand fractions modeled here consist of very fine to medium sized median grain sizes and are the same as in FTN FLOW-3D modeling done previously (i.e., 83 μ, 125 μ and 250 μ). Thus, both wash-load and bed-material can be modeled in Delft3D which helps to identify the distinct capture behavior of sand by various types of intake-invert elevation combinations.

To develop a consistent distribution of grain size, FTN obtained sediment size and corresponding percentage classification data from WI/CPRA from two available monitoring sites, namely, BCS and Myrtle Grove. An analysis of the percentage breakdown of sand and fines data from these sources including the final sediment distribution selected for the present modeling is presented in Table 3.2.

The percentage of sand and fines in the total sediment load is a function of the hydrograph (McCorquodale et al. 2016) and is represented by the specification of Hysteresis Sediment Rating Curves (HSRC) (Esposito et al., 2017) and Total (Sand) Rating Curve (TRC) (Allison et al., 2012). The fines load is obtained by subtracting the sand load from the total sediment load. An example of the sediment load distribution for Year 1 (Historical Year 1963) and Year 50 (Historical Year 2013) from WI's Basin-Wide model river hydrograph are presented in Figure 3.15. As can be seen, the total fines load is about 80-90% of the net annual sediment load. Therefore, fines are expected to dominate the diverted sediment load.

For all hydrograph-based runs sediment is input into the model as depth-averaged concentration, uniform across the river cross-section at the upstream MR boundary at RM 66. The upstream boundary (RM 66) is far enough from the diversion site (RM 60.7) for the study purposes and provides an adequate length of river domain in the model to allow a natural cross-sectional distribution of flow and sediment arriving at the diversion location. For all runs involving long term morphology change, an equilibrium bed sediment distribution was developed by running the model for about 6-8 months (a typical operational year) initially before the start of the production runs. This approach ensured a proper spatial distribution of bed material grain size that is similar to the native river bed and enabled the model to reproduce the appropriate spatial distribution of near-bed concentration and bedload transport which determine the cross-sectional distribution of suspended and bed load flux across the river.

Table 3.2. Sediment Size classification for sand and fines used in FTN Delft3D modeling based on analysis of MR monitoring data and WI basin-wide model hydrograph at RM 66. Fines are distributed as 75% silt and 25% clay following WI recommendations and is the same as that used in WI basin-wide model boundary.

Data Source	**Data Type**	**Sand (d_{50}≥63 µ, Non-cohesive)**			**Total Sand**	**Fines (d_{50}<63 µ, Cohesive)**		**Total Fines**
Sediment Type		Medium	Fine	Very Fine		Silt	Clay	
d_{50}		250µ	125µ	83µ		N/A	N/A	
Data from Bonnet Carre Spillway Monitoring (WI, June 2011)	Concentration (mg/l)	13.2	21.0	5.0	39.2	63.4		63.4
	% of Total Sand or Fines	34%	53%	13%	100%	100%		100%
Isokinetic Analysis from Myrtle Grove Monitoring (Meselhe et al., 2012)	Sediment Load (t/d)	30,024	34,437	32,655	97,116	233,539	25,805	259,344
	% of Total Sand or Fines	30%	37%	33%	100%	90%	10%	100%
Present Intake Screening Modeling	% of Total Sand or Fines	30%	37.5%	32.5%	100%	75%	25%	100%

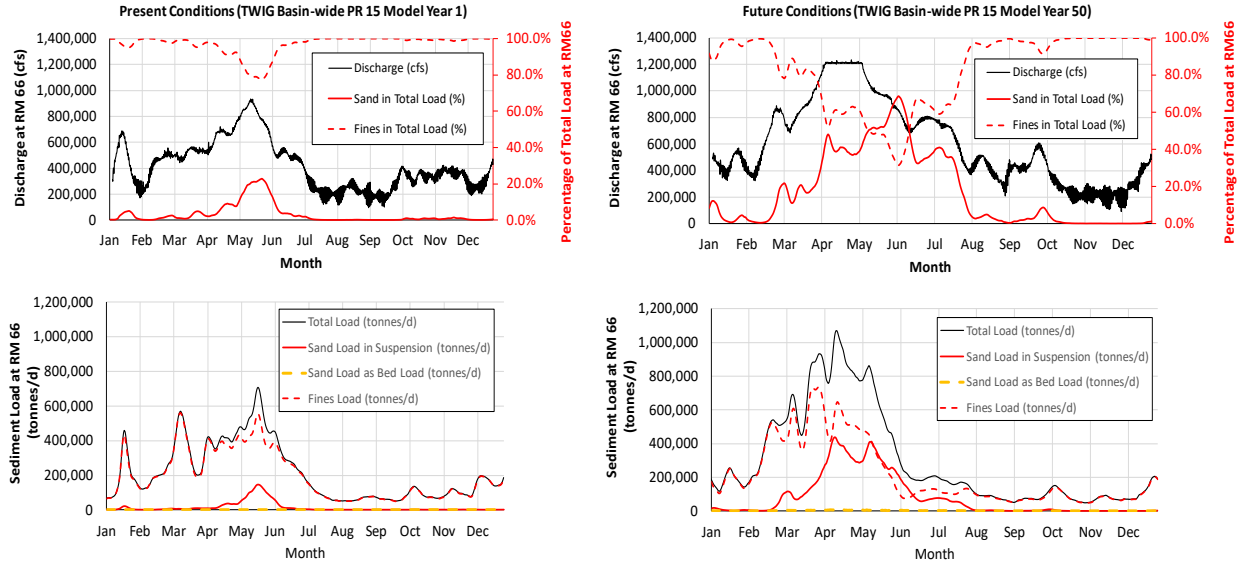

Figure 3.16. WI basin-wide model time series of discharge and sediment loads at RM 66 for present (left column) and future conditions (right column). Top panels show discharge on left axis and percentage of sand and fines on the right axis; Bottom panels show river loads in tones/day. (Data provided by WI/CPRA).

For the calibration (October 2008-October 2010 period) and the validation (October 2010-May 2011 period) runs, the boundary conditions for sediment were obtained using the HSRC and TRC curves at Belle Chasse from the observed historical hydrograph for the 2008-2011 period and imposed at RM 66. All sediment modeling with the 10-mile FTNMS/ FTNMSDI/ FTN2Comp models are performed in three-dimensions, so the simulation of secondary currents and effects on morphology are explicitly included in the modeled results and no separate parametrization is necessary. In the next section however, where the results of the two-dimensional FTNULMR Delft3D model results are presented, parametrization of secondary currents on bedload is included and calibrated. Observed data collected between 2008-2011 by Allison, et al. (2011) were used for the calibration/validation of the FTNMS model. The 2012 USACE bathymetry, which is the same bathymetry used for all production runs was chosen as the initial bathymetry. Even though the WI/CPRA conducted a bathymetry survey towards the end of 2008 after the MR flows had fallen below 400,000 cfs, this bathymetry was not used because it covered the Alliance sandbar only - unlike the 2012 USACE bathymetry that covered the entire model domain. Since the primary purpose of this model is to help in design of

structural components and not to perform a rigorous hind-casting of the exact bed elevation, the use of the 2012 bathymetry as the initial bathymetry is a reasonable approach. The bed was allowed to evolve and develop a self-armored bed composition by running the model initially at high flow for two months.

All the river models involving sediment transport and morphology change were run with a Morphology Acceleration Factor (MorFac) of 40 which is within the recommended range of 40-80 (McCorquodale et al., 2016).

The model was set up and calibrated for water surface elevation, depth-averaged velocities and vertical profiles of velocity for the April 9, 2009, flow conditions. The main parameter used to calibrate the hydrodynamics was the bottom roughness of the river channel. A uniform Manning's roughness coefficient *n* of 0.024 provided the best results in terms of water surface slopes and depth-averaged velocities. The same value of roughness was used in Gaweesh et al., (2016) which independently confirms the choice of the roughness coefficient.

A secondary parameter that was also calibrated was the background eddy viscosity with the 3D model using 1 m^2/s and the 2D model 0.001 m^2/s, based on the calibration results. The 3D sediment transport models also required specification of background eddy diffusivity and a value of 10 m^2/s was used similar to WI's modeling work.

No turbulence model is used for the 2D models while for the 3D models the k-ε (Rodi 1984) turbulence model was used and is the same as that used in the previous WI work (Gaweesh et al. 2016).

The calibrated hydrodynamic model was used as the basis for developing the sediment transport model. Model calibration involved adjusting sediment transport parameters, particularly those concerning sand transport, by comparing the model results with the isokinetic sediment concentration profiles and total sediment load measured at the Myrtle Grove location. It is to be noted that the FTN Delft3D models are based on the calibrated WI OMBA model which is itself based on the 3D Delf3D model for the MR developed by the WI (McCorquodale et al., 2016) and this is expected to be acceptably calibrated for sediment transport. Nevertheless, FTN reviewed the extensive sediment calibration parameters and revised some of the parameters to achieve better agreement with the field data. The sediment transport parameters adjusted were

more extensive than those for the hydrodynamics. This calibration process involved a total of about 160 2D and 3D model runs. The main parameters investigated were the following:

1. *Three sediment transport formula for sand (non-cohesive transport): Van Rijn (1984a,b), Van Rijn (1993) and Van Rijn (2004):*

   WI used the Van Rijn (1984a,b) formula for the 3D Delft3D MR model, the Van Rijn (1993) formula for the early MBSD planning phase modeling (Meselhe et al. 2014) and the Van Rijn (2004) formula for the later stage OMBA land building models (Esposito et al., 2017). FTN tested all three formulas and found Van Rijn (1993) to best reproduce the sediment transport concentrations in the river for the calibration and validation cases.

2. *Multiplication factor for suspended sediment reference concentration factor.*

   It was found that the suspended sediment reference concentration multiplication factor had a dependence on the river discharge and the default value of 1.0 yielded best results for the lower flow (approximately 720,000 cfs) April 2009 observation while a value of 0.6 was appropriate for the high flow (approximately 990,000 cfs) Mar 2011 observation. A mean value of 0.8 was used for this parameter for the continuous hydrograph runs.

3. *Multiplication factor for bed-load transport vector magnitude.*

   The bed-load transport vector multiplication factor was also found to have a dependence on the river flow and a value of 1.7 was found appropriate for the lower flow (720,000 cfs) April 2009 observation while a value of 2.0 was found to be suitable for the high flow (approximately 990,000 cfs) Mar 2011 observation.

4. *Spatial variability of the thickness of the sand deposit on the bed (stratigraphy) and proper definition of non-erodible zones such as revetments*

   FTN received the stratigraphy definition file used in the WI OMBA model and adjusted for the sand bar extents based on the geotechnical boring data collected in 2013 as provided by Eustis Engineering Services (Eustis), the geotechnical team member of the Design Team. Elevations -40 ft, NAVD88 and shallower are protected by USACE revetments and are non-erodible. The sand bar was observed to start from about -50 ft, NAVD88 and cover the deeper elevations up to the near the thalweg at the diversion site. Figure 3.16 shows the stratigraphy definition as used in the model and the extent of the sand bar from the graphic provided by Eustis. It was found that accurate definition of the sand bar extent as well as the non-erodible revetment zones was an important criterion for matching the sediment concentration profiles for both calibration (low flow) and validation (high flow) observations, due to the contribution of the locally sourced sand to the suspended sediment in the water column in addition to the wash load.

3.3.2 Results

Figure 3.17 shows the comparison of the final calibrated and validated modeled and observed MR discharge and total sediment load at RM 61.6 (i.e., at location "MGUp" in Allison et al., 2011). The modeled discharge and sediment load match well with the observed data. Differences in the modeled and sediment loads for the April 2010 observation can be attributed primarily to the difference in observed and modeled fines (silt and clay) loads (shown later in the top panel of Figure 3.18). Note that the prediction accuracy of the modeled fines load (which settles very little between RM 66 and RM 61.6 and have a travel time of less than 1 day over the 5-6 miles) largely depends on the HSRC boundary conditions prescribed at RM 66. The HSRC curve itself is developed for Belle Chasse (RM ~76) which is approximately 10 miles upstream of the actual RM 66 boundary. At MR flows greater than 450,000 cfs the modeled fines load at the RM 61.6 is seen to be always smaller than the boundary conditions at RM 66 (HSRC-TRC predicted fines at boundary plotted with black diamonds). However, for the April 2010 observation, the observed fines load is significantly higher than the boundary condition (RM 66) predicted value. It is unclear whether the measurement uncertainties were responsible for this single outlier or the inherent statistical nature of the HSRC.

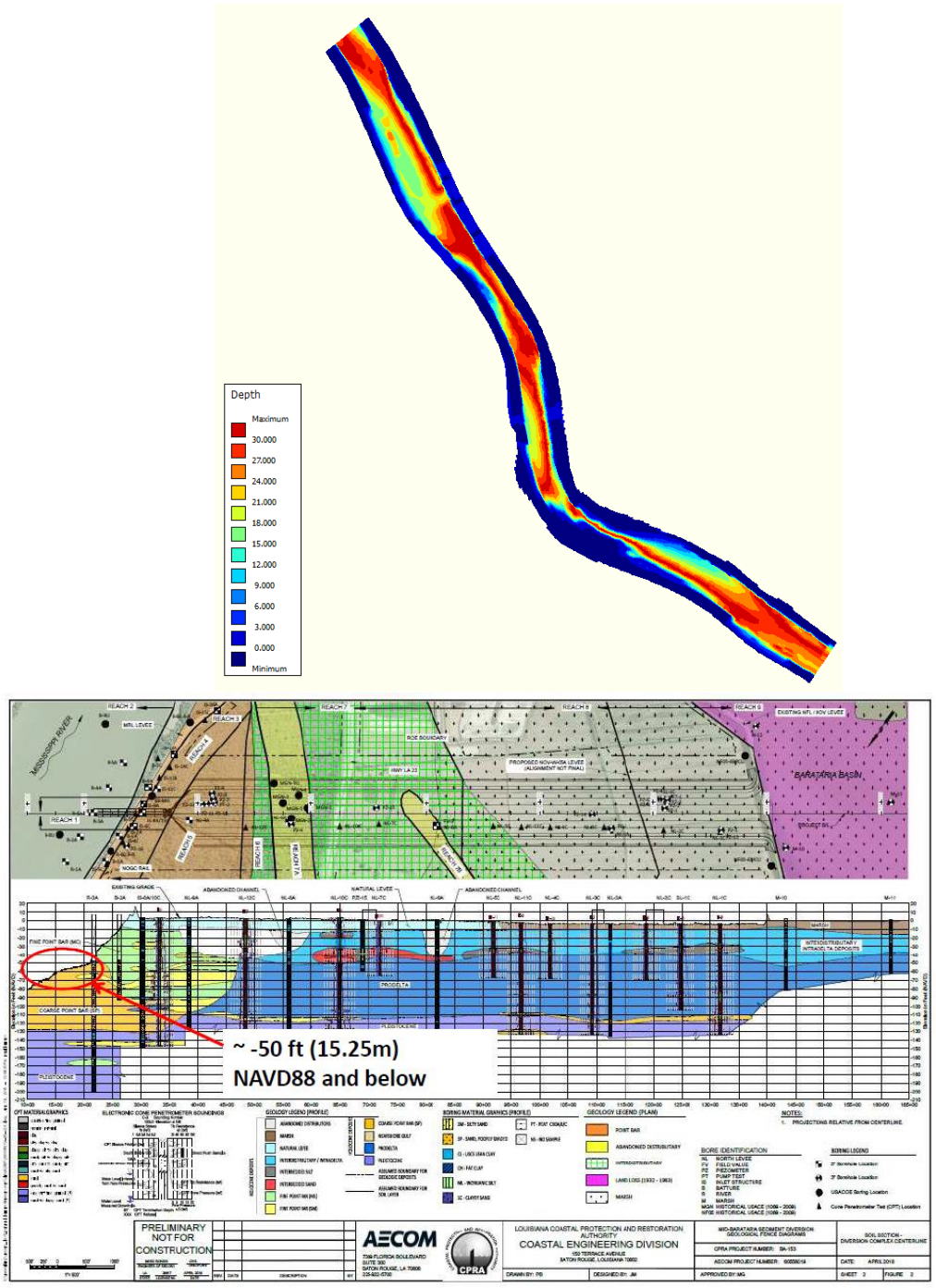

Figure 3.17. Top panel. Definition of model stratigraphy. Sediment thickness represented as depth below the river bed (in feet). Note the revetments (blue areas near the river banks mostly at or above -40 ft NAVD88) are set as non-erodible. Bottom panel: Geotechnical info-graphic showing that the sand bar starts from -50 ft NAVD88 and extends below to deeper inverts at the diversion site.

Figure 3.18 shows the comparison of modeled suspended (middle panel) and bed-load (bottom panel) for sand with observed data at RM 61.6. Overall, the model results match well with the observed data. The underestimation of the April 2009 data point is likely due to local hysteresis effect in the sand transport which cannot be captured in the TRC rating curve. As the bed storage of sediment evolves, the model seems to be able to recover the hysteresis effect, (March 2010 and 2011 were only two falling limb observations). Most of the variation between observed and modeled bed loads is due to the temporal effects. The model predicts the range of bed load well. Even though the variation in predicted and modeled bed load is greater than the suspended load, the bed load itself forms a small percentage (5-10 %) of the suspended sand load at MR flows greater than 900,000 cfs (Figures 3.19 and 3.20). In summary, the model is able to predict overall sediment transport of fines and sand over the 3-year hydrograph within the observed uncertainties and can be further used for the estimation of diverted loads under with structure scenarios.

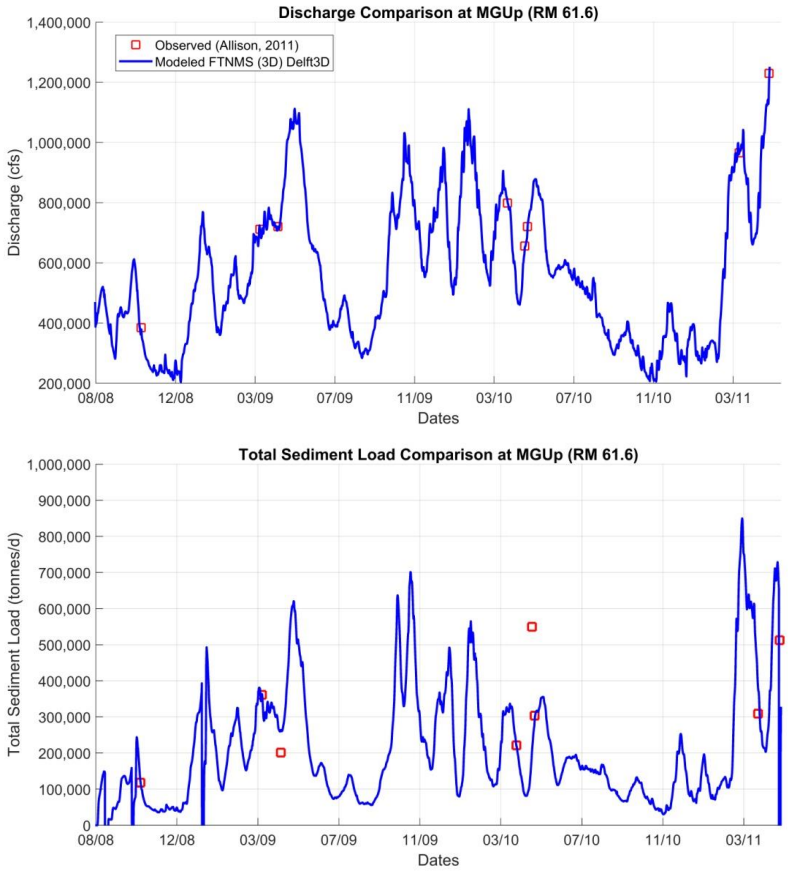

Figure 3.18. Comparison of modeled and observed discharge (top panel) and total sediment load (sand and fines, bottom panel) at the MBSD location RM 61.6.

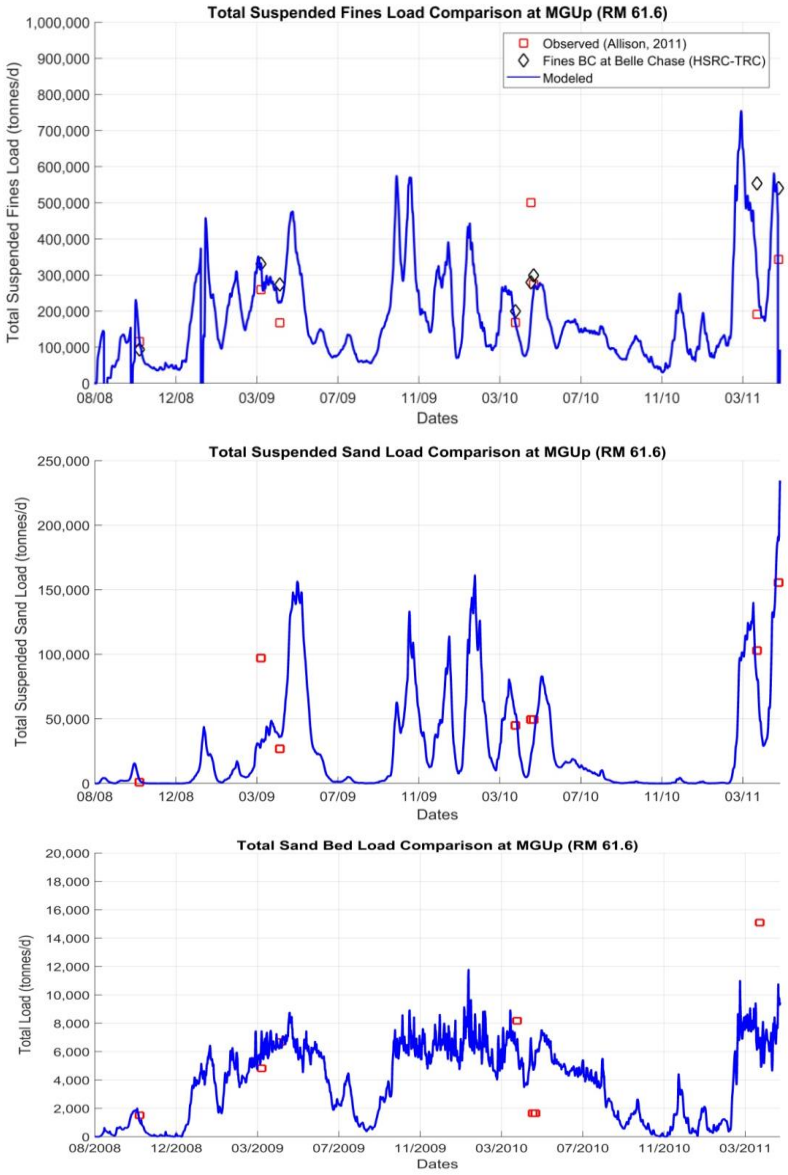

Figure 3.19. Comparison of modeled and observed fines (silt and clay) in the top panel, suspended sand loads in the middle panel, and bed load in the bottom panel at location RM 61.6.

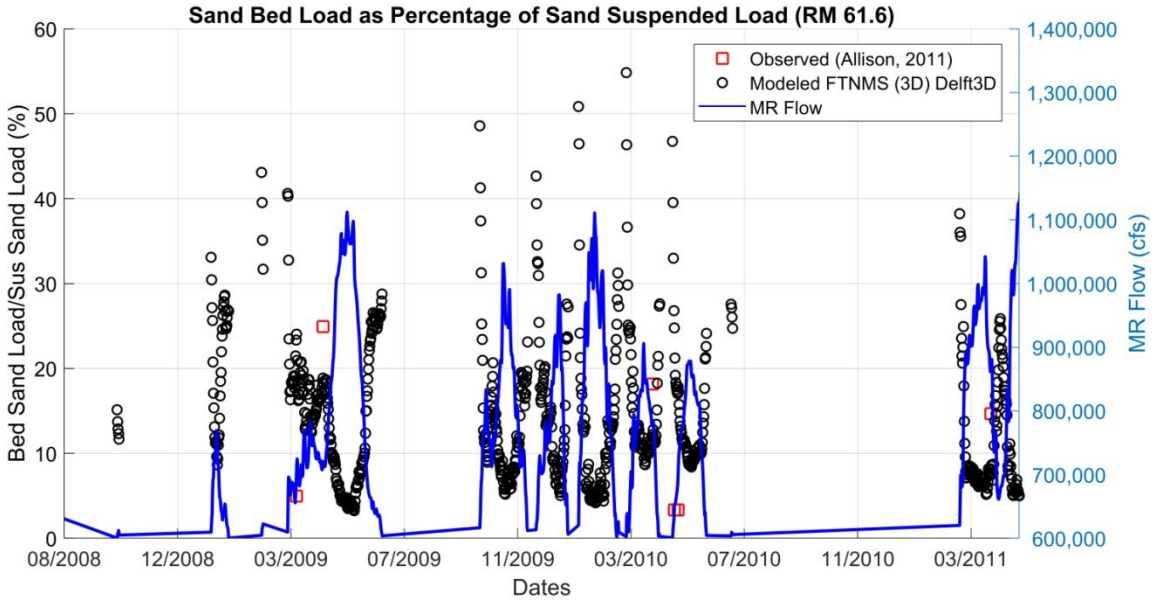

Figure 3.20. Modeled sand bed load as percentage of modeled sand suspended load. Observed data is shown in red squares. For MR Flow (>600,000 cfs) when most of the sand enters into suspension, the bed load varies between 5-60 % of the suspended load.

The final calibrated and validated hydrodynamic model results for cross-sectional depth averaged velocities in the river (cross-section looking upstream) are shown in Figures 3.21 and 3.22 compared with field data along the locations as shown before in Figure 3.5. The 2D model matches the depth-averaged velocities slightly better near the thalweg than the 3D model, while the 3D model gives better estimates of the lower velocities near the RDB. The differences in 3D modeled velocities from 2D (rigid bed) are possibly due to the differences in the predicted bathymetries in the model compared to the observed bathymetries. Another reason could be the possible effect of parked barges downstream of Alliance along the RDB and/or CHS terminal upstream on the near-bank (at or below -40 ft, NAVD88) RDB velocities. The barge parking location is expected to be removed post-construction, so the model without the barge effect is used for all production runs. Note that even though the 2D model is not used for sediment transport, it is used later for rigid bed hydrodynamic runs for determining water levels and diversion capacity (in FTNOMBA) so it was necessary to calibrate it for hydrodynamics at this stage.

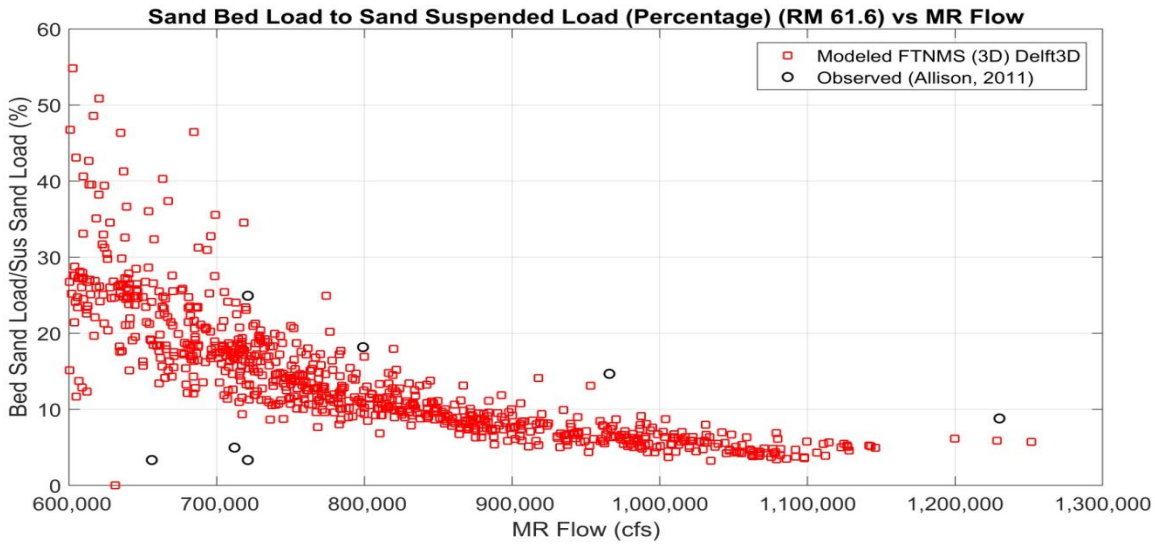

Figure 3.21. Modeled sand bed load as a percentage of the modeled sand suspended load plotted against MR Flow (>600,000 cfs). Observed data shown is in black circles. Modeled values match well within the variation of the observed data.

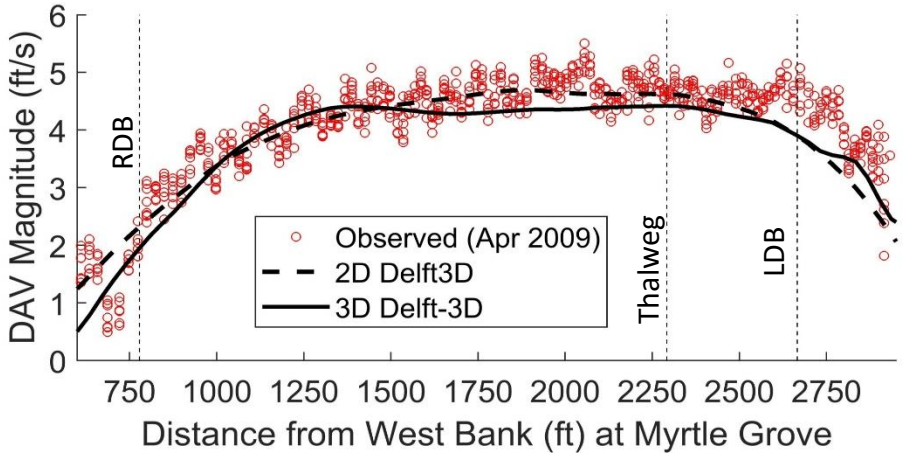

Figure 3.22. Model calibration using April 2009 depth-averaged velocities. Depth-averaged velocity compared with field observations from CPRA's 2008-2011 MR monitoring at the Myrtle Grove (MGUp2) location near the diversion site.

The comparison of vertical velocity profiles with field measurements for the 3D model shows a good correlation (Figure 3.23 and 3.24). Overall, the model results are within the acceptable range of error in the field observations and match the velocities at the RDB (near the proposed diversion) well.

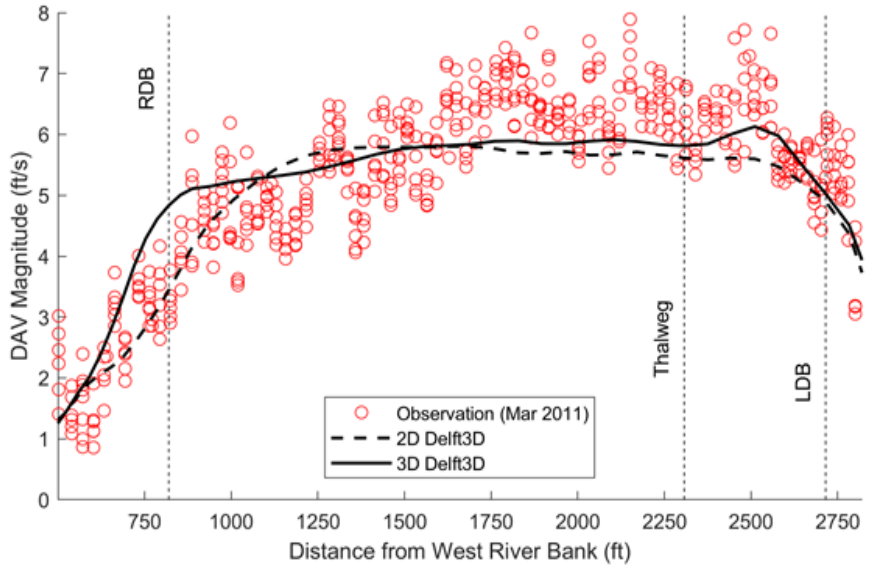

Figure 3.23. Model validation using March 2011 depth-averaged velocities. Depth-averaged velocity compared with field observations from CPRA's 2008-2011 MR monitoring at Myrtle Grove (MGUp2) location near the diversion site.

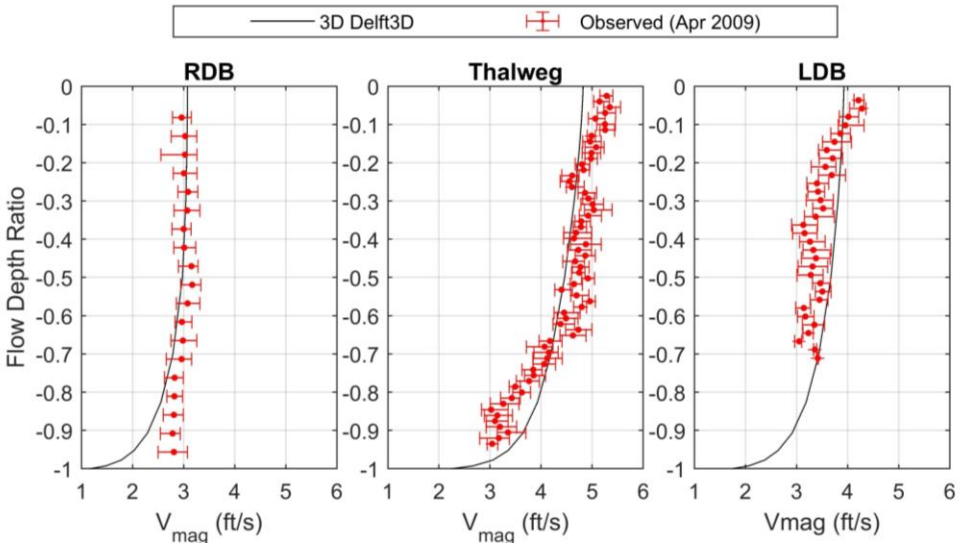

Figure 3.24. Model calibration using April 2009 vertical velocities. Vertical velocity profiles compared with field observations from CPRA's 2008-2011 MR monitoring, at the three locations on Figure 8.7.

Figure 3.25 shows the suspended sediment profiles (sand and fines) at the three locations; west, middle and east on Figure 3.5 from the calibration period (April 2009). At all three locations the profiles match well with the observed data. The model also represents the well-distributed vertical profile of the fines (cohesive sediment) in addition to the typical Rousian profile of the sand (non-cohesive sediment). Figure 3.26 shows the suspended sediment profiles (sand and fines) at the same three locations for the validation period (March 2011). The slight difference in near-bed concentrations at the west and the east location for the calibration and validation cases can be attributed to difference in model and observed bathymetries within the bottom 10% of the depth where no data is available. Overall, the 3D Delft3D model is able to match sediment concentration profiles for sand and fines for both low and high flows well as the Suspended Sediment Concentration (SSC) profiles.

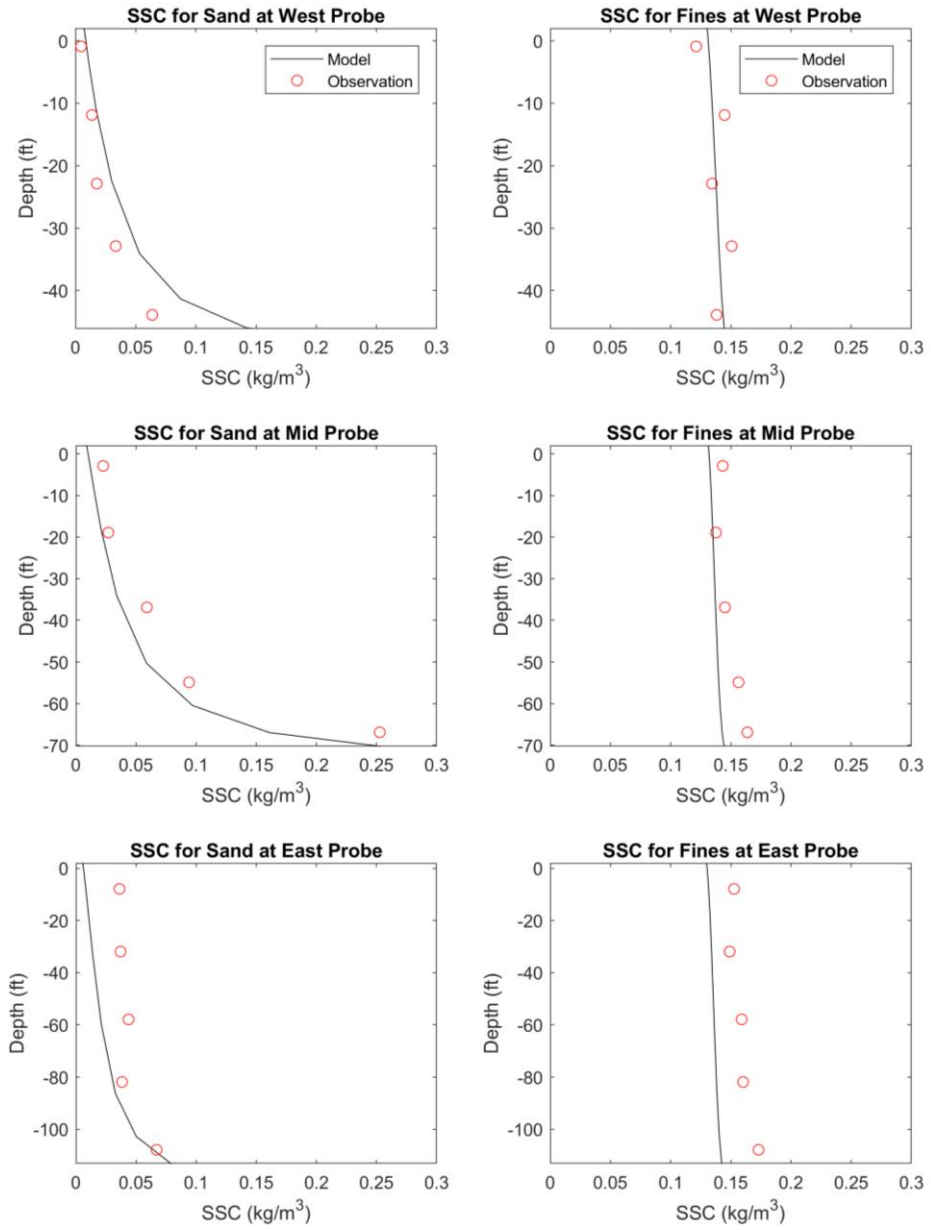

Figure 3.25. Sediment calibration (April 2009): Suspended sediment concentration (SSC) profiles for sand (left) panels and fines (right panels) at West (near RDB), Mid (near thalweg) and East (near LDB) probes as shown on Figure 3.5.

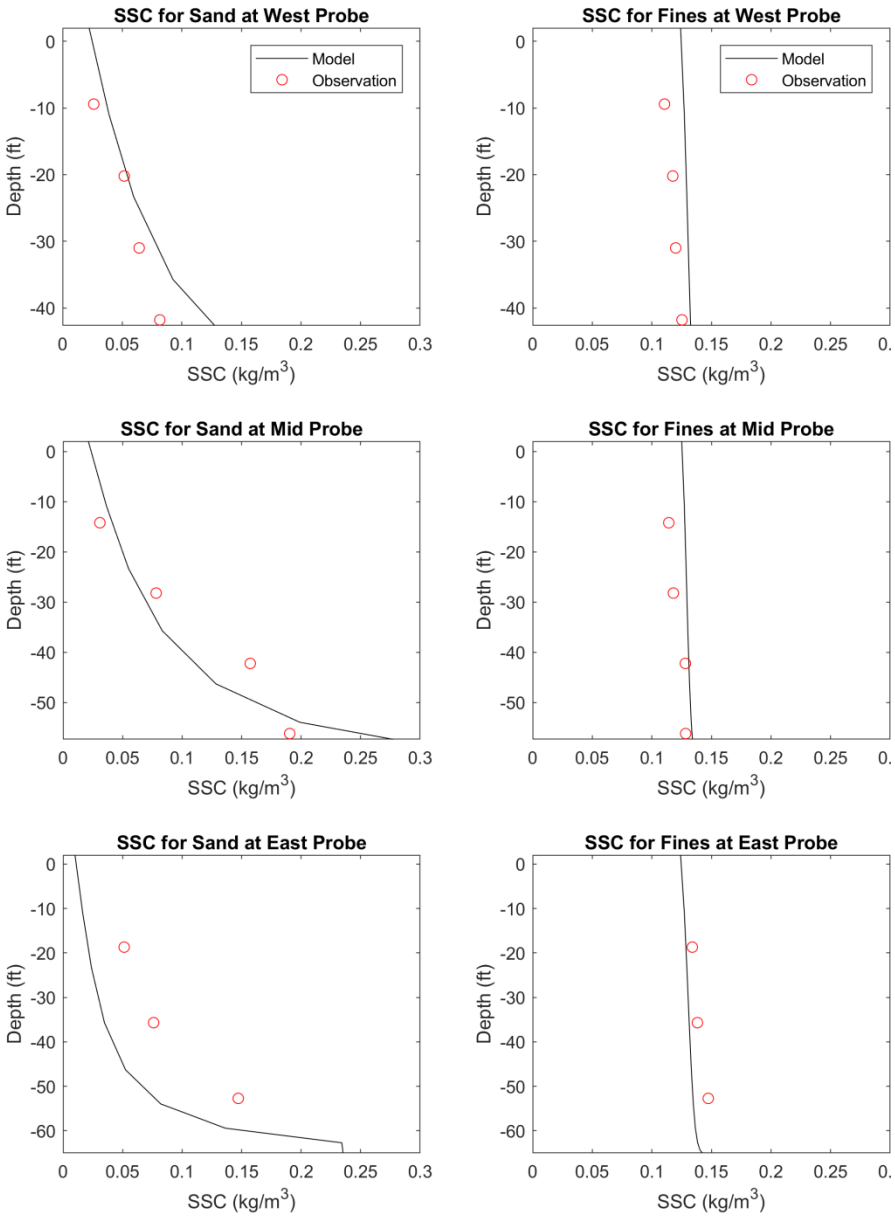

Figure 3.26. Sediment validation (March 2011): Suspended sediment concentration (SSC) profiles for sand (left) panels and fines (right panels) at west (near RDB), mid (near thalweg) and east (near LDB) probes as shown on Figure 3.5.

The Delft3D model, despite being a hydrostatic model, is well-documented in its ability to model secondary flows at river bends (Kalkwijk and Booij 1986; Frolke 2016; Banda et al. 2017). Figure 3.27 shows that the 3D Delft3D model, similar to the FLOW-3D model, is able to produce the secondary currents at the Myrtle Grove bend, immediately downstream of the diversion. It is to be noted that the secondary currents are negligible upstream of the diversion location and are not expected to affect or play a significant role in the sediment capture performance of the MBSD diversion. The Myrtle Grove bend is of particular interest in its proximity to the diversion due to its prograding sand bar that encroaches into the ship channel. A potential for deposition as a result of the lack of stream power in the river, due to diversion operations, is analyzed through modeling later in Chapter 9. The comparison of the calibrated suspended sediment transport profiles locally at this bend are shown in Figure 3.28.

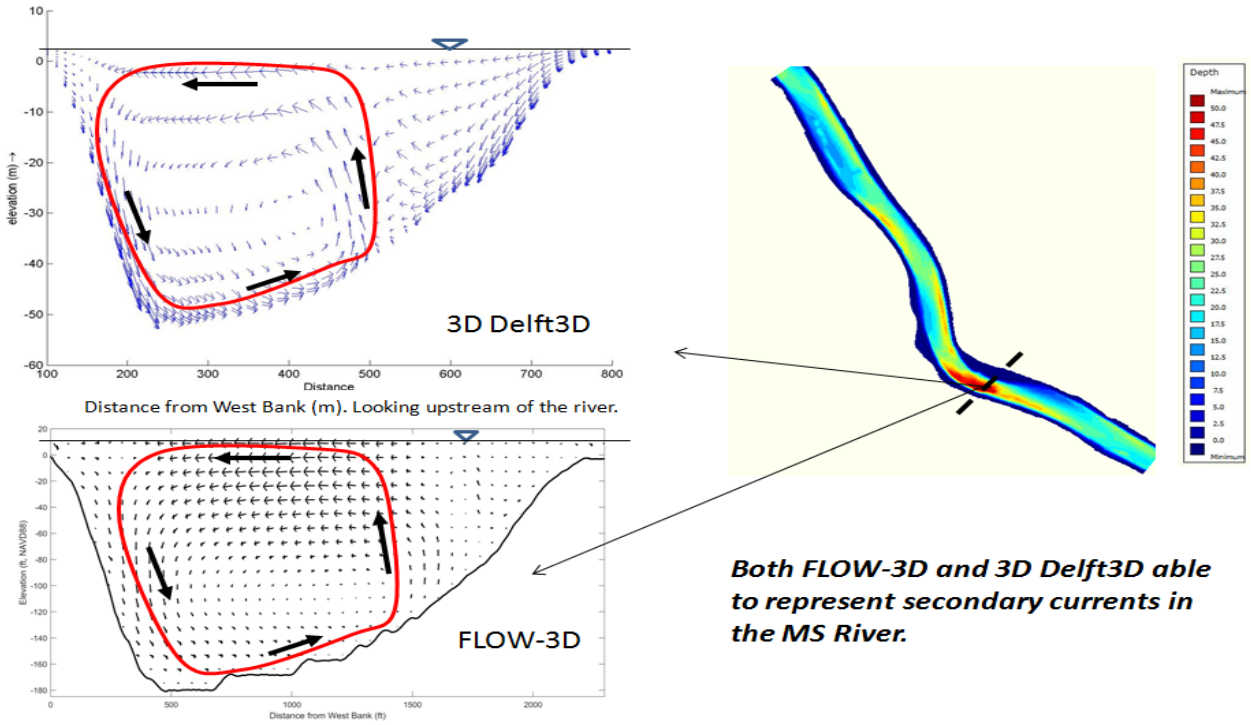

Figure 3.27. Both the 3D Delft3D and the FLOW-3D model are able to represent the secondary currents at the Myrtle Grove (downstream of MBSD diversion location) bend.

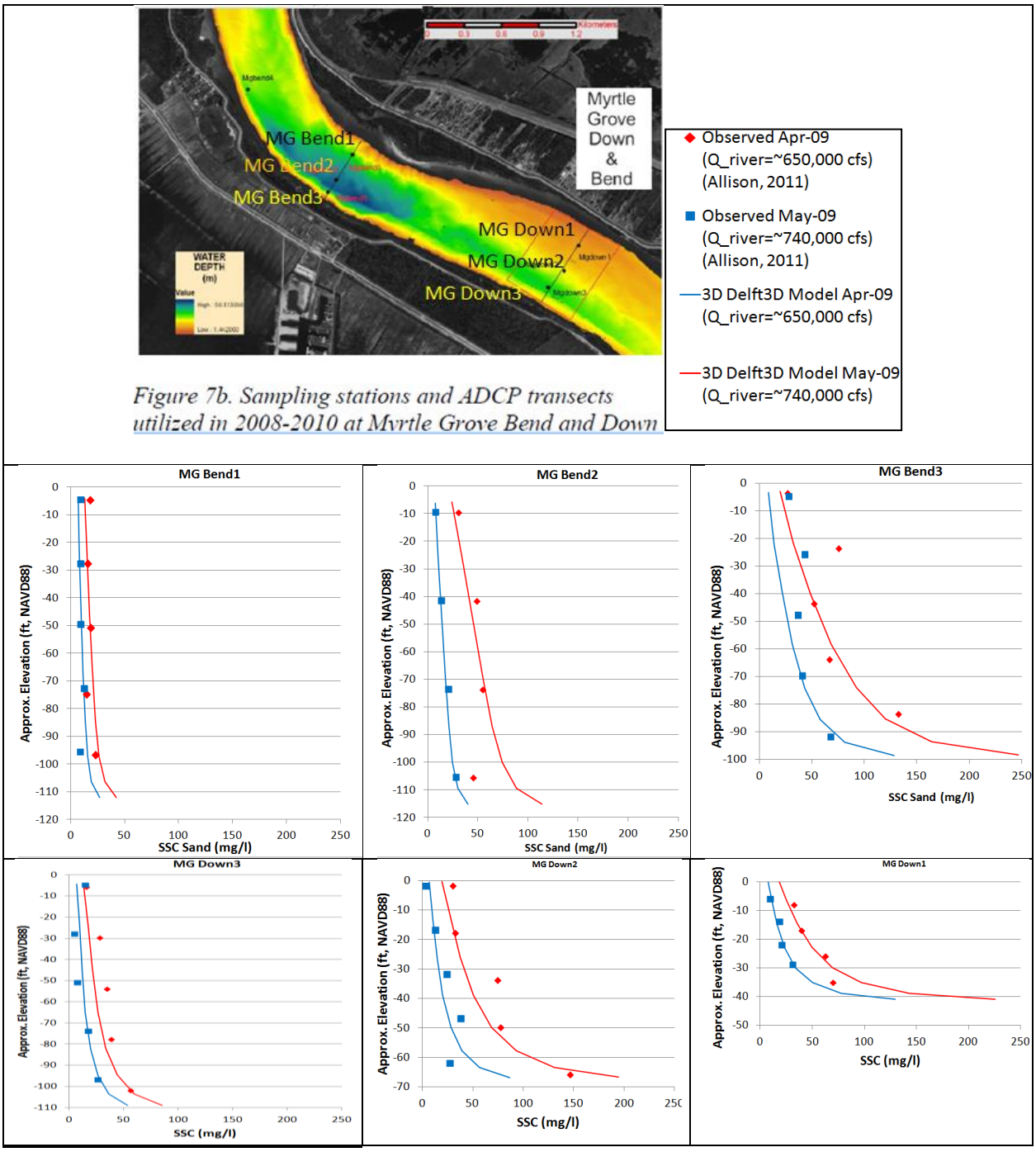

Figure 7b. Sampling stations and ADCP transects utilized in 2008-2010 at Myrtle Grove Bend and Down

Figure 3.28. Top panel shows locations were observed suspended sand concentration (SSC) data is available (Allison 2011) as well as the legend for the figures in panels below. Middle and bottom panels show the comparison of SSC at those locations within the 2008-2011 study period.

Figure 3.30 shows the comparison of cross-sectional transects 2, 4, 6, 8 and 10 (see Figure 3.29 for the locations) with observed and modeled bathymetries for the 2008-2012 model period. The purpose of this figure is to examine the implications of using an arbitrary starting bathymetry (USACE-2012 in this case) for simulation of a historical period. This exercise allows the assessment of the performance of the model in predicting the overall morphology change and to assess whether the model predictions are within the natural variation of the overall sandbar elevations within this reach. Ideally, for a long-term morphology prediction, the initial starting bathymetry should not be a factor. In fact, the exact staring bathymetry is seldom available for the entire domain at the beginning of a river morphology simulation. The focus instead is to estimate whether the model is able to reliably capture the sediment flux variations with discharge and naturally variable but consistent flow driven change in the morphology over several flow hydrographs. The focus is also on assessing whether the model can evaluate the design aspects of diversion-induced aggradation/ degradation as a comparative analysis of with- and without-project conditions. The figure shows that most of the bathymetric changes that are ongoing without the presence of the diversion are below -40 ft, NAVD88. Note that the USACE Alliance revetments currently extend up to -40 to -50 ft over this portion of the river along the RDB and is seen to limit any large scale (>2-3 ft of dune deposition) elevation change along the banks. The most ‘active’ part of the sand bar, as was shown in Chapter 2: Field Data Analysis, is between about -40 to -80 ft, NAVD88 where most of the dunes/sand waves cross the Alliance bar. These variations within this zone are unlikely to be affected by the diversion which is designed at -25 ft, NAVD8 invert. It is seen to influence the sediment transport in a limited zone (about 600-800 ft from the west bank or up to inverts -30 to -45 ft, NAVD88) of the river near the right descending bank, as will be shown later in Chapter 4: Intake Modeling. Thus, the natural historic variations of the bar elevations seen here are likely to remain even after the diversion is built. Figure 3.30 shows that the modeled morphology variations are within the historic variations of the sandbar change. For a more detailed historical analysis of the Alliance sand bar since 1964 to 2018 see Chapter 2.

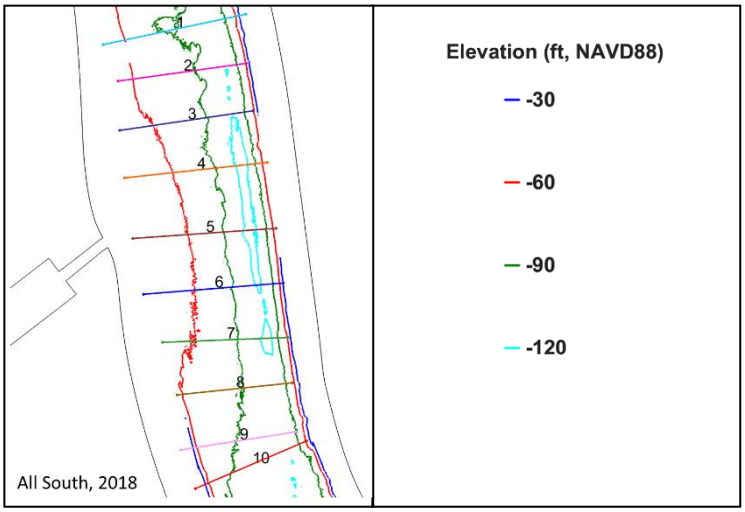

Figure 3.29. Location of transects analyzed and compared with model results in Figure 3.30 later. For a full analysis of the historical change of the Alliance Sand Bar bathymetry see Chapter 9: Modeling of Riverside Effects of Diversion Operations.

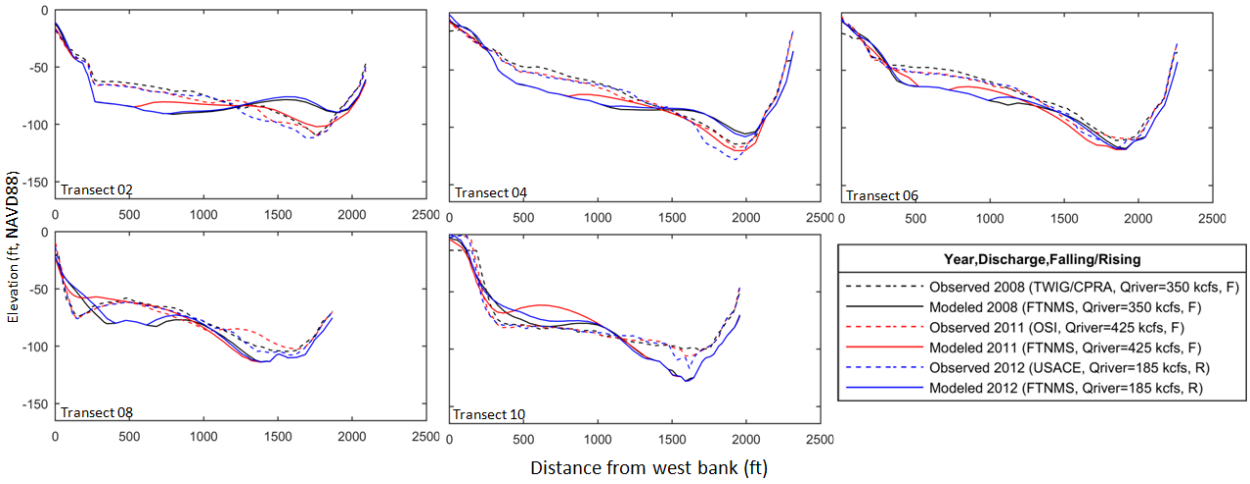

Figure 3.30. Comparison of modeled and observed bathymetries.

Figure 3.31 shows the snapshots of the modeled bathymetry at different times when similar flow conditions existed in MR. The results show the complex nature of bathymetry evolution which depends not only on the river flow but also on the history of the hydrograph.

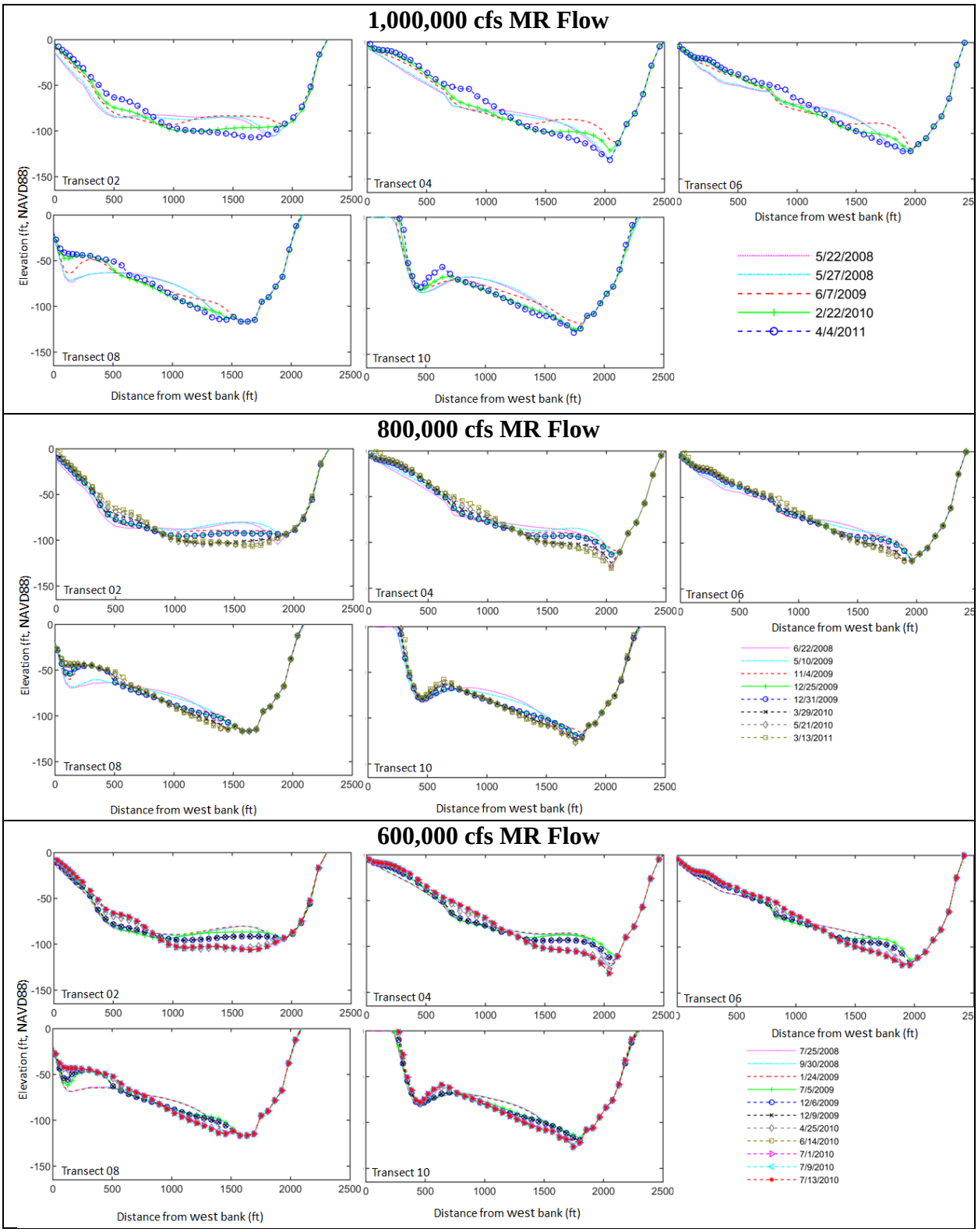

Figure 3.31. Modeled bathymetries grouped by similar MR flows during the 2008-2011 period. Results show a highly variable elevation

The 3D morphology model does show a tendency of thalweg deepening and bar accretion over time, particularly near the bends and at high flows (> 900,000 cfs which is near the effective discharge of this reach). This is also possibly due to the absence of the flow months below the trigger flow (450,000 cfs) where sand mostly flows as bedload through the thalweg and reshapes it. The phenomenon of progressive thalweg deepening is noted both in the 1964-2018 long term analysis (presented in Chapter 9) as well as the 2008-2012 short term observations (Figure 3.30). However, for the purposes of the present study where the focus is on modeling the river distribution of sediment flux and the morphological impact of the diversion on the bar itself (presented later in Chapter 9), it is appropriate to apply the model for with- and without-project modeling conditions without the loss of generality. Therefore, even though the rates of deposition and erosion within the thalweg and the sand bar may not be exactly as that needed to match the observed bathymetries, the limitations of the model in predicting the exact historical bathymetry snapshots are acceptable for the purposes of the presented comparative analysis of with- and without-project conditions later in Chapter 9.

The FTNMS model is additionally validated for hydraulics and sediment using the data from river monitoring surveys collected in 2018. The upstream (RM 66) boundary conditions for water and sediment discharge were specified by the same HSRC and TRC sediment rating curves used before and as shown in Figure 3.32. Table 8.6 shows a summary of the results of model validation. Comparison of performance for each parameter is discussed below.

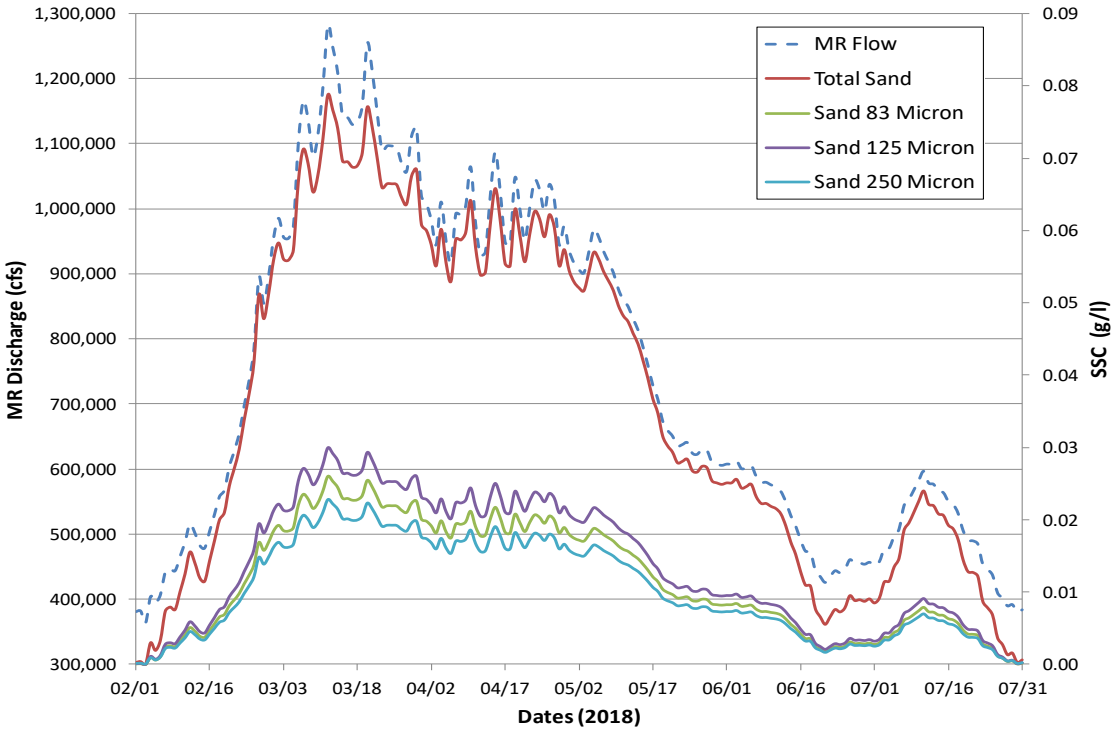

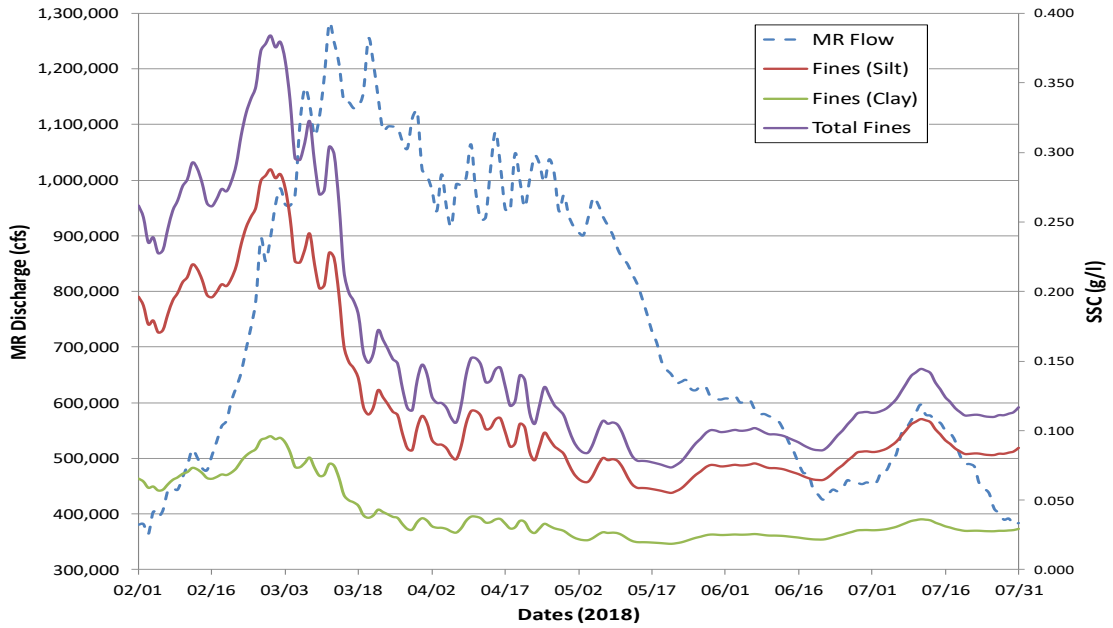

Figure 3.32. Model boundary conditions at RM 66: Sand concentrations (top panel) and fines concentrations (bottom panel).

Table 3.3. Summary of the FTNMSI Delft3D model validation results using the 2018 data.

Parameter	Observed	Modeled	% Error
WL at Alliance (ft, NAVD88)	Event 1: 8.0 Event 2: 5.3	Event 1: 8.2 Event 2: 5.2	Event 1: +2.5% Event 2: -1.9%
Avg Discharge passing PP-01, PP-02 and PP-03 (cfs)	Event 1: 1,038,304 Event 2: 616,735	Event 1: 1,021,692 Event 2: 627,889	Event 1: -1.6% Event 2: +1.8%
Avg Susp Sand Load passing PP-01, PP-02 and PP-03 (t/d)	Event 1: 91,806 Event 2: 16,386	Event 1: 90,260 Event 2: 19,076	Event 1: -1.7% Event 2: +16.4%
Avg Susp Sand Conc. at PP-01, PP-02 and PP-03 (mg/l)	Event 1: 36.2 Event 2: 10.9	Event 1: 36.1 Event 2: 12.4	Event 1: -0.1% Event 2: +14.4%
Avg Bed Load (Sand) passing PP-02 (t/d)	Event 1: 15,674 Event 2: 477	Event 1: 15,642 Event 2: 3,759	Event 1: -0.2% Event 2: +688%

Figure 3.33 (top panel) shows the comparison of modeled water levels with observed values at the USACE Alliance gage. The Root Mean Square Error (RMSE) was 0.3 ft. The model is able to reproduce the observed water levels very well throughout the hydrograph, particularly along the rapidly rising and falling limbs of the hydrograph

Figure 3.33 (bottom panel) shows the comparison of modeled discharge with observed mean discharge (between PP01, PP02 and PP03) at the MBSD diversion location and shows less than 5% variation from observed values (Table 3.3).

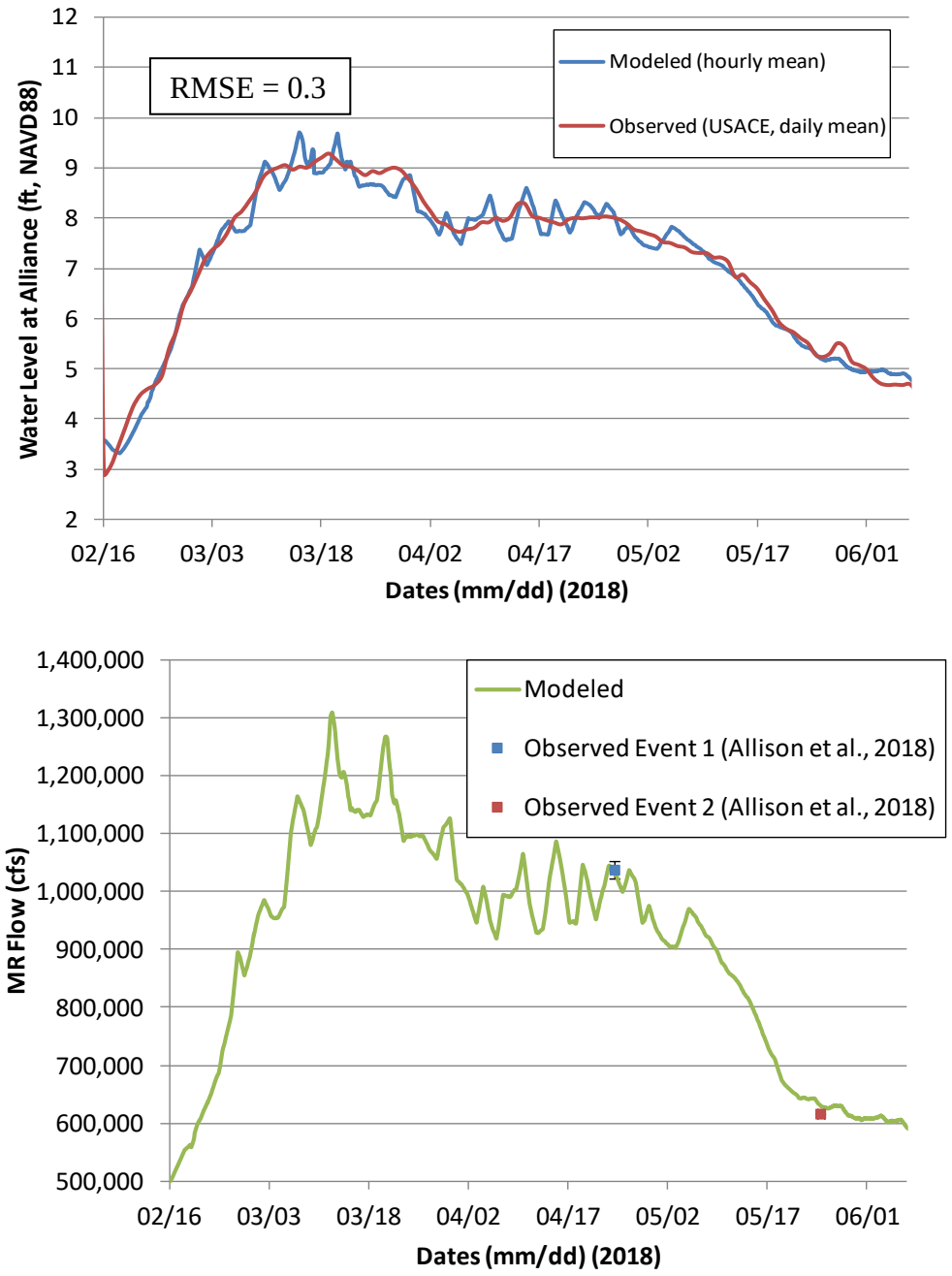

Figure 3.33. Top panel: Comparison of modeled water levels with USACE Alliance gage values. Bottom panel: Comparison of modeled discharge with observed discharge (average of PP01, PP02 and PP03).

The initial model calibration and validation (Figures 3.21 and 3.22) was performed with a constant roughness (Manning's n of 0.024) for the entire river cross-section. It was found that at high flow regime, the model over-predicted the velocities near the 750 ft distance the west bank by about 1 ft/s. The 2018 data represented a high flow regime (> 1,000,000 cfs) as well as a low flow regime (617,000 cfs) and transects were available at three separate cross-sectional locations (Figure 3.34). This allowed FTN to examine the variability of the roughness near the diversion location with greater resolution at different flows using a series of steady state runs. Figure 3.35 and 3.36 shows the comparison of modeled depth averaged velocity magnitudes across the river cross-section with observed ADCP velocities for the high and low flow events in 2018. It was found that while at lower flows (617,000 cfs) the choice of a constant Manning's n (0.024) sufficed to reproduce a good comparison with the river cross section velocities, at higher flows an improved comparisons with the cross-sectional velocities could be achieved by 'tuning' the Manning's n to account for the possible sheltering effects of the parked barges and upstream CHS terminal, the along shore shallow vegetated zones and the shore protection structures along the RDB. A technique described in (Demissie & Bacopoulos 2017) was followed where successive steady state model iterations were performed using Event 1 at high flow (1.06 M cfs) regime to reproduce observed velocities. A total of 11 iterations were performed to develop the Manning's n distribution map shown on Figure 3.34 which provided the best match for velocities. Note that it is not possible to vary Manning's n both spatially and temporally at the same time in the current version of the Delft3D software, so this distribution cannot be used for a time-varying hydrograph run. This exercise was intended to show the importance of the effects of the existing local river features immediately upstream and along the bank that may influence the velocities close to the proposed diversion intake. Note that the current barge parking facility is slated to be removed post construction and the actual velocities may be somewhat higher (by about 1 ft/s) than the current conditions in presence of these barges. FTN used a constant Manning's n of 0.024 $s/m^{1/3}$ for all production runs. For models involving a Chezy coefficient presented later, a value of Chezy 65 $m^{1/2}/s$ is found to match Manning's n of 0.024 $s/m^{1/3}$ results well. In the future, as more data becomes available and model features are improved, it may be possible to introduce a temporally varying Manning's n distribution for simulations involving time-varying hydrographs.

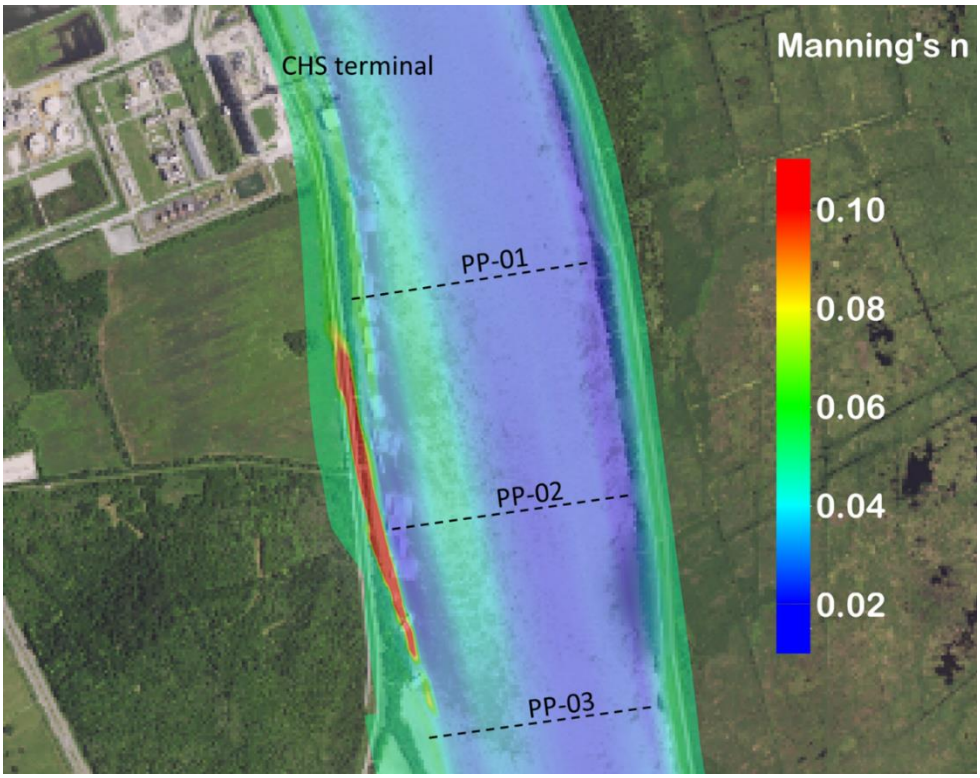

Figure 3.34. Manning's n distribution for steady state Event 1 run (1,060,000 cfs MR flow).

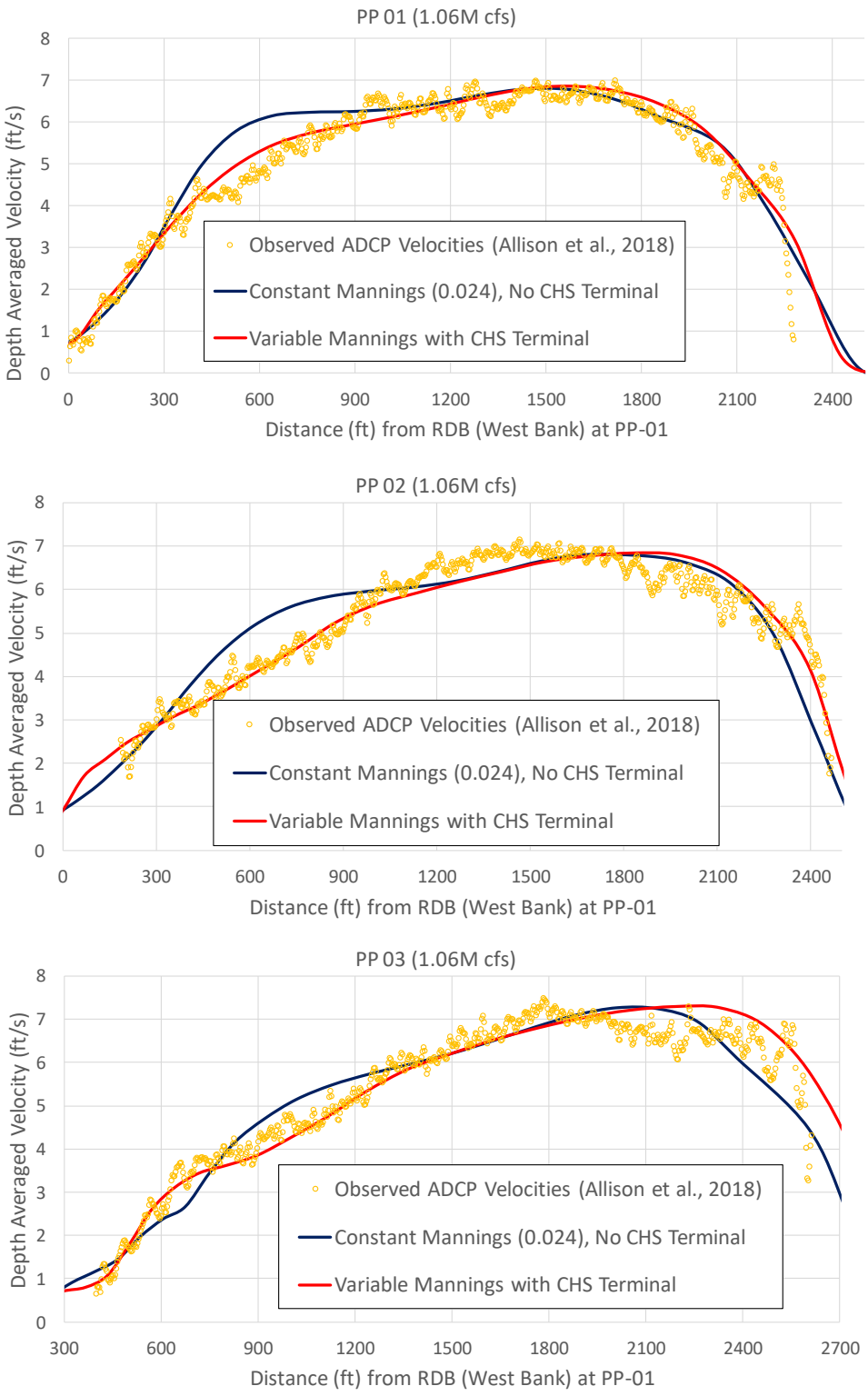

Figure 3.35. Event 1: Comparison of modeled and observed river cross-section velocity magnitudes.

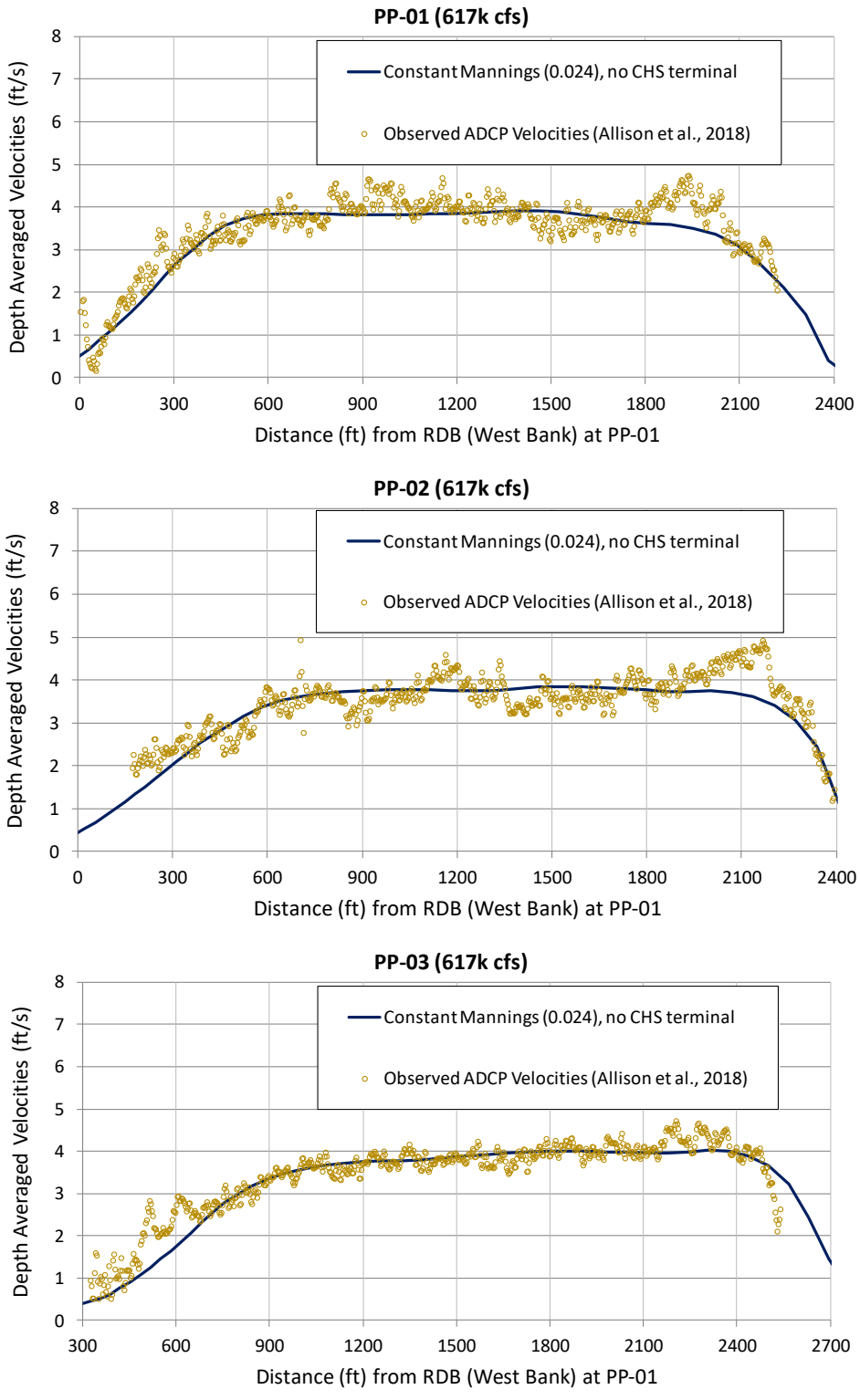

Figure 3.36. Event 2: Comparison of modeled and observed river cross-section velocity magnitudes.

Figure 3.37 shows the comparison of suspended (top panel) and bed load (bottom panel) sediment passing the MBSD location. The suspended load is averaged across the three sections while the bed load is compared for the PP02 section only as this is the closest location to the proposed intake and likely to be entrained mostly into the diversion. Table 3.3 shows that both the suspended and bed loads match very well with observed data at high flows (<2% variation) while the model overpredicts the loads at low flows. This is due to the use of constant-in-time multiplication factors for bedload transport vector magnitude and the suspended load reference concentration values. Delft3D does not allow the temporal variation of this factor with the hydrograph which is a model limitation. In principle, a separate calibration could be done to match the observed values better at low flows, but for future production runs with the diversion structure, the high flow setting is recommended. In other words, because the sand loads are 3-4 times higher at around 1,000,000 cfs than at around 600,000 cfs, a model that matches the higher flows better would lead to better estimates of diverted loads. Some uncertainty also exists regarding the precision of observed bedload transport data at lower flows. Data in the literature suggest large scatter in bed load transport rates at lower flows ([<700,000 cfs] see Allison et al., 2018, Nitrouer et al., 2008). From a practical standpoint the bed load in the river has a greater chance of entrainment into the diversion only at high flows, when dune activity starts near the sand bar portion around the -40 to -60 ft, NAVD88 inverts (Ramirez et al., 2013). The influence of the diversion extends only a few hundred feet into the river.

Figure 3.38 and3.39 show the comparison of vertical profiles of the modeled suspended sand concentrations with the observed isokinetic data for Event 1 and Event 2, respectively. In general, the model shows good comparison with the observed data. The profiles match better for Event 1 and over-predict for Event 2, particularly at locations B and C. This is likely due to the same reason as the total suspended loads which are over estimated for Event 2, the low flow event. In general, at location A, both events show somewhat higher near-bed suspended sand concentrations in the model than the observed data. In particular at low flows, it is difficult to explain the almost well-mixed sand concentration profiles in the observed data. It can possibly be due to the effect of the upstream dock structures that are within 1-2 miles and/or parking activities of large ships at the docks. Unfortunately, the barge/ship parking information and ship traffic information at the time of sampling was not available.

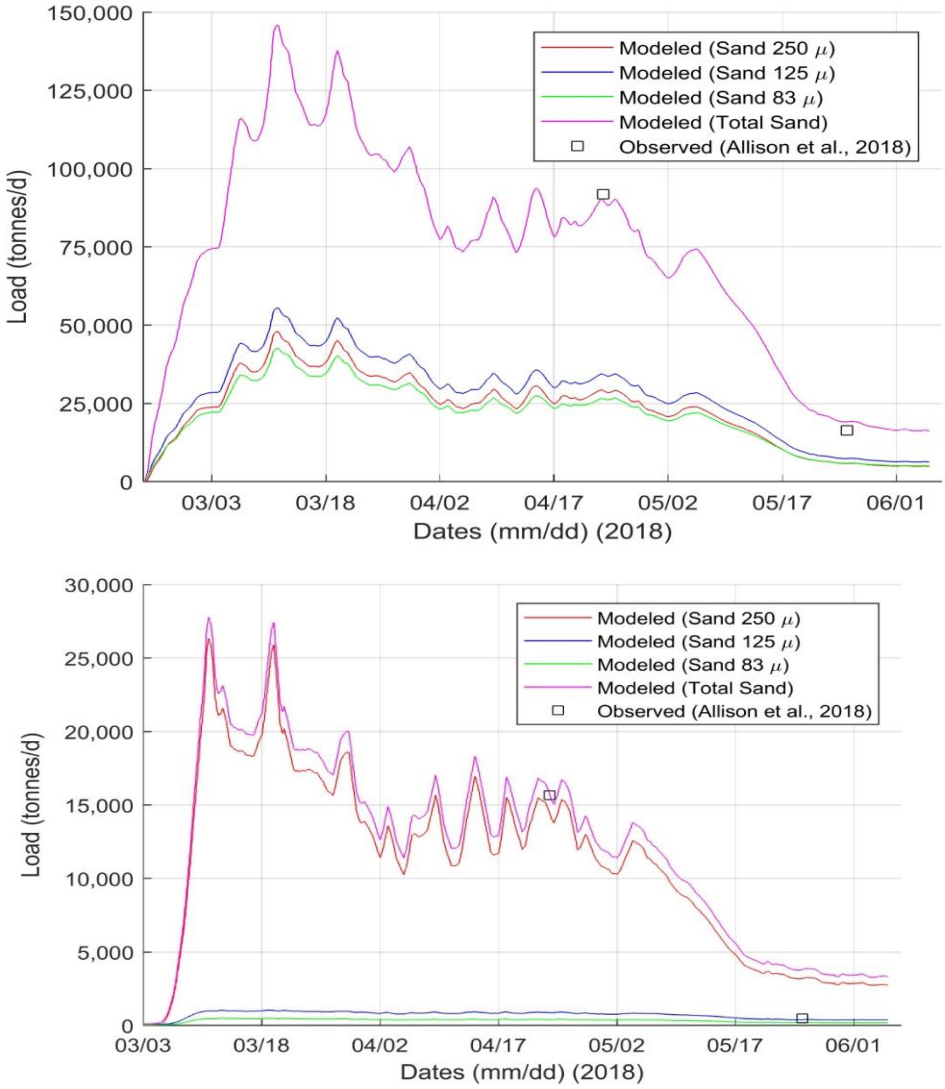

Figure 3.37. Comparison of observed total suspended sand load (averaged across the three sections) with modeled *suspended* sand loads (top panel) and comparison of observed total *bed load* at the central transect PP02 (closes to the diversion inlet) with modeled bed loads (comprised of sand only) in the bottom panel

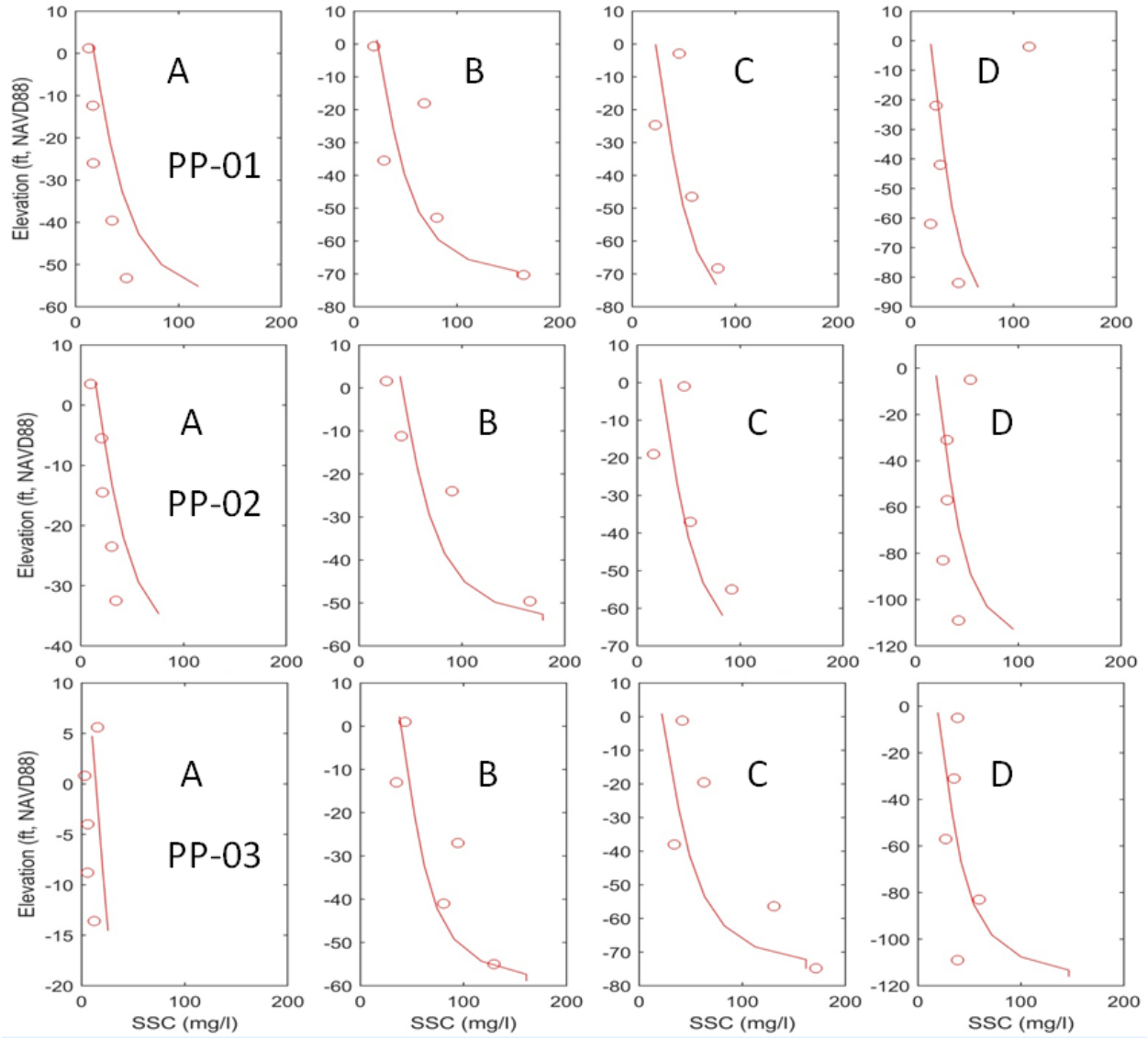

Figure 3.38. Comparison of modeled suspended sediment concentration profiles with observed isokinetic data for sand at three transects (four locations, A, B, C and D along each transect as shown, location details in Allison et al., (2018) for Event 1.

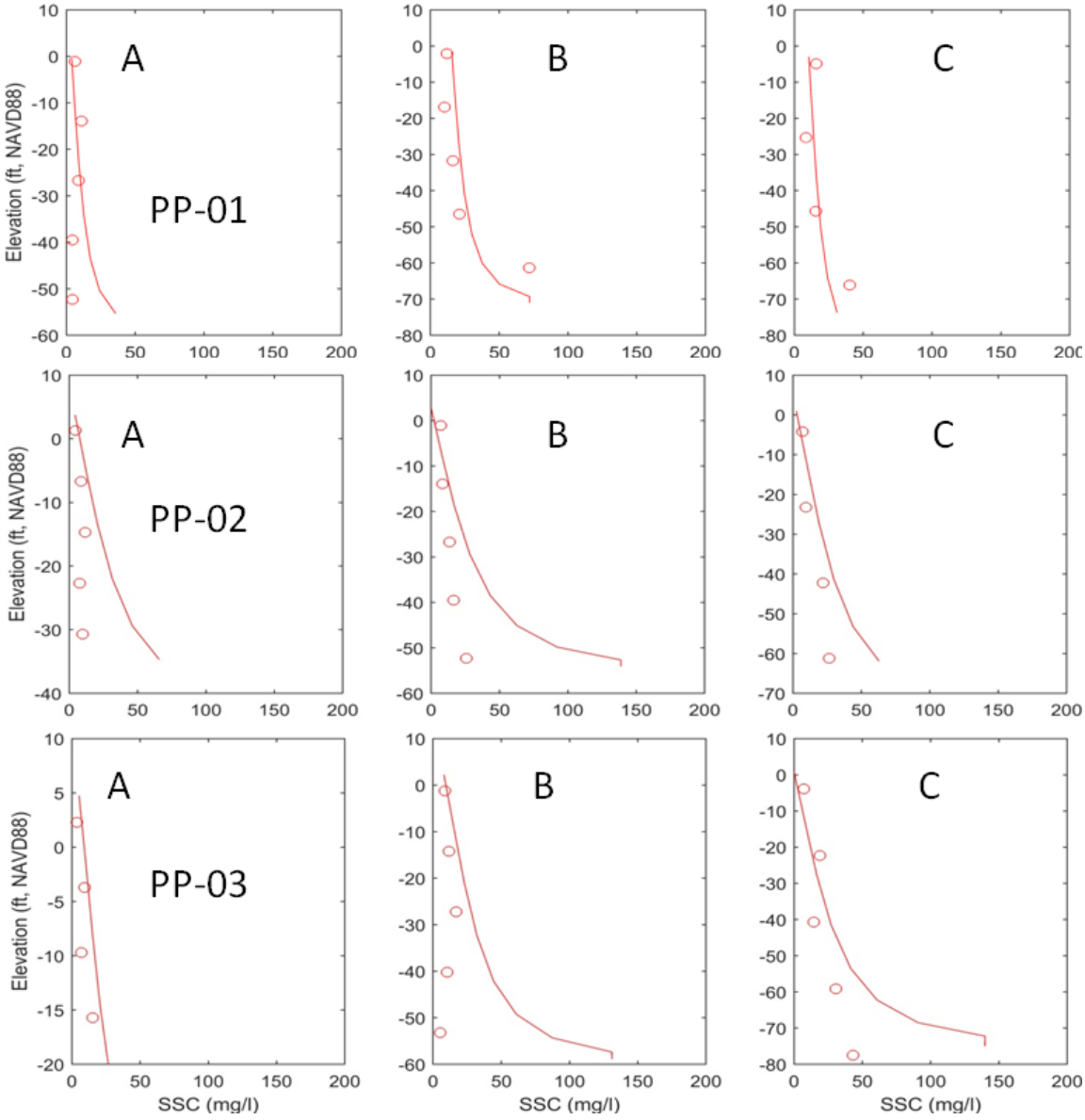

Figure 3.39 Comparison of modeled suspended sediment concentration profiles with observed isokinetic data for sand at three transects (four locations, A, B, and C along each transect, location details in Allison et al., (2018) for Event 2.

Figure 3.40 shows the comparison of observed backscatter data predicted sand concentrations with modeled sand concentrations at the three locations (PP01, PP02 and PP03) for Event 1 (1,060,000cfs). The model shows good comparison overall with observed contours. The contours of concentration over the sand bar are predicted better than those at the thalweg.

Since the model does not simulate dunes explicitly, it does not predict the spatial variation of the concentrations around the thalweg very well, where most of the dune activity occurs. The concentration gradients, however, are predicted relatively well near the -40 to -60 ft, NAVD88 elevations indicating that the model can be relied on to provide reasonable estimates of diverted loads into the intake. It is also worth noting that this method of estimation of suspended concentrations from backscatter data has larger relative error based on the scatter in the backscatter calibration itself (Allison et al., 2018). However, as more and more data become available and repeatability of observations is established, such datasets can become very valuable in conjunction with isokinetic point-based data to provide insights into sand bar dynamics.

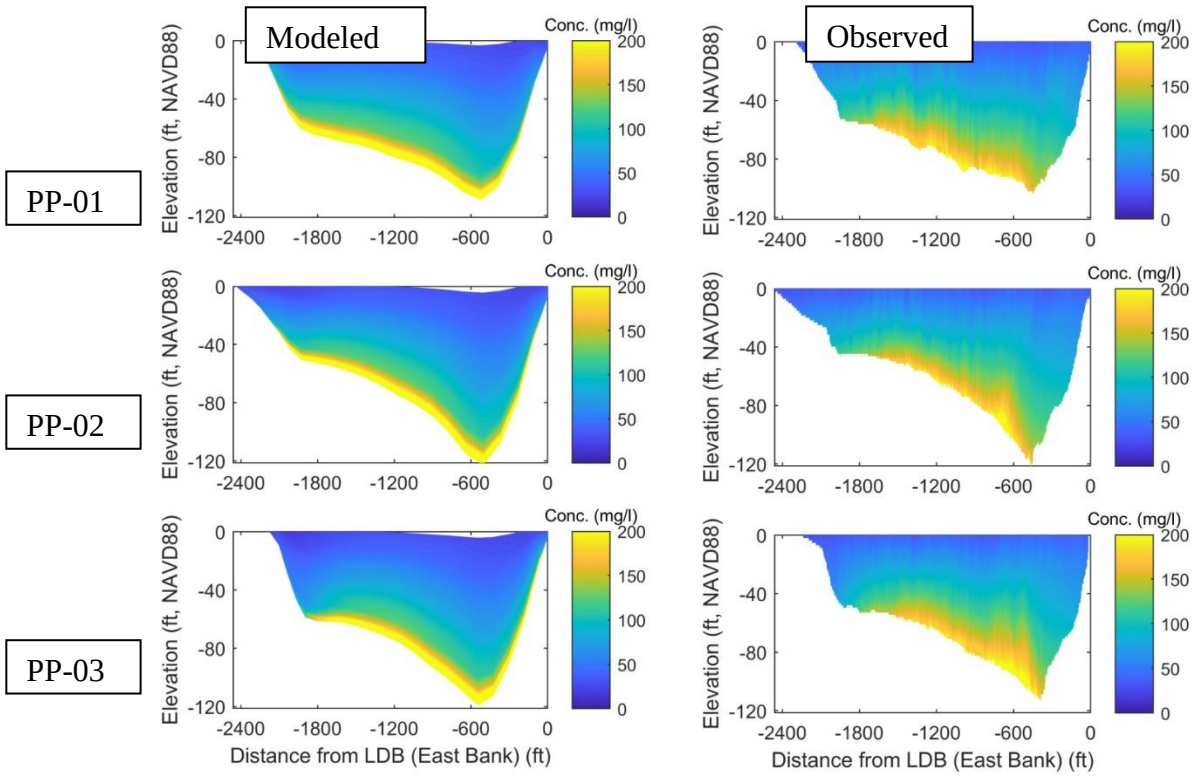

Figure 3.40. Comparison of modeled sand concentration with observed values at the three locations PP01, PP02 and PP03 for Event 1. The observed values were obtained from backscatter data of ADCPs

3.4 Delft3D 2D (FTNULMR) Model

The FTN Upper Lower Mississippi River (FTNULMR) 2D Delft3D model is developed here to study the effects of the MBSD and MBrSD joint and separate diversion operations on the MR water levels and morphology in a far scale context compared to the near-field modeling of the previously discussed 10-mile long FTNMSDI models.

3.4.1 Model Setup

Figure 3.41 shows the model domain stretching from RM 140 near Reserve, LA to about RM 48.7 at the West Pt A La Hache USACE gage. The model bathymetry was created using the USACE 2012 MR Channel Survey data and USACE 2017 MR Revetment Survey data. At the upstream at RM 140, the boundary condition is specified as a discharge time-series. For the hydrodynamic event-based calibration and validation runs, the inflow discharge time series was developed by adding leakages between RM 140 and Belle Chasse (i.e., BCS, Davis Pond and Caernarvon diversions) to the observed discharge at USGS Belle Chasse gage. This approach was flowed instead of, say, prescribing the observed discharge at USGS Baton Rouge station at RM 140 because initial modeling with the Baton Rouge flows revealed water mass balance issues in the observed data between Baton Rouge and Belle Chasse which cannot be explained by MR flow leakages in between the two gages. In fact, Lewis et al. (2017) indicates observational error at either or both USGS gages may be responsible for this lack of flow balance. Since the USGS Belle Chasse gage is accepted by CPRA and adopted by DT for all diversion related monitoring, it was decided to adopt this gage as the 'truer' of the two and reconstruct the RM 140 discharge by adding the intervening leakages. This approach also provided a consistent water level trend downstream of BCS from the model results. The discharge time series at Davis Pond and Caernarvon were obtained from USGS resources and the flows exiting BCS were specified from the USACE published discharges for the 2018-2020 events.

For the 2008-2017, 10-year sediment transport and morphology calibration/validation, the observed discharge at Belle Chasse is directly imposed at the upstream boundary and all intervening leakages are closed. This approach, while simpler than the one before, was adopted

because the purpose of the morphology model is to investigate mainly the river channel in between (RM 73 to RM 60) and downstream (up to RM 48.7) of the diversions. Initial tests with the discharge boundary including the leakages did not reveal any difference in morphology results in this region which occur mostly downstream of Belle Chasse and therefore independent of discharge specification upstream. It is to be noted that diversion induced morphology change does not extend much above RM 71 even though hydrodynamic effects, i.e., the water level effects are seen to extend even up to BCS and beyond. The sediment boundary condition for the sediment transport run is set using the HSRC and TRC rating curves and is shown in Figure 3.43 later. The sediment classifications used were the same as those developed for the FTNMS model described in the previous sections. The Van Rijn (1984) sediment transport model for non-cohesive sediment is used. The secondary current (spiral flow, Espir) parameter, the suspended (Sus) and bedload (Bed) coefficients, as discussed before were similarly calibrated. A value of 10 was chosen for the spiral flow parameter, 0.4 for the Sus factor and 5.5 for the Bed factor. Note that these values are different from the 3D FTNMS models developed before and applicable only for the 2D FTNULMR model. A uniform Chezy of 65 $m^{1/2}/s$ is used for the entire domain for the sediment transport runs since the morphological effects of the diversions are confined well downstream of RM 70. This portion is well represented by a uniform Chezy for both falling and rising limbs. The model was run for 8 months of a complete operational year (2008-2009) to develop an equilibrium bed grain size distribution before the actual 10-year production cycle began. Note that since the boundary of the FTNULMR model is far away (RM 140) from the test sections of MBrSD (RM 68) and MBSD (RM 61) and because the model was run with a Morphological Acceleration Factor, the upstream sediment boundary condition has little effect on the actual sediment fluxes simulated at those transects. In fact, they are determined by the local bed material flux movement over a few bar lengths upstream. The only role of the sediment boundary is to adequately develop a bed material gradation which can produce the required site-specific sediment fluxes.

The downstream boundary was a water level boundary from the observed USACE West Pt A La Hache gage data for all event-based runs and as a Q-H boundary (Figure 3.14) for all sediment transport runs. For the with-structure event-based runs presented later in Chapter 9,

the time series of water level at the downstream boundary was adjusted dynamically based on the Q-H predicted water level difference given the known discharge difference passing the boundary at the previous time-step.

For the with-structure runs presented later in Chapter 9, at the two diversions, time series of discharge (capped at 75,000 cfs) were imposed based on the Q-Q (diversion discharge vs MR discharge) relation developed for each diversion. The MBrSD Q-Q is based on the 15% design and as supplied to FTN by the Stantec DT through CPRA. The MBSD Q-Q relation is as developed in Chapter 8 for the three-component model.

For the event based hydrodynamic runs since the ultimate goal is to understand the impact of the diversion operations on the water level set-down at Bonne Carre and downstream, the model was first carefully calibrated to observed water levels without the diversions, in the rising and falling limb of the 2018-2019 hydrograph. It was found that while a uniform Chezy of 65 $m^{1/2}/s$ produced a reasonable match of observed and modeled water levels, for the falling limb a piecewise hydrograph based variable Chezy was required. As shown in Figure 3.42, for the falling limb, above 750,000 cfs MR flow, upstream of Harvey Lock a rougher value ($C=50\ m^{1/2}/s$) was needed while below IHNC lock $C=65\ m^{1/2}/s$ was needed. The rougher Chezy requirement, as inferred from qualitative inspection of USACE channel and revetment surveys in this region, is most likely due to the growth of bedforms during the falling limb as a result of increased deposition resulting from the closure of BCS. The increased sinuosity of the MR channel between the BCS and IHNC also creates a somewhat flat water surface profile locally in this region indicating that the reach averaged skin friction shear stress drops significantly in the falling limb post Bonnet Carre opening. Below 750,000 cfs, however, a further change is also necessary upstream of BCS which is set as $C=60\ m^{1/2}/s$ as shown in Figure 3.42 bottom right panel. This latter change is possibly required due to Lower Mississippi River backwater induced effects at low flow affecting deposition upstream of the BCS and a slight roughening of the bed. The zone between the BCS and Harvey Lock is set to $C=55\ m^{1/2}/s$ for this phase of the hydrograph.

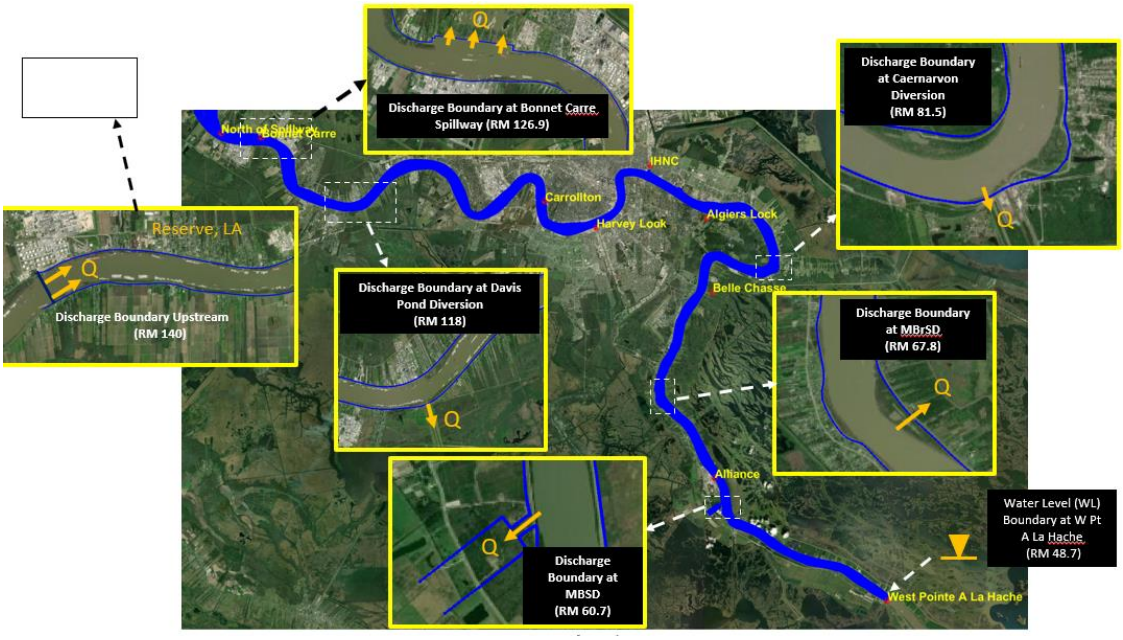

Figure 3.41. FTNULMR 2D Delft3D model domain and the boundary conditions.

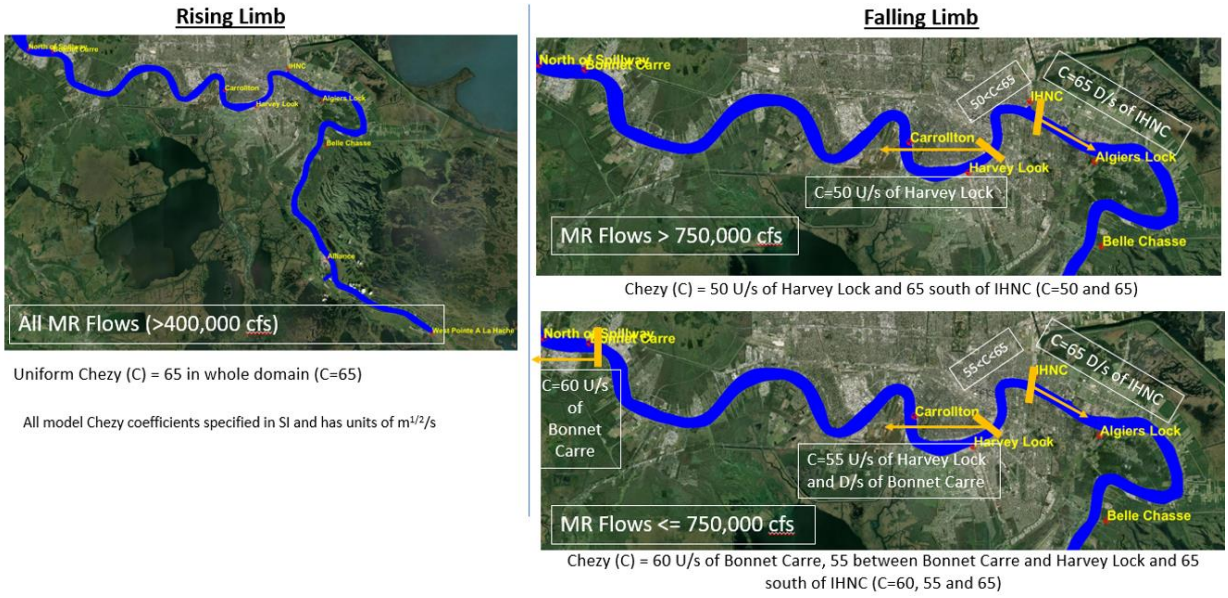

Figure 3.42. Calibration of MR bed roughness based on rising and falling hydrograph sequences.

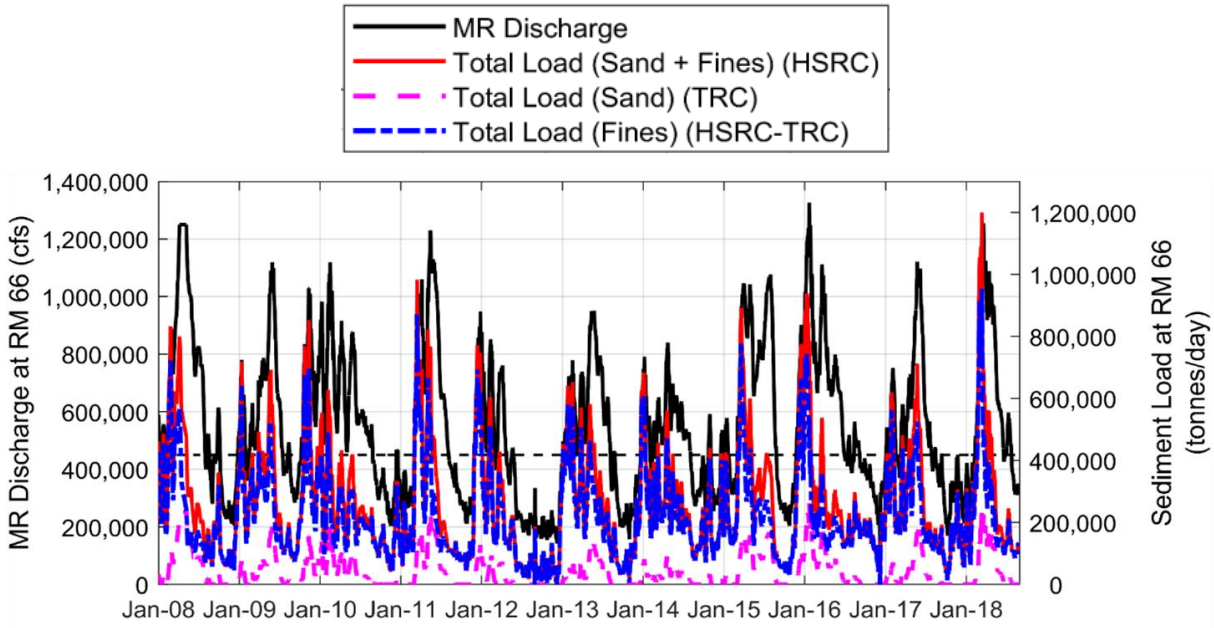

Figure 3.43. Boundary condition at RM 140 for the 2008-2018 FTNULMR 2D Delft3D Sediment Transport Model.

3.4.2 Results

Figures 3.44 and 3.45 show the model and observed time series comparison from the rising and falling limbs of the hydrographs, respectively. The event-based runs show an RMSE of 0.18 to 0.77 ft among the gages compared and are well within the natural variability in the water levels year to year.

Figure 3.46 shows the comparison of the modeled water levels from the calibration/validation period (2008-2020) to the observed data (2008-2018) over the 10-year period. The model results fall well within the observed water level variability and can be extended to with-structure modeling to evaluate effects of operations of the diversions.

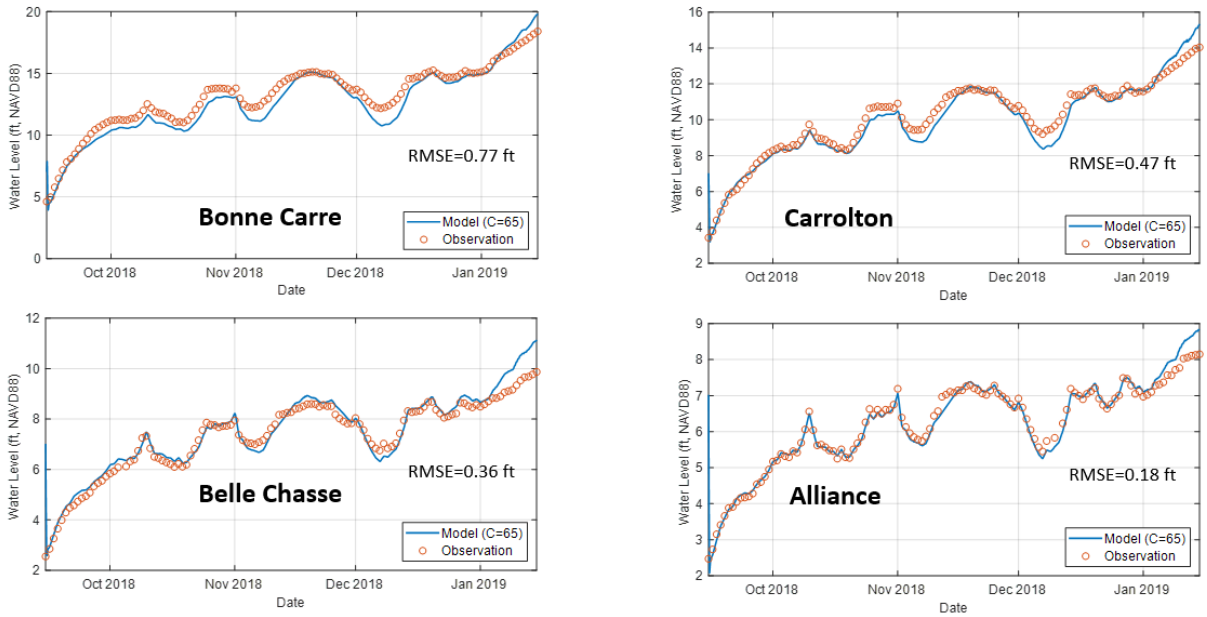

Figure 3.44. Rising limb model calibration.

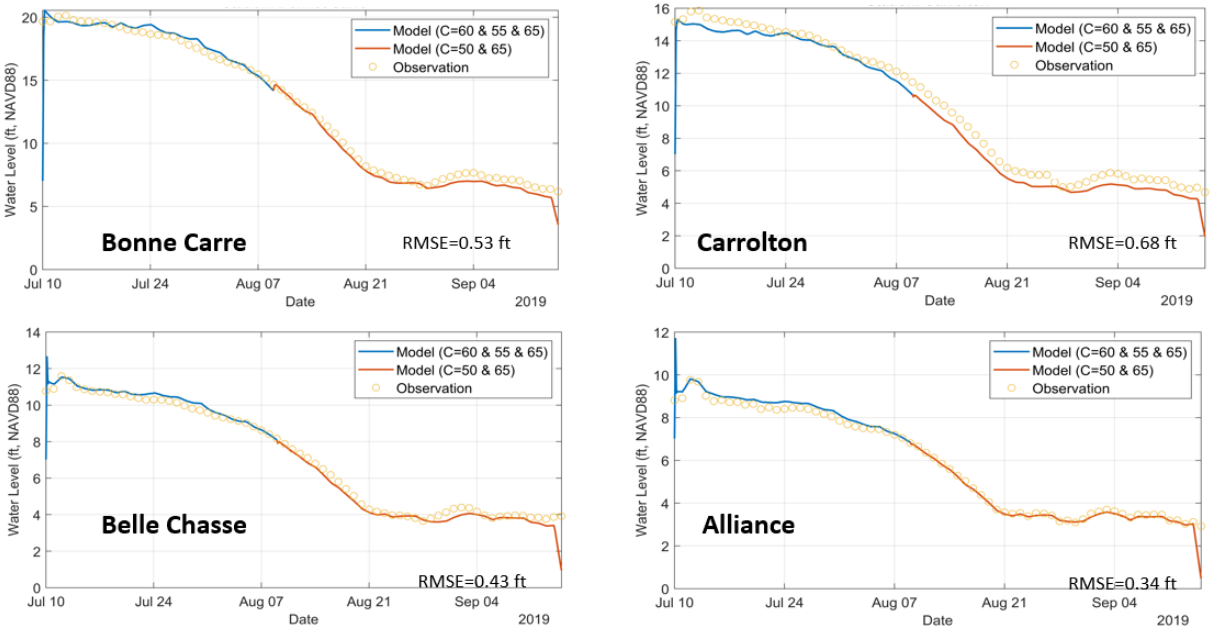

Figure 3.45. Falling limb model calibration.

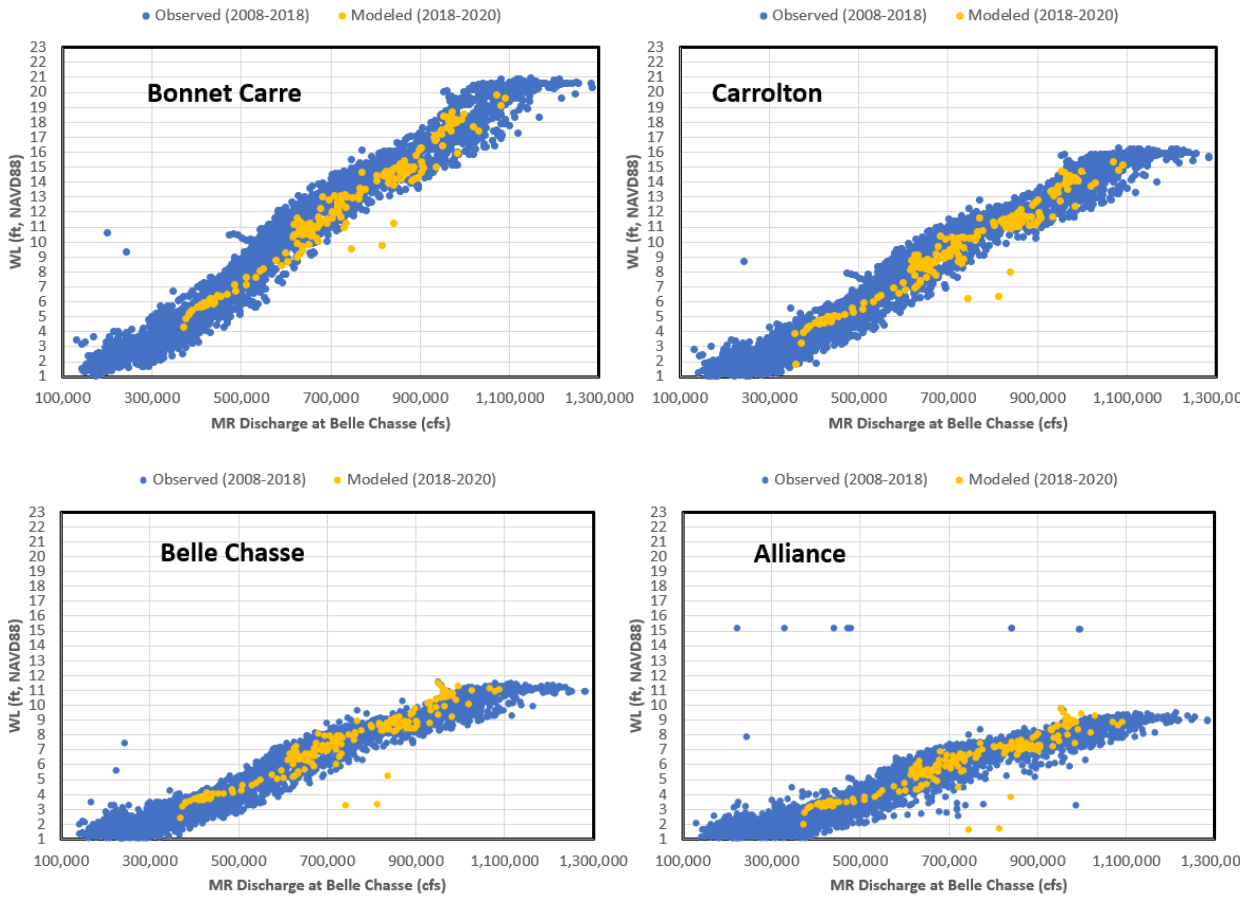

Figure 3.46. Discharge-Stage (Q-H) Scatter Plots of Observed (blue) and Modeled (yellow) data from the FTNULMR Delft3D (2D) model. Most of the modeled data lies well within the natural range of variation of the observed water level at a given river discharge.

Figure 3.47 shows the modeled sediment rating curves of the calibrated model compared with the observed data. The validation period (2018-2020), including observed data from recent 2018-2020 MR monitoring are also included in the results. A total of 26 model runs (each of a 12-year period) were conducted to arrive at the final choice of parameters for the calibrated model results.

Figure 3.48 shows the comparison of modeled sediment rating curve at the MBrSD location with observed data. It shows that the model parameters are able to represent the sediment flux well at this site for flows below 1,000,000 cfs. Above this value, the few

observation results, are affected by possible submarine retrogressive sand bar failure (Torrey et al., 1988) which entrains locally suspended sand rich plumes at this cross-section. Such phenomenon was not modeled in Delft3D and is beyond the scope of the discussions here. Nonetheless, the model is shown to be able to simulate sediment fluxes at different locations between the diversions within the observed variability in the data and can be extended to multi-year with and without-project analysis.

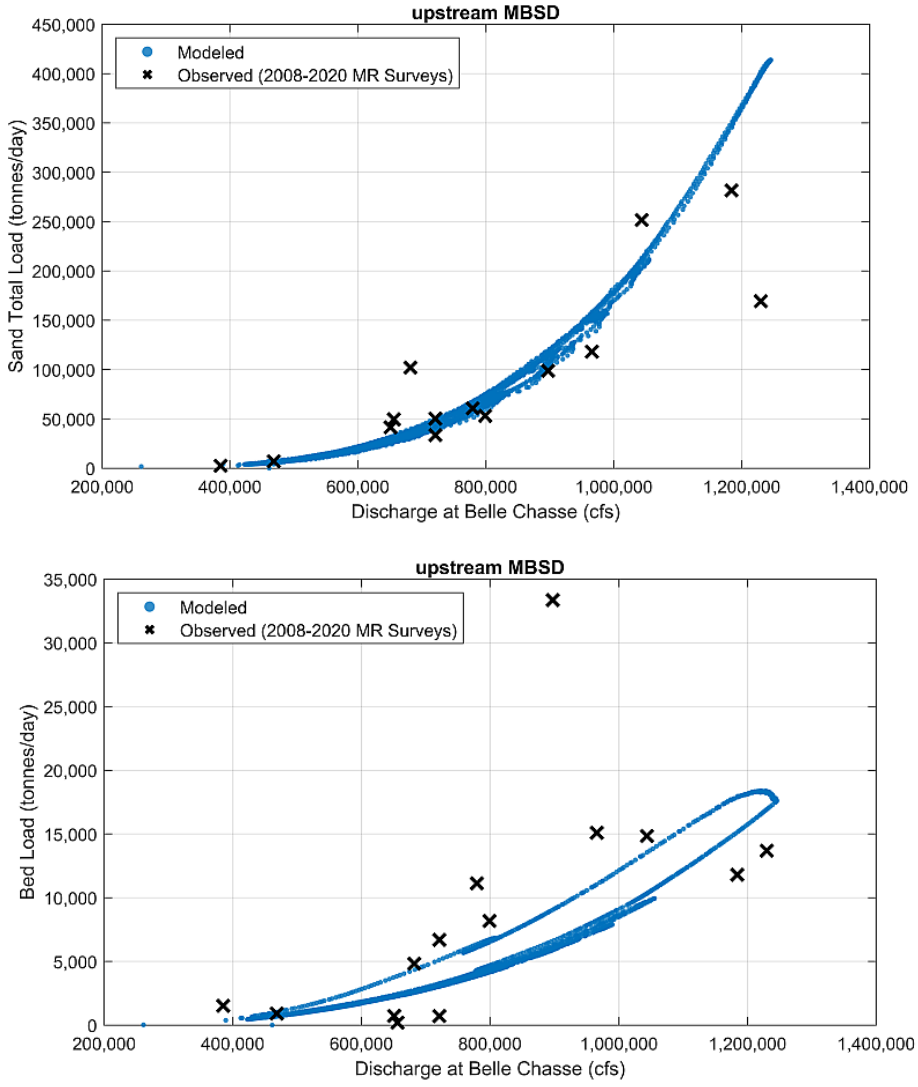

Figure 3.47. Comparison of modeled suspended (top panel) and bedload (bottom panel) sand fluxes a the MBSD location without structure and under current conditions.

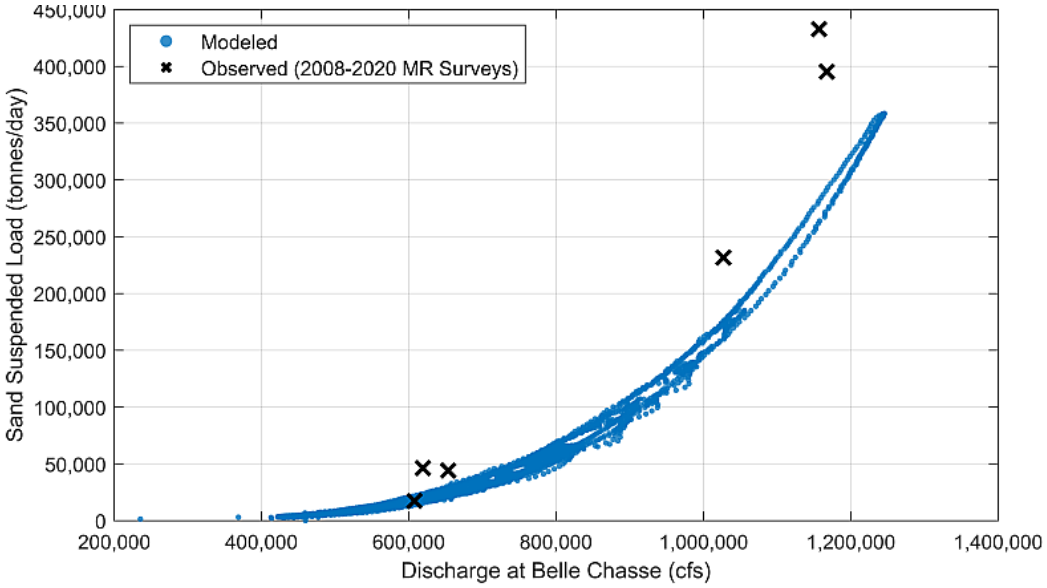

Figure 3.48. Comparison of modeled suspended sand flux at the Mid-Breton diversion location. The model somewhat underestimates the sediment load above 1,000,000 cfs at this location primarily due to the fact that the observations are affected by locally occurring submarine retrogressive sand bar failure induced short term sediment injection in the water column which are beyond the scope of the current model.

3.5 Conclusions

Three separate models, the Mississippi River three-dimensional FLOW-3D (hydrodynamics and particle transport), two-dimensional Delft3D (hydrodynamics only) and the three-dimensional Delft3D (hydrodynamics and sediment transport) models were successfully calibrated and validated with the observed MR hydrodynamic and sediment monitoring data from 2008-2018. The FTNULMR two-dimensional Delft3D model was also calibrated and validated for water levels (2018-2020) and suspended and bedload sediment fluxes (2008-2020).

For the FLOW-3D model the river bed roughness value was calibrated to match observed velocity distributions while for the sediment transport simulations using mass particles the upstream seeding plane location, seeding rate and vertical extent were adjusted. The particle specific factors such as diffusion coefficient were also calibrated. The model results matched the cross-sectional distribution of velocity at both low and high flows, the vertical profiles of velocity and the suspended sediment concentration well. An underprediction of concentration,

particularly at high flow was noted on the bar near the thalweg indicating that to some extent the model may underpredict the net cross-sectional summation of sediment load and therefore overpredict the absolute values of sediment water ratio (whose denominator include the sediment load in the river) computed from the model results from FLOW-3D. Therefore, the FLOW-3D SWR values were only used for relative comparison between different intake configurations. The modeled sediment distribution near the proposed intake, however, matched well with observations and the model can be used to evaluate sediment capture performance under with-structure conditions.

The 2D and 3D Delft3D models were calibrated for water level, cross-sectional velocity distribution and discharge. The 3D Delft3D model was further extended for sediment transport and morphology modeling. It was calibrated and validated with the observed vertical velocity profiles, vertical suspended transport profiles, net suspended and bed load fluxes over a large number of events at different MR flows between 2008-2018.

The 2D Delft3D FTNULMR model was developed to analyze joint diversion operations. It was calibrated and validated for hydrodynamics. A hydrograph (rising or falling limb) phase dependent Chezy roughness distribution was developed to match the model water levels to the observed data at various gages between BCS and Alliance. For sediment transport modeling, a re-calibration of the suspended and bedload factors was necessary to what was adopted for the FTNMS 10-mile-long model. Also, the Van Rijn (1984) sediment transport model was used for the FTNULMR model instead of the Van Rijn (1993) formulation used in the 3D FTNMSD model for non-cohesive sediment. The secondary current effect on the bedload for the 2D model was parametrized by calibrating the spiral flow factor. The models described in this Chapter are applied to evaluate with-structure scenarios in the following Chapters.

4.0 RIVER INTAKE MODELING

4.1 Introduction

The proposed MBSD intake headworks is a controlled lateral opening on the lower MRL. The headworks consists of the intake portion in the river, the U-Frame with three bays, the bulkhead gate structure and the intake transition to the conveyance channel. The purpose of the diversion complex is to divert sediment and fresh water from the Mississippi River to the Barataria Basin.

The main hydraulic design goal was to design an intake that will allow at least 75,000 cfs diversion flow at 1,000,000 cfs MR flow as measured at Belle Chasse, under current (2020) conditions. The secondary goals were to maximize the operational efficiency of the diversion as defined by two principal criteria: 1) Minimize the headloss at the intake and thereby maximize diversion flow for a given MR flow and 2) To maximize the SWR of sand, defined as a ratio of the sand concentration in the diversion to the sand concentration in the river. Since the fines (silt and clay) are relatively well mixed in the river cross-section, modeling studies have shown (Meselhe et al. 2012, Meselhe et al. 2014) that fine sediment SWR ranges around 1.0. In other words, the concentration within the intake is similar to that averaged across the river for fines. Meeting the first criterium will automatically satisfy the goal of maximizing the captured sediment load which is a product of sediment concentration and the diversion discharge. Also, since sand concentration increases in the river with flow and at or above 1,000,000 cfs MR flow sand concentration can be 5-6 times that at or below 600,000 cfs (Nittrouer et al. 2008), the headworks was designed with the goal to prioritize the sand capture for diversion discharge of 75,000 cfs at a river flow of 1,000,000 cfs.

A complex three-dimensional (3D) flow field is found to be developed in the river and in the U-Frame of the intake structure as flow enters the diversion and transports river sediment, particularly sand into the intake. The purpose of the numerical modeling was to assist the Design Team in selecting an invert for the structure and the type of the intake structure based on sediment capture efficiency and energy loss through the structure. The hydraulic and sediment results from the currently advanced intake structure at the 60% phase are presented here.

Two numerical models were used for the analysis, namely, FLOW-3D and Delft3D. FLOW-3D is a fully 3D CFD code and is used to compute the energy head through the system but has limited sediment transport capabilities. It is also used to estimate the SWR of the suspended sand load. The Delft3D is a physically-based sediment transport model and includes bedload transport, the contribution of locally sourced sediment to suspension and is able to compute areas of sediment scour and deposition. However, Delft3D solves the shallow water equations (i.e., does not represent vertical accelerations) which provides a less accurate solution of the rapidly varied flow field near the intake. To evaluate the intake performance, results of both models are used along with the results from a 1:65 scale undistorted physical model that has a live bed described in a separate report.

4.2 Modeling Methodology and Setup

4.2.1 FLOW-3D

The FTNMSDI FLOW-3D model domain consists of the FTNMS (MR only) domain as well as the intake headworks, the intake transition and part of the conveyance channel. See Chapter 3 for a complete description of the FTNMSDI setup including boundary conditions.

To model friction losses in the FLOW-3D intake model, in addition to specifying 0.6 m as the roughness height of river (calibrated from FTNMS model), the roughness height for the U-Frame concrete portion of the intake headworks diversion was set to 0.006 m. All rip-rapped zones were assigned the same roughness as the river based on initial sensitivity analyses of rip-rap median size.

The FTNMSDI model required an additional specification of boundary at the conveyance channel. A water level boundary was defined for this purpose. A series of runs with varying water levels at this boundary location were first run and the water levels that diverted 75,000 cfs at 1,000,000 cfs (High Flow Scenario) MR flow, 48,000 cfs at 600,000 cfs (Low Flow Scenario) MR flow and 34,000 cfs at 450,000 cfs (Trigger Flow Scenario) were chosen for the production runs. Note that the choice of diversion discharge for the Low and Trigger flows scenario were guided by initial WI modeling rating curves obtained from CPRA (Liang et al., 2017) for a different diversion design developed in the planning phase. As will be shown later in Chapter 8,

where the complete rating curve of the 60% E&D phase diversion design is developed, the diversion discharge is 48,300 (range 40,000-53,000 cfs considering natural variability of river and basin water levels due to tides/wind) at 600,000 cfs MR flow and 29,000 cfs (range 28,000-35,000 cfs) at 450,000 cfs MR flow for the final 60% E&D phase design. Therefore, the initially chosen steady state discharge values could be regarded as reasonable approximations within the observed range.

To quantify the conveyance performance the total energy head loss was quantified. The total energy head is defined as:

$$Total\ Energy\ Head = \frac{v^2}{2g} + WSE \quad \ldots\ldots. (1)$$

Where: v indicates the depth-averaged velocity along the centerline of the structure,

g is the gravitational acceleration, and

WSE is the water surface elevation referenced to the NAVD88 datum.

The total energy loss between the center of the MR at the diversion location and the end of the intake transition is used to evaluate the total hydrodynamic friction and turbulent expansion and contraction losses caused by the intake headworks.

To quantify the sand capture performance using particle modeling in FLOW-3D, the sediment water ratio at steady state was used and it is defined as:

$$\text{Steady State Sediment Water Ratio (SSSWR)} = \frac{\frac{\text{SSSL}_d}{\text{SSSL}_r}}{\frac{SSQ_d}{SSQ_r}} = \frac{\frac{\text{ParticleRate}_d}{\text{ParticleRate}_r}}{\frac{SSQ_d}{SSQ_r}} \quad \text{.....(2)}$$

Where: SSSWR denotes the steady state sediment water ratio,
SSSL is the steady state sediment load,
SSQ is the steady state discharge, and
Particle Rate indicates the steady state particle passing rate at any given location.

The subscripts *d* and *r* indicate quantities at the diversion and the river transect locations, respectively. The diversion transect location was placed at the end of the gate complex within the intake, while the river transect location was placed at the proposed MBSD diversion location (RM 60.7) in the river only (no diversion structure) scenario. Note that this is a slightly different definition from that used in Delft3D SWR computations where a reference plane about 1 mile upstream is used to compute all SWR and CSWR computations. The Delft3D upstream reference plane, could have been too near the seeding plane in the FLOW-3D setup and boundary effects could not have been eliminated, hence the difference in choice. However, this difference does not affect comparison of SWR values for a given model. The river transect was placed at the proposed diversion location in the river-only setup to capture the natural cross-sectional variability of sediment due to the presence of the sand bar. Also, defining it in the river-only model (instead of the river model with diversion structure) eliminated any near-field influence of the different diversion intakes on the values in the denominator of the SWR definition and enabled us to do a true independent comparison of performance of various intakes.

FLOW-3D near-bed velocity model results were used to compute the skin-friction shear stress. Shear stress is calculated based on the law of the wall,

$$u_\tau = \frac{u*\kappa}{\ln(\frac{y}{y_0})} = \sqrt{\frac{\tau_w}{\rho}} \text{ ..... (3)}$$

$$y_0 = \frac{k_s}{30}$$

Where: u_τ is the shear velocity (m/s),

u is the velocity magnitude 2.5 m from the river bed (m/s),

κ is the Von Kármán constant with a value of 0.41,

y is distance from the boundary wall with a value here of 2.5 m,

$\frac{y}{y_0}$ is the dimensionless distance from the wall,

k_s is the wall surface roughness (m),

τ_w is the wall shear stress (Pascals or N/m^2), and

ρ is the fluid density (kg/m^3).

4.2.2 Delft3D

The Delft3D FTNMSDI model, similar to the FLOW-3D model, is composed of the FTNMS model, the intake, the intake transition and the conveyance channel. Detailed description of the setup of the Delft3D FTNMSDI model can be found in Chapter 3.

For the sediment transport model runs performed in this Chapter, the 3D Delft3D model was used to run a three-year 2008-2011 hydrograph. The upstream boundary conditions in the MR are shown in Figure 4.1. The conveyance channel of the FTNMSDI model was extended up to 4000 ft downstream of the transition (approximately the mid-point of the conveyance channel) to eliminate boundary effects on sediment results within the headworks, particularly morphology changes in the transition. This model, henceforth termed as the FTN2Comp (for FTN 2 Components) model was subsequently used to model sediment diversion over the three-year hydrograph. A discharge boundary was used at the conveyance channel end. This discharge was obtained by first running the FTNOMBA 2D model that includes the river and the entire

Barataria basin (Figure 1.2) for the same 3-year period. These simulations are described in Chapter 7. The diversion discharge was capped at 75,000 cfs flow in the FTN2Comp model to simulate gate operated flow restriction above this flow. No base flow (i.e., below 450,000 cfs MR flow) condition was modeled and the diversion was only operated at or above the 450,000 cfs MR flow trigger.

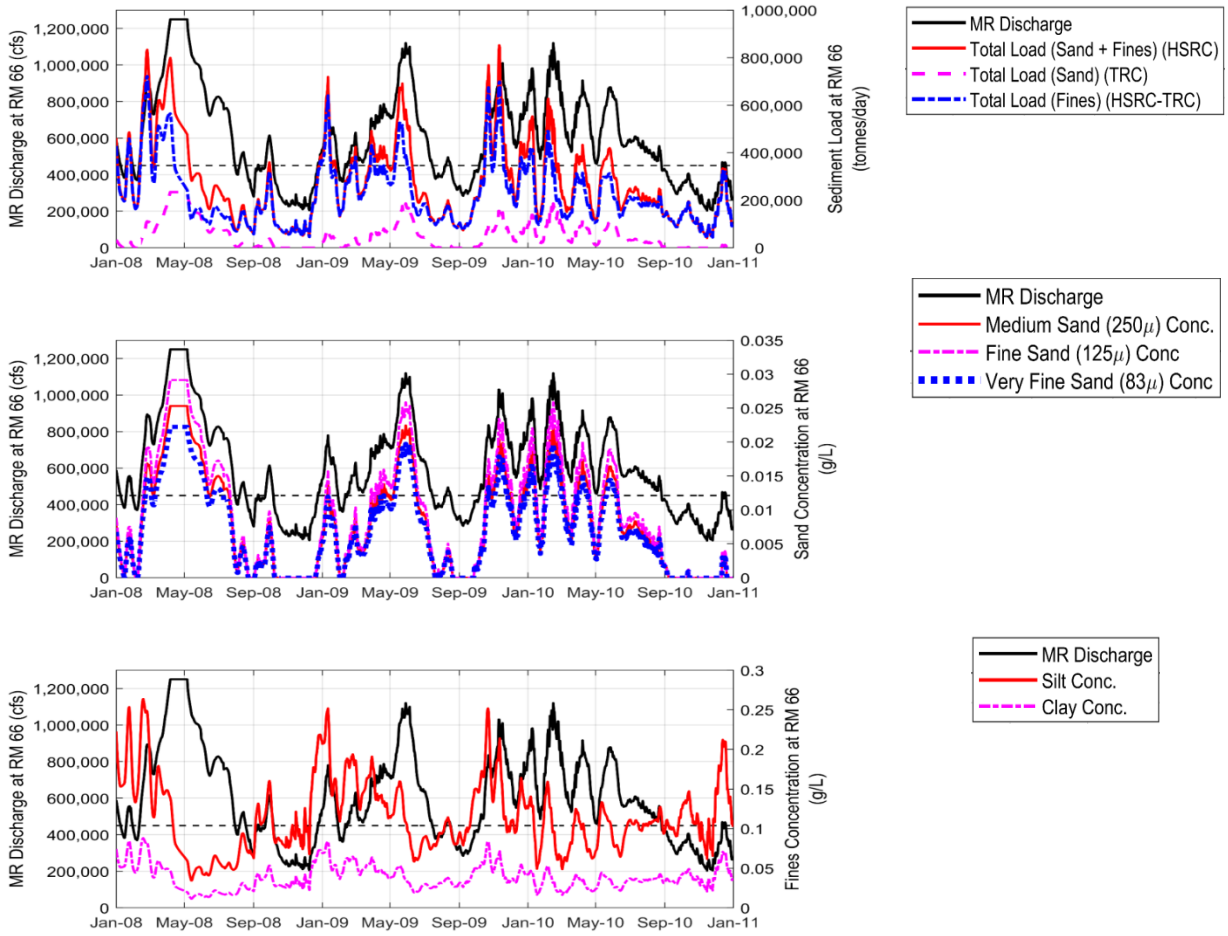

Figure 4.1. The 3-year (2008-2010) upstream boundary conditions applied at RM 66.

The sediment water ratio in Delt3D is defined as,

$$Sediment\ Water\ Ratio\ (SWR) = \frac{Sediment\ Load\ at\ Intake\ Plane / Discharge\ at\ Intake\ Plane}{Sediment\ Load\ at\ River\ Plane / Discharge\ at\ River\ Plane}$$

As mentioned before the river concentration (Sediment Load/Discharge) was obtained from an upstream plane from the with-structure model for the denominator of the SWR expression in the FTN2Comp model and not from the without-project run as in the case of FLOW-3D.

4.3 Model Results

4.3.1 FLOW-3D

The FLOW-3D FTNMSDI model which includes the FTNMS model (MR only without diversion) domain, the diversion intake headworks and about 2,500 ft of the conveyance channel, was used to model the intake hydrodynamics.

Figure 4.2 shows the comparison of depth averaged velocities and flow patterns (streamlines) with and without diversion structure at MR flow of 1,000,000 cfs. The right panel is from the FTNMS model. It is seen that under with-project conditions, the velocities within the river portion of the intake are ~4-6 ft/s and higher (by 2-2.5 ft/s than without project) under with project conditions. There is a general acceleration of flow towards the diversion and velocity increases to over 8 ft/s close to the U-Frame inlet. Close to the dolphin, between 0 to -15 ft, NAVD88 elevations, some local flow acceleration is seen on either side as the flow separates around the dolphin. A well-defined recirculation zone downstream of the dolphin is visible and can be (as will be shown later in bed shear stress map in Figure 4.5) a local zone for sediment deposition. Notice the streamlines bending into the diversion from deeper zones (-20 to -30 ft, NAVD88). The presence of the dolphin can aid in reducing the risk of impact of any loose barge flowing down the river with the upstream flared wall of the diversion.

In Figure 4.3, a zoomed-in view of the intake flow dynamics shows the rapid flow acceleration as the flow enters the U-Frame. Velocities reach 12-13 ft/s within the intake U-Frame. The centerline velocity through the headworks is also shown later in Figure 4.6 by line plots. The velocity distribution within the intake were provide to the DT to guide the decisions of rip-rap extent and sizing, placement of the dolphin and protection, optimum angle of flare of the intake walls, engineered slopes as well as navigation simulations.

Figure 4.4 shows the near bed (white) and surface (cyan) streamline patterns leading into the intake. Only streamlines that lead into the diversion are shown. Notice that the diversion can draw the water from farther (about 150-200 ft) regions of the river at deeper layers (elevations about -40 to -50 ft, NAVD88) than at the surface layers. This is because of the lower velocities (lower inertia of motion) in the bottom layers of the river compared to the surface layers, which enable the diversion to divert deeper waters with greater ease than the surface waters. As discussed later, this is also the reason why a relatively shallow (-25 ft, NAVD88) diversion can be effective in diverting near-bed sand for the same discharge capacity as a deeper diversion.

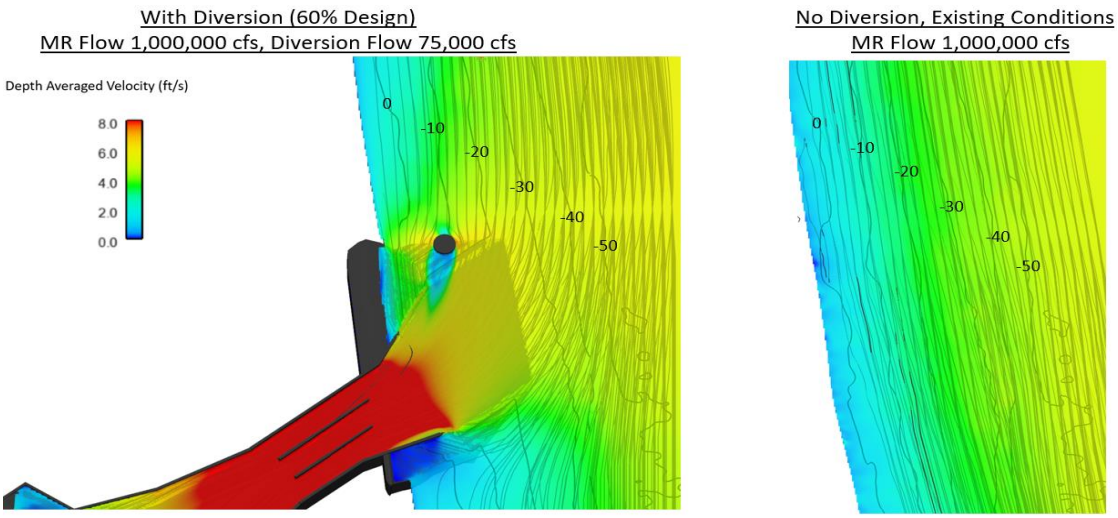

Figure 4.2. Flow velocity and streamlines for with (left panel) and without (right panel) structure scenarios. MR Flow is at 1,000,000 cfs and diversion flow is 75,000 cfs for the with structure (left panel) case shown. Bathymetry contours (ft, NAVD88) are marked at every 10 ft intervals.

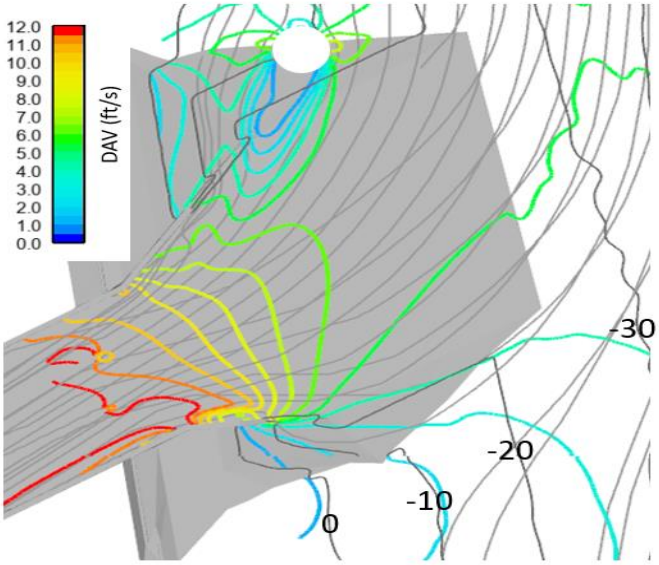

Figure 4.3. Zoomed in view of left panel in Figure 4.1 showing depth averaged velocity contours and flow acceleration into the intake. MR flow 1,000,000 cfs, diversion flow 75,000 cfs. Bathymetry contours (ft, NAVD88) are marked at every 10 ft intervals.

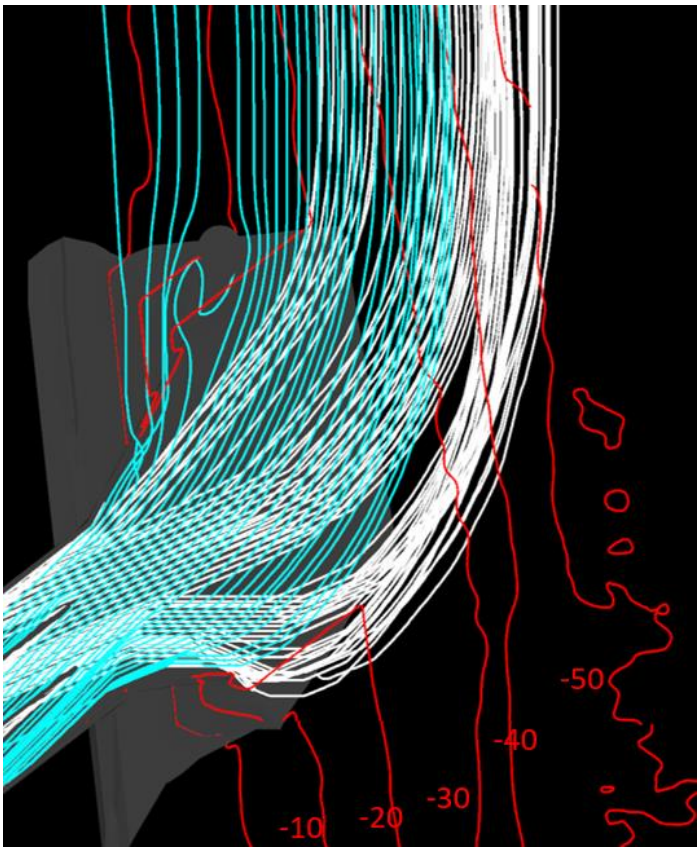

Figure 4.4. Plot showing near-bed (white) and surface (cyan) streamlines curving into the diversion intake. Notice that the intake draws water from farther regions of the river at deeper layers (up to -40 to -50 ft, NAVD88) than at the surface layers (up to about -30 ft, NAVD88). More near-bed streamlines turn into the upstream than the downstream bay. Bathymetry contours (ft, NAVD88) are marked at every 10 ft intervals.

Figure 4.5 shows the bed shear stress distribution calculated using Equation (3) and methodology described before. The shear stresses in the river are about 6 to 12 Pa at 1,000,000 cfs MR flow and is consistent with the observations by Nittrouer et al. (2008). Within the intake, a distinct hight shear stress zone (>13 Pa) is noted as the flow accelerates over the intake and leads into the U-Frame. It is sufficient to bring all intake bedload sand into suspension as it enters the U-Frame. A low shear stress zone sheltered behind the dolphin is visible as well as immediately downstream of the diversion at river bed elevations shallower than -10 ft,

NAVD88. Local depostion may occur in these zones. This issue is addressed later in Chapter 9 on river effects modeling where the near- and far-field deposition effects of the diversion are discussed. It is important to note that shear stress is a function of both velocity and roughness, therefore the shear stress in the model is affected both by velocity and rip-rap bed roughness.

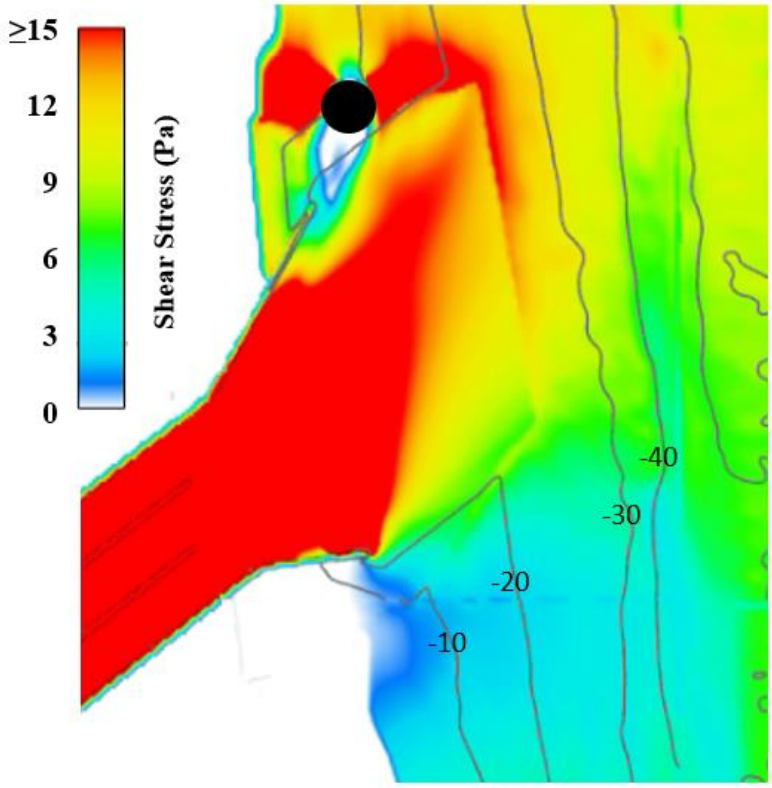

Figure 4.5. Bed shear stress distribution at 1,000,000 cfs MR flow and 75,000 cfs diversion flow. Bathymetry contours (ft, NAVD88) are marked at every 10 ft intervals.

Figure 4.6 shows the centerline variation of the velocities, water level and the total energy head (computed using Equation 1) through the intake headworks. Flow accelerates from 4-6 ft/s in the river to 12-13 ft/s in the diversion intake bays and decelerates to about 6 ft/s in the conveyance channel. The contraction and expansion energy losses together with the friction loss is manifested as the total energy loss within the intake structure. Between the mid-river location and the beginning of conveyance channel (end of transition) about 1.17 ft of total energy head drop is observed from the FLOW-3D model results. Note that Figure 4.6 only extends up to

about 800 ft riverward of the start of the U-Frame and does not reach the center of the river. The water level drops from about 8 ft to about 5.5 ft in the U-Frame due to the high velocity induced drawdown and again rises to about 7 ft towards the start of the conveyance channel. Note that the water level in the river ranges from 7.2-8.2 ft when the diversion is operational at 1,000,000 cfs MR flow at this river reach and includes the effect of the drawdown of the diversion on the river as will be shown later in Chapters 8 and 9. So the 8 ft water level in the river simulated here may be considered a specific but likely scenario. Changes in water level of 1 ft within this range is not expected to change the velocities or energy head drop to any significant extent. Historical observations show that at 1,000,000 cfs the water level in river has ranged between 6.6 ft and 8.2ft, NAVD88.

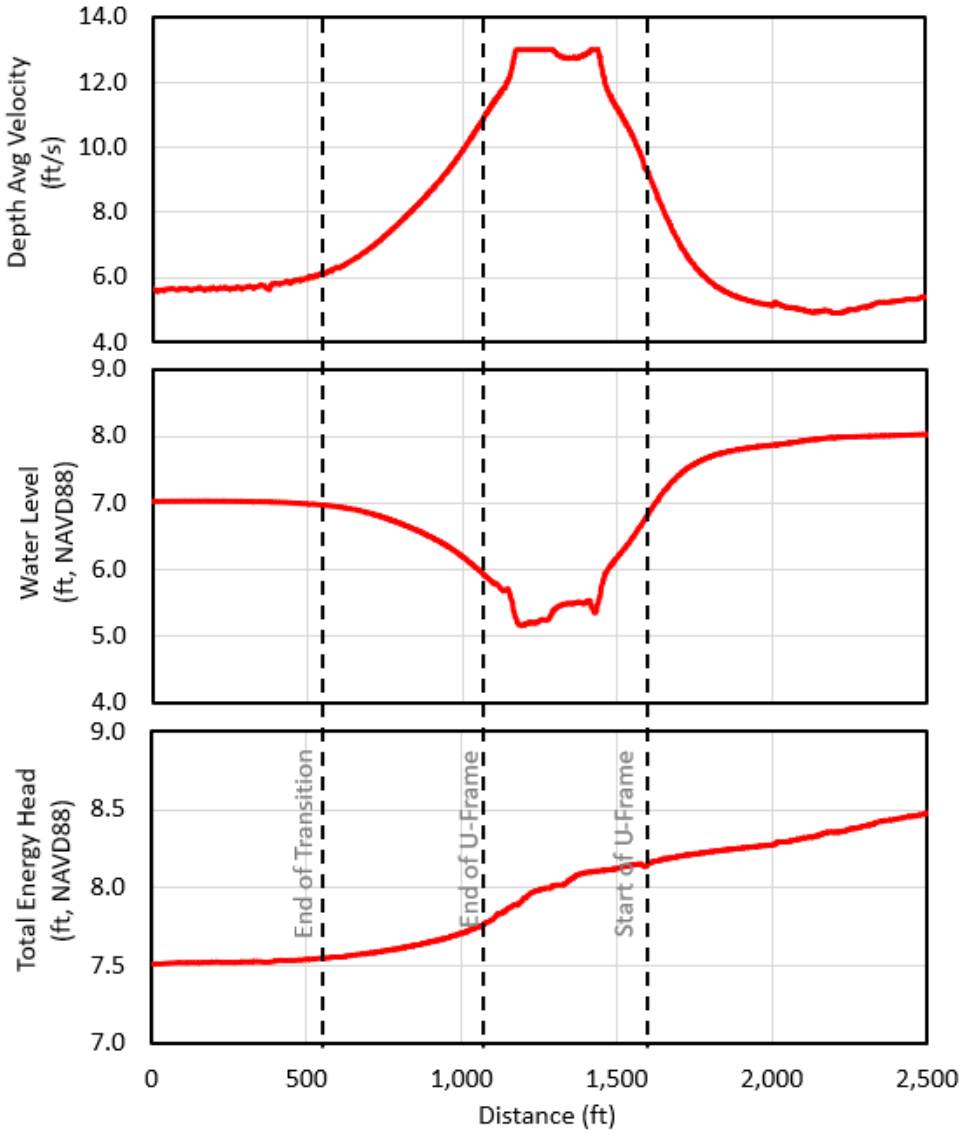

Figure 4.6. Centerline depth averaged velocity (top panel), water level (mid-panel) and total energy head (bottom panel) through the diversion intake headworks. MR flow is 1,000,000 cfs and diversion flow 75,000 cfs.

In addition to the modeling at High Flow (1,000,000 cfs MR) scenario, a Low Flow (600,000 cfs MR) and Trigger Flow (450,000 cfs MR at which flow all diversion gates are to be opened) were also conducted. The diversion discharge of 48,000 cfs and 34,000 cfs were set for Low and Trigger flow based on the same WI rating curve. In addition to estimating head loss through the structure, the intake velocities, particularly in the -25 ft river portion of the intake

were examined for these low and trigger flow runs. The design of the intake must allow sand movement even at these low flows to reduce the risk of deposition. The intake is designed to enable velocities of at least 4 ft/s at the start of the U-Frame at 450,000 cfs MR flow. Table 4.1 lists the head loss and intake velocities at the High, Low and Trigger flows modeled and shows that intake velocities remain above 4 ft/s even at the trigger flow. The head loss is also found to decrease with decreasing flow because of the reduction of flow velocity through the intake.

Table 4.1. Summary of FLOW-3D Total Energy Loss between mid-river and start of the conveyance channel and intake velocities at start of U-Frame.

Structure Type	Invert (ft, NAVD88)	Total Energy Head Loss (ft)/ Intake Velocity @ Start of U-Frame (ft/s)		
		High Flow (MR=1M cfs/ Div=75K cfs)	Low Flow (MR=600K cfs/ Div=48K cfs)	Trigger Flow (MR=450K cfs/ Div=34K cfs)
Open Channel 60% BODR	-25	1.03/9.2	0.61/6.5	0.32/4.5

Particle transport modeling was only conducted for the High Flow (1,000,000 cfs MR Flow, 75,000 cfs Diversion Flow) scenario as the FLOW-3D particle modeling is most appropriate when most of the sand is in suspension. Figure 4.7 shows the distribution of the three particle sizes modeled, namely, medium (250 micron), fine (125 micron) and Very Fine (83 micron) sand. It is seen that the highest concentration of the medium sand (red particles) is in the upstream-most bay and decreases towards the downstream bays. This is due to the same mechanism described in Figures 4.3 and 4.4 where water from the deeper, farther region of the river, which tends to be rich in the coarser sands, tends to be drawn into the diversion and favors the upstream bay due to the strong helical secondary currents developed as a result of the diversion flow. This effect shown by modeling here is qualitatively similar to the Bulle effect (Bulle 1926, Dutta and Garcia 2018), a phenomenon which causes the ratio of bedload entering the diversion to the bedload passing in the main channel to be higher than the flow ratio between the diverted and main channel flow. The confirmation of this effect will also be shown later in the Delft3D modeling section describing the CSWR impact of the Bulle effect on each sand fraction. In addition to the Bulle effect, the transverse variation in the distribution of the particles

across the river also aids the distribution of sand sizes diverted. In the west bank region (where the diversion is located), the depths are shallow (10-40 ft) and the source of the suspended sand is primarily the bed material load on the sand bar which is coarser than the sand in the wash load from the upstream. Towards the thalweg of the river with depths of 70 to 120 ft, the source of suspended sand at the same elevation as the diversion invert is mostly from the suspended river load coming from upstream and is made up of finer sand which is easier to suspend. This cross-sectional distribution of sand sizes causes coarser sand sizes to be concentrated near the diversion on the sand bar while the finer sand is relatively evenly distributed across the river resulting in the relative enhancement of coarser sand over the finer fraction near the diversion intake.

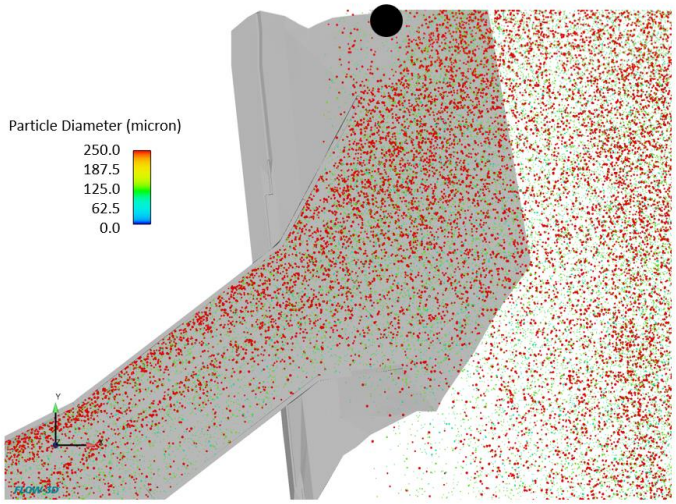

Figure 4.7. Particle distribution into the intake shown by three particle sizes (Medium Sand by red, Fine Sand by Green and Very Fine Sand by Cyan). Notice the greater tendency of the coarser particles (particularly the 250-micron medium sand) to concentrate towards the upstream bays due to the strong secondary helical currents developed at the intake as the water and coarser sediment from the deeper part of the river enters into the diversion as shown in Figures 4.2 and 4.3.

The steady state sand SWR computed in the 60% E&D phase design for each sand class is shown in Table 4.2. Notice that SWR increases with particle size and qualitatively confirms the Bulle effect described earlier and shown by modeling of flow patterns.

Table 4.2. FLOW-3D Sand SWR at 1,000,000 cfs MR Flow and 75,000 cfs diversion flow

Structure Type	Invert (ft, NAVD88)	SWR: Total Sand	SWR: 250 µ Sand	SWR: 125 µ Sand	SWR: 83 µ Sand
Open Channel 60% BODR	-25	1.03	1.14	1.06	0.85

3.1.1.1 Inter-Model Calibration of Intake: FLOW-3D and Delft3D

The FLOW-3D model results were used to calibrate the 2D and 3D Delf3D models. Results from High flows (75,000 cfs diverted flow when MR flow is 1,000,000 cfs) were used to calibrate the intake Chezy roughness distribution. Low flow (48,000 cfs diverted flow when MR flow is 600,000 cfs) was used to validate the results. This method allowed a consistent model performance for hydrodynamics for Delft3D similar to FLOW-3D in absence of any real-life data for head loss through the structure. Physical model results were used to validate the choice of roughness coefficients subsequently.

The main parameter adjusted was the Chezy coefficient at the intake (entrance, neck and conveyance channel transition) to simulate the turbulence contraction/expansion, grade change, and friction losses. The aim was to match the Delft3D losses to the FLOW-3D predicted head loss under the given river and diversion discharge conditions. Figure 4.8 shows the calibrated Delft3D model comparisons of centerline water level, velocities and total energy head through the intake with the FLOW-3D results. The underprediction of velocity in the intake U-Frame and corresponding overprediction of water level in Delft3D is due to the lack of geometry details of the bay walls in the Delft3D model where they are represented as thin dams. This representation does not constrict the flow through the bays as much as in FLOW-3D where U-Frame walls are resolved in the model grid. It is not possible to resolve these walls in Delft3D. Moreover, the non-hydrostatic near-field flow physics within the U-Frame bays cannot be adequately reproduced with a hydrostatic flow model such as Delft3D. Therefore, an ‘averaged’ approach is followed in Delft3D where the net head loss within the headworks is matched with FLOW-3D. FLOW-3D is used for all near-field intake headworks modeling (e.g., Transition and gate modeling) and Delft3D is used only for long term applications of the larger 3 component system.

Figure 4.9 shows the distribution of the calibrated Chezy coefficient used in the model. Note that the MR is set to a constant Chezy of 65 $m^{1/2}/s$ which matched with previously

presented FTNMS results with Manning's n of 0.024 previously calibrated in Chapter 3. The decision to shift to a Chezy based model for the diversion components was partly due to the need to build a consistent Delft3D model to be used for basin wide application later which used Chezy based trachytope formulations.

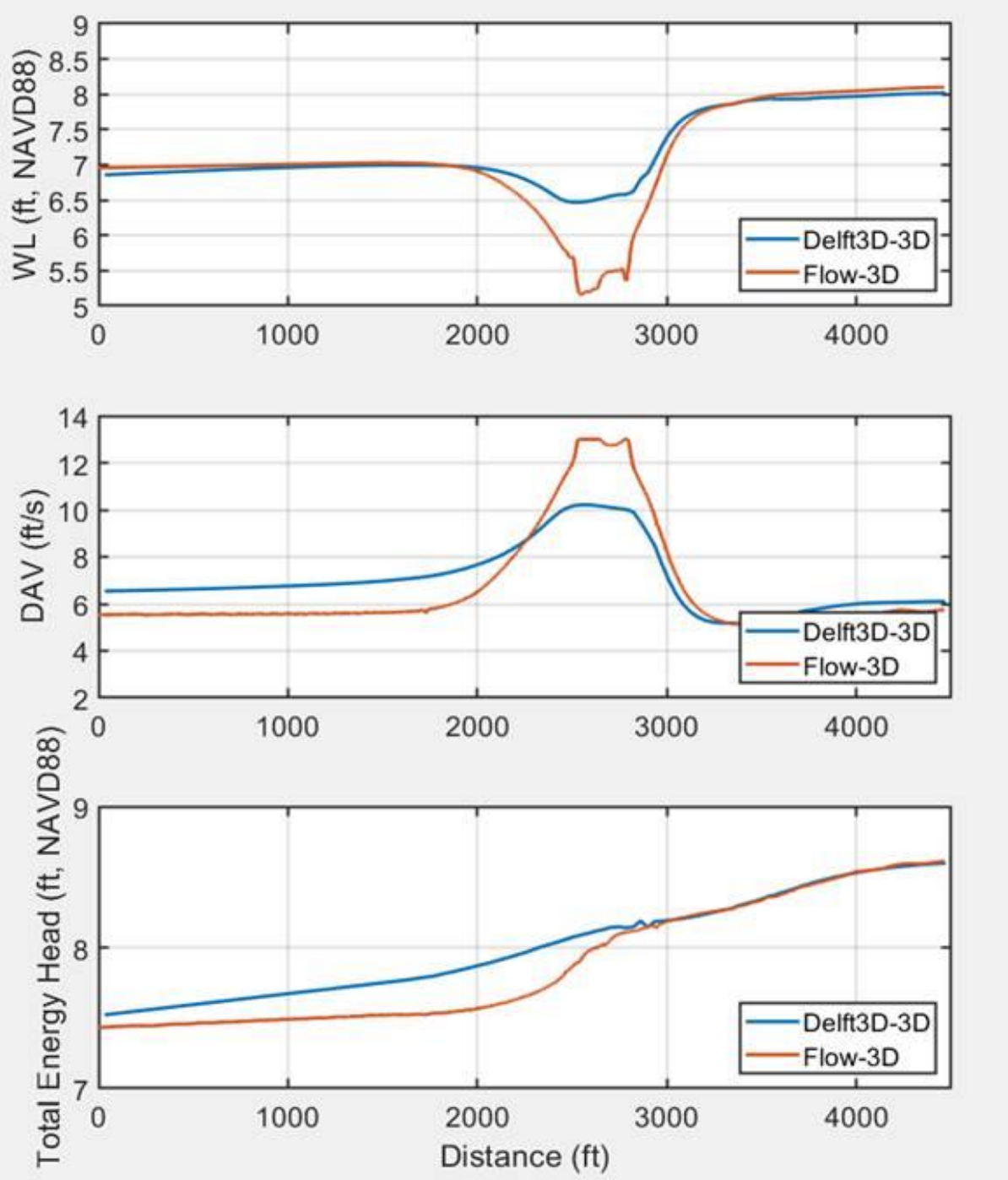

Figure 4.8. Calibration of Delft3D model with FLOW-3D intake structure centerline model results.

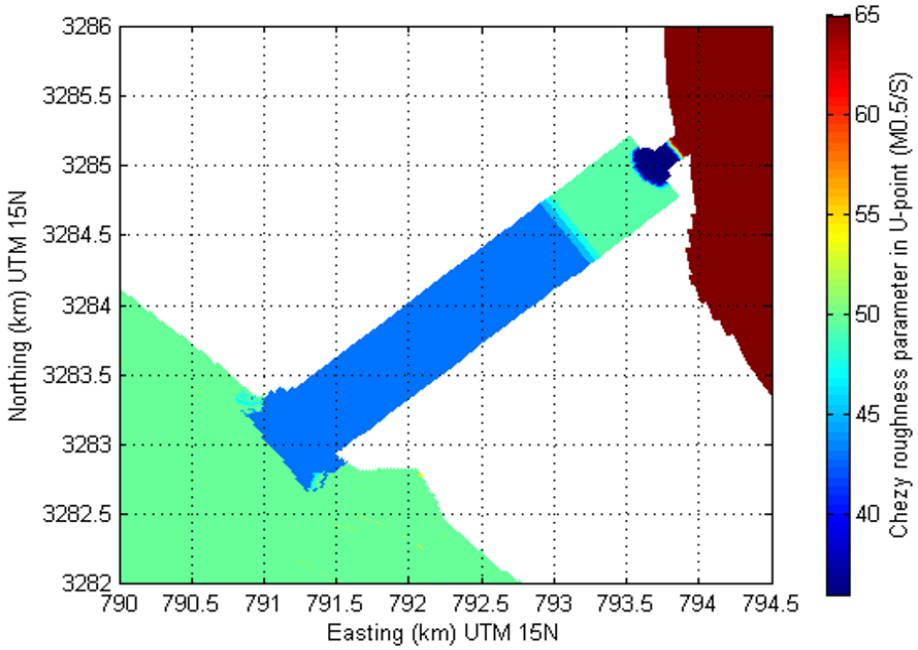

Figure 4.9. Distribution of Chezy coefficient at the intake and the conveyance channel. The three-component model domain is shown here for completeness even though only part of the conveyance channel exists in the FTNMSDI model.

4.3.2 Delft3D

The modeled annual water volume, sediment load and detailed distribution of the different fractions of sand and fines are shown in Table 4.3. The sediment loads in the river compare well with the observed data by Allison et al., (2012) at Belle Chasse and Alliance indicating the ability of the calibrated model to reproduce the yearly sediment budget in the river.

It is seen that the diverted sediment load varies between 5.2 to 8.2 Mil tonnes per year. The fines sediment load which comprises of about 70% (Year 2008) to 85% (Year 2009) of the total load increases with the number of days of operation. The diverted sand load on the other hand is more sensitive to the number of days of Medium to High Flow (800,000 cfs to 1,000,000 cfs or above) operations. As seen from Figure 4.1, year 2008 experienced a prolonged (almost 2 months) of flow above 1,000,000 cfs while 2009 experienced much lesser number of such High Flow periods. 2010 experienced several pulses of flow that peaked between 800,000 cfs to 1,000,000 cfs. Therefore, the sand portion of the diverted load in both 2008 and 2010 showed are about the same (1.5 Mil tonnes per year) while for 2009 it is about half of that (0.8 Mil tonnes per year).

Table 4.3. Detailed water volume and sediment load estimates from 2008-2011 Delft3D (3D) FTN2Comp model, passing the river and the diversion intake.

	Upstream River Plane			Downstream River Plane			Diversion Intake Plane		
Time frame for each cycle	**Feb08-Aug08**	**Dec08-Jul09**	**Sep09-Sep10**	**Feb08-Aug08**	**Dec08-Jul09**	**Sep09-Sep10**	**Feb08-Aug08**	**Dec08-Jul09**	**Sep09-Sep10**
Number of days in the cycle	**171**	**190**	**324**	**171**	**190**	**324**	**171**	**190**	**324**
Total Water Volume (Trillion Cubic Feet)	13.6	11.2	19.6	12.5	10.3	18.0	1.0	0.9	1.5
Total Sand 250 μ Load (Million tonnes)	4.8	2.2	4.3	4.2	1.9	3.6	0.5	0.3	0.5
Total Sand 125 μ Load (Million tonnes)	7.2	3.3	6.2	6.5	2.8	5.4	0.6	0.3	0.6
Total Sand 83 μ Load (Million tonnes)	6.6	2.8	5.1	5.9	2.5	4.6	0.4	0.2	0.4
Total Silt Load (Million tonnes)	36.8	43.7	62.8	33.7	40.0	57.7	2.8	3.4	5.0
Total Clay Load (Million tonnes)	12.3	14.6	20.9	11.2	13.3	19.3	0.9	1.1	1.7
Total Sand Load (Million tonnes)	18.7	8.3	15.6	16.6	7.2	13.6	1.5	0.8	1.5
Total Fines Load (Million tonnes)	49.0	58.2	83.7	44.9	53.3	77.0	3.7	4.5	6.7
Total Sediment (Sand+Fines) Load (Million tonnes)	67.7	66.5	99.3	61.5	60.5	90.7	5.2	5.3	8.2

Table 4.4. Cumulative Sediment Water Ratio (CSWR) results from the modeled sediment loads in Table 4.3.

	Upstream SWR			Downstream SWR		
Time frame for each cycle	**Feb08-Aug08**	**Dec08-Jul09**	**Sep09-Sep10**	**Feb08-Aug08**	**Dec08-Jul09**	**Sep09-Sep10**
Number of days in the cycle	**171**	**190**	**324**	**171**	**190**	**324**
CSWR Sand250μ	1.23	1.28	1.31	1.30	1.37	1.40
CSWR Sand125μ	1.10	1.15	1.17	1.13	1.19	1.21
CSWR Sand083μ	1.03	1.08	1.10	1.05	1.10	1.12
CSWR Silt	1.02	1.01	1.02	1.02	1.01	1.02
CSWR Clay	1.01	1.00	1.01	1.01	1.00	1.01
CSWR Total Sand	**1.12**	**1.17**	**1.19**	**1.15**	**1.21**	**1.24**
CSWR Total Fines	**1.01**	**1.00**	**1.01**	**1.02**	**1.00**	**1.01**
CSWR Total Sediment (Sand+Fines)	**1.04**	**1.02**	**1.04**	**1.05**	**1.03**	**1.05**

Table 4.4 shows the yearly distribution of the CSWR for sand and fines. Both upstream and downstream reference planes are used to compute the results. It is seen that the sand CSWR (Upstream Plane) varies between 1.12 and 1.19 while that for fines is about 1.0 to 1.01. Since the fines constitute over 80% yearly average of the diverted sediment, the CSWR of the total sediment approaches around 1.0 as well. The total sediment CSWR is around 1.02 to 1.04.

4.3.3 Delft3D Intake Morphology Modeling: Intake Flushing Study

Morphology modeling with the diversion closed for an extended period of time, presented in detail later in Chapter 9, indicated possible deposition of silt and sand in the river portion of the intake either in the form of bedload from the bar or deposits from the low flows. It is intuitive that the depression in the river bank may act as a sediment trap when the diversion is closed and can possibly be a maintenance issue when the diversion is subsequently opened if sufficient diversion flow is not available. The goal of this section of the intake study was two-fold: (1) Determine if diversion capacity is affected by partially blocked intake when the diversion is opened at Trigger Flow (450,000 cfs) in a following year after intake is deposited (2) Test the self-cleaning (flushing) efficiency of the diversion flow measured as number of days after diversion opening. required to achieve an equilibrium bathymetry or regain the initial intake bathymetry by clearing away or reducing the deposition at the intake.

The initial sediment deposited bathymetry came from the 10-year river response morphology modeling done later in Chapter 9. In that exercise, model runs were conducted with the diversion open and diversion closed under the same hydrograph conditions for 10 years. Figure 4.10 shows the Year 0, Year 1, Year 5 and Year 10 conditions at the intake. Only bathymetry contours shallower than -30 ft, NAVD88 are shown as the concern for deposition is only above -25 ft, NAVD88 intake. To answer (1) above, the FTNOMBA model (including the Barataria and MR domains) was first executed in a steady state setup for each of the 3 deposited river bathymetries with MR flow at 450,000 cfs. The model results showed that the 1-, 5- and 10-Year deposition-induced blockage had only a minor impact on the diverted discharge. The discharge reductions were 500 cfs (29,500 cfs vs 30,000 cfs with no deposition), 900 cfs (29,100 cfs vs 30,000 cfs) and 3,700 cfs (26,300 cfs vs 30,000 cfs) for the three cases. This

indicates that at Trigger Flow under current head difference between the basin and the river, adequate flow capacity is available and the reduction in diversion flow due to the deposition induced blockage is small.

The question (2) was answered by running a continuous hydrograph morphology simulation starting at trigger flow. Starting with each of Year 1, 5 and 10 bathymetries, simulations were started at the start of trigger flow in the hydrograph of year 2008 (Figure 4.1) and model runs were continued till the flow in the river reached 1,000,000 cfs or above in the rising limb. Approximately 34 days passed till the flow reached 1,000,000 cfs after opening and 30 days till 800,000 cfs. The influence of the presence of consolidated silt in the deposit along with sand was also tested by setting a critical shear stress of erosion of silt as 1.5 Pa, typical of riverine consolidated deposits. The deposit was allowed to scour as the diversion was opened. An initial 1 day was given when no morphology change occurred to allow the model to attain hydrodynamic equilibrium and avoid sudden 'shock' induced erosion of the bed.

Figure 4.11 shows the evolution of the deposit as a series of line plots. The Start of Run condition indicate the deposited intake profiles. The End of Run indicates the end of 30 days or when the flow reached about 800,000 cfs. The End of Run (1M cfs) indicates the end of the 34-day period when the flow reached 1,000,000 cfs. The model result where only sand was considered (no consolidated fines fraction) is also shown with (Sand) in parentheses. It is seen that an equilibrium bathymetry is reached fairly quickly within 30 days and the deposited bed erodes to about the same -18 ft, NAVD88 from the starting (-15 ft for Year 1, -10 ft for Year 5 or -5 ft for Year 10). Further acceleration of the flow to 1,000,000 cfs reduces the deposit to -22 to -23 ft, NAVD88 showing a rate of slowing down of erosion of the deposit. When only sand is considered, the deposit erodes faster and reaches an invert of -22 to -23 ft, NAVD88 fairly quickly at 800,000 cfs MR flow. This exercise indicates that adequate flushing flow that can erode deposits as high as -5 ft, NAVD88 is available under current conditions at 450,000 cfs and an average of 30-35 days can clear away most of the deposit from the intake if the river reaches above 800,000 cfs.

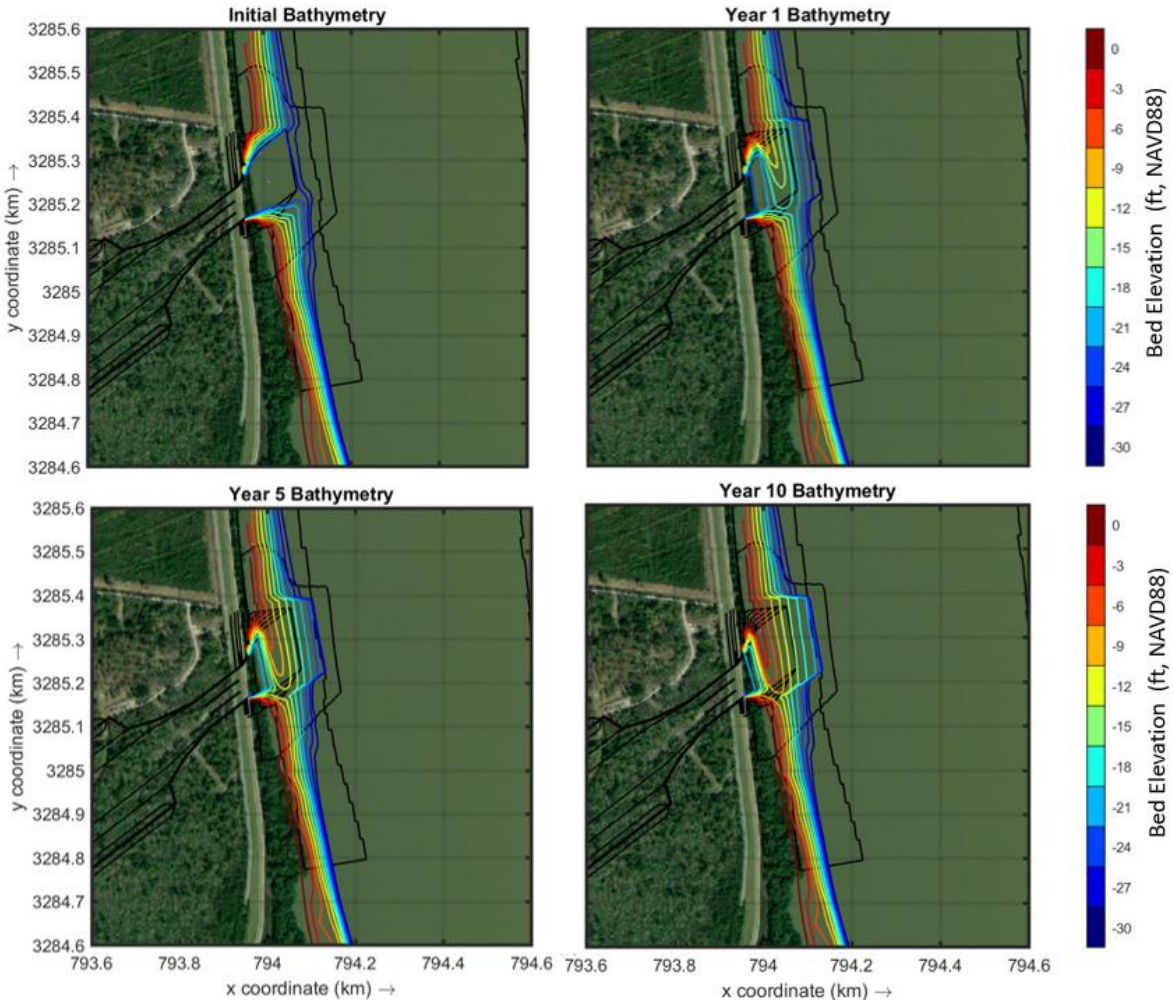

Figure 4.10. Sediment filled in part of the river portion of the intake over time. Clockwise from top left: initial (Year 0) with no sediment deposition in the intake, after 1 year of closure (Year 1) with partially deposited intake- a very likely scenario if diversion closed for maintenance, after 5 years of closure (Year 5) with additional deposition shown-an unlikely scenario and after 10 years (Year 10) with almost the entire intake shut and the river having regained its previously existing bank profile- a very unlikely scenario.

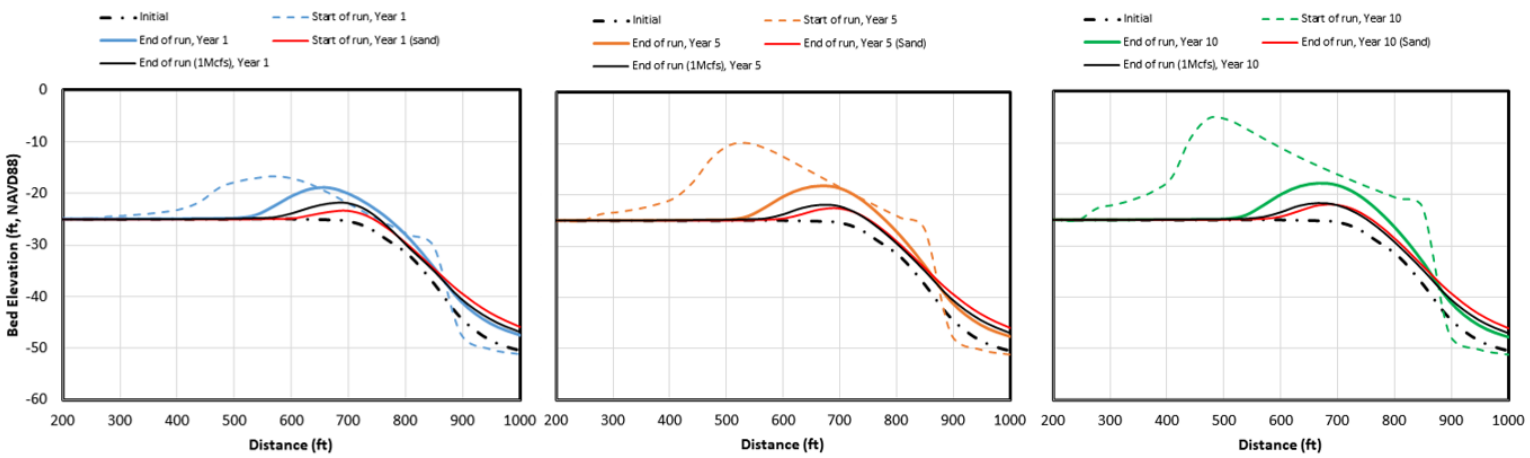

Figure 4.11. Bed elevation evolution along the centerline of the river portion of the intake structue for the three flushin scenarios. Year 1 (left panel), Year 5 (mid-panel) and Year 10 (right panel) initial deposited bathymetries were eroded until an equilibrium bathymetry was reached. Effect of only sand in the deposition versus both sand and silt (consolidated to 1.5 Pa) was studied.

4.4 Minor Change in Intake Design from 60% to 90% Phase:

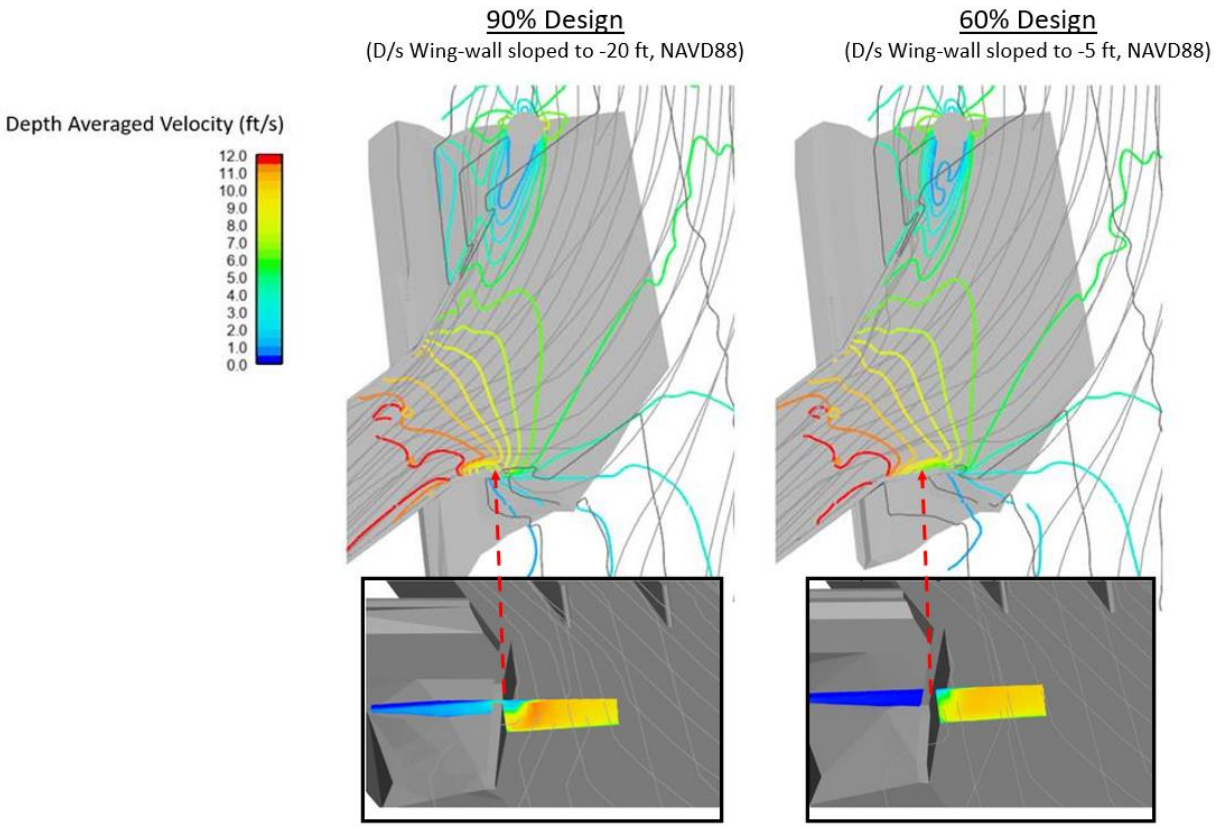

Figure 4.12. Comparison of flow at the intake: The latest design (90%, left panel) has a sloping downstream wing-wall which reaches to -20 ft, NAVD88 while the previous 60% design had the wall sloping up to -5 ft, NAVD88.

Figure 4.12 shows the minor change to the intake from the 60% to 90% design phase. The end point of the downstream wing wall which extends from the U-Frame into the river was lowered to improve flow distribution between the bays. The wing-wall in the 90% design ends at -20 ft, NAVD88 versus -5 ft, NAVD88 in the 60% design. This allowed for a slight improvement in water flow as well as sand SWR in the downstream most bay. The total sand SWR as reported in Table 6.2 improved from 1.03 to 1.05 with the benefit mostly in the very fine sand which tends to get entrained in the downstream most bay from the locally reversing flow from the downstream zone of the diversion near the right descending bank of the MR. The

difference in headloss between the two intake designs was however insignificant. No other notable hydraulic changes were observable for the 90% intake over the 60% intake.

4.5 Conclusions

Two numerical models (FLOW-3D and Delft3D) were used to evaluate the head loss and sediment capture performance of the 60% Three Bay -25 ft, NAVD88 MBSD diversion intake headworks. FLOW-3D was used to:

- Quantify energy head losses at High, Low and Trigger flows,
- Determine the velocity, flow patterns and the shear stress around the diversion intake,
- Provide hydrodynamic data for inter-model calibration with Delft3D and
- Determine the SWR using a discrete particle modeling method.

Delft3D was used to:

- Determine the sediment loads diverted and CSWR for a period of three years (2008-2011) under varying MR hydrograph and sediment conditions,
- Evaluate flushing of intake deposits when diversion operations begin at 450,000 cfs MR flow.

The modeling indicates that adequate design capacity to divert 75,000 cfs at 1,000,000 cfs MR flow is available with an estimated 1.17 ft of head loss within the intake. The final diversion rating curve for various flows will be developed in Chapter 8 later. The FLOW-3D sand SWR was about 1.05 while the CSWR for sand varied from 1.15 to 1.19 year to year in Delft3D. Overall the total sediment CSWR for sand and fines was between 1.02 to 1.04 from Delft3D.

5.0 INTAKE TRANSITION MODELING

5.1 Introduction

This chapter describes hydraulic modeling of the intake transition feature that connects the intake U-Frame to the conveyance channel. All model results are from the FLOW-3D model.

The intake transition is an expanding structure that connects approximately 220 ft wide rectangular cross-section of the intake U-Frame to the trapezoidal cross-section of the conveyance channel. The conveyance channel has a 300 ft bottom width, approximately 715 ft top width and 1:4 side slopes with approximately 100 ft wide berms at +2 ft, NAVD88 elevation where the transition meets the channel. The U-Frame and the conveyance channel bed elevations are same as the river intake invert, i.e., -25 ft, NAVD88. The entire transition is armored by rip-rap.

The main hydraulics design goals of the intake transition are to:

- Improve the hydrodynamic performance of the intake headworks by reducing expansion energy loss through the transition by minimizing flow separation and large eddies that cause most of the energy losses.
- Reduce potential sediment, particularly sand, deposition zones by reducing low hydraulic shear stress areas, particularly along the flared sides of the transition.

The final transition design presented here was refined through a series of numerical model runs with different intermediate transition geometries, each varying in either one or all of the following: length, flare angle and number of stages (i.e., the number of successive flare angles within the transition). Results from only the as-designed transition configuration currently advanced in the 60% E&D phase is presented here. One of the transition designs was also validated with physical modeling (Alden, 2020) which showed that the modeling procedure described here was able to arrive at a transition of economical length, provide adequate length for a uniform flow transition without significant flow separation within the main channel flow and also showed no significant deposition issues. Figure 5.1 shows the sketch of the currently advanced transition design. It is made of 3 stages with flare angles of 11-, 21- and 70 degrees from the upstream to the downstream direction. The conveyance channel berms start at the end of the second transition (beginning of the 70-degree flare). There is about 100 ft section with a concrete bottom between the gates and the beginning of the transition which is part of the U-Frame.

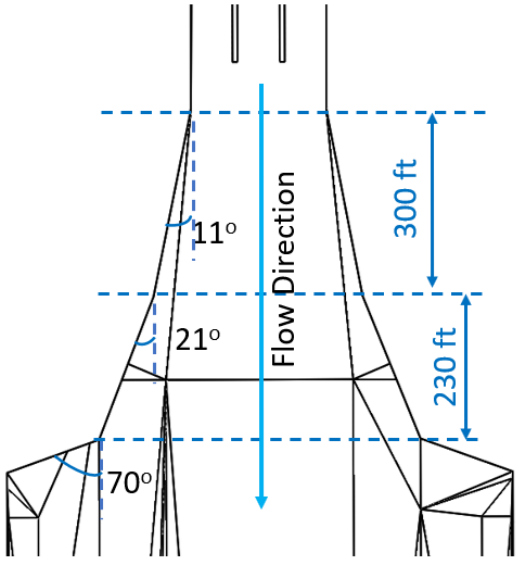

Figure 5.1. Sketch of the transition section of the MBSD headworks advanced in the 60% E&D phase.

For the bulkhead gate modeling, the results presented in this section are for an emergency opening/closing scenario where the flow coming underneath the partially opened gates are shown to enter the downstream section at a high velocity. The model results provide an insight into the jet dissipation length. This information of velocity and length is helpful for the designers in designing rip-rap size and concrete portion behind the gates. For detailed head loss estimates by bulkhead see physical modeling (Alden, 2020) conducted which will be used later in operations modeling in the 90% E&D phase.

5.2 Model Setup

For the transition and the bulkhead gate modeling, a truncated version of the FTNMSDI FLOW-3D model, hereby called the FTNGATE3Bay model is used. Figure 5.2 shows the difference in the domains. Details about the FTNMSDI model is described in Chapters 3 and 4. The FTNGATE3Bay consists of the U-Frame, the intake transition and part of the conveyance channel (length of about 4000 ft or half of the channel). Table 5.1 and 5.2 show the distribution of grid sizes compared between the two models. Even though the FTNGATE3Bay is much

smaller domain than FTNMSDI, the resolution of the former is about 3-4 times higher in the vertical (0.8-1.0m in FTNGATE3Bay vs. 1.8-3.5m for FTNMSDI within the intake) and about 1-4.5 times higher in the horizontal (1.3m uniform in FTNGATE3Bay vs. 1.3-6.0m in FTNMSDI). The higher resolution and fairly uniform grid resolution were required because the FTNGATE3Bay was run with the Large Eddy Simulation (LES) method for turbulence modeling while the FTNMSDI model used the Reynolds-averaged Navier-Stokes (RANS) method for turbulence closure. The LES model in FLOW-3D, being inherently explicit (i.e., the sub-grid scale turbulence length), is a function of the grid size. Therefore, a higher resolution grid was needed to adequately model the 'large' eddies important for the energy extraction from the main flow and to preserve the energy cascade without excessive diffusion. Initial sensitivity tests indicated a length scale of about 1 m was adequate below which results for velocity and head loss became insensitive to the choice of grid size. A 3D grid of 1.3 m x 1.3 m x 0.8 m has about $(1.3 \times 1.3 \times 0.6)^{1/3} = 1.1$ m of LES filter length scale (defined later) and is therefore sufficiently fine to model the important large eddies which range from a few feet corresponding to the roughness scale of the bed to the scale of the transition length itself (i.e., hundreds of feet).

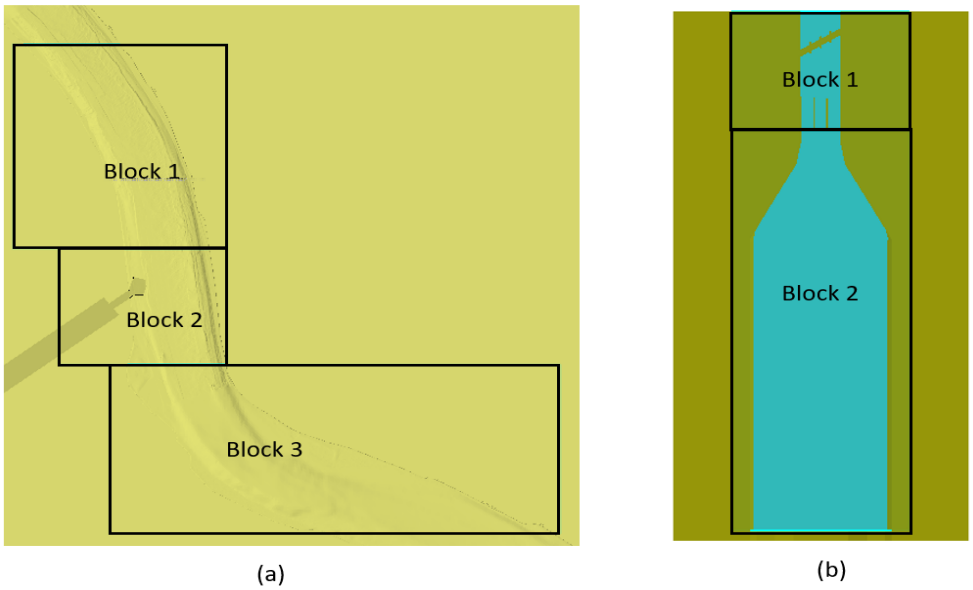

Figure 5.2. Mesh blocks for FLOW-3D (a) FTNMSDI (RANS) domain and (b) the FTNGATE3Bay (LES) domain.

Table 5.1. Mesh sizes for the mesh blocks for the FTNMSDI (RANS) model.

Block No.	Δx (m)	Δy (m)	Δz (m)
1	4.5-10.0	6.0-10.0	1.8-3.5
2	1.3-6.0	1.3-6.0	1.8-3.5
3	4.5-10.0	6.0-10.0	1.8-3.5

Table 5.2. Mesh sizes for the mesh blocks in FTNGATE3Bay (LES) model.

Block No.	Δx (m)	Δy (m)	Δz (m)
1	1.3	1.3	0.8-2.1
2	1.3	1.3	0.8-1.0

Smagorinsky's (1963) Large Eddy Simulation (LES) turbulence model was used for these computations. The 3D LES-filtered Navier-Stokes equations in FLOW-3D resolve larger eddies, in this case the horizontal eddies that form as the water exits the intake's U-Frame. These eddies induce recirculation, drain energy from the main flow and can create sediment deposition areas by reducing mean velocities in the sheltered zones caused by the upstream flow separation. The effects of the sub-grid scale smaller eddies are modeled using a turbulent eddy viscosity term (μ_t) which is computed from the strain rate (S_{ij}) of the resolved flow field (FLOW-3D, 2018) and a constant Smagorinsky's constant, C_s, set here as 0.2 based on physical model tests of jet dissipation from the intake, as follows:

$$\mu_t = \rho(C_s\Delta)^2\sqrt{(2S_{ij}2S_{ij})} \quad \text{..... (1)}$$

$$\text{Where, } \Delta = (\Delta_x\Delta_y\Delta_z)^{1/3} \quad \text{..... (2)}$$

The symbol Δ is defined as the characteristic filter length scale and is the cube root of the product of the grid sizes in three dimensions ($\Delta_x, \Delta_y, \Delta_z$).

The advantage of the LES models over the RANS models is the former's ability to more accurately model and capture the flow structures of larger eddies.

Meshing of the transition model consists of two mesh blocks as is shown in Figure 5.2b and Table 5.2. As mentioned before the LES filter size was 1.11 m calculated using Equation (2) and is smaller than the smallest eddy size of importance such as the eddies generated from the rip-rap bed. These small eddies have length scales equal to the Nikuradse's roughness scale ($2.5d_{50}$) of the bed. For 0.6 ft of median rip-rap size, these are about 1.5 ft in length scale and are much smaller than the largest eddy size (the length of the smallest transition stage, i.e., 230 ft).

For the transition modeling, a discharge boundary of 75,000 cfs was set at the upstream of intake channel. The downstream boundary at the channel was set as a continuative (zero gradient) boundary, therefore water level was free to adjust based on the calculated gradient which allowed for testing of head loss for various intermediate designs. The roughness height for the intake section was set to 0.006 m (0.02 ft) corresponding to concrete lining while the roughness height for the conveyance channel with transition was set to 0.457 m (1.5 ft) which corresponds to rip-rap lining of stone with about 0.6 ft diameter. The FLOW-3D model was run for a duration of 5,000 seconds which was sufficient to reach a steady state for discharge.

5.3 Results

The model results of velocity and shear stress through the transition structures are presented for the fully-open and emergency closure gate scenarios.

5.3.1 Gates fully open scenario

The results from the modeling simulations were examined in terms of the recirculation zones, shear stresses and velocity distribution through the transition. Figure 5.3 shows the distribution of velocities and skin-friction bed shear stress in the intake transition zone. The mean velocity magnitude of the flow entering the transition is about 8 ft/s. The main flow core remains fairly unaffected because separation occurs only along the shallow berms where the channel carries little flow. This was possible because of the three-stage transition within an economical length. The bed shear stress contours indicate that instantaneous magnitude could range from 5 Pa (in the conveyance channel) to about 30 Pa (immediately after the gate, over rougher rip-rap). Most of the transition itself has a shear stress of about 15-20 Pa and is high enough to keep sand in suspension (typically 0.5 Pa threshold for coarse to medium sand). Also, the velocities are much higher than the 4 ft/s typically present in the river where the sand is already in suspension. Therefore, most of the intake transition is expected to be free of any significant deposition. Some areas (white color) indicative of low shear stress occurrence scattered on the shear stress map. These are simply due to the instantaneous nature of the flow field captured by the LES model indicating the fluctuating shear stress as a result of turbulence in the intake transition interacting with the bed. The time averaged (10 mins) velocity and streamline plot confirms that the mean velocity remains in the 4-8 ft/s range over almost all of the intake transition.

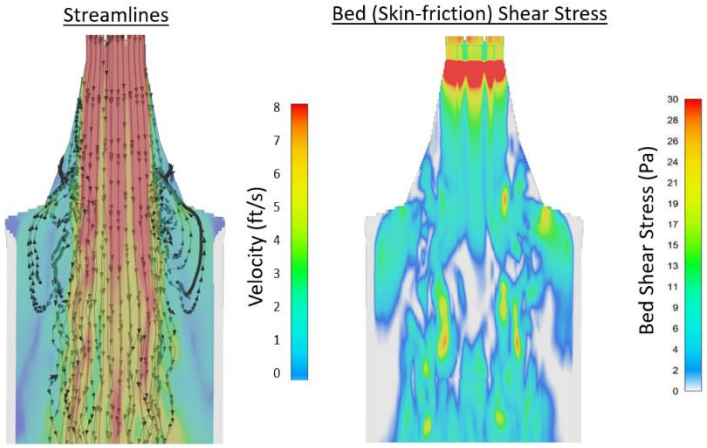

Figure 5.3. Time-averaged velocity contours and streamlines (left panel) and instantaneous skin-friction bed shear stress (right panel).

Figure 5.4 shows the cross-sectional distribution of the time average (30 mins) velocity magnitude, the instantaneous fluctuation as Root Mean Square Deviation (RMSD) and the ratio of RMSD to the mean velocity. The figure shows that over the 300 ft bottom width of the channel, the mean velocity remains above 4 ft/s with very low turbulent velocities (fluctuating component about 0.25 ft/s) accounting for only 6% of the mean velocity. The turbulent fluctuations increase and mean velocity magnitude decrease only near and on top of the shallow berms and is unavoidable to keep an economic length. These regions about 200 ft from the center of the channel on either side berms have mean velocities of 1-2 ft/s and turbulent fluctuations from 0.5-1 ft/s or about 50% of the mean velocity. These will likely lead to some deposition of sand and coarse silt on the berms immediately downstream of the transition but is unlikely to block the main channel or the transition flow where higher velocities are predicted. As will be seen later in Chapter 6, some deposition in this area is seen from the Delft3D sediment transport modeling. However, since the flow over the berm is very small compared to the bulk of the flow through the channel, this local deposition just downstream of the transition does not decrease the channel flow capacity.

The final design as incorporated into the FTNMSDI model showed the least head loss among all the designs tested and amounted to about 0.1-0.15 ft of total head loss between the end of the U-Frame and the conveyance channel. Details of head loss can be found in Chapter 4.

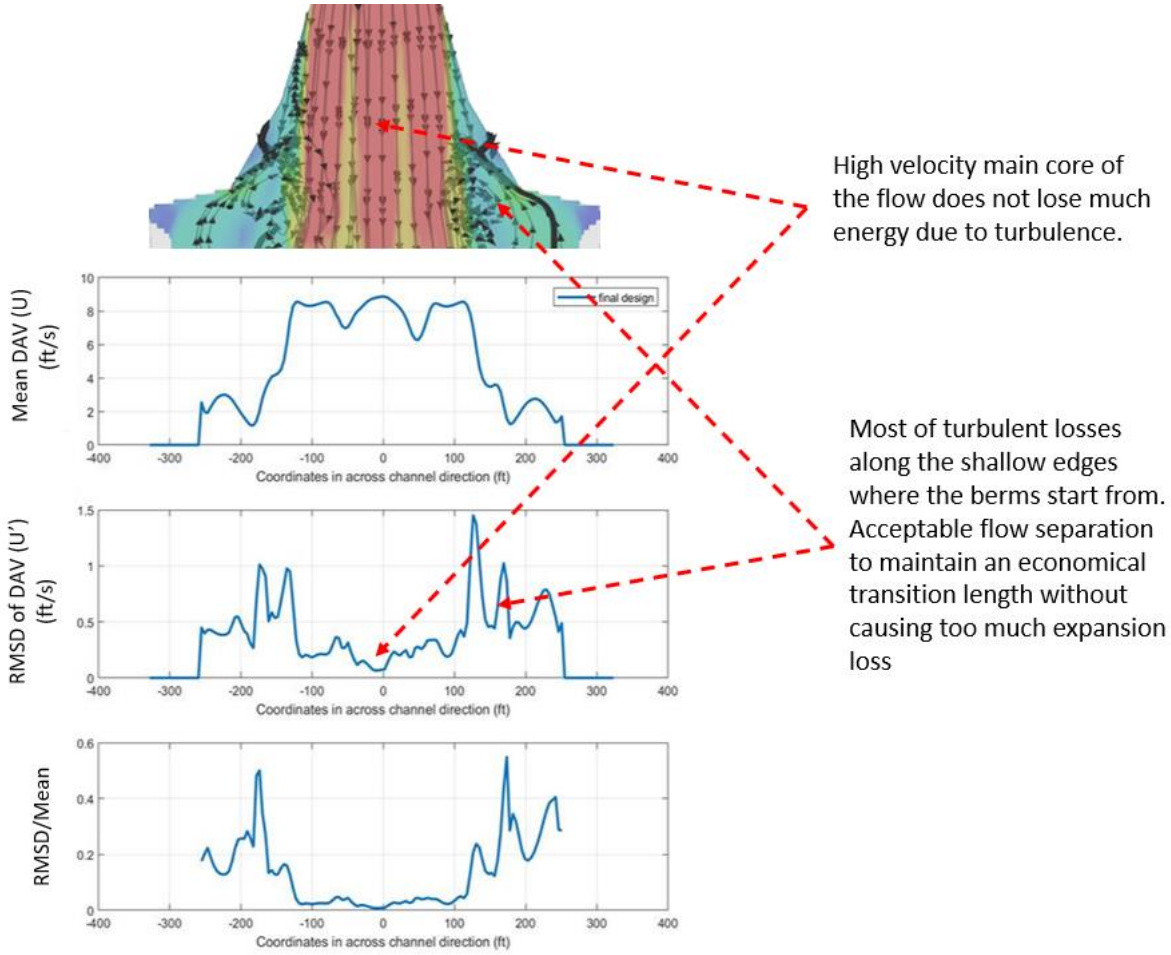

Figure 5.4. Top panel: Velocity and flow pattern reproduced from Figure 5.3, followed by panels of the Mean Velocity Magnitude (averaged over 30 mins), Root Mean Square Deviation of Instantaneous Velocity and the ratio of RMSD to the Mean velocity.

5.3.2 Emergency gate-closure scenario

Figure 5.5 shows the results from the gate modeling scenario where all the three bulkhead gates are open only 5 ft from the U-Frame bed and the MR stage (upstream) is at 9 ft, NAVD88 while the conveyance channel of the FTNGATE3Bay is set to 0 ft, NAVD88, likely minimum water level in the basin during the operational period. The flow condition in the river corresponds to a 1,250,000 cfs MR flow. The scenario therefore can be thought to be an emergency opening or closing scenario which might be warranted in case of river or basin side emergencies. Since the bulkhead gates take a certain time (on the order of hours) to operate, it is

useful to understand the peak velocities over the beginning portion of the rip-rapped intake that may occur under this scenario to inform rip-rap design. The diversion flow was about 20,000 cfs and was found to yield the largest velocities. Note that at opening greater than this, the diverted flow increases but the peak velocities under the gate falls due to larger cross-sectional area. On the other hand, for opening smaller than this causes reduction of flow and hence the velocity. Therefore, the selected flow case was found to a reasonable example of the extreme velocity conditions that may occur at the beginning of the intake. Figure 5.5 shows that the peak jet velocity under the gate reaches about 26 ft/s immediately downstream but dissipates quickly largely due to turbulence losses as the submerged jet mixes with the water above it. The peak velocity, approximately 2.5 ft from the bed decreases from about 26 ft/s to 13 ft/s over a distance of 150 ft (of which the distance between the gate to the transitions start is 75 ft) downstream of the gates. Therefore, it is recommended that either adequate length be provided downstream of the gate for the jet to dissipate or the rip-rap design within the first 75 ft of the transition design take this scenario into account, even though this may be a rare occurrence.

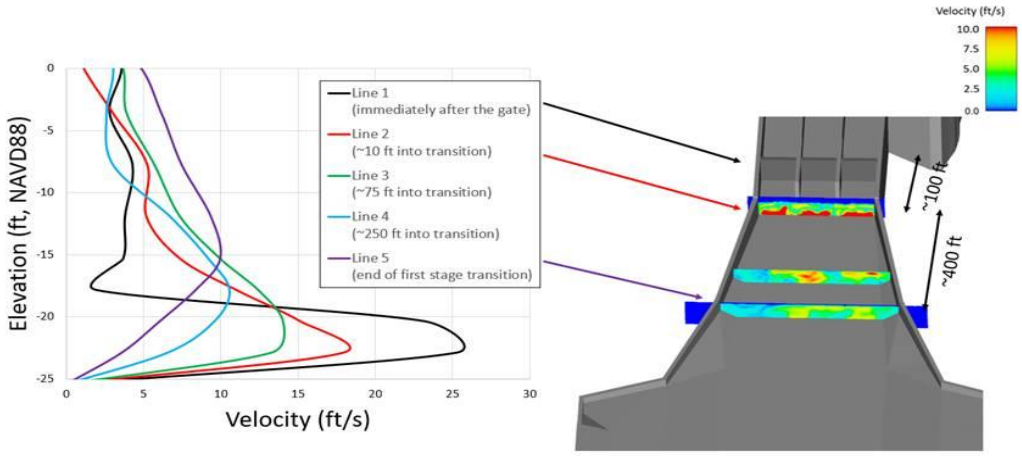

Figure 5.5. Modeling of emergency closure/opening condition for the bulkhead gates under highest expected head difference and MR flow. All gates are open 5 ft from the U-Frame bottom. MR flow is 1,250,000 cfs or about 9 ft, NAVD88 stage in MR at the diversion intake while the conveyance channel downstream is at 0 ft, NAVD88. Diverted flow is about 20,000 cfs. Left panel: Vertical velocity magnitude profiles at successively downstream locations from the gate. Right panel: 3D perspective view of the flow coming out of the small opening below the gates and impinging on the rip-rapped transition bed.

5.4 Change in Intake Transition Design from 60% to 90% Phase due to Channel Design Change

The conveyance channel design was altered from 1:4 (V:H) side-slopes and a 300 ft bottom to a 1:7 side-slope and a 250 ft bottom width design in 90&% phase to accommodate stability requirements due to a change to the construction method from in the wet to in the dry design. Model results for the updated 90% channel can be found later in Chapter 6, Section 6.4. In this section, the model results for the updates to the 90% design intake transition are shown only and compared with the old 60% design results. As will be shown here in this section, there is no significant difference between the performance of the two intake designs and the updated design performs as well as the previous design in terms of reducing head loss by retaining the core flow structure without excessive turbulence within the channel proper and also allowing for high enough shear stress to keep the intake sides clear of sand deposits. The total headloss along the intake transition length remained less than 0.15 ft for the updated 90% design similar to the 60% design, which is about 10% of the entire headworks.

Figure 5.6 shows the comparison of the intake design layouts of the updated 90% design (left panel) and previous 60% design (right panel). The change in the channel slopes from 1:4 to 1:7 means a longer side slope width and therefore resulted in a widening of the surface distance at which the intake transition met the channel at the top of the downstream end from the previous design, which in turn necessitated a lengthening of the transition without changing the flare angles at the three stages. Iterative modeling of designs with difference transition flare angles while trying to keep the length of the transition the same as before resulted in sub-optimal designs, primarily due to pre-mature flow separation along the sides before the flow reached the third transition stage. This restricted the change in the flares angles and the angles were decided to be kept the same with only an increase in linear length. Also, the bottom width of the channel being reduced to 250 ft from 300 ft meant that there was no need to widen the bottom the from the intake (220 ft) to the channel and avoided the need for flaring the bottom along the flow direction.

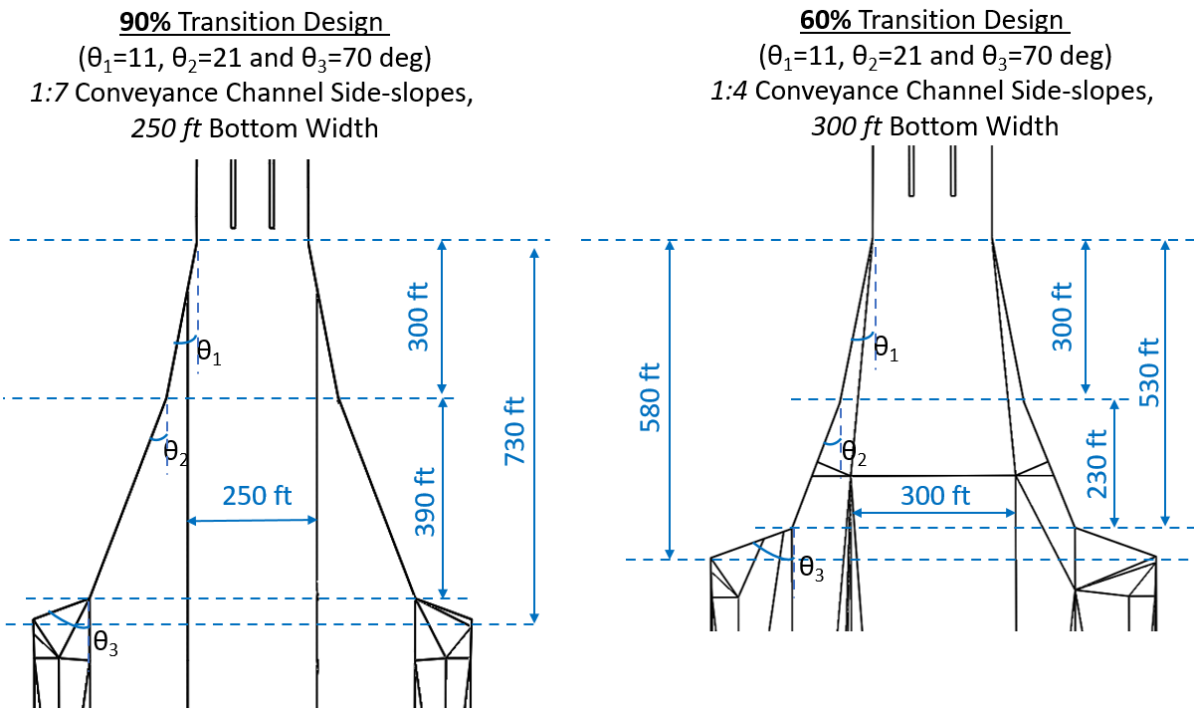

Figure 5.6. The updated 90% intake design (left panel) compared with the previously designed 60% design (right panel). Figures are not to scale.

Figure 5.7 shows the results for depth averaged velocity and streamlines in the top row with the 90% design shown on the left and the 60% to the right. The bottom rows show the bed shear stress results. The results in the right panel for the 60% design are the same as shown before in Figure 5.3. The figures show that the 90% design performs as good as the 60% in keeping the main flow core concentrated at the center and most of the intake transition is expected to be free of any significant deposition.

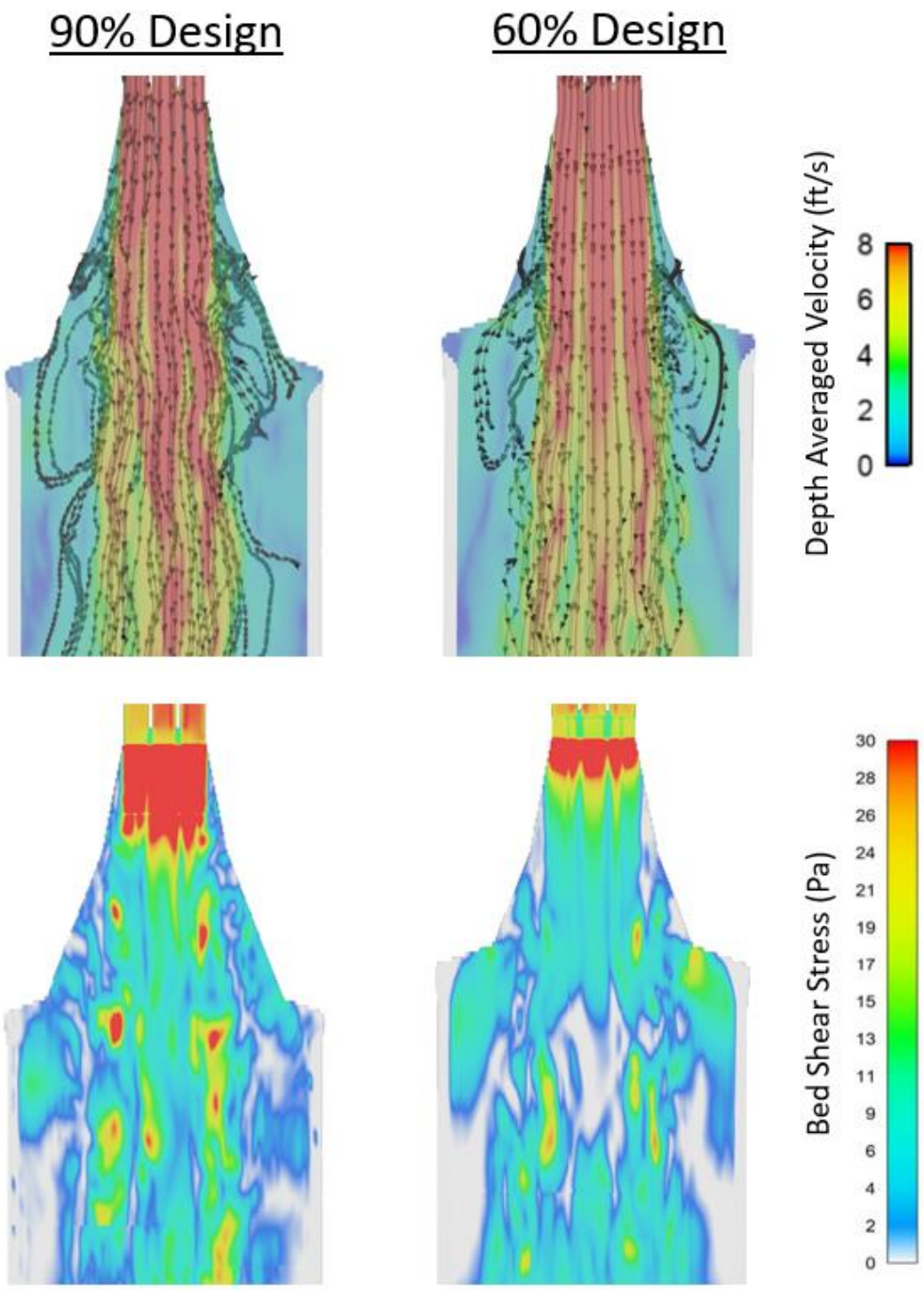

Figure 5.7. Top row: Comparison of time-averaged velocities and streamlines. The updated 90% design results are shown on the left and the previous 60% design results on the right. Bottom row: Comparison of instantaneous bed shear stresses for the same two designs.

Figure 5.8 shows the comparison of the cross-sectional distribution of the time average (30 mins) velocity magnitude, the instantaneous fluctuation as Root Mean Square Deviation (RMSD) and the ratio of RMSD to the mean velocity for the two designs. The results for 60% design are the same as before in Figure 5.4. Figure 5.8 shows that there is no significant difference between the mean velocities at the channel center or within 200 ft distance on either side of the intake transition where the main flow is concentrated. The 90% design shows somewhat reduced velocity (2 ft/s) to the 60% design (3 ft/s) primarily due to a slightly shorter berm (by about 50 ft) due to the widening of the channel. The mean velocity still remains above 2 ft/s, the threshold for silt deposit. It is possible that sand may deposit in the immediate downstream area over the berms of the channel just downstream of the intake as also indicated by morphology modeling later in Chapter 6, which was taken into consideration during levee and berm design by the geotechnical team. Even though the turbulent fluctuations show a slight increase by about 0.5 ft/s near the channel center for the 90% design from the 60%, the ratio of RMSD to the mean velocity remains less than 10% for both designs. The slight increase of turbulence in the DAV was traced to about 1 ft/s increase in turbulent surface velocity stemming from an increased shear between the widening flow at the surface and the somewhat constant flow maintained by a constant width intake transitional channel bottom for the updated design which is not there in case of 60% where the bottom width also widened somewhat along with the surface width. The shallow water jet globally still remains fairly stable and undergoes a seamless transition into the conveyance channel for both designs.

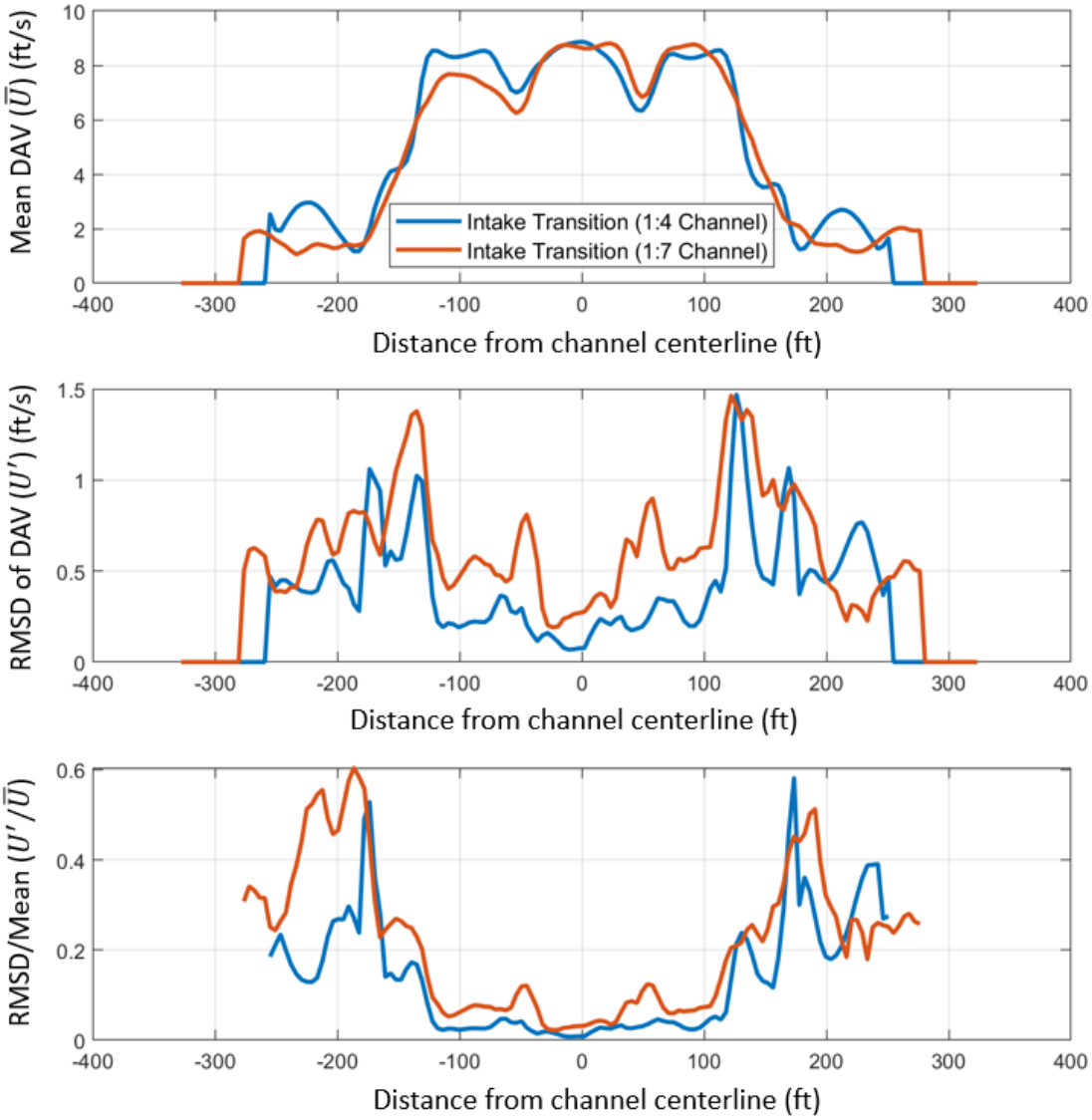

Figure 5.8. Comparison of updated 90% design with previous 60% design results. Top panel: Mean Velocity Magnitude (averaged over 30 mins), Root Mean Square Deviation of Instantaneous Velocity and the ratio of RMSD to the Mean velocity.

5.5 SUMMARY

FLOW-3D LES modeling was performed for the design of the transition keeping the economical length, and minimizing head loss and deposition areas for the 60% E&D. The 90% current transition design is about 730 ft long and gradually widens from the intake U-Frame to the conveyance channel in stages of 3 flare angles of 7-, 11- and 70 degrees.

The mean velocities, fluctuating component (turbulence) velocities and detailed flow structures were identified within the intake transition and used to develop a transition which keeps the main core of the flow unaffected by expansion losses. Bed shear stresses were computed and used to identify the potential areas of deposition. Minor deposition along the side berms downstream of the intake was identified but it is not expected to affect flow capacity. The transition showed head loss of only 0.1-0.15 ft which is about 10% contribution of the entire intake headworks head loss.

6.0 CONVEYANCE CHANNEL MODELING

6.1 Introduction

In this chapter the sediment transport and morphology modeling of the conveyance channel as it concerns regarding the hydraulic design of the MBSD system is presented. The conveyance channel design currently advanced at the end of the 60% E&D phase is an approximately 9,750 ft rip-rapped open channel with a uniform trapezoidal cross-section of 300 ft bottom width and 1:4 side slopes at a constant -25 ft, NAVD88 invert. The channel connects the intake headworks to the outfall transition feature.

Sediment and morphology modeling of the intake headworks (Chapter 4) indicated that the channel has enough sediment transport capacity to carry most of the very fine to medium sand loads from the river in suspension at the design peak flow of 75,000 cfs (high flow). The sand moves mostly along the bottom one-third to half of the channel depth. At low to medium flows (30,000 cfs to about 55,000 cfs) the conveyance channel was seen to move the sand load mostly as bedload with intermittent suspension during flood acceleration phases. For flows above 55,000 cfs the near-bed velocity is high enough such that the turbulence from the rip-rap cause bedload to be suspended. Therefore, long term deposition of sand in the conveyance channel bottom and on the side-slopes is not predicted by the modeling as long as the diversion is operated every year and allowed to reach flows greater than 55,000 cfs. However, deposition of fines on the side berms which slope from about +2 ft, NAVD88 to about -4 ft, NAVD88 is a distinct possibility as the easily suspended fines, particularly silt is found to deposit on the berms where velocities are mostly below 2 ft/s (low shear stress) even at the peak flow (Figure 6.1, showing a transect near the middle of the channel from the 3D FTN2Comp model). The berms extend about 100 ft from the foot of the levees towards the channel and have a very mild slope smaller than 1:20 at most places.

The first part of this chapter investigates through modeling the possible maximum deposition thickness on the berms. To this end, two cases of critical bed shear stress for silt are considered. The low value case corresponds to a ‘freshly deposited’ condition and a high value case corresponds to a ‘consolidated deposit’ condition. Since silt is the most abundant deposit indicated among the fines (clay settling velocity is too small to be able to settle on the berms)

deposits on the berms, silt critical shear stress was the focus to explore the possible influence of deposited sediments sitting on the berms on the diversion flow as well as provide the geotechnical engineers design surcharge information for levee or slope stability concerns.

The second part of this chapter describes base flow induced sediment deposition at the bottom and sides of the channel, in the outfall areas, and its implication on the diversion capacity. A base flow of 5,000 cfs maximum diversion flow when MR flow is below 450,000 cfs is currently specified by CPRA and modeled here. In additional channel flushing, which is defined as flow exceeding 5,000 cfs by opening all the gates during the base flow period, as and when there is enough available head between the river and the basin, is shown to remove deposition during base flow.

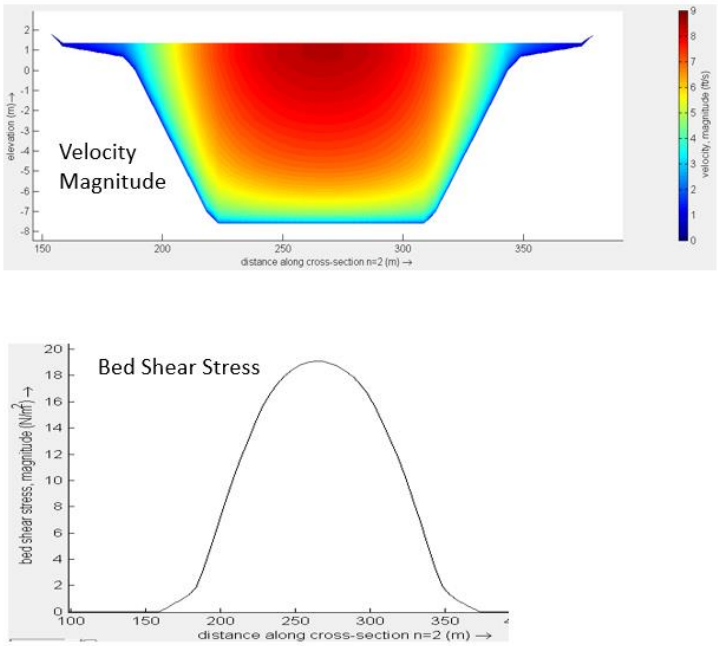

Figure 6.1. Top panel: Typical velocity distribution along a cross-section near the middle of the channel at 75,000 cfs diversion flow and Bottom panel: Bed shear stress. FTN2Comp (3D) Delft3D model results.

6.2 Model Setup

Two different models were used for the first and second tasks as described below.

6.2.1 Conveyance channel berm deposition modeling

A 3D Delft3D model consisting of the intake U-Frame, the intake transition and the entire conveyance channel was used for the modeling of sediment deposition on the channel berms. This model domain is similar in extent to the FTNGATE3Bay model described in Chapter 5. The 2008 MR hydrograph was simulated as an example. The diverted discharge (capped at 75,000 cfs) time series from the 2008-2011 modeling performed in Chapter 4 with the FTNOMBA (2D) Delft3D model was used as the upstream boundary at the U-Frame entrance. A water level boundary condition was also specified at the downstream end of the conveyance channel domain obtained from the same 2008-2011 FTNOMBA (2D) model results. The sediment concentration for sand (3 classes, very fine, fine and medium) and fines (silt and clay) introduced at the upstream boundary was specified as a cross-sectional uniform concentration calculated from the diverted sediment loads from the 2008-2011 modeling performed in Chapter 4 with the 3D Delft3D FTN2Comp model. Therefore, this model prescribes the same hydrodynamic conditions as simulated in the FTNOMBA model and also introduces consistent sediment loading rates at the upstream with the 2008-2011 modeling performed before. A morphology acceleration factor of 40 was used for the runs.

The following four specific scenarios were simulated with current and future conditions and varying critical shear stress for erosion of silt:

1. Current conditions
    a. Water levels from the FTNOMBA run with current bathymetry and 0.82 ft, NAVD88 water level at the Gulf
    b. Silt critical shear stress of 0.092 Pa. This value of critical shear stress for silt is representative of fresh deposits and does not consider consolidation induced strength gain. It was also used in the WI/CPRA's coastal master plan models.
2. Future conditions
    a. Water levels from the FTNOMBA run with future bathymetry as predicted from WI's 50-year land building model run and 50-year RSLR from the 1.5 m in 100 years. scenario
    b. Silt critical shear stress of 0.092 Pa.
3. Current conditions
    a. Water levels from the FTNOMBA run with current bathymetry and 0.82 ft, NAVD88 water level at the Gulf

b. Silt critical shear stress of 1.5 Pa. This value of critical shear stress for silt is representative of consolidated deposits (Kombiadou and Krestinitis 2012, Van Rin 2020, Lo et al., 2014).

4. Future conditions
   a. Water levels from the FTNOMBA run with future bathymetry as predicted from WI's 50-year land building model run and 50-year RSLR from the 1.5m in 100 years scenario
   b. Silt critical shear stress of 1.5 Pa.

6.2.2 Base flow induced deposition modeling

The FTNOMBA (2D) Delft3D model (without the MR) as described in Chapter 7 in detail was used for the modeling of the base flow induced deposition effects in the channel and the outfall. The 1968-1973 (5 year) historic hydrograph was modeled as the 2020-2025 period. This period was selected as it is part of the 50-year (1968-2018 representative of the 2020-2070 period) modeling period being modeled for land-building modeling for the 90% design tasks. The implication of choosing this period will be discussed in the results later.

Figure 6.2 shows the as-simulated 2020-2025 period hydrograph. Note that compared to the 2008-2011 period, this historical period had fewer number of MR peak flows that exceeded 1,000,000 cfs. Such periods are considered 'dry' years. Since lower MR flows can also lead to decreased diversion flows, choosing the relatively wet years seen in the recent decade 2008-2018 may, therefore, show somewhat less deposition than the results from the, dry, 1968-1973 period. Nevertheless, as will be shown later concern still exists regarding inability of the 5,000 cfs base flow to adequately keep the channel clean.

The diversion discharge in Figure 6.2 is obtained by the interpolation technique described in Chapter 3 and accounts for the variability in river water levels and Gulf water levels. The diversion discharge time series is imposed at the upstream boundary (mid-channel location) of the FTNOMBA model with no MR domain and only the Barataria Basin. The diversion discharge is capped to 75,000 cfs and is specified with or without base flow periods. Sediment concentrations at the mid-channel boundary are specified by a rating curve developed correlating the river concentrations to the diversion concentrations. River concentrations for sand and fines being calculated using the Hysteresis and Total Sand rating curves respectively as described in Chapter 3, includes the natural variation of sand and fines with river discharge.

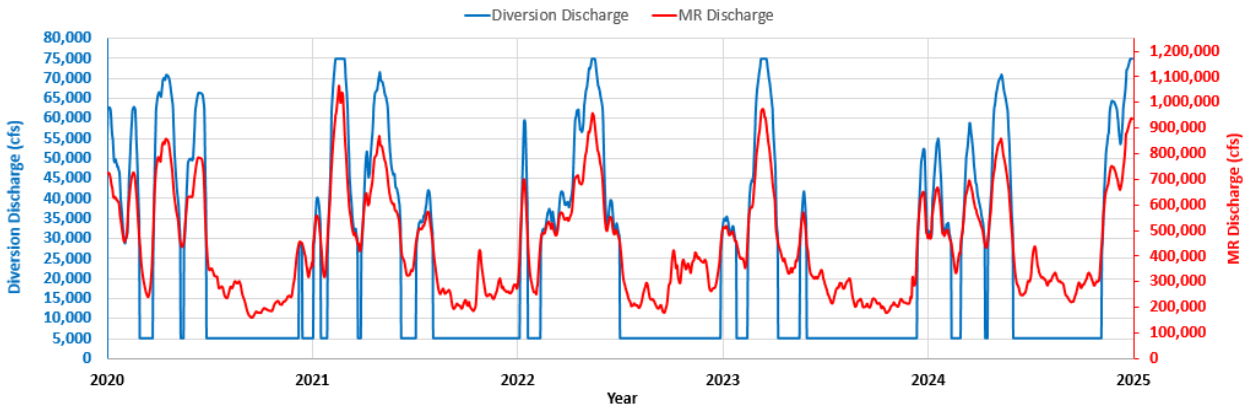

Figure 6.2. The historical MR hydrograph (in red, shown on the right y-axis) from 1968-1973 (5 years) used to simulate the 2020-2025 period. The diversion discharge (in blue, shown on the left y-axis) is obtained using the interpolation technique from a matrix of steady state runs and accounts for the variability in river discharge induced water levels and the Gulf of Mexico water levels as described in Chapter 8.

6.3 Results

6.3.1 Conveyance channel berm deposition modeling

Figure 6.3 shows the model results of the four scenarios together. The top panel shows the sediment deposition thickness over the berms. A cross-sectional averaged value over the two berms is shown at each location along the channel. Flow is from right to left. The bottom panel shows the existing average berm elevation. Adding the deposit thickness to the bathymetry will yield the elevation of the deposited bed. The top of the deposit elevation under the compact marsh sediment case (high critical shear for silt, 1.5 Pa) aligns with the maximum water level during operations. The difference in the future and current conditions results is about 0.8-1 ft difference in water levels within channel due to land-building and RSLR when maintenance dredging is performed in the basin.

From Figure 6.3 it is seen that when no compaction effects of the deposited sediment are assumed, the deposition on the berms extends about 2,200 ft along the channel from the start of the channel. As was explained in Chapter 5, this deposition immediately out of the intake transition is caused by the flow separation on the shallow berms and is unavoidable. However, the deposit thickness averages only about 2 ft. Thus, under the fresh silt deposit assumption it might be said that the channel berms can remain relatively self-cleaning. When a consolidated condition for the silt is assumed, the deposit with higher critical shear becomes impossible to

erode. Over time an equilibrium elevation, which is close to the maximum water level in the channel, is reached. Note that the increased deposition on the berm blocks most of the flow on the berms and causes a reduction of only about 2-3% of the diversion flow. While it may not be a major concern from the perspective of the hydraulic performance of the channel, the geotechnical design must consider these likely deposits for any levee/channel stability designs. Additionally, if left un-dredged, the deposits are likely to encourage undesirable vegetation growth.

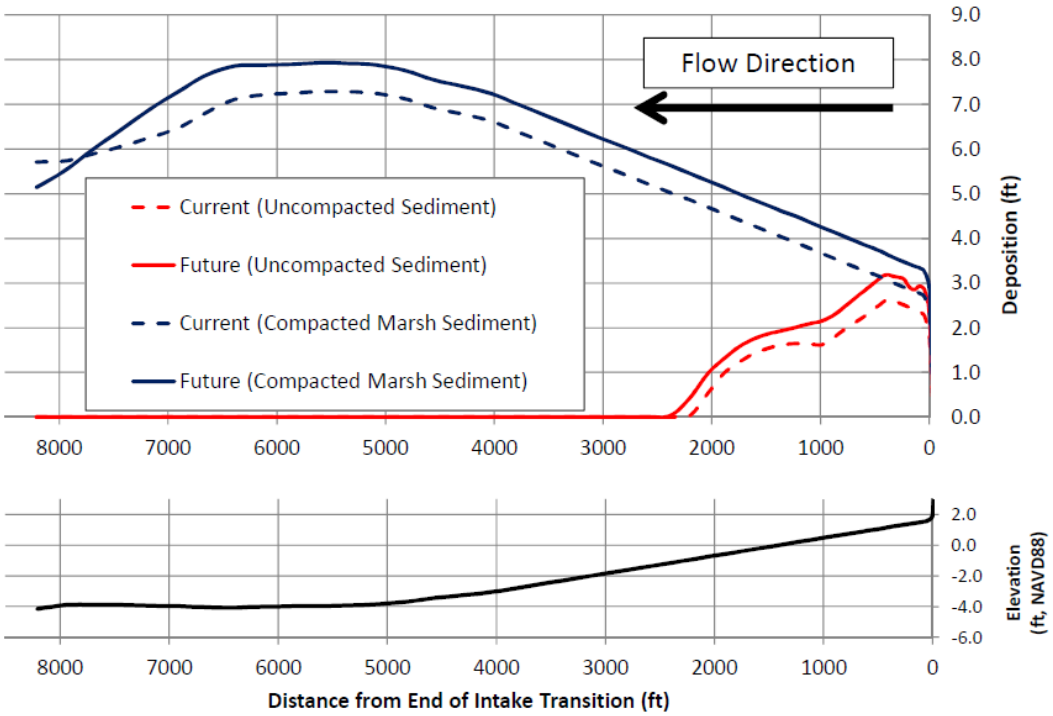

Figure 6.3. Top panel shows the average sediment deposition thickness on the berms. Two cases are shown, without assuming compaction of sediment (red) and with assuming compaction of sediment and consolidated of fines (blue). Bottom panel: As-designed average bed elevation of the berms.

6.3.2 Base flow induced channel deposition modeling

Figure 6.4 shows the bed elevations after 5 years (2020-2025) with (left panel) and without (right panel) base flow. It is seen that in presence of base flow the immediate vicinity of the outfall changes rapidly to a predominantly depositional environment as evident from the emanating deltaic channels much closer to the crevasse generated scour hole at the end of the

Outfall Transition Feature. Emerging sand bars are visible as well much closer to the outfall feature. They are likely to elevate the tailwater due to increased marsh resistance to flow and the resulting backwater effect. Note, for the 5 years modeled, a reduction in discharge is not assumed in year resulting from the base flow induced progressive outfall deposition. Within the red box shown in the figure the scenario with the base flow shows an increase in average bed elevation of about 0.4 ft compared to the without base flood scenario. Thus, in addition to meeting the EIS requirements, the base flow contributes to land building as a result of continuous supply of sediment even during the non-operational period.

Figure 6.4 also shows the transect in the conveyance channel where cross-sectional evolution is compared as an example of channel deposition analysis in Figure 6.5. It is seen that base flow induced deposition causes about 25% reduction in flow cross-section within the channel while for the no base flow scenario the reduction is only 5%.

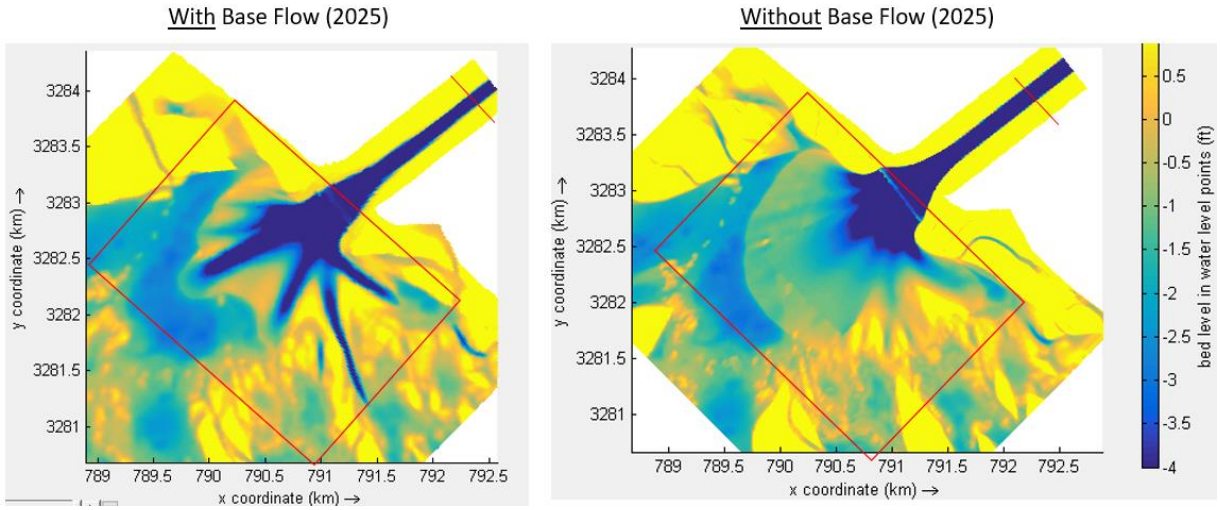

Figure 6.4. Bed elevations at the end of the 5-year period (2020-2025) in the outfall area with (left panel) and without (right panel) when base flow.

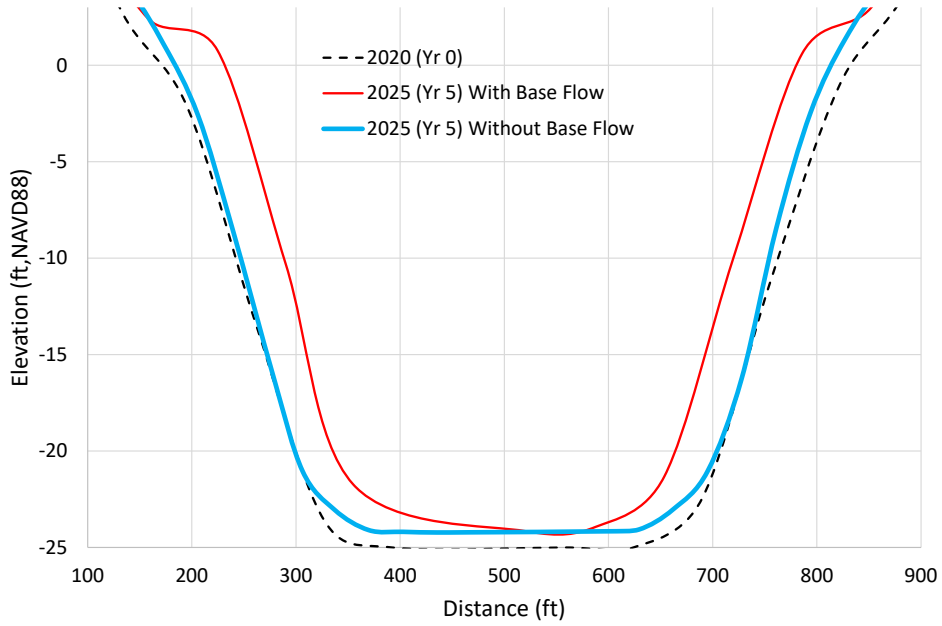

Figure 6.5. Evolution of the conveyance channel cross-section (Transect location shown in Figure 6.4).

In order to estimate the impact on the diversion discharge performance as a result of base flow, the year 2008 hydrograph was rerun with the bathymetries from the end of 5 years as a rigid bed (no morphology or sediment transport) including the river domain. Results of diversion discharge for each MR discharge range were then arranged in a tabular form as shown in Table 6.1. In addition to testing the bathymetries with and without base flow, the channel for the with base flow case was also dredged and run. This third case was run to understand the performance if only channel maintenance is performed but the outfall allowed to deposit under base flow. It is seen that compared to the scenario with no deposition, the current conditions scenario without base flow shows about 9-10% reduction below 750,000 cfs while above this the reduction is only about 2-3%. On the other hand, for the scenario with base flow and no channel maintenance the reduction in discharge ranges from 25-33% across the diversion flow range and is a significant adverse effect on diversion operations. If, however, only the conveyance channel is dredged keeping the outfall vicinity un-dredged, the reduction in discharge is only about 10-15% below 750,000 cfs and about 4-5 % above it. Therefore, the effect of the channel blocking up due to deposition has a greater influence on the diversion capacity than the outfall deposition.

Table 6.1. Influence of base flow induced deposition on diversion discharge.

Daily MR Discharge (cfs)	Daily Diversion Discharge			
	No Deposition in Channel/Outfall (cfs)	Without Base Flow: Deposition in Outfall and Minimal Deposition in Channel	With Base Flow: (Increased) Deposition in Outfall Only (Channel Dredged) (cfs)	With Base Flow: (Increased) Deposition Both in Outfall and Channel (cfs)
450,000	28,500	25,000 (-25%)	24,000 (-16%)	19,000 (-33%)
600,000	45,600	41,700 (-9%)	41,100 (-10%)	31,100 (-32%)
750,000	64,700	58,100 (-10%)	57,300 (-11%)	44,400 (-31%)
900,000	73,700	71,800 (-3%)	70,500 (-4%)	55,000 (-25%)
1,000,000	79,800	77,200 (-3%)	75,600 (-5%)	59,000 (-26%)
1,250,000	94,900	92,900 (-2%)	91,100 (-4%)	69,100 (-27%)

Figure 6.6 shows the time series of the diverted discharge together with the silt concentration. The silt concentration is chosen here because, as will be seen in Figure 6.9, almost all of the sediment coming in the diversion channel during the base flow period is silt. This is because the fines which follow the Hysteresis Sediment Rating Curve show increased or near-peak concentration in the rising limb i.e., before the river and diversion discharge peaks are reached. When the base flow is restricted to 5,000 cfs, only about 6.7% of the peak discharge flow of 75,000 cfs is available to transport silt concentration loadings which on the other hand are similar to the medium and high flows. In fact, as seen from Figure 6.7, the velocities in the channel are about 1 ft/s or lower under base flow conditions. The lack of sediment (silt) transport capacity of the 5,000 cfs flow in the conveyance channel needs a modification of the operations strategy, possibly by intermittent increase of the base flow for a few days to flush the channel. A more detailed analysis of the flushing slows, days and criteria will be developed as part of the 90% E&D phase.

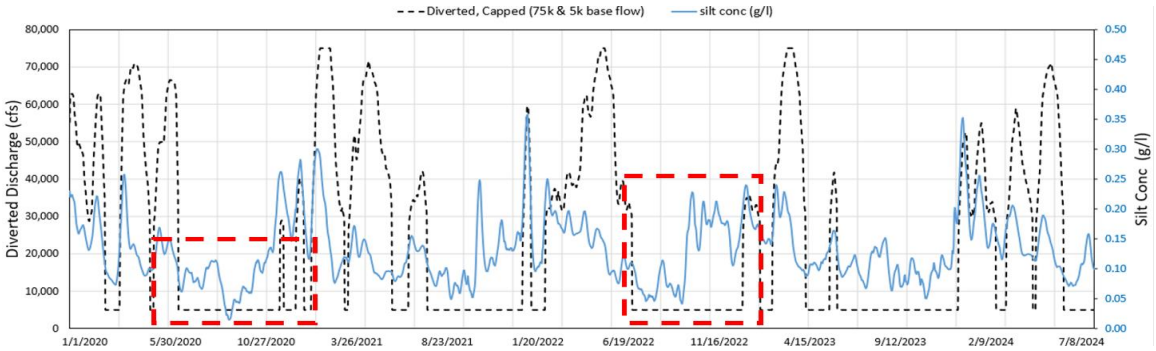

Figure 6.6. Time series of diversion discharge (left y-axes) and silt concentration in the intake (right y-axis). The diverted silt concentration is similar to that in the river as silt SWR is almost 1.0. The red dashed boxes show periods of base flow. Notice that silt concentration in this period remains comparable to the concentrations at medium to high flow (100-200 mg/l).

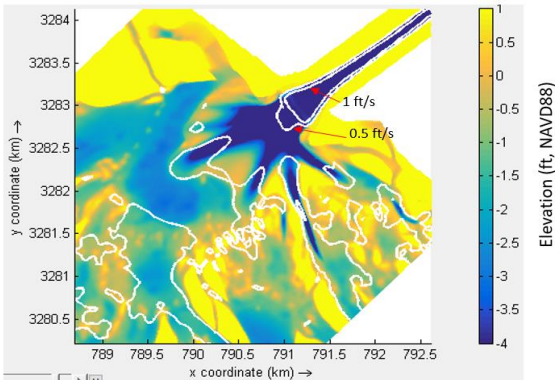

Figure 6.7. Contours of velocity at 0.5 and 1.0 ft/s marked by white solid lines due to 5,000 cfs diversion flow overlaid on the year 5 bathymetry.

Another important aspect of the base flow is the number of days and the sediment loading. Figure 6.8 shows the frequency of occurrence of the 5,000 cfs base flow. Data over the 5-year period is averaged on a yearly basis to show the number of days per year that the diverted flow will remain at a given discharge range. The error bars indicate maximum and minimum days per year. It is seen that 140-260 days (average about 205 days) are possible in a year when only base flow will occur. The number of days of base flow exceeds 50% of the year. Note that since the 1968-1973 period is considered here, the number of days may be somewhat larger if a more recent decade with a greater number of days above 450,000 cfs are considered.

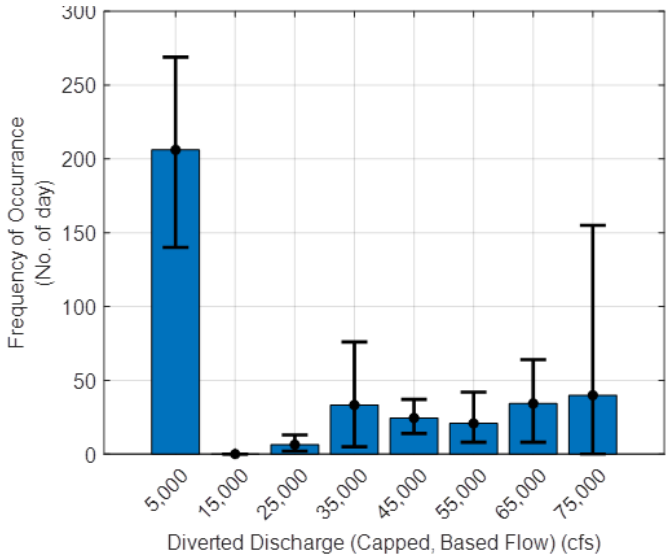

Figure 6.8 Frequency of occurrence of diversion flows based on the period 1968-1973. Mean values of days shown along with the range.

Figure 6.9 shows the combined effect of the number of days of 5,000 cfs flow and the greater availability of silt in the diverted load on the diverted sediment load distribution. The data is presented as the amount of sediment diverted by the diversion per year corresponding to each diverted discharge bin. As seen from the bottom and mid-panel the silt load in the river (about 400,000 tonnes/yr) at 5,000 cfs diversion flow is comparable the mean silt load between 25,000 to 55,000 cfs, even though only a fraction of the flow is available. This analysis explains the abundance of silt in the base flow deposits and the hysteresis phenomenon inherent in the fines which at the same time enhance land building but also pose a maintenance challenge in the channel and the near-field of the outfall.

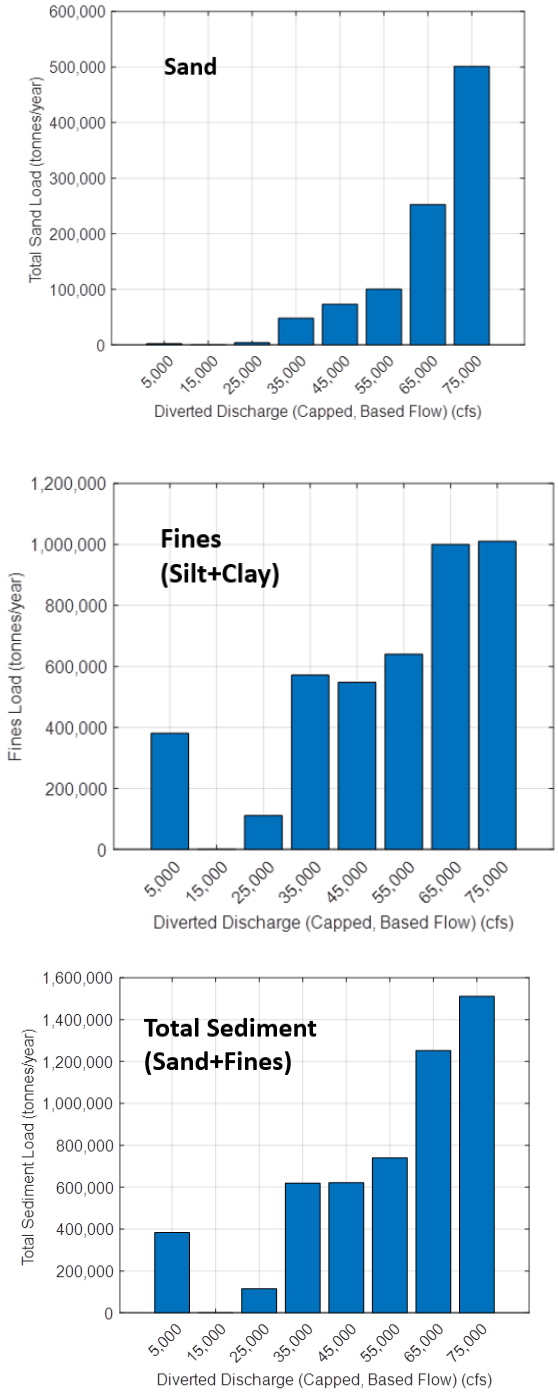

Figure 6.9. River sediment load variation with diversion discharge for sand (top panel), fines (middle panel), and total sediment (bottom panel). Notice that at 5,000 cfs sand load is negligible the sediment depositing is mostly silt.

6.4 Changes to Conveyance Channel Geometry in 90 percent Design

The conveyance channel side slopes were modified to 1:7 (V:H) in the 90 percent design from 1:4 as in the 60% design, whose results were shown in the sections before. The bottom width was also reduced from 300 ft in 60% design to 250 ft in 90 percent design. The changes were necessitated due to moving from an in the wet construction method to the in the dry method and the 1:7 channel with the 250 ft bottom width allowed the necessary stability requirements without increasing the overall footprint of the channel including the levees, during in the dry construction. The change in channel cross-section yields about 7.5% of additional flow area at the upstream end to 9% in the downstream end for the 1:7 design over the 1:4 design within the channel proper and excluding the berms. As will be seen later this also slightly reduces the headloss in the channel and increases flow capacity. This section shows updated modeling results that investigate the performance of this updated design, particularly from the perspectives of headloss, velocity distribution and concern for sediment deposition along the channel sides and on the berms similar to the analysis before in Section 6.3.1. Note that the berm elevations still are retained at the natural ground elevation as in the 1:4 channel, hence the widening of the channel proper resulted in slight shortening of the berms.

The typical velocity distribution along a channel cross-section located near the mid-channel where Hwy 23 bridge crosses the structure is shown in Figure 6.10. In addition to the 1:7 full length channel adopted in 90% design another design which had a hybrid configuration with 1:4 slope east of Hwy23 and 1:7 side slope west of Hwy23 was initially also considered that is shown here. The 1:7 full length was ultimately adopted based on ease of construction and also based on the fact that there was no significant difference in performance between the two designs. The solid lines are from calibrated Delft3D model results against FLOW-3D three-component models of the same. The dots are from the FLOW-3D model with the 1:7 channel slope West of Hwy23 only shown as reference. Two different flows were analyzed using steady state runs, the 75,000 cfs which is the maximum permitted flow and the 40,000 cfs which is the approximate lowest operational flow (when MR flow >450,000 cfs). The main aim of this analysis was to determine if the channel cross-section has adequate distribution of velocities exceeding 2 ft/s which is regarded as the threshold of resuspension of silt and hence can be expected to be deposit free. Sand is not the main sediment of concern here as sand moves

mostly along the lower one-third of the water column for this channel and very little sand moves up to settle on the berm. As seen from the figure, the 1:7 full length design shows a slight drop in centerline velocities from the 1:4 design, from a maximum of about 7.1 ft/s to 6.3 ft/s at 75,000 cfs but a gain of about 0.5-0.8 ft/s towards the channel sides at about 200-300 ft from the channel center. At high flows, most of the channel velocity however remains above 2 ft/s and deposition are not a concern for either design including the berms.

At the lowest flow, 40,000 cfs, a portion of the channel sides, shoreward of about 225 to 250 ft from the centerline shows velocities less than 2 ft/s and is a possible zone of deposition. Note that even though the zone of deposition for the 1:7 appears less (green arrow length) than the 1:4 (blue arrow length) around the channel sides and the berms, the 1:7 has a longer possible perimeter because of the lower slopes. Also, the berms for 1:7 are shorter in width and start further away from the channel center than the 1:4. This means on a per unit length basis, the 1:7 channel may apparently show greater deposition on the sides, where in fact with respect to distance from the centerline, deposition would have still happened on the 1:4 berm as well. The deposition results from the morphology modeling done later confirm this initial inference.

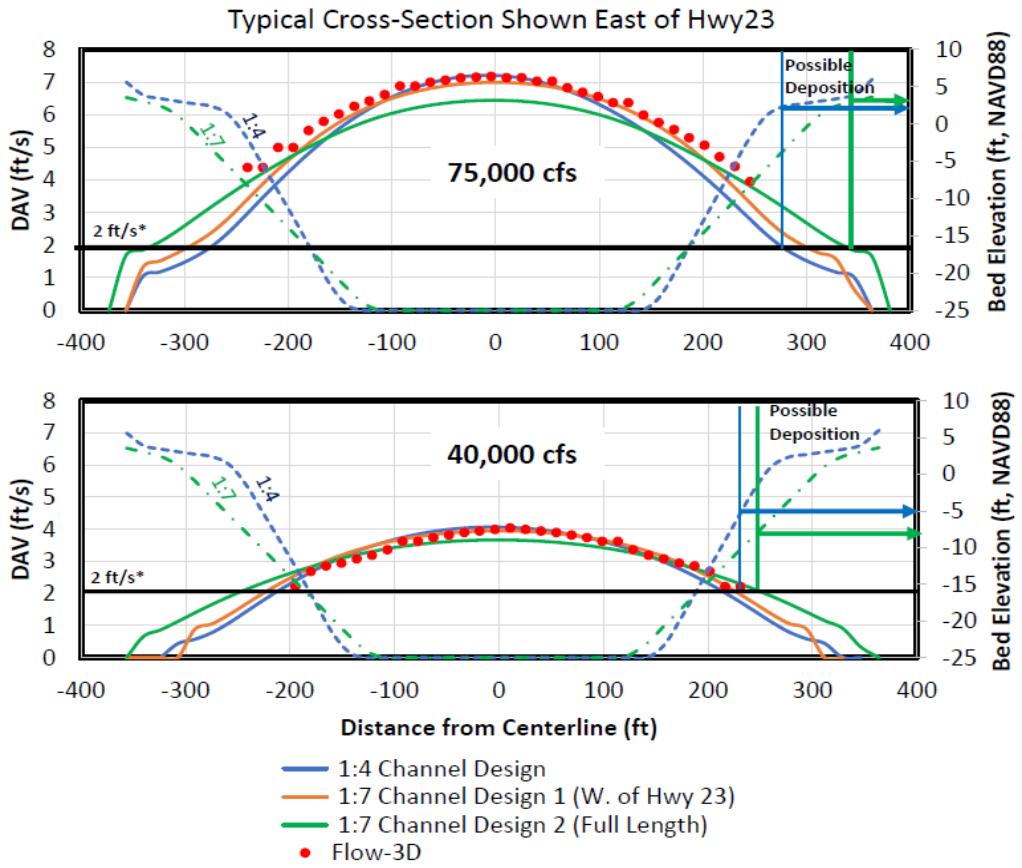

Figure 6.10. Comparison of depth-averaged velocity distribution along a cross-section located near the middle of the channel for the 1:4 and 1:7 designs. The 1:7 full length channel design was adopted finally.

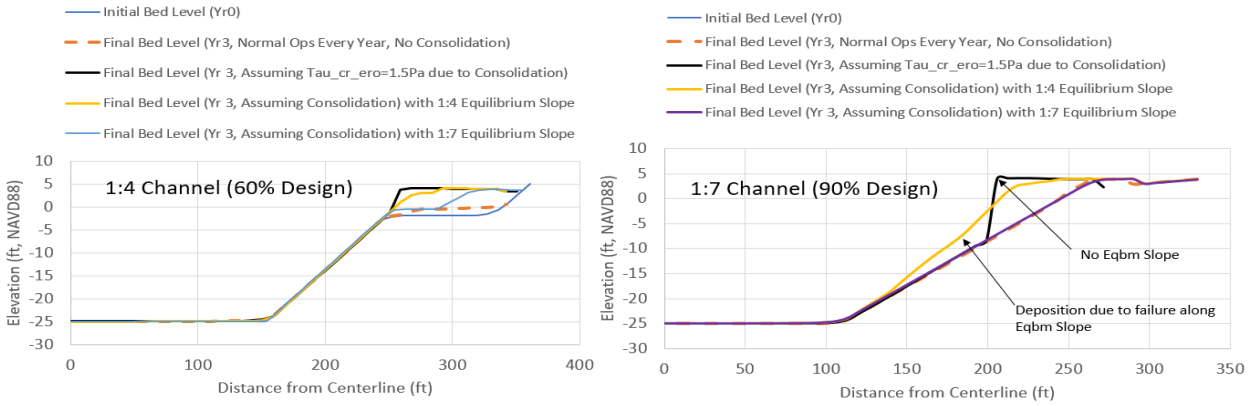

Figure 6.11. Deposition profiles along the channel cross-section showing possible areas of deposition for the 1:4 and 1:7 designs with and without assumptions of consolidation and or equilibrium slopes.

Figure 6.11 shows the results from the morphology model runs using the FTNGATE3Bay Delft3D 3D model as described before. The sediment properties and model setting are the same as used before the for-berm deposition modeling gin Section 6.3.1. A three-year model, simulating the 2008-2011 MR hydrograph with normal diversion operations with base flow was modeled. Silt, which is the principal deposited material was assumed to have unconsolidated critical shear stress of 0.09 Pa. Effect of consolidation was tested by restarting the model after every year and assigning the deposited sediment to a class of higher critical shear stress (1.5 Pa). This way every year, the successive layered deposition and consolidation could be modeled. The 1.5 Pa for consolidated cohesive material is a reasonable choice based on available literature on consolidation effects of fine-grained material in estuarine environments (Lo et al., 2014; van Rijn 2020). In addition to modeling the consolidation effects of the deposited sediment, the effect of an equilibrium slope on the deposited material was also tested. Generally, Delft3D does not allow for the failure of slopes to be modeled explicitly other than the provision for erosion of adjacent dry cells. However, the model does allow for specification of a stable slope for a deposit along the bank, such that if the are slope is exceeded material is caved off and deposited below the equilibrium slope and is available for further transport. This way the caving off of an unstable slope can be modeled in the morphology model without explicit slope stability modeling. In this case two additional slope thresholds 1:4 (typical stable slope under fully wet conditions) and 1:7 (typical stable slope under dry conditions) was simulated. These two envelopes can be regarded as a band of natural uncertainty for stable slope of the sediment deposited along the berm and the shallow portions of the berms. As seen from Figure 6.11, the results show that if no consolidation effects are assumed, almost no deposit forms on the berms for the 1:7 channel. This is actually a slight improvement over the 1:4 design where some deposit would still have formed for the 1:4. By shortening the berm width and making the channel banks deeper at the same distance from the channel center, the 1:7 design actually increases the sediment transport efficiency along the channel banks. If consolidation is assumed, while all the model results showed that deposits in the 1:4 channel would have sat entirely on the berm, for the 1:7 channel some deposit could be seen forming on the shallow portions, particularly shallower than -10 ft, NAVD88 along the channel. The results for the 1:7 channel also show variability based on what equilibrium slope is assumed. If the 1:7 equilibrium

slope is assumed, there is almost no deposition even with consolidation effects. On the other hand, if 1:4 equilibrium slope is assumed, some consolidated deposit could be seen sitting on the channel banks shallower than -10 ft, NAVD88, which would need some manual maintenance cleaning so that the channel cross-section is not reduced over time. If no equilibrium slope is specified, an unusually steep deposit is seen to be sitting for the 1:7 case. In summary it can be said that based on the natural uncertainty of consolidation, stable slope of the deposited sediment, some deposition could form along the channel banks of the 1:7 channel that may need occasional maintenance every 3 years or so to prevent constriction of the channel cross-section. A steady state run with the reduced cross-section as shown by the 1:4 equilibrium slope and consolidation effects indicated a 9% reduction in flow capacity for the diversion. However, given the fact that the 1:7 channel flow cross-section itself is about 8% more than the 1:4 channel cross-section, the 9% reduction did not significantly reduce the performance to what it would have been for the 1:4 channel without deposition and the 1:7 channel design could be recommended for construction given the immense benefits in cost savings it would offer from construction perspective. Detailed flow capacity comparison between the 60% and 90% designs are shown later in Section 8.3.3 across the entire MR hydrograph.

6.5 Channel Sediment Flushing Modeling during Base Flow Period (MR<450,000 cfs)

Base flow induced channel deposition as identified in section 6.3.7 before and occasional channel flushing was proposed to clean these deposits. Channel flushing flow may be defined as flow exceeding the maximum 5,000 cfs base flow and is affected by opening the diversion gates fully for a short period of time when MR<450,000 cs. Such flows can occur for a few days to a week as and when river and basin conditions allow for a high enough head difference (typically 0.4 ft or above) and mostly happens when 450,000 cfs < MR flow < 300,0000 cfs.

In this section, morphology modeling with and without channel flushing model results using the FTNGATE3Bay 3D Delft3D model are presented and discussed. Note that no consolidation is assumed of the channel deposits here as flushing is expected to be conducted within two to three months of maximum interval in between two flushing events or after diversion closure, so that it is unlikely that sediment in the channel will have enough time to

consolidate. Typically, the base flow period when MR<450,000 cfs lasts between mid of July to early December and the diversion gates are expected to be only partially open to divert a maximum of 5,000 cfs. A number of different operational scenarios are possible and are modeled here to understand the efficacy of flushing for each scenario. The scenarios consider insights gained from operations modeling presented in Chapter 11 later where 300,000 cfs MR flow is identified as the threshold for intra-daily reverse flow (at least one hour a day flow reverses from basin to river) and around 225,000 cfs MR flow as the threshold for inter-daily reverse flow (flow is from basin to river for the entire day) due to tidal influence. Flow-reversal is undesirable from a water quality perspective for the river as well as prospect of fine sediment being lost to the river, hence the diversion may be kept closed below either threshold at the discretion of the operations manager. The scenarios investigated here are:

- **Run 1:** *No flushing simulated*. 5,000 cfs constant diversion flow throughout base flow period, when MR flow < 450,000 cfs. This is the scenario simulated for CPRA's EIS modeling (GEC, 2021) and does not consider the head difference across the diversion. This was the same scenario that was modeled in section 6.3.2 and was found to induce excessive channel deposition.
- **Run 2:** *With flushing simulated*. 5,000 cfs maximum diversion flow for 300,000 < MR Flow < 450,000 cfs but diversion closed below 300,000 cfs to prevent intra-daily reversal flow.
- **Run 3:** *With flushing simulated*. 5,000 cfs maximum diversion flow for 300,000 < MR Flow < 450,000 cfs but diversion kept fully open below 300,000 cfs, except for the period of inter-daily flow reversal (mostly below MR <225,000 cfs) when diversion is kept fully closed.

The 1980 MR hydrograph from June 1980-February 1981 or ~7.5 months, which saw one of the longest base flow periods in over 54 years of record, is chosen intentionally to examine the worst possible effects of deposition in the channel due to base flow operations with and without flushing. Basin conditions are assumed current (2020) which determines the tidally averaged daily diverted discharge conditions simulated. Figure 6.12 shows the MR hydrograph in the second vertical axis to the right (black solid line) and the diversion discharge modeled for each scenario in the left vertical axis. There were two flushing period available during these 7.5 months, one in August and another in late January lasting 15 days and 8 days respectively.

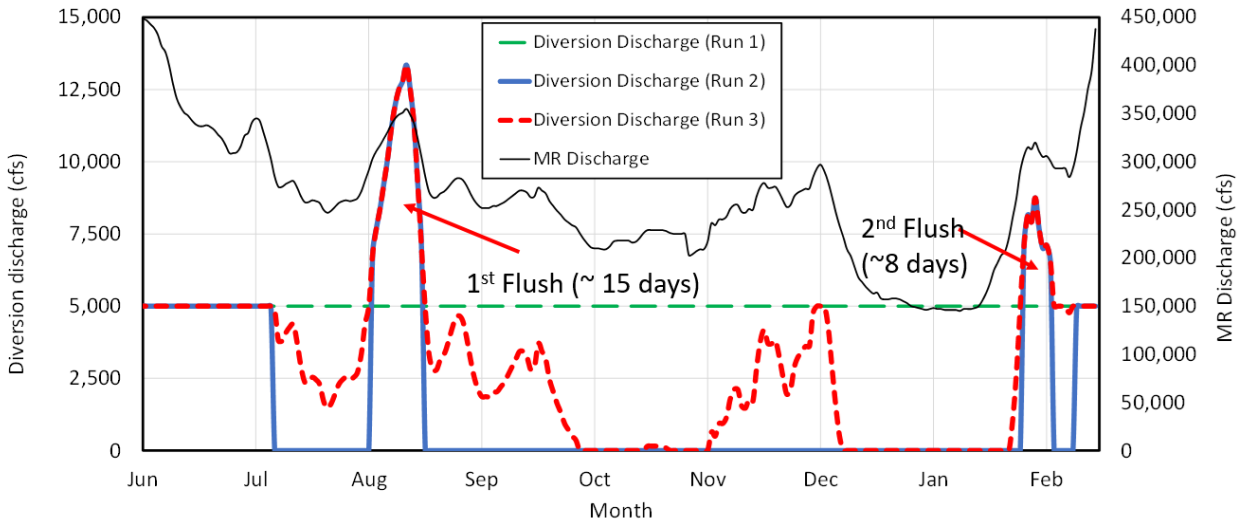

Figure 6.12. 1980 MR hydrograph modeled for channel flushing simulations.

Figure 6.13 shows the deposition depths (over the initial as constructed channel bottom) in the channel after the end of the 7.5 months period. Run 1 which is with constant 5,000 cfs base flow showed the highest deposition in the channel due to the maximum sediment delivery to the channel and the consistently low sediment transport capacity due to lack of flushing. Sediment buildup is more in the upstream half of the channel which over the years may be expected to spread along the entire length of the channel. Note that this scenario is highly improbable as it is shown later from tidally based head driven model runs later in Chapter 11, a constant river to basin flow of 5,000 cfs daily is not available during the low flow period. In this case the 1980 hydrograph had a considerable period below 300,000 cfs which this scenario does not capture. Nevertheless, the model results are insightful to understand the probable effects on the channel, as was shown before in 6.3.2 which assumed this scenario, if flushing is not conducted. Run 2 which in which flushing is conducted but the diversion remains closed below 300,000 cfs MR flow, showed the least deposition in the channel among the three scenarios due to reduced sediment delivery to the channel (diversion mostly closed late Aug-January when MR falls below 300,000 cfs) as well as due to the two flushing flow events which help in cleaning the channel. This shows that even for the worst base flow year (longest period) chosen, it is possible that channel deposition may not be a real concern if the diversion is closed for most of the period and flushing is done at least once. From a purely channel deposition perspective therefore it is

recommended to keep the diversion closed below 300,000 cfs as well. Run 3, in which flushing is conducted but the diversion remains closed under 225,000 cfs showed more deposit sitting than Run 2 but far less than Run 1. Most of the channel deposition depth remains below 2-3 though and can also be recommended as an acceptable scenario. One of the major differences between this and the Run2 is that since the diversion is kept fully opening below 300,000 cfs it allows for the diversion discharge to fall below 5,000 cfs and brings in additional sediment load to the basin that is otherwise lost in Run 2. Therefore, there is some obvious benefit to this scenario from maximizing the efficiency of land-building and as will be shown later in Chapter 10, base flow is an important factor for offsetting land loss against rising sea levels and subsiding land. The land-building modeling performed in Chapter 10 use this scenario for the 50 yr modeling for the base flow, even though no flushing is performed there. The channel is instead manually dredged out every year in those runs, to simulate flushing effects indirectly.

Figure 6.13. Depth of deposition and distribution at the end of the about 7.5 months of base flow period.

6.6 Channel Self-cleaning after Diversion Full Opening (MR>450,000 cfs)

This section demonstrates the ability of the diversion operational flow (MR>450,000 cfs) to clean a previously deposited channel that occurred during a prior low flow period. Since the exact deposition pattern and distribution in the channel can be highly variable at the end of the base flow period and before the diversion operations begin for the next flood year, a few hypothetical depths of deposits were assumed within the channels. Since Figure 6.13 indicates mostly a 2- 5 ft deposition depth within the channel during base flow (Run 2 and 3), two runs with a 2 ft uniform deposition across and along the channel and a 5 ft uniform deposition are modeled. In this case both unconsolidated and consolidated deposits are modeled in order to also consider the unlikely scenario that the diversion is not operated for a year and is now starting with consolidated deposit as old as a full year back.

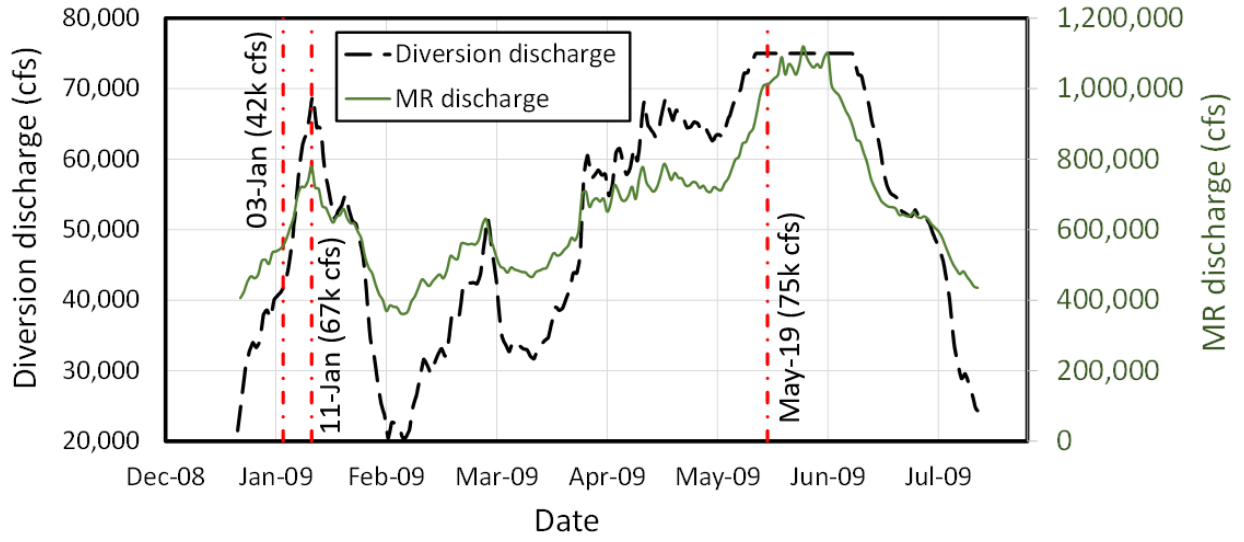

Figure 6.14. MR hydrograph from 2008-2009 modeled to determine self-cleaning ability of channel during normal diversion operations (MR>450,000 cfs).

Figure 6.14 shows the MR hydrograph modeled from Dec 2008-Jul2009 as a demonstration of diversion operational year. This hydrograph was selected because within the recent decade (2008-2018) this hydrograph allowed for multitude of rise and falls and the diversion channel would likely undergo repeated deposition and erosion during the falling and rising limb of the hydrograph. In reality after the diversion gates are fully opened in December, even though the MR fell below 450,000 cfs for a few days in February 2009, the diversion is unlikely to be closed due to too short a time window. The morphology results are presented at three specific dates where the diversion flow hit a certain threshold and demonstrates the efficacy of the operational flows cleaning the channel.

Figure 6.15 and 6.16 show the change in channel cross-section when starting with the 2 ft and the 5 ft initial deposit thickness along the channel bottom. If no consolidation is assumed (green dashed line), it seen that the channel deposits are more or less completely cleaned by January 3rd, or in about 17 days from the start of the modeling on December 18 when MR hits 450,000 cfs for the first time. This without consolidation, similar to the channel flushing runs, the minimum operational diversion flows of even 30,000-40,000 cfs for a week or two is sufficient to clean the deposits.

For the consolidated deposits (red dashed-dot line in Figs. 6.15 and 6.16), the results show a gradual cleaning process from bottom up with a certain equilibrium slope developing (1:4 to 1:5) for elevations shallower than -10 ft, NAVD88. It is seen that as the diversion flow quickly rise from 42,000 cfs to 67,000 cfs within about 8-9 days (January 3rd to January 11th), most of the channel cross-section deeper than -10 ft, NAVD88 cleans itself fully. As the MR flow and therefore the diversion flow undergoes a series of rise and falls in the next 4 months, the deposits shallower than -5 to -10 ft NAVD88 continue to remain. The results are very similar to those demonstrated in Figure 6.11 before for berm deposition modeling and confirms the conclusion that for the 1:7 channel maintenance dredging of the shallow channel banks (shallower than -10 ft, NAVD88) may be necessary of the deposits are allowed to consolidate over time there. It is possibly best to perform regular flushing during base flow every year and operate the diversion at least for a few days at the peak flow to reduce any possibility of consolidated material building along the shallow banks which can become costly to manually dredge later.

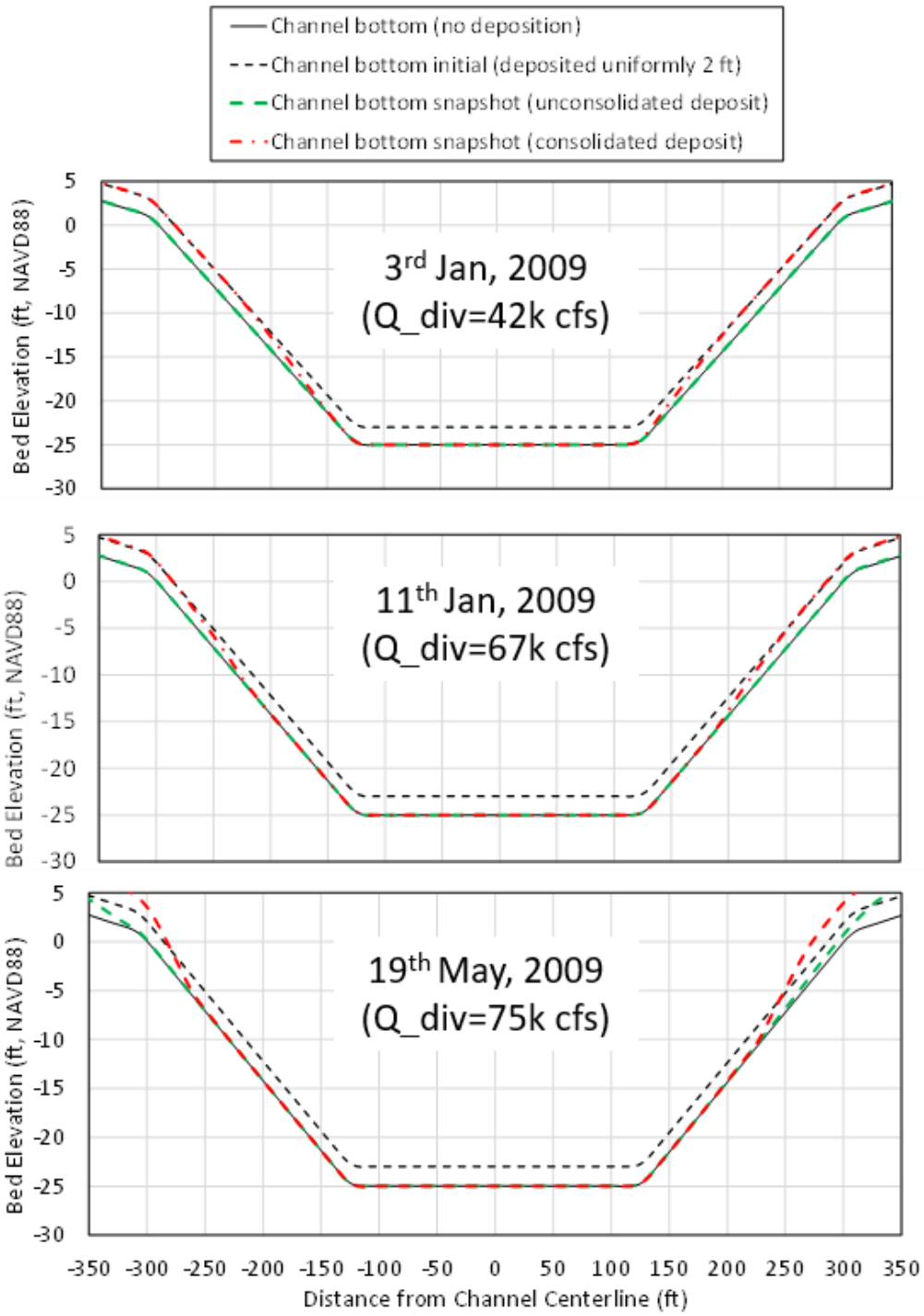

Figure 6.15. Initial deposit 2 ft: Cross-section along a representative section near the mid-channel bed elevations with and without consolidation of deposit at the three dates in Figure 6.14.

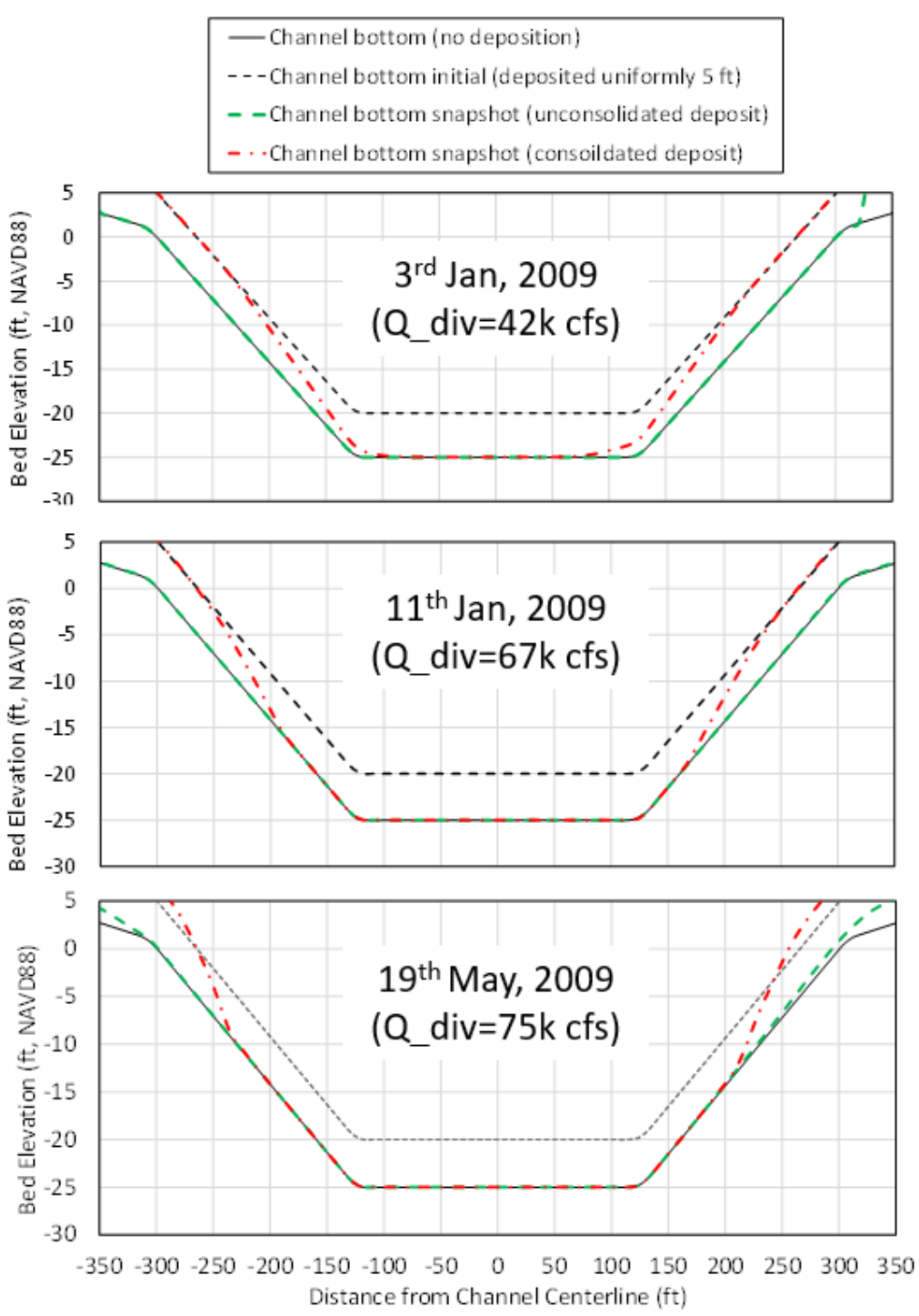

Figure 6.16. Initial deposit 5 ft: Cross-section along a representative section near the mid--channel bed elevations with and without consolidation of deposit at the three dates in Figure 6.14.

6.7 Conclusions

In this chapter deposition on the channel berms during regular operations and on the channel bottom under base flow operations were modeled, analyzed and discussed. It is seen that deposition on the berms during the full-capacity diversion operation is not a significant design concern for the hydraulic performance of the channel. During the base flow operation, the deposition of the silt load in the channel may reduce diversion capacity significantly. The silt deposition during base flow is a combined effect of lack of sufficient transport capacity at base flow and a comparatively abundant supply of silt in the diverted flow.

In order to reduce the possibility of deposition during base flow it is recommended that the diversion be kept closed below 225,000 cfs and regular flushing be carried out as and when the head difference across the diversion allows for discharge capacity to exceed 5,000 cfs. Typically, a week-long flushing is seen to be effective in reducing deposition significantly. If the deposited material is allowed to consolidate, even after the diversion is fully opened it may not clean away the material at the shallower zones, typically less than -10 ft, NAVD88 and some maintenance dredging may be necessary. It is probably best to allow the diversion to flow at peak capacity at least for a few days every year to prevent any consolidation of deposited material along the banks.

The 1:7 side slope channel design in the 90% phase shows about 5-16% improvement in diversion flow capacity along the entire MR hydrograph. Any improvement of discharge capacity is desirable from a future performance standpoint as it can significantly reduce dredging volumes in the basin as well as increase sediment load delivered over time. The 1:7 channel is also cheaper to construct in the dry and is the favored choice for the final 90% design.

7.0 OUTFALL TRANSITION MODELING

7.1 INTRODUCTION

The Outfall Transition Feature (OTF) is an engineered transition between the diversion or conveyance channel (invert -25 ft, NAVD88) and the marsh floor (elevation of about -4 ft, NAVD88) on the basin side. The primary function of the OTF is to distribute the high velocity diversion outflow with maximum depth averaged velocities of 5-7 ft/s exiting the channel into the basin with sediment in suspension. The sediment, particularly sand, also must transport far enough into the basin such that immediate deposition of sand within the outfall area does not create a 'healing crevasse' condition too early in the operational life of the diversion. This chapter describes the modeling activities performed till the 60% E&D phase related to the OTF morphology evolution which was simulated during the first three years of the diversion operation. Initial designs tested with a short rip-rapped OTF indicated that the scour bottom elevation could reach as deep as -60 to -80 ft, NAVD88 within a few years. The scour hole has the potential to migrate as a typical head-cut upstream, which may undermine the structural integrity of the back-levee tie-ins and possibly the conveyance channel. Subsequent modeling efforts were focused on investigating the factors responsible for scour, improving the spreading of the flow exiting the OTF by a step-by-step modification of the OTF geometry, armoring extents and also keeping the OTF to an economical dimension. As will be shown in the later sections, the extent of the rip-rap on the OTF, the ability to achieve a relatively uniformly distributed flow at the OTF edge without excessive flow separation and the erosion characteristics of the native soil were the most important aspects of design to minimize the scour depth. The final design at the end of the 60% design showed a projected scour bed elevation of approximately -11 ft, NAVD88 or about 7 ft deep below the -4 ft, NAVD88 marsh bed.

FTN also reviewed the available literature on similar existing outfalls in the LMR area for scour issues. Three relevant case studies that demonstrate the genesis and evolution of crevasse-splay induced scours are discussed to draw qualitative parallels with the model results and provide additional evidence to the design team.

Additionally, the Delft3D morphology model was validated for determination of crevasse induced scour at the West Bay Diversion intake site. This exercise was intended to improve

confidence in the model setup for use at MBSD OTF site, the West Bay site has its own site-specific scour issues and should not be used as a direct indicator at the MBSD OTF site.

The morphology and scour models have inherent large uncertainty. Therefore, an initial sensitivity analysis of model parameters was performed and presented here as well. Due to the large modeling uncertainties, a holistic approach is recommended in design of the countermeasures. Such an approach considers field observations of scour holes, experience from the Subject Matter Experts and additional site-specific soil erodibility sampling. Due to inherent uncertainties of the erosional properties of the soil a safety factor of 2, i.e., a minimum of 14 ft deep wall below the marsh bed was recommended for the depth of any head-cut mitigation measures such as a sheet pile wall or toe wall at the OTF edge.

7.2 Hydrodynamics: Water LEVELS and Velocity and Bed Shear Stress Distribution in the Barataria Basin

The 2D Delft3D FTNOMBA (Table 1.1, Figure 1.2) model was run as a series of steady state runs with different diversion flows, to develop water level (WL) distribution and velocities in the vicinity of the OTF required for design and/or basin-side effect concerns. The water level at the Gulf of Mexico (GoM) boundary was held constant at +1.0 ft, NAVD88, the approximate 2020-2021 Mean Water Level (MWL). The basin was set to a constant Chezy roughness coefficient of 50 with the diversion channel Chezy roughness set at 40 as indicated from three-component inter-model calibration shown in Section 9. Therefore, no tidal effects and/or river water level induced OTF variations were modeled here which has been presented later in Chapter 9 as part of the Operations Modeling. Figures 7.1 to 7.3 show water level distributions in the basin with diversion flow of 30,000 cfs, 50,000 cfs and 75,000 cfs respectively.

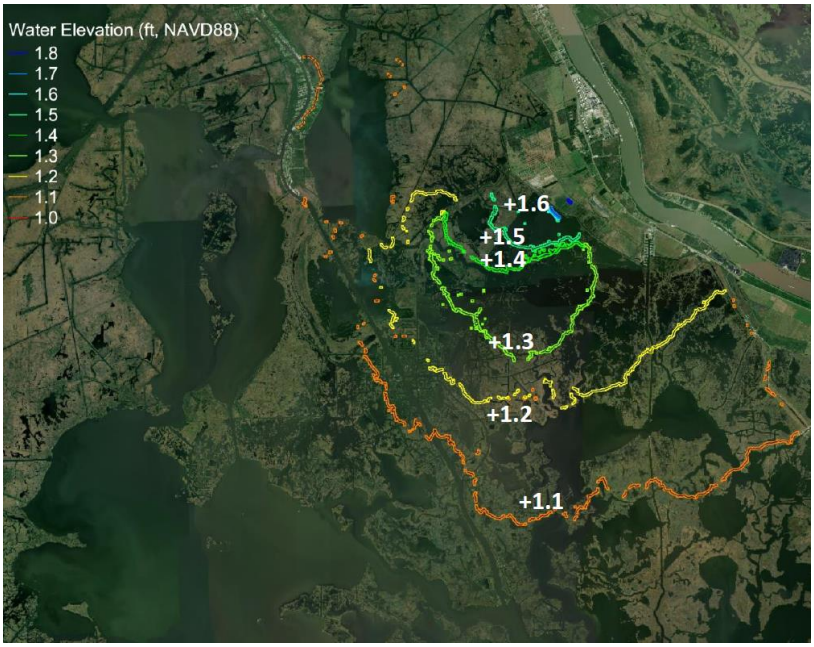

Figure 7.1. Water level distribution in Barataria Basin with 30,000 cfs diversion flow and +1.0 ft, NAVD88 WL at GoM.

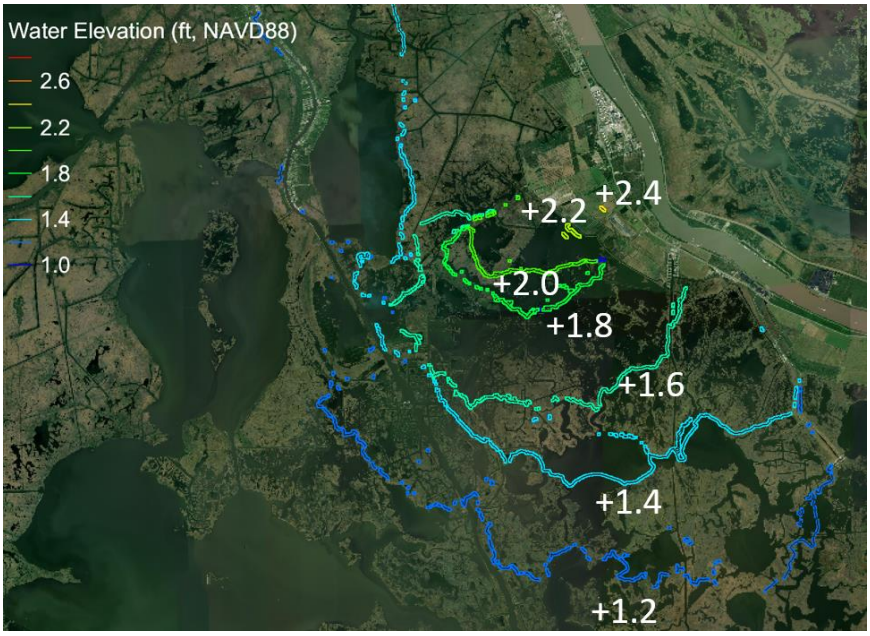

Figure 7.2. Water level distribution in Barataria Basin with 50,000 cfs diversion flow and +1.0 ft, NAVD88 WL at GoM.

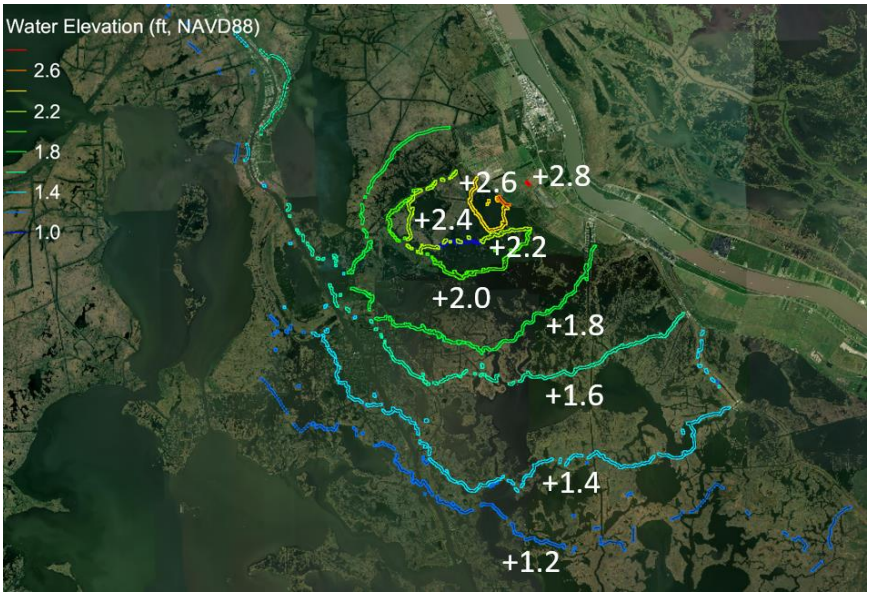

Figure 7.3. Water level distribution in Barataria Basin with 75,000 cfs diversion flow and +1.0 ft, NAVD88 WL at GoM.

As seen from the figures, the water level varies between 1.6 to 2.6 ft in the immediate vicinity of the diversion outfall and decreases in the basin to the ambient water level in over an approximately 3 to 5-mile zone. This zone may be thought to be the immediate zone from the OTF where the kinetic effects of the diversion flow may be most dominant.

Figure 7.4 shows the depth averaged velocity distribution in the basin at 75,000 cfs diverted flow and shows that the velocity decreases from about 6 ft/s to about 2 ft/s over a distance of 1 to 1.5 mile from the OTF.

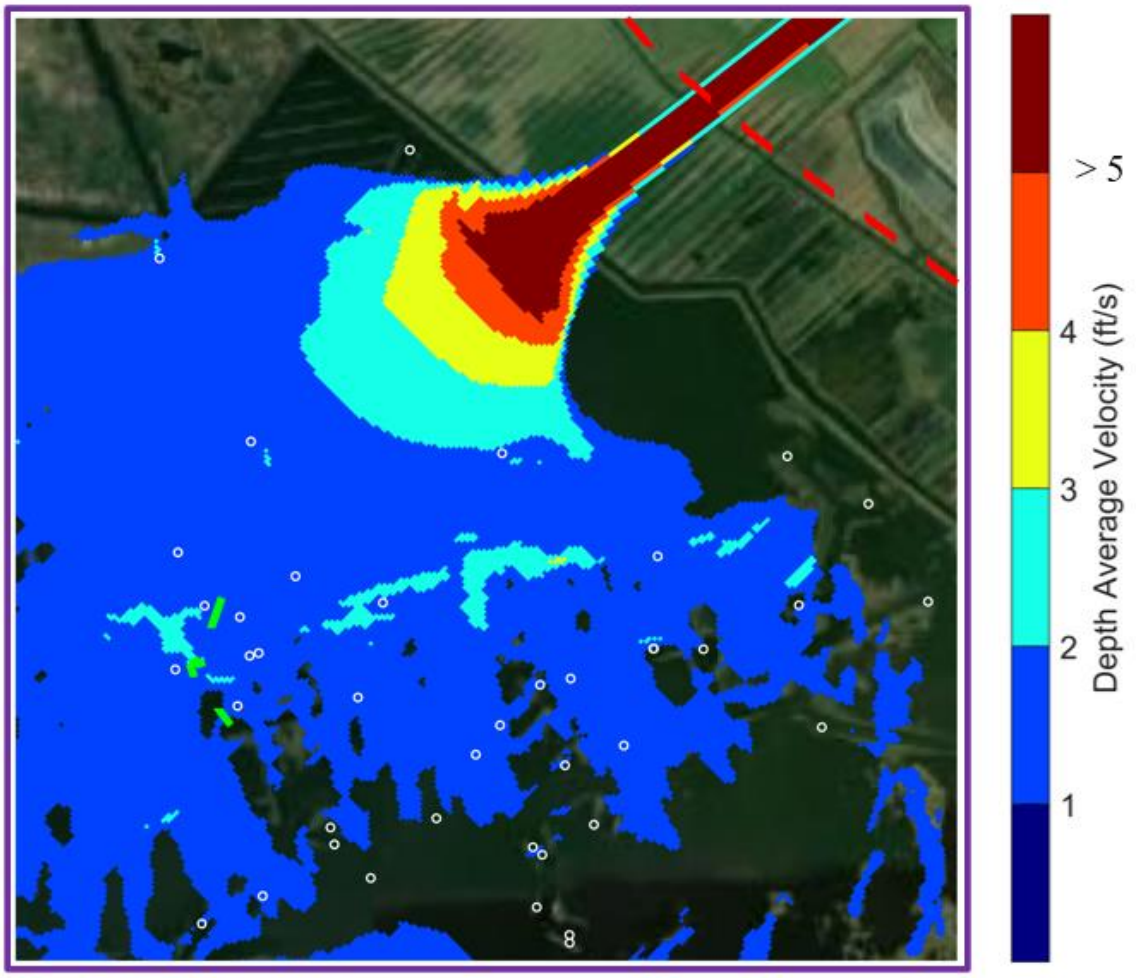

Figure 7.4. Velocity distribution near the MBSD Outfall at 75,000 cfs diversion flow and +1.0 ft, NAD88 WL at GoM.

7.3 SEDIMENT TRANSPORT And Morphology Modeling: Investigation of Scour at Outfall Edge

This section begins by reviewing scour at similar MR outfall areas and then describes the modeling and results from the MBSD OTF scour evolution runs performed to arrive at the current design.

7.3.1 Case Studies of Scour at existing similar MR Outfall Areas

Below is a brief review of three studies from the existing literature that provide information on scour observations at lateral outlets along the Lower Mississippi River at the

West Bay diversion, the Southwest Pass outlets, the Mardi Gras Pass, and the Davis Pond diversion canal. A modeling study performed by the WI during the MBSD planning phase is also summarized.

7.3.1.1 Morpho-dynamics of the Erosional Phase of Crevasse-Splay Evolution and Implications for River Sediment Diversion Function

Yuill et al. (2016) describes the evolution of a crevasse splay at the Mississippi River West Bay diversion from the opening in 2004 up to 2014.The unlined diversion channel was created originally at an invert of -25 ft, NAVD88 similar to the proposed MBSD conveyance channel. The diverted discharge varied from about ~3,500-7,000 cfs to about ~39,000 cfs during the annual flood within the initial 5 years (2004-2009) but increased to ~70,000 cfs from 2009-2014 period. The long-term trend of the diverted flow shows a steady linear rise over 8 years (Figure 7.5) due to the widening and scouring of the main diversion channel. Figure 7.6 shows the evolution of the thalweg of the diversion channel from 2004 to 2014. As seen from the figure, the deepest channel invert (in 2012), representative of an in-channel scour hole, developed down to -33 m, NAVD88 (-100 ft, NAVD88) within the narrowest section of the channel. Channel widening and infilling reduced the scour depths somewhat (to -60 ft, NAVD88) from 2012 to 2014. In the case of the MBSD, the conveyance channel is lined by a rip-rap. Therefore, the invert deepening observed for West Bay is likely to occur at the outfall where the rip-rap lining ends.

Figure 7.7 (top panel) shows the bed shear stress distribution from the Delft3D modeling by Yuill et al. (2016) under the 2004 diversion conditions. Note the high hydraulic shear stress zone (>10 Pa) at the end of the diversion channel. A similar zone can be expected at the MBSD outfall. Figure 7.7, bottom panel (left side), shows the cross-section near the end of the conveyance channel (beginning of the outfall transition, flow direction is into the plane of the paper) from the FTN2Comp 3D Delft3D model at 75,000 cfs diversion flow. The velocities at the core of the flow (within the flat portion of the trapezoidal channel section) range from 8-9 ft/s at the surface to 2-3 ft/s near the bed. This results in peak bed shear stress of about 19 Pa. As the flow travels from -25 ft, (-7.63 m) NAVD88 (beginning of outfall transition) to -4 ft, (-1.22 m) NAVD88 (end of outfall transition), the high velocity surface stream is expected to hit the soft

marsh soils with a critical shear stress of 1.5-2.5 Pa (analysis of critical shear stress from geotechnical parameters and SEDflume studies as presented later in in Section 7.3.3) and is a significant erosion concern. As seen on the right side of the bottom panel of Figure 7.7, the typical cross-sectional velocities in the core of the West Bay diversion channel were much lower (0.6-1.2 m/s or ~2-4 ft/s) compared to the velocities expected to enter the MBSD outfall transition. Therefore, a scour hole of similar depth as the West Bay diversion can be expected in the case of MBSD outfall if the channel is simply merged over an unarmored transition. Furthermore, the central core for the West Bay diversion channel undergoes lateral reorientation due to the widening of the channel cross-section reducing, the velocities which in turn helps in scour reduction. In the case of MBSD, the fixed, constructed channel will maintain 75,000 cfs flow and the high velocity core will remain constant in orientation and strength throughout the life of the project, thereby concentrating the flow at the center of the OTF edge.

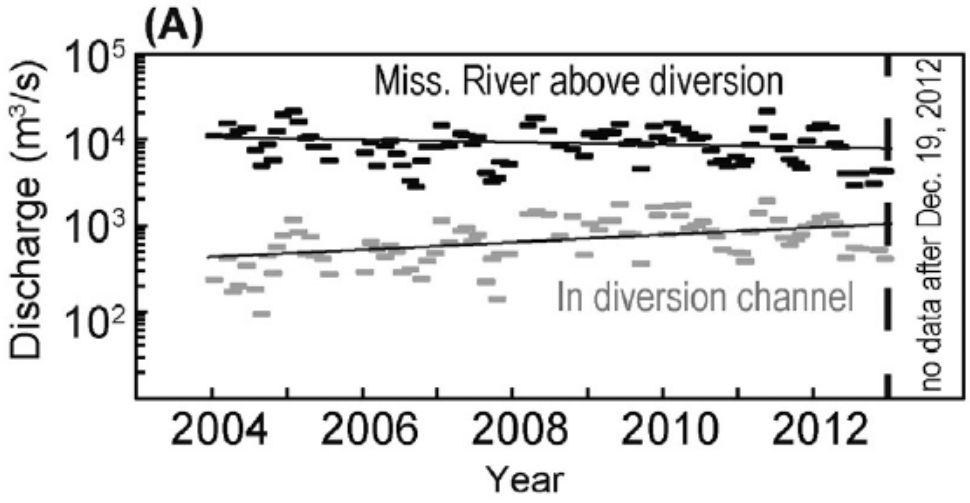

Figure 7.5. West Bay diversion discharge and MR flow upstream of diversion location (figure adapted from Yuill et al. 2016)

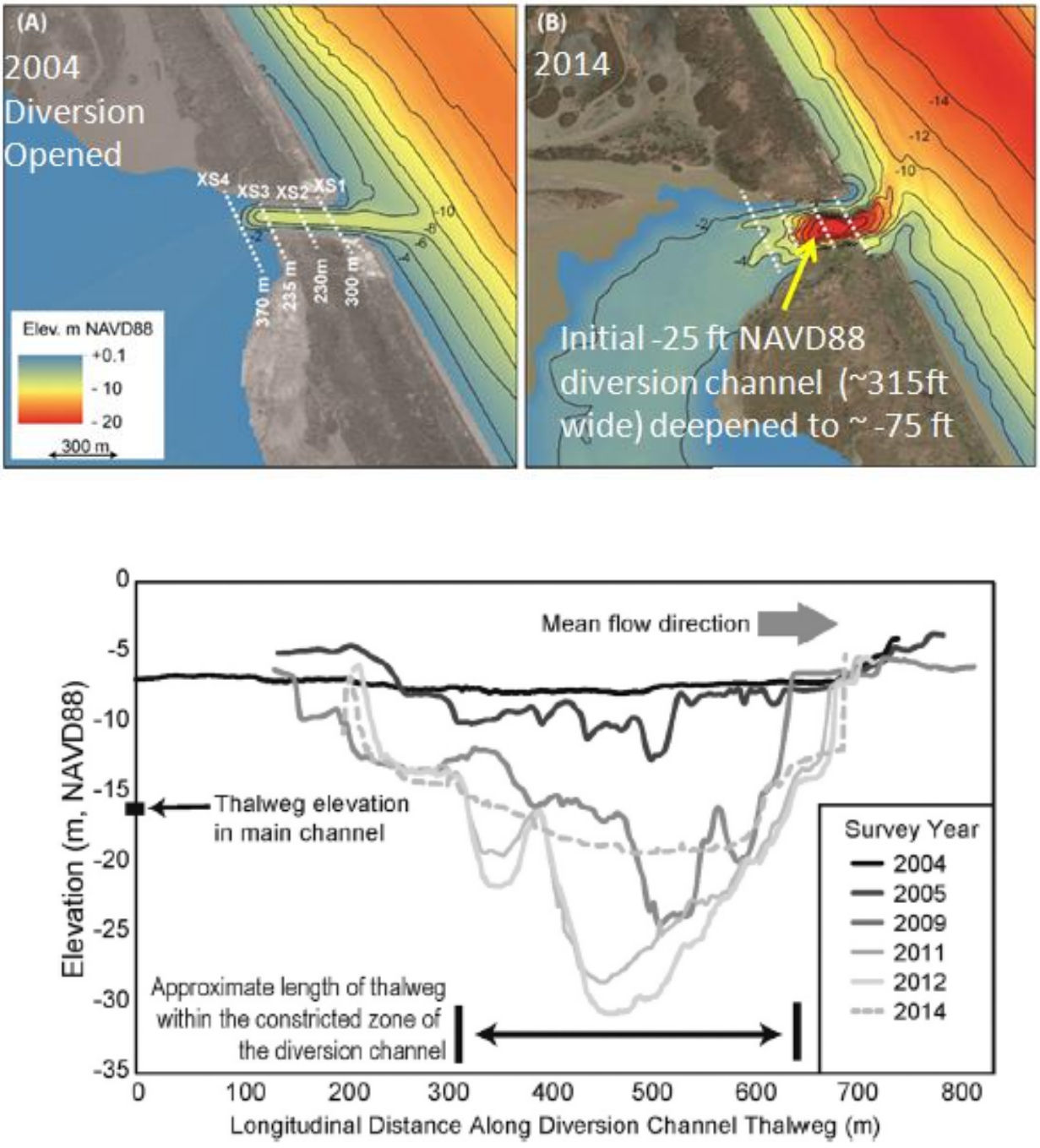

Figure 7.6. Top Panel: Plan view of contours showing evolution of crevasse-splay induced scour and diversion channel widening between 2004 (diversion opening) and 2014. Bottom Panel: Deep scour holes ~-100 ftNAVD88 visible along the diversion channel thalweg (figures adapted from Yuill et al., 2016). Channel widening and infilling reduces the scour depths somewhat (to -60 ft NAVD88) between 2012 to 2014.

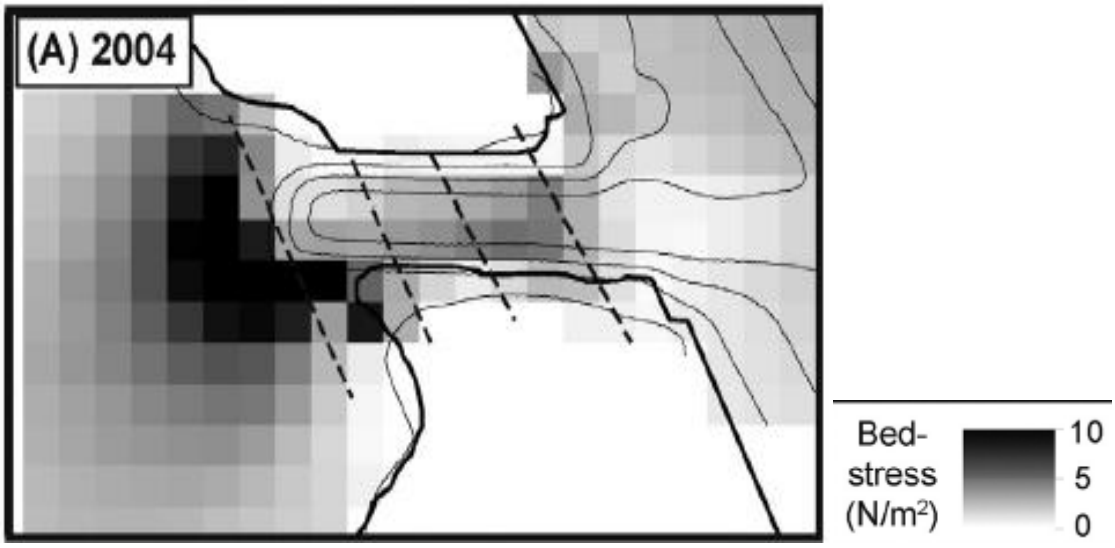

FTN2Comp 3D Delft3D Model for MBSD

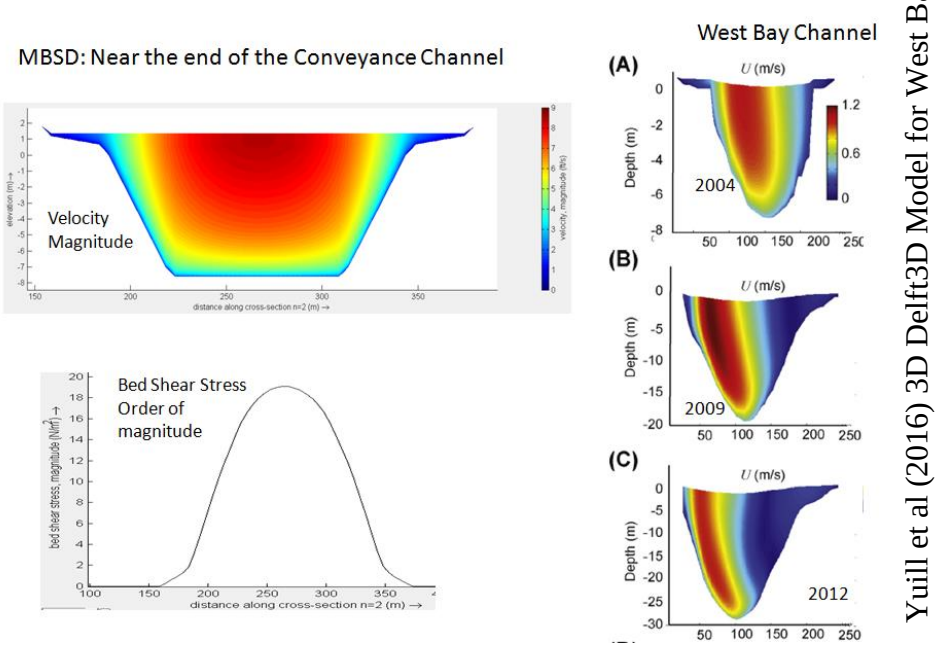

Yuill et al (2016) 3D Delft3D Model for West Bay

Figure 7.7. Top Panel: Bed shear stress distribution from Yuill et al. (2016) Delft3D model for West Bay diversion at the time of diversion opening (2004). Bottom panel: Velocity distribution and bed shear stress at end of conveyance channel (beginning of outfall transition) from FTN2Comp 3D Defl3D model (left figures) at 75,0000 cfs diverted flow for MBSD compared against velocity distribution (right figures) of the West Bay diversion channel.

7.3.1.2 Ayres (2015) Southwest Pass Outlets Bathymetry and Flow Distribution Assessment

Ayres (2015) describes the bathymetry (multi-beam) and flow (ADCP) distribution through the Southwest Pass Outlets of the Mississippi River. Figure 7.8 shows that scour holes with a bottom elevation ranging from about -50 ft, NAVD88 to about -110 ft NAVD88 exist at the four Southwest pass locations. In these outlets, the scour holes are observed at the river entrance to the diversion channel (crevasse initiation zone). The exception is Burrwood Bayou (bottom right) where the deepest hole forms at the open water end towards the Gulf side due to the presence of the emergency control structure. All these locations show scour hole formation whenever flow exits a narrow cross-section (similar to West Bay) into the soft soils that are typical of the Louisiana coast. The close-up of Outlet W-1 shows the deepest hole of ~-110 ft (NAVD88) with steep (~1:2.3 V:H) side slopes along the upstream end. Information such as past surveys and geotechnical cores that would have aided in understanding the historical evolution of these scour holes was not immediately available for use in this report. Nevertheless, based on the publicly available historical stratigraphy information of the Bird's Foot (Balize/Plaquemines) delta area (Kulp et al. 2002, Chamberlain et al. 2018), it is possible that the bottom elevation of these scour holes may be limited by the presence of high shear strength and highly consolidated clay substrata (forming the Pleistocene/Holocene interface zones). The hydrodynamics alone cannot explain such deep scour hole formations. Table 7.1 shows the distribution of discharge through each of these passes. Note that the discharge through Outlet W-1 is only 429-498 cumecs (~15,200 cfs – ~17,700 cfs, much smaller than the 75,000 cfs peak discharge through the MBSD channel) and yet has the potential to cause a ~-110 ft NAVD88 deep scour hole. Considering this, it is reasonable to expect local scour holes as deep or possibly deeper (depending on the depth of the Pleistocene layer) at the MBSD outfall location if no scour mitigation is considered within the MBSD OTF design.

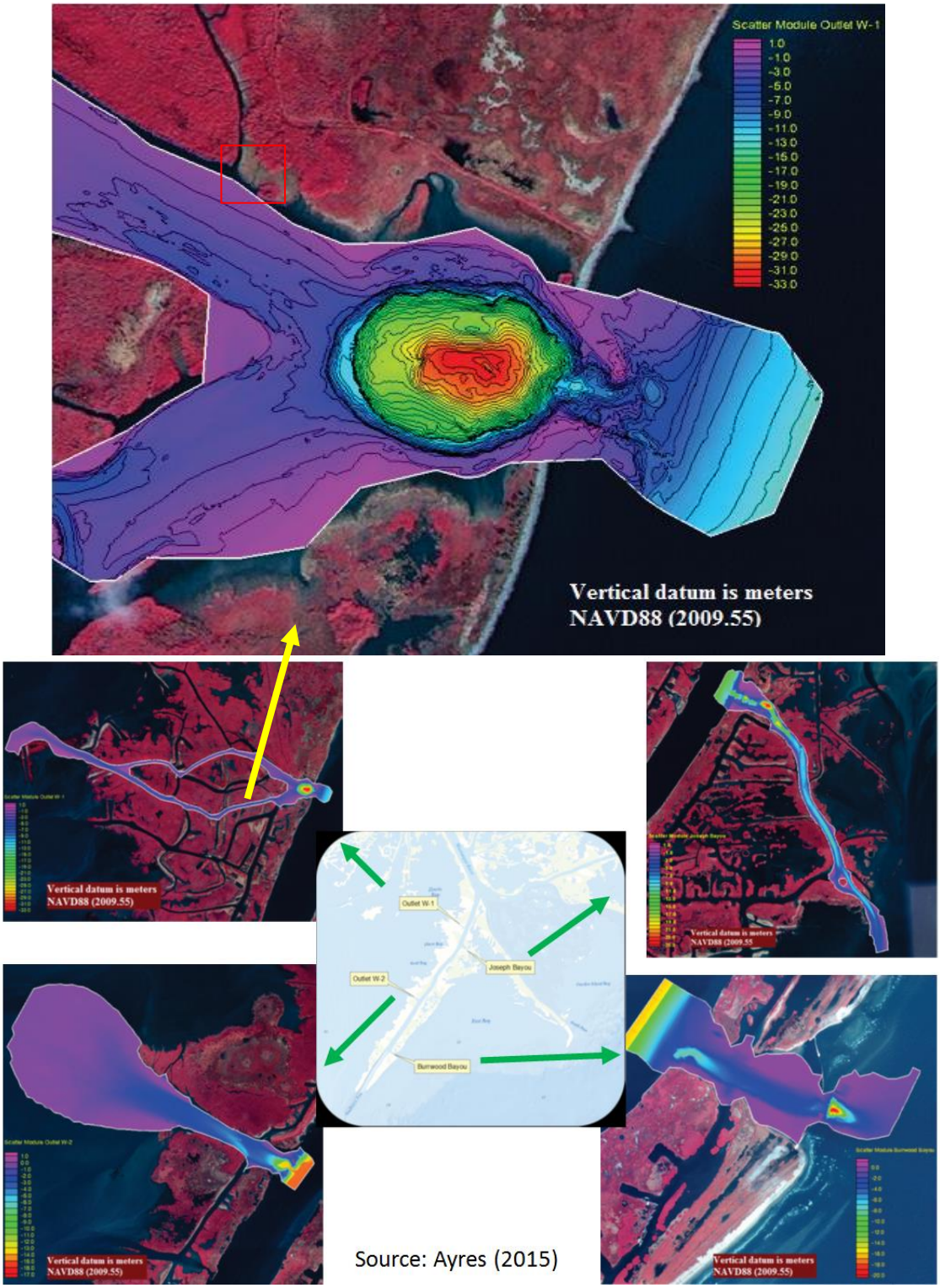

Figure 7.8. Scour holes at four Southwest Pass Outlets. The scour hole bed elevations range from about -50 to -110 ft, NAVD88. The topmost panel shows the close-up of the Outlet W-1 which shows deepest depths of ~-110 ft NAVD88. (Adapted from Ayres [2015]).

Table 7.1. Flow distribution through various Southwest Pass outlets at ebb (top panel) and high-tide (bottom panel) conditions from ADCP data (from Ayres, 2015).

The ADCP measurements summarized in this table were conducted on 14 March 2014 between 1600 and 1845 GMT.	Average Transect Flow $m^3 s^{-1}$	Portion of Total Southwest Pass Flow %	Portion of Southwest Pass Flow at the Outlet %
Southwest Pass Upstream of Outlet W-1	6210	100.0	
Outlet W-1	429	6.9	6.9
Southwest Pass Downstream of Outlet W-1	5596	90.1	
Southwest Pass Upstream of Joseph Bayou	5263	84.7	
Joseph Bayou	709	11.4	13.5
Southwest Pass Downstream of Joseph Bayou	4536	73.0	
Southwest Pass Upstream of Outlet W-2	4596	74.0	
Outlet W-2	870	14.0	18.9
Southwest Pass Downstream of Outlet W-2	3537	57.0	
Southwest Pass Upstream of Burrwood Bayou	2912	46.9	
Burrwood Bayou	380	6.1	13.0
Southwest Pass Downstream of Burrwood Bayou	2601	41.9	
Four Outlets total percentage for this tide condition		38.4	

The ADCP measurements summarized in this table were conducted on 15 March 2014 between 1320 and 1700 GMT.	Average Transect Flow $m^3 s^{-1}$	Portion of Total Southwest Pass Flow %	Portion of Southwest Pass Flow at the Outlet %
Southwest Pass Upstream of Outlet W-1	5619	100.0	
Outlet W-1	498	8.9	8.9
Southwest Pass Downstream of Outlet W-1	5081	90.4	
Southwest Pass Upstream of Joseph Bayou	5181	92.2	
Joseph Bayou	894	15.9	17.2
Southwest Pass Downstream of Joseph Bayou	4003	71.2	
Southwest Pass Upstream of Outlet W-2	4479	79.7	
Outlet W-2	793	14.1	17.7
Southwest Pass Downstream of Outlet W-2	3490	62.1	
Southwest Pass Upstream of Burrwood Bayou	3482	62.0	
Burrwood Bayou	505	9.0	14.5
Southwest Pass Downstream of Burrwood Bayou	2927	52.1	
Four Outlets total percentage for this tide condition		47.9	

7.3.1.3 Evolution of Mardi Gras Pass of the Mississippi Delta in Southeast Louisiana: March 2012 through December 2013

Lopez et al. (2014) describes the evolution of the Mardi Gras Pass (MGP) which was originally disconnected from the Mississippi River and was formed from two preexisting conveyance canals associated with the now defunct Bohemia Diversion. MGP first showed signs of development during the Mississippi River flood of May 2011, when overbank flooding during the receding flood cut a new, 630-foot-long channel across the crest of the river's natural levee. This resulted in the connection of two preexisting conveyance canals. Subsequently, during the early high water of the 2012 annual flood, headward erosion started progressing upstream through a forested river bar. Scour holes as deep as 34-50 feet were visible in 2013 (Figure 7.9). Headward erosion during January and March 2012 propagated the MGP channel further upstream through the forested bar until it reached the Mississippi River during February 2012 (i.e., Mardi Gras season). The peak diverted discharge through MGP during this period was only 2,300 cfs (Figure 7.10), yet it led to a fast head-cut propagation. This rapid head-cut propagation triggered from the downstream scour holes typically propagates in the form of mass erosion (Figure 7.11), physical processes that cannot be captured by simple morphology-based models and demonstrates that an uncontrolled scour propagation is an important consideration for the outfall design.

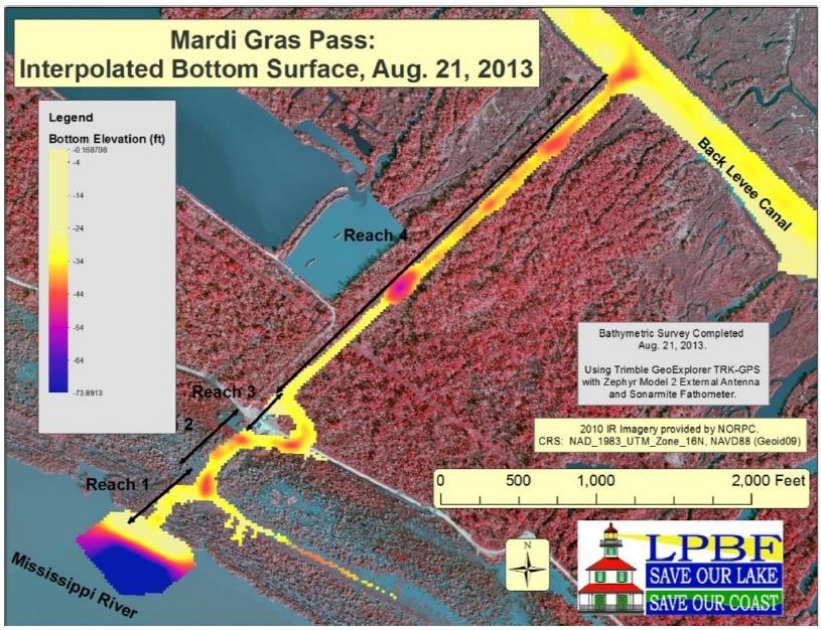

Figure 7.9. Bathymetry showing location of scour holes along Mardi Gras pass after the head-cut reached the river (Lopez et al., 2014)

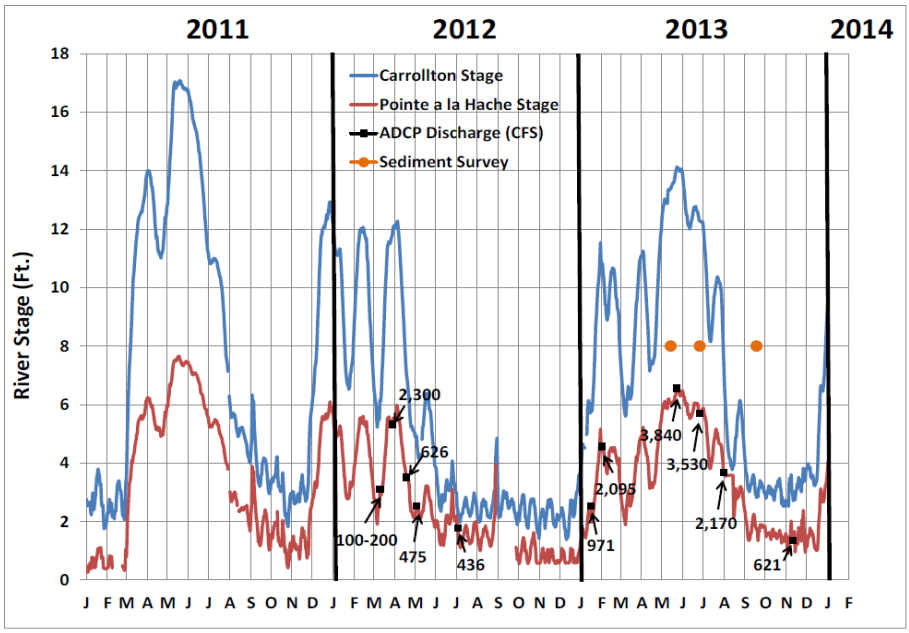

Figure 7.10. Mississippi River stage and corresponding diverted discharge though MGP during the period of head-cut reaching the river. Discharge ranged from 100-2,300 cfs during January-March 2012 when head cut propagated upstream and joined with the Mississippi River (Lopez et al., 2014).

Figure 15: Collapse of slump and tree root ball due to undercutting and bank erosion in Reach 1 of Mardi Gras Pass, January 23, 2013.

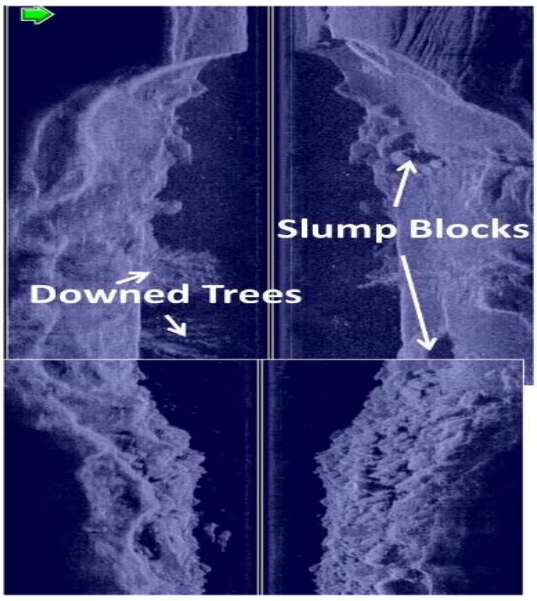

Figure 7.11. Head-cut processes in pictures. Head-cut propagated within 2-3 months (Jan-Mar 2012) through a wooded area and joined with the Mississippi River. Evidence of mass erosion as slump blocks along banks and underwater downed trees in side-scan sonar. (Lopez et al., 2014).

7.3.1.4 TO5 Outfall Management: Mid-Barataria and Mid-Breton diversions. The Water Institute of the Gulf. Technical Report to the LA CPRA.

A two-dimensional Delft3D coupled flow and morphology outfall model study conducted by WI using the WIOMBA (Esposito et al. ,2017) model predicted scour hole formations at the OTF location at MBSD (Figure 7.12) with elevations below -55 ft, NAVD88 for both Highly Consolidated (HC) (critical shear stress 1.0 Pa) as well as Very Highly Consolidated (VHC) (critical shear stress 2.5 Pa) clay scenarios within 1 to 5 years.

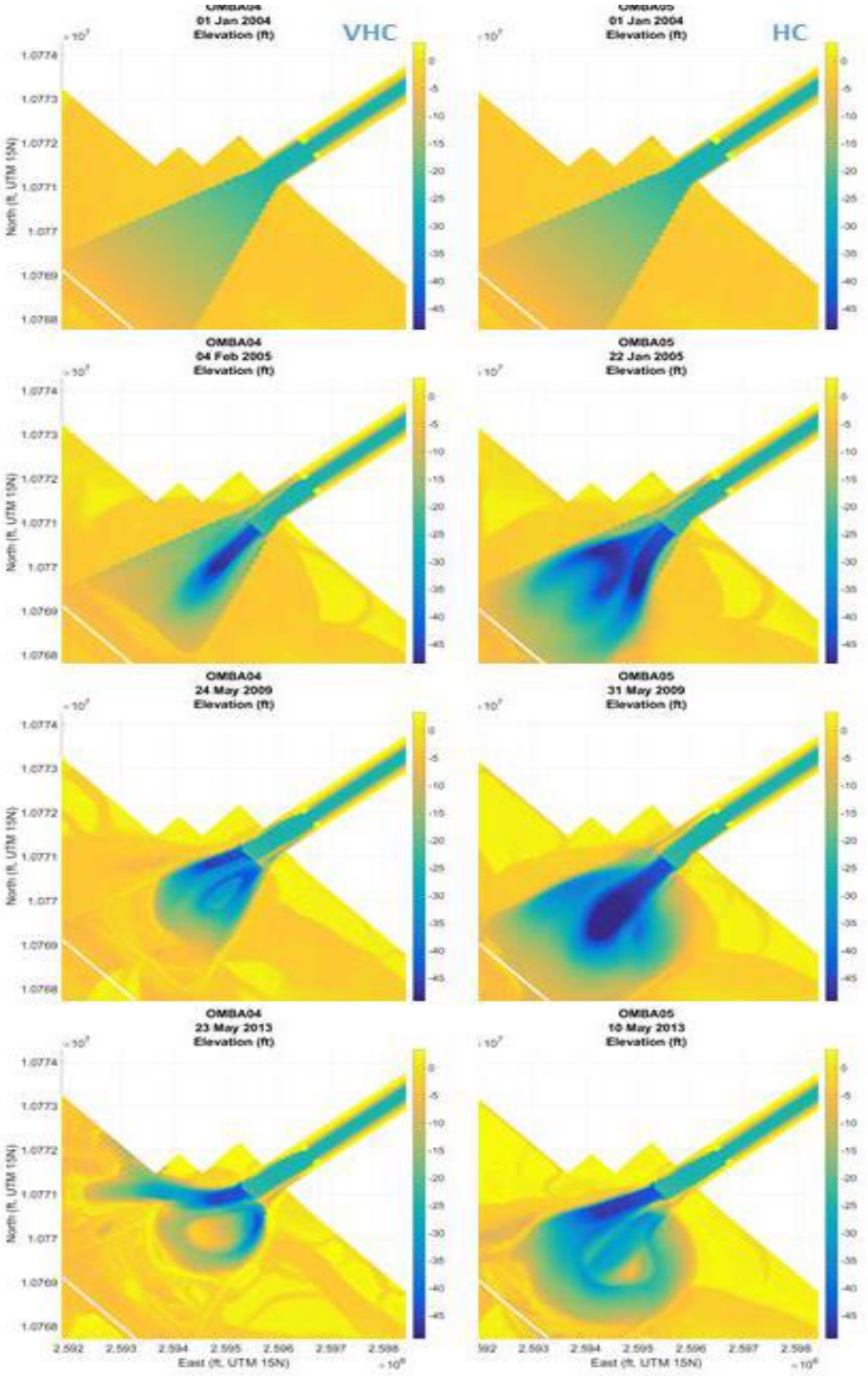

Figure 7.12. WIOMBA Very Highly Consolidated (VHC) run to the left and Highly Consolidated (HC) run to the right. Deep scour holes (bed elevations lower than -55 ft NAVD88) appear in the first year (2nd row from top) which fill to some extent as simulation progresses. HC shows deeper holes even after 3 years than VHC. (Esposito et al. 2017).

7.3.1.5 Davis Pond Diversion Canal Scour Observations

The Davis Pond diversion is located near Luling, LA, on the west bank of the Mississippi River in St. Charles Parish at River Mile 118.4. The diversion flow is determined by specified salinity targets at two locations in Barataria Basin. The operation plan calls for a minimum diversion flow of 1,000 cfs and the maximum flow of 10,000 cfs (CPRA 2020). The topographic survey of the diversion canal conducted by the USACE in 2015 were provided by CPRA as shown in Figures 7.13 and 7.14. The scour in the canal was observed to reach up to -20 to -25 ft NAVD88 over a 1.5-mile zone starting from the outfall and extending into the outfall channel.

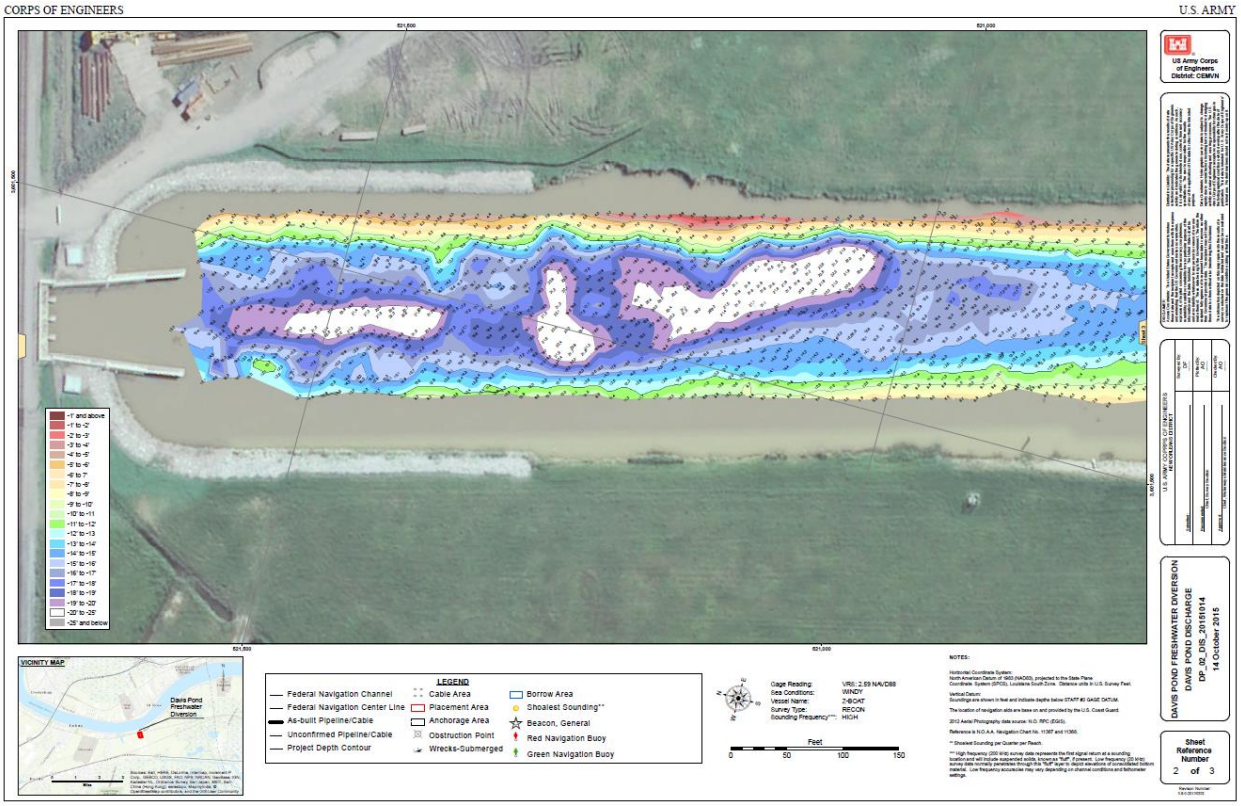

Figure 7.13. Topographic survey of the Davis Pond diversion canal Segment 1.

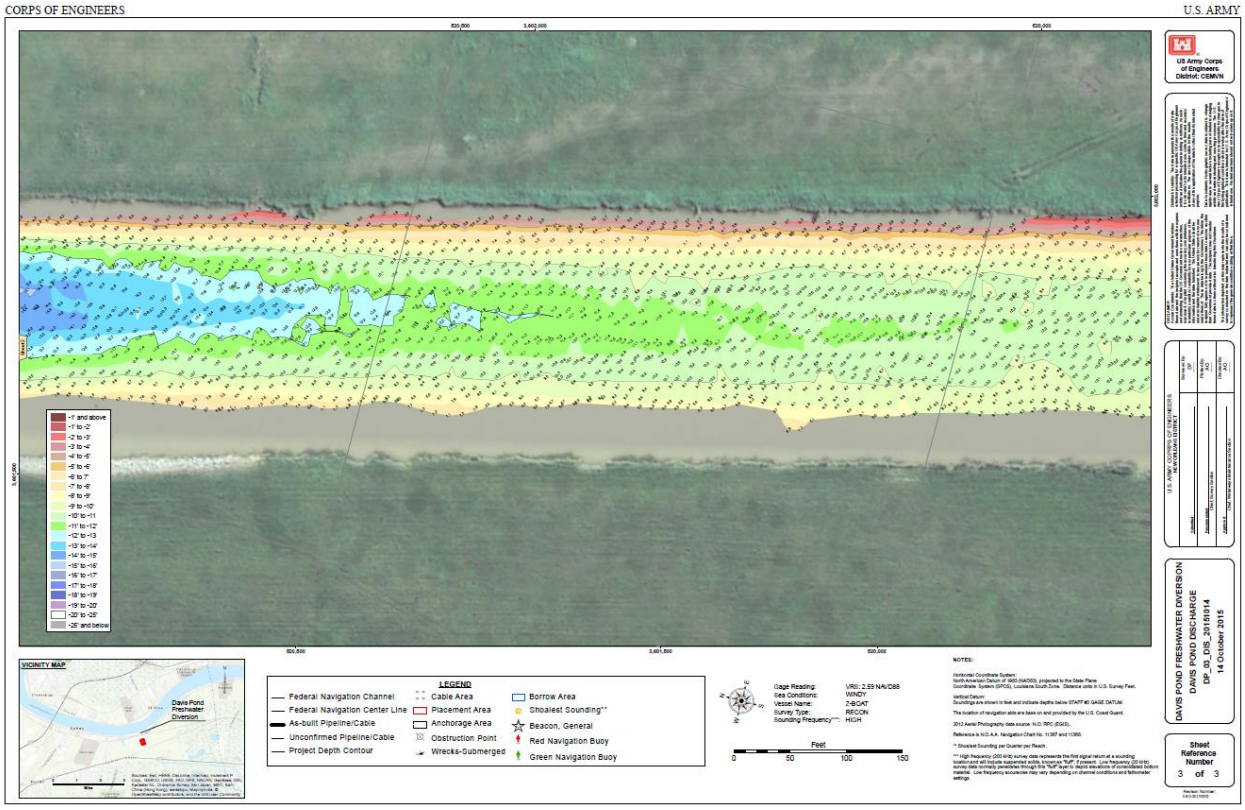

Figure 7.14. Topographic survey of the Davis Pond diversion canal segment.

7.3.2 Outfall Morphology Model Setup

The 2D Delft3D FTNOMBA fully coupled FLOW-Morphology model was used to model the outfall scour evolution. The Delft3D model uses the linear Partheniades-Krone (Partheniades, 1965) formulation to calculate the erosive flux for cohesive sediment as follows:

$$E = M\left(\frac{\tau_b}{\tau_{cr}} - 1\right) \text{ ..... (I)}$$

Where, $\tau_b = \frac{\rho g U|U|}{{C_{2D}}^2}$ ..... (II) is the bed shear stress calculated using the quadratic law of bed friction for 2D model. The law uses the Chezy coefficient, $C_{2D} = \frac{h^{1/6}}{n}$, where h is the water depth and U the depth-averaged velocity and n is the Manning's coefficient.

Therefore, the two principal main input parameters of stratigraphy definition to the model are the critical shear stress of erosion (τ_{cr}) and the erodibility parameter (M).

The FTNOMBA model was refined by a factor of 4 (i.e., the grid size was refined by a factor of 2 in each of X and Y directions) within an approximately 3-mile radius of the outfall. The refined FTNOMBA model, henceforth termed as FTNOMBARefined has a uniform grid size of 7 m (~23 ft) within this zone. The FTNOMBA model had a 15m (~49 ft) uniform grid size within this zone. This refinement was necessary to adequately resolve the scour hole evolution and propagation within the outfall vicinity.

The Barataria Bay bathymetry uses the current bathymetry (Year 0) as supplied by CPRA while the river bathymetry is set as the US Army Corps of Engineers (USACE) 2013 bathymetry as was used in previous modeling with FTNOMBA. During the initial design phases, the OTF lengths of 1,500 ft (with 850 ft non-erodible), 1,500 ft (all non-erodible, 3,200 ft (all non-erodible) and 4,500 ft (all non-erodible), where distances are calculated from the end of the existing NOV back-levee were evaluated for scour evolution.

For the upstream MR boundary at RM 66, a discharge hydrograph (Figure 7.15) observed during the 2008 annual flood (February 10, 2008 through July 31, 2008) when the MR flow exceeded 400,000 cfs was used. The 400,000 cfs start for the simulation was selected to allow sufficient time for model initialization before it reached the 450,000 cfs flow, the currently adopted trigger for diversion operation. Further, the year 2008 was selected for evaluation because the river reached well over 1,000,000 cfs and remained over ~900,000 cfs for about 3 months that would allow modeling a continuous diversion flow of 75,000 cfs for 3 months. Analysis of the MR hydrograph over the last 10 years (2008-2018) suggests such high flow years are becoming increasingly common and it is not unusual to consider years such as 2008 for the design evaluations of the outfall. The downstream boundary of the MR at RM 56 used a Q-H (stage-discharge) relation. The southern Gulf of Mexico boundary was set to a 0.25 m (0.82 ft) constant water level representative of the current MWL at Port Fourchon.

To simulate a conservative scenario for the OTF design, no river sediment was introduced into the model. Moreover, the amount of river sediment is not expected to be significant over a one-year hydrograph to “fill in” the hole. Therefore, relying on the river sediment to mitigate the concerns over the large-scale scour propagation, a relatively rapid process, is not recommended for design. A morphological acceleration factor (MorFac) of 80 was selected for all production runs. Sensitivity analysis (presented later) indicated that the scour

evolution is less sensitive to MorFac (range 20-80) compared to the other model parameters. The bed stratigraphy was defined as a top 'marsh' layer above -5 ft, NAVD88 underlain by a relatively consolidated 'compact' layer. Note that within the immediate outfall area (~ 1 mile) the average basin elevation being at ~-4ft, NAVD88 and most of it is submerged under water, so there is no marsh layer in the vicinity where the scour hole forms.

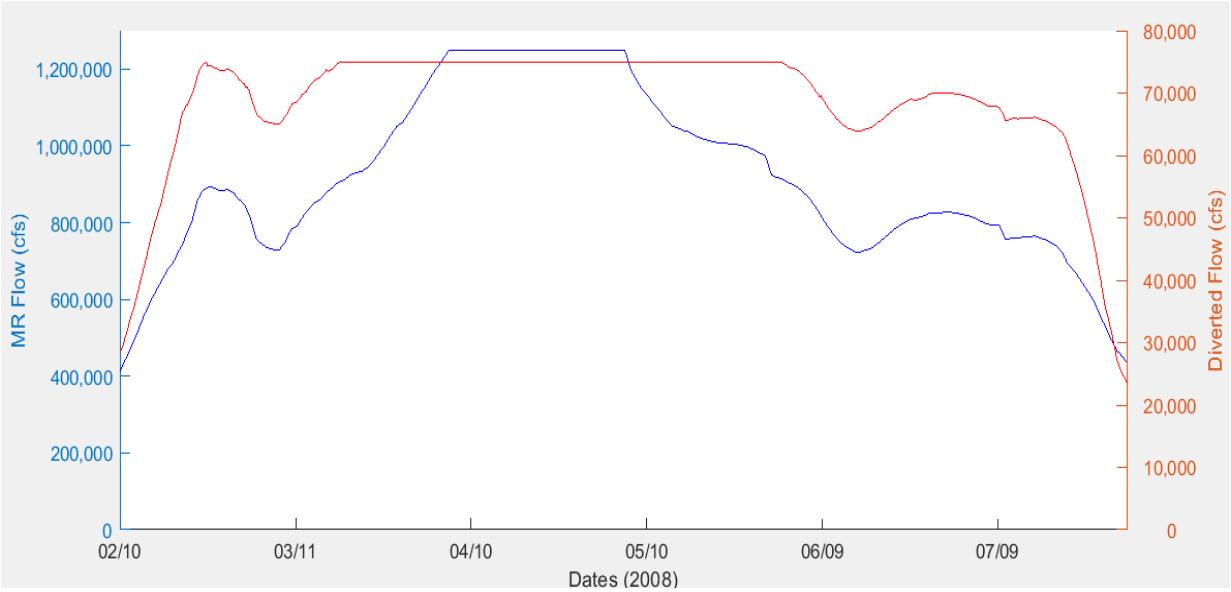

Figure 7.15 MR Flow hydrograph (in blue, left axis) and MBSD diverted discharge (in red, right axis) for the 2008 flood year hydrograph.

7.3.3 Estimation of Critical Shear Stress of Erosion and Erodibility of Native Marsh Soil

Two different approaches were used to determine the erosion properties for the native marsh soil for use in the Delft3D model. The first approach involved estimating the critical shear stress of erosion and erodibility from observed geotechnical parameters. Later in the design phase SEDflume (Integral 2020) methodology was used to estimate the critical shear stress and erodibility from laboratory erosion tests on collected cores.

For critical shear stress estimation from the geotechnical properties of the outfall borings collected at the site (Figure 7.16) established equations from peer-reviewed literature (Winterwerp and vanKerstern 2004, Winterwerp et al. 2012, Mitchener and Torfs 1996, Smerdon and Beasely 1959) for cohesive soil were used. These equations relate the common geotechnical

properties to the two model parameters. The borings OF1 through OF6 were collected in the outfall area within 4,500 ft from the end of the conveyance channel.

Figure 7.17 shows the depth variation of bulk density, dry density and the plasticity index for the 6 cores. The depth is measured below the existing mudline at ~ -4 ft to -5 ft, NAVD88. The first 10 ft below the mudline shows a large scatter in all the geotechnical parameters and is likely due to the large organic content that is expected in these wetland soils. The plasticity index shows values greater than 100%, representative of very high liquid limits and were excluded as they fell beyond the range of applicability of the equations. The remaining data was used to calculate critical shear stress of erosion (Figure 7.18) for all the samples using the three independent equations as given below. The plasticity index values (Figure 7.17, bottom panel) as well as the visual classification of the samples (Table 7.2) suggests that mostly high plasticity fat clays are present 15 ft below the mudline and relationships developed for purely cohesive high plasticity cohesive soils are appropriate. The purpose of using three independent formulations is to reduce the uncertainty inherent in these formulations. Uncertainties in estimates of critical shear stress from geotechnical parameters stem from the difference in erosion test apparatus, experimental conditions (particularly the consolidation state of the test material), hydraulic parameterization of the bed shear stress in the equations themselves, percentage of sand/silt/clay present, and organic content in the sample among other factors. For engineering design, it is important to consider estimates from different sources of these equations and carefully consider the applicability of the range of these estimates for the field conditions.

Winterwerp et al., (2012) combined data from a number of experiments and sites to arrive at a single best-fit relation that relates critical shear stress of erosion (τ_{cr}) to the plasticity index of the soil (PI %) as follows:

$$\tau_{cr} = 0.7 * PI^{0.2} \quad \text{(III)}$$

The limits of the spread in the data for this fit are given by the relations,

$$Low: \tau_{cr} = 0.35 * PI^{0.2}$$
$$High: \tau_{cr} = 01.4 * PI^{0.2}$$

Equation III, is applicable for soils with PI>7%.

This relation implicitly includes the effects of the sediment composition (sand-mud ratio) and of organic material on the critical shear stress because the Atterberg limits (PI=Liquid Limit-Plastic Limit) themselves directly depend on the sediment composition and organic material.

Mitchener and Torfs (1996) suggested the following relation which relates critical shear stress of erosion with the bulk density (BD) of the soil,

$$\tau_{cr} = 0.015 * (16.02 * BD - 1{,}000)^{0.73} \quad \text{(IV)}$$

The factor 16.02 converts bulk density in lb/ft^3 to kg/ m^3. Samples with bulk density greater than 2600 kg/m^3 very near the submerged mudline are neglected from this calculation.

Smerdon and Beasley (1959)'s relation also considers the plasticity index (PI %) and is applicable for PI<70% as follows,

$$\tau_{cr} = 0.105 * PI^{0.82} \quad \text{(V)}$$

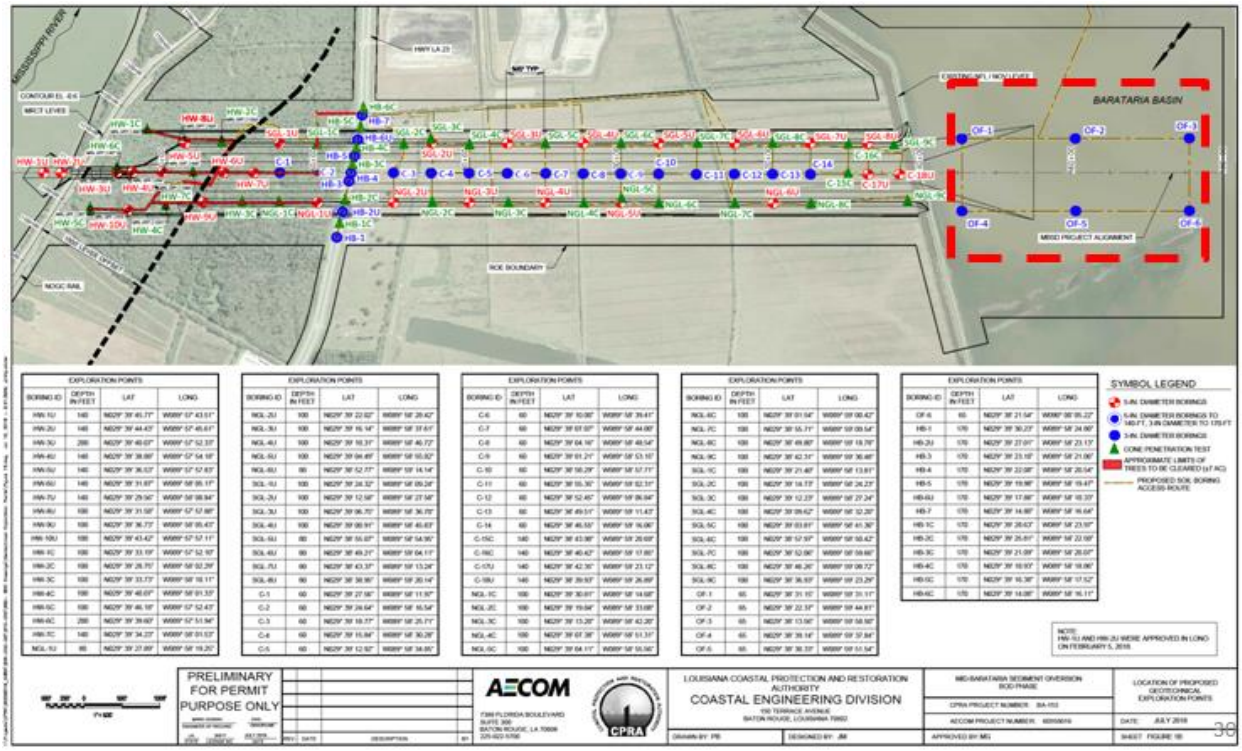

Figure 7.16. Outfall boring locations (OF 1-6, marked inside the red dashed line box to the right) within ~4,500 feet of the end of the conveyance channel, the region of potential scour.

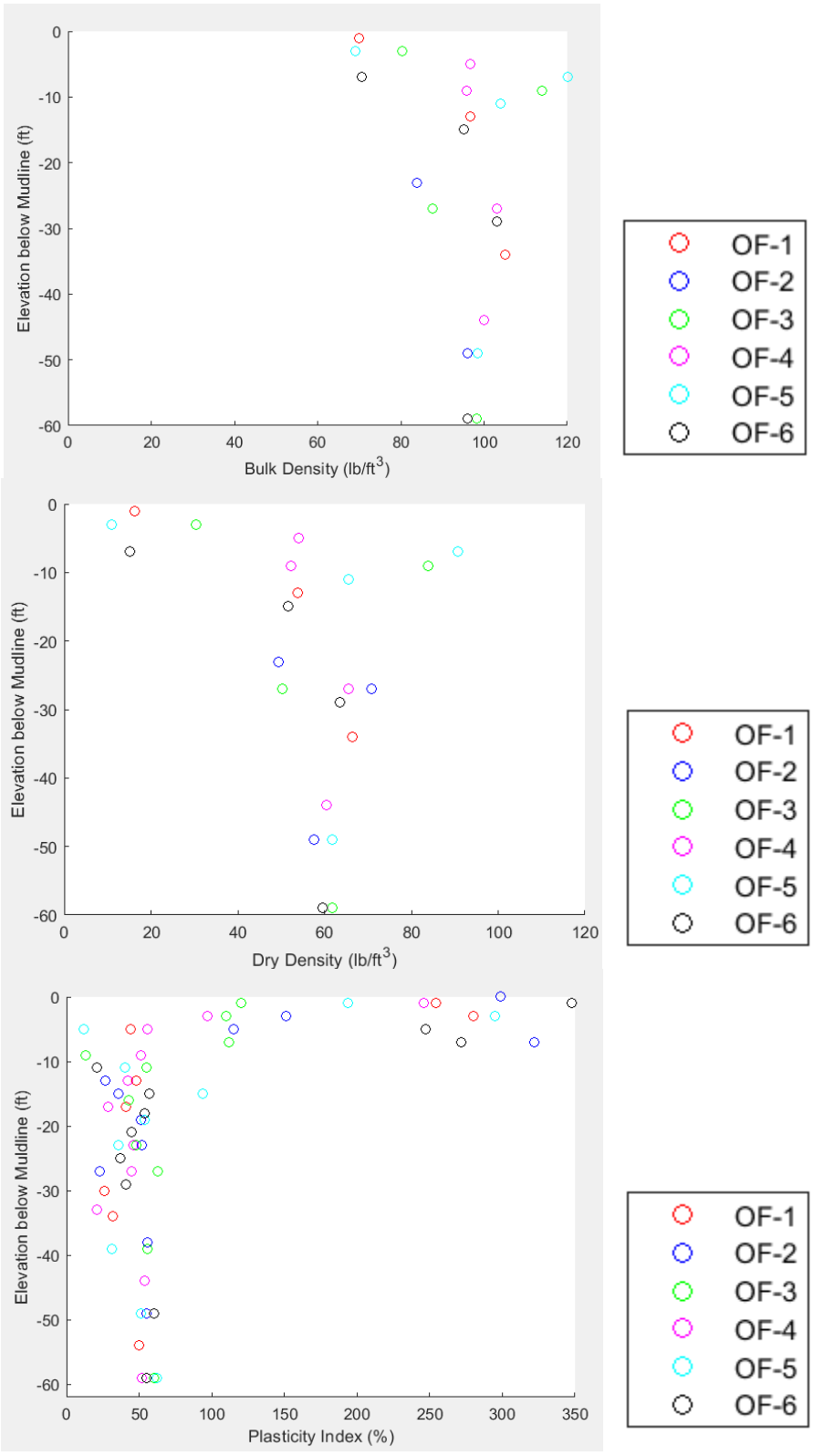

Figure 7.17. Depth variation of Bulk Density, Dry Density and Plasticity Index at the six outfall boring locations. Depth is measured below the existing mudline at ~-4 ft, NAVD88.

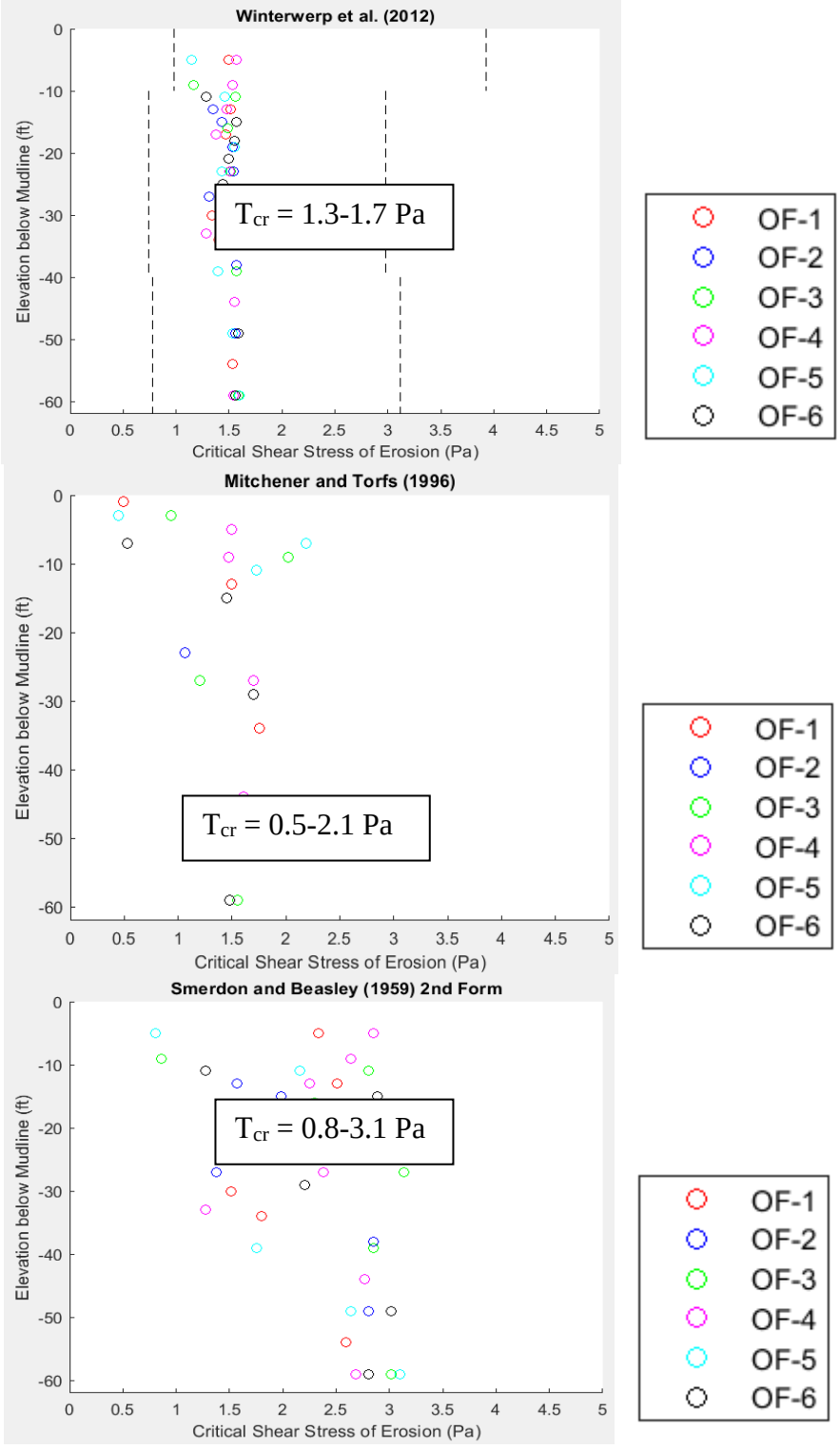

Figure 7.18. Critical shear stress of erosion calculated using Winterwerp et al., 2012 (top panel), Mitchener and Torfs, 1996 (middle panel) and Smerdon and Beasley, 1959 (bottom panel). The inset boxes show the range of the shear stress values from each relation.

Table 7.2. Visual classification of the samples collected at OF 1-6 sites.

BORING	SAMP_NUM	DEPTH (ft)	LAB_USCS	LAB_CLASS
OF-1	1A	0	PT	VSO DGR PT
	1B	1	CHOC	VSO DBR CHOC
	7B	13	CH3	VSO GR CH3 W/ ARS ML
	16B	34	CH2	SO GR CH2
OF-2	3B	5	CHOC	VSO GR CHOC W/ RT
	12B	23	CH3	VSO GR CH3 W/ ARS ML & SP
	14B	27	CL6	VSO GR CL6 W/ SIF
	19B	49	CH4	SO GR CH4 W/ ARS ML
OF-3	2B	3	CHOB	VSO GR CHOB W/ RT, SIF, ARS SP
	5B	9	CL4	SO GR CL4 W/ ARS SP
	14B	27	CH4	VSO GR CH4 W/ ARS ML
	21B	59	CH3	SO GR CH3 W/ ARS ML
OF-4	3B	5	CH4	VSO GR CH4 W/ ARS ML & SP
	5B	9	CH3	VSO GR CH3 W/ ARS ML, O
	14B	27	CH3	VSO GR CH3 W/ ARS ML & SP, O, SIF
	18B	44	CH4	SO GR CH4 W/ ARS ML
OF-5	2B	3	CHOC	VSO DBR CHOC
	4B	7	ML	GR ML W/ ARS CH & SP
	6B	11	CH3	VSO GR CH3 W/ ARS ML
	19B	49	CH3	SO GR CH3 W/ ARS ML
OF-6	4B	7	PT	VSO BR PT
	8B	15	CH4	VSO GR CH4 W/ ARS & LNS ML
	15B	29	CH3	VSO GR CH3 W/ ARS ML & SP
	21B	59	CH4	VSO GR CH4 W/ ARS ML

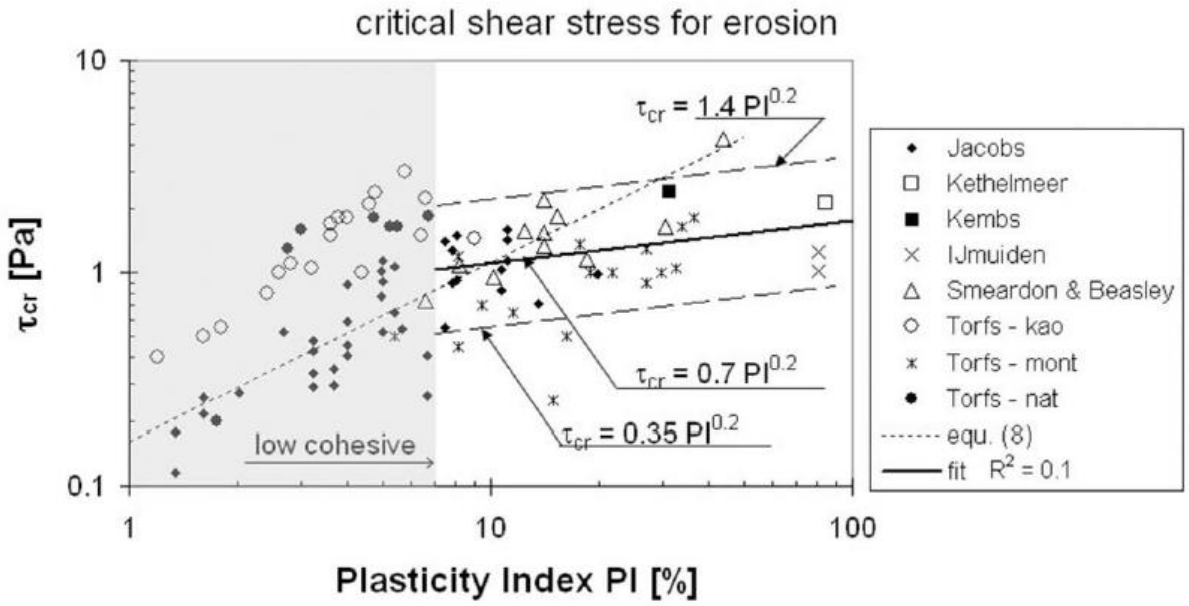

Figure 7.19. Critical shear stress of erosion relation for cohesive soils (Figure adapted from Winterwerp et al., 2012).

The above relations (III, IV, and V) were used to calculate critical shear stress for erosion of all the samples as shown on Figure 7.18. The inset boxes show the range of variation of the shear stress values calculated from each relation. Based on these results the critical shear stress range is most likely between 1.5 Pa and 2.5 Pa, which was subsequently selected for sensitivity testing in the model.

For the erodibility parameter, a wide range of values can be found in the literature ranging from 0.01 x 10^3 to 0.5 x 10^3 kg/m^2/s for fairly fresh deposits (Whitehouse et al. 2000). For the consolidated clay deposits this value can be much lower. According to Winterwerp et al. (2012) the scatter in the unconfined, consolidated coefficient (C_v) is prominent in the observed specimens and depends on the state (over-consolidated/ under consolidated) of the sample when it is subjected to the erosive forces. An example of this can be found in the studies by Briaud et al. (2017) who conducted erosion tests on various samples of clay. The CL (low plasticity clay) and CH (high plasticity clay) sample results for erosion rate are shown on Figure 3.6. The figure shows that unlined critical shear stress erodibility is not a simple function of the plasticity. The slope of the lines through this data provides the erodibility estimate and shows a spread of 4 orders of magnitude. Assuming a mean dry bed density of 1000 kg/m^3 (62.5 pcf) (Figure 3.2)

and a mean critical shear stress of 2 Pa, the medium range slope yields an M value (erodibility parameter) of ~$9x10^{-4}$ kg/m^2/s. In their Delft3D morphology modeling on the east side of the river, the WI used a value of $1x10^{-3}$ kg/m^2/s based on the field data collected at Breton Sound (Meselhe et al., 2015). Considering the variability discussed above, a range of $1x10^{-4}$ to $1x10^{-3}$ kg/m^2/s was selected to test the sensitivity of the erodibility parameter, M.

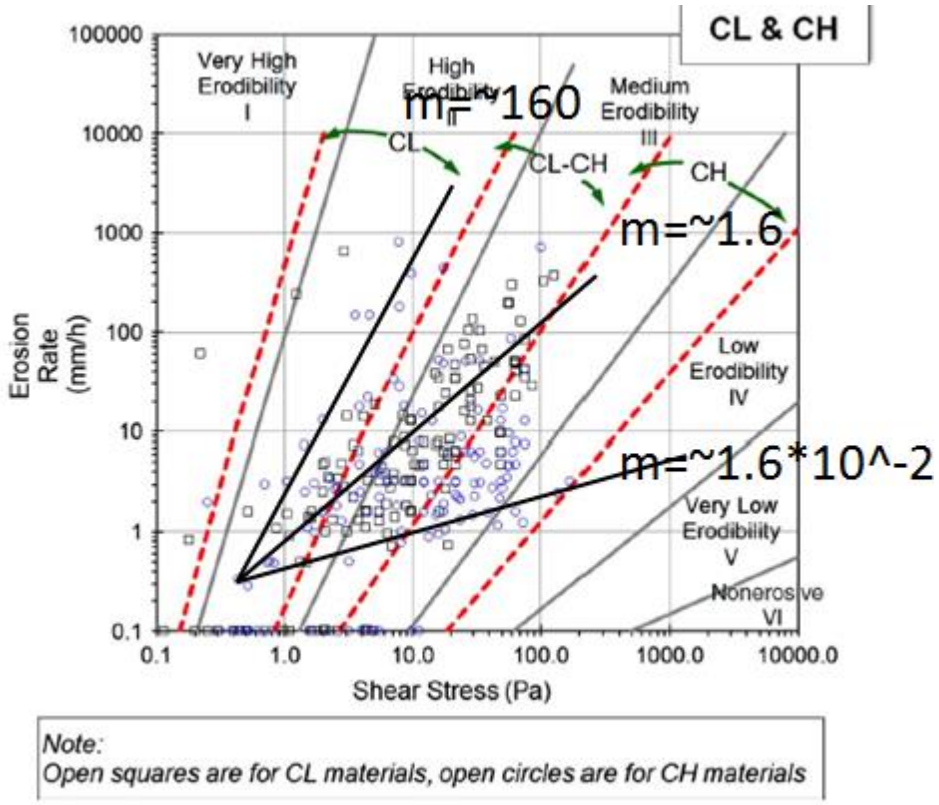

Figure 7.20. Erosion rate as a function of critical shear stress for consolidated clay samples (Figure adapted from Briaud et al., 2017). Black lines are drawn to indicate approximate High, Medium and Low fit slopes through the data.

In addition to geotechnical data, SEDflume (Integral, 2020) data analysis was conducted from about 120 samples collected at the OTF site (Figure 7.21). The laboratory data for erosion rate and imposed critical shear stress was plotted for every sample as in Figure 7.22 and a linear Partheniades-Krone (Equation I) was fitted to it. Critical shear stress and erodibility was obtained as the regression parameters of this fitting. Since most of the hydraulic shear stresses expected in the field are below 15 Pa, only the linear portion of the data erodibility between 0 to 15 Pa of

imposed shear stress was used for fitting. Further for most samples mass erosion is expected to occur above 15 Pa as dynamic pressure of the fluid on the sample surface is expected to exceed 2-3 times the direct shear strength (Cu) of the soil and the erosion model is not applicable for mass erosion.

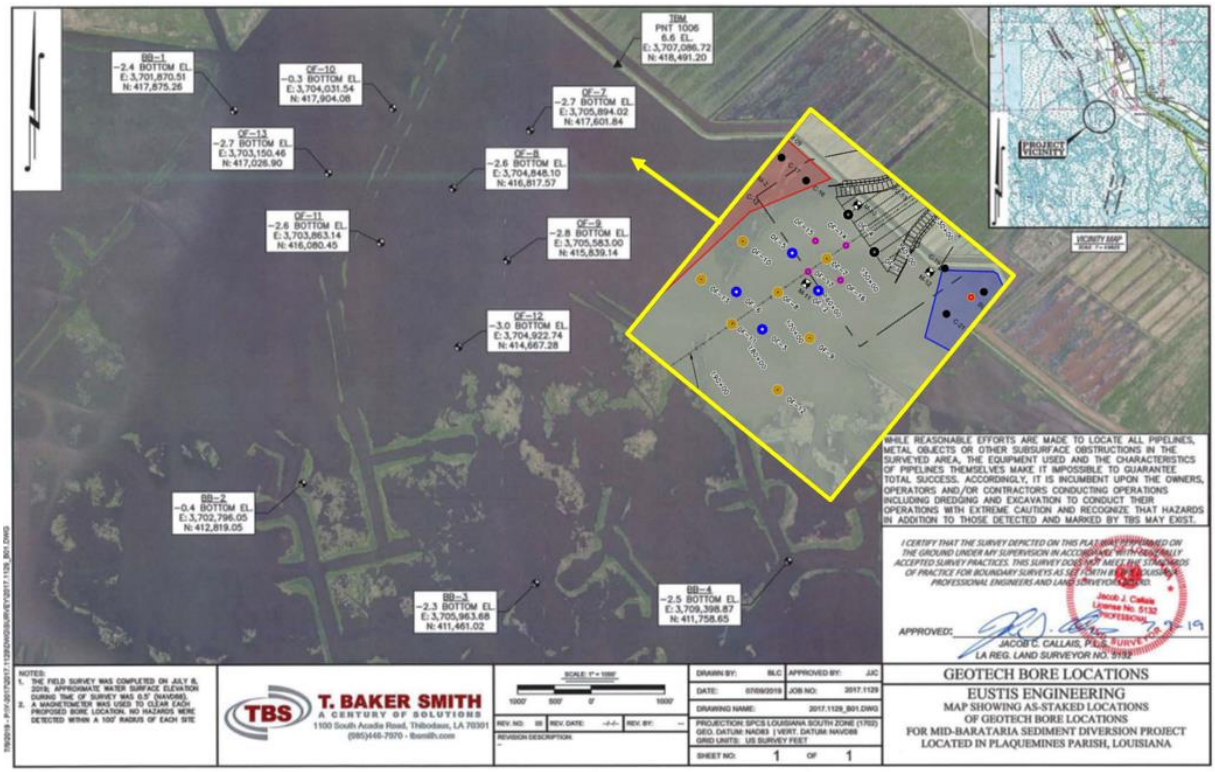

Figure 7.21. Locations at which samples (up to about 120 ft below mudline) were collected for SEDflume analysis.

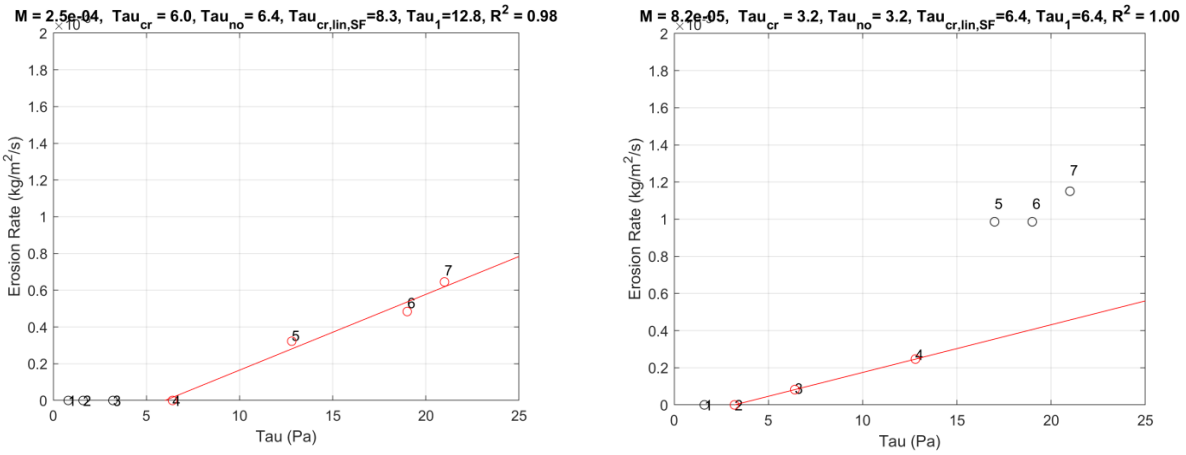

Figure 7.22. Example of linear Partheniades-Krone type erosion model fitting to observed SEDflume data from a given sample shown here. The process was repeated for more than 100 samples. Only the linear portion of the data between 0-15Pa was utilized for fitting.

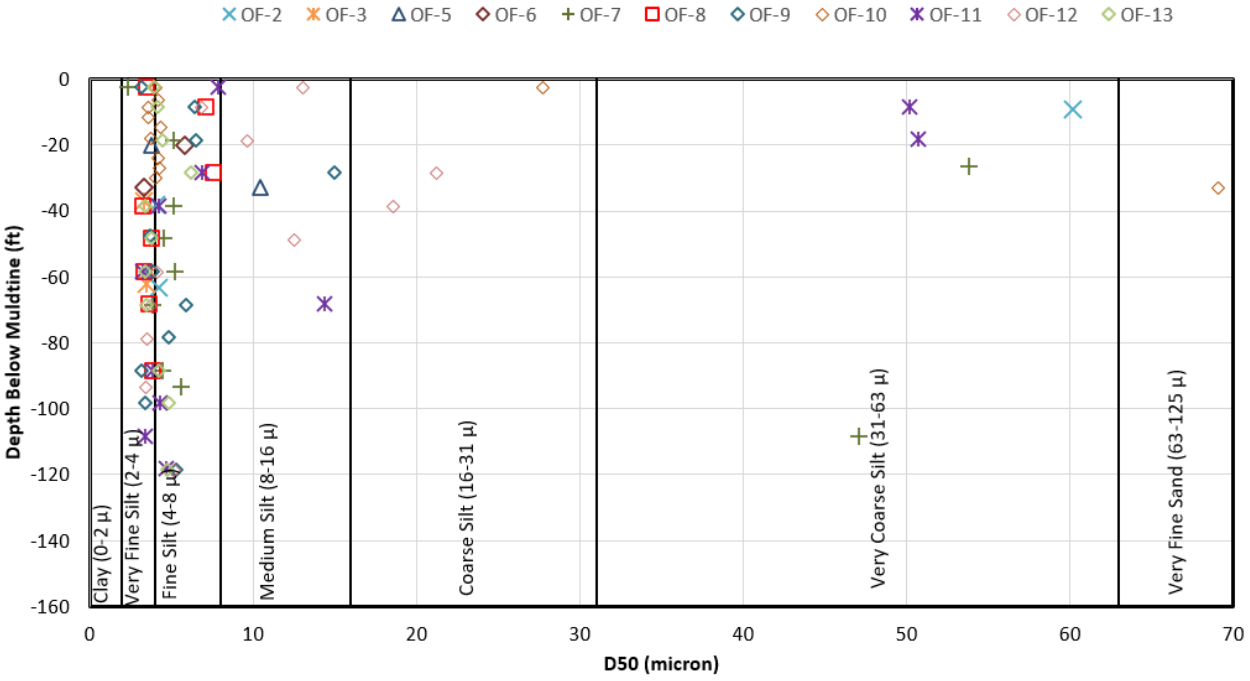

Figure 7.23. Grain size analysis (Beckman-Coulter method) of the collected sample cores plotted against depth below mudline. Data shows that most of the layer above 60 ft below the mudline in the OTF area is composed of very fine to fine silt with intervening layers of medium to very coarse silt.

In addition to critical shear stress, the grain size distribution was analyzed and the median size (D50) of the samples were calculated. The depth variation of the samples (Figure 7.23) indicated that while the majority of the samples at the outfall location were composed of very fine to fine silt (2-8 micron), the layer above 60 ft below mudline had numerous intervening layers of medium to very coarse (8-63 micron) silt as well.

The critical shear stress and erodibility from the SEDflume analysis along with the sediment type is shown in Table 7.3. The results show that the critical shear stress of erosion increases with decrease in median grain size due to increase of cohesive properties of the material. Very coarse to coarse silt ranged between 0.5-2 Pa while medium to fine silt ranged between 1-5 Pa median critical shear. In particular large scatter was observed for fine and very fine silt samples and critical shear stress ranged between 0.3-17 Pa.

Figure 7.24 shows the frequency distribution (number of samples) at any given range of critical shear stress and shows that the bulk of the samples had critical shear below 4 Pa with the maximum between 1-2 Pa. In view of the large range of variation of the critical shear stress for fine and medium silt, the presence of intervening coarse to very coarse silt layers within 60 ft below mudline and the fact that the majority of the OF samples had a critical shear between 1-2 Pa, it was decided to use 1.5 Pa as the spatially uniform critical shear for the Delft3D production runs for scour estimation comparing different designs. Note that attempts to create a spatially variable distribution of the stratigraphy was not successful because of the very large horizontal variability spatially (even over 10s of meters) and only a few meters vertically. The fact that critical shear stress is very sensitive to the silt classification and the change in erosion characteristics due to factors beyond the scope of this study (e.g., salinity effects on cohesion, consolidation effect on cohesion, difference in structural characteristics depending on deposition mechanism, bioturbation, etc.) it was decided to use a spatially averaged ‘most probable’ value for the modeling. Nonetheless sensitivity analysis in the 1-2.5 Pa range was performed to quantify its effect on the modeled scour depths.

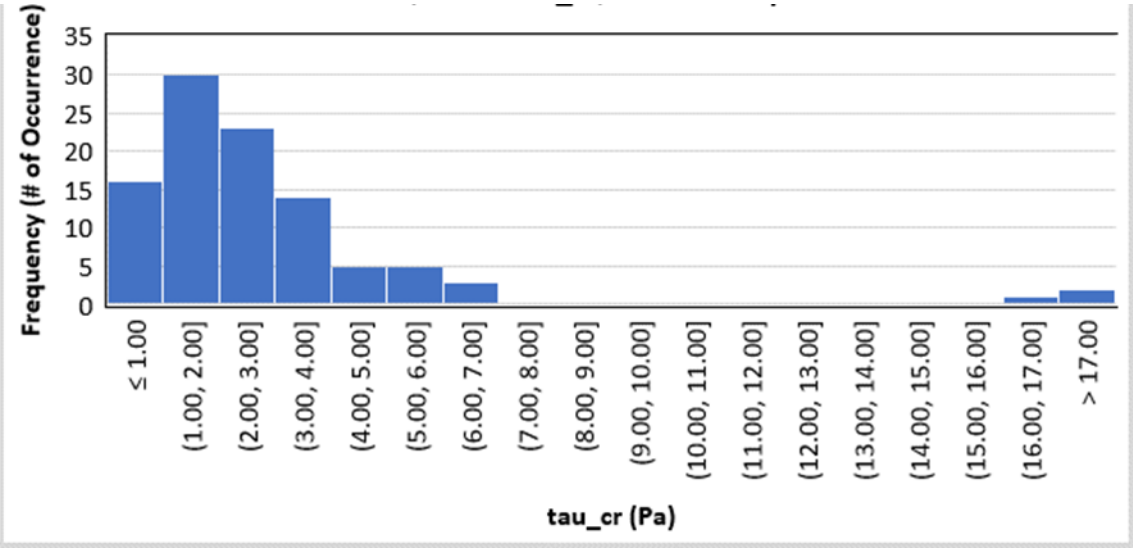

Figure 7.24. Histogram of critical shear stress from SEDflume experiments.

Table 7.3. SEDflume results.

Sediment Type (USGS)	D50 (micron)	Tcr (Pa)			Erodibility (kg/m^2/s)		
		Median	Upper Limit (d*<0.3)	Lower Limit	Median	Upper Limit	Lower Limit
Fine Silt	≤4.0	3.5	17.0	0.7	3.2E-4	1.0E-3	2.6E-5
	8.0	1.0	4.6	0.3	6.3E-4	1.6E-3	2.3E-4
Medium Silt	12.0	5.4	N/A	N/A	9.3E-4	2.3E-3	3.7E-4
	16.0	3.2	N/A	N/A	1.2E-3	3.1E-3	4.9E-4
Coarse Silt	20.0	2.1	N/A	N/A	1.5E-3	3.9E-3	5.2E-4
	24.0	1.5	N/A	N/A	1.8E-3	4.6E-3	5.5E-4
	28.0	1.2	N/A	N/A	2.2E-3	5.4E-3	5.7E-4
Very Coarse Silt	32.0	0.9	N/A	N/A	2.5E-3	6.2E-3	5.9E-4
	36.0	0.8	N/A	N/A	2.8E-3	6.9E-3	6.1E-4
	40.0	0.7	N/A	N/A	3.0E-3	7.1E-3	1.2E-3
	63.0	0.4	N/A	N/A	7.0E-3	7.2E-3	4.8E-3

Another important parameter that was also tested is the dry density of the bed. Values of dry density that were tested as upper and lower limits of the sample based on the data shown on Figure 7.17 were 848 kg/m^3 (53 pcf) and 1,200 kg/m^3 (75 pcf).

7.3.4 Insights from Initial Outfall Design Modeling

To evaluate the response of outfall morphology to the OTF configuration, the following OTF lengths were simulated initially.

- 1,500 ft OTF, 850 ft non-erodible (rip-rapped) length;
- 1,500 ft OTF, 1,500 ft non-erodible (rip-rapped) length;
- 3,200 ft OTF, 3,200 ft non-erodible (rip-rapped) length; and
- 4,500 ft OTF, 4,500 ft non-erodible (rip-rapped) length.

Figure 7.25 shows the bathymetry of the outfall area at the end of the one-year flood hydrograph simulation. It shows that a deep and long scour hole has formed over a distance of 6000 ft from the end of the conveyance channel extending into the basin at the end of the non-erodible limit.

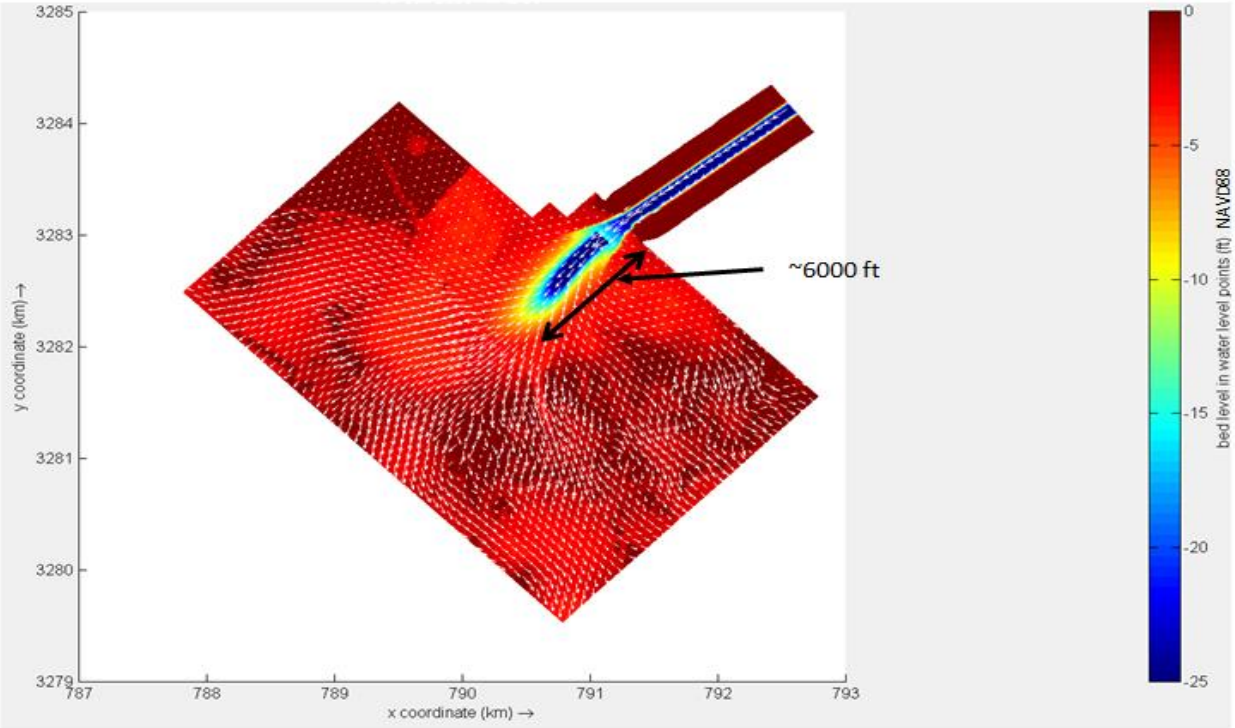

Figure 7.25. Bathymetry contours at the end of the first year shows an ~6000 ft long scour hole. The deepest point is ~-80 ft NAVD88 at the edge of the 850 ft non-erodible extent. Bed elevation contours are at the end of the run (one-year flood).

Figure 7.26 upper panel shows the longitudinal (i.e., along the thalweg) variation of this scour hole starting from the end of the conveyance channel (origin) while the bottom panel shows the transverse variation. It is seen that the 1,500 ft outfall with the 850 ft non-erodible extent shows a very deep scour with bottom elevations of about -80 ft, NAVD88 immediately downstream of the non-erodible limit. The lower panel of Figure 7.26 shows the corresponding transverse view of the scour hole through the deepest portion. The predicted maximum scour bottom elevations for the tested outfall lengths and non-erodible extents are listed in Table 7.4. Note that Delft3D cannot model head-cutting, channel stabilization or geotechnical slope stability failures. Also, the 2D model applied here cannot simulate the complex 3D hydraulic features (e.g., nappe formation, vertical eddy structures) at the edge of the non-erodible limit. In real life, in the absence of any head-cut prevention structure at the end of the non-erodible limit, the steep slope will possibly cause the non-erodible segment to fail and cave into the scour hole and cause the head-cut to propagate upstream. Also, the side banks will possibly collapse and create a wider hole than predicted by modeling. Therefore, the model results are more representative of scenarios where a head-cut prevention structure is already in place at the end of the non-erodible extent. Considering these limits and uncertainties, the modeled scour depths are more reliable than the predicted lateral extents.

Table 7.4. Predicted maximum scour bottom elevations for the tested outfall lengths and non-erodible extents.

Approximate OTF Length from the End of Conveyance channel (ft)	**Non-erodible extent from End of Conveyance Channel (ft)**	**Maximum Scour Bottom Elevation (ft, NAVD88)**
1,500	850	-80
1,500	1,500	-14
3,200	3,200	-11
4,500	4,500	-8

A decrease in scour depth (from -80 to -14 ft, NAVD88) is noticed when the non-erodible portion is extended from 850 ft to 1,500 ft. Extending the non-erodible portion beyond 1,500 ft achieves only minor additional reductions in scour depth (-11 ft, NAVD88 for 3200 ft and -8 ft, NAVD88 for the 4,500 ft). This can be explained by Figure 7.27 which shows the longitudinal

variation of the depth-averaged velocity (top panel) and bed shear stress (bottom panel) along the scour hole at 75,000 cfs peak diverted flow. The depth-averaged velocity (DAV) in the scour hole at the end of the 850 ft non-erodible extent of the 1,500 ft OTF length is about 5.5 ft/s which produces a bed shear stress of about 3.5 Pa. Therefore, the erosion rate (following equation I) is much higher compared to the 1,500 ft non-erodible OTF length where the velocity in the scour hole at the edge of the non-erodible extent of the OTF (850 ft) is lower, about 3 ft/s, and the corresponding bed shear stress of 1.75 Pa is very close to the 1.5 Pa critical shear stress. Thus, in this 2D Delft3D morphology-based model the initiation and progression of the depth of the scour hole depends very much on the velocity and bed shear stress within the scour hole at the edge of the non-erodible sections.

Figure 7.28 shows the contour plots of bed elevation (top row) and depth-averaged velocity (bottom row) for the 850 ft and 1,500 ft non-erodible extents on the same 1,500 ft OTF. Note the different legend limits for the bathymetry contours. This figure illustrates the relative benefit of extending the non-erodible limit to where the high energy core has spread laterally and reduced the discharge per unit width. This will be the main goal of the analysis in the next phase where different modifications to the flare angle will be tested. so that head-cut countermeasures are cost-effective. An additional consideration in the OTF design is sand (particularly the medium 250 micron) dropping out of suspension too soon (within a short distance from the OTF) and the potential for a ‘healing crevasse’ forming early in the operational life of this diversion. The ultimate goal is to manage the hydraulics, sand transport and scour through a combination of structural design of the OTF, diversion operations and outfall maintenance (dredging/additional armoring).

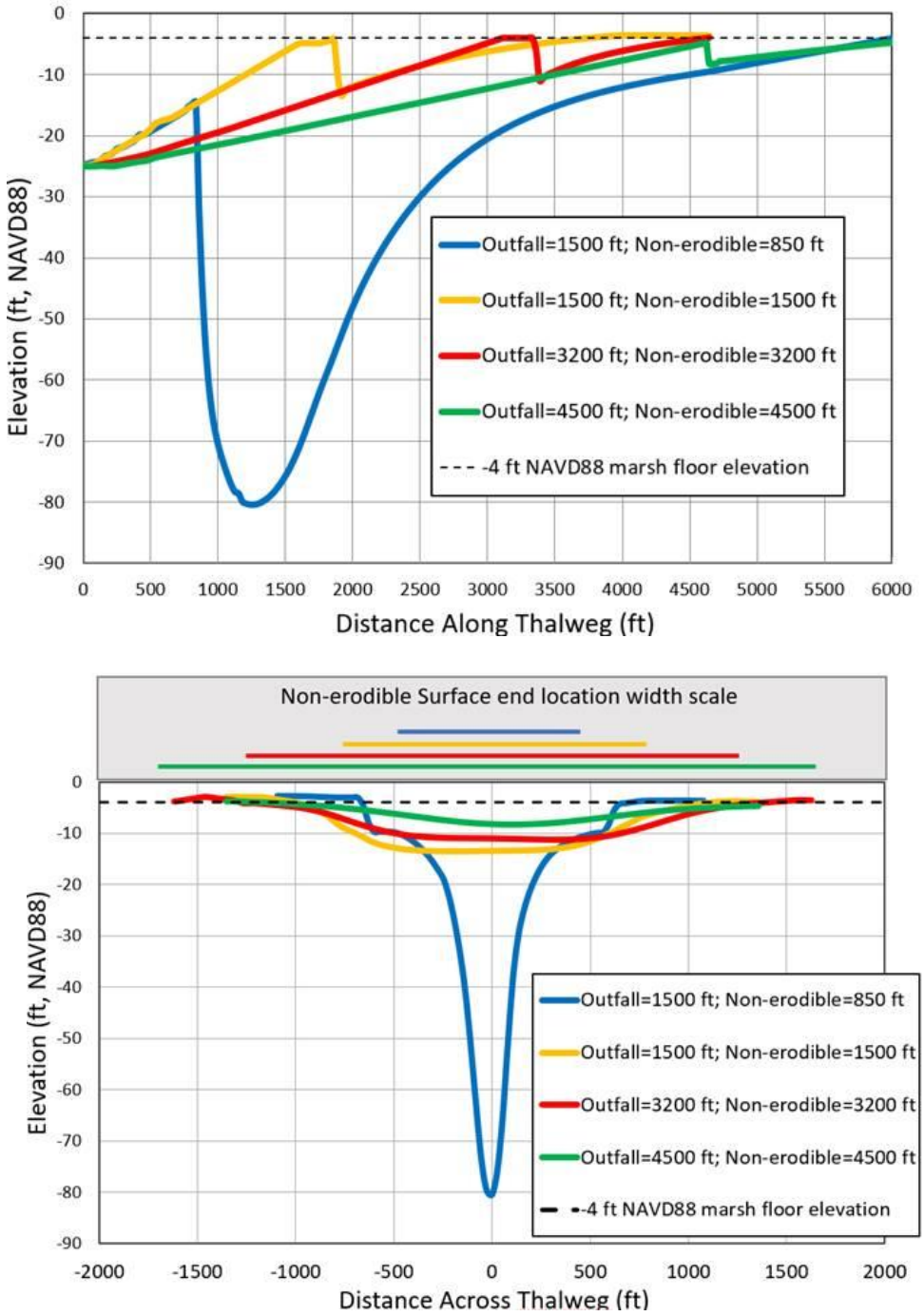

Figure 7.26. Upper panel: Longitudinal (along thalweg) variation of scour bed elevations, origin is at the end of the conveyance channel, flow is from left to right. Bottom Panel: Transverse (across thalweg) variation of scour bed elevation, origin is at the center of the deepest point of the hole, flow is in the direction normal to the plane of paper. Scour elevations are at the end of the simulation (one flood year).

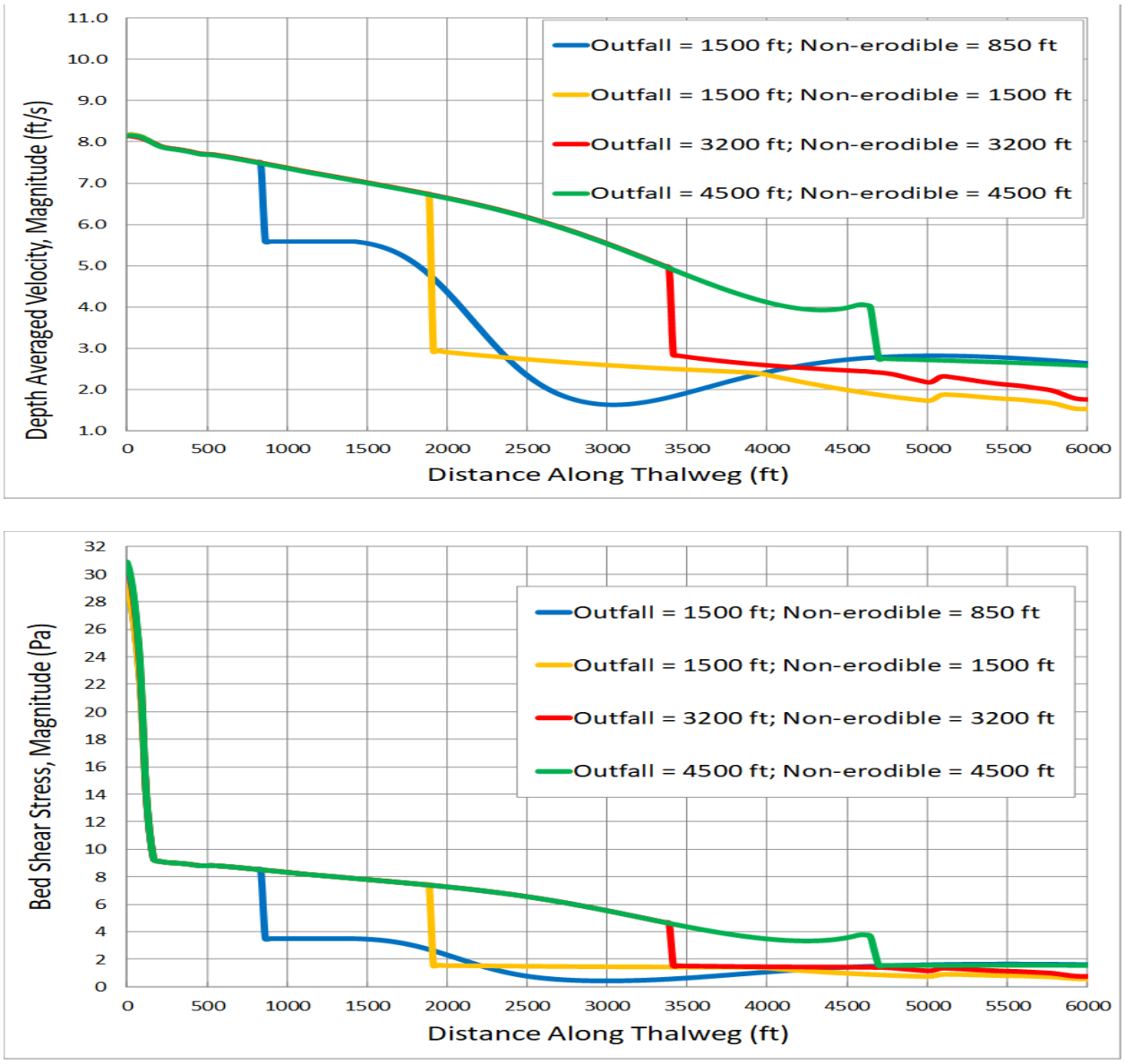

Figure 7.27. Upper panel: Longitudinal (along thalweg) variation of depth-averaged velocity, origin is at the end of the conveyance channel. Bottom Panel: Longitudinal (along thalweg) variation of bed shear stress, origin is at the end of the conveyance channel. Flow is from left to right for all the figures. Diverted flow is at 75,000 cfs.

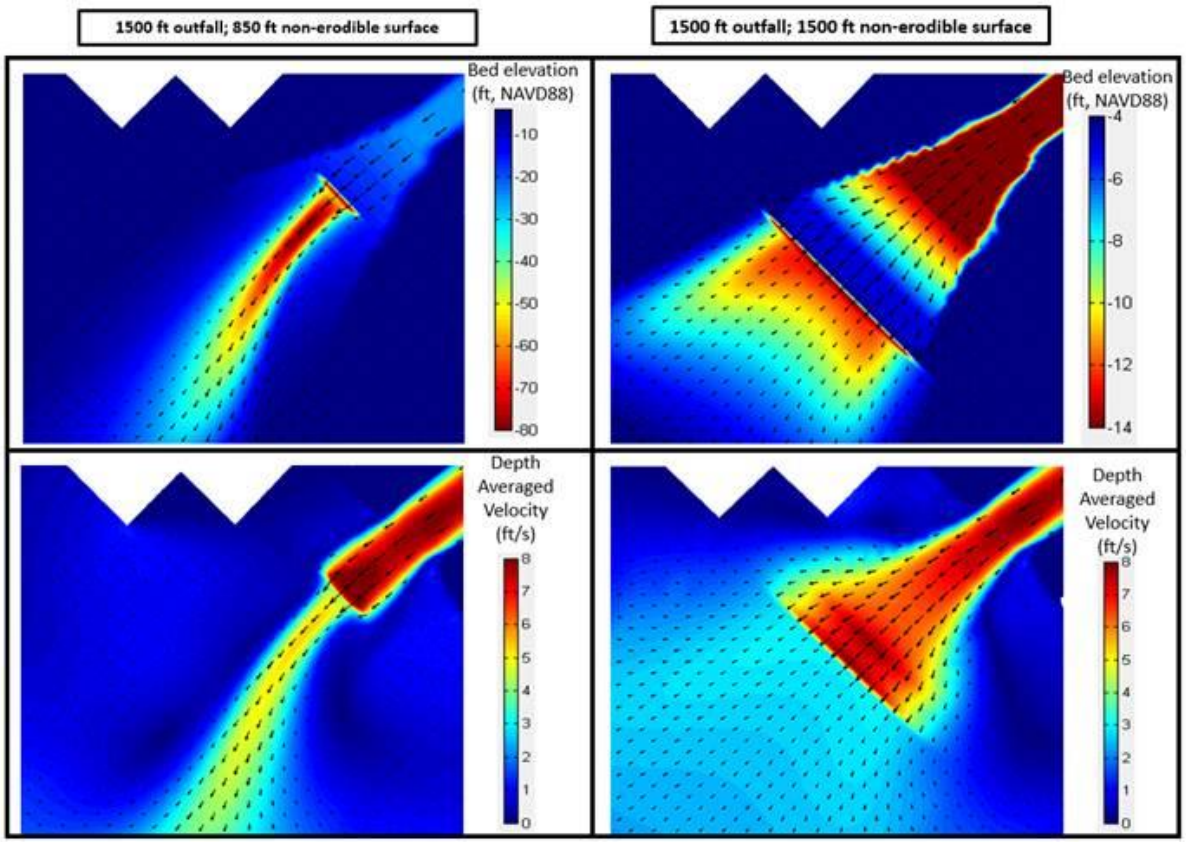

Figure 7.28. Upper row: Color contours of bed elevation with arrow velocity vectors, Bottom row: Color contours of depth-averaged velocity with arrow velocity vectors. Notice the different legend limits for the bed elevation color contours.

Another important concern in the early years of operation (possibly within 3 years) is the lateral migration of the scour hole. Observational evidence from natural delta propagation studies suggests that dendritic channels emanate from the initial crevasse erosional phase. A design concern here is the scouring from a dendritic channel encroaching the OTF from the sides. To design adequate protection for the sides of the OTF it is important to quantify the critical design velocities expected in this zone. Figure 7.29 upper panel shows the variation of hydraulic bed shear stress as calculated by the model using Equation II for varying depth-averaged velocities. Assuming a constant Manning's n=0.018 (i.e., for smooth sandy channels) for the wetlands, this figure shows that depth-averaged velocities greater than a threshold of 2 ft/s can cause potential scour within the outfall area. The lower panel of Figure 7.29 shows contours of depth-averaged velocities at 75,000 cfs diverted flow (~900,000 cfs MR flow) and 96,000 cfs diverted flow at ~1,250,000 cfs MR flow. This setup was with a fully non-erodible basin (no morphology model).

Since the formation of a scour hole reduces the velocity and horizontal extent of the scour is uncertain, it is recommended to use the velocity contours from this setup as an initial guideline to design the lateral extent of the head-cut mitigation feature.

7.3.5 Outfall Evolution Model Sensitivity Analysis

The scour depth sensitivity to four principal model parameters, namely, the critical shear stress of erosion (T_{cr}), erodibility parameter (M), morphology acceleration factor (MorFac) and the dry density (DD) were analyzed and compared against the base case (1,500 ft long OTF with 850 ft non-erodible zone) as shown in Table 7.4. All the runs used the same boundary conditions and were run with the one-year (2008) flood hydrograph. Only one parameter ('Parameter of interest' in Table 7.5) was varied from the base case to evaluate its impact. The range of the parameter values for this sensitivity analysis were selected based on the discussions in the previous sections.

Table 7.5. Sensitivity analysis performed for different model parameters.

Run No.	Parameter of interest	T_{cr} (Pa)	M (kg/sqm/s)	MorFac	DD (kg/m^3)
1	Base Case	1.5	$1.0x10^{-3}$	80	848
2	T_{cr}	2.5	$1.0x10^{-3}$	80	848
3	M	1.5	$0.5x10^{-3}$	80	848
4	T_{cr} & M	2.5	$0.5x10^{-3}$	80	848
5	M	1.5	$0.1x10^{-3}$	80	848
6	T_{cr} & M	2.5	$0.1x10^{-3}$	80	848
7	MorFac	1.5	$1.0x10^{-3}$	20	848
8	Dry Density	1.5	$1.0x10^{-3}$	80	1200

The results from the sensitivity tests are shown on Figures 7.30 to 7.34. They show that the outfall scour bottom elevations vary from -80 ft (Run1, Base Case) to -20 ft (Run 6, T_{cr} =2.5 Pa and M=0.1x10^-3 kg/sqm/s). The erodibility appears (M) to be the most sensitive parameter followed by the critical shear stress (T_{cr}), the dry density (DD) and MorFac in the decreasing order of sensitivity. The joint variation of critical shear stress and erodibility (Figure 7.31) shows the highest ranges of variation in scour depth. The sensitivity of scour depth to dry density and MorFac is relatively low.

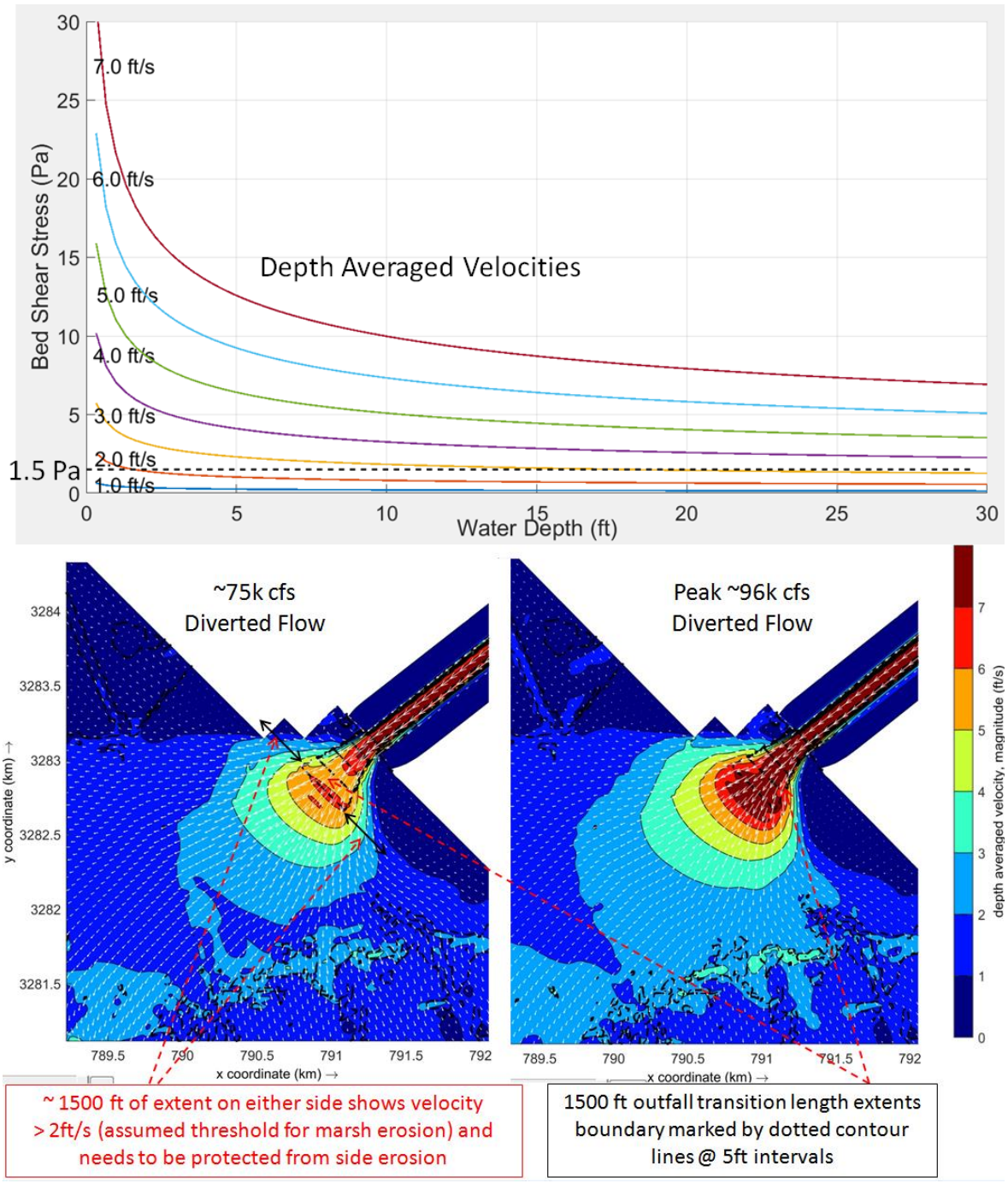

Figure 7.29. Upper panel: Variation of hydraulic bed shear stress with water depth for different depth-averaged velocities. The critical shear stress threshold 1.5 Pa is marked by a dotted line. Bottom panel: Contours of depth-averaged velocities (at 1 ft/s interval) in the immediate outfall area. 75,000 cfs is the peak operational discharge, ~96,000 cfs is the maximum discharge the diversion can deliver to the basin under current conditions (all gates open at 1.25M cfs MR flow).

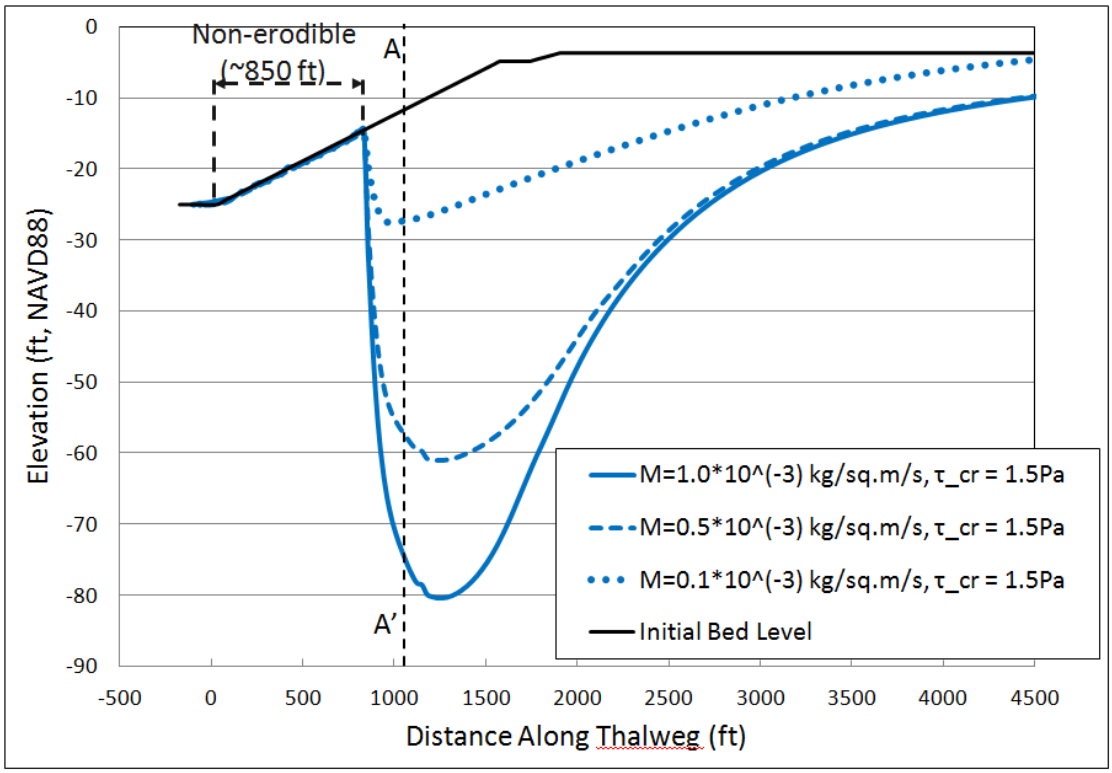

Figure 7.30. Sensitivity of modeled scour bed elevations to the erodibility parameter (M) for constant critical shear stress (T_{cr}). Longitudinal (along thalweg) scour bed elevations shown here, flow is left to right and origin is at the end of the conveyance channel. Section A-A' represents the location of the transverse section view (shown on Figure 3.16). OTF is 1,500 ft long and non-erodible length is 850 ft.

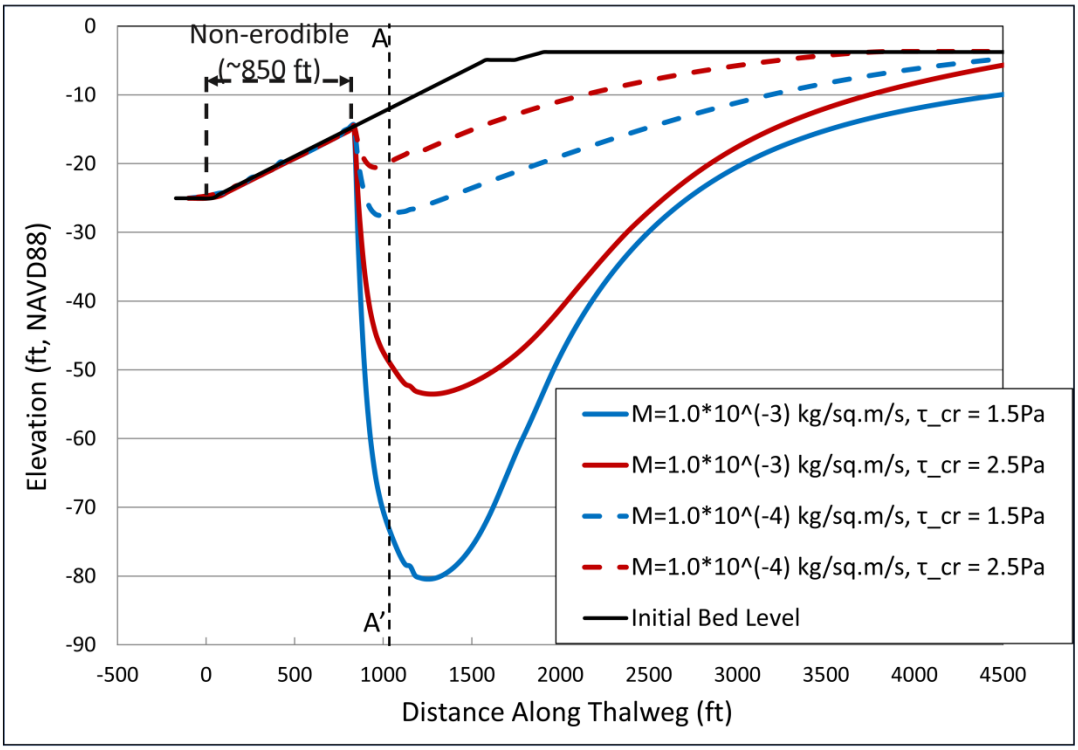

Figure 7.31. Sensitivity of modeled scour bed elevations to both the critical shear stress (T_{cr}) erodibility parameter (M). Longitudinal (along thalweg) scour bed elevations shown here, flow is left to right and origin is at the end of the conveyance channel. Section A-A' represents the location of the transverse section view (shown on Figure 3.16). OTF is 1,500 ft long and non-erodible length is 850 ft.

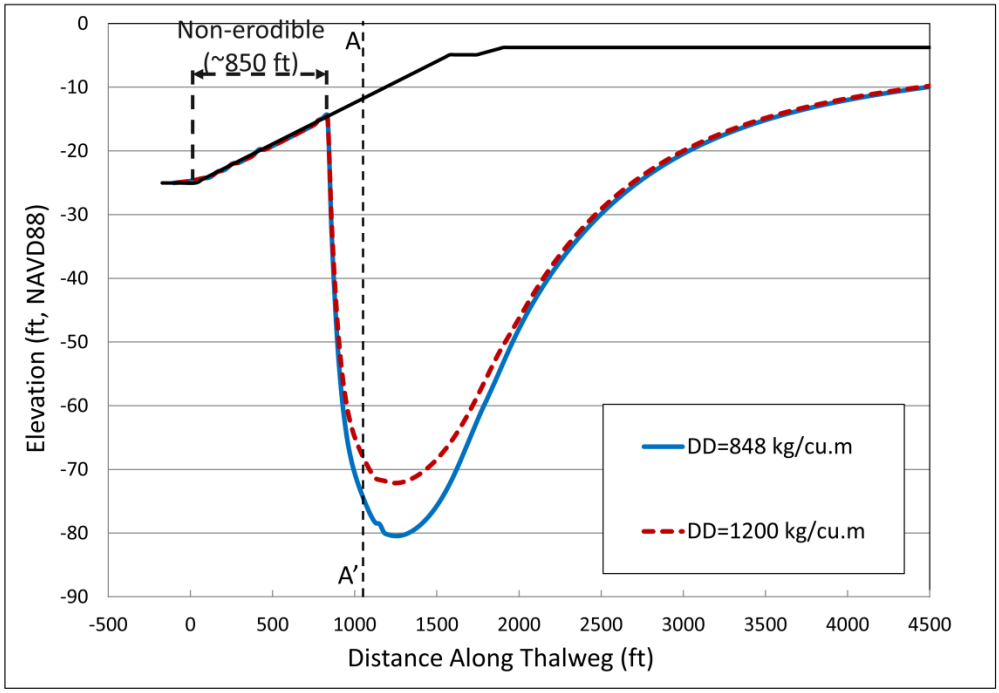

Figure 7.32. Sensitivity of modeled scour bed elevations to dry density (DD) of the soil. Critical shear stress was set at 1.5 Pa and erodibility parameter 10^{-3} kg/sq.mm/s. Longitudinal (along thalweg) scour bed elevations shown here, flow is left to right and origin is at the end of the conveyance channel. Section A-A' represents the location of the transverse section view (shown on Figure 3.16). OTF is 1,500 ft long and non-erodible length is 850 ft.

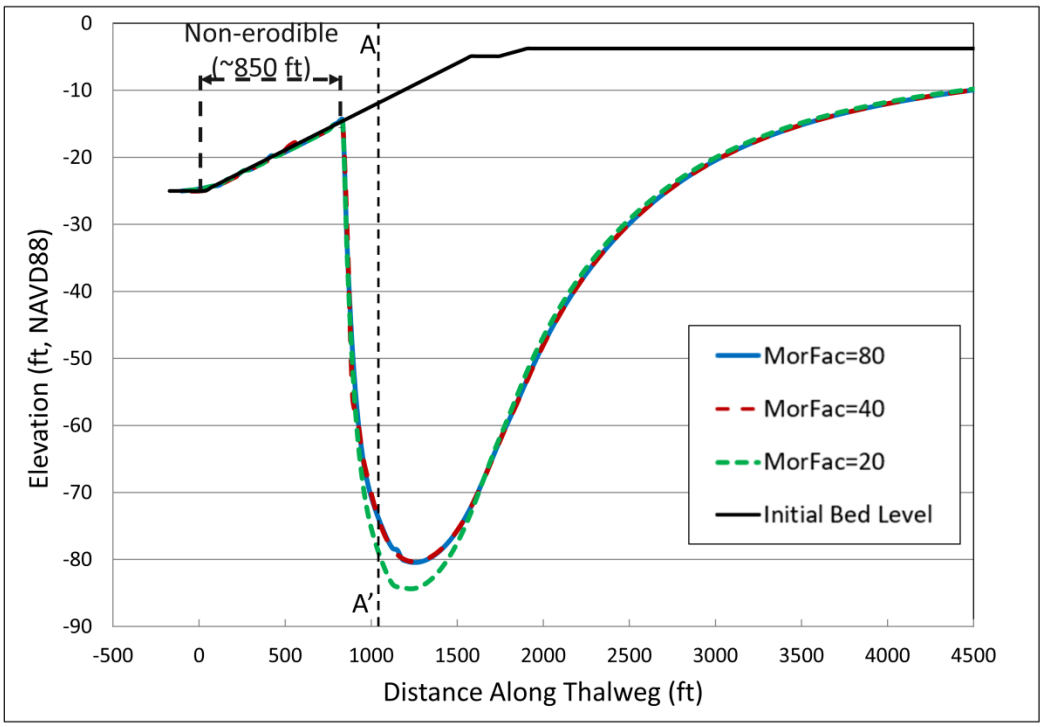

Figure 7.33. Sensitivity of modeled scour bed elevations to morphological acceleration factor (MorFac). Critical shear stress was 1.5 Pa and $M=10^{-3}$ kg/sq.mm/s. Longitudinal (along thalweg) scour bed elevations shown here, flow is left to right and origin is at the end of the conveyance channel. Section A-A' represents the location of the transverse section view (shown on Figure 3.16). OTF is 1,500 ft long and non-erodible length is 850 ft.

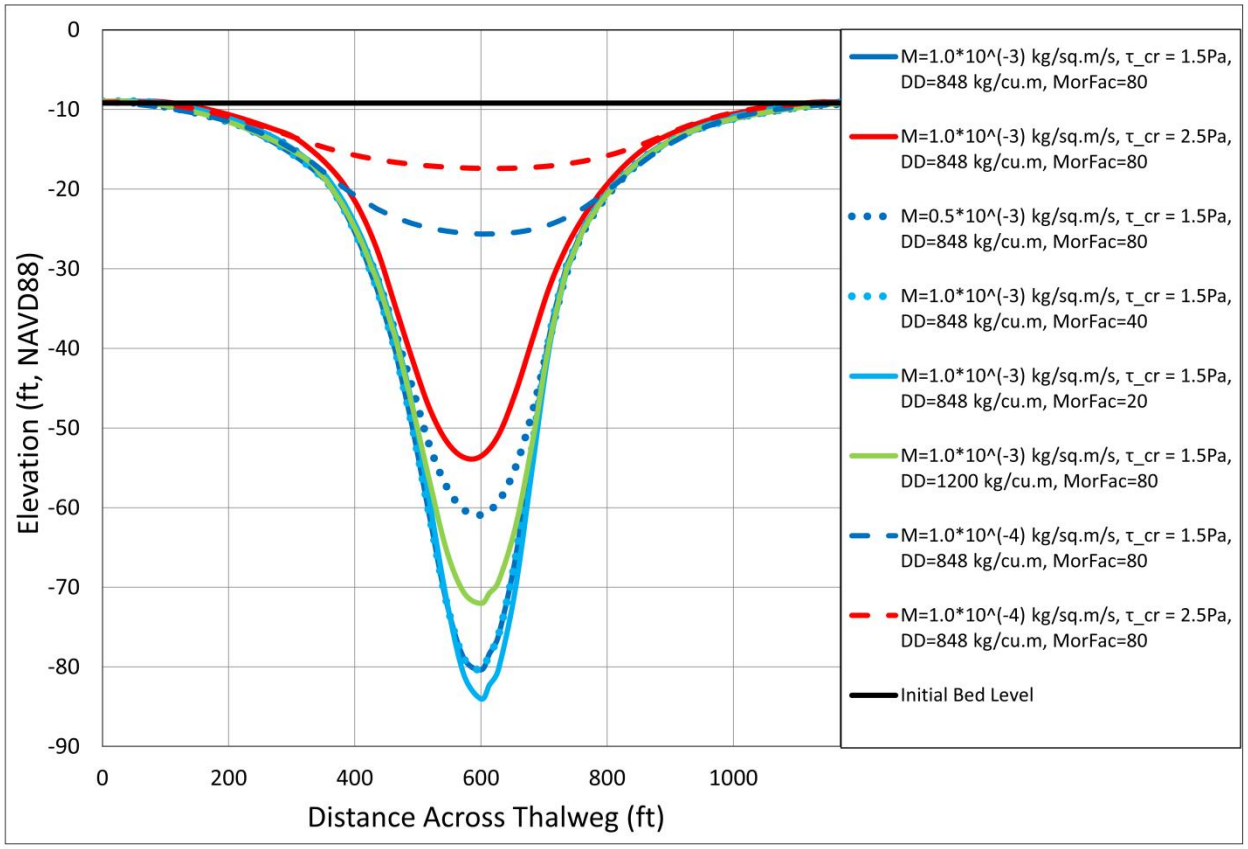

Figure 7.34. Sensitivity of modeled scour bed elevations to all the four parameters. Transverse (across thalweg) scour bed elevations shown here along section A-A' marked on Figures 19-23. Flow is perpendicular to the plane of paper. OTF is 1,500 ft long and non-erodible length 850 ft.

7.3.6 Rigid-bed FLOW-3D Modeling of Velocities and Bed Shear Stresses and comparison with 2D Delft3D results

A FLOW-3D fully 3D rigid-bed model (hydrodynamics only, no sediment transport or morphology evolution) was developed to understand the hydrodynamics, quantify bed shear stress and compare results with the previously completed 2D Delft3D hydrodynamics. Figure 7.35 shows the model extents and the boundary conditions. Table 7.6 lists the grid sizes used for the three different mesh blocks shown in the figure. Note the highest resolution mesh Block No. 2 (2.5 m x 2.5 m x 0.3-0.6 m) which covers the OTF geometry.

Table 7.6. 3D Mesh sizes used for each block.

Block #	Δx (m)	Δy (m)	Δz (m)
1	5	5	0.3
2	2.5	2.5	0.3-0.6
3	10	10	0.3

Two different bathymetry/ topography configurations of the 1,500-ft OTF design were evaluated in FLOW-3D as shown in Figure 7.36. The left panel shows the uneroded (initial) bathymetry while the right panel shows scoured bathymetry after one year. The scoured bathymetry is obtained from Delft3D model after one-year run (Figure 7.28, left panel). The uneroded bathymetry is expected to provide insight into potential jet separation at the outfall as well as evaluating the efficacy of the designed 1,500- ft OTF when rip-rapped along its entire extent (i.e., fully non-erodible). The deepest scoured bathymetry (bottom elevation approximately -80 ft, NAVD88) and the shallower (bottom elevation approximately -14 ft, NAVD88) were selected due to the need to understand the validity of the 2D hydrodynamics that cause such a deep hole when a shorter rip-rap extent is used. Moreover, this test is also expected to shed light on the possible hydrodynamics that are responsible for creating the deep scour holes at a short distance downstream from the crevasse occurring in some of the field sites described in the case studies mentioned before.

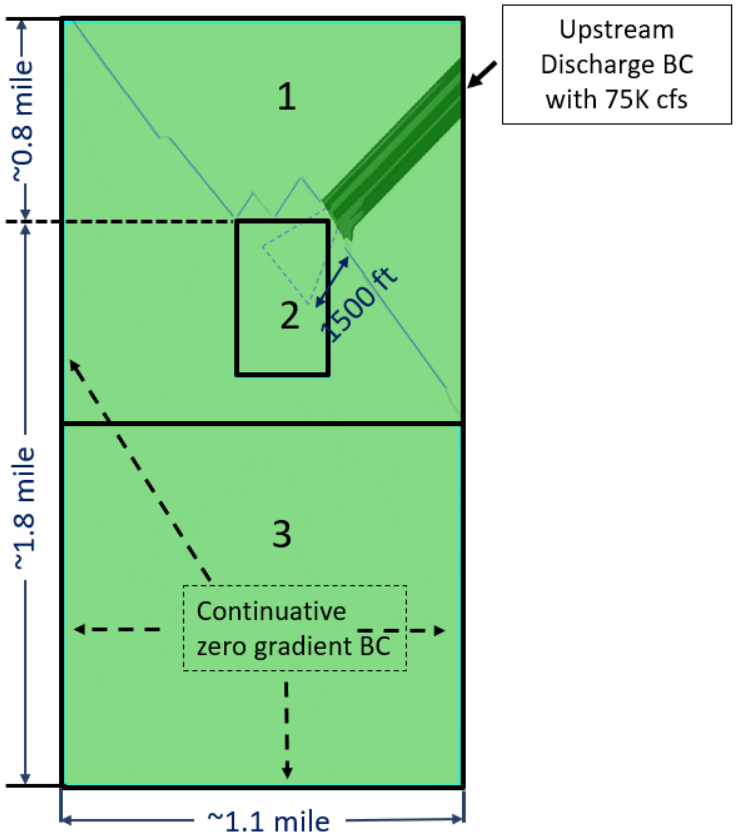

Figure 7.35. 3D FLOW-3D OTF model domain showing 3 mesh blocks and the boundary conditions (mesh sizes in Table 5.1).

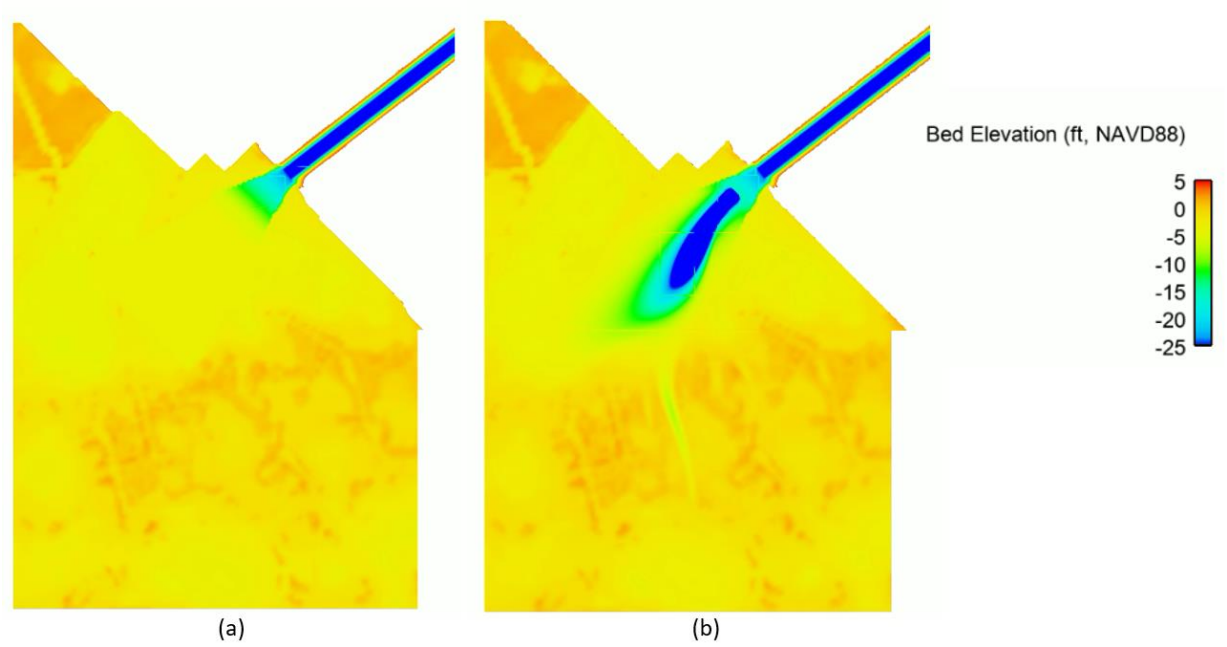

Figure 7.36. Bathymetry/ topography of the basin and the 1,500-ft OTF evaluated in the FLOW-3D model. (a) Initial OTF before erosion; entire OTF and basin non-erodible (b) Only 850-ft non-erodible, Scour geometry after 1 year.

Figure 7.37 shows a snapshot in time of the flow velocities and patterns predicted by the FLOW-3D model for the two tested OTF geometries. The flow pattern for the unscoured OTF is somewhat symmetrical with some weak circulation. The velocities and flow patterns shown by the scoured geometry shows the hydrodynamics dominated by the hole. Strong eddies constrict the outfall discharge to the center of the OTF. Note that the horizontal eddies shown are a snapshot in time. In reality these eddies will shift position over time due to jet instability. A closer view of the 3D flow field is shown in Figure 7.38. The vertical variation of longitudinal velocity in Figure 7.39 shows that the velocities in the scour hole are about 4 ft/s.

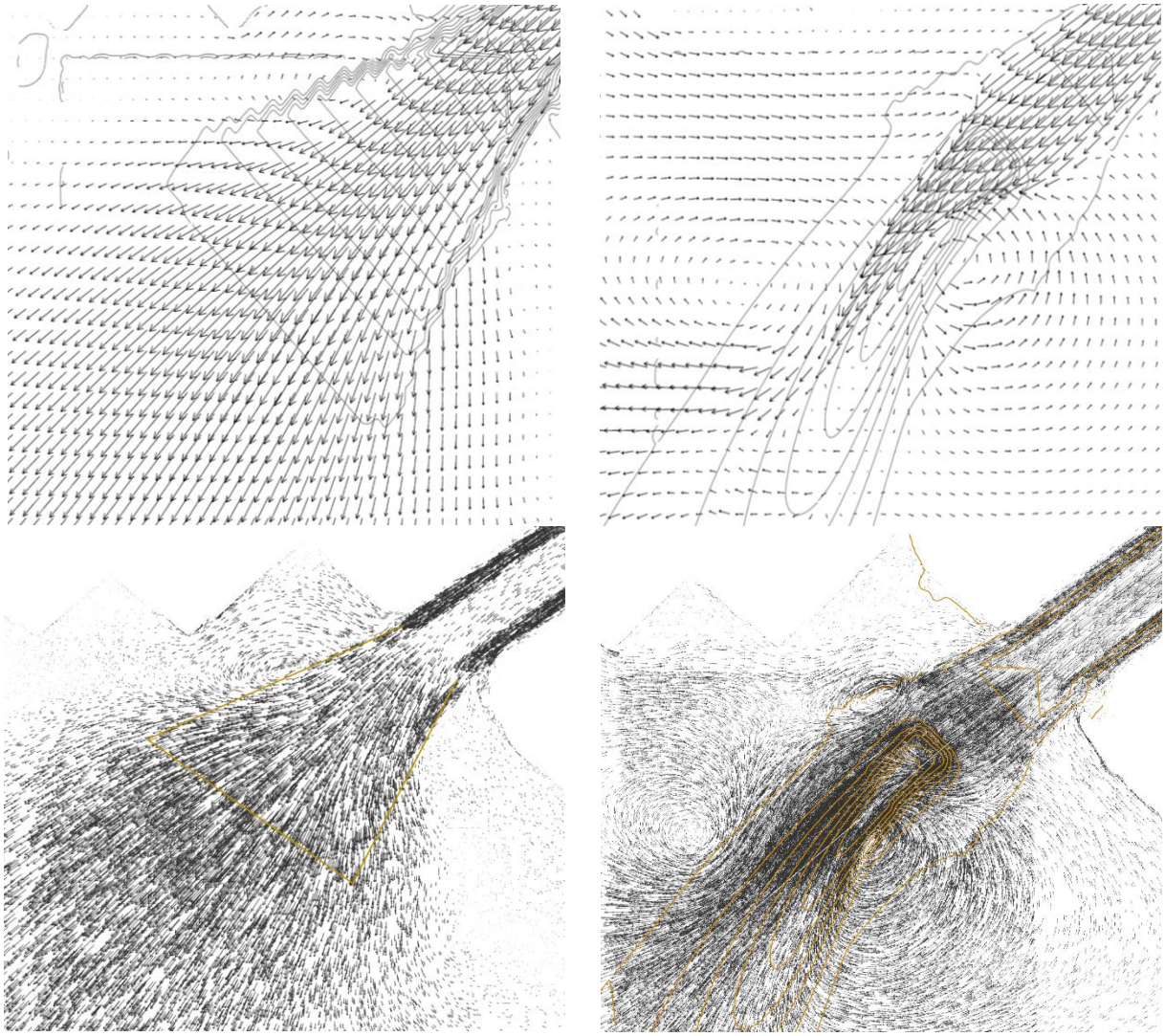

Initial OTF without scour

OTF with deep scour at the end of 850-ft non-erodible length

Figure 7.37. Instantaneous flow pattern in and around the two tested OTF geometries. Top panels show depth-averaged velocity vectors plotted at 100 ft interval and indicate depth-averaged flow features, while the bottom panels show all vectors throughout the depth and indicate the complex 3D nature of the flow at the scour hole.

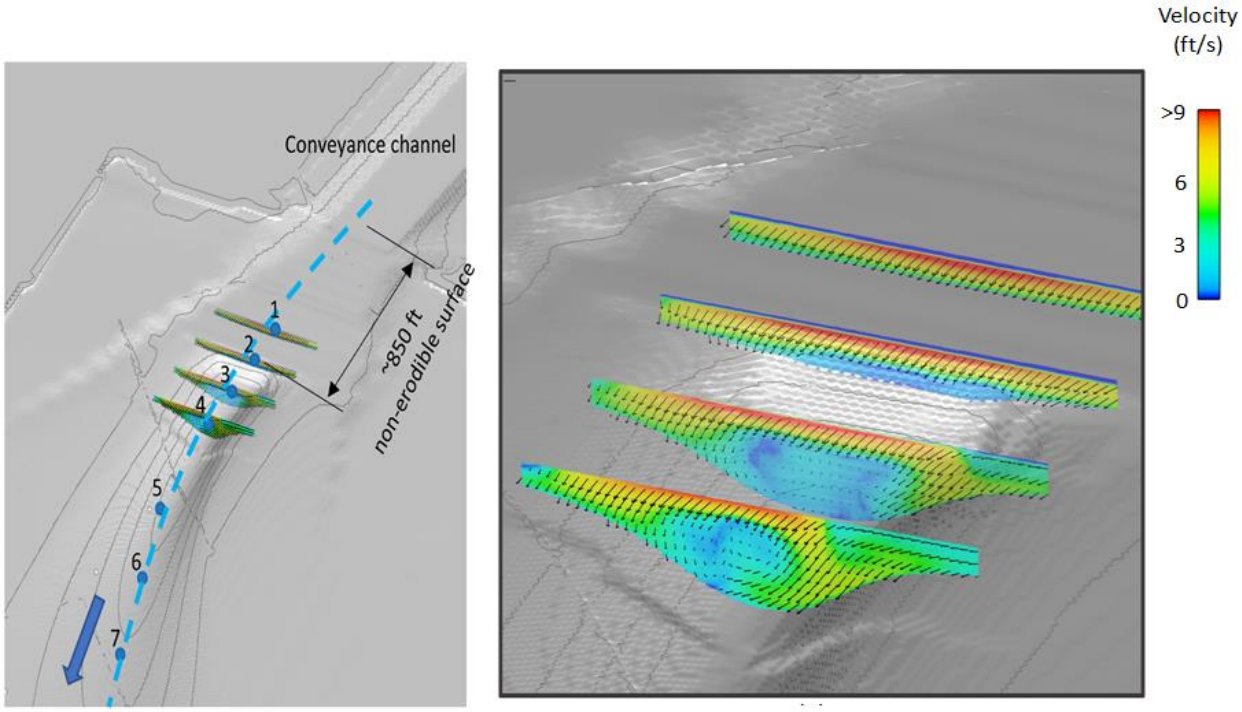

Figure 7.38. Three-dimensional flow pattern along the scoured OTF. Notice the inward rushing flow of water from the sides into the scour hole which keeps the near bed velocities at or above 4 ft/s.

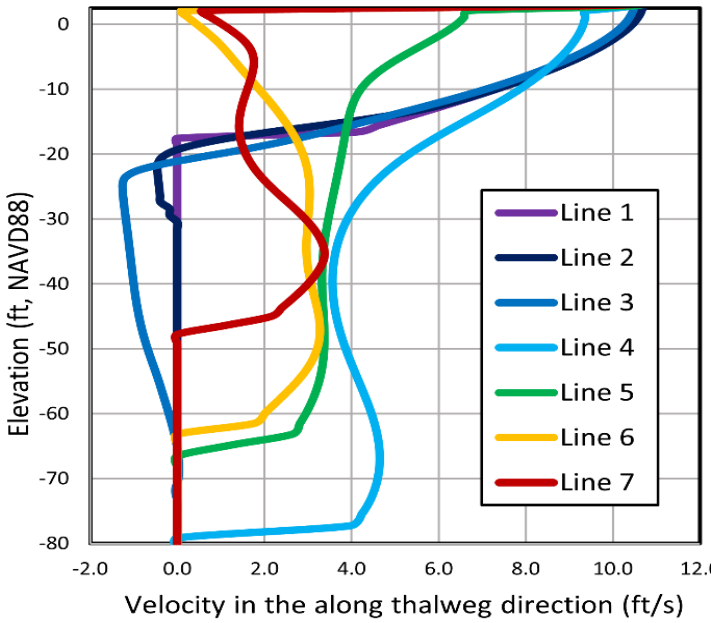

Figure 7.39. Vertical variation of longitudinal velocities at the locations indicated in the left panel of Figure 5.4. Note similar near-bed velocity within the hole (lines 4, 5 and 6) with the deepest point (line 4) having velocities of about 4 ft/s.

A view of the vertical velocity field along the longitudinal direction is shown in Figure 7.40. Notice the attached roller where the velocities are lower than 4 ft/s. The flow reverses forming a clinging nappe at the upstream edge of the hole. Downstream of this feature, the near-bed flow velocities range between 4 to 5 ft/s within the hole. This indicates that the scour hole predicted by the 2D model may be closer to the non-erodible edge than expected. It also suggests that the scour hole depths are likely to be physically realistic due to the higher near bed velocities.

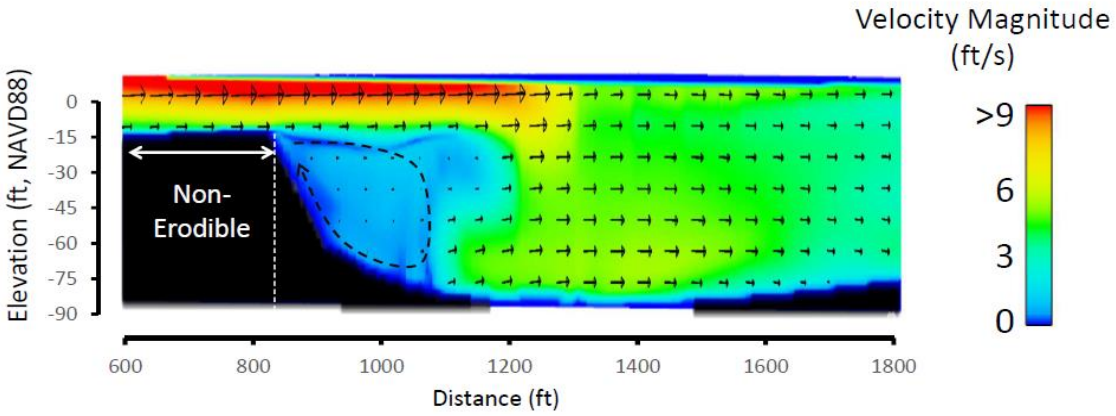

Figure 7.40. Flow pattern and velocity distribution along the vertical section (shown as blue dotted line in Figure 5.4 left panel) along the thalweg of the scour hole.

Figure 7.41 compares the depth-averaged velocities and the bed shear stresses from the 2D Delft3D and 3D FLOW-3D models. Notice the reduction of DAV and the associated reduction of bed shear stress immediately downstream of the OTF edge indicating the roller (clinging nappe) zone of low stress. Further downstream the DAV recovers and reaches almost 6 ft/s at the hole location with bed shear stress of about 6 Pa. The velocity predictions between two models are similar. Note that bed shear stress in the 2D Delft3D model is calculated using the quadratic law using the Chezy coefficient while the bed shear stress in FLOW-3D uses the law of the wall including a Reynolds-averaged Navier-Stokes (RANS) model for turbulence. Similarities in the bed shear stress in the 2D model with the 3D model provides greater confidence in the hydrodynamics that cause the predicted scour hole depth, while acknowledging that the location of the scour hole may be slightly further downstream in reality that predicted by the 2D model.

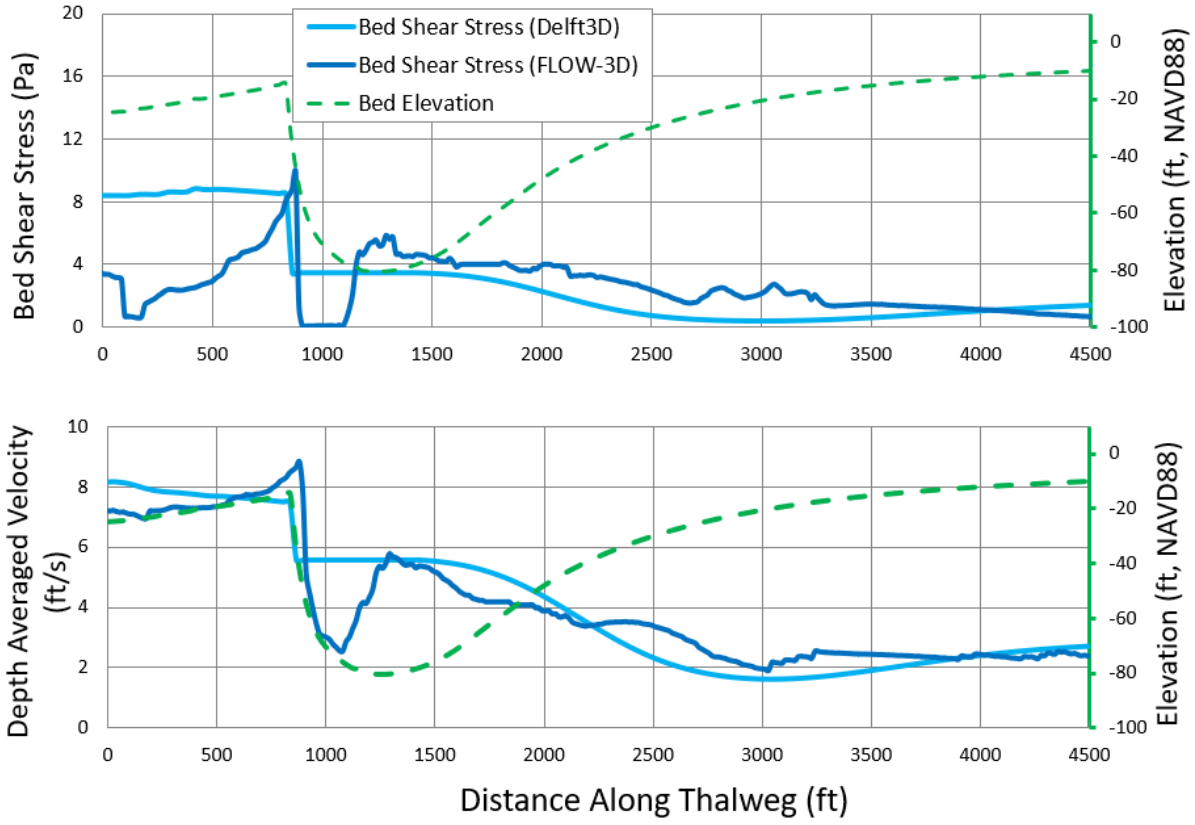

Figure 7.41. Comparison of the depth-averaged velocities and the bed shear stresses from the 2D Delft3D and 3D FLOW-3D model at 75,000 cfs diverted flow for the same scoured geometry (1,500-ft OTF, with 850-ft non-erodible extent and about an 80 ft scour hole).

The 2D Delft3D model results presented in Section 3 were further analyzed in terms of the unit discharge and scour progression. The 3D mechanism of flow concentration into the scour hole at the edge of the OTF described in Section 5 manifests itself as a rise in unit discharge in the 2D model (Figure 7.42).

Results of the DAV, bed shear stress, and unit discharge for both the 850 ft non-erodible extent (blue line) and 1,500 ft non-erodible extent (black line) cases are shown in Figure 7.42. The left panel shows the decrease in the DAV within the hole as the hole deepens. The hole formed at the edge of the 1,500 ft non-erodible extent shows a steep, decreasing DAV gradient with depth due to the lack of the flow concentrating within the hole, unlike that in the 850 ft non-erodible extent case which has a much lower DAV decrease. The initial increase in DAV for both cases is because the model runs a continuous hydrograph where flow reaches the peak 75,000 cfs after some finite number of days. The middle panel shows the decrease of bed shear stress associated with the decrease in DAV with a similar consequence the depth needed to attain a value near the critical shear (1.5-2.5 Pa), is much deeper for the 850 ft non-erodible case than the 1,500 ft case. The right panel shows the 2D representation of the phenomenon observed in the 3D FLOW-3D modeling (Figure 7.38 right panel) where the unit discharge within the hole keeps rising and is almost 10 times larger; if the non-erodible extent is shorter (850 ft) while when the hole is formed at the edge of the longer non-erodible extent (1,500 ft) the unit discharge tends to flatten out with only limited scour. All these results demonstrate the cascading nature of a scour hole formation where a hole if developed within the 1,500 ft OTF length, where the flow is still relatively concentrated (e.g., at the edge of the 850 ft non-erodible case), the hole tends to increase in depth due to the concentration of flow within the hole from the rest of the OTF width. However, a hole generated at the end of the 1,500 ft OTF, does not scour as much due to the relatively shallow jet already having spread, which prevents concentration of the jet within the hole.

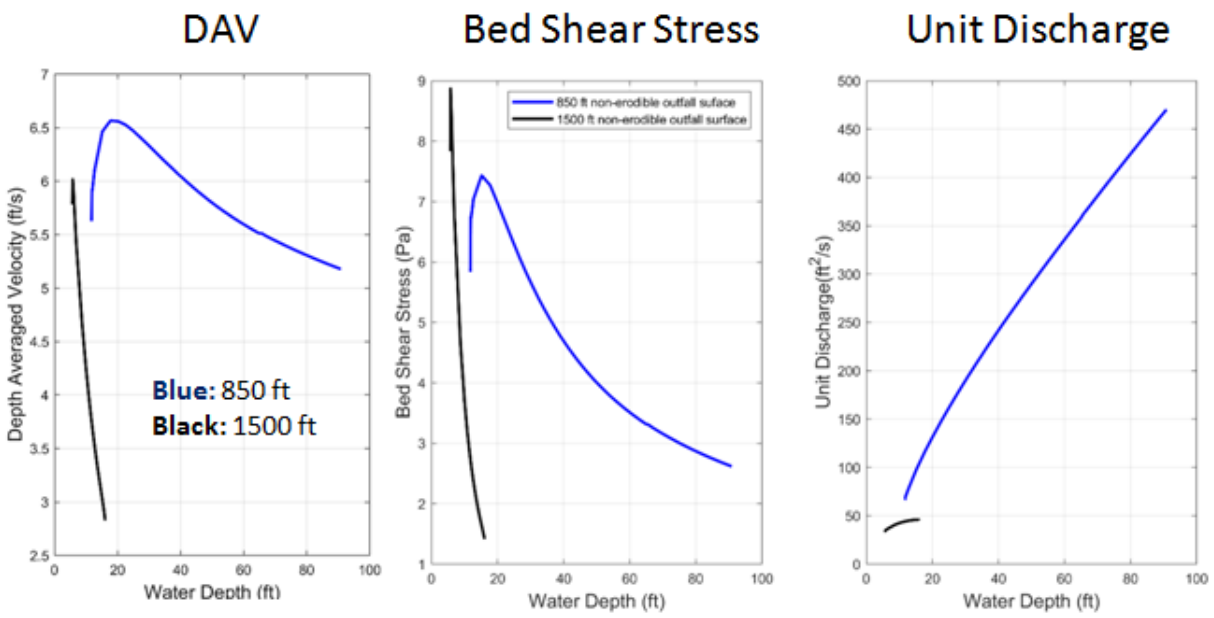

Figure 7.42. Results from the 1 yr (2008 hydrograph, Figure 3.1) 2D FTNOMBARefined extracted at the deepest point in the hole as shown in Figure 3.8 are presented here to explain the evolution of depth-averaged velocity (left panel), bed shear stress (mid-panel) and the unit discharge (right panel) during the process of scour hole development (water depth in the hole in X axis).

Figure 7.43 shows the variation of unit discharg along the scour thalweg. It shows that the unit discharge for the scoured (about -14 ft NAVD88 scour elevation) 1,500 ft non-erodible OTF (erodible basin) is not significantly different from the initial (non-erodible basin) value between the -1,500 ft to -2,500 ft mark, indicating the jet is sufficiently spread before reaching the the edge of the outfall for both these cases, such that the concentration potential is low in the scoured hole. On the other hand, the approximately 10 times greater unit discharge for the scour hole (about -80 ft NAVD88 scour elevation) at the edge of the 850 ft non-erodible extent explains the significant cascading effect and scouring potential of the concentrating jet.

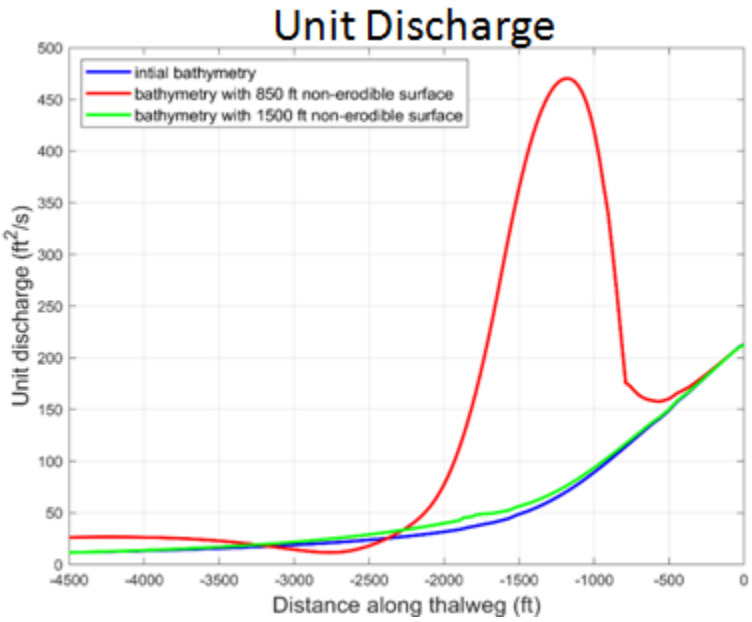

Figure 7.43. Unit discharge variation along the length of the outfall under scoured conditions (red and green lines representing the 850 ft non-erodible and 1,500 ft non-erodible extents) at 75,000 cfs diverted flow. The blue line indicates the initial (non-erodible 1,500 ft OTF and non-erodible basin condition).

Figures 7.44 and 7.45 show the variation of the scour hole elevation, scouring rate and depth-averaged velocity within the hole as the diverted discharge changes for the 850 ft non-erodible and 1,500 ft non-erodible (both with the same 1,500 ft OTF) cases. For both cases, the main scouring occurs during the rising limb and the peak flow part of the hydrograph and indicates the rapid nature of the scour hole formation (2-3 months) in context of the life of the diversion. It is observed that for the 850 ft non-erodible case, the scouring process starts at about 50,000 cfs diverted flow, while for the 1,500 ft non-erodible case, the scouring process starts sooner at about 42,000 cfs diverted flow. This is due to the relative shallower initial elevation (about -4 ft NAVD88) of the initial bathymetry versus the deeper (about -10 ft NAVD88) edge of the non-erodible extents. The velocity at which the scour is initiated is about 3-4 ft/s. The rate of scour for the 850 ft case is approximatelky 2-3 times that of the 1,500 ft case. The rate of scour increases non-linearly above 60,000 cfs for the 850 ft case and reaches about 1 ft/day at the onset of the first peak (about 75,000 cfs) flow, while the 1,500 ft case shows gradual flattening of the scour rate above 65,000 cfs with scour rates much lower (about 0.4 ft/day). Note that once

the first peak flow is reached, the scour rate is lower for subsequent peak flows as the scour hole has sufficiently deepened, velocities are reduced, and the bed shear stress approaches the critical shear stress of the native material. This knowledge of the quantitative behaviour of scour evolution with the diversion discharge can aid in choosing operational peak flows during the first few years of the MBSD operation. It also provides the operations the option for mitigation of excess scour (should it occur) without risking a detrimental scour failure of the structure. Regular surveys of the OTF are recommended during the first few months of diversion operation to determine if excess scour is occuring.

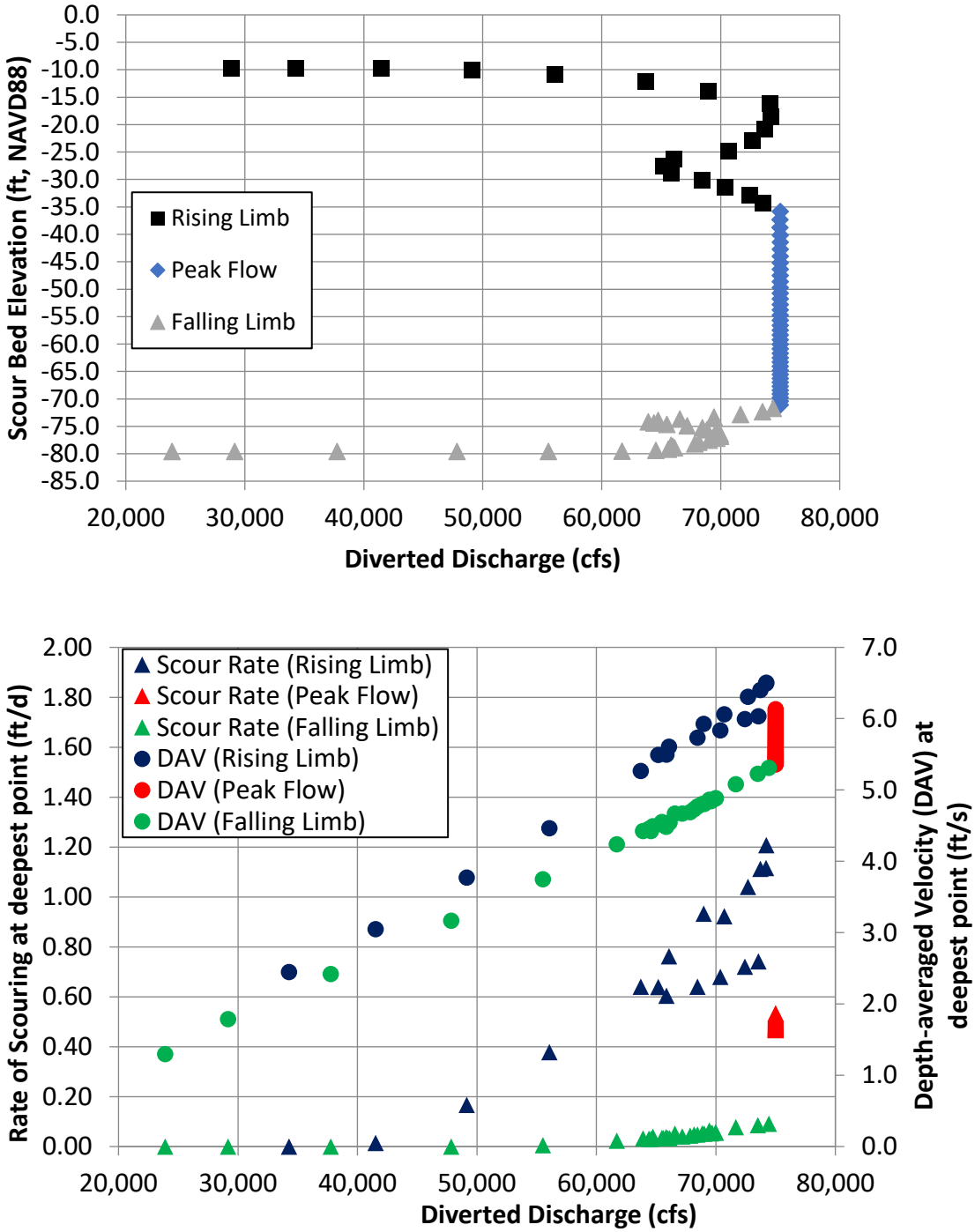

Figure 7.44. 850 ft non-erodible, 1,500 ft OTF 1Yr (no river-sediment run). Upper Panel: Variation of scour bed elevation at deepest point with diversion discharge; Lower Panel: Rate of scouring (left Y axis) and Depth-averaged Velocity (rigth Y axis) variation within the point with diversion discharge (X axis).

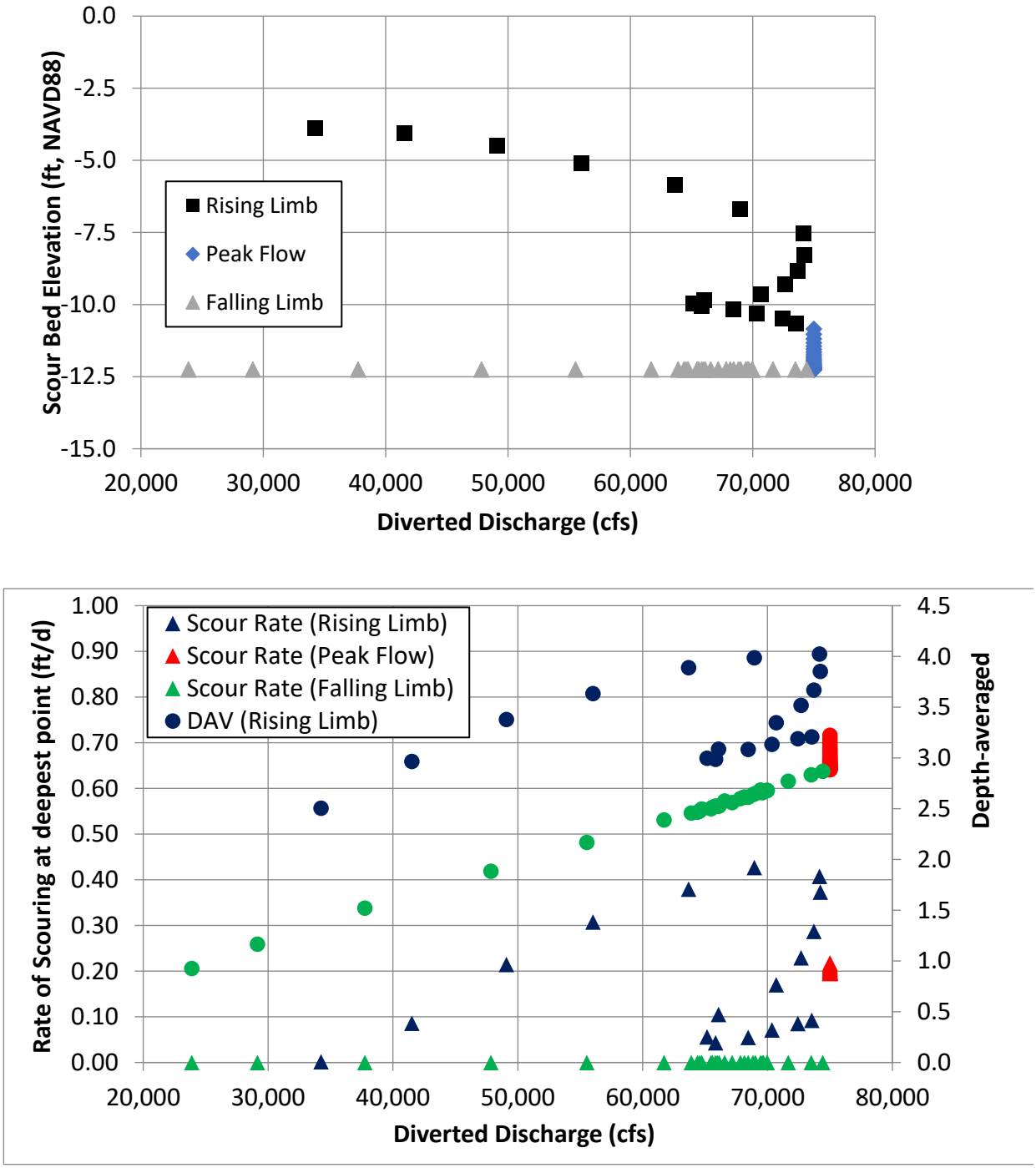

Figure 7.45. 1,500 ft non-erodible, 1,500 ft OTF. Upper Panel: Variation of scour bed elevation at deepest point with diversion discharge; Lower Panel: Rate of scouring (left Y axis) and Depth-averaged Velocity (rigth Y axis) variation within the point with diversion discharge (X axis).

Figure 7.46 shows the results from an idealized test where a constant 75,000 cfs diversion discharge was introduced for 365 days (one calendar year) without simulating the effect of the natural rise and fall of the river discharge. This idealized test was done to get an estimate of the approximate geomorphic timescales of the scour evolution at peak discharge without running very long, multi-year simulations. Results from the 850 ft non-erodible extents are shown by solid lines while those from the 1,500 ft non-erodible extent are shown with dotted lines. It is seen that the progression of scour hole deepening occurs quickly in 3-6 months if a continuous discharge of 75,000 cfs is imposed for both cases. The 1,500 ft non-erodible OTF shows that equilibrium depth is fairly shallow, about -15 ft, NAVD88, and once attained additional scour is unlikely over a long term if the OTF flare is maintained (i.e., the jet is kept spread out).

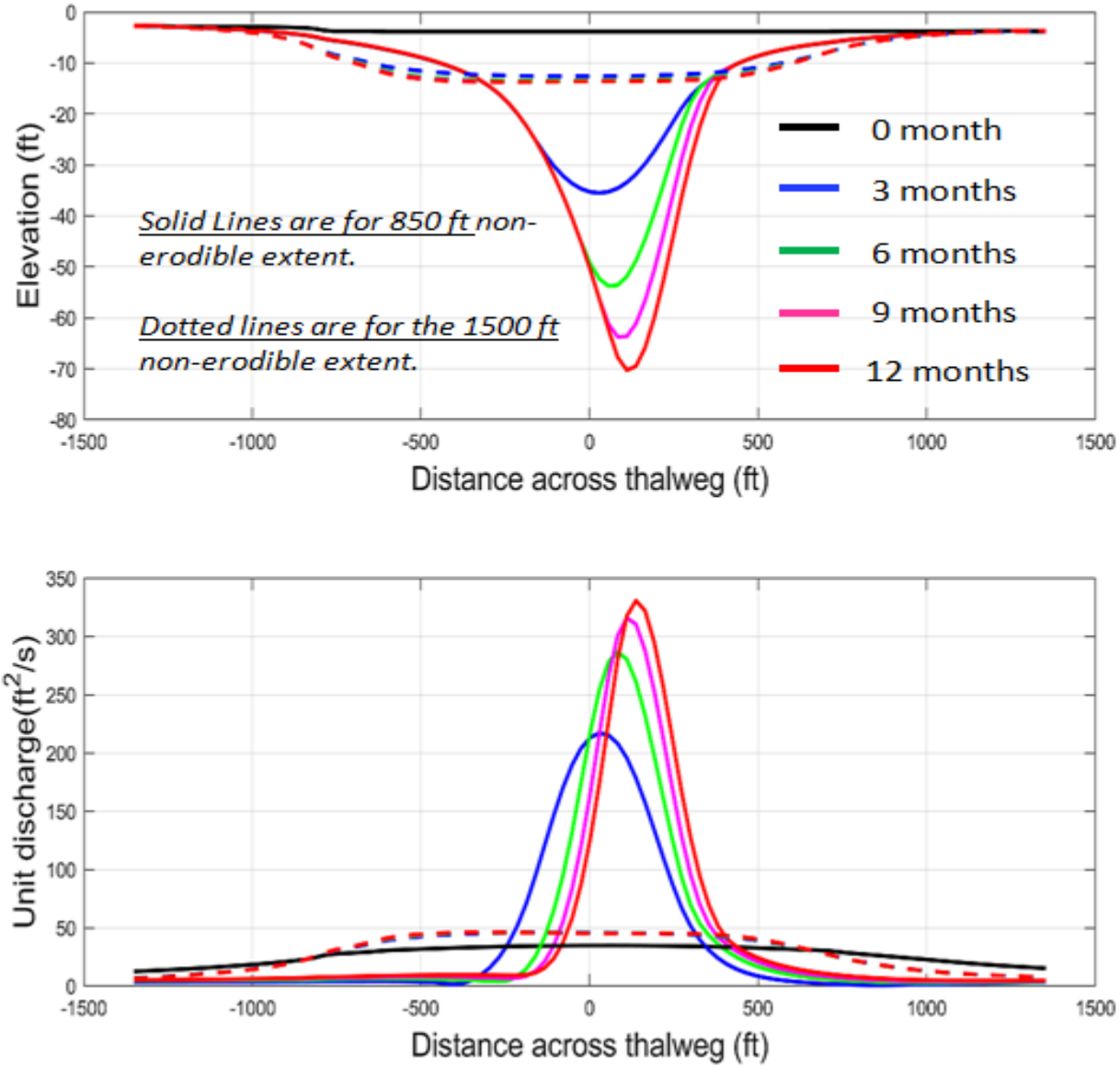

Figure 7.46. Scour hole elevation and associated unit discharge evolution for constant peak diversion flow over 1 calendar year (steady state constant diversion discharge of 75,000 cfs over 365 days).

7.3.7 Scour Evolution with River Sediment Supply

To evaluate the effect of the river sediment, particularly the armoring due to the sand contribution from the river, the 2D Delft3D (FTNOMBARefined) model was re-run with sediment input from the 3D Delft3D (FTN2Comp) model. Figure 7.47 shows the respective model domains and the boundary conditions.

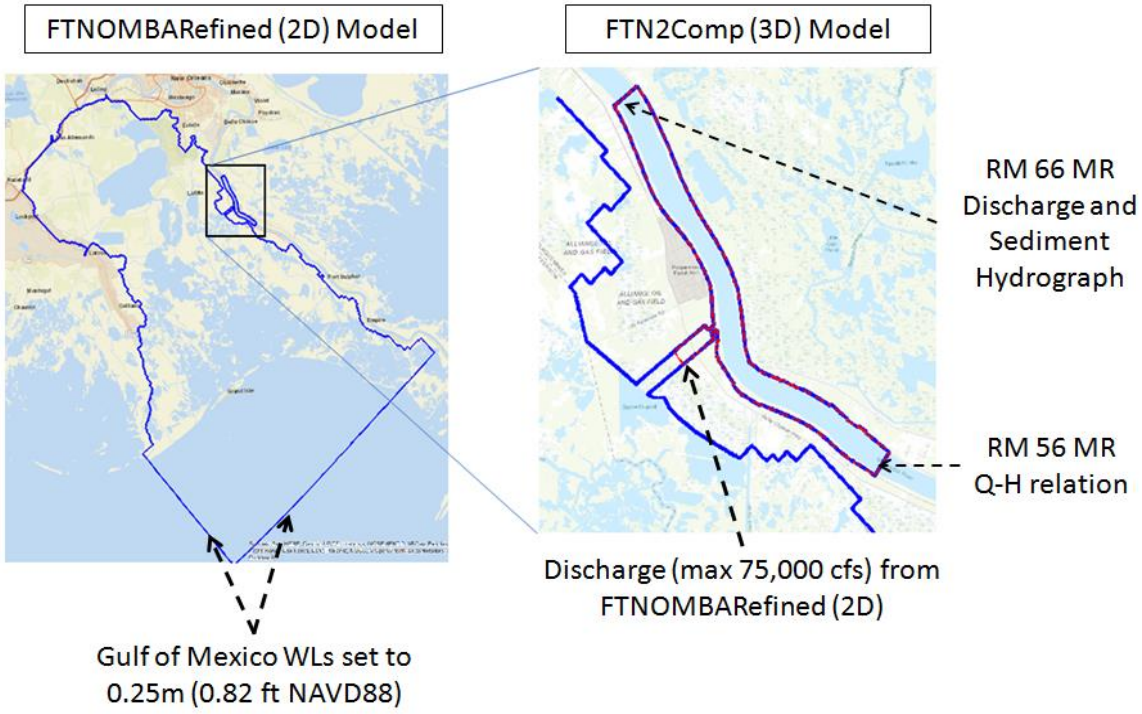

Figure 7.47. FTNOMBARefined (left) 2D Delft3D and FTN2Comp (right in red) 3D Delft3D model domains and the boundary conditions.

The scour evolution was evaluated using a 3-year flow and sediment hydrograph from 2008 through 2010 as shown in Figure 7.48. The model was run only for the period when the MR flow exceeded 450,000 cfs (i.e., the trigger flow for the diversion operations) denoted by the black dotted horizontal line. The model was run continuously for the consecutive operational periods with the operational periods sequenced one after another in time. The sediment was input as a uniform cross-sectional averaged concentration. The total sediment load was divided into

sand and fines as specified using the Hysteresis Sediment Rating Curve (HSRC) for total load and Traditional Rating Curve (TRC).

The following steps were followed to compute the flow and sediment load input for the FTNOMBARefined (Flow+Sediment) Model:

- Step 1: Perform a 3-year (2008-2010) run with the 2D FTNOMBARefined (Flow only) model to obtain water level (WL) time-series at the mid-channel location
- Step 2: Extract WL time series at mid-channel location to specify as an input boundary condition to the 3D FTN2Comp (Flow-Sediment) Model
- Step 3: Perform a 3-year run with the 3D FTN2Comp (Flow+Sediment) model with the same 3-year flow hydrograph (2008-2010). Specify sediment loads at RM 66 using HSRC and TRC rating curves. The diverted discharge from the 3D FTN2Comp model is capped at 75,000 cfs.
- Step 4: Extract cross-sectionally averaged diverted sediment concentration at mid-channel location from the 3D FTN2Comp model output and input to the 2D FTNOMBARefined (Flow+Sediment) model as a boundary for mid-channel. The river domain of the 2D model is removed in this step.
- Step 5: Perform a 3-year (2008-2010) 2D FTNOMBARefined (Flow+Sediment) run
- Step 6: Extract bathymetry/ topography at the end of the 3-year period from the 2D FTNOMBARefined morphology run and perform a steady state run with the 2D FTNOMBARefined (Flow Only) Model with MR flow at 1M cfs to verify that the diversion capacity is above design capacity of 75,000 cfs.

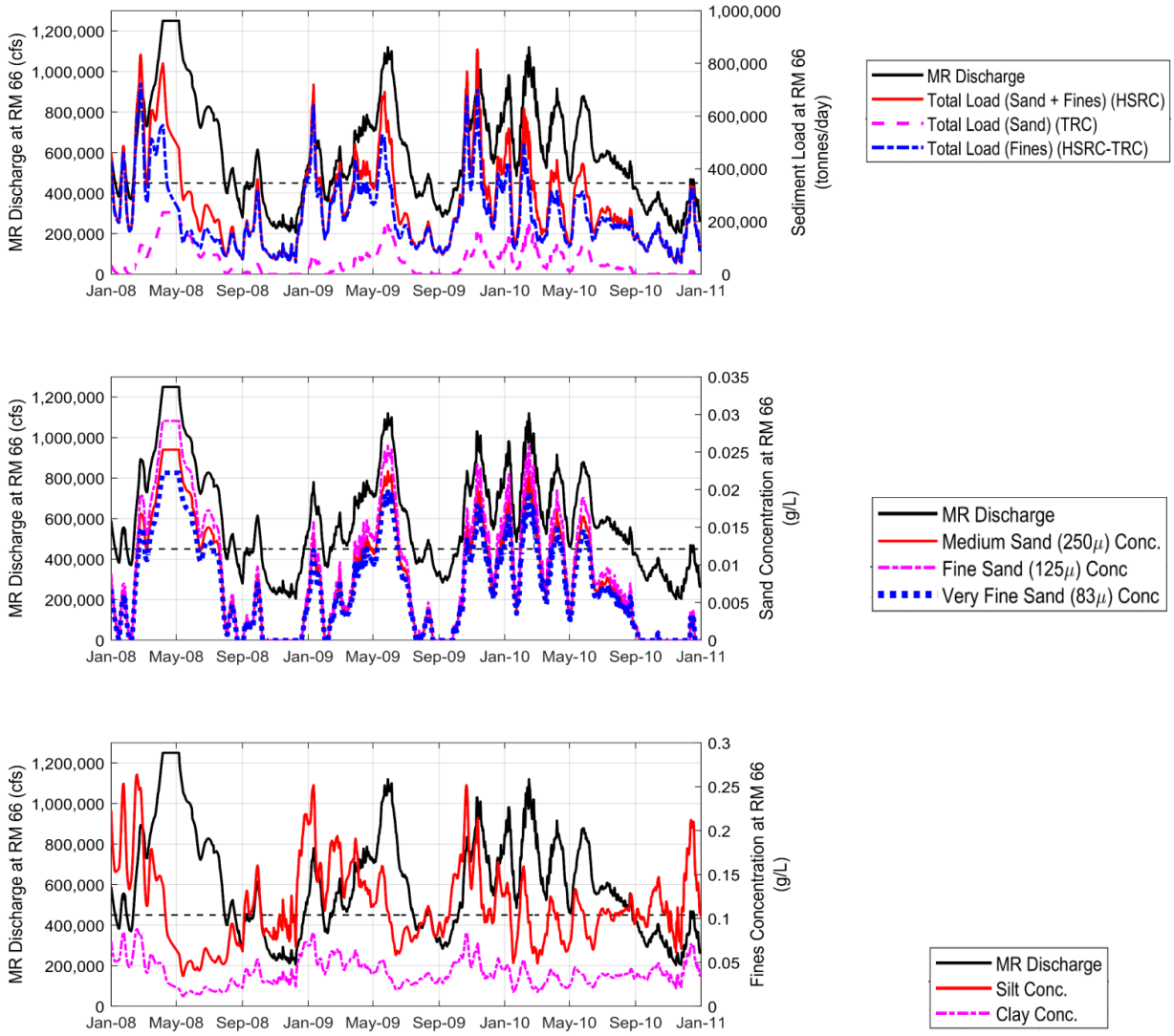

Figure 7.48. The 3-year (2008-2010) boundary conditions applied at RM 66.

Figure 7.49 shows the variation of the bed elevation along the thalweg of the scour hole as predicted by the models. It is seen that at maximum scour elevation is about -63 ft at the end of Year 1 when diverted sediment is considered versus -80 ft when river sediment is not considered. This is due to the increase in critical bed shear stress and erodibility of the scour hole as a result of armoring by the river sand and also the increase in bedload supply from the incoming sediment from the river. However, even though the scour hole is shallower with river

sediment at end of Year 1 with river sediment, the scour hole keeps deepening in the subsequent years and reaches about -78 ft at the end of Year 3. This elevation is similar to the scour elevations at the end of Year 1 for the no-river-sediment case. This implies that for the design of scour mitigation, use of the end of Year 1 scour hole bed elevations is reasonable. The rate of deepening decreases from Year 1 to Year 3 indicating a tendency for an equilibrium depth. This modeling analysis validates the presence of a significantly deep outfall hole with the base design even in the presence of river sediment and explains why such deep holes exist at other locations along the LMR outlets described previously (Section 2).

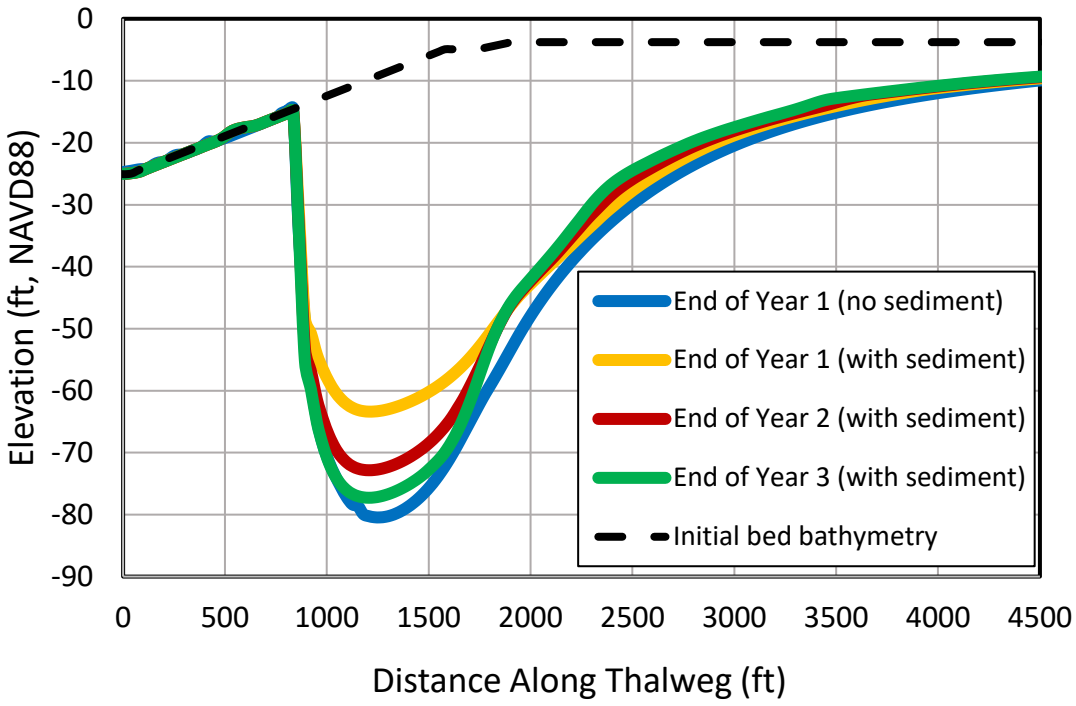

Figure 7.49. Bed elevation along the thalweg of the scour hole for the 3-year (with river sediment) and the 1-year (no river sediment) simulations. The OTF is 1,500-ft (850-ft non-erodible). Critical shear stress of erosion of the native material was 1.5 Pa.

Figure 7.50 shows the scour hole thalweg elevations for the critical shear stress specifications of 1.5 Pa and 2.5 Pa. The 2.5 Pa case shows a shallower hole (about, -45 ft, NAVD88) at the end of Year 3 (with river sediment) compared to a deeper (about, -53 ft, NAVD88) at the end of Year 1 when river sediment is not considered. Based on the predicted rate of progression, it appears that the scour hole has approached equilibrium.

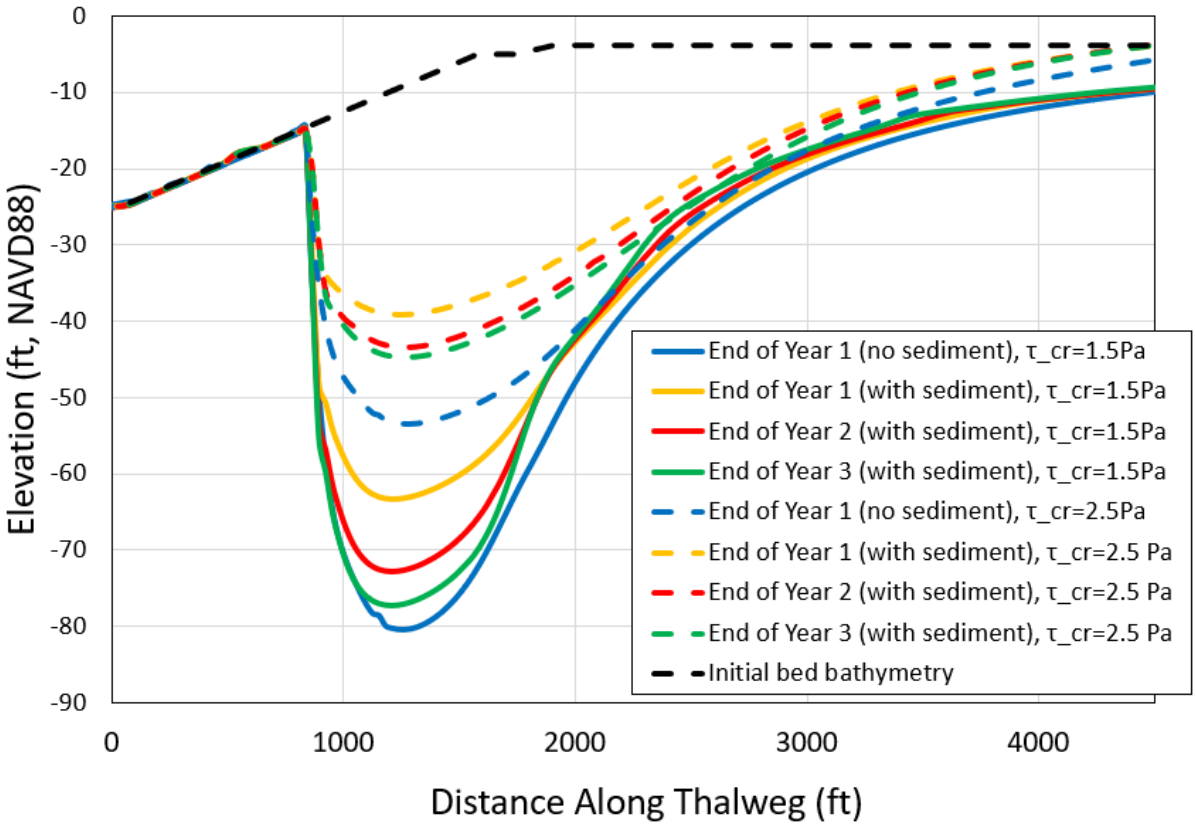

Figure 7.50. Sensitivity of the scour hole depth to the critical shear stress of erosion of the underlying stratigraphy (below -10 ft, NAVD88). The OTF is 1,500-ft (850-ft non-erodible).

The OTF configuration of 1,500 ft length with the entire length being non-erodible was also evaluated. Figure 7.51 shows the comparison of scour elevations from the 3-year (with river sediment) run with the 1-year (no river sediment run). It is seen that at maximum scour elevation of about -11 ft, NAVD88 at the end of Year 1(with river sediment) is similar to the elevation of about -14 ft, NAVD88 at the end of Year 1without the river sediment scenario. Note that the rate of progression of the maximum scour is very slow and reaches about -14 ft.

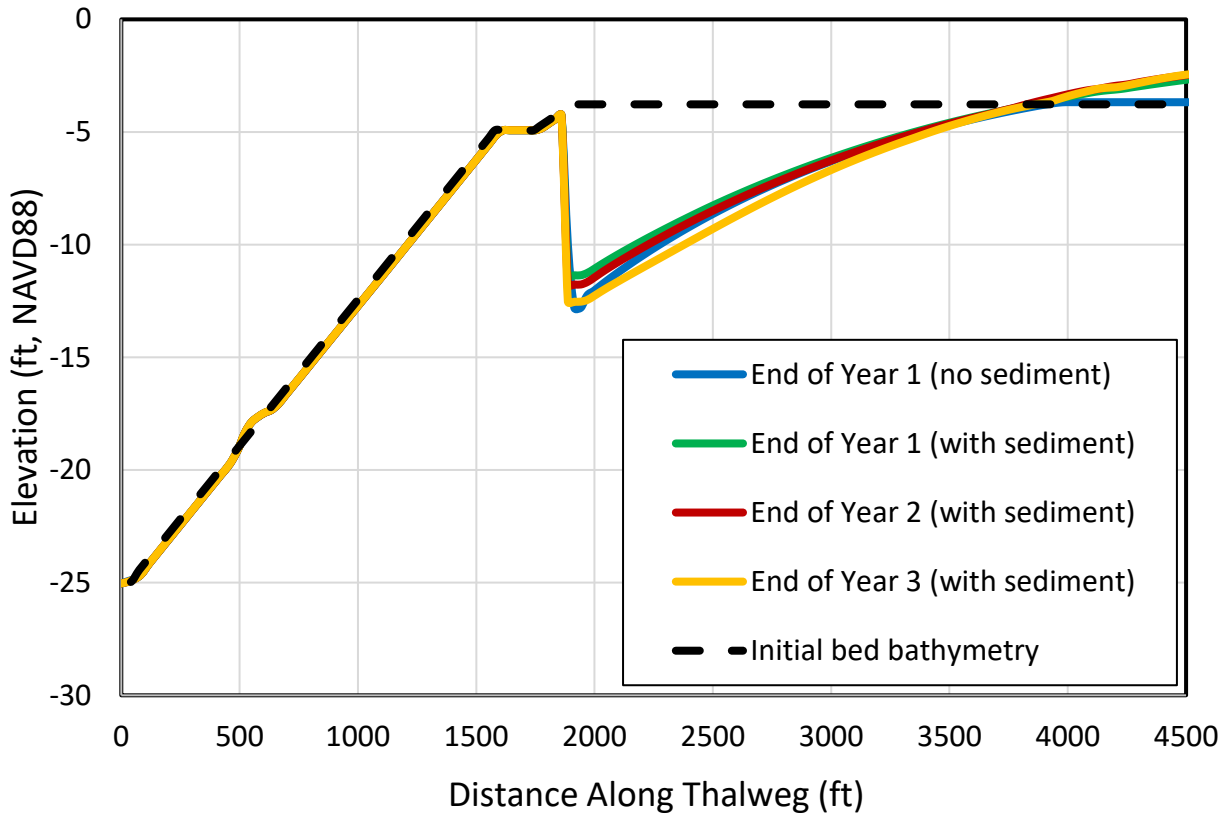

Figure 7.51. Bed elevation comparison along the thalweg of the scour hole with river sediment (3-year run) and without river sediment (1-year run). The OTF is 1,500-ft (all non-erodible).

Figure 7.52 shows the comparison of bathymetry/topography from the end of Year 3 of the FTNOMBARefined model with that from the published WIOMBA model results (Esposito et al., 2017). It is seen that the general deltaic network distributions are similar, indicating the relative insensitivity of the deltaic network to the choice of the applied river hydrograph. Note that the WIMOBA05 model had a 4,500 ft erodible OTF while the FTNOMBARefined model in this case has a 1,500 ft OTF with the first 850 ft as non-erodible.

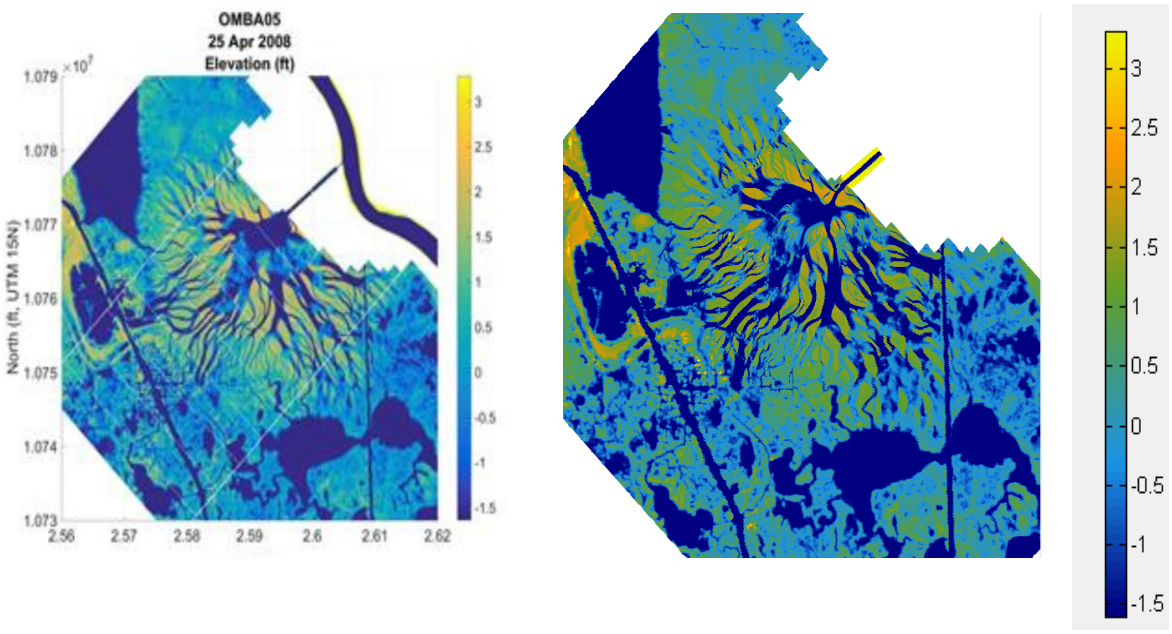

Figure 7.52. Comparison of bathymetry/ topography predicted at the end of 4.5 years (left panel) from the WIOMBA05 model (Esposito et al., 2017) model with that predicted at the end of 3 years from the FTNOMBARefined (right panel).

7.4 Development of the Three-Stage OTF Design at60% E&D phase

As shown in the previous sections, the 1,500-ft (all non-erodible) OTF leads to a much shallower scour hole (about -14 ft, NAVD88) compared to the 1,500-ft (850-ft non-erodible) OTF scour hole (about -80 ft, NAVD88). To reduce the cost of the OTF rip-rap, the DT and CPRA decided to evaluate an OTF layout that is pulled back into the conveyance channel. The proposed design was a 2,000 ft long single stage (only 1 flare angle) OTF. Similar to the previous OTF modeling evaluations, the 2,000-ft OTF was also evaluated with a 1-year (no river sediment) hydrograph (Year 2008) as well as a 3-year (with river sediment) hydrograph (Year 2008-2010).

The most important finding from this design was that a single stage pulled back OTF with lateral guide walls is insufficient to prevent flow separation along the OTF shoulders which causes sheltered areas where sediment deposits. Note that the 1,500 -t OTF designs which extended in the open marsh beyond the existing NOV levee, did not need guide walls as flow was allowed to spill over the OTF sides. As seen in Figures 7.53 and 7.54, the deposition along the raised guide levees of the 2,000-ft OTF extends all along its length, while for the 1,500-ft

OTF which does not have levees, the deposition extends only up to about the middle of the OTF from the end of the channel. This is because the outflowing water from the 1,500-ft OTF can spread more, particularly in the south-east direction.

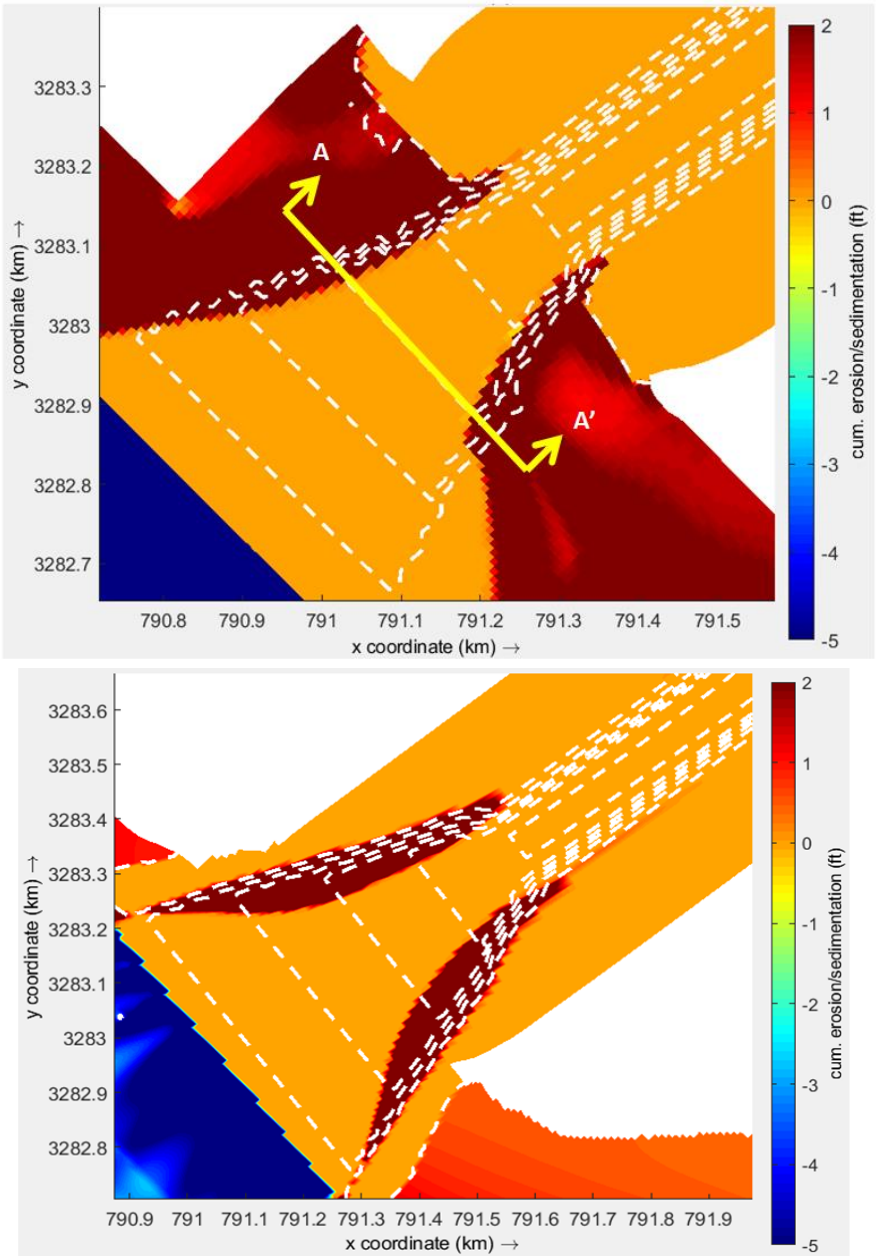

Figure 7.53. Comparison of predicted erosion/deposition at the end of Year 1 for model runs with river sediment included for the 1,500-ft OTF (upper panel) and the 2,000-ft pulled back OTF. Color bar represents cumulative erosion (-ve, blue)/ deposition (+ve, red).

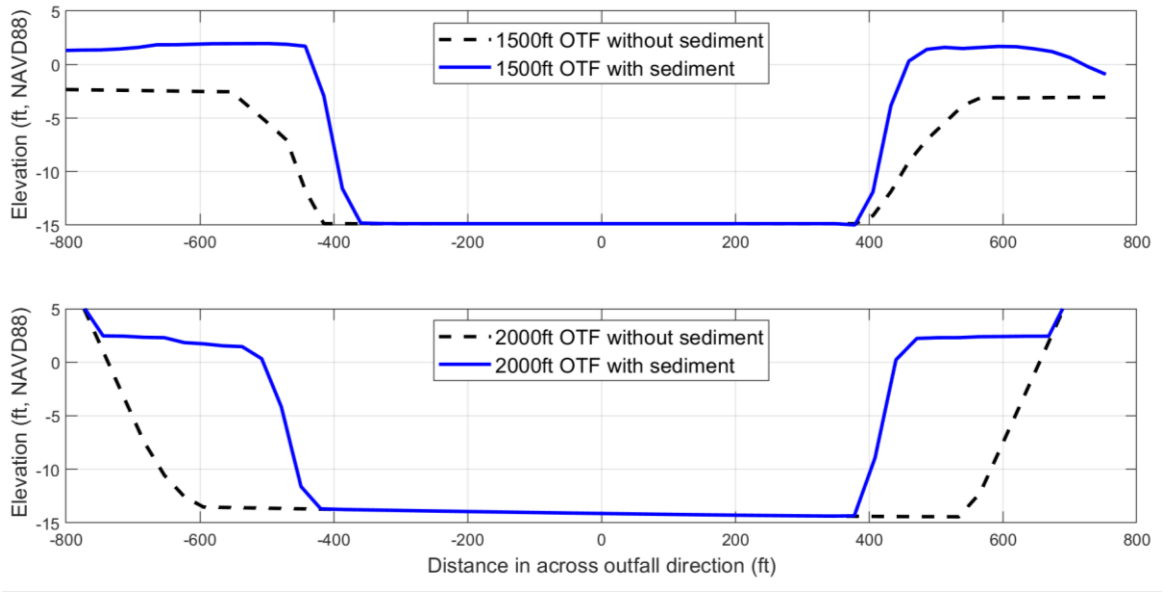

Figure 7.54. Scour hole cross-section (A-A' in Figure 8.6) at the end of Year 1(with- and without-river-sediment) for the 1,500-ft (upper panel) and the 2,000-ft pulled back OTF.

The above lateral deposition induced scour enhancement is confirmed by the unit discharge analysis as shown in Figure 7.55 which shows the centerline variation of unit discharge for the two OTF designs (1,500 ft and 2,000 ft pulled back) with and without river sediment. It is seen that the 2,000-ft OTF enhances the unit discharge for the with-sediment run (green line) compared to the without-sediment (red dotted line) run. The lack of extended lateral guide levees and reduced deposition of the 1,500-ft within the OTF keeps the unit discharge similar to the without-river sediment case. Even though the deposition of the sediment reduces the cross-section of the flow within the OTF somewhat in the first year, this deposition seems to have reached equilibrium and little further reduction of the cross-section is observed in the subsequent years.

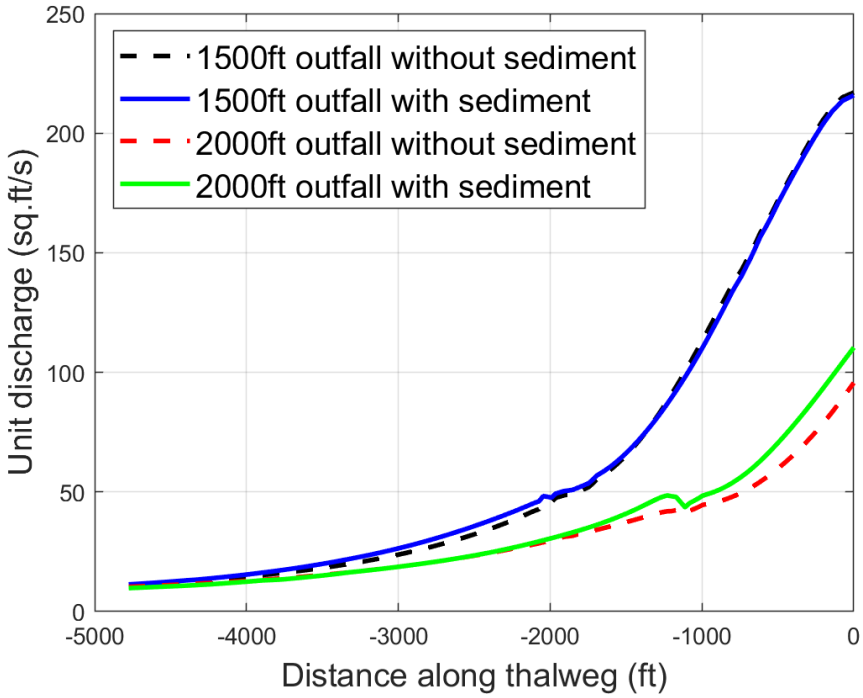

Figure 7.55. Unit discharge variation along the thalweg of the scour hole at the end of Year 1 for the with- and without-river-sediment runs for the 1,500-ft and 2,000-ft OTFs.

Using findings from the previous designs, a series of OTF designs were evaluated using FLOW-3D by varying the angle of flare, stages of flare (i.e., one, two or three stages of flare) with the aim of keeping separation to a minimum along the sides of the OTF confined by the guide walls, yet keeping an economical transition length. The currently advanced design is a three-stage OTF as shown in figure 7.56. The figure shows flow velocity vectors along with 2 ft/s or below velocity contours. Silt deposition is expected only on the shallow berms at or less than 1 ft/s indicating that the main flow path from the OTF can remain relatively free of deposition. The reduction of flow separation was also found to reduce expansion head loss by 4-5%.

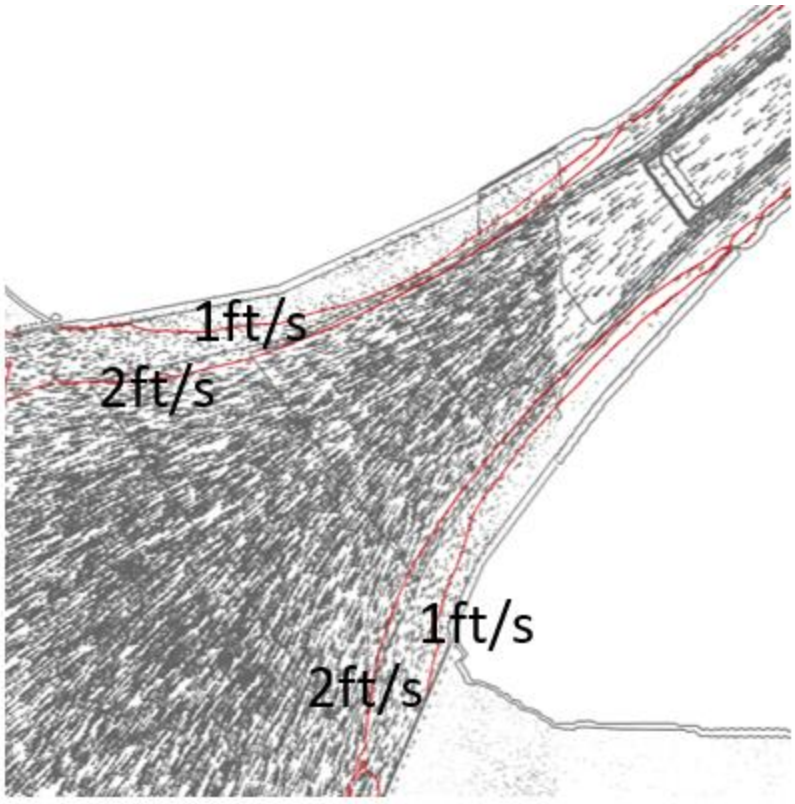

Figure 7.56. Three-stage OTF design with velocity vectors and contours of velocities at or below 2 ft/s shown with red lines. Deposition is mostly expected along the shallow berms (< 1 ft/s) and the main OTF channel is expected to remain relatively clean.

The end result was reduced scour at the end of three years (Figure 7.57) by about 4 ft due to reduced deposition at the shoulders and better spreading of flow along the OTF edge. Scour was found to reach -11 ft, NAVD88 or about 7 ft deeper than the existing -4 ft, NAVD88 marsh surface. In light of the inherent uncertainties of the erosion properties as discussed before as well as the model sensitivity to the critical shear stress of erosion it is suggested a safety factor of at least 2 be used for design of any head-cut prevention feature (e.g., a toe wall). Also, a sacrificial armor of about 50 to 100 ft is recommended at the end of the OTF edge to allow self-adjustment of the scoured face assuming a 1:4 stable rock slope after scour formation.

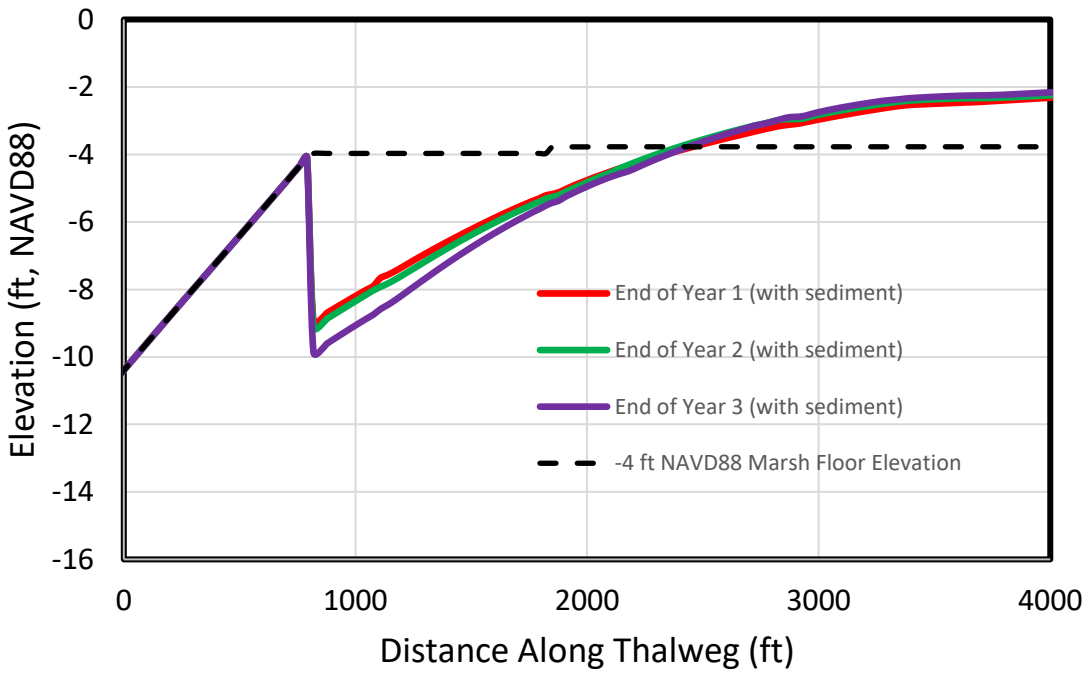

Figure 7.57. Evolution of scour hole over three-years for the three-stage OTF geometry design.

7.5 Access Channel Route Modeling

Two access channel routes (Figure 7.58) are considered by the DT during the construction phase. The following modeling was conducted to evaluate the impact on outfall scour if either of these channels are left in place post-construction.

Figure 7.59 shows the bed elevations after 3 years following the start of diversion operations with either or none of the access channels left in place. It is seen that most of the new deltaic land forms beyond a mile from the OTF end and is unaffected by the access channel layouts. The access channels influence the scour propagation in the basin as scour is seen to follow the access channel initially. The major length of the southern access channel which crosses the southerly flow from the diversion is expected to start filling up by emerging deltaic sand bars while the northern access channel remains relatively clear of deposition. This is further confirmed by cross-sections shown in Figure 7.60 across the channels.

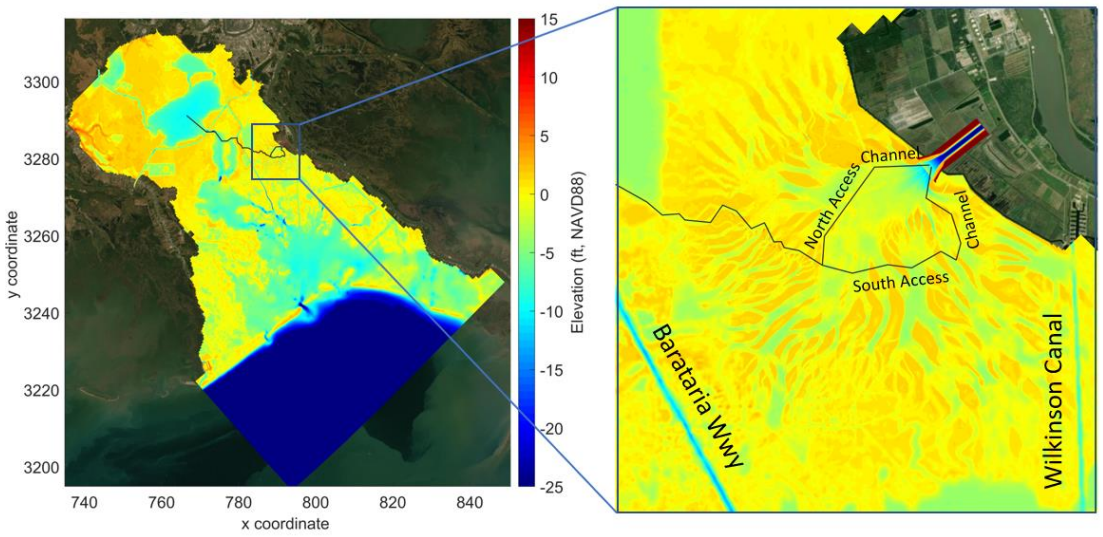

Figure 7.58. Two access channel routes investigated.

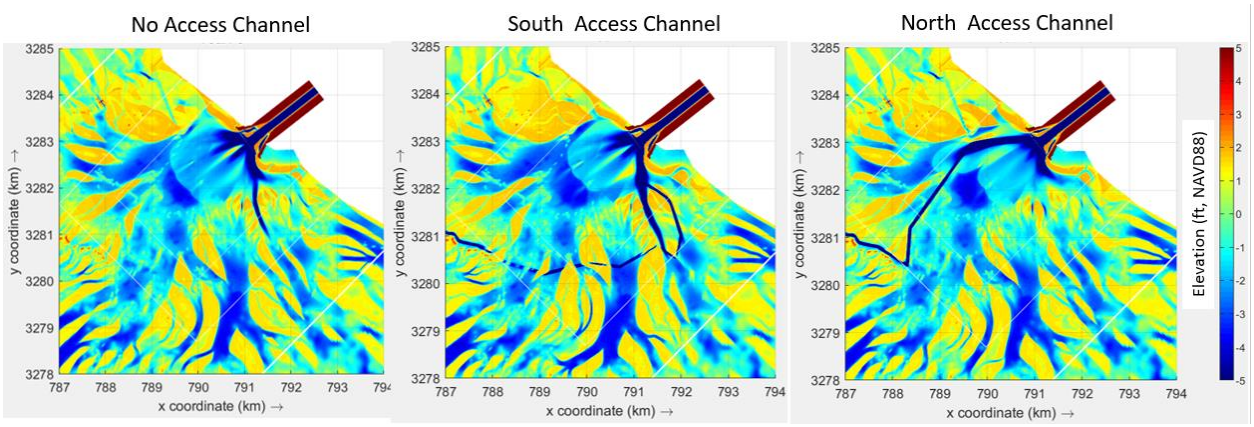

Figure 7.59. Bed evolution after three years with and without access channel left in place at the start of operations.

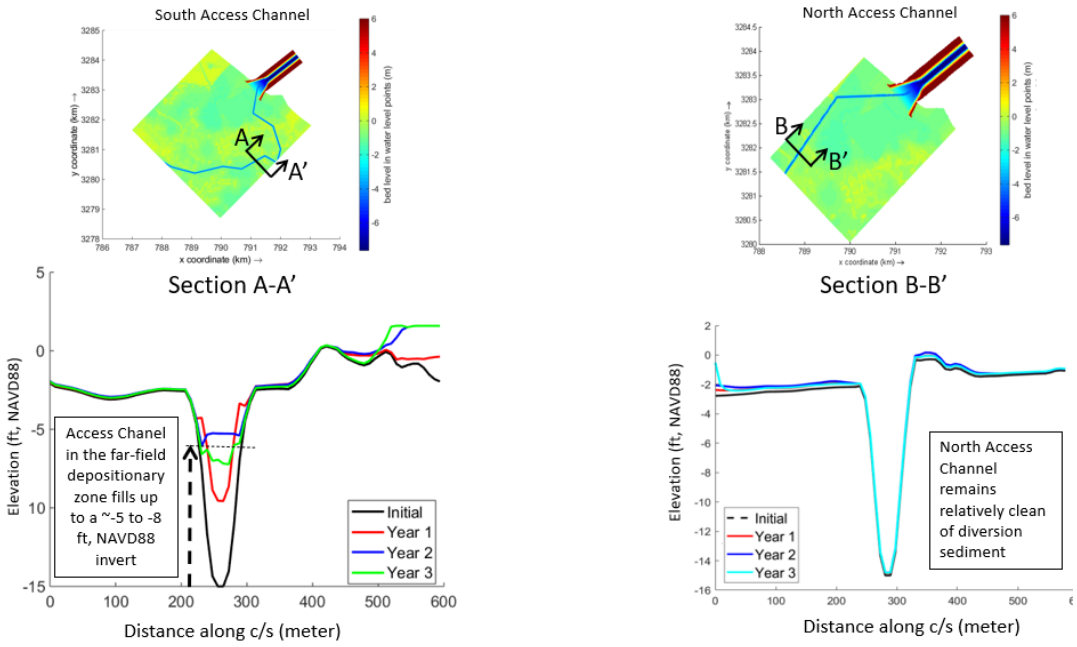

Figure 7.60. Southern access channel is starting to fill up while the northern access channel remains relatively clean. Cross-sections looking upstream.

Figure 7.61 shows the impact of the access channels on the scour at the end of the OTF. The presence of both the access channels increases scour by concentrating flow from the OTF in the vicinity of their channel axis. One of the differences seen between the north and south channels is that bank cutting induces channel migration towards the *right* where the main core of the flow is concentrated for the northern access channel while little to no bank cutting is seen for the southern channel. Both channels show deeper scours, -20 to -25 ft, NAVD88 for the north channel and -30 to -35 ft, NAVD88 for the south channel than the -11 ft, NAVD88 for the no channel case. No significant impact to preferential sand movement is seen through the channels as sand settles relatively small distance from the OTF due to lack of necessary shear stresses to transport further into the basin.

In summary, it is recommended that if an access channel is built, it be blocked after construction so flow cannot concentrate along the edge of the OTF. Either channel can be built, but the southern channel fills in far-field of the diversion, so if post-construction use of the channels is planned, the northern channel is preferred.

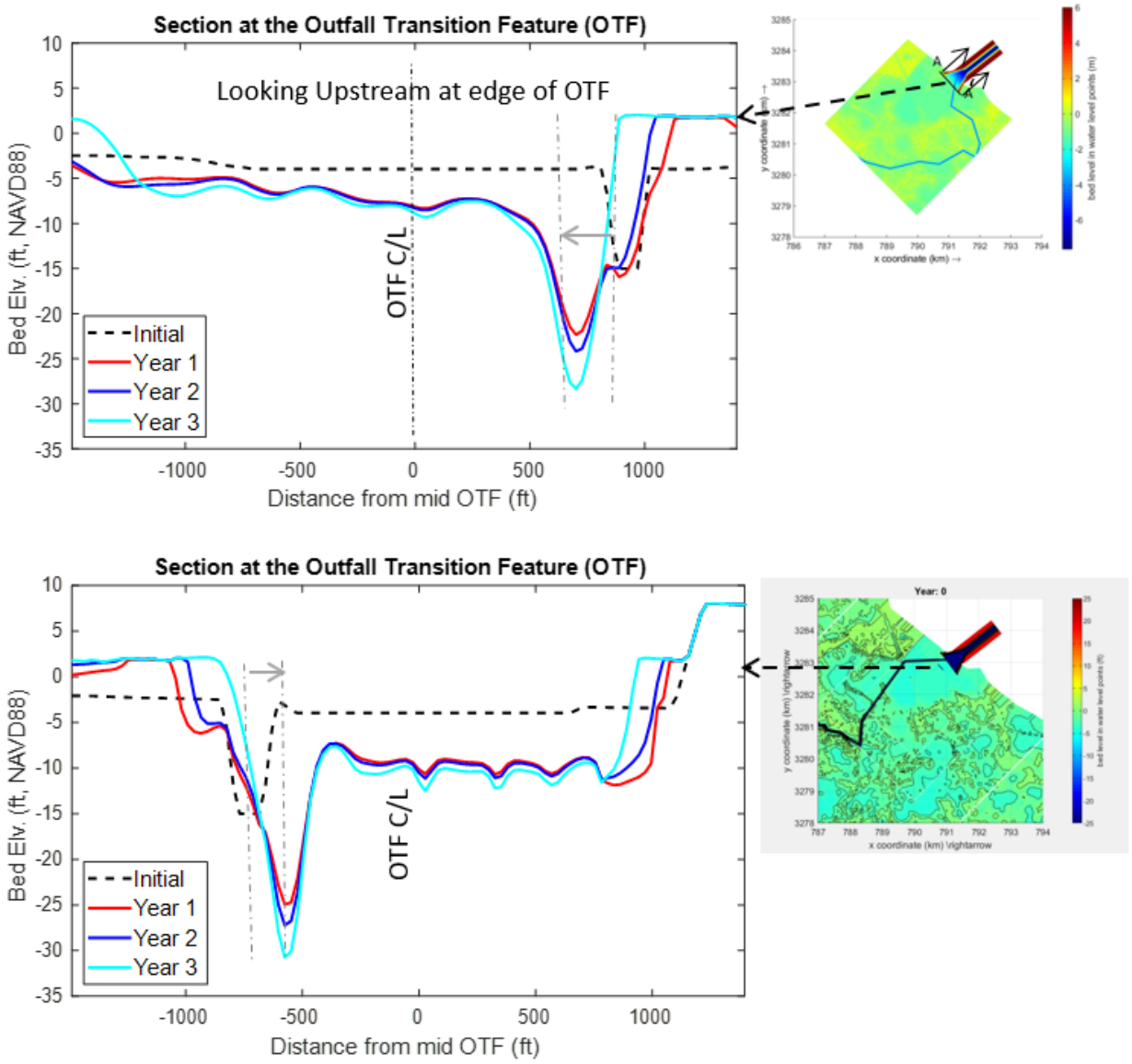

Figure 7.61. Scour evolution across the OTF edge in presence of the access channels. Upper panel is for the south channel and the bottom for the north channel. Cross-sections looking upstream.

Figure 7.62 shows the velocities in the near-field of the OTF guide walls. It shows that velocity reduces quickly as the flow exits downstream of the wall and the non-flow side of the wall remains sheltered. Over time sediment is expected to fill this sheltered place up between the levee and the walls.

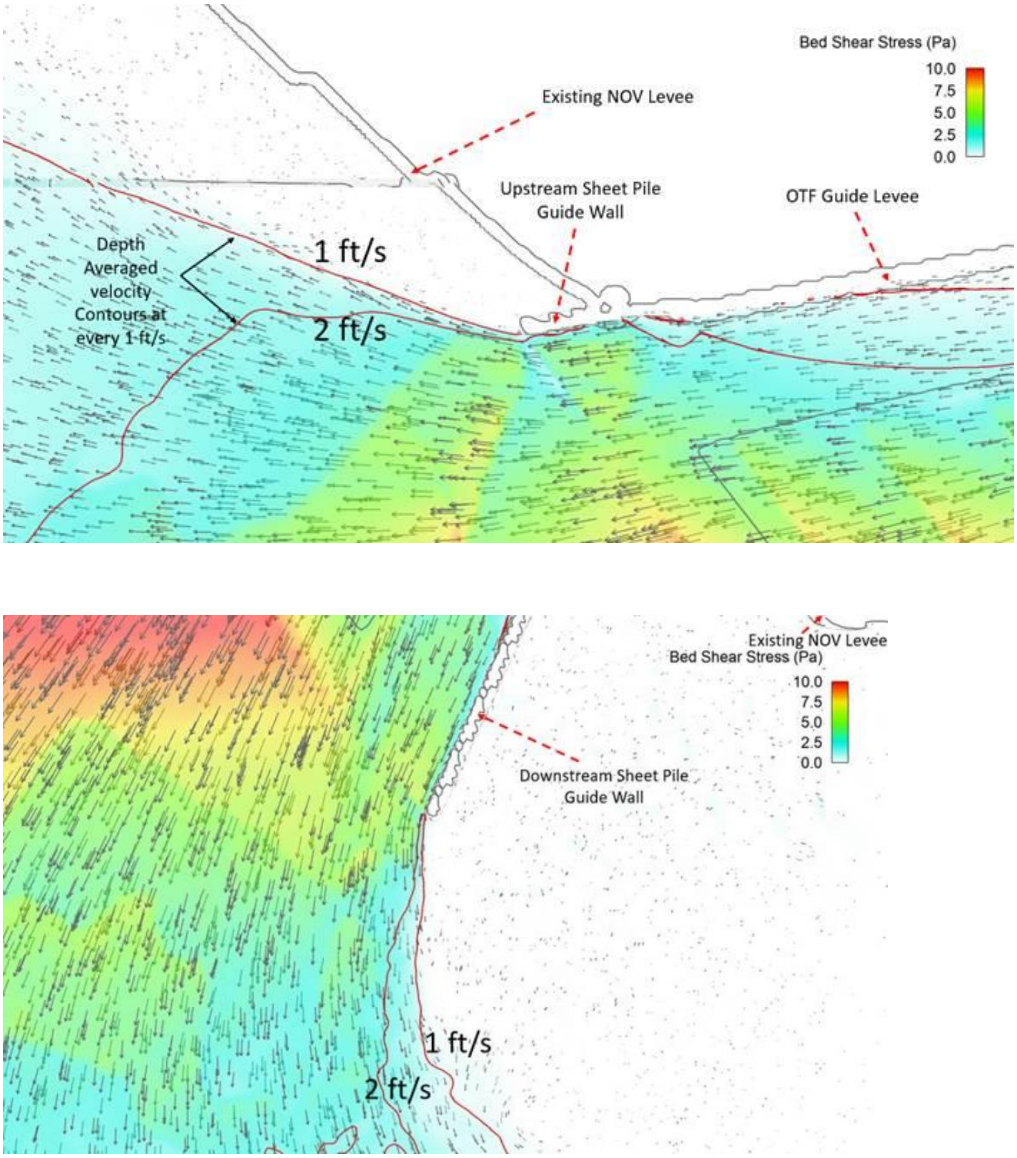

Figure 7.62. Velocities near OTF guide walls.

7.6 Conclusions

It was recognized and demonstrated that a significant potential exists for development of a scour hole at the end of the outfall depending on the configuration of the Outfall Transition Feature. The numerical modeling showed a large range of scour depths of 7-75 ft depending on the length of the non-erodible outfall length, input parameters for erosion and geometry of the OTF. Due to the large uncertainty in the numerical morphology models, information from

multiple resources, such as observations of existing scour holes and field experience of the experts should be used to design countermeasures.

The following conclusions can be reached from the numerical modeling performed to date:

1. Scour elevations are very sensitive to the critical shear stress of native material, erodibility and less sensitive to the inclusion of river sediment in the outfall models.
2. In initial designs with a 1,500-ft, 850-ft non-erodible, OTF, the model predicted a deep scour hole (bottom elevation about -55 to -80 ft, NAVD88) at the end of the riprap. The shallow jet also showed separation once a deep hole is formed. Jet separation within the OTF is not desired as it increases the unit discharge leading to an increase in scour.
3. In case of the 1,500-ft, all non-erodible, OTF, the model predicted shallower scour hole (bottom elevation about -15 ft, NAVD88) at the end of the riprap. This is because the outflowing water is able to spread out all the way along the 1,500-ft length of the OTF.
4. The design of the OTF was evolved subsequently to be pulled back into the NOV levee and a three-stage final design which minimizes flow separation, reduces lateral deposition and yields the least scour while also keeping an economic transition length was developed at the end of the 60% design phase.
5. The 3D hydraulic modeling of the scoured outfall vicinity showed that the hydraulic results from the 2D morphology model are reasonable. It also showed that if a scour hole forms at a point far enough upstream of the OTF where the jet has not spread out enough, then it can keep deepening through a feedback mechanism.
6. Scouring starts at about 50,000 cfs. In the initial years of operation, it is recommended to carefully monitor the scour by keeping the maximum flow at or below this and gradually ramping up in the years. More information on operational modeling and control of scour will be provided in 90% design.
7. For the tested river hydrograph (Year 2008), model predicted that most of the scour occurs during the rising limb of the diversion above 60,000 cfs flow as flow reaches the peak flow (75,000 cfs) over a period of 1-2 months. It is recommended that the diversion flow be closely monitored and the OTF regularly surveyed during the first year of operation to prevent any catastrophic rapid progression of scour.
8. River sediment slows down the rate of scouring but cannot be relied upon to fill in scour holes from a design perspective.

At this 60% phase in the E&D, the 2,000-ft, pulled back, 3 stage flare angled, all non-erodible OTF is the preferred alternative.

8.0 THREE COMPONENT MODELING

8.1 Introduction

The three-component modeling results described in this chapter relate to the FLOW-3D (3D) FTN3Comp model and the Delft3D (2D) FTNOMBA (including the 10-mile MR) domain. Once all the individual components of the diversion structure as described in previous chapters: 4 (Intake), 5 (Intake Transition), 6 (Conveyance Channel) and 7 (Outfall Transition Feature) were designed, the modeling was carried on combining the three components (the Intake Headworks, the Conveyance Channel and the Outfall Transition Feature) together. The construction and modeling of this three-component domain is important because even though the diversion components were initially modeled separately to identify the best design that meets the overall requirements of capacity and sediment transport as well as their individual performance metric, this is the first time all of the components are brought together and their effect as a system can be evaluated including the net head loss through the MBSD system.

The FLOW-3D model was first constructed with the three components together and run for specific steady state conditions. The Delft3D model was then calibrated against the FLOW-3D results. The calibrated Delft3D model was then applied for the secondary tasks described later.

Therefore, the objectives of the three-component modeling were as follows:

1. Calibrate the Delft3D (2D) FTNOMBA model against the FLOW-3D (3D) model results for head loss, velocity and water level for the three-components.
2. Use the Delft3D FTNOMBA model to develop diversion discharge performance rating curves under current conditions.
3. Use the Delft3D FTNOMBA model to perform select operations analysis such as base flow frequency, situations of reverse flow from the basin to the river to inform design.

8.2 Model Setup

A FLOW-3D (3D) FTN3Comp model as well as the FTNOMBA (2D) Delft3D model were used. The details about the FTNOMBA model can be found in Chapter 3 (river-side) and

Chapter 7 (basin-side) and are not repeated here. Only those specific boundary conditions are discussed that are used for the purposes of the modeling tasks discussed in this chapter.

8.2.1 FLOW-3D FTN3Comp Model

The FLOW-3D three-component model domain is shown on Figure 8.1. It consists of the same FTNMSDI domain (intake headworks and the river) along with the full length of the conveyance channel (9,750 ft) and 3 miles of the basin from the outfall in the Barataria Bay. The distance of 3 miles to the tailwater boundary conditions was determined sufficient from initial sensitivity tests to eliminate tailwater boundary influences on the diversion discharge. The tailwater boundary in the basin is determined from a previously run Delft3D FTNOMBA (2D) run with a constant 75,000 cfs diversion discharge. Note that even though the 75,000 cfs discharge condition is possible under a variety of MR water levels, typically in the range 7.2-8.2 ft, the water level 3 miles downstream of the outfall is more or less constant as it is determined by the discharge coming out of the outfall alone. The tailwater boundary may be affected by Gulf of Mexico (GoM) water level though, but this does not affect the FLOW-3D results as both Delf3D and FLOW-3D are reproducing the same condition when the GoM water level is the Mean Water Level (MWL) of 2020 which is 0.82 ft, NAVD88.

Table 8.1 lists the grid-sizes in the various mesh blocks in the domain. Uniform expansion was used to make a smooth transition from block to block. Similar to FTNMSDI model setup (Chapter 3), the MR is set to a roughness value of 0.6 m, the intake concrete U-Frame to 0.006 m, the intake transition, the conveyance channel and the Outfall Transition Feature to 0.457 m. The Barataria Basin is set to a uniform roughness value of 0.06 m.

The river bathymetry is the USACE 2012 bathymetry as described in Chapter 3. The intake headworks, the conveyance channel and the outfall transition feature bathymetries were developed as stereolithography (STL) files from as-designed 3DAutoCAD drawing file renderings. The Barataria Basin bathymetry was taken from the FTNOMBA Delft3D model and validated with recently (2019-2020) collected bathymetry by the design team.

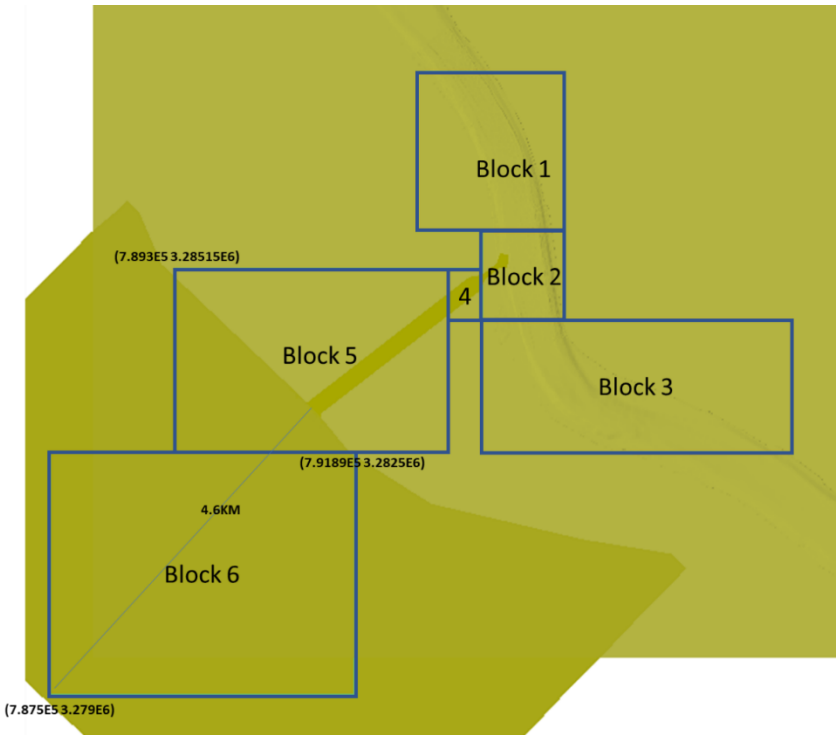

Figure 8.1. FLOW-3D FTN3Comp Grid and domain extents. The mesh block numbers correspond to grid resolution descriptions in Table 8.1.

Table 8.1. FLOW-3D FTN3Comp Model Mesh resolution.

Block #	Δx (m)	Δy (m)	Δz (m)
1	4.5-10.0	6.0-10.0	1.8-3.5
2	1.3-7.0	1.3-6.0	1.8-3.5
3	5.0-10.0	5.0-8.0	1.8-3.5
4	1.3-5.0	1.3-5.0	0.8-1.0
5	5.0-11.0	7.8-8.0	0.5-0.6
6	1.3-5.0	1.3-5.5	0.8-1.0

8.2.2 Delft3D FTNOMBA Model

For all steady state runs with FTMOMBA, a representative mean or most likely design condition was chosen in the basin. To this end, the GoM water level in the FTNOMBA model was held constant at 0.82 ft (0.25 m) NAVD88 based on the observed MWL at Port Fourchon for 2020. The downstream MR boundary at RM 56 uses the same stage-discharge (Q-H) relation

developed in Chapter 3. The steady state runs were also used to model the water levels and velocities through the diversion components under current and future conditions as described in the Design Document Report (DDR).

For the calibration runs, the Delft3D model had a vegetation cover consisting of various marsh vegetation species and was defined from the 2013 observed Louisiana Coastwide Reference Monitoring Stations (CRMS) data. In Delft3D trachytope formulation based on Baptiste et al., (2007) was used to model the vegetation induced roughness change. Thus, the model indirectly simulates the vegetation drag induced backwater effect at the diversion outfall. Note that since much of the Barataria Basin in the vicinity of the outfall is devoid of intertidal flats, vegetation is sparse in this area and therefore, under the current conditions, vegetation drag contributed very little to the energy dissipation in the main kinetic dissipation zone of the diversion flow. However, the approach was still retained since additional modeling under future conditions, when land building will cause development of intertidal emergent vegetated islands and thereby modify flow, is ongoing.

The calibrated FTNOMBA model was also used to explore the possible variation of the discharge capacity under varying MR hydrograph, MR water level and GoM water level conditions. Since the number of possible combinations are too large to be modeled individually, a technique based on interpolation of results from a Monte Carlo type combination of many steady states runs under a variety basin water levels and/or river discharge and water levels was adopted. The 2008-2019 observed time series of Port Fourchon water levels were used. For these runs, the GoM water level was varied from -1.0 to +3.0 ft, NAVD88 and the MR upstream was set at steady state between 100,000 cfs (lowest observed flow) to 1,250,000 cfs (highest observable flow) at 50,000 cfs intervals. For the period when the MR flow is below 450,00 cfs and the diversion flow is possibly affected by wide fluctuations in daily water levels from tides and wind, the role of the variation of the MR water level with discharge was also addressed. For this purpose, two additional Q-H curves downstream of MR at RM 56 (Figure 8.2) were also developed and included in the modeling. The observed daily MR discharge hydrograph, the daily observed GoM water level and the RM 56 (downstream MR boundary) daily water levels (interpolated from USACE Alliance and W Pt A La Hache gages) were used as the basis for the

interpolation of the results from the steady state Monte Carlo runs. Obvious reverse flow conditions when the MR water level at the diversion intake (RM 60.7) was below the GoM water level were eliminated from the runs. A total of 161 steady state runs were simulated for flows below 450,000 cfs and about 75 for above 450,000 cfs.

The above exercise also yielded valuable information on availability of base flow discharge of 5,000 cfs and the feasibility of maintaining it with the current design when the MR flow is below 450,000 cfs. The modeling also addresses frequency of occurrence of reverse flow either below or above 450,000 cfs based on the observed CRMS and MR intake water levels at RM 60.7 from the 2008-2018 period as an example. The analysis on reverse flows is extended to the future as well based on available sea level rise information. Note that all the analysis conducted here is based on daily averaged data. Therefore, while it does include spring and neap tide effects as present in the observed data, the analysis does not include diurnal tidal variations. The analysis considering diurnal tidal variations will be presented in the 90% E&D phase but is unlikely to change any results significantly because analysis of tidal phase lags in the basin and the river shows little difference indicating that effect of tides on the diversion discharge will be small, possibly much smaller than the monthly variation.

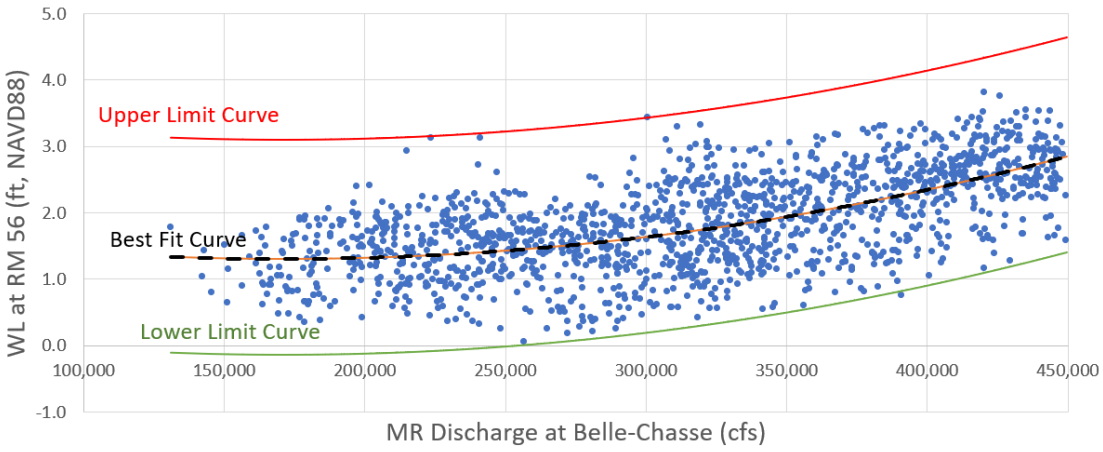

Figure 8.2. Two additional Q-H curves (Upper Limit and Lower Limit) in addition to the Best Fit Curve developed in Chapter3 developed for modeling at conditions below diversion trigger flow (< 450,000 cfs) where tidal effects are evident. The curves encompass the possible range of observed water level and discharge combinations in the 2008-2018 period.

8.3 RESULTS

In this section first the calibration results between FLOW-3D and Delft3D are presented followed by application of the FTNOMBA Delf3D model for capacity estimate and base flow analysis.

8.3.1 Calibration of Delft3D model with FLOW-3D model

A series of Delft3D FTNOMBA model runs were performed systematically varying the conveyance channel roughness coefficients but keeping the calibrated roughness coefficients in the river domain (Chapter 3) unchanged to match the FLOW-3D diverted discharge, the diversion centerline water surface elevation and the depth-averaged velocity. The final comparison of calibrated results for these three quantities along the three-component diversion centerline is shown on Figure 8.3. Figure 8.4 shows the final calibrated Chezy roughness coefficients comparison with Delft3D and FLOW-3D for the three-components and the Barataria Bay. A separate Manning's based roughness calibration was also performed and was validated by physical model results for the conveyance channel roughness.

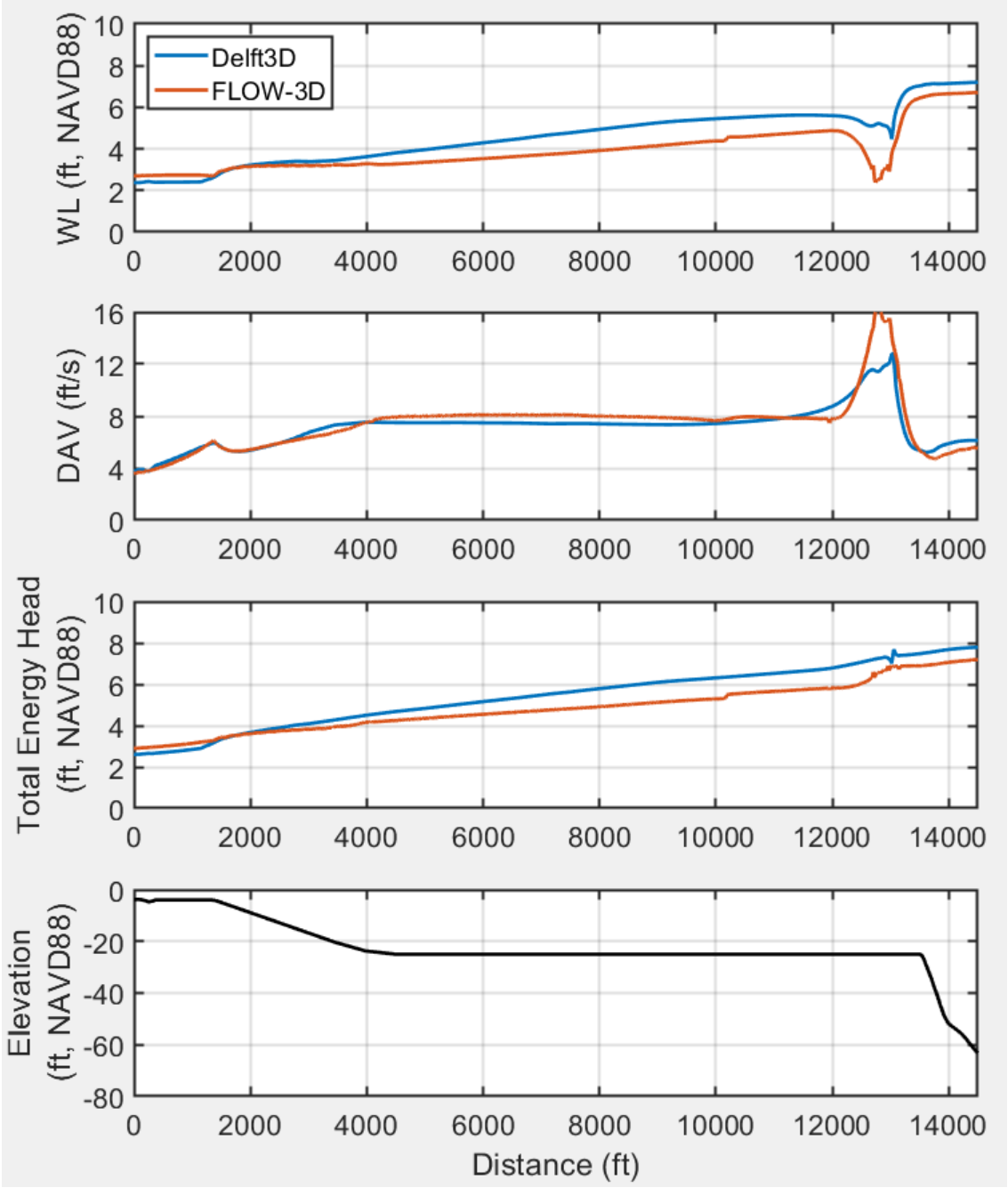

Figure 8.3. Calibrated centerline plots of three-component Delft3D FTNOMBA model with FLOW-3D FTN3Comp model. From top to bottom, Water Level (WL), Depth-Averaged Velocity (DAV), Total Energy Head and Bathymetry.

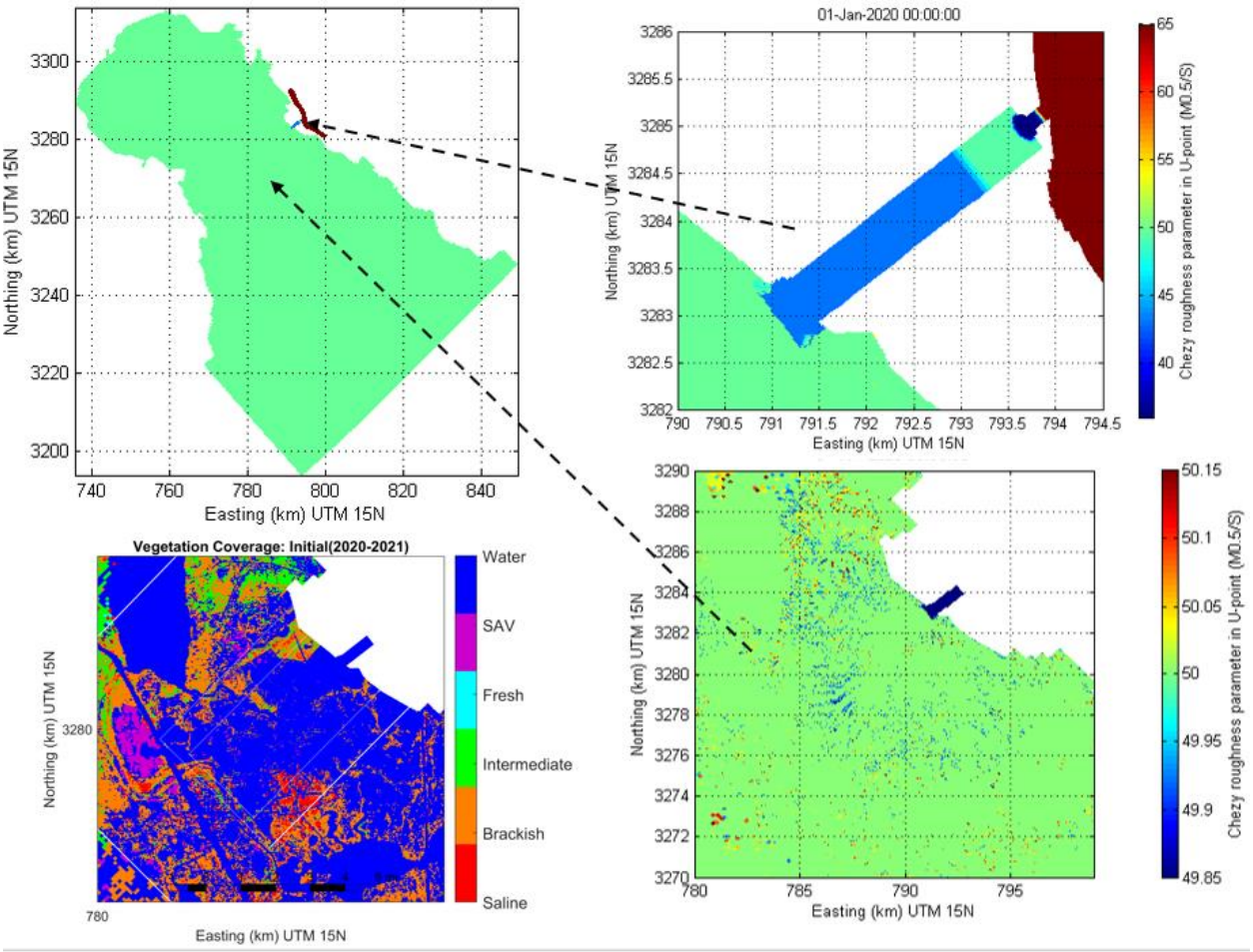

Figure 8.4. FTNOMBA Chezy roughness distribution in the three-component system (top right) and vegetation (left bottom) induced roughness modification in the basin (bottom right).

8.3.2 Modeling of base flow and reverse flow frequency when MR flow is less than 450,000 cfs

The current Environmental Impact Statement for the MBSD project (GEC, 2021) assumes a 5,000 cfs continuous base flow for MBSD. However, the EIS models do not have a head driven diversion system. Instead, the diversion flow is specified as a flow boundary at the start of the conveyance channel. Moreover, it does not consider the structural dimensions and head losses based on the actual as designed conditions. Therefore, as part of the initial operations modeling study it was decided to investigate how many days of 5,000 cfs or more diversion flow

may be actually possible and how many days of flow below 5,000 cfs or reverse flow can occur. Currently the understanding is that the gates will remain completely closed below 5,000 cfs to prevent reverse flow situations. At flows below 450,000 cfs when reverse flow can probably occur, diurnal variations can range up to 5,000 cfs due to tides. Therefore, if strictly no reverse flow is allowed, it is probably better to close the gates if the possibility exists that flow can fall below 5,000 cfs. Of course, even if the capacity is available, the gates will restrict the flow to 5,000 cfs mean daily flow.

There are fundamentally three boundary variables that affect the diversion discharge: the river discharge, the river water level (which is influenced by tides and wind and hence can vary for a given discharge) and the GoM water level. Figure 8.5 shows the time series of the reconstructed diversion discharge for MR flow less than 450,000 cfs from the observed data using the matrix of 161 Monte Carlo runs.

Figure 8.6 shows the average number of days in a given month when the daily flow in the MR is below 450,000 cfs as observed from the 2008-2019 period. This figure shows that between 7 (in July) to 27 (in September) days of base flow periods may be possible in the typical July-Dec non-operational period of the diversion.

Figure 8.7 is based on the analysis of the diverted discharge reconstructed time series shown in Figure 8.5 which shows that up to 8 days per year in the months of October to December on an average is possible when the gates may have to be completely shut to prevent flows below 5,000 cfs or any chance of reverse flow from the basin to the river.

Figure 8.8 shows the monthly distribution of the mean daily discharge and the maximum and minimum discharge values using error bars. The monthly averaged daily discharge varies from about 15,000 cfs (January) to about 30,000 cfs (April). The maximum and minimum daily values range from 1,000 cfs (January) to 43,000 cfs (Sep). Reverse flow conditions are not included in the monthly discharge computations and is assumed zero as the gates are assumed to be closed. Thus, a wide variation of discharge is possible and under current conditions adequate flow capacity exceeding 5,000 cfs base flow is available. This information is important when developing channel flushing maintenance requirements that will be explored in the 90% E&D phase.

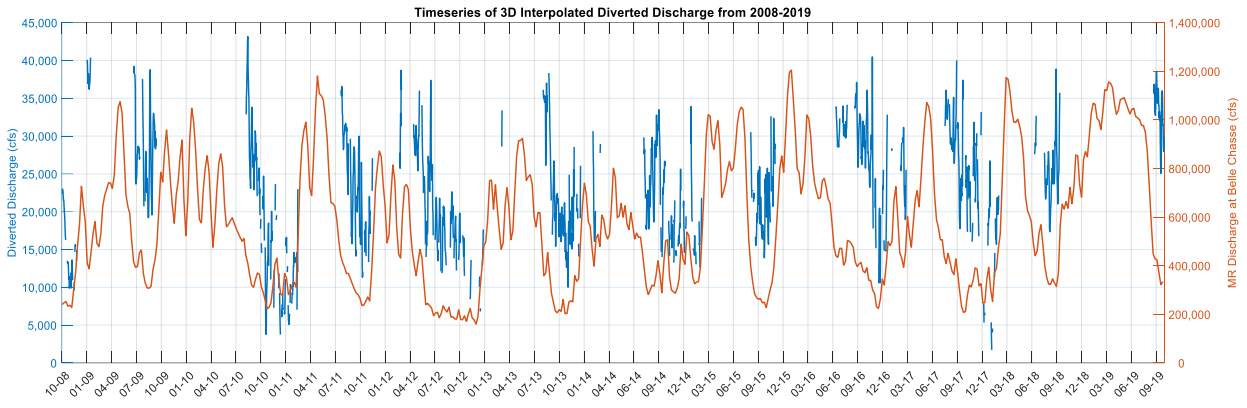

Figure 8.5. Reconstructed time series of diversion flow (left y-axis) in blue and observed MR discharge in red (right y-axis) for the 2008-2019 period when MR < 450,000 cfs from the 3D interpolation of the Monte Carlo matrix of steady state runs.

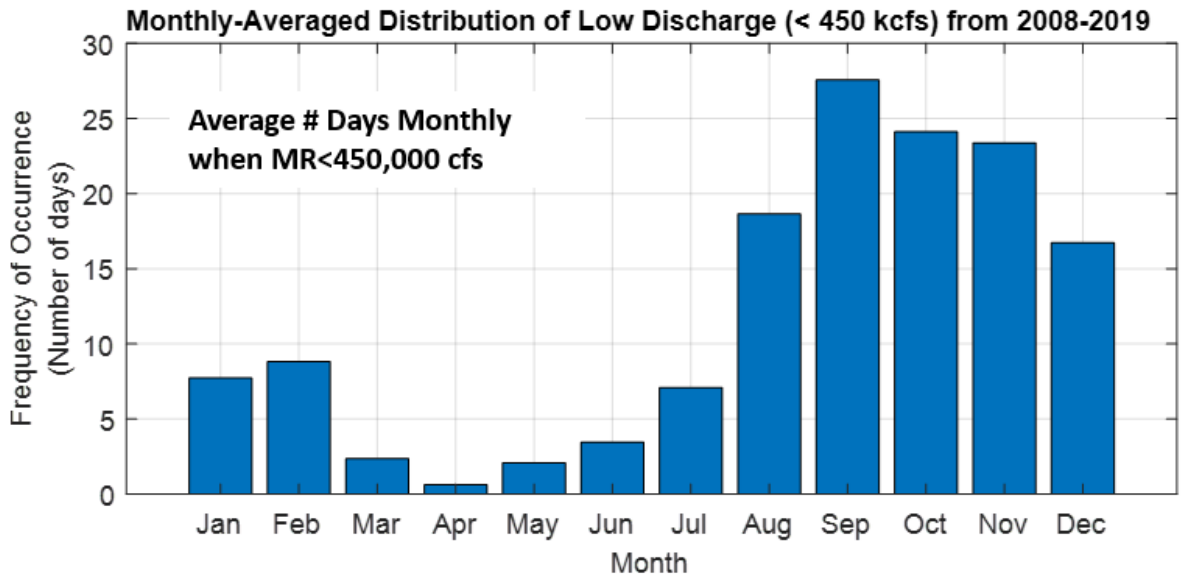

Figure 8.6. Average number of days in a given month when the daily MR flow is below 450,000 cfs based on the 2008-2019 MR hydrograph.

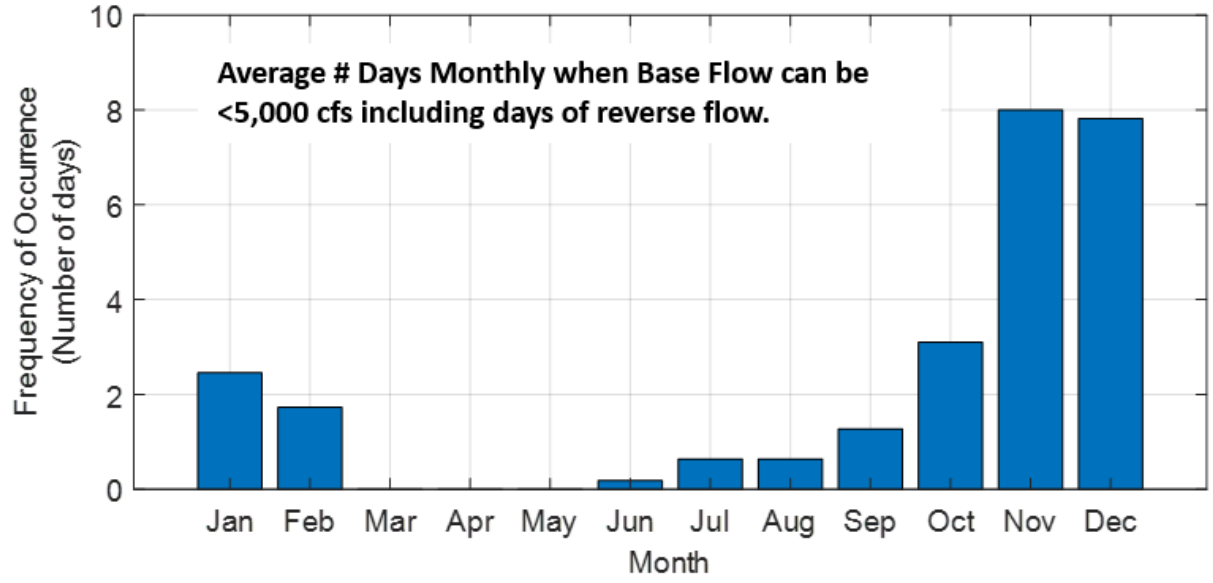

Figure 8.7. Average number of days when base flow of 5,000 cfs cannot be maintained, including the days of reverse flow.

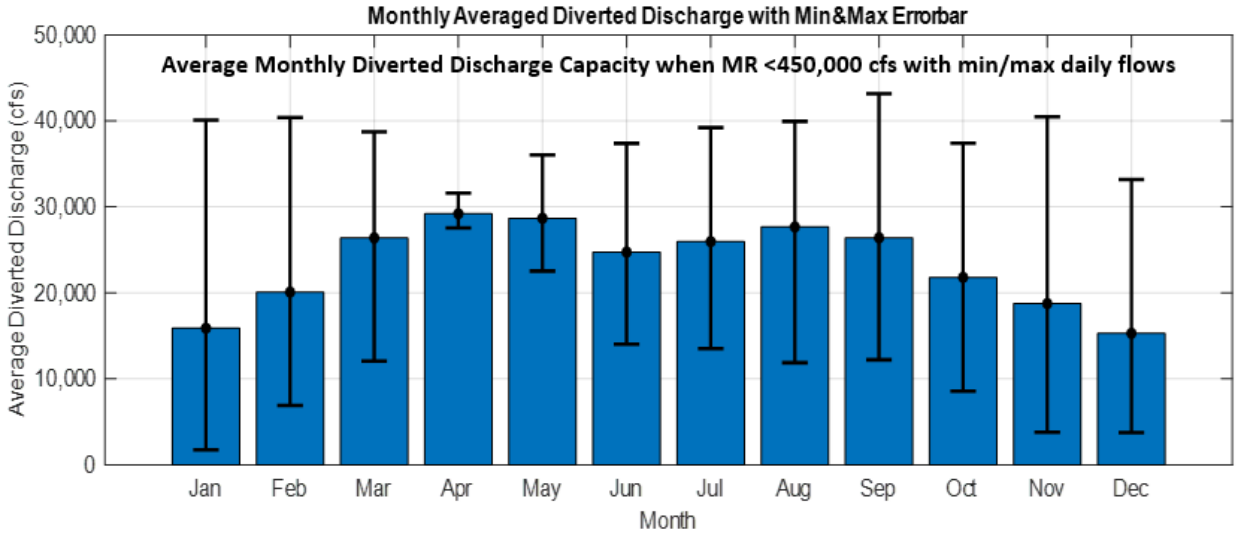

Figure 8.8. Monthly average and range of the daily discharge based on the 2008-2019 MR hydrograph.

8.3.3 Reverse flow analysis for MR flow above 450,000 cfs under future conditions

Figure 8.9 shows the future conditions for possible number days of reverse flow in a year. For the future conditions, Relative Sea Level Rise (RSLR) of 1.5 m in 100 years (Figure 8.10,

CPRA, 2012) was added to the observed CRMS (2018-2019) water levels in the basin. Note that no adjustment to water levels in the MR is done for future conditions modeling as existing studies (Karadogan et al. 2009) as well as FTN's data analysis of the WI Basin Wide model results indicate that RSLR effects are negligible in the future as far upstream the MR as RM 60.7 where the diversion is located. Since at the reverse flow condition, no connection exists between the river to the basin (flow is zero theoretically) no modeling was actually required. The water levels in the basin and the river were simply compared as a desktop analysis to develop the histograms. In the future the possibility of reverse flow even at MR flow greater than 450,000 cfs increases. In the future 50-years, particularly in the last decade, the diversion may have to be kept closed for as much as 25 days a year on average, even above 450,000 cfs to prevent reverse flow. This is tantamount to a loss of about one month of diversion operations. It is needless to say that in the future, base flow will be unavailable for a greater number of days even above 450,000 cfs than what is available currently.

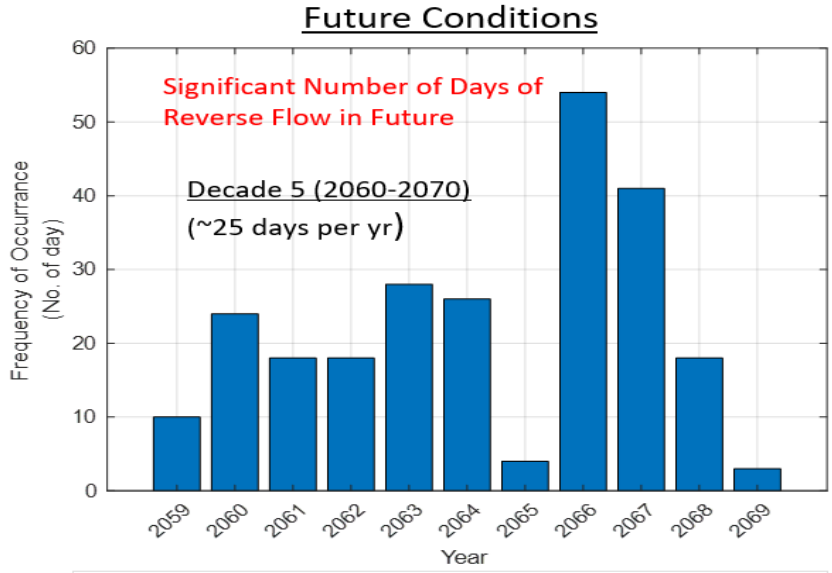

Figure 8.9. Annual number of days of reverse flow when MR > 450,000 cfs during the 50-years of operation. Left panel: Current conditions (first decade) insignificant potential for reverse flow. Right panel: Future conditions (last decade), average 25 days per year of reverse flow is possible due to RSLR.

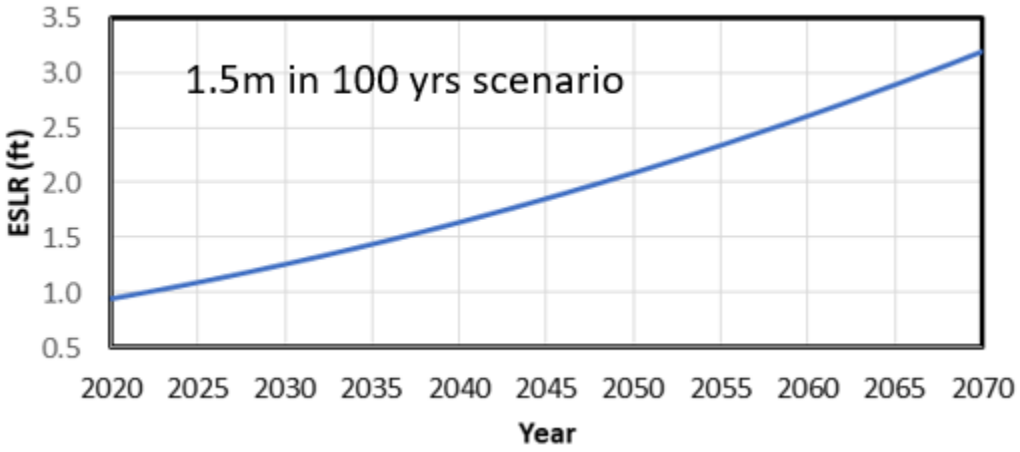

Figure 8.10. RSLR scenario used for computation of number of days of reverse flow possible now and in the future as in Figure 8.9.

8.3.4 Estimation of Diversion Discharge vs. MR Discharge (Q-Q) Rating Curve

The discharge capacity of the 1:4 (60%) and 1:7 (90%) side slope design channels without deposition is compared in Figure 6.13 for the full range of MR discharge. The FTNOMBA model was used for this purpose after calibrating with the FTN3Comp FLOW-3D model for either channel geometries. The FTNOMBA model was run using the same Monte Carlo technique discussed later in Chapter 8 with a variety of Gulf of Mexico water levels and varying MR discharge hydrograph to yield a statistically averaged diversion discharge at a given MR discharge range. The modeling indicates that on an average the 1:7 allows for a 5-16% increase in discharge capacity with respect to 1:4 channel with the benefit being highest around 650,000 cfs MR flow and lowest at about 1,250,000 cfs MR flow assuming all gates open. If gates are operated and flow restricted to 75,000 cfs this translates to a lower operating trigger for gate operations. For the 1:4 channel the diversion gates were expected to be partially closed at about 930,000-980,000 cfs. For the 1:7 channel this now becomes 830,000-920,000 cfs based on the natural water level variability between the river and the basin. The immediate benefit to this change is not only somewhat greater capacity at the highest flows but an overall increase across the entire hydrograph which translates to increase in sediment load diversion across the entire hydrograph, the detailed results of which are shown later in the basin side analysis in Chapter 10.

Another benefit to this increase in capacity is that it offsets any uncertainty of discharge capacity loss from the intake headworks from physical modeling which showed about 10% lesser capacity (Alden, 2020). A discussion on the numerical model results which were calibrated with the physical model are separately given in Chapter 11 which discusses operations modeling.

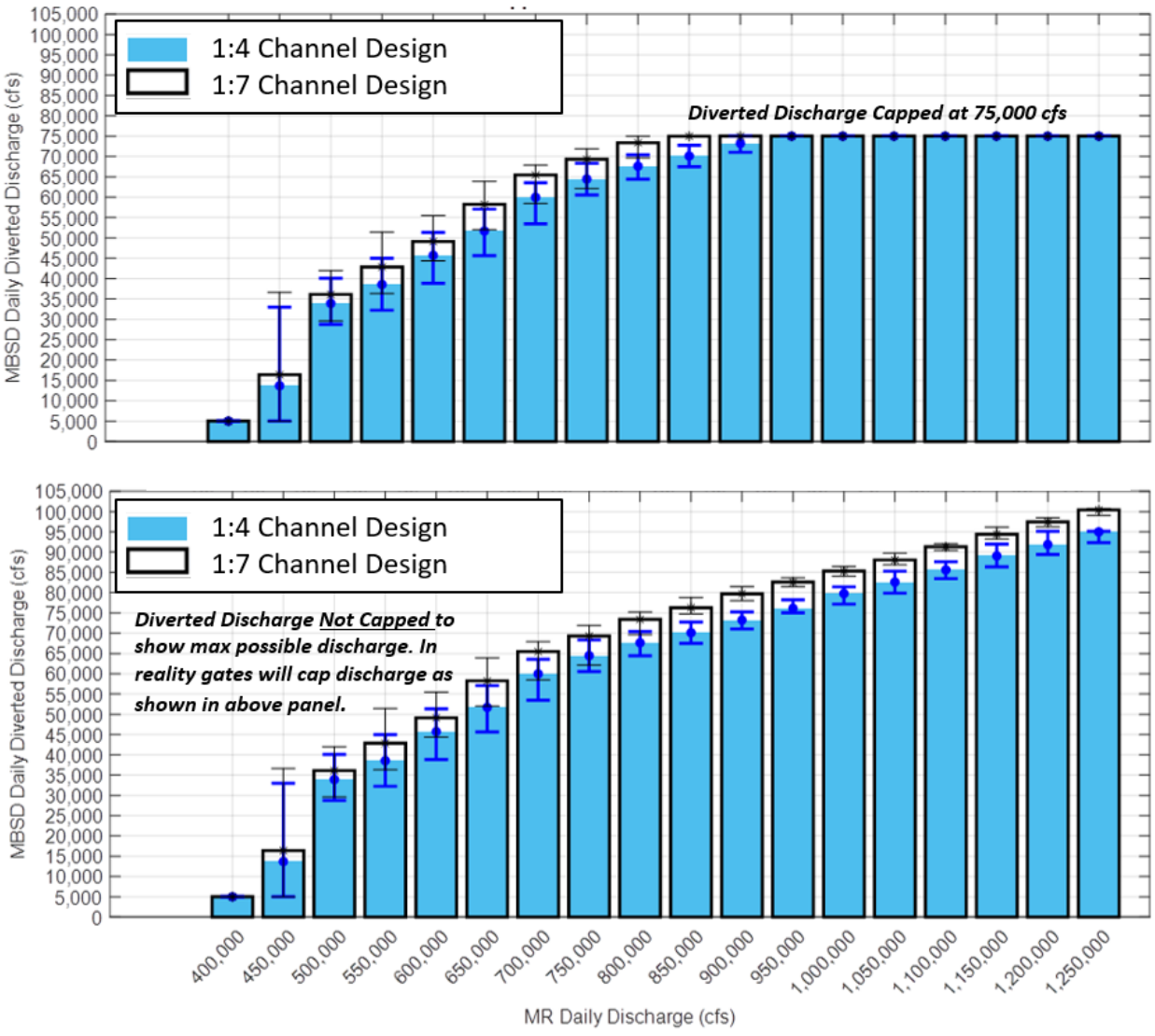

Figure 8.11. Comparison of Diversion discharge vs MR discharge (Q_div-Q_MR) for the two channel designs. Both channels are free of any deposits. The 1:7 Channel Design is adopted in 90% design stage. The 1:4 Channel Design was presented in 60% design stage.

Table 8.2 shows the simplified summary of the data with the diversion discharge values being represented by a statistical mean value over a 100,000 cfs spread around the MR flow value in the first column. It shows that at 450,000 cfs about 28.500 cfs diversion discharge is possible on an average while at 1,000,000 cfs currently about 79,800 cfs capacity exists. Note that even though the capacity above 75,000 cfs currently exists at 1,000,000 cfs, gate operations will prevent flow exceeding this limit. At about 921,000 cfs the diversion is seen to divert 75,000 cfs under current conditions. Thus, even with the MBrSD operations (at 75,000 cfs and hence allowing only 925,000 cfs MR flow at MBSD location) there is just enough capacity for the diversion to divert 75,000 cfs.

Table 8.2. Summary of Diversion Discharge at a given MR Discharge.

MR Daily Discharge (cfs)	Daily Diversion Discharge 60% Design (3Bay, -25 ft invert) (cfs)	Daily Diversion Discharge 90% Design (3Bay, -25 ft invert) (cfs)
450,000	28,500	32,500
600,000	45,600	49,500
750,000	64,700	69,800
900,000	73,700	79,900*
1,000,000	79,800*	85,700*
1,250,000	94,900*	100,200*
920,000	75,000	82,000
850,000	70,700	75,000

*For actual operations, maximum discharge will be restricted to 75,000 cfs by gates. The extra capacity is for future reserve due to rising tailwater due to land-building and RSLR.
All results rounded to nearest 100 cfs. There is a +/-5 to 8% variation in discharge due to varying river WL which is not shown here.

8.4 Change in Three-Component Model from 60% to 90%

The conveyance channel and the intake transition geometry were the main changes in the three-component design from 60% to 90% phase. Those changes and their individual modeling are documented in Chapter 5 and 6. In this section, model results showing re-calibration of the Delft3D FTNOMBA model based on the revised FLOW-3D FTN3Comp model is presented.

Figure 8.12 shows the results of the calibration between Delft3D and FLOW-3D models. This model setup and design geometry and was used for modeling done henceforth with the 1:7 channel, which includes the land-building runs with Low SLR and the High SLR without

base flow in Chapter 10 as well as operations modeling in Chapter 11. This can be compared with Figure 8.3 before for the 60% design and shows and improvement in calibration as well.

Table 8.2 is also updated with the 90% discharge capacity results across the MR hydrograph. The rating curve of the 60% design and the 90% design has been compared in Chapter 6.

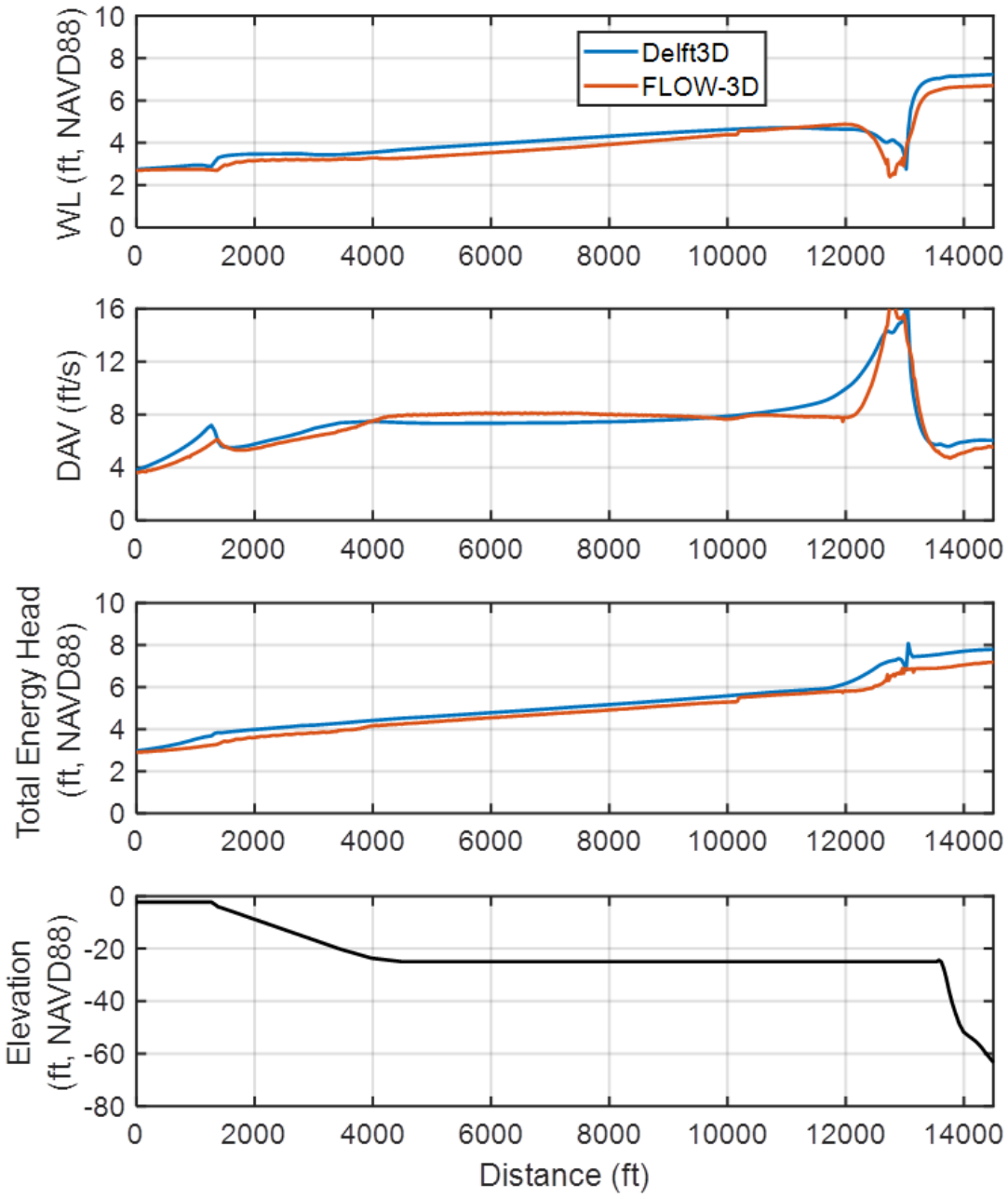

Figure 8.12. 90% Phase Design with 1:7 Conveyance Channel and Intake Transition: Calibrated centerline plots of three-component Delft3D FTNOMBA model with FLOW-3D FTN3Comp model. From top to bottom, Water Level (WL), Depth-Averaged Velocity (DAV), Total Energy Head and Bathymetry.

8.5 Conclusions

In this chapter the development of a three-component (includes the intake headworks, the conveyance channel and the outfall transition feature) FLOW-3D model is described. The FLOW-3D model was used to calibrate the Delft3D (2D) FTNOMBA 3 component roughness. The FLOW-3D and Delft3D results are independently validated with physical model channel roughness estimates as well. The specific conclusions from this chapter are as follows

1. Under current conditions, below 450,000 cfs MR flow, base flow of 5,000 cfs may not be available for about 8 days per month from during the months from October to December. It is recommended that the gates be closed in those days to prevent reverse flow.
2. Other than those days about 25,000 cfs average base flow per month may be available from July to December indicating that short term flushing flows if required to flush the channel of sediment or to maintain water quality may be available at current conditions.
3. Under current conditions, at least during the first decade (2020-2030) the potential for the reverse flow conditions is negligible at MR flows above 450,000 cfs. However, in the future, particularly in the last decade (2060-2070) reverse flow potential exists for as many as 25 days on an average per year shortening the diversion operational period by a month.
4. In the operational range, the average diversion flow can range from 32,500 cfs (at MR flow of 450,000 cfs) to 86,000 cfs (at MR flow of 1,000,000 cfs). However, the gates will cap the diversion flow to 75,000 cfs which starts at MR flow of about 850,000 cfs. The maximum diversion flow capacity possible is about 100, 200 cfs with no gates and MR flow of 1,250,000 cfs. The extra capacity currently available above 1,000,000 cfs can help offset to some extent any future loss in capacity due to land building and/or RSLR effects.
5. Under current conditions, MBSD can divert 75,000 cfs daily flow even with MBrSD operational at 75,000 cfs peak flow.

9.0 MODELING OF RIVERSIDE EFFECTS OF DIVERSION OPERATIONS

9.1 Introduction

This chapter describes the numerical modeling performed to evaluate the hydrodynamic and morphological effects of the MBSD project on the Mississippi River. The effect of MBrSD (RM 68) jointly operating with MBSD (RM 60.8) is also analyzed. The hydrodynamic effects are manifested mainly as water level set-down in the river as a result of the MBSD operations and are analyzed up to BCS (RM 127). The morphological effects are mainly manifested as deposition downstream of the diversion as a result of loss of stream power and also as local erosion immediately upstream of the diversion intake.

To evaluate the effects of diversion(s) operations on MR water levels, the 92-mile long (RM 140 to RM 47.8) FTNULMR 2D Delft3D model was used. The model setup, boundary conditions, calibration and validation are described in detail in Chapter 3

For the sediment transport and morphology modeling, two different model setups are used. First is a 10-mile long (RM 66 to RM 56) FTN2Comp 3D Delft3D model and the second is a 92-mile long FTNULMR 2D Delft3D model same as the one used for the hydrodynamic modeling above. The descriptions of the model setup, calibration and validation were discussed before in Chapter 3. The FTN2Comp model only simulates the effect of the MBSD diversion but the longer FTNULMR model simulates joint (MBSD and MBrSD) diversion-induced channel morphology effects. Note that the 3D model explicitly simulates the secondary current effects on bedload transport through the MR bends and sandbars while the 2D model uses a spiral flow parameterization to model the same effects. The 3D model also simulates the near-field (within 1000-2000 ft) effects of the flow and sand capture by the diversion intakes. Both models were independently calibrated and validated for suspended and bedload sand flux using observed data as described in Chapter 3. The comparison of results from both 2D and 3D morphology models enable us to understand the uncertainty in results associated with these two morphology modeling methods.

The simulation period selected for the morphology modeling was a ten-year period from 2008 through 2018, mainly because of the ready availability of hydraulics, sediment

(Allison 2011, Allison et al. 2018) and bathymetry data (USACE 2013 Hydro-surveys and 2017 Revetment surveys) against which the model is calibrated/validated (Chapter 3). Also, the last 10 years of the MR hydrographs have been one of the highest flow periods in the recent history with 7 out of 10 years exceeding 1,000,000 cfs MR flow below BCS, namely, 2008, 2009, 2010, 2011, 2015, 2016, 2017. This record provides a reasonable basis of riverside design conditions at this reach. Additionally, the Belle Chasse gauge, which has data available from 2008 onward, provides an excellent set of sediment rating curves which were developed by the WI and made available to DT for this study.

9.2 MODEL SETUP

The general setup of the FLOW-3D FTMSDI and Delft3D FTN2Comp (3D) and FTNULMR (2D) Delft3D models is described Chapter 3. The following section describes only those aspects of the setup which are different for the purpose of the current modeling tasks.

9.2.1 FLOW-3D FTNMSDI

The FLOW-3D FTNMDI model was run in steady state mode on rigid bed (no morphology modeling) at 1,000,000 cfs MR flow and 75,000 cfs diversion flow, the latter being imposed as a discharge boundary at the conveyance channel location under both diversion open and diversion closed conditions as shown in Table 9.1. The main purpose was to investigate secondary current effects at the Myrtle Grove bed which is a likely site of sediment deposition when MBSD is operated. It was also used to confirm the strength of the secondary currents modeled in FTN2Comp Delft3D rigid bed model under similar conditions and bathymetry.

9.2.2 Delft3D FTN2Comp (3D)

The FTN2Comp model was used for the morphology modeling for the 10 years (2008-2018) MR hydrograph period for the MBSD diversion only under fully open and fully closed conditions for the entire period. The differential change in the MR bed due to diversion operations can be quantified by subtracting the change in bed elevations of the closed scenario from the diversion open scenario. This approach removes any bias arising from the boundary conditions and initial conditions, and allows isolation of the effect of only the diversion on the

river morphology. Also, if the initial USACE 2012 bathymetry is considered as an equilibrium bathymetry representative of the medium term (say, 10 years) in the future, then the possible future bed elevations due to the diversion operations may be assumed to be entirely due to the differential erosion/deposition between the closed and open diversion scenarios. For every year, this differential bed change can be obtained by subtracting the bed elevations of the open- from the closed-diversion scenario bed elevations. Subtracting this from the initial bed elevation thus yields the net change in bed level due to the diversion operation only.

Figure 9.1 shows the boundary conditions for flow and sediment at the upstream boundary (RM 66). The model was run only for the period when MR flow exceeded 450,000 cfs which is the proposed flow trigger for start and stop of the diversion operation. To generate a continuous hydrograph without the closed-diversion periods, the hydrographs for each year were stitched together sequentially after removing the period when MR flow was less than 450,000 cfs in between the annual hydrographs. Therefore, an important assumption in this model is that the river morphology does not evolve significantly at MR flows below 450,000 cfs. Since the sand mostly enters into suspension above 450,000 cfs (Allison, 2012, Ramirez et al., 2013) within this reach of the Lower Mississippi River (LMR), this is a reasonable assumption in order to reduce model computation times. Note that only sand (medium, fine and very fine) was considered for modeling here as sand is the principal component of the bed stratigraphy in the river at flows exceeding 450,000 cfs (see bed material load data analysis in Allison, 2011). Even though the effect of fines (silt and clay) on the bed material load can be significant at MR flows less than the trigger flow, this effect is not considered here as the model was not run when MR flows were less than 450,000 cfs.

Figure 9.2 (top panel) shows the discharge boundary condition applied at the MBSD diversion location. The diversion discharge is capped at 75,000 cfs to mimic gate operations that will cap flows at 75,000 cfs. The bottom panel shows the discharge boundary at the MBrSD location based on a diversion discharge to MR discharge (Q-Q) relation provided by the MBrSD Design Team based on their 15% design. This boundary was used for the FTNULMR (next section) runs which includes both diversions.

In addition to running the model with revetments, a scenario was also simulated where the Alliance revetments were removed. This was done to evaluate the maximum erosion possible

at the intake assuming absence of revetment protection. In reality, the design will include rip-rap armor protection even riverward of the revetments in the vicinity of the intake whose extents were designed based on the location of any intake degradation seen in the model.

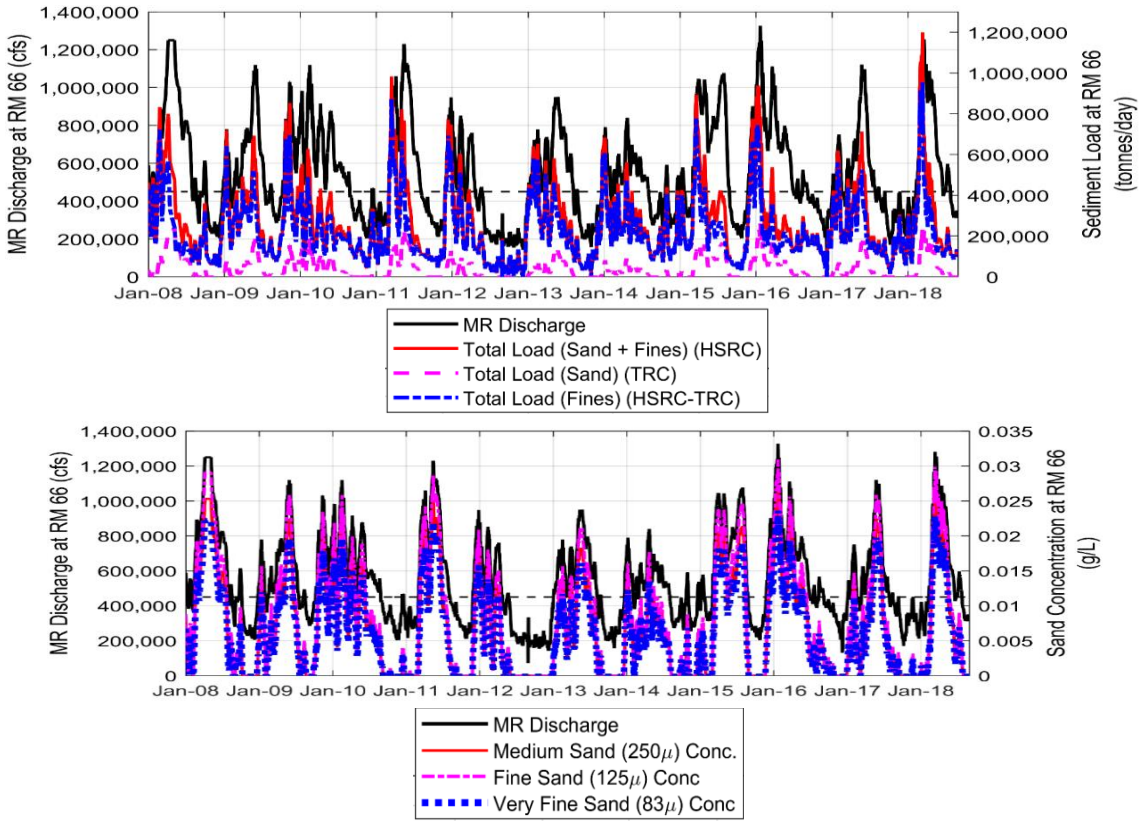

Figure 9.1. Discharge and sediment (sand only modeled) hydrograph for the 2008-2018 period. Note the diversion is operated only when the river exceeds 450,000 cfs (black dashed line) MR flow.

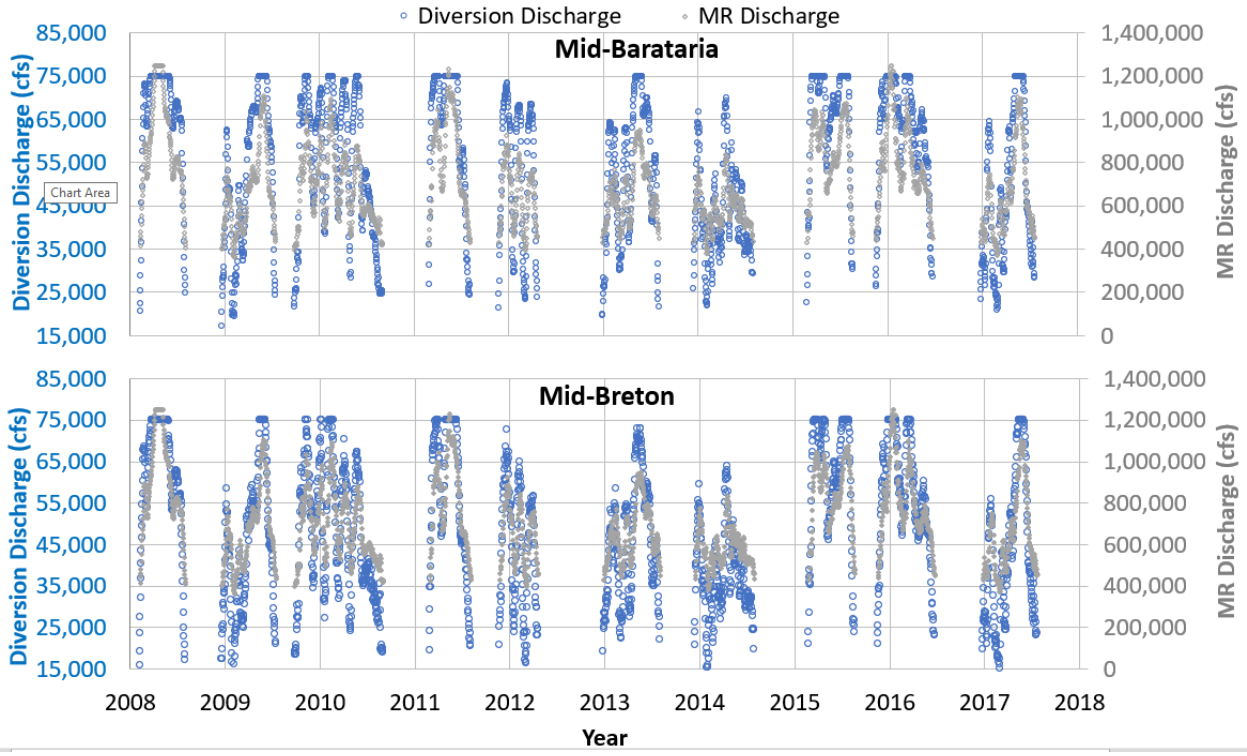

Figure 9.2. Diversion flow (capped at 75,000 cfs) time-series boundary condition (blue points) imposed at diversion locations for the 10-year runs. Only Mid-Barataria (top panel) is modeled in FTN2Comp while both Mid-Barataria and Mid-Breton (bottom panel) are modeled in FTNULMR model. The MR discharge is shown in grey symbols.

9.2.3 Delft3D FTNULMR (3D)

The detailed hydrodynamic and morphology setup, calibration and validation of the 2D Delft3D FTNULMR model is described in Chapter 3. For the hydrodynamic runs simulating the effect of the diversion induced set-down, the 2018 calibration period (Chapter 3) was used. The observed downstream (West Pt A La Hache, RM 48.7) water level time-series boundary used for the no-structure run in Chapter 3 was adjusted in the with-structure case presented in this chapter to account for the effect of the diversion induced drawdown downstream based on the Q-H relation. The diversion discharge at or both MBSD and MBrSD sites were specified by the discharge boundary developed for the 2018 hydrograph similar to the one shown in Figure 9.2.

For morphology modeling, the FTNULMR upstream boundary was setup with the same RM 66 boundary condition as the FTN2Comp model, even though this meant that the sand boundary conditions developed for Belle Chasse (Figure 9.1) were actually applied at RM 140 at

Reserve, LA. This is appropriate because as discussed in Chapter 3, when Delft3D is run with the Morphological Acceleration method the time scales of morphological changes over multiple years are squeezed into simulated changes over a few months (e.g., with a MorFac of 40, a 10-year simulation becomes an approximately 3-month simulation). This time is often not sufficiently long for the upstream sand introduced into the river domain to travel to the area of interest rendering the morphology results far downstream insensitive to the boundary conditions. This was confirmed by an independent run as well without a boundary for the zone below RM 70 which is the current area of interest and where most of the diversion effects on river morphology are visible in the river. Most of the bedload that affects the morphology changes in the model within the area of interest is actually travelling either as bedload or suspended loadsourced locally from a few sand bars upstream within the short period of the runs compared, to the actual multi-year scales they represent. This is the reason why an initial stratigraphy was developed carefully for the FTNULMR model by running the MR only model for 6-8 months (about 20 years of real-world time) before the actual start of the production period. The Delft3D model being a physically based model where sand transport module is driven by the Van Rijn equations, determines the fluxes of suspended and bedload for sand as a function of the local sediment grain size and the imposed bed shear stress. Therefore, during this initial stratigraphy development, before calibration, careful attention was paid to attain an equilibrium bed material size distribution that closely matched survey data at Alliance and Myrtle Grove bars before the stratigraphy was deemed acceptable for the production runs. Also, the secondary current effects on the bedload allowed the model to redistribute and sort the sand material cross-sectionally and was confirmed by the development of sand bars. Once the stratigraphy cover was developed the model was run and further refined to allow sufficient erodible sand reserves in areas where bedload movement was visible. This was considered important because the sand bars should not run out of sand before the simulation ends which will artificially create sediment-starved conditions. The thickness of the erodible substrate was also adjusted on the sand bars to mimic consolidated conditions in areas where the MR sand bars do not show erosion below a certain depth from available surveys. The pathways of bedload transport across the MR channel, particularly downstream of BCS was carefully observed from USACE historic revetment surveys from 2017-2018 and the model was confirmed to be able to mimic such distributions visually. As

presented in Chapter 3, the model was validated against observed bedload and suspended load data from available MR surveys between RM 70 and RM 58, particularly on the sandbars where the two diversions are located.

9.3 Results

9.3.1 Analysis of change in river hydrodynamics due to open diversion

The changes in the river hydrodynamics due to the presence of the diversion are analyzed in this section with rigid bed models. Only MBSD is modeled here with the FTN2Comp model. This exercise helps explain the forces that drive the morphological response of the river to the diversion operations discussed in the subsequent sub-sections.

The simulations used for this analysis were FTN2Comp FLOW-3D steady state runs with MR flow of 1,000,000 cfs and diversion flow of 75,000 cfs. The model was run for both the diversion open and diversion closed conditions. The Delft3D simulation MR flows were at 1,250,000 cfs (75,000 cfs diversion) and 600,000 cfs (48,000 cfs diversion).

For with- (diversion open) and without-project (diversion closed) analysis the FTN2Comp (3D) Delft3D model domain was used. This meant that the diversion geometry is present in both the cases with the only difference being that thin dams were used in Delft3D to block the diversion at the intake gate location to simulate the without-project (or diversion closed) condition. This technique made it possible to calculate the differences of hydrodynamic quantities on a common model grid.

Figure 9.3 shows the bed shear stress distribution at two river flow conditions. The highest possible river flow conditions scenario at this location is shown in the upper panel. The low flow 600,000 cfs condition scenario is shown in the lower panel. The differences (closed-open diversion) of bed shear stresses due to the presence of the diversion are show for each flow conditions. It is seen that peak shear stresses in the river at low flow (about 2-3 Pa) are 4-5 times less than at those at the highest flow (about 10-12 Pa). The corresponding differences in shear stresses between the closed and the open conditions are 2-3 times less at low flow (about 0.6-1 Pa) than at high flows (1.8-2 Pa). The positive (red) shear stress areas experience higher shear stresses under closed condition, or lower under open conditions indicating the potential for sediment deposition under with-project (open) condition. The negative (blue) shear stress areas,

due to the local action of the intake, are the areas where bed shear stresses are higher under open conditions indicating potential for erosion under with-project (open) condition. The exception to the latter is the blue zone just downstream of the diversion along the Right Descending Bank (RDB) which can still possibly experience sediment deposition due to the increased supply of sediment that can migrate towards the RDB being attracted by the diversion flow. Note that generally the river bed shear stress (1-3 Pa) is sufficiently greater than the theoretical Shields critical shear stress for resuspension (~0.2-0.25 Pa for medium sand) even at 600,000 cfs flow. The existing (closed condition) typical bed elevations can only be maintained if this equilibrium sand transport (where supply and sediment transport balance each other locally) is maintained under open conditions as well. However, when the diversion is opened, this equilibrium is going to be disturbed (reduced deposition in the blue areas and increased deposition in red areas). As a result, the sand transport within the blue areas will rise and then fall below the current equilibrium in the red areas. Therefore, the results presented later showing areas of degradation (erosion) and aggradation (deposition) are not simply native bed erosion or deposition but a consequence of this dynamic balance between the sediment supply rate, sediment transport potential and the hydrograph forcing. The competition between the supply and sediment transport capacity over years of hydrograph cycles will ultimately lead to an equilibrium condition. The present modeling results are just one example of such an equilibrium.

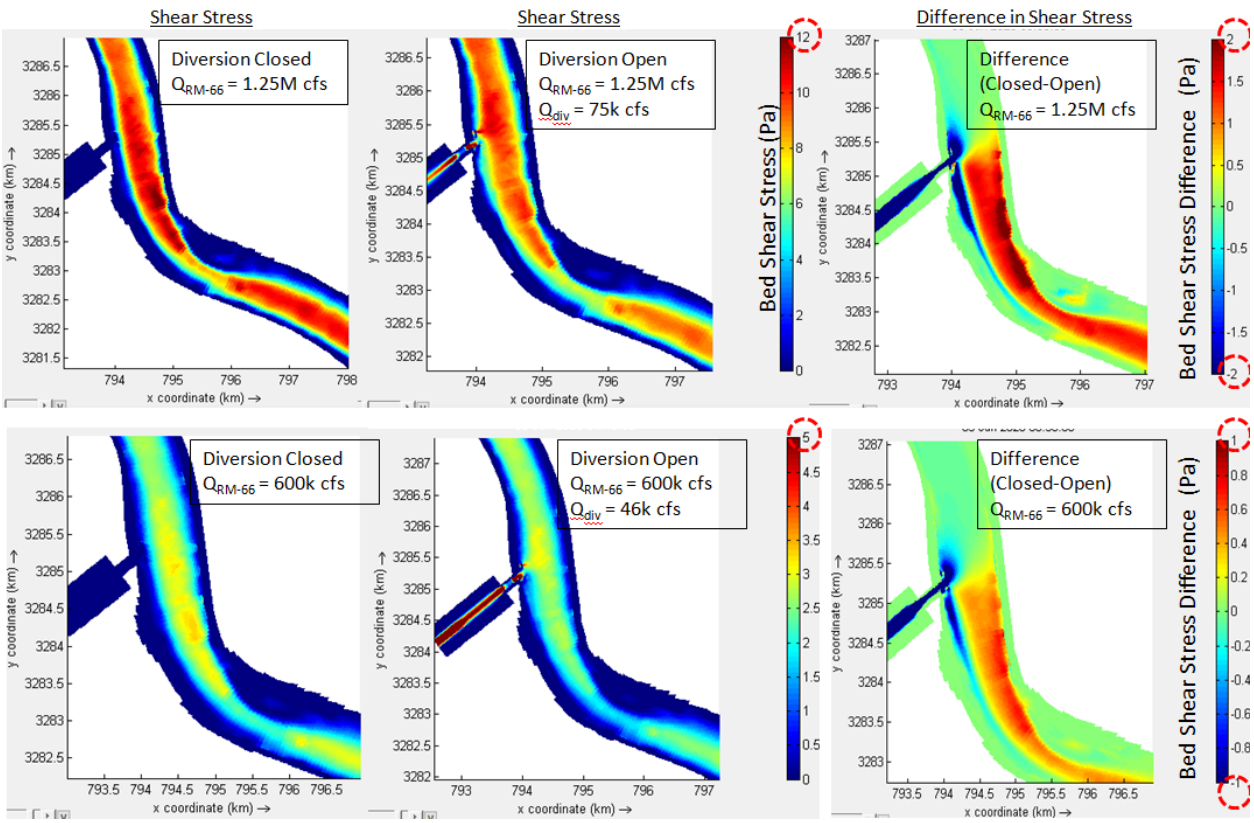

Figure 9.3. Bed shear stress (diversion close, open and difference) results from the 3D Delft3D model for the 1,250,000 cfs and 600,000 cfs MR flow scenarios. Note the difference in legend limits, circled by red dotted lines.

Figure 9.4 shows analysis of stream power at two locations marked in the upper panel. The stream power time series at these two locations is shown in the middle panel. The stream power is calculated as ρgQS, where, ρ is the density of water, *g* is the acceleration due to gravity, Q is the river discharge and *S* is the slope of the water surface. The Q and S values are from the 10-year simulation period from 2008 to 2018 under diversion-open scenario. A reduction of stream power is analyzed which can be associated with a reduction in the sediment transport capacity downstream of the diversion. The bottom panel shows the stream power at the upstream plane at a given MR flow on the left y-axis (blue solid bars) and the corresponding stream power loss percentage between the upstream and downstream planes (red outlined bars) on the right y-axis. The plot summarizes the quantitative effect of the diversion on the stream power and hence the sediment carrying capacity of the river. The figure shows that most of the loss in stream power is less than 1,000 kg.m/s^3 below a river flow of 900,000 cfs. However, above this

flow the stream power loss rises rapidly up to 3,000 kg.m/s^3. Interestingly, the percentage of stream power loss between the two planes remains more or less constant between 12-18% of the stream power upstream for the entire MR flow range above 400,000 cfs. This indicates that while the reduction of the stream power and hence the sediment conveyance efficiency may be more or less uniform due the diversion operations along the entire hydrograph, the absolute loss of stream power above 900,000 cfs is about 3 times the loss of stream power below that flow. Thus, a flow of about 900,000-1,000,000 cfs may mark a threshold above which the diversion operations will likely lead to greater deposition downstream than when operated below this threshold.

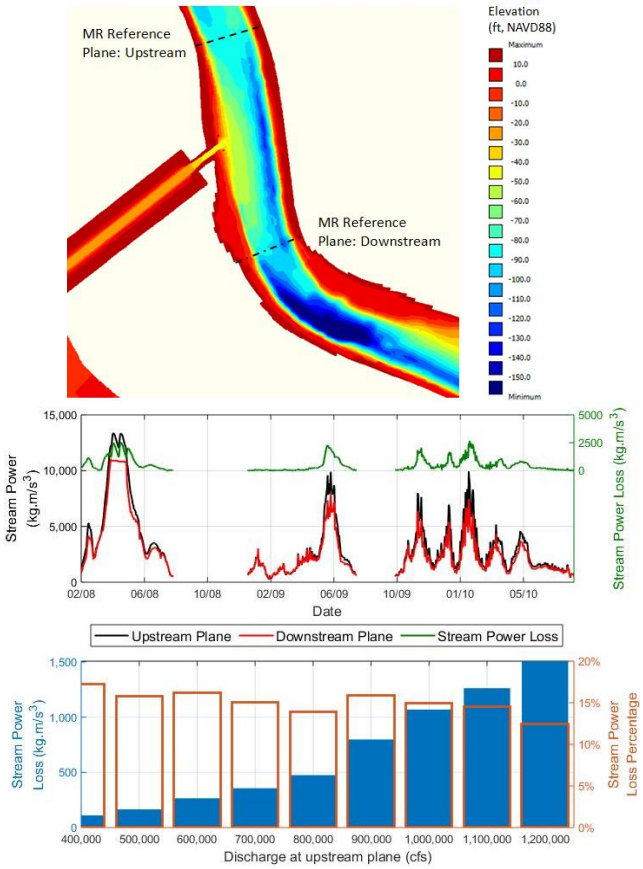

Figure 9.4. Estimated river stream power at an upstream and a downstream location about 1 mile away from the diversion intake and the difference in stream power variation with river flow. Top panel shows the location where the stream power is calculated. Mid-Panel shows the time-series of stream-power at the two planes (left axis) and the difference in stream power (right panel). Only a 3-year period out of the 10-year simulation is shown for brevity. Bottom panel shows the variation of the stream power loss (left panel) and percentage stream power loss (right panel) with discharge at the upstream plane for the full 10-year (2008-2018) period.

Initial modeling indicated a potential for deposition at the Myrtle Grove sand bar immediately downstream of the diversion. This sandbar extends into the ship channel. As will be shown later, the sand bar is currently an actively depositional bar possibly maintained by occasional submarine retrogressive bar failure. In order to evaluate the local river response, it was deemed particularly important to examine the hydrodynamics near the Myrtle Grove bend where a sandbar and secondary (in a cross-sectional plane) currents exist.

Figure 9.5 shows the secondary currents produced by the FLOW-3D model run at 1,000,000 cfs MR flow with a 75,000 cfs diversion flow. The comparison of the FLOW-3D and Delft3D secondary currents were made in Chapter 3. Here we discuss more the horizontal flow distribution implication of the secondary current at this bend, which together with the bedload flux at the bar bottom actively causes deposition at this bend. The river channel cross-section in the bottom panel shows the presence of secondary currents at Transects 1 and 2. As the flow goes downstream from Transect 1 to 2, there is a lateral shift in the core of the streamwise velocity away from the inner bank towards the outer bank. Consequently, the flow separates and forms a horizontal reverse flow zone attached to the bar edge. It is likely that this reduced velocity zone causes deposition of the sediment along the shallower portions of the bar edge and causes bar accretion in addition to bedload brought in at the bar foot. Notice the fairly steep slope of the sand bar at this location. It is likely that bar sloughing and periodic sediment erosion during the receding river flows are present at this location. Morphology modeling confirmed that the use of an equilibrium slope correction factor was needed to be able to correctly model the equilibrium bar shape. Review of the Google Earth imagery at lower flows (mid-panel of Figure 9.5) shows the sub-aqueous bar being exposed and streaming sediment into the main river flow. It is to be noted even though bank erosion is modeled in the Delft3D model using dry cell erosion factor, bank collapse/ undercutting is not explicitly modeled, though the use of the equilibrium bank slope indirectly simulates the steep side slopes where present.

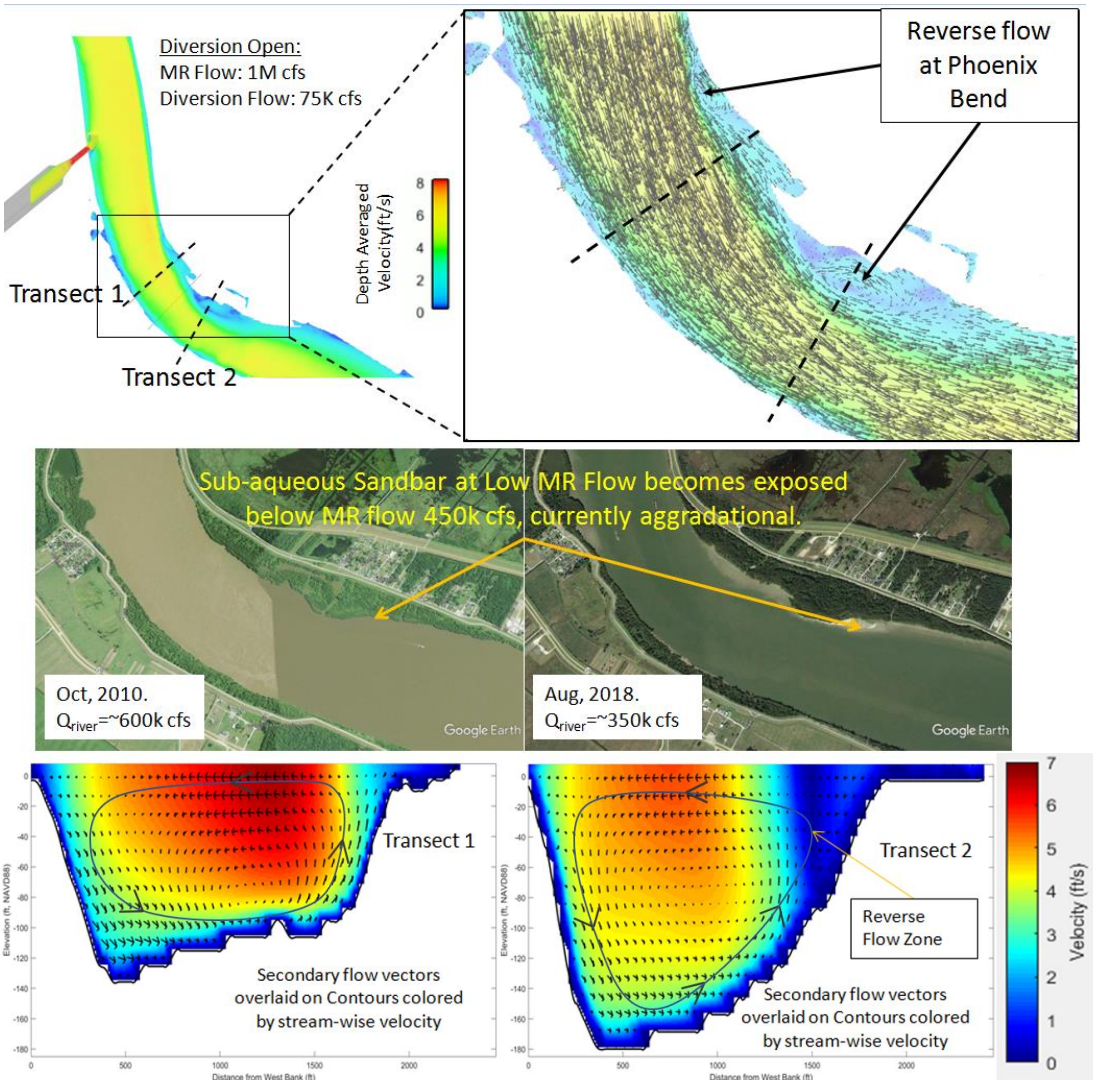

Figure 9.5. FLOW-3D model results of secondary currents at the Myrtle Grove bend shown as vectors (bottom panel) for the 1,000,000 cfs river flow. Sketched arrow lines represent the general direction of the secondary current. Top panel shows depth-averaged velocities and the horizontal circulation. Middle panel shows existence of a shallow sub-aqueous bar exposed at low flows as seen in the Google Earth imagery.

A FLOW-3D simulation was also carried out for this case and is shown with the Delft3D velocity results in Figure 9.6. A reverse flow pattern similar to FLOW-3D is observed on the batture at this bend, which explains the natural accretion of the sand bar under current (without project) conditions discussed later.

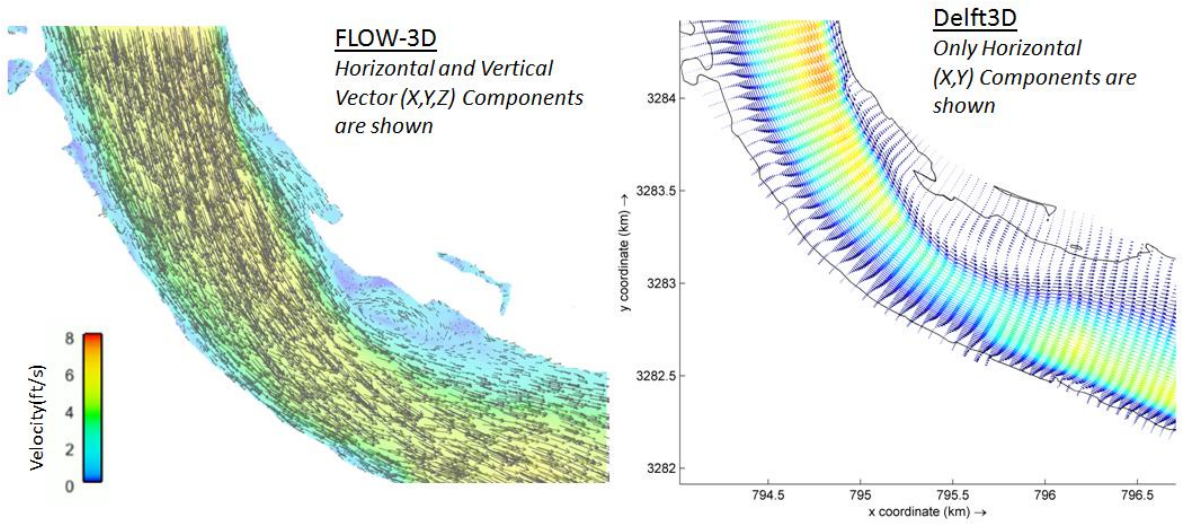

Figure 9.6. Comparison of Delft3D (right panel) and FLOW-3D (left panel) velocities at the Myrtle Grove bend.

The comparison of the strength of the primary (longitudinal) and the secondary (transverse) velocity field at the bend (Transect 2 looking upstream) is shown in Figure 9.7 for diversion closed and open conditions. The secondary velocity vectors are plotted on the color contours of the primary velocity (top panel) and the secondary velocity (bottom panel). These are FLOW-3D FTNMSDI model results for a steady state simulation with MR flow at 1M cfs and with the diversion either closed or open.

The results show that, when the diversion is open, only 925,000 cfs (75,000 cfs less than 1,000,000 cfs) flows past the bend, reducing the primary and the secondary velocity magnitudes. The figure in the bottom-right shows the ratio of the secondary velocity magnitude of the closed diversion condition to the open condition. When the diversion is open, the flow away from the bend at the surface is weaker (red areas with ratio contours greater than 1) while the flow towards the bend near the base of the bar is stronger (blue areas with ratio contours less than 1).

The combined effect is that there is less exchange of flow between the outer thalweg zone and the bar. This is likely to cause sand, which moves mainly in the lower half of the water column as it comes downstream from the Alliance South sandbar, to be transported towards the inner bend and more likely to be deposited at the base of the bar at or below -100 ft, NAVD88 (in the blue zone).

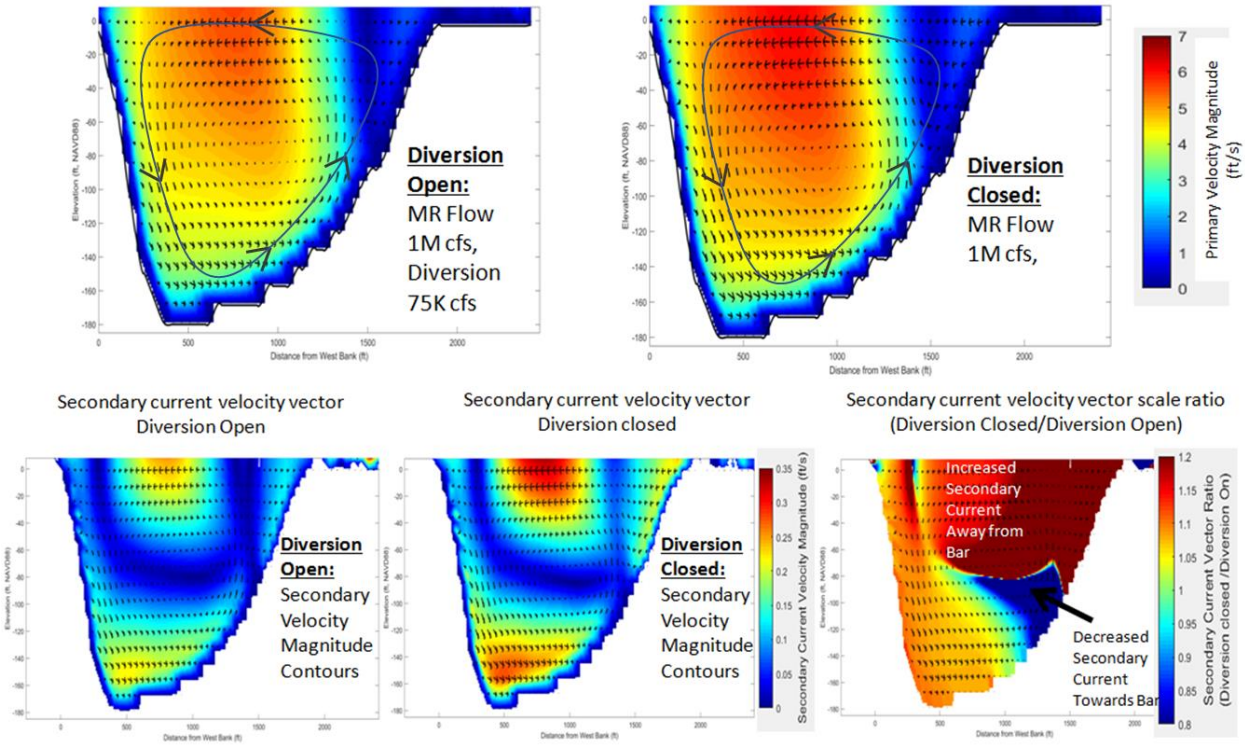

Figure 9.7. Secondary velocity vectors plotted on the color contours of the primary velocity (top panel) and on the contours of the secondary velocity (bottom panel) for diversion open and closed condition. Results at the Myrtle Grove bend from a FLOW-3D simulation with MR inflow of 1,000,000 cfs with 75,000 cfs diversion flow.

The effect of the secondary current on the sediment transport at the bend is shown in Figures 9.8 and 9.9 which together provide a 3D view of the sediment transport mechanism at this bend. Figure 9.8 shows the bedload bypassing the sandbar through the deeper part of the bend due to the secondary current effect. The results demonstrate that a well-calibrated 3D Delft3D sediment transport model can simulate the exchange of sediment between alternating bars at river bends as reported in the field studies (Nittrouer et al., 2008 observations from Audubon Park bend). As was explained in Figure 9.8, any reduction of the secondary current will likely cause deposition along the bar edge (below about -100 ft, NAVD88 contour) which can slowly encroach into the existing ship channel (dotted black lines in figure 9.9) left panel. The portion of the ship channel closer to the bar edge is currently at an average elevation of about -70 ft, NAVD88 which is much below the required -55 ft ship draft. The average is taken along the entire width of the channel.

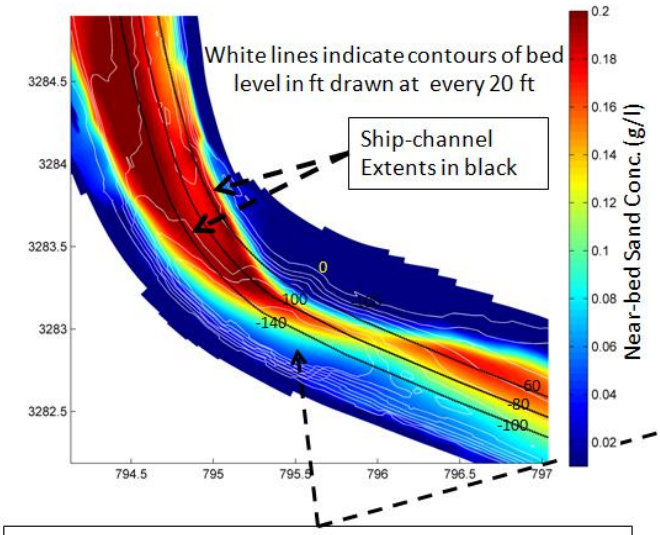

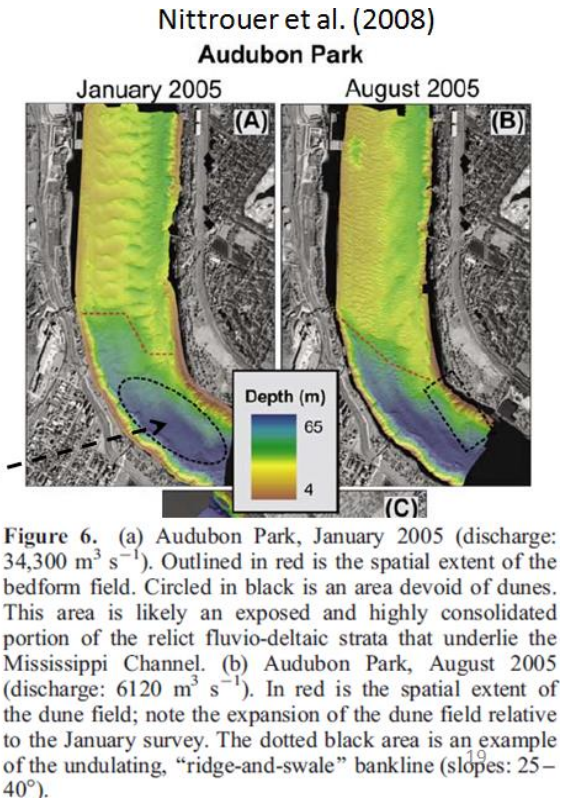

Figure 6. (a) Audubon Park, January 2005 (discharge: 34,300 m^3 s^{-1}). Outlined in red is the spatial extent of the bedform field. Circled in black is an area devoid of dunes. This area is likely an exposed and highly consolidated portion of the relict fluvio-deltaic strata that underlie the Mississippi Channel. (b) Audubon Park, August 2005 (discharge: 6120 m^3 s^{-1}). In red is the spatial extent of the dune field; note the expansion of the dune field relative to the January survey. The dotted black area is an example of the undulating, "ridge-and-swale" bankline (slopes: 25–40°).

Figure 9.8. Effect of secondary currents on the Myrtle Grove bed sandbar. Left panel: Near bed sand concentration contours overlaid on the bed elevation contours in white (interval 20 ft) along with the ship-channel extents. Right panel: Reproduced from Nittrouer et al. (2008) showing the absence of dune fields over the deeper part of the bend based on the multibeam survey data.

9.3.2 Analysis of Morphology Evolution in the Vicinity of the Intake

Figure 9.9 shows the evolution of the sandbar in the vicinity of the intake. The left-side figures show results from the as-designed condition, i.e., with the intake rip-rap cover and the USACE revetments in place. The right-side figures show results from a hypothetical (extreme) condition where all of the rip-rap and revetment is assumed to be removed and the natural river bank exposed. The reason for conducting the hypothetical second test is to provide the designers with an assessment of a severely degraded bed elevation for adequate safety factor consideration in scour mitigation design. In reality the cofferdam cutoff portions below river bed will be left in place after construction and will act as natural toe cut off wall for any potential scour, so it is highly unlikely that the hypothetical situation shown in the right will happen. The upper panels show maps of aggradation/ degradation of the bed derived as the difference in bathymetry

between year 10 and year 0. Note that the river bathymetry evolves for both the close and open diversion conditions. The estimated morphology change due to the open diversion is the difference of these two bathymetries. This difference is added to the initial bathymetry to give an indication of bathymetry evolved solely due to the influence of diversion. This bathymetry is plotted in the cross-section profile.

Under the as-designed conditions (left-side figures in Figure 9.9), it is seen that the maximum bed elevation change on the sandbar is about 8-10 ft and occurs in front of the intake reaching an equilibrium fairly quickly.

In view of these results, it is recommended that the rip-rapped zone extends up to -45 ft, NAVD88 river bed elevation upstream of the intake to adequately protect the intake from any degradation. Regular monitoring of the intake area is recommended and, in some cases, the diversion may need to be closed for a period of time (possible one annual flood) for the sandbar near the intake to regain its bed elevations. Wet years (MR flow exceeding 1,000,000 cfs) tend to bring in large amounts of sediment that can fill this area quickly.

Under the hypothetical extreme scenario where no revetment or rip-rap protection is placed at the intake, the degraded bed levels were predicted to deepen to about -50 ft, NAVD88 (25 ft below the existing elevation) near the intake U-Frame. The progressive deepening of this zone is a design concern and indicates the protective role of the rip-rap. It is recommended that the designers critically evaluate this condition to include an adequate safety factor due to phenomenon that cannot be addressed by numerical modeling, retrogressive sand bank failure, settlement of rip-rap, scour within and undercutting of the rip-rapped bed, and failure of the revetment due to damage or loss of soil underneath.

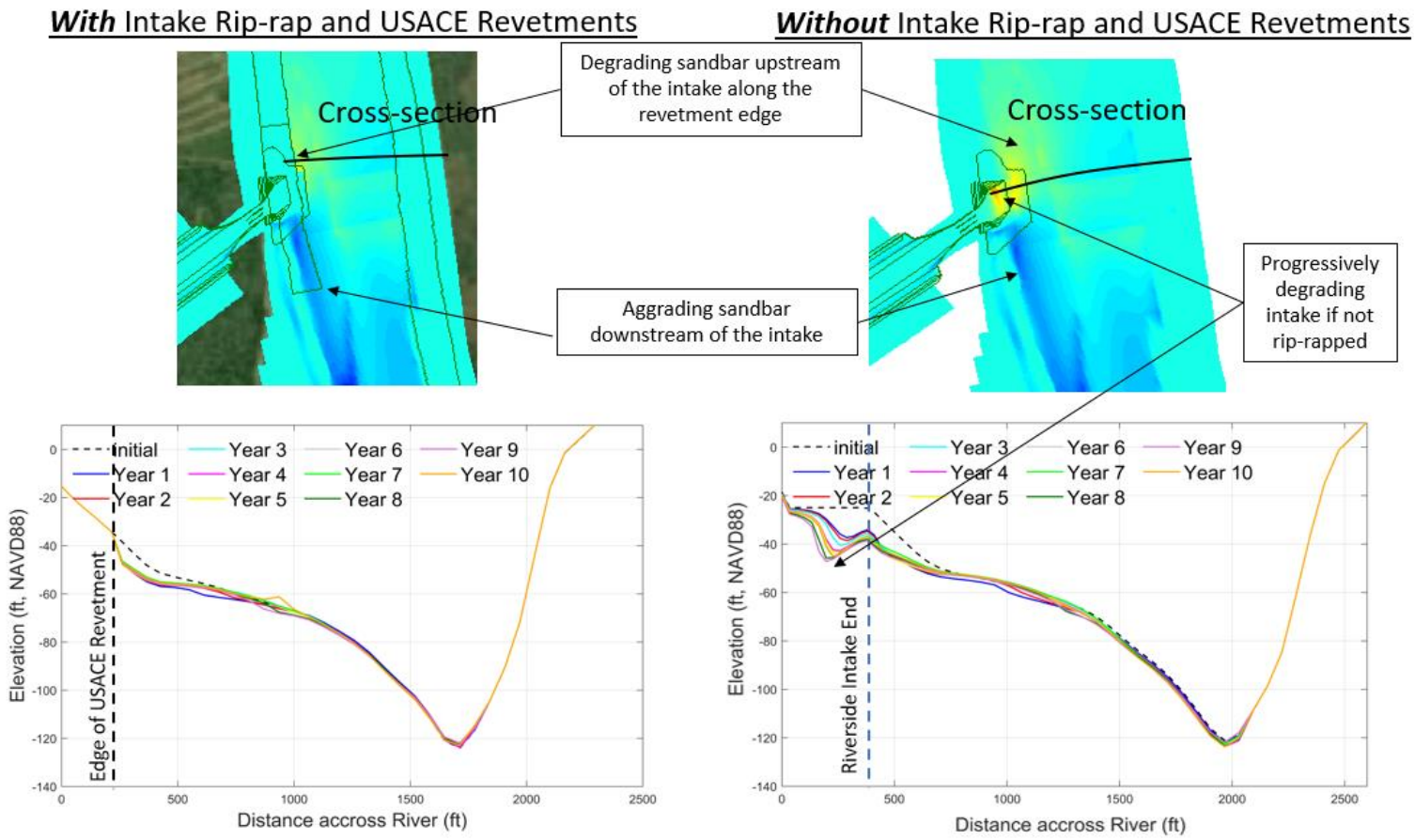

Figure 9.9. Model results (FTN2Comp, 10-year, 3D Delft3D) of morphology evolution near the upstream intake vicinity. Left panel shows results with both riprap placed as designed and the existing USACE revetments. Right panel shows a hypothetical condition with no riprap and no USACE revetment. The maps in the upper panel show the difference in the Year 10 and Year 0 (initial) bathymetry. The cross-section profiles in the bottom panel are developed by adding evolved bathymetry difference between the diversion closed and open conditions to the initial bathymetry and therefore show the resultant change due to diversion effect only.

A separate analysis was also performed to examine the differences in morphology evolution between the wet and dry MR flow periods. A period is considered dry when the MR flow does not exceed 1,000,000 cfs and is considered wet otherwise. The 2008-2010 period is considered as a wet period because the MR flow exceeded 1,000,000 cfs on all 3 years compared to the subsequent 3-year period (2012-2014) which is a dry period because the MR flow never exceeded 1,000,000 cfs. For this testing, the model was started from 2012 and run for 3 years (2012-2014) instead of 2008 and compared with the 2008-2010 period. It showed that in presence of the as-designed rip-rap and revetment, the degradation of bed elevations at the end of 3 years is comparatively less (3-4 ft) during the dry years compared to the wet years (about 8 ft). Also, for the scenario when no rip-rap or revetment protection is present the degradation is less by 10-12 ft at the end of the dry period compared to the wet period. This indicates the benefits of opening the diversion for the very first time during a year when the MR is expected to be relatively "dry". This will expose the intake and the sandbar to a milder river condition will give operational managers ample time to monitor and mitigate any intake scour.

The modeling analysis presented in this section was considered in comparison with the observations at the West Bay diversion (Appendix B1). The West Bay diversion (Yuill et al. 2016) is a natural diversion with no hard structure or riprap at the intake and has a smaller diversion capacity (approximately 50,000 cfs in 2014) than MBSD. Figures 9.10 and 9.11 show the effect of the West Bay diversion on the MR bed elevations near the vicinity of the intake. The diversion channel which was originally built at an invert of -25 ft, NAVD88 with a downstream orientation has realigned itself. It has also resulted in a degradation of the sandbar near the immediate upstream vicinity of the intake qualitatively similar to that indicated by modeling of the MBSD. It should be noted that unlike at MBSD, at the West Bay site the sandbar was initially shallower along the bend. The degradation along the thalweg for the West Bay diversion is likely due to dedicated dredging of the ship channel by USACE during the 2004-2013 period. Note that no rip-rap/revetment protection existed at the intake of the West Bay diversion unlike at MBSD, nor is the intake channel at MBSD was allowed to re-orient after opening. So even if the possibility and hydrodynamic forcing exist, the chances of such a large degradation are minimal with the as-designed rip-rap extents at MBSD.

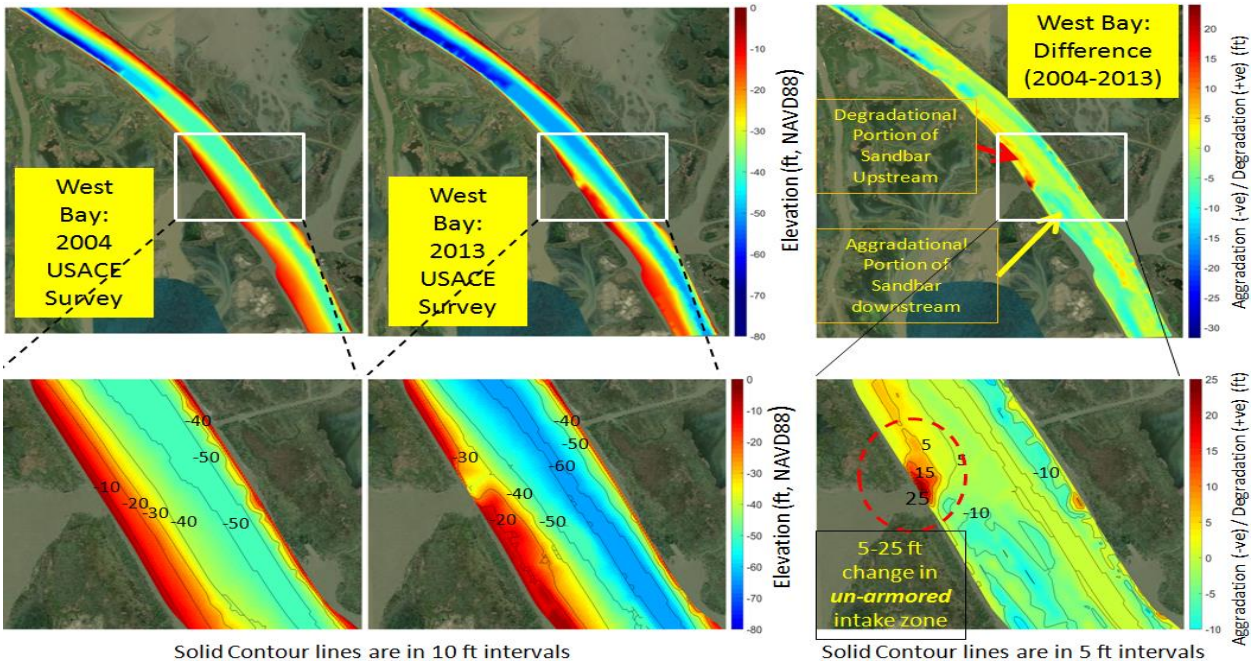

Figure 9.10. Analysis of West Bay diversion riverside bathymetries (USACE 2004 and 2013). The vicinity of the intake is showing a degradation of river bed elevation while the sandbar has aggraded in the downstream area.

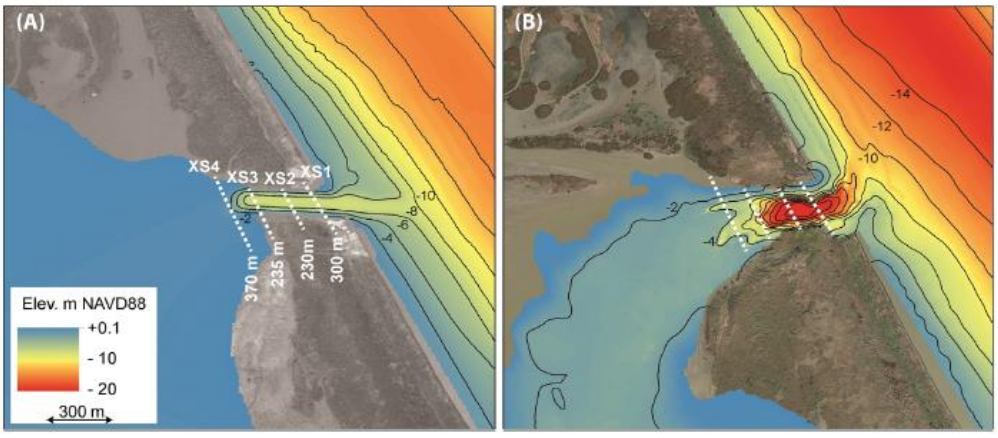

Fig. 2. Bathymetric maps for the West Bay diversion, (A) 2004 and (B) 2014. Contour lines delineate elevation change at 2-m intervals. Also shown are the location and width for four reference cross sections used to examine model velocities within the diversion channel. These maps were created from bathymetric data reported in the results section of this manuscript.

Figure 9.11. Diversion channel and river bed elevation evolution from 2004-2014 at West Bay (Reproduced from Yuill et al., 2016).

Figure 9.12 compares the relative upstream extent of this degradation zone on the sandbar with the MBSD project. In the case of MBSD the degradation zone extends to about 0.2 miles upstream (left panel) while at the West Bay site this zone extends to about 1.8 miles (right

panel). The likely shorter distance at the MBSD location is due to the steeper natural upstream slope of the bar. Also as described in Chapter 4, the near-bed suspended sediment and bedload is more likely to be entrained into the diversion but is limited by the extent from which the river water and sediment can enter the diversion which is only a short distance, about 1,000 ft upstream of the intake.

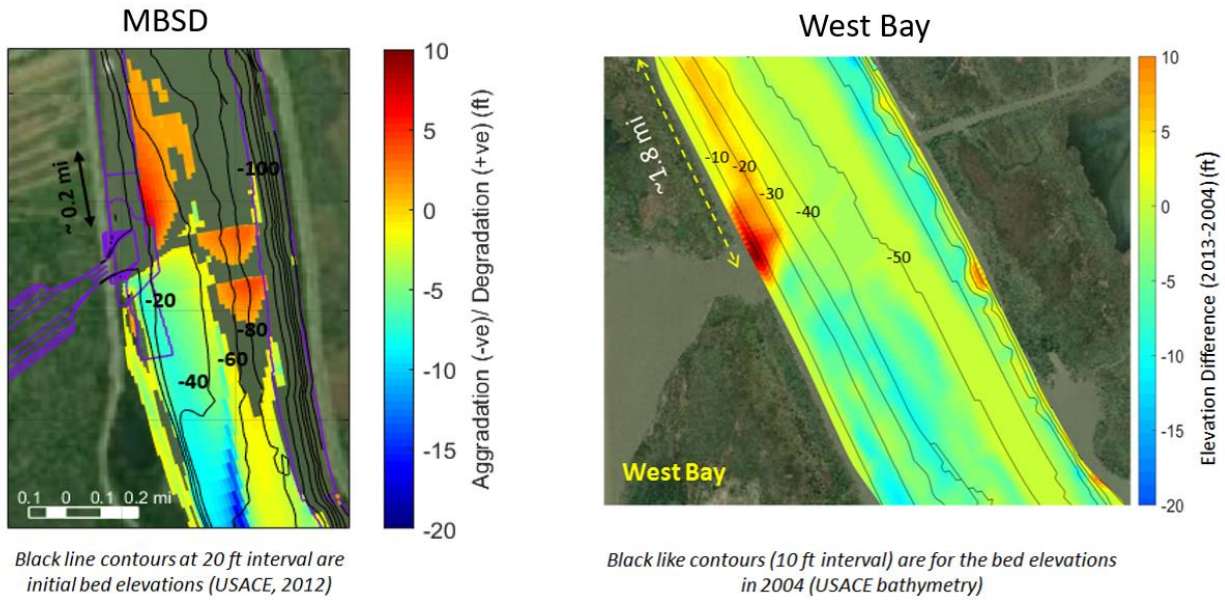

Figure 9.12. Comparative upstream extents of the sandbar degradation zone for the MBSD (left panel) and West Bay (right panel) sites. Downstream deposition is visible for both cases.

9.3.3 Analysis of Morphology Evolution downstream of the diversion location

As discussed in Section 9.3.1, the decrease of stream power downstream of the diversion can lead to potential deposition. It should be noted that even though the CSWR for sand is greater than 1 (Chapter 4), it will not eliminate downstream deposition concerns at least within the 5-10 miles of the intake. According to Brown et al., (2013), for a water diversion ratio of 0.075 (75,000 cfs diverted flow at 1M cfs MR flow), to reduce the long-term deposition effects, the sediment diversion efficiency or the CSWR will need to be at least 1.75. The CSWR will need to be at least 4.75 to reduce the short-term effects. Since neither of these conditions are fulfilled, some downstream deposition is expected.

Before delving into the model results, an analysis of the historical bathymetry (USACE 1992, 2004 and 2013 channel surveys) of the downstream reach of the diversion, particularly in the vicinity of the Myrtle Grove sandbar and the deep thalweg near the RDB is presented in Figure 9.13. The lower panels in the figure show the regions in red that have shown aggradation (+ve) from 1992 to 2004 (left panel) and from 2004 to 2013 (right panel). Blue and green areas represent net degradation (-ve) during the same period. The Myrtle Grove sandbar is seen generally to be aggradational throughout this period with the period between 1992-2004 showing greater aggradation than the 2004 to 2013 period. It also appears that the deep thalweg along the RDB is filling in. The bar itself seems to have eroded somewhat between 2004 to 2013, but net accretion has occurred at the deep bend. This is in agreement with the finding presented earlier (Chapter 2) regarding the long-term evolution of the Alliance sandbar. The Alliance sandbar appears to have evolved downstream until 1992. Overall, the Alliance sandbar appears to have been relatively stable since 2004 though there has been some thalweg deepening in 2013 and 2018. Downstream of the Alliance bar, near the RDB of the Myrtle Grove bend it appears that the thalweg is actually filling in.

The 20-year (1992-2013) trend seems to indicate that the Myrtle Grove bar area is already an actively accreting area. An interesting observation is that there appears to have been some erosion at the edge of the Myrtle Grove bar where the ship channel crosses it between 2004-2013. It is unclear if the impact of ship activity in this area and/or retrogressive submarine bar failures affects the bar shape. Further investigation of this observation is beyond the scope of the current study as these effects are likely to continue even when the diversion is operational. Table 9.1 shows the net volume change in this area. Even though this period shows net degradation, most of the degradation appears to be downstream of the bar.

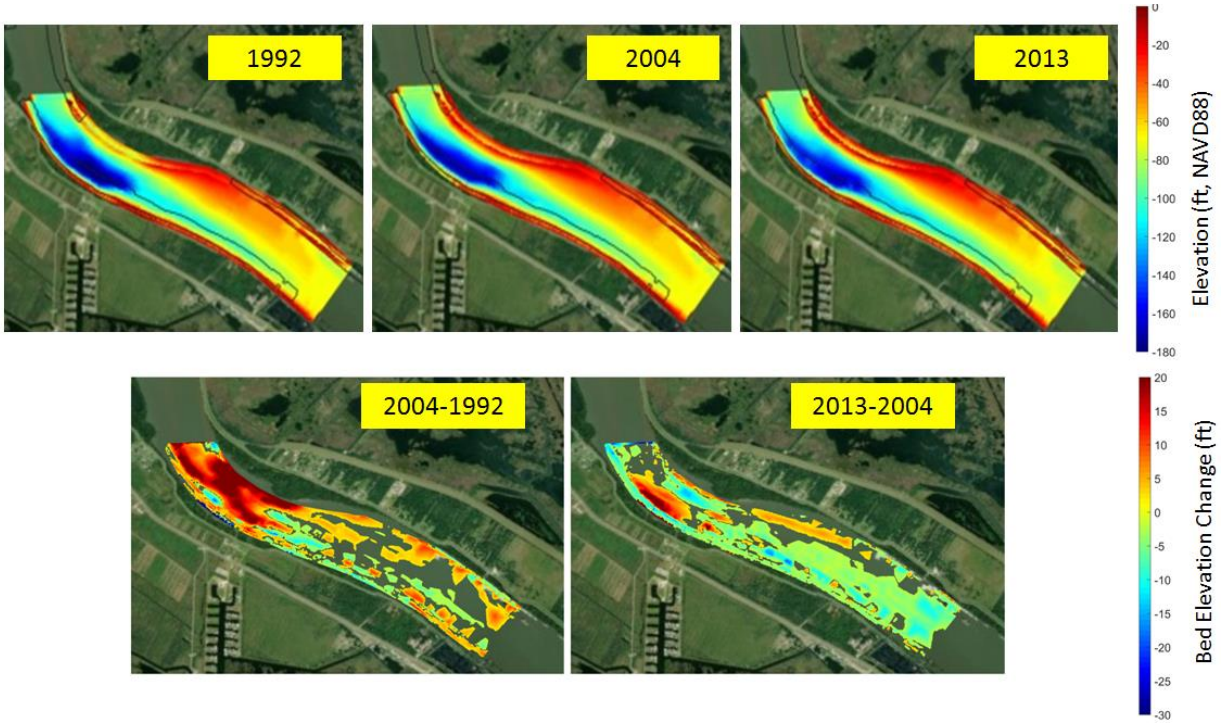

Figure 9.13. Historical bathymetric surveys from 1992, 2004 and 2013 by the USACE in the upper panel. Lower panel shows the bathymetry difference between the years indicated. The elevation changes in the [-2, 2] ft range set transparent for readability.

Table 9.1. Net volume change within the area shown in Figure 9.13.

Net Change within Period	Years	Volume Change (+ve Aggradation, -ve Degradation) (CY)	Average Yearly Change (CY)
1992-2004	12	4,428,500	+370,000
2004-2013	9	- 2,031,500	-226,000
Net Change: 1992-2013	**21**	**+ 2,397,000**	**+ 144,000**

Figure 9.14 shows the bathymetry evolution over the 10-year (2008-2018) in the right column of panels. It is representative of the net elevation difference due to the diversion effects only assuming that the initial bathymetry is a current equilibrium condition. The difference between the closed and the open conditions are shown in the left column of panels. The ship channel extents are shown by dotted black lines along with a centerline. Model results show that, the general trend of the Myrtle Grove bar to accrete and encroach into the deep thalweg

continues in the future. There are downstream changes on the Myrtle Grove bar, too. Of particular interest is the evolution of bathymetry along the ship channel, especially between RM 57 to RM 58 where the channel passes close to the edge of the Myrtle Grove bar. In this stretch of the river an active accretion is predicted by the model similar to the past observations (Figure 9.13). The results show that the deposition in the bend is mostly at the deeper elevations at the base of the Myrtle Grove bar and does not appear to reduce the available ship channel draft.

Note that for this FTN2Comp model, the RM 56 boundary is set as a uniform cross-sectional boundary for water level and discharge and it likely affects the results in the last mile of the model domain. This modeling exercise was intended to study only the short-term downstream morphology response within 5 miles of the diversion. For a longer-term simulation the model domain the longer FTNULMR model presented later shows ship channel deposition up to about RM 50.

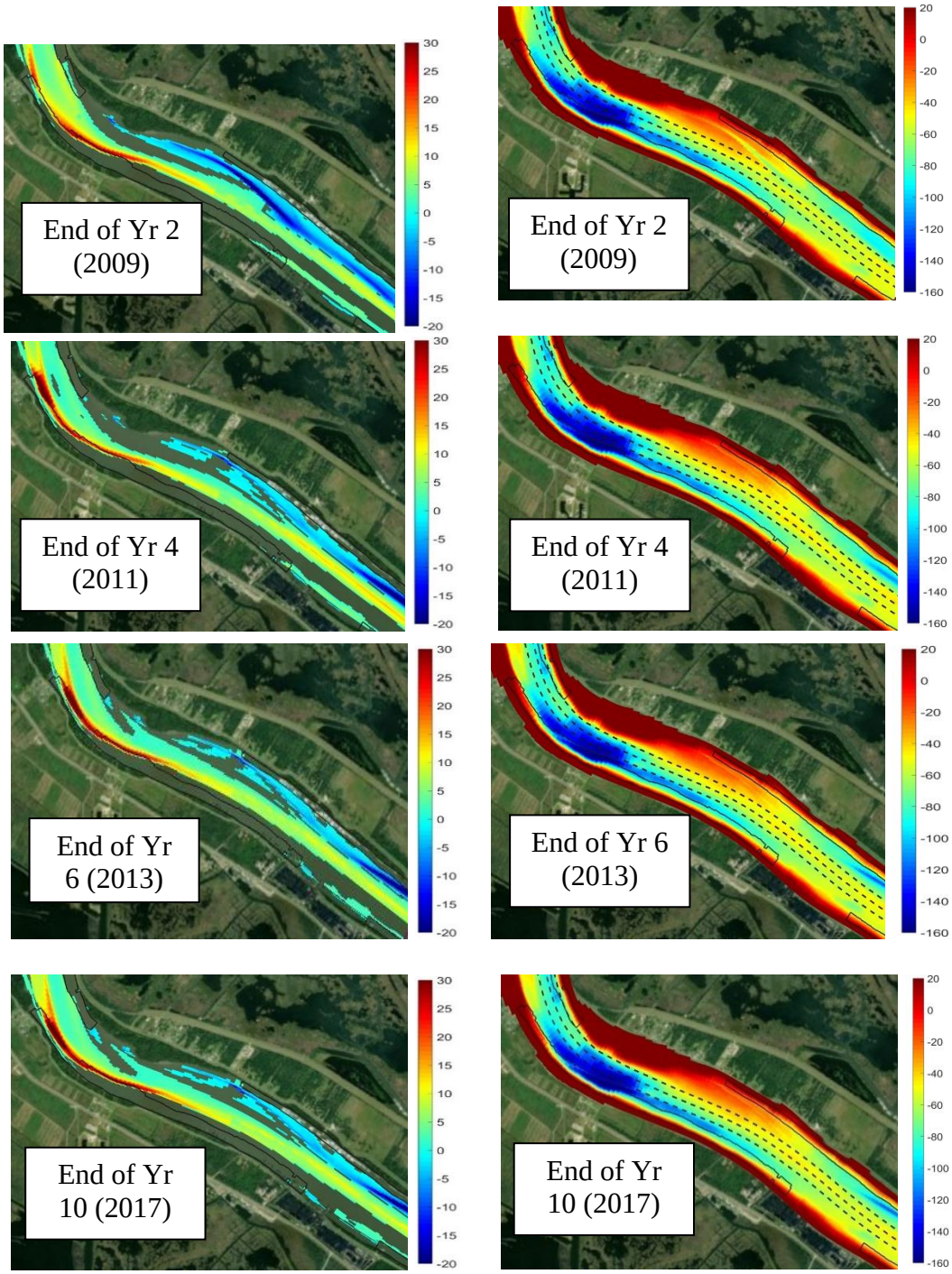

Figure 9.14. Left column of panels show the change in bed elevation (positive is Aggradation, negative is degradation) over 10 years (2008-2018). The right column of panels shows the corresponding bed elevations. The ship channel extents and the mid-line is shown by dotted black lines. An equilibrium appears to be reached after 5-6 years at the Myrtle Grove bend.

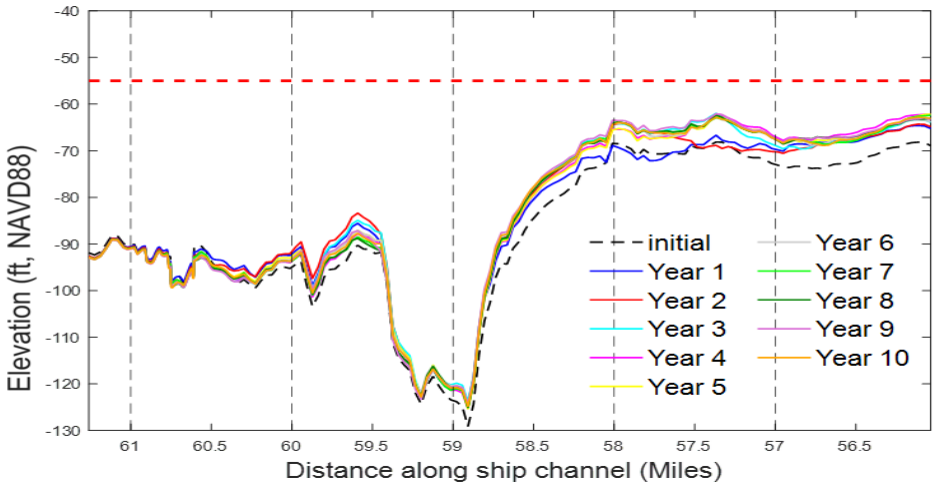

Figure 9.15. Evolution of cross-sectionally averaged (along the width of the ship channel, dashed line Figure 9.14) bed elevations of the ship channel. Red dotted line indicates the -55 ft, NAVD88 elevation level which is the USACE proposed mandated ship channel elevation in the near future.

Figure 9.15 shows the evolution of the cross-sectionally averaged (across the width of the ship channel) ship channel bed elevation profile for the simulated10 years (2008-2018). The elevations were obtained by adding the difference between the closed and open conditions to the initial bed level (assumed to be the equilibrium bed elevation for this period). This method of allows calculations of bathymetric change from diversion operations induced deposition effects only. The model results show that even though the Myrtle Grove sand bar shows some accretion, the bed elevations within the ship channel are well below -60 ft, NAVD88 and are unlikely to reach the required -55ft NAVD88 draft clearance. The ship channel deposits seem to attain an equilibrium bed in 5-6 years.

Figure 9.16 shows the cross-sectional bathymetry of the ship channel at the end of each of the 10 years at three transects. It shows the spatial distribution of the depositional trend within the ship channel. The ship channel extents are marked by the magenta dashed vertical lines. Notice that the ship channel itself currently crosses over bed that is shallower than -55 ft, NAVD88. The differential plot (Figure 4.23) indicates that bed levels are unlikely to get shallower than -55 ft. The deposits do not block the ship channel and at Section 2, the deposit is located below -100 ft, NAVD88 (i.e., at the base of the sand bar) due to the mechanism explained by the reduction of the secondary and primary flows (Figure 9.7).

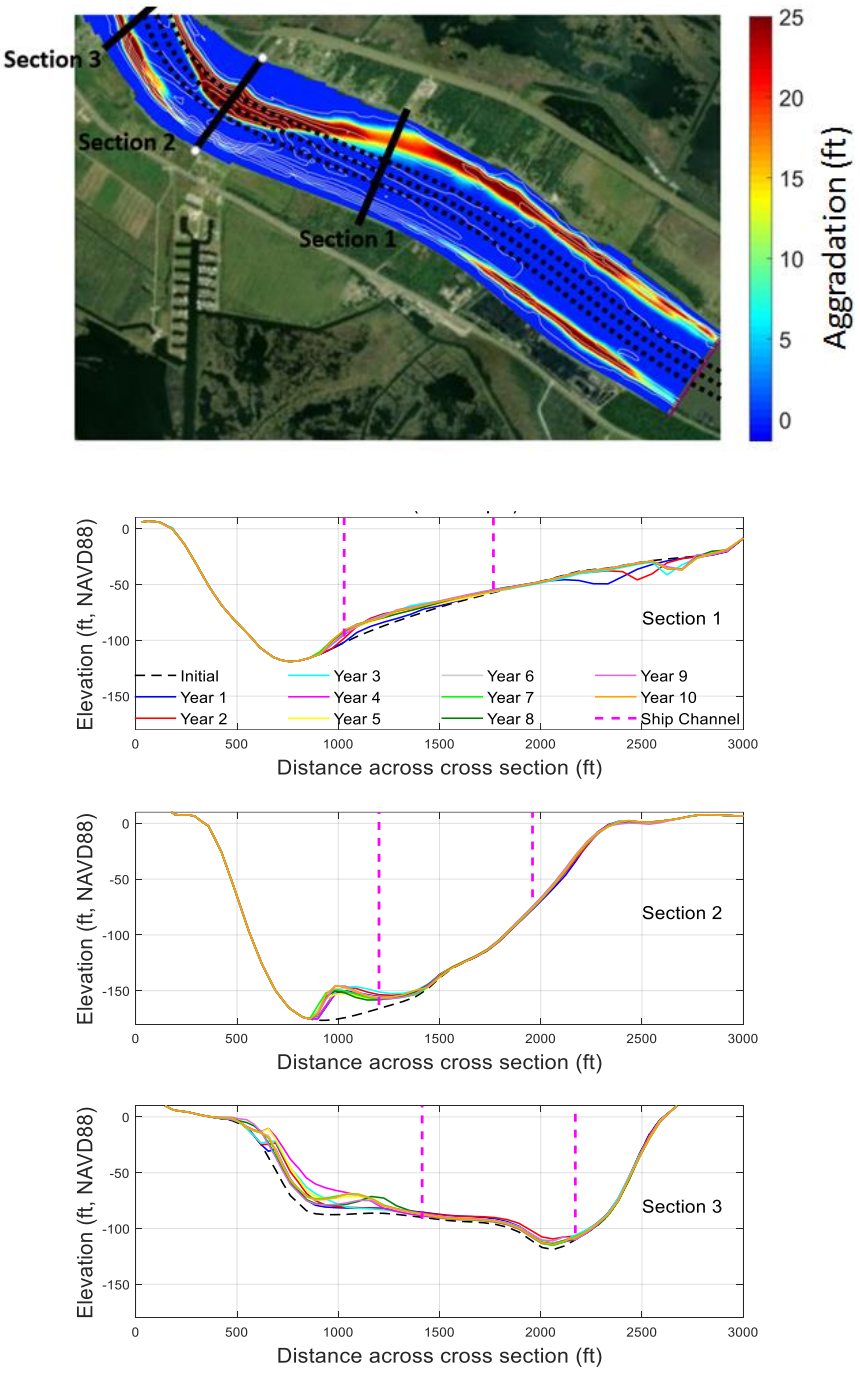

Figure 9.16. Cross-sectional plots showing bathymetric change at across the ship channel at three cross-sections at the Myrtle Grove bar. Solid lines along with the black dotted line (initial bed) show evolution of the sand bar through time. Vertical magenta dashed lines indicate extents of ship channel and its relative location with respect to the sand bar at these sections. Net deposition due to the diversion operation is likely to occur at the base of the sand bar (deeper than -100 ft).

Table 9.2 shows the change in volumes expressed as aggradation (+ve) or degradation (-ve). The volumes are calculated within the ship channel extents and between the length from RM 61.6 to RM 56. Note that the maximum yearly change for all cases occurs during the first year (2008). This is primarily due to the unusually large number of days (almost 3 months) of operation during 2008 when the MR flow remained well over 900,000 cfs. The choice of this starting year is thus conservative from an impact standpoint. Also, the quick response of the river channel to the hydraulic and sediment forcing enable the river to reach downstream equilibrium fairly quickly such that the deposited volumes for the subsequent years are about an order of magnitude lower than for the first year. It is likely that the use of MorFac which assumes a linear change in bed elevation in response to change in discharge also contributes to the rather large change in the first year. In reality it will probably take 5-6 years to reach a local downstream equilibrium. Therefore, the volumes averaged over the 10-year are better indicators of the expected change in the ship channel. Approximately, 109,000 CY of yearly averaged deposition of sand, with year-to-year variations ranging from about -150,000 CY to +130,000 CY, is predicted in the ship channel as a direct effect of MBSD operations. The year-to-year variations correspond usually to the nature of the flood hydrograph with wet years showing net deposition and dry years showing net erosion.

Table 9.2. Model predicted volumes deposited (+ve) or eroded (-ve) within the ship channel from a 10-year with- and without-project run including differential effects due to MBSD operations.

End of Yr	Without Project Aggradation (+ve)/Degradation (-ve) Volumes within Ship Channel (CY)		With Project Aggradation (+ve)/Degradation (-ve) Volumes within Ship Channel (CY)		Effect of MBSD (With Project – Without Project) Aggradation (+ve)/Degradation (-ve) Volumes within Ship Channel (CY)	
	Yearly Change (A1)	Cumulative Change (A2)	Yearly Change (B1)	Cumulative Change (B2)	Yearly Change (B1 –A1)	Cumulative Change (B2 –A2)
2008 (Yr 1)	2,364,059	2,364,059	3,476,217	3,476,217	1,112,158	1,112,158
2009 (Yr 2)	76,236	2,440,295	203,298	3,679,515	127,062	1,239,220
2010 (Yr 3)	3,414,860	5,855,155	3,396,956	7,076,471	-17,903	1,221,317
2011 (Yr 4)	2,010,256	7,865,411	1,871,647	8,948,118	-138,609	1,082,708
2012 (Yr 5)	-168,576	7,696,834	-166,093	8,782,026	2,484	1,085,192
2013 (Yr 6)	1,664,270	9,361,104	1,687,046	10,469,072	22,776	1,107,968
2014 (Yr 7)	967,257	10,328,361	1,024,616	11,493,688	57,359	1,165,327
2015 (Yr 8)	62,480	10,390,840	-83,287	11,410,401	-145,766	1,019,561
2016 (Yr 9)	-4,045,728	6,345,112	-3,929,091	7,481,310	116,638	1,136,198
2017 (Yr 10)	3,482,607	9,827,719	3,437,633	10,918,943	-44,974	1,091,224
Average Change / Yr	**982,772**	**N/A**	**1,091,894**	**N/A**	**109,122**	**N/A**

9.3.4 Analysis of far-field morphodynamic effects due to joint diversion operations

In this section, results from the FTNULMR (2D) Delft3D morphology model are presented, with particular emphasis on understanding and quantifying the change in river bathymetry between the two diversions, impact on the anchorage areas of interest downstream of MBrSD and, deposition on a larger extent of the ship channel beyond what was analyzed in the previous section with the near-field FTN2Comp model.

Figure 9.17 shows the net change in bed elevation due to diversion operations at the end of 10 years. In terms of deposition downstream of MBSD, it is seen that the maximum deposition near the Myrtle Grove bend occurs when both diversions are operations, followed by MBSD alone and MBrSD alone. Being closer to the bend, MBSD has a greater effect on the immediate downstream deposition at this location than MBrSD. The influence of MBrSD is visible in the

portion of the MR between the two diversions. Most locations show less than 10 ft of deposition in between the diversions. The spatial variability in the deposition occurs due to complex, secondary current-induced bedload interaction with the bends as well the proximity of the sand bar to the diversions. For example, when operating alone both MBSD and MBrSD show some erosion in the vicinity of the intakes. Note that except for the intake, no armoring was assumed at the MBrSD intake which also lacks revetment protection. The model is also not sufficiently fine in resolution to be able to capture the MBrSD intake in detail. The purpose of this exercise was primarily to capture the far-field effects, so the results of erosion near the MBrSD intake should be verified through independent near-field modeling which is beyond the scope of this study. Nonetheless, the model is able to reproduce expected deposition trend of sand bars aggradation between the diversions when both the diversions are operational. Under joint diversion operation scenario, it appears that the upstream intake degradation at MBSD is considerably reduced, possibly due to additional bedload supply from the bar upstream of Alliance as a result of the stream power reduction due to MBrSD. The additional bedload comes from what would have been additional suspended load travelling downstream as bedload due to the stream power deficit. This may possibly be a positive aspect of the joint diversion operations. Note that most of the excess bedload is still traveling deeper in the river along the distal parts of the Alliance bar and cannot be easily entrained into the MBSD diversion unless mechanical means are used to dredge it and place it near the zone of influence of the MBSD diversion. Therefore, so in terms of CSWR no significant additional benefit could be found from the joint operations scenario.

In addition to the ship channel, the anchorage areas were also analyzed for bed elevation change within the 10-year modeling period.

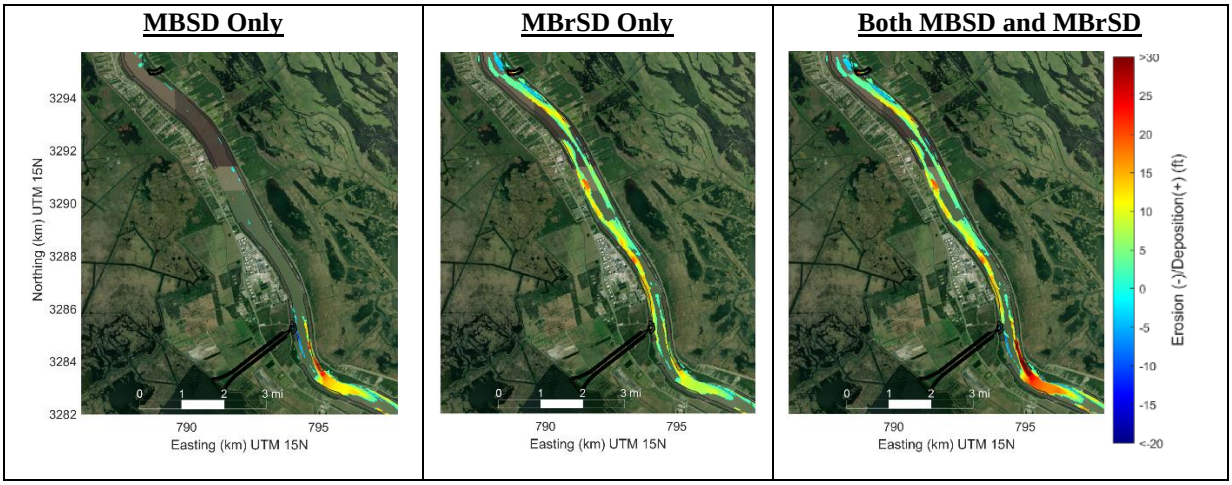

Figure 9.17. Cumulative bed elevation change in 10 years after the start of the diversion operations. Positive values indicate aggradation or deposition and negative values erosion or degradation.

Figures 9.18 and 9.19 show the evolution of the averaged ship channel bed elevation through the 10 years under single and joint diversion scenarios, respectively (similar to Figure 9.15 showing the nearfield results). These plots allow a closer inspection of the ship channel deposition over a longer extent. As was shown before, MBSD operation alone or when both diversions are operated simultaneously the two major areas of deposition are the Myrtle Grove bar and the Harlem-Gravolet reach. Note that the river narrows considerably at Harlem-Gravolet reach and the ship channel passes through an extended shallow zone (-70 to -90 ft, NAVD88). The highest bed elevation predicted at the Harlem-Gravolet reach is around -60 ft, NAVD88 and comparable to the Myrtle Grove sand bar deposited bed elevation. Therefore, it is recommended that these two zones be surveyed regularly within the first 5 years of diversion operation and probably every 5 years thereafter to keep the ship channel bed elevations monitored and if needed perform local dredging at those locations. It appears that equilibrium channel elevations are established in 5-6 years as the rate of deposition slows down after this period.

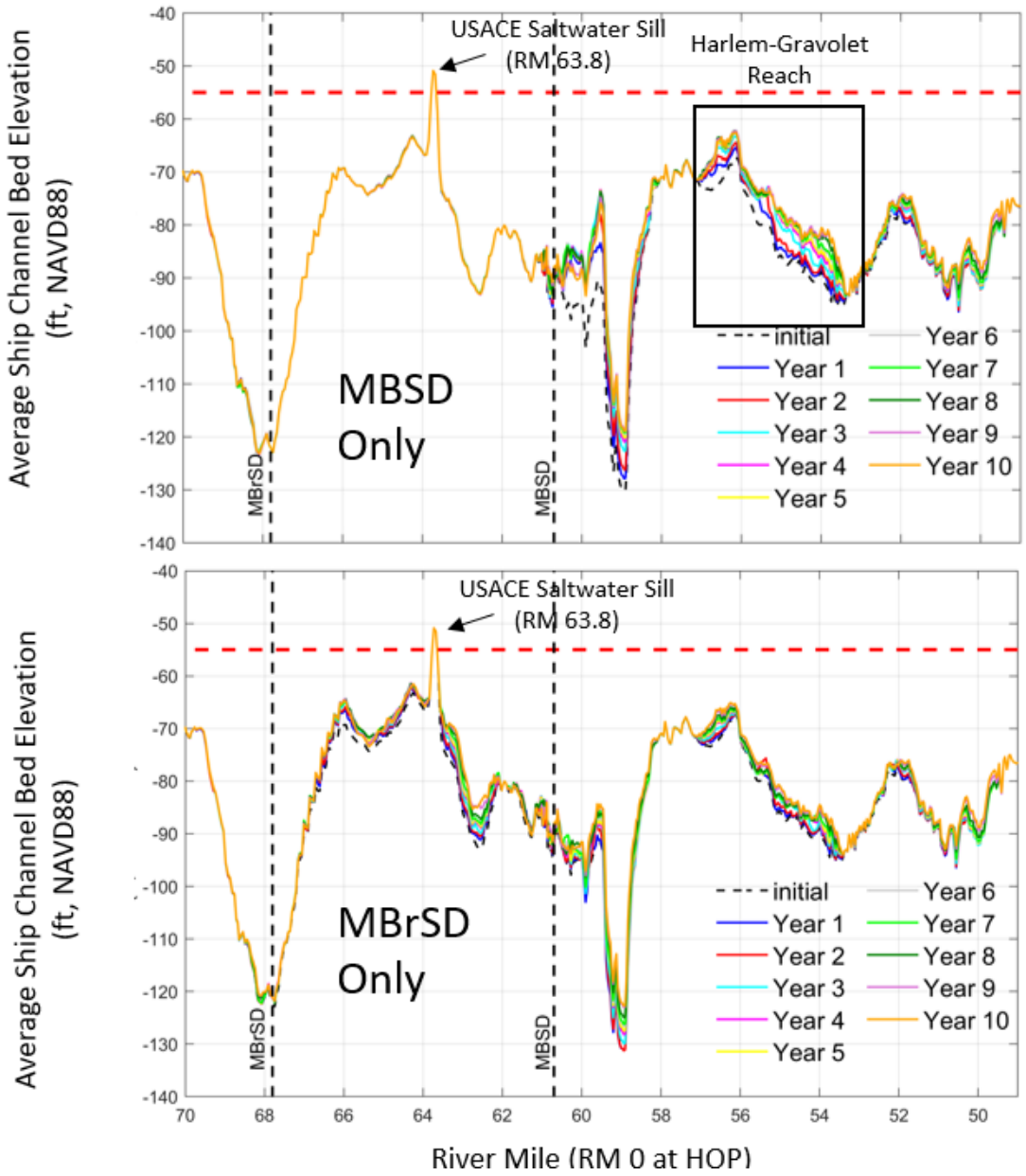

Figure 9.18. Ship channel cross-sectional averaged bed elevation evolution in 10 years under single diversion (MBSD only or MBrSD only) scenario. The USACE saltwater sill was set as a non-erodible morphology feature so it does not evolve. The Harlem-Gravolet reach is the single highest deposition zone of all the reaches between RM 70 to RM 50.

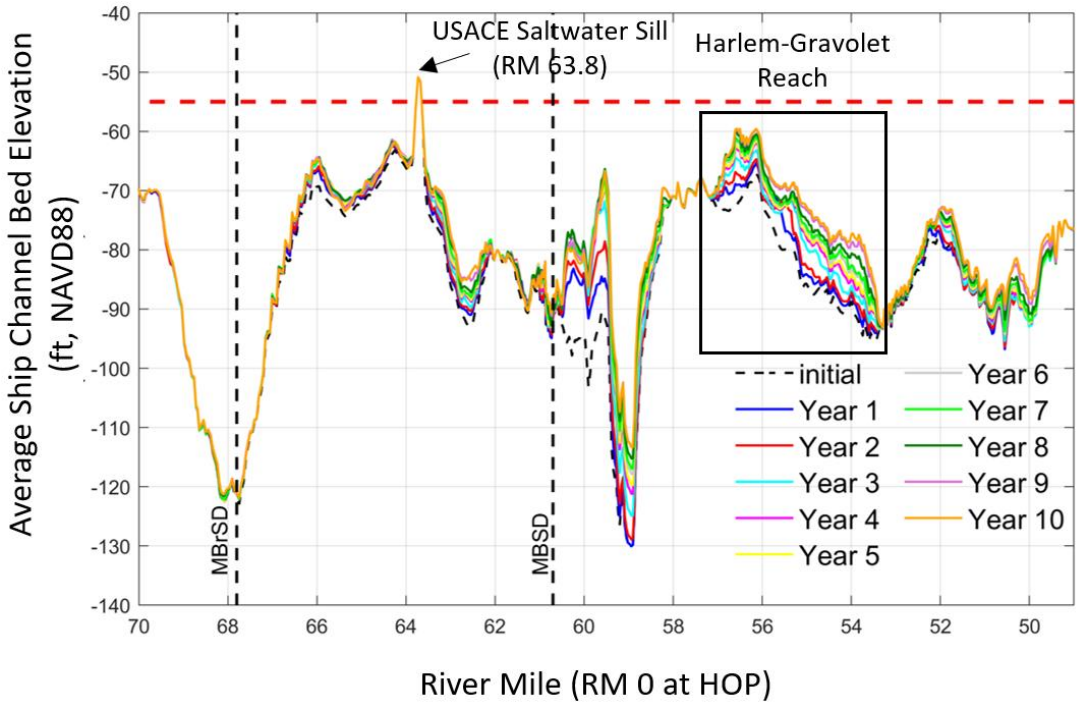

Figure 9.19. Ship channel cross-sectional averaged bed elevation evolution in 10 years under joint diversion operations (both MBSD and MBrSD) scenario. The USACE saltwater sill was set as a non-erodible morphology feature so it does not evolve. The Myrtle Grove bar near RM 58 to 60 along with the Harlem-Gravolet reach are the main deposition zoned of all the reaches between RM 70 to RM 50.

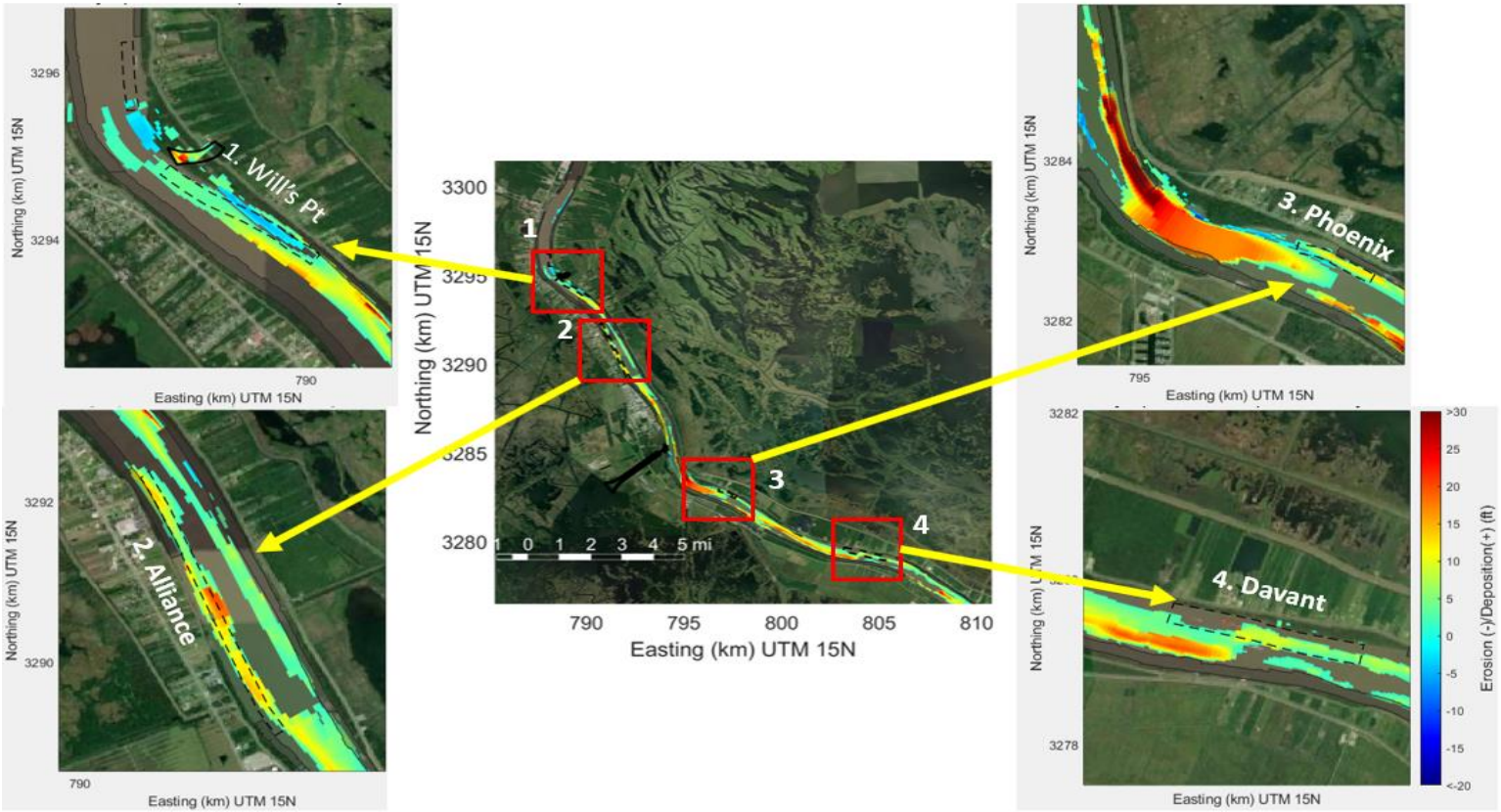

Figure 9.20. Anchorage locations analyzed for average elevation change in 10 years as shown in Table 9.3. Figure shows cumulative bed change contours for the joint diversion operation case.

Figure 9.20 shows the locations of the anchorages of interest downstream of MBrSD in the reach of interest from the point of view of deposition as a result of diversion operations. In the figure, the 10-year cumulative morphology change is shown as an example. Table 9.3 provides detailed the 10-year net change of the spatially averaged elevation in each anchorage area. The bounding area is defined by the dashed anchorage lines obtained from USACE navigation maps. The table also lists the minimum, maximum and the standard deviation values of spatial variation of bed elevation change in this zone. Note that even if the 10-year mean value is reported and in generally not significantly affected by yearly operations, once a certain equilibrium is reached in 5-6 years, the minimum and maximum values may change significantly from year to year due to yearly hydrograph variations and localized changes. Table 9.3 shows that Alliance is the most affected anchorage area by the MBrSD alone and the joint operations with a mean gain in elevation of 8.5 ft and locations with a deposition as high as 20 ft. The Phoenix anchorage is the next highest point of deposition and is mostly attributed to MBSD operations with the average gain in elevation 5 ft due to MBSD alone and 6 ft due to joint diversion operations.

Table 9.3. Summary of predicted bed elevation changes over 10 years at the anchorage locations in Figure 9.20. Positive values are deposition, negative values are erosion.

Anchorage Zone	Scenario	Mean Bed Elevation Change over 10 years (ft)	Min to Max Range of Annual Bed Elevation Change (ft)	Standard Deviation of Annual Bed Elevation Change (ft)
1. Will's Point	MBSD Only	-0.3	-0.9 to +0.1	0.2
	MBrSD Only	+1.6	-5.1 to +13.7	2.7
	Both MBSD+MBrSD	+1.3	-5.4 to +13.7	3.0
2. Alliance	MBSD Only	-0.1	-0.7 to +0.3	0.2
	MBrSD Only	+8.5	-0.3* to +19.7	4.9
	Both MBSD+MBrSD	+8.5	-0.3* to +20.0	5.0
3. Phoenix	MBSD Only	+5.0	-2.1 to +13.6	4.6
	MBrSD Only	+1.7	-2.9 to +12.5	2.8
	Both MBSD+MBrSD	+6.0	-1.7 to 13.3	4.3
4. Davant	MBSD Only	+1.8	-0.1 to +8.3	2.6
	MBrSD Only	+0.9	-0.5* to +5.5	1.5
	Both MBSD+MBrSD	+2.2	-3.3 to 11.3	3.1

*This specific model point possibly impacted by non-erodible revetment underneath.

9.3.5 Water level set-down effects at Bonnet Carre due to diversion (s) operations

The FTNULMR model calibrated and validated in Chapter 3 was used here under with-structure conditions to estimate the water level set-down effects at Bonnet Carre Spillway (BCS) location. The main purpose of this study is to quantify and demonstrate that there is an appreciable water level set-down at BCS to warrant a possibly reduced or delayed opening of the spillway. This can potentially aid operational managers to manage the spillway operations in coordination with the downstream diversion (s).

The model was run with the 2018 hydrograph for with- and without-structure(s) conditions. The output was then categorized into discharge vs. water level bins. The statistical mean of each discharge bin was computed and compared between the with- and without-structure(s) conditions. This approach is different from running a steady state model with- and without- structure(s) which was also tested initially but proved to be unphysical for addressing the set-down questions as the water level in a domain as long as the FTNUMLR is highly dynamic being dependent on the water surface slopes that varies in time and space and cannot be captured by an idealistic steady state run. Reproducing the dynamic nature of the rise and fall of the water level was important in achieve accuracy below 0.3 ft which is of the same order of magnitude as the set-downs.

Figure 9.21 shows the set-down of water levels at Bonnet Carre and downstream USACE gage locations. It is seen that the effect of set-down is the highest immediately upstream of the diversions and decreases upstream and downstream. The predicted set-down at Bonnet Carre is 1.4 ft at 1,000,000 cfs MR flow and 1.7 ft at 1,250,000 cfs MR flow when both diversions are operational. When only one of the diversions is operated the set-down ranges from 1.1 ft to 1.3 ft at 1,000,000 cfs and 1,250,000 cfs MR flow, respectively. MBrSD, being slightly closer to BCS, has a slightly more (by 0.1-0.2 ft) sert-down than MBSD.

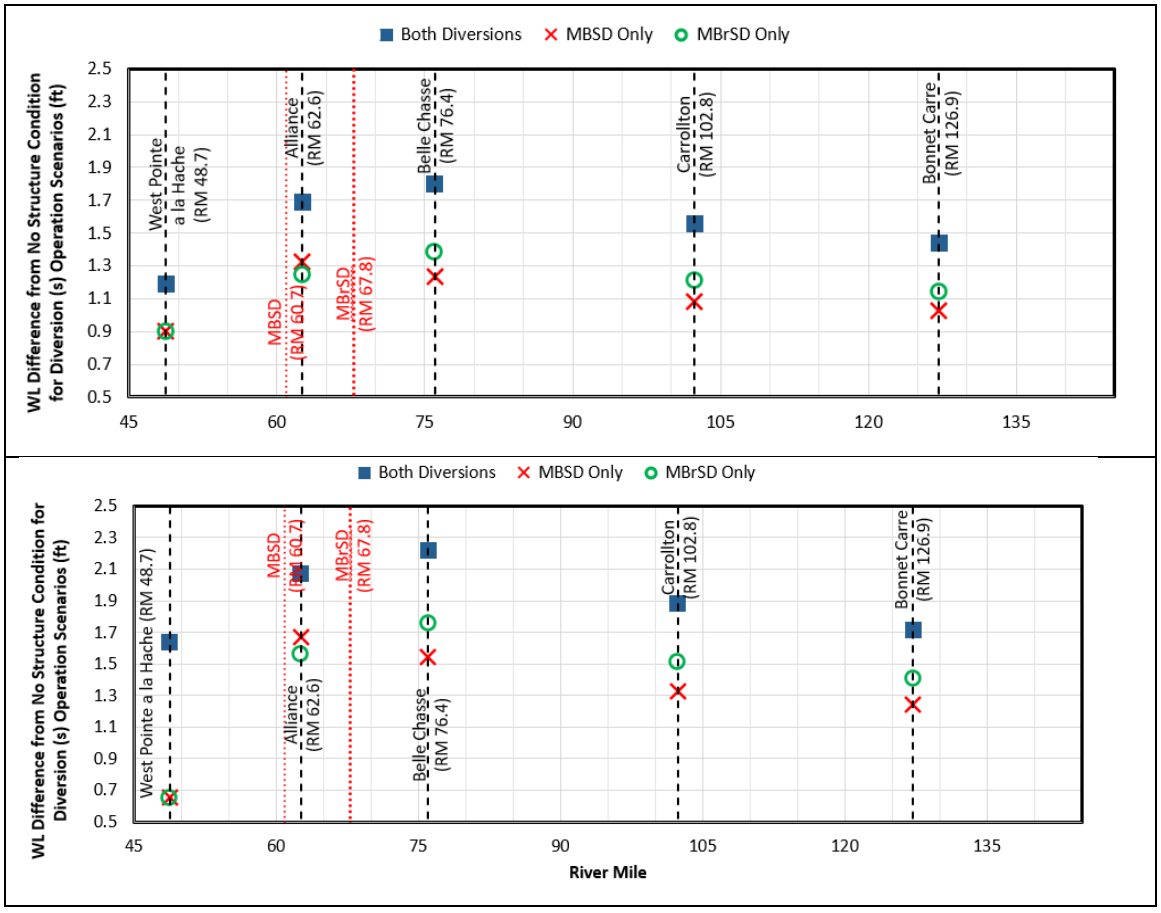

Figure 9.21. Water level set-down under different diversion(s) operating scenario at Bonnet Carre and below for MR flow at 1,000,000 cfs (top panel) and 1,250,000 cfs (bottom panel).

9.4 Conclusions

The near-field hydrodynamic and morphological response of the MR to the MBSD was evaluated through a series of sediment transport simulations using a 3D Delft3D model (FTN2Comp) model and a FLOW-3D hydrodynamic simulations where necessary. In addition, a 2D Delft3D (FTNULMR) model is also developed and used to analyze the morphology effects in the river as a response to the diversion operations. The FTNULMR was further used to estimate the water level set-downs near the at Bonne Carre Spillway due to combinations of diversion operations.

The following are the findings from this study:

1. The MBSD operation modeling over a 10-year (2008-2018) period shows a degradational upstream zone near the RDB revetment extending for about 0.2 miles upstream on the MBSD sandbar. This is similar qualitatively to the observations at West Bay over a 9-year period (2004-2013).
2. Without adequate rip-rap and revetment protection, the upstream degradational zone can potentially cause a loss of invert elevation of the diversion intake itself. The invert shows deepening up to -50 ft, NAVD88 (i.e., 25 ft below the intake invert) in about 10 years. With proposed rip-rap and existing revetment the change in elevation is much less; about 5-8 ft over 10 years. The interannual variability of this elevation change is 3-4 ft. Note that the model does not account for scour under the revetment edge or under the rip-rap or for bank collapse. Therefore, the model results of degradation should only be used qualitatively. The structural designers of the mitigation measures should use near-field model velocities, adequate safety factor and appropriate accepted empirical methods.
3. Opening the diversion during a potentially dry period can reduce the immediate (first year) impacts of the sandbar degradation. It is recommended that regular annual surveys be performed to monitor this area and if bed elevations exceed structurally mandated minimum levels, the diversion may have to be kept closed for a year to allow the sandbar near the intake zone to rebuild itself.
4. Downstream of the diversion, the MR channel shows aggradation particularly at the Myrtle Grove sandbar, which is seen to accrete into the deeper portion of the bend.
5. The model results indicate that under diversion open conditions, aggradation downstream of the diversion may will not cause shallowing of the average ship channel draft south of RM 70 over -55 ft, NAVD88 over 10 years, even though there may be few locations like the Myrtle Grove sand bar and the Harlem-Gravolet reach depositing more than other location. Approximately, 109,000 CY of sand is estimated to be deposited annually as a result of the MBSD operations within the ship channel between RM 61.6 and RM 56 over the 10-year period.
6. Diversion induced average bed elevation at the four main anchorage sites below RM 69 indicate that Alliance is most affected by the MBrSD operations and the Phoenix bend by the MBSD operations. Joint operations tend to increase deposition south of the MBSD site.
7. Water level set-down at Bonnet Carre due to diversion(s) operations indicates a 1.4-1.7 ft of set-down at MR flow of 1,000,000 – 1,250,000 cfs.

10.0 BASIN-SIDE EFFECTS OF DIVERSION: 50 YR LAND-BUILDING AND MAINTAINENCE DREDGING MODELING

10.1 Introduction

In this chapter the 50 Yr land-building modeling, which includes both the morphological change in the basin due to the mineral sediment contribution from the diversion and the non-mineral vegetation growth induced vertical accretion of the ground, modeled using the Louisiana vegetation (LAVEG) model, is presented. In addition, effects of self-weight consolidation of the deposited sediment and the Relative Sea Level Rise (RSLR) (spatially varying subsidence and temporally varying Eustatic Sea Level Rise) are also included for the 50-year modeling. This model will hitherto be abbreviated as FTNOMLV-CONSOL (FTN's Outfall Model with LAVEG including Consolidation). The modeling includes salinity and water level effects in the basin on the vegetation dynamics. Therefore, even though model results presented here include salinity variations in the basin and vegetation distributions, this is not meant to replace those results from the independent EIS study (GEC, 2021) which is the official permitting document and include a more exhaustive investigation of scenarios. The land-building, salinity and vegetation results here should be considered as representative of diversion effects mostly within the first 8-mile radius of the outfall where the model is mostly active in land-building. For the scenarios that are similar to those in EIS, the model results here could be taken as a refinement of those results however, given the fact that a refined diversion geometry (and hence flow rating curve) as well as greater resolution within the this 8-mi zone is possible in this modeling. As will be discussed later number of detailed scenarios are modeled here including effects of High and Low SLR as well as with and without base flow (defined as a minimum flow during when MR<450,000 cfs). In addition, the effects of maintenance dredging in the basin are also investigated here.

One of the important additions to the existing investigations by CPRA (GEC,2021) is that the FTNOMLV-CONSOL model is a head-driven based model, meaning that the diversion capacity can change based on the head difference available between the riverside and the basin side of the diversion and therefore can dynamically change the rating curve (Diversion Discharge

vs River Discharge) over the 50 yrs of modeling as dictated by RSLR and future land-building effects. This is a very important requirement to validate that the diversion design is indeed able to perform effectively during its entire design life. In the 30% design, it was identified that the MBSD diversion may not be able to maintain its target capacity of 75,000 cfs at 1,000,000 cfs MR flow up to Year 50 due to RSLR and land-building effects induced macro-roughness increase in the basin. While that hydrodynamic only modeling used decadal bathymetries from the Water Institute's Basin Wide modeling (Meselhe et al., 2017) to provide dredged estimates every 10 yrs, the current modeling improves on that by performing dredging on the bathymetry directly outputted from the current hydrodynamic-morphology coupled modeling itself. This approach not only provides a consistent model platform for land-building and dredging at the same resolution but also eliminates the need for depending on another model for the morphology modeling part. Therefore, the current modeling also includes an investigation into the dredging estimates in the future as well as modeling a scenario where no dredging can be performed for the 50 yrs. This chapter begins by explaining the model setup of the FTNOMLV-CONSOL modeling, then provides a description of the scenarios modeled and finally the results are presented.

10.2 Model Setup

10.2.1 Delft3D (2D) Coupled Flow and Morphology (OM) Module

The two-dimensional (2D) Delft3D model (FTNOMBA) coupled hydrodynamics (HD) and morphology (OM) model described in Section 1.7 and used in the Outfall Transition Feature (OTF) modeling in Chapter 7 was extended to model the entire 50 years of diversion operations. A detailed description of key model parameters is shown in Table 10.1.

Table 10.1. Key Model Input Parameters for 2D Delft3D (OM) Model used for 50 yr modeling.

Model Parameter Class	Parameter Name	Value and Units		Description
Model Bed Roughness	Chezy Coefficient	*Diversion Three-Component:* Variable spatially, see Fig 4.9. *Basin:* Variable spatially and temporally with vegetation characteristics, distribution and water depth, see Figure 8.4.		Baptiste et al. (2007) used to specify basin Chezy, see Section 8.2.2.
Sediment Types and Characteristics	Sand (Non-cohesive): Very Fine (d_{50}=83μ), Fine (d_{50}=125μ) and Medium (d_{50}=250 μ) Fines (Cohesive): Silt (2μ<d_{50}<63μ) and Clay ($d_{50}\leq$2μ) Special Class (Cohesive): Marsh (Root Mat Layer) Compact (Compact Sediment)	*Dry Bed Density:* Sand= 1,600 kg/m^3 Fines=500 kg/m^3 Special Class: Marsh=152 kg/m^3 Compact=848 kg/m^3	*Settling Velocity:* Sand: Variable, from Van Rijn (1993) model. Fines: Silt=7.1x10^{-3} m/s Clay=2.75x10^{-6} m/s Special Class: Marsh=1x10^{-4} m/s Compact=1x10^{-4} m/s	Model parameters are similar to CPRA models used in LA Coastal Master Plan.
Critical Shear Stress of Erosion	$\tau_{cr,ero}$	Sand (Non-cohesive): Computed from Shields' curve, Van Rijn (1993) model. Fines (Cohesive): Silt=0.092 Pa, Clay=0.0093 Pa. Special Class (Cohesive): Marsh=1.5 Pa Compact=1.5 Pa		Cohesive sediment model parameters are similar to CPRA models used in LA Coastal Master Plan. For the Compact class of sediment 1.5Pa was used based on SEDFLUME analysis, Table 7.3 and Figure 7.24.
Erodibility Parameter	M	Sand (Non-cohesive): Not applicable as erosion of sand is determined by dynamic concentration gradient at the bed and vertical diffusion coefficient calculated from hydrodynamics. Fines and Special Class: M=1x10^{-3} kg/m^3		--
Sediment Transport	Sediment Transport Model Formulations Used	Sand (Non-cohesive): Van Rijn (1993) Fines and Special Class: Linear Partheniades-Krone (1965) for erosion and deposition		--
	Sediment Transport Model Specific Constants	Sand (Non-cohesive): Bed-slope effect on bed-load=Yes, Bagnold (1966) Hiding/Exposure Modeled=No Stream-wise and Transverse Bed Gradient Factors=1.5 and 0.5 Multiplication factors for suspended and bed-load transport=0.8, 1.85 Van Rijn's reference height factor=0.1		--
Horizontal Eddy Viscosity and Diffusivity	--	1 m^2/s and 10 m^2/s		--

The coupled flow and salinity model is run for the a given cycle by splitting it up into 15-day intervals. A cycle for HD-OM modeling is defined as the period between 450,000 cfs MR flow in the rising limb of the current flood cycle to 450,000 cfs of rising limb of the next year's flood cycle and includes both operational period as well as the base flow non-operational period. During the operational period (OP), which lasts between the start of the cycle and the day the MR flow again comes down to 450,000 cfs in the falling limb, the diversion gates remain fully open unless to limit flow to 75,000 cfs, typically above 1,000,000 cfs MR flow. During the non-operational period (NOP), which is any time the MR flow drops below 450,000 cfs, the base flow (diversion flow between 0 and 5,000 cfs) is the only diversion flow modeled. Each of these 15-day intervals within the main cycle, is termed as a sub-period (SP) and forms of a standalone hydrodynamics and salinity model. All of the SPs in a given cycle are run parallelly during execution of one HD-OM cycle in a massively parallel High-Performance Computing (HPC) system. This approach allows a whole HD cycle (about a year) to be run within the same time (about 1 day of wall clock time) it takes to complete the OM cycle, which is accelerated by morphological acceleration and allows for an entire HD-OM-LV-CONSOL cycle to be completed in roughly 1 day. What makes this method even more attractive is that the HD model retains the natural variability in salinity like from seasonal variation in the Gulf of Mexico and water levels, including effects of daily and Spring and Neap tides in the basin, all of which contribute to the statistical and physical variation in WL and salinity that is expected due to the interaction of tides, diversion flow and the bathymetry. A detailed step by step approach of the HD model is given below:

1. Divide the whole cycle into Operational Period (OP) (MR flow >450,000 cfs when diversion if fully open or closed only to limit diversion flow to 75,000 cfs) and Non-Operational Periods (NOP) (MR flow<450,000 cfs and diversion max flow restricted to 5,000 cfs). The relation between diversion flow and MR flow is known beforehand at the start of a cycle from rating curves updated every 5 years as described later.
2. Split OP into Sub-Periods (SP) of ~15 days, keeping individual months intact.
3. Split NOP into SPs of ~30 days, keeping individual months intact.
4. Identify starting and ending date & time of the SPs.
5. Define all boundary conditions for each SP.

6. Initialize each SP with the end conditions for water level, velocity and salinity of the corresponding SP in the previous cycle which is approximately at the same period of the year.
7. Set up separate SP model files and sync with HPC system.
8. Run models in parallel in HPC system.
9. After all model runs have ended sync and post process results files from HPC system for statistical calculations.

While the HD-OM module runs every year, the module to update the diversion discharge rating curve and perform dredging runs every 5 years. This is done because primarily it is computationally more time intensive to run the HD model with the river domain as the Courant number requirements are tighter (smaller time steps) due to the high velocity at the intake (see Chapter 4) and it was determined through initial test runs that the change in rating curve within 5 years was not significant with diversion flow changes at a given MR flow varying less than 3% within each 5-year period. Also, the iterative dredging technique, where several dredge templates are tested one by one to improve design capacity to the target within each 5-year period, requires manual oversight to determine which channels are most suited for dredging. The Monte Carlo simulation module, described later which provides a continuous time series of diversion discharge for the next 5-year cycle runs several runs in parallel and takes about 2 calendar days to complete. The entire dredging and diversion flow rating update can be done in about 2-3 days of wall-clock time with a 3-person team. The main outputs from the model are an updated diversion discharge time series for the subsequent 5-year cycle, dredging volume and dredged template at every 5-year interval, required to maintain 75,000 cfs peak flow at 1,000,000 cfs MR flow. A detailed step by step approach of the Dredging and Diversion Flow Update Module is given below:

1. Run every 5 years starting from 2025 and ends in 2070.
2. Perform dredging performed if diversion flow falls below 75,000 cfs at 1,000,000 cfs MR flow. Final dredging volume and template is obtained by an iterative process. The basin is dredged incrementally following existing deltaic channels pathways as a trapezoidal cut with side slopes no steeper than 1:5 and the diversion capacity checked through a series of steady state runs, until capacity reaches 75,000 cfs. The final dredged bathymetry is then used to perform the Monte Carlo type analysis below.

The Monte Carlo type analysis described before in Section 8.2.2 discharge time series is used in this module. This analysis runs a series of steady state runs with temporally constant boundary conditions, MR flow and Gulf of Mexico water level, to prepare a seed matrix of diversion discharge within which diversion discharge data can be interpolated given other combinations of boundary conditions whole values lie within the steady state-run boundary envelopes. This module produces the continuous diversion discharge time series, given known boundary conditions of water level at Gulf of Mexico and MR flow for the next 5 years. The water levels and MR flows are known beforehand for the entire 50 years as shown later in Figures 10.x and 10.x based on historical hydrograph and the ESLR scenario modeled. The basin bathymetry is held constant during all the steady state runs and is the same produced by the HD-OM run just preceding the beginning of the next 5-year Dredging and Flow Update module. The river bathymetry is held constant as the current (Yr 0, 2020) bathymetry. Detailed steps of this analysis are given below:

1. Perform 3 separate runs with the same historical MR hydrograph, with MR flow ranging from 200,000-1,250,000 cfs, each with a Maximum, Minimum and Mean GoM WL as computed from analysis the subsequent 5-year record of GoM WLs, the period for whom the diversion discharge is being forecasted. This is meant to encompass the full envelope of water levels at GoM possible during the interpolation procedure.
2. From the above 3 runs, a 3D matrix can be generated comprising, the modeled daily diverted discharge for each of the three GoM WL conditions and the entire range of daily MR flows simulated. Therefore, given the MR hydrograph and the daily GoM WL record of the next 5 years, which are both known beforehand for the entire 50 yrs., it is possible to perform a three-dimensional (3D) interpolation where the simulated diversion discharge in step #1 is interpolated to find the daily diversion discharge for each day in the next 5 years.

This module obviously assumes that the diversion discharge can be linearly interpolated for the range of GoM WL and river discharges and a steady state condition is possible to be attained each day. Both these assumptions have been verified to be valid through independent in-house event base hydrograph modeling of a test period and the error from the interpolation method is found to be less than 3% of discharge.

The sediment transport and morphology (OM) module is run with the discharge time series at the mid-channel location similar to modeling in Chapter 7, that is there is no river domain modeled as it is not pertinent for basin effects. For detailed description of the model setup the reader is referred to that chapter. The detailed OM module sediment transport and morphology parameters are given in Table 10.1. A morphological acceleration (MorFac) factor if 80 is used for the OP periods and a value of 160 for the NOP periods. Initial tests with variable MorFac found no significant difference in land building over decadal scales within these ranges. The final bathymetry at the end of the OM module is updated for vegetation accretion and self-weight consolidation as described in next sections before being fed to the HD-OM module of the next cycle.

10.2.2 Louisiana Vegetation (LAVEG) Module

The Louisiana Vegetation (LAVEG) module comprises of a collection of Python and Matlab based model scripts that incorporate temporally averaged but spatially varying hydrodynamic model results from the HD module to model vegetation growth, species allocation, vegetated area distribution, marsh collapse (senescence) and finally updates the vegetation cover (percent area occupied by a given species of vegetation) for use in basin roughness modeling using Baptiste et al., 2007 formulation. For technical details of the module the reader is referred to WI publication (Jung et al., 2019).

CPRA provided the LAVEG framework, including the initial Matlab and Python scripts to FTN. FTN incorporated the model framework to be used with a domain decomposition Delft3D model, developed additional scripts in the LAVEG pre-processor to efficiently perform computations in the cloud without large data transfers and corrected minor technical bugs in the code (e.g., definition of summer period was corrected to April -August instead of July-Sep to be consistent with Visser et al. 2013). A brief description of the key components of the LAVEG module are given below:

10.2.2.1 LAVEG Preprocessor Module

A series of MATLAB based scripts that computes the spatial annual and summer statistics (mean and standard deviation) for Water Depth and Salinity from the spatially and temporarily varying model results of the whole year from the HD module. Since one cycle (about a year) of the HD module run comprises of many sub-periods each 15 days long, this module first reconstructs the time series of salinity and water depth at every grid cell for the entire cycle first. Then the mean and standard deviation of annual and summer values of the modeled salinity and water depth quantities are computed for every cell. Land-water indexes (0 for land, 1 for water) for every cell are also computed based on the mean water level (MWL) of the year being modeled, where the MWL changes year to year based on ESLR scenario modeled as in Figure 10.5 later. If the elevation of a given cell falls at or below the MWL of the year then it is considered to be in water and if above the MWL it is considered land. The LAVEG preprocessor module then passes the following quantities for every cell in the model, for the current cycle, to the main LAVEG processor module described below: Summer mean water depth, summer mean salinity, annual standard deviation of water depth, annual mean salinity and land-water index. The LAVEG processor module also requires the mean summer temperature which is held constant at 21.6 deg C based on last 10 years of meteorological data.

10.2.2.2 LAVEG Processor Module

This module includes a Python based model that implements the Louisiana Vegetation (LAVEG) model (Visser et al., 2013). to develop a spatial distribution of vegetation cover to be used by the hydrodynamic and morphology modules for the next cycle. This module also includes growth and senescence functions based on input hydrodynamic statistics from the preprocessor module described above and allows for plant species exchange in response to hydrodynamic conditions year to year.

In addition, this module also includes a series of MATLAB scripts that implements Marsh Collapse algorithm and updates the trachytope (roughness) distribution settings of the basin. The Marsh Collapse algorithm (WI) starts with the initial vegetation cover produced by the LAVEG Python codes described above and uses the hydrodynamic data to modify them based on a set of rules given below. This module therefore specifies in a given cell the amount of

area occupied by each type of vegetation as well as water and bare ground. This information is then fed as trachytope (*uv) files to be used by the Baptiste et al. (2007) formulation within Delft3D during the next to the main Delft3D during the next HD and OM cycle. Marsh collapse rules:

- **Fresh marsh**: Land will convert to water if land elevation is at, or below, the annual mean water level for the year and the maximum two week mean salinity during the year is above 5.5 ppt.
- **Intermediate Marsh**: Land will convert to water if the annual mean water depth over the marsh is greater than 0.36 m.
- **Brackish Marsh**: Land will convert to water if the annual mean water depth over the marsh for is greater than 0.26 m
- **Saline Marsh**: Land will convert to water if the annual mean water depth over the marsh is greater than 0.24 m

10.2.3 Percent Organic Matter (POM) Accretion Module

This module includes a set of MATLAB scripts that computes the Percent Organic Matter (POM) accretion on the basin surface as a result of plant growth and senescence. The percent vegetation coverage occupied in a given cell by a given vegetation species, as modeled by the Marsh Collapse module before is converted to vertical accretion (mm/yr) based on a series of accretion curves reverse engineered from the WI BW PR4V3 model data and developed by the WI. For more details on these curves and the assumptions behind them the reader is referred to WI publication. POM accretion is added to the marsh composition of the existing stratigraphy layer and the resultant change in bathymetry due to organic matter accumulation obtained by dividing the total vegetation contribution from all species in a cell by the dry density of vegetation matter, assumed as constant 152 kg/m^3 and same as the ‘Marsh’ component in the morphology (OM) module shown in Table 10.1. Therefore, when the subsequent morphology model cycle is restarted not only is the bathymetry adjusted but also the composition of the top most layer of the bed updated to reflect the added organic matter.

10.2.4 Subsidence and Self-weight Consolidation (CONSOL) Module

Basin subsidence, due to continental existing continental scale subsidence, is included in the model by specifying a subsidence file for the 50-year model run as shown in Figure 10.1, which shows the total subsidence happening in the basin in 50 years. This dataset is the same as used in CPRA's LA coastal master plan modeling and is meant to remain consistent with existing models. The subsidence is applied linearly, where the model divides the total subsidence by the number of timesteps during the model run and the bathymetry is lowered by that amount incrementally at every time step. No additional modification to the bathymetry data is therefore needed offline, for subsidence effects.

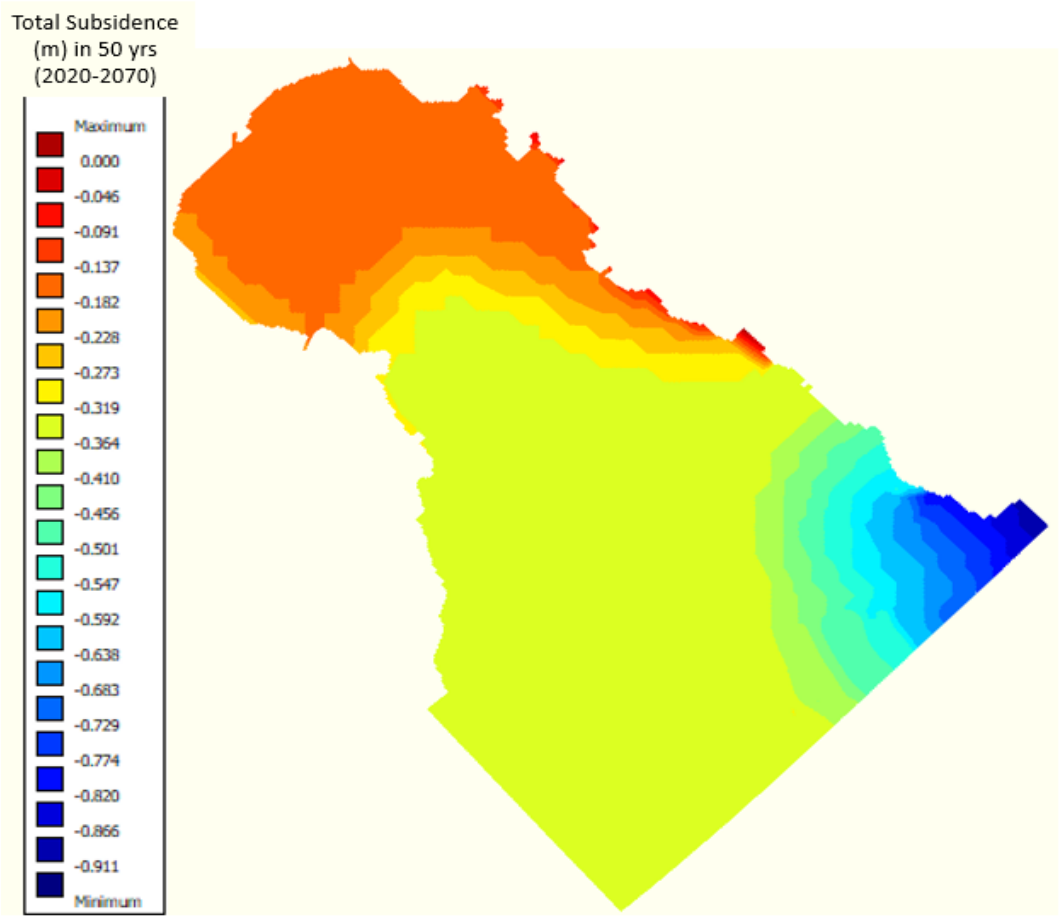

Figure 10.1. Total subsidence over 50 years (2020-2070). Subsidence is applied linearly for during each model cycle (year) implicitly during the modeling process.

Self-weight consolidation is modeled on a per cycle (about a year) basis as it depends on the amount of sediment (mineral and vegetation) sitting on top of the consolidable layer during the cycle. The consolidation module considers the spatially varying deposition by modeling every domain of the cell separately. Specific details of the CONSOL module, which is written in MATLAB is given below. This module is an improvement to the existing OMLV framework provided by CPRA.

- Terzaghi's 1-D consolidation theory applied to compute self-weight consolidation due to the deposited load. Each model grid cell in the basin is considered as an independently consolidable land.
- At a given cell, the spatially and temporarily variable consolidation problem is solved with consolidation applied at the end of every cycle of HD-OM-LV run. A constant load, equal to the mean yearly load, is assumed to be applied over the full current cycle in order to compute consolidation over the cycle.
- The deposited load and overburden pressure are computed as a weighted average of the loads of each constituent sediment fraction (sand, silt, clay and marsh) based on their volume fractions and individual densities.
- Consolidation coefficients (Cc, Cv) can vary both as a function of imposed load and depth. Relations were developed from analysis of laboratory consolidation tests conducted over 40 soil core samples taken in the basin.
- CONSOL Module validated against Tornqvist et al. (2008)'s data. For more details see below.
- Both primary and secondary consolidation processes considered. However secondary consolidation contribution was found to be negligible due to the transient nature of loadings (repeated erosion/sedimentation) and large t95 values compared to the life of the project and was neglected from the final results.
- Consolidated soil is considered always to be in an over-consolidated state, no swelling is modeled.

The CONSOL module was independently validated with Nienhuis et al. (2018) model data as shown in Figure 10.2, which shows a test case of deposition at 12cm/yr for 100 years. The values of consolidation coefficient (Cv) and compression index (Cc) were altered in the CONSOL model until the model matched the observed data best. A value of Cv=2.8 ft^2/d and Cc=1.0 was found to match the data best. Note that the purpose of this validation was simply to determine if the model algorithm is properly implemented, the exact values of Cv and Cc will

come from the field data at MBSD site. The fact that Nienhuis's model validation Cv=2.8 ft^2/d equaled the value from analysis of samples from within 10 ft depth below mudline shown later was purely a co-incidence but also possibly a validation of Nienhuis' which was itself validated against long term Tornqvist's (2008) data.

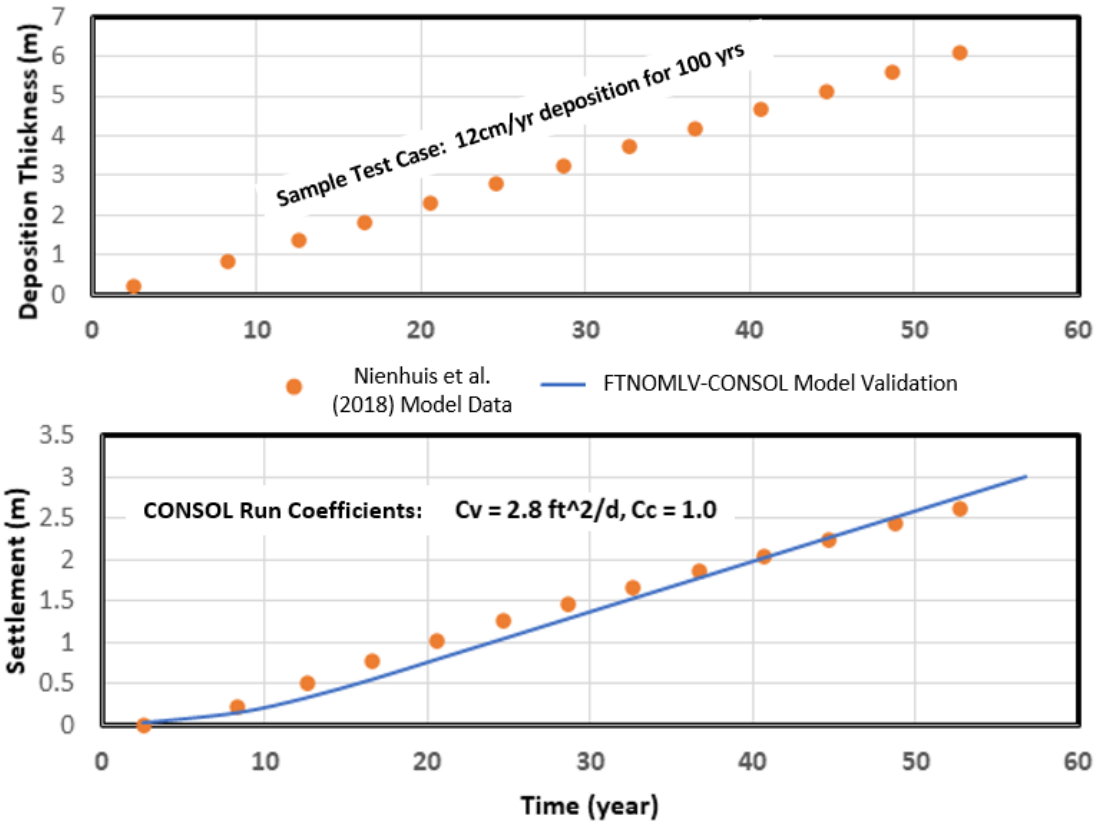

Figure 10.2. Validation of CONSOL module with Nienhuis et al. 2018 model data.

EUSTIS collected extensive samples from the Barataria Basin (Figure 7.21, Chapter 7) from which consolidation tests were conducted on about 110 samples. FTN analyzed the data to construct the input coefficients for the CONSOL module. The median Cc was found to be 0.76 and the mean value of 0.79. No meaningful spatial or depth trends were found for the Cc value and a constant Cc=0.8 was adopted for the entire domain. On the other hand, Cv variability was found to be best modeled by dividing the consolidable layer (assumed at 40 ft below mudline similar to findings of Tornqvist, 2008) into specific ranges and computing the variability

with pressure within each range. The top two deoth ranges between less than 10 ft and between 10 and 15 ft had too much scatter in the observed data to produce a meaningful correlation and a mean value for Cv were chosen as constant value for the entire depth. The Cv values deeper than 15 ft were assigned a power function based on a best fit regression line. Figure10.3 shows the analysis of Cv ranges as a function of depth and overburden pressure. Both Cv and Cv were held spatially constant horizontally in the whole domain.

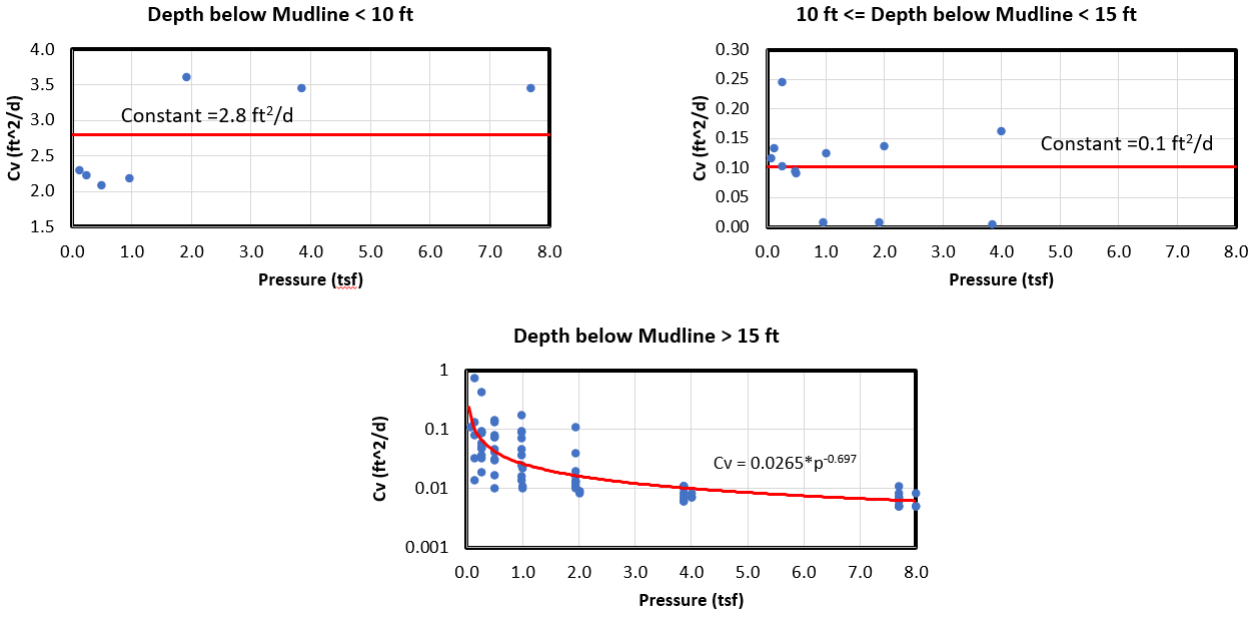

Figure 10.3. Variation of coefficient of consolidation (Cv) with depth and overburden pressure.

10.2.5 Coupling of FTNOMLV-CONSOL Modules

The coupling of the FTNOMLV-CONSOL modules is achieved mainly through a series of hierarchical Matlab codes that work with minimal human intervention in outputting data from a previous module, processing and transferring the required input data for the subsequent module. Figure 10.4 shows the flow-chart showing the interaction of the modules and what data is transferred between the modules.

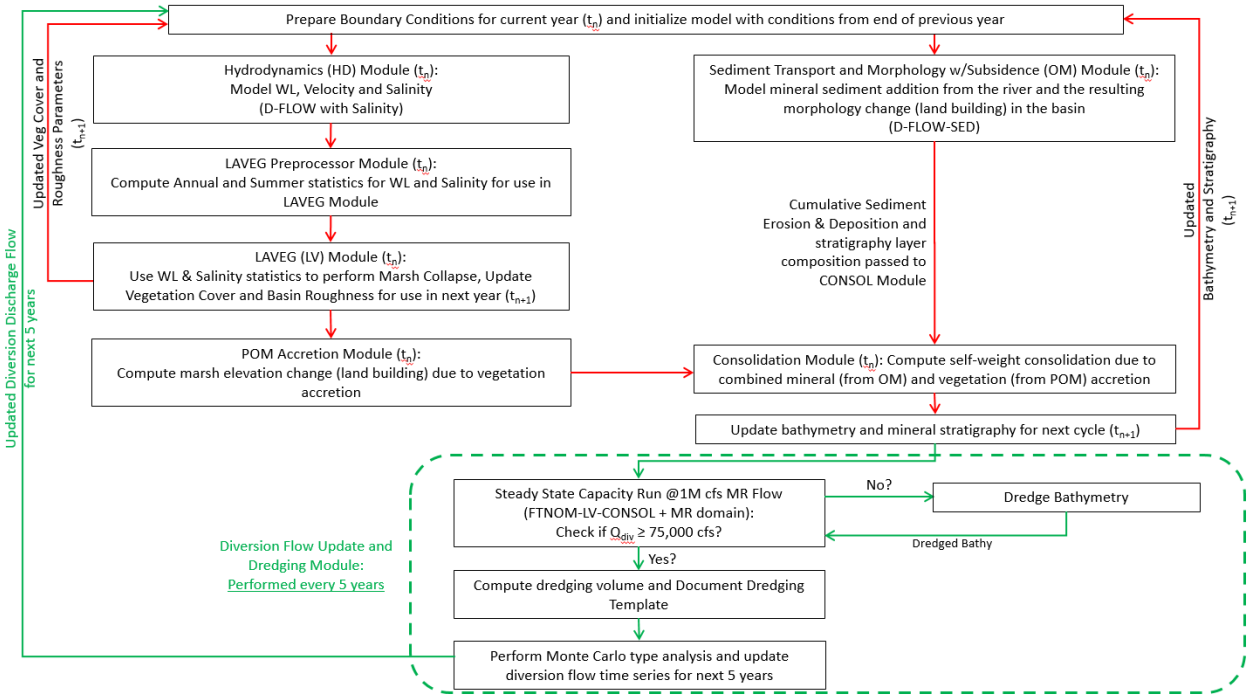

Figure 10.4. Flow-chart showing the coupling of various FTNOMLV-CONSOL modules.

10.3 Model Scenarios and Boundary Conditions

Table 10.2 shows the four 50-year scenarios modeled and presented here. While not all combinations of variables were possible to be investigated, the modeling followed instructions from CPRA for the conditions to be investigated here. For all modeling a maximum of 5,000 cfs base flow is allowed below 450,000 cfs MR flow with a minimum of 0 cfs, that is no reverse flow from basin to river is permitted and is consistent with recommendations from reverse flow analysis in Section 8.3.3 before. Since the FTNOMLV-CONSOL model is a head driven model that determines the diversion discharge for each 5-year period, it automatically adjusts for flow availability based on head difference below 450,000 cfs MR flow and therefore can have flows below 5,000 cfs and even periods of no flow (when reverse flow conditions are predicted) as well. Therefore, the with base flow modeling here is different from WIBW-PR4V3 modeling which assumed a constant 5,000 cfs base flow when MR was below 450,000 cfs without considering periods of non-operation due to lack of head availability of reverse flows.

Table 10.2. 50-Yr Modeling Scenarios investigated using FTNOMLV-CONSOL Model

Sea-level Rise by 2100 (meters)	Base Flow of max 5,000 cfs when MR <450,000 cfs?	Dredging Conducted?	Description
0.5	Yes	Yes	With Dredging, with Base Flow, Low SLR
1.5	Yes	Yes	With Dredging, with Base Flow, High SLR
		No*	Without Dredging, with Base Flow, High SLR
	No**	Yes	With Dredging, without Base Flow, High SLR

Eustatic Sea Level Rise (ESLR) is applied to the water level boundary for the HD-OM module. The water level for the HD runs is specified hourly while that for the OM model uses a constant annual mean water level calculated from the ESLR curve. This is because the tidal variations in the HD module is necessary to model the physically realistic water level and salinity variations in the basin, the statistical analysis of which forms an important basis of the LAVEG module described in the next section. In order to develop a realistic tidal forcing, the 10-year period 2008-2018 water level data at Port Fourchon is used as a basis to reconstruct future 50-year water level boundary. The tidal oscillations about the annual mean water level are first separated and then added to the adjusted future annual MWL based on the ESLR prediction. The process is described in Figures 10.5 and 10.6.

Figure 10.5 shows the USACE High (1.5 m by 2100) and USACE Intermediate (0.5 m by 2100) ESLR curves, including a rate of change of ESLR plotted in the secondary y axis. Note that the curves begin from 1992 as defined by USACE convention. These two scenarios will henceforth be termed High SLR and Low SLR scenarios for the discussions of results in this chapter. The figure shows the rapid acceleration of ESLR for the High SLR scenario over the Low SLR scenario and as will be shown later is the most important factor identified in estimating land remaining at the end of the 50-year period.

Figure 10.6 shows the actual water level boundaries (hourly in blue and annual mean in red) in Gulf of Mexico used for the HD and OM runs for the two ESLR scenarios modeled here.

As mentioned before the 10 year hourly tidal oscillations are repeated every decade after adjusting for the rising annual MWL. The addition of the statistical variability in tidal data also enables secondary statistical calculations of water level variability in the basin. Note that all tropical storm and hurricane periods were filtered out of the data as the diversion is planned to be closed during this period. Also, no tropical storms or hurricanes are modeled here.

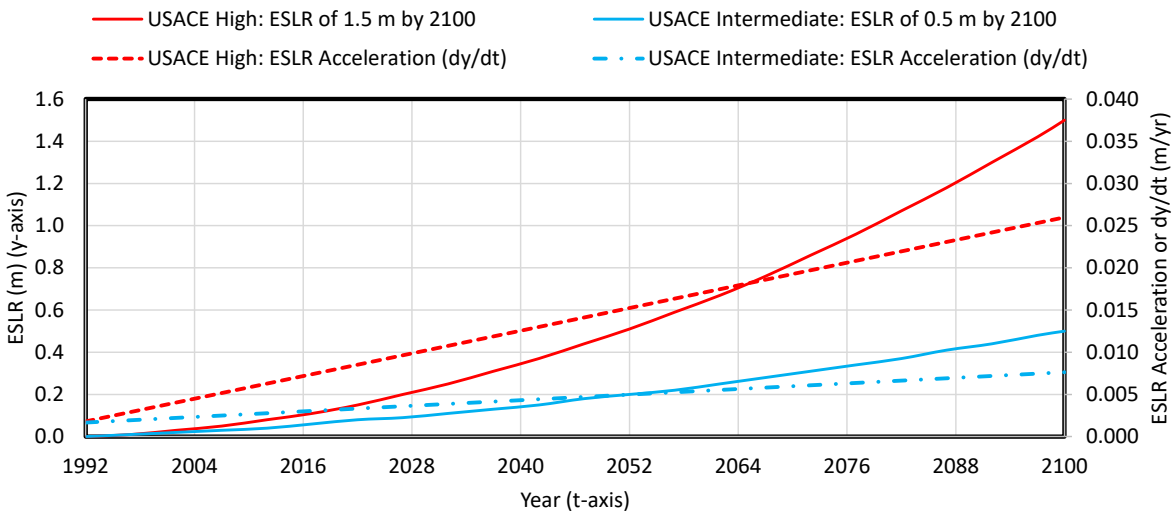

Figure 10.5. USACE High and Intermediate Eustatic Sea Level Rise (ESLR) scenarios investigated. The secondary y axis to the right shows the rate of increase (acceleration) of the ESLR over time.

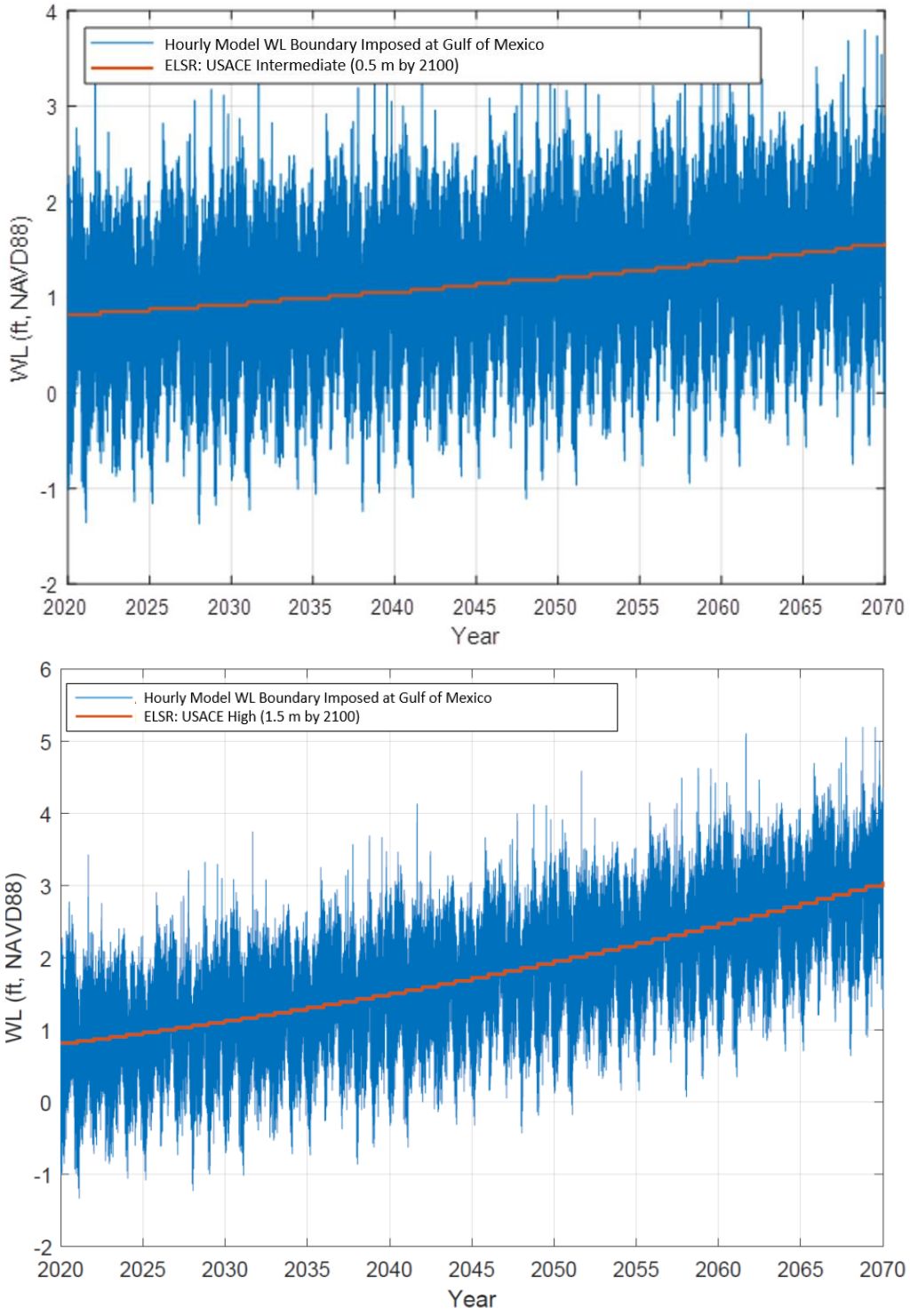

Figure 10.6. Gulf of Mexico water level boundary used for the 50 Yr (2020-2070) FTNOMLV-CONSOL runs for the two scenarios: USACE Intermediate ESLR (top panel) and USACE High ESLR (bottom panel).

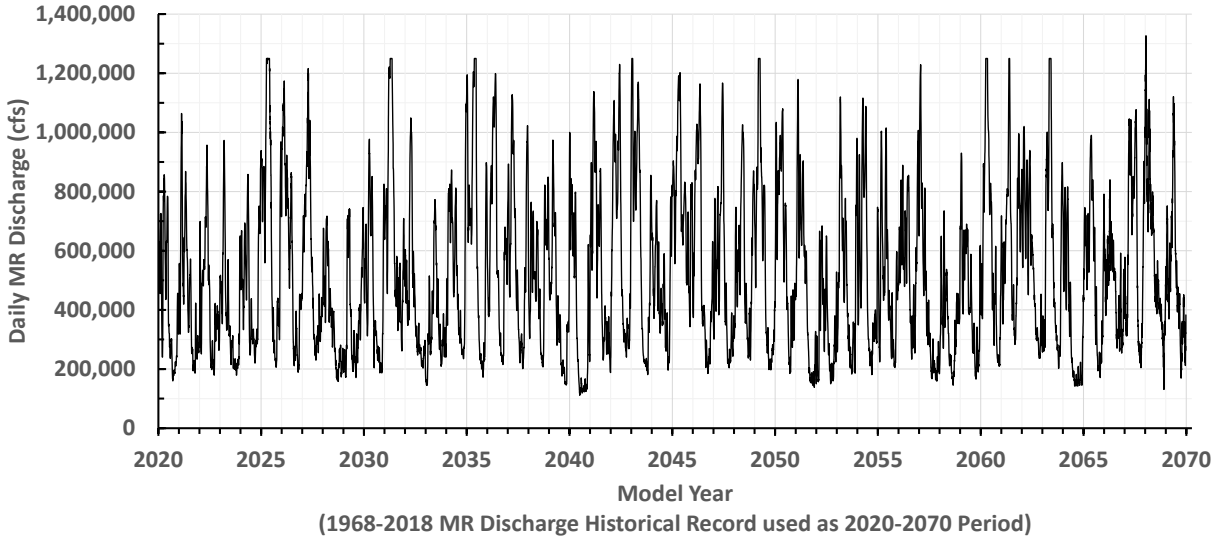

Figure 10.7. Mississippi River (MR) Discharge Boundary used for the 50 Yr (2020-2070) FTNOMLV-CONSOL runs. The 1968-2018 historical MR hydrograph is simulated as the 50 yrs (2020-2070) period in the model.

Figure 10.7 shows the historical MR hydrograph, 1968-2018 modeled as the future 50-year hydrograph (2020-2070) for the FTNOMLV-CONSOL modeling here. CPRA specifically instructed the use of this period for all modeling to be consistent with other mid-basin diversion models being conducted. The MR hydrograph before 2008 is obtained from USACE Tarbert landing gage and after capping to 1,250,000 cfs MR flow which is the mandated maximum flow before Bonnet Carre is opened. For the 2008-2018 period, data from USGS Belle Chasse is used directly without the need for any capping. The MR hydrograph shows mostly variability between 150,000-1,250,000 cfs with a diversion operation stating at the 450,000 cfs mark in the rising limb starting from late December to early January and ending at 450,000 cfs again in the falling limb between June and July.

In addition to freshwater input from the diversion outfall, there are two additional significant sources of freshwater, the Davis Pond Diversion (DPD) and Gulf Intracoastal Waterway (GIWW), in the Barataria basin that require modeling here. Even though these sources generally have less than 5,000 cfs of monthly mean input flow and are not significant sources of water for water level influences, near the diversion outfall, their impact on the background salinity in the basin cannot be ignored. Figure 10.11 shows the locations of the GIWW and DPD

freshwater input locations. For both these locations a mean monthly discharge is specified as discharge boundary for the 50-year modeling and is held constant for all years. Based on the limited monthly variations and the fact that mean monthly flows are more important drivers of salinity rather than a few days of flow changes makes this a reasonable approach. Note that these two inputs are only modeled in the HD model and the OM model does not need any of these inputs as they are not significant sources of sediment.

Figure 10.8 shows the analysis of the observed data from 2002-2019. The error bars represent maximum and minimum values. The mean monthly discharge data from this analysis is used to model the DPD boundary in the 50-year HD model. The with project discharge at DPD is not likely to change as this is a regulated source and there is enough excess head available between the MR and the basin at the DPD location that a forced discharge boundary is applicable under with project condition as well.

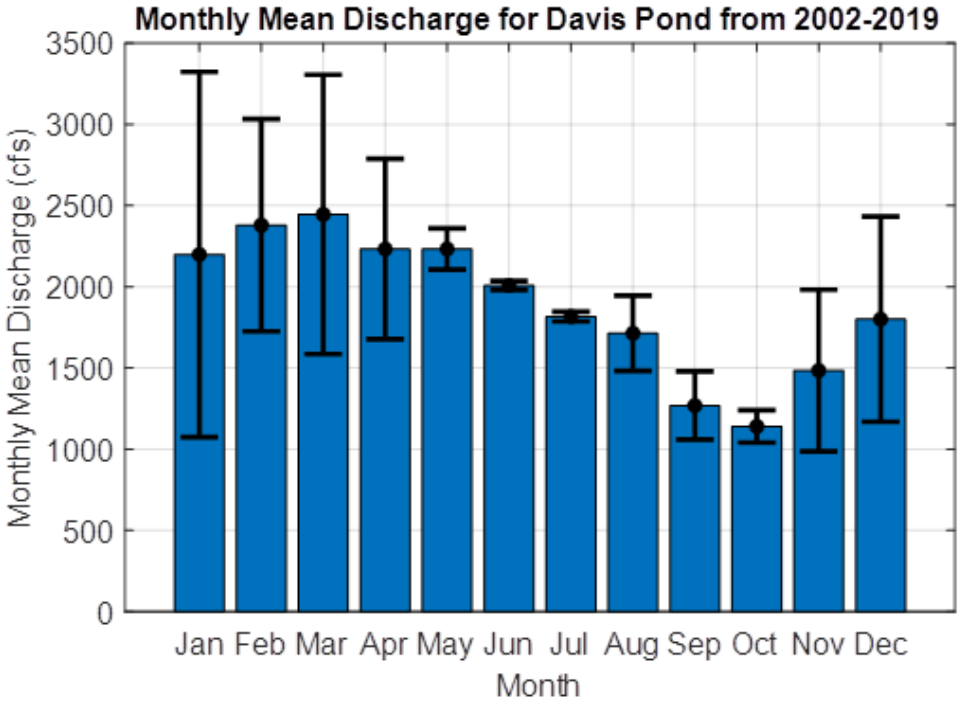

Figure 10.8. Davis Pond Diversion discharge boundary specified as mean monthly values.

In order specify the boundary conditions at GIWW which is a forced discharge boundary under with project conditions, it was first necessary to quantify the amount of reverse flow that could occur during diversion operations in the Barataria basin and resulting increase of water levels in the Barataria basin (east of GIWW) and the Terrebonne basin (west if GIWW). First a rating curve under existing without project conditions, relating the discharge through the GIWW gap and the water level difference at gages that are positioned at sufficiently far-field of the gap was developed as shown in Figure 10.9. These are the USGS gage at Houma to the west and USGS gage at West of Little to the east. Based on this rating curve it is thus possible to develop discharge through GIWW which can even be negative (flow east to west). The monthly averaged water levels from the USGS W of Little Lake location taken from a previously conducted, With Project 3-year run (2008-2011) was then used along with the observed monthly averaged water levels at Houma to estimate the updated GIWW flows using the rating curve developed before. This approach assumes therefore that Houma water levels are not impacted by MBSD. Figures 10.10 show the mean monthly GIWW discharges with and without MBSD. The right panel showing with project (MBSD) conditions is used as the boundary conditions for the 50-year modeling. It is seen that for the months of Dec-June when the diversion is mostly active, the predominant flow is from Barataria to Terrebonne basin at GIWW (negative flows indicate east to west) due to the primarily higher water levels in the Barataria basin. For the months from July-November, when the MBSD is only operating at base flow, there is negligible change in GIWW flows from without project conditions. Therefore, there may be additional freshwater benefits to Terrebonne basin from Barataria flows due to MBSD operations.

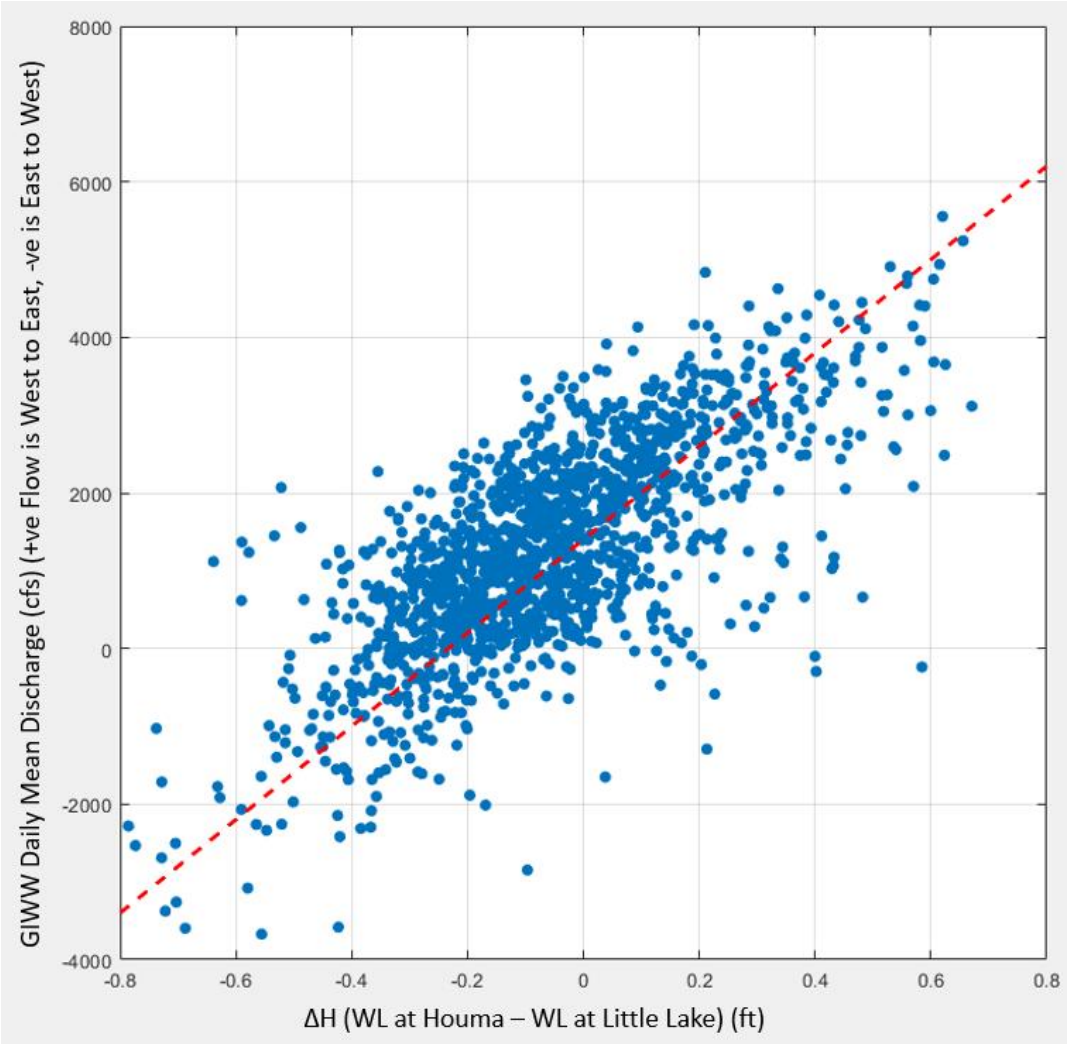

Figure 10.9. Rating curve at GIWW reconstructed from relating flow and head difference on either side, Houma (west) and Little Lake (east). Positive flow is west to east.

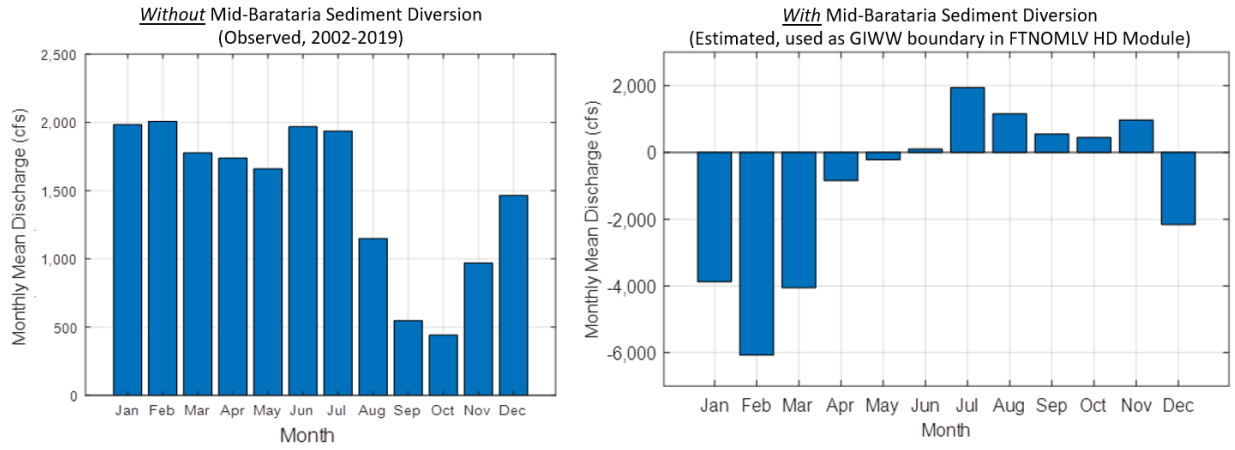

Figure 10.10. Gulf Intracoastal Waterway (GIWW) Monthly Mean Discharge (Q) from 2002-2019 with minimum and maximum error bars. Both without project (observed, left panel) and with project (modeled and estimated, right panel) are shown. The without project mean monthly data was used for the 50 Yr (2020-2070) FTNOMLV-CONSOL runs.

10.4 Model Calibration and Validation

The coupled hydrodynamic and salinity (HD) module was calibrated and validated for water level and salinity using observed data from two separate two-month periods. The October-November 2014 period was used for calibration of the model and the October-November 2015 period was used for validation. The main reason for picking the October-November periods was that during this time of the year, the diversion is likely to be closed and salinity and water level variations in the basin becomes important for controlling the mean annual values of those quantities. In addition, this period of the year also tends to show the strongest non-tropical storm wind events, resulting from cold fronts which typically can have a major influence on the spatial distribution of salinity particularly within the north eastern part of the mid-basin area where the diversion outfall is located and the main region of interest for delta building. However, no wind is currently modeled in the 50-year modeling done here as it was considered unnecessary for the statistical mean quantities of interest here. Therefore, picking this period lets us evaluate the model performance in its ability to reproduce those mean quantities effectively. Since mean annual and summer salinity and water levels are the main drivers of vegetation growth for the LAVEG models performed here, greater attention was paid to reduce model bias than say to match every peak or trough in salinity and water level, which is difficult

to reproduce without exact wind field availability and since the exact wind events cannot be predicted in the future, wind effects were neglected here. Another reason to neglect wind in the modeling is that the wind effects are event based and the statistically significant effect on the MWL can be variable year to year. Applying a predefined wind condition can bias those results. As will be seen later in spite of neglecting wind effects, the model performs reasonably well in matching the mean quantities for salinity and water levels.

Figure 10.11 shows the distribution of gages in the model where model data is compared with observed data. The gages are divided into USGS stations in the south, the CRMS stations near the diversion outfall and the USACE station at Jean Lafitte to produce a spatially intuitive picture of model performance in the basin. The CRMS stations are an important indicator of the general salinity and water level conditions near the diversion where the vegetation effects are most important. The USGS stations provide estimates of salinity and water level in the lower bay where environmental concerns are of important and evaluates the model's capability in that region for use later in salinity modeling. The USACE station provides a water level datum consistency across three agencies (USGS, USACE, CRMS) and is primarily meant to demonstrate the uncertainties in water levels in the CRMS stations found as will be explained later. The only two freshwater sources of significance modeled here are the Gulf Intra-coastal Waterway (GIWW) and the Davis Pond Diversion as shown in Figure 10.11.

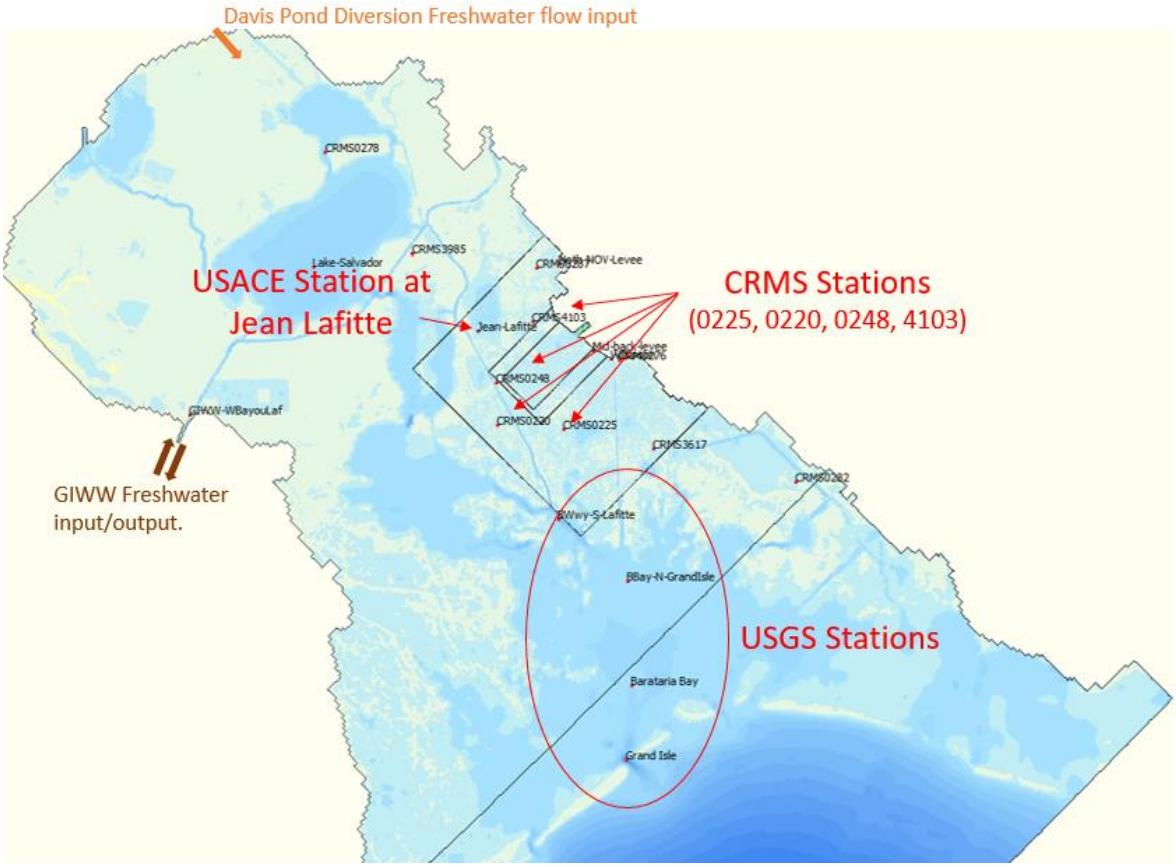

Figure 10.11. Location of gages in the Barataria basin where the model data is compared with the observed data for the calibration and validation runs. For all these runs, there is no diversion discharge from MBSD. The only existing freshwater input sources in the model are Davis Pond diversion to the north of the basin and the Gulf Intracoastal Waterway (GIWW) to the west of the basin.

Figure 10.12 shows the time series of observed discharge at Davis Pond from October-November 2014 and October-November, 2015 used for the calibration and validation runs. The GIWW was also forced by a discharge boundary condition for the October-November, 2014 period from the observed data as in Figure 10.13. No data was available for the GIWW location for the 2015 period and hence the same boundary as in 2014 was used in 2015 as well. All discharge data was specified as daily averaged in the model. Negative values for discharge at GIWW indicate flow from Barataria to Terrebonne basin (East to West). The general flow direction is therefore from West to East during this period, punctuated by reverse flow periods influenced by Spring and Neap tides and wind effects. Note that GIWW flows which are correlated well with Atchafalaya flows in the Terrebonne basin show increased flows in Jan-June and mean monthly flows are between 500-1,000 cfs during the calibration-validation period (Figure 10.10 left panel), so it has relatively less influence in salinity control in the Barataria Basin than in say summer months.

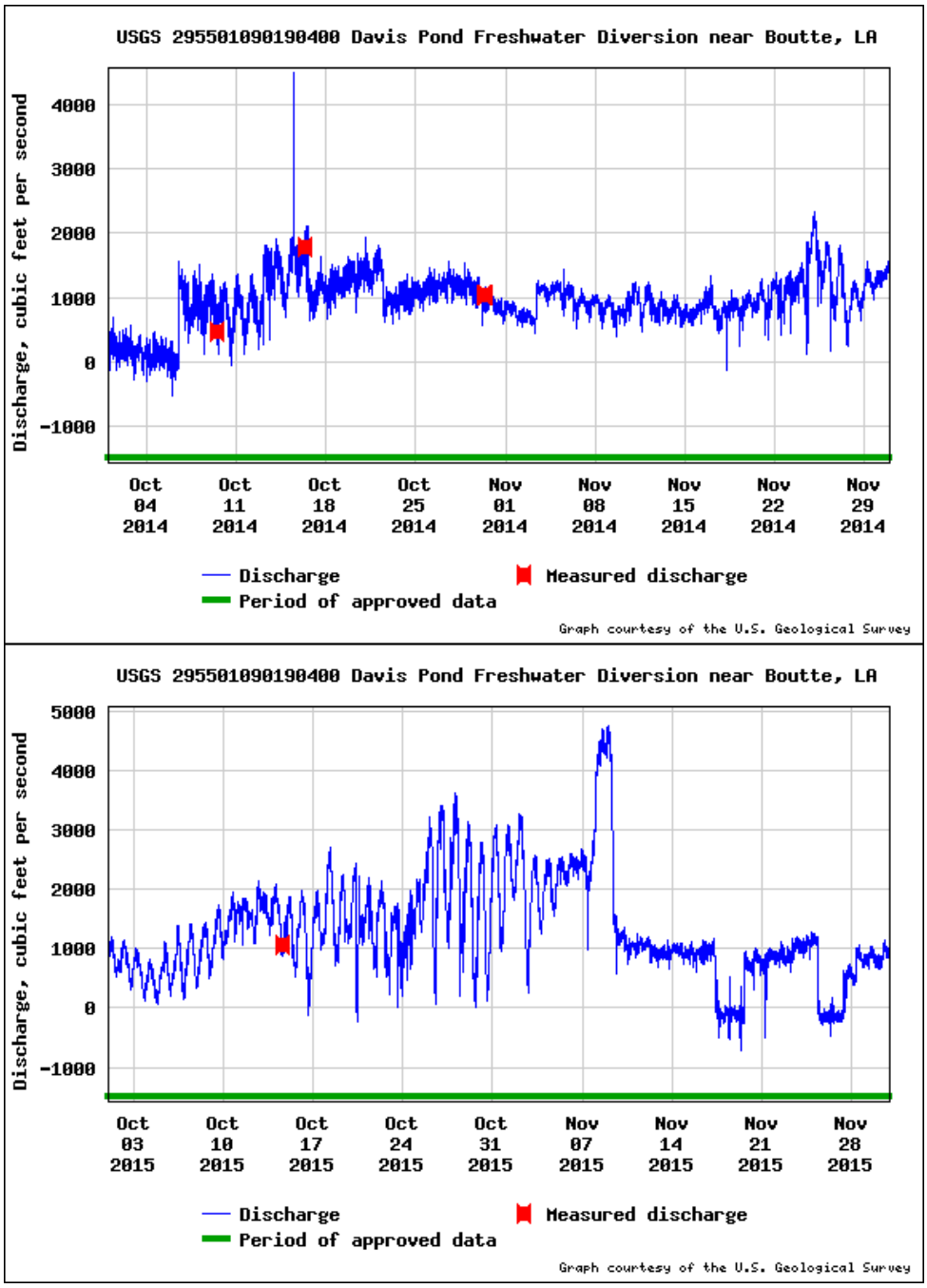

Figure 10.12. Davis Pond Diversion discharge for calibration period (October-November, 2014) in top panel and for the validation period (October-November, 2015) in bottom panel. Figure courtesy https://nwis.waterdata.usgs.gov/. Data from USGS 295501090190400.

10.4.1 Water Level Calibration and Validation

The calibration for water level involved varying bare ground Chezy roughness in the basin. The Chezy approach was used as in the calibration validation modeling to remain consistent with the roughness framework of the FTNOMLV-CONSOL runs where the vegetation properties set the Chezy roughness in the basin following Baptiste et al. (2007) formulations. The same formulation was used here as well. A value of bare ground Chezy=50 $m^{1/2}/s$ was found to yield the least bias in mean water levels compared with observed data. Figures 10.14 to 10.16 show the calibration results for water level at the USGS, CRMS and USACE stations respectively. While the USGS and USACE station all has bias less than 0.16 ft, the CRMS stations has relatively more bias with the model data overpredicting the observed data at the CRMS stations by about 0.4-0.6 ft. Similar range of bias was also noted for these stations for the validation period as shown Figures 10.17 to 10.19, where the model data at CRMS stations overestimated the observed data by about 0.4-0.5 ft, while the bias at the USGS stations were all below 0.1 ft. It is worth noting that the CRMS observed water levels have a consistent bias with the USGS stations to the south, as well as with the USACE station to the north. Therefore, the model results at the CRMS stations are consistent with the USGS stations in the south, it's just that the CRMS observed data shows a lower mean water level. It is not exactly clear why this is there in the CRMS observed data and can be attributed to a variety of reasons, some important ones are discussed below:

- Water exchange between open water and sheltered wetland zone are often non-linear with time, shallow wetland locations are often restricted and may be guided by complicated flow paths that are not resolved in the model. This could result in lower observed mean water levels.
- Meteorological factors (temperature and pressure) and groundwater percolation are known to affect water level readings within sheltered wetlands.
- Wind effects are not modeled and differential wind drag over sheltered wetland sites and open water can affect the mean water level readings.
- NAVD88 datums of CRMS stations are not rigorously validated against USGS gage datums so the datum uncertainty is unknown.

Note that in spite of the apparent bias of the model data at the CRMS stations, these stations being sufficiently far away from the kinetic dissipative zone of influence of the diversion flow, this bias is not expected to affect with the outfall transition feature tail-water under project conditions, which is an important parameter for capacity estimation modeling. Given the fact that even in absence of wind effects the modeled mean water levels have insignificant bias (less than 0.1 ft) in the open water stations indicate that it is appropriate to neglect wind for the with-project production runs. This validated simplification is important to complete modeling of one cycle (1 yr) HD module simulation completion in 1 day within the greater FTNOMLV-CONSOL 50 yr run framework, and makes it compatible with the relative efficiency of other modules and enables CPRA to obtain a single 50 yr model sequence result be available in about 2.5 months. The 0.1 ft bias noted at the USGS stations is well below the uncertainty of the datum at the USGS/USACE stations which are sinking continuously due to subsidence and being revised regularly in typically 7-10 yr intervals.

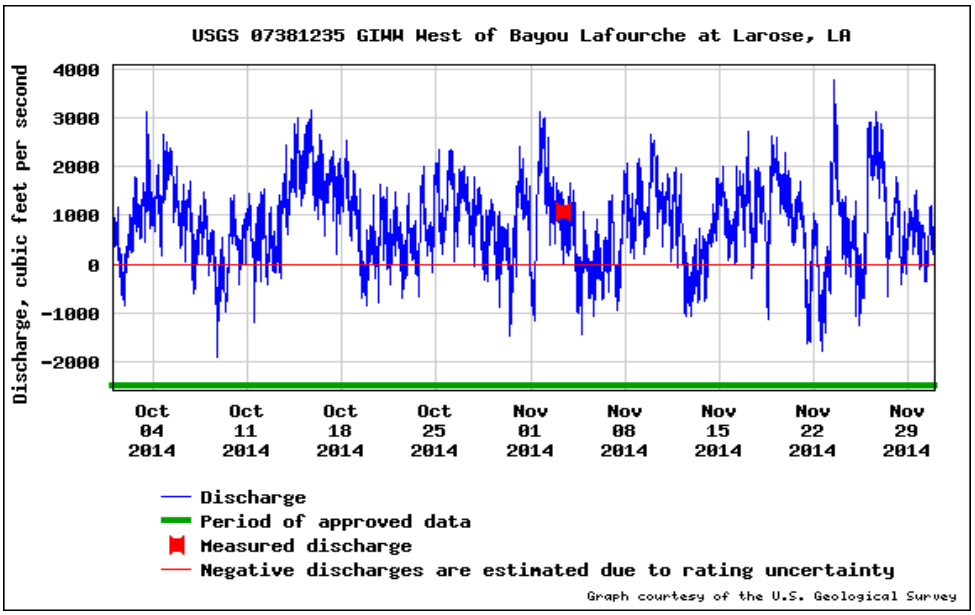

Figure 10.13. GIWW discharge measured at USGS GIWW W of Bayou Lafourche at Larose station for the calibration period (October-November, 2014). Data was unavailable for the validation period and hence was not used in the model. Figure courtesy https://nwis.waterdata.usgs.gov/.

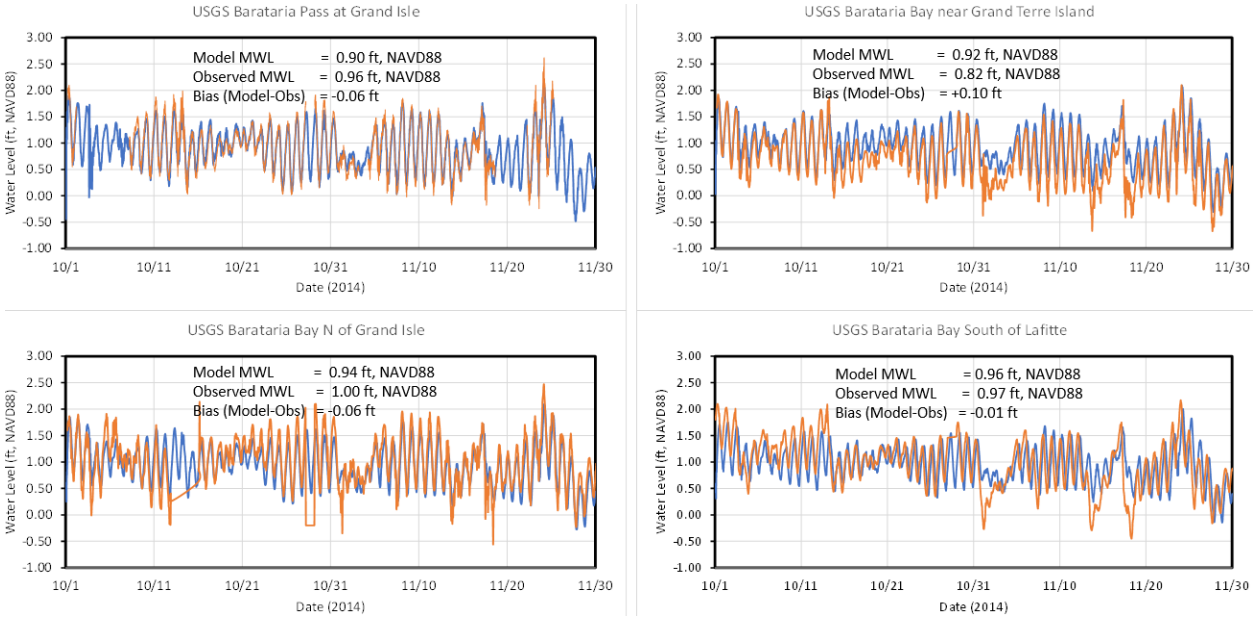

Figure 10.14. Water level calibration (October-November, 2014): USGS Stations.

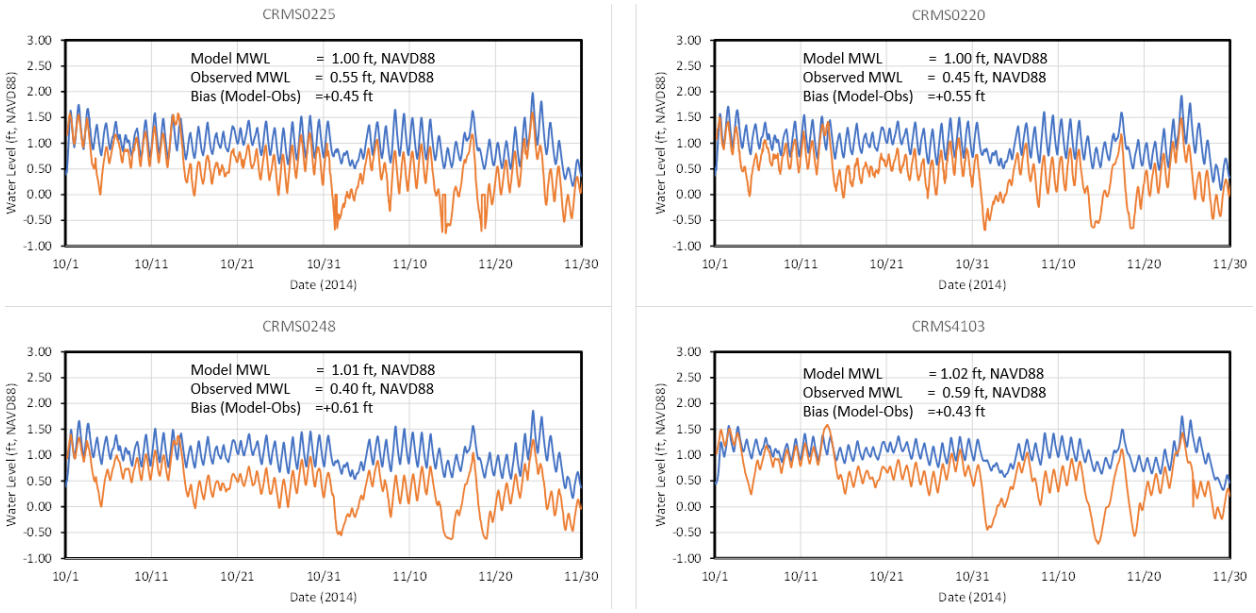

Figure 10.15. Water level calibration (October-November, 2014): CRMS Stations.

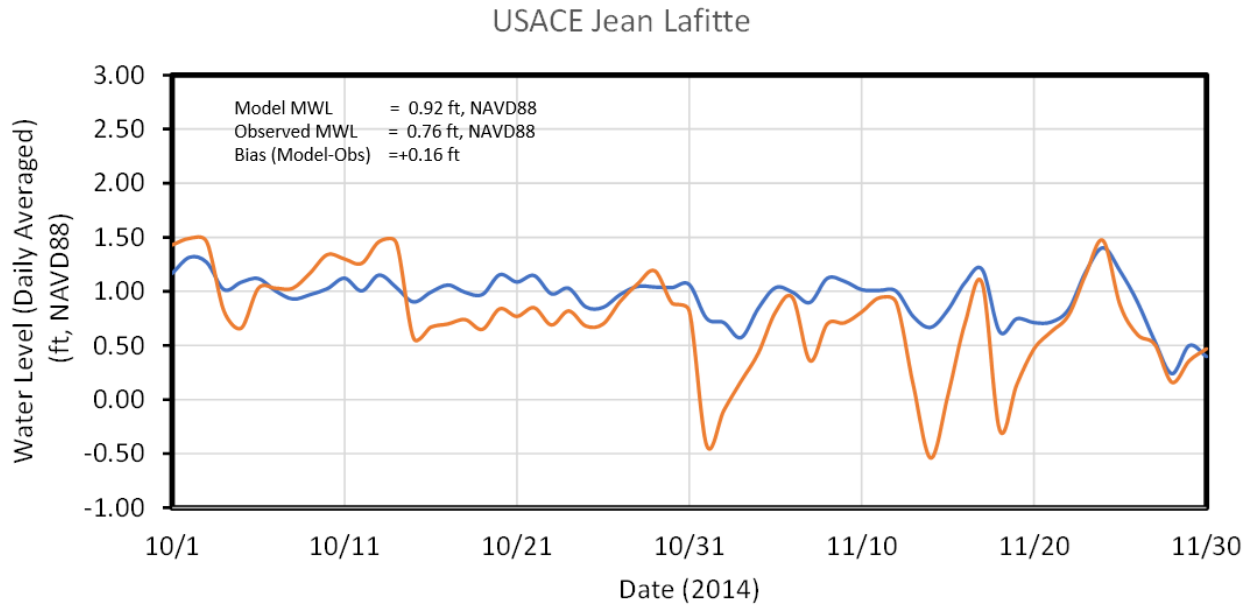

Figure 10.16. Water level calibration (October-November, 2014): USACE at Jean Lafitte station.

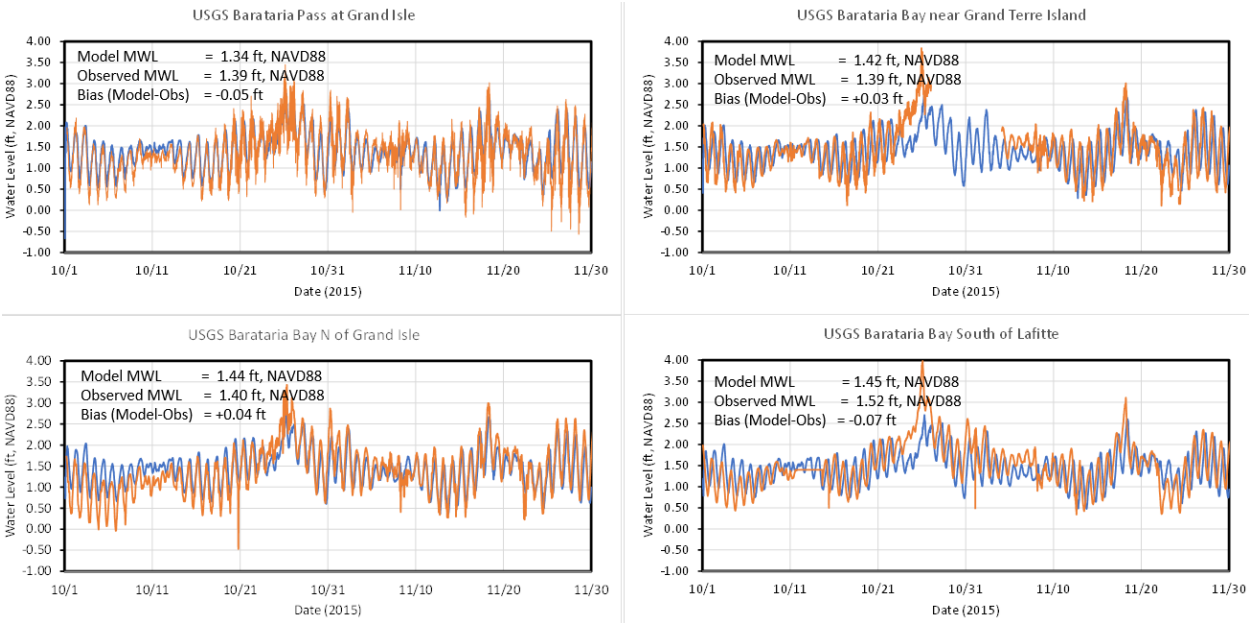

Figure 10.17. Water level validation (October-November, 2015): USGS Stations.

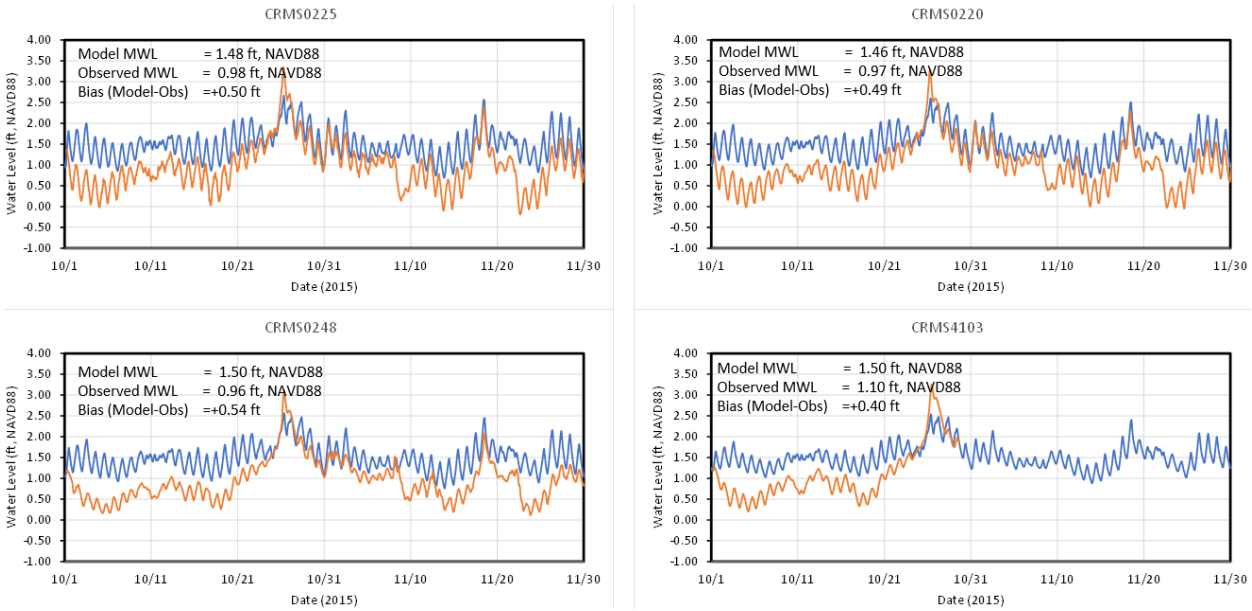

Figure 10.18. Water level validation (October-November, 2015): CRMS Stations.

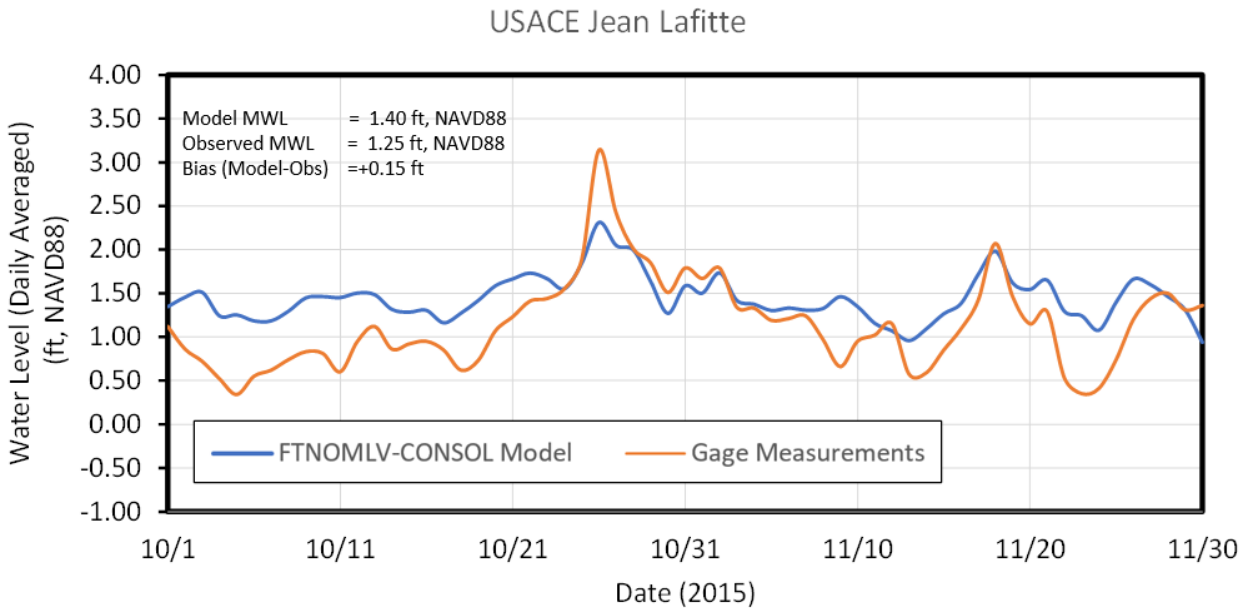

Figure 10.19. Water level validation (October-November, 2015): USACE at Jean Lafitte station.

10.4.2 Salinity Calibration and Validation

The main parameters adjusted for salinity calibration are the eddy diffusivity and viscosity parameters in the 2D Delft3D model. The model being split up into several domains (domain-decomposition or DD method, Figure 10.20) with different grid sizes, a variable eddy diffusivity was required within each domain that approximately scales with the grid size, to be able to model the salinity spread through each connected domain in a consistent manner. The layout of the domain decomposition is shown in Figure 10.20, with the grid sizes shown in Table 10.3. The final calibrated eddy diffusivity and viscosity values that showed least bias at the gages were chosen for validation and are shown in the same table. Eddy viscosity and diffusivity values were smoothed at the DD domain interfaces to avoid steep jumps.

Figures 10.21 and 10.22 show the calibration of salinity at the CRMS and USGS stations. The USACE station has no observed salinity data so it is not shown. As seen from the figures, the mean salinity over the model period matches well with the observed data particularly at the CRMS stations where the influence of salinity on the vegetation is particularly important. The model bias at the CRMS stations is below 0.6 ppt. The model does tend to underestimate the salinity somewhat (bias about 2-3 ppt) at the USGS stations near Grand Isle and at Barataria Bay near Grand Terre Island where the influence of wind forcing on salinity through the narrow barrier island passes are particularly important and unable to be resolved by the model which does not have wind effects. Given the fact that the modeled mean salinity trends match reasonably well with the observed mean salinity for the most important areas that influence FTNOMLV-CONSOL results, particularly near the diversion outfall (CRMS stations) where the salinity influences the vegetation dynamics most, the model can be considered to be well calibrated for the purpose. The validation period, as shown in Figures 10.23 and 10.24, the maximum salinity bias remains 0.6 ppt at the CRMS stations and is considered well validated. It is important to note that since there is no wind in the model, the salinity peaks and troughs and therefore the range of temporal variations cannot be adequately modeled in this framework and is an acceptable compromise given that the LAVEG module only needs the mean annual and summer statistics which means reproducing spatial variability in mean salinity distributions are more important than the temporal variability.

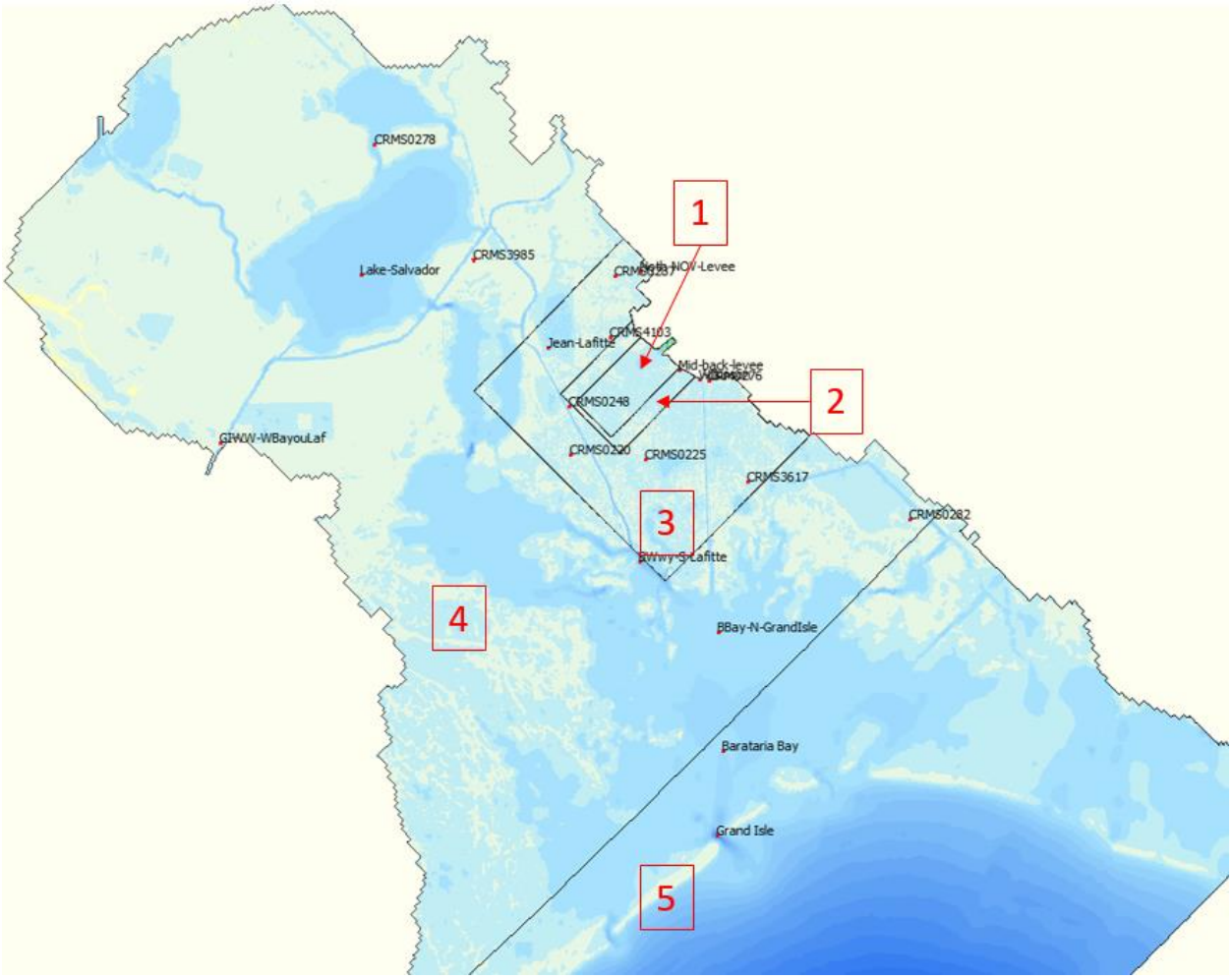

Figure 10.20. Domain decomposition (DD) domains and their numberings for the FTNOMLV-CONSOL basin domain. The river domain is not shown here as it was not used during calibration/validation.

Table 10.3. Calibrated and validated domain-wise eddy diffusivity (for salinity) and eddy viscosity settings for each Domain Decomposition (DD) domain as in Figure 10.20. Note that the values scale with the grid size. Viscosity and diffusivity values were smoothed at the DD domain interfaces to avoid steep jumps.

DD Domain #	Grid Size	Eddy Diffusivity (m^2/s)	Eddy Viscosity (m^2/s)
1	15.0 m (49.2 ft)	3.0	0.1
2	15.0 m (49.2 ft)	3.0	0.1
3	50.0 m (164.0 ft)	4.5	0.3
4	150.0 m (492.1 ft)	45	0.9
5	150.0 m (492.1 ft)	45	0.9

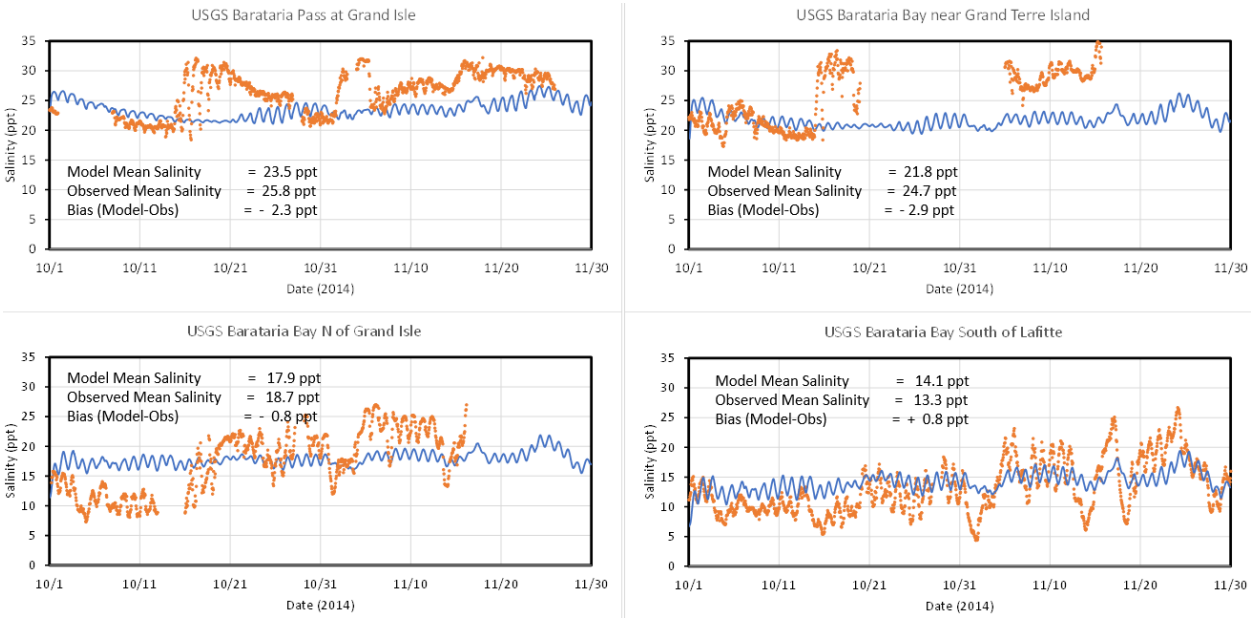

Figure 10.21. Salinity calibration (October-November, 2014): USGS Stations.

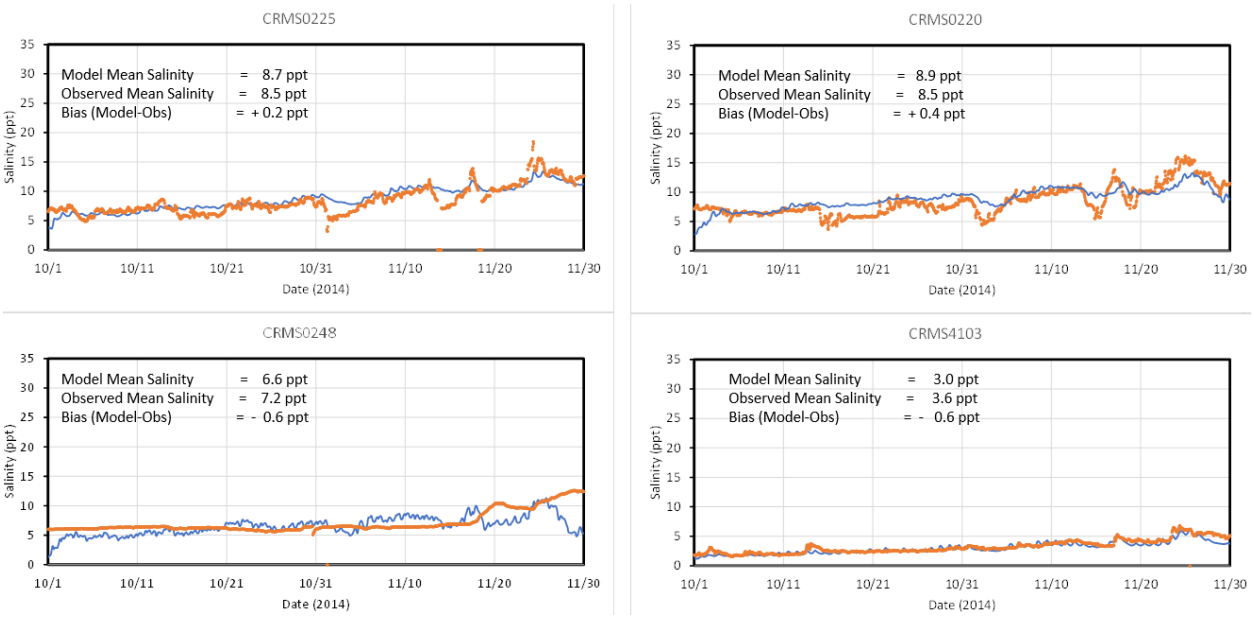

Figure 10.22. Salinity calibration (October-November, 2014): CRMS Stations.

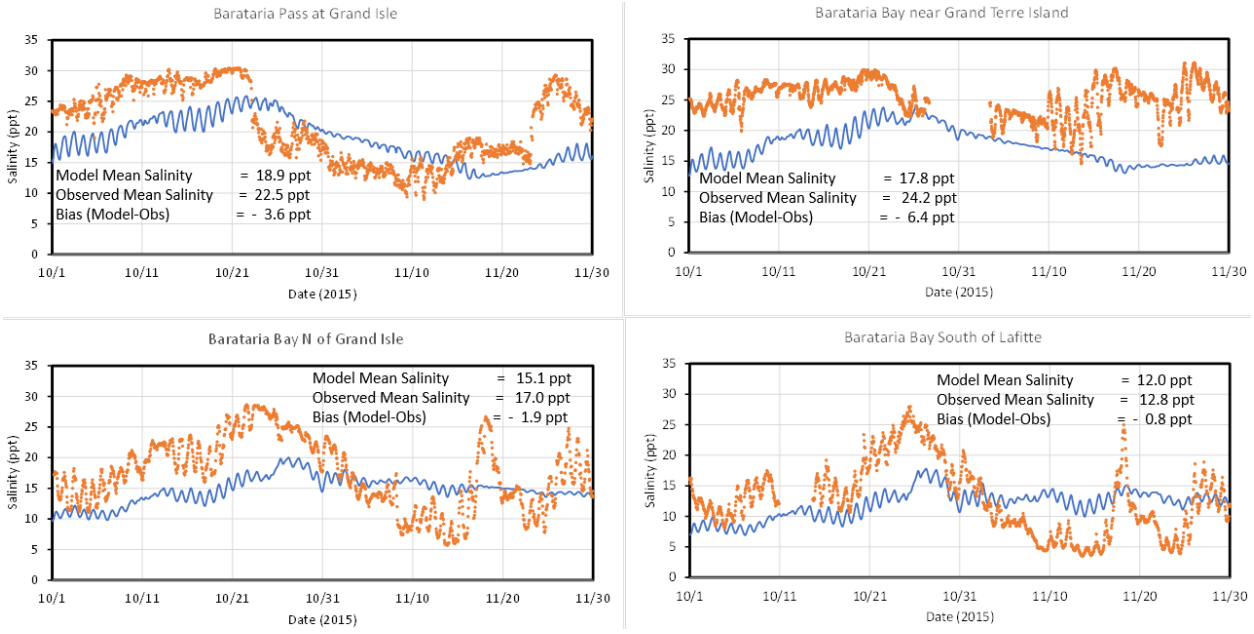

Figure 10.23. Salinity validation (October-November, 2015): USGS Stations.

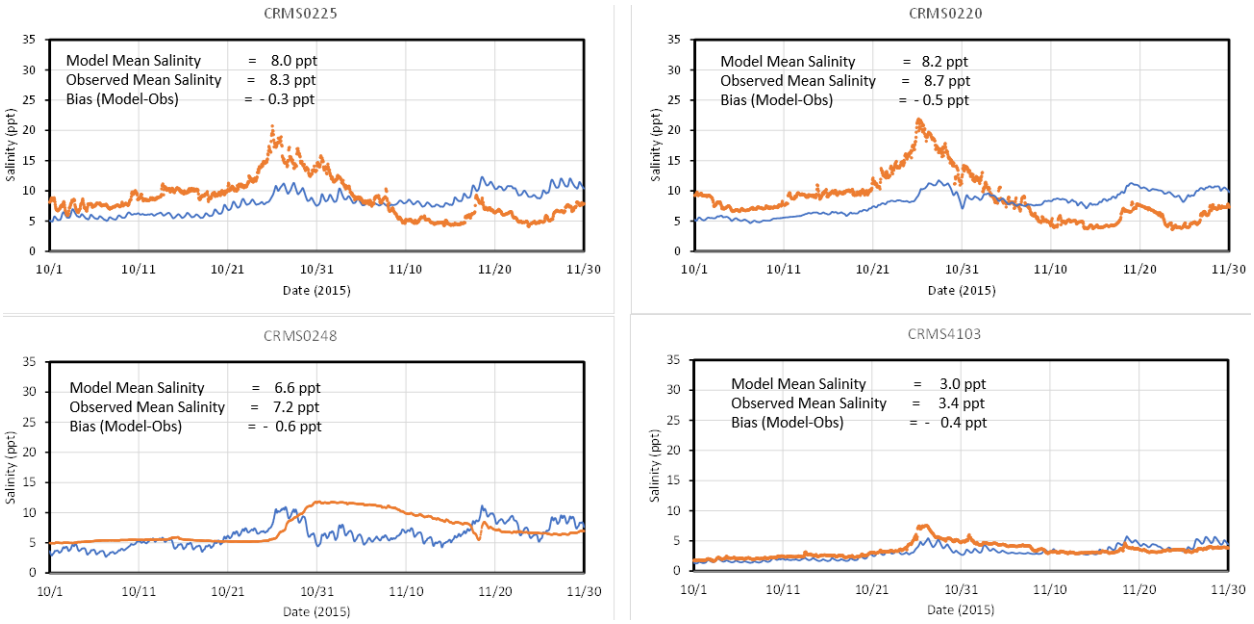

Figure 10.24. Salinity validation (October-November, 2015): CRMS Stations.

10.5 Model Results

10.5.1 Land Building and Dredging Estimates

This section presents the 50-year model results of sub-aerial land area built (or sustained) for the four scenarios investigated here. In addition, for the three 'with basin dredging' runs (High ESLR with Base Flow, High ESLR no Base Flow and Low ESLR with Base Flow), the required dredging volumes needed to maintain target capacity in the future are also presented. Dredging volumes for Barataria Waterway and Wilkinson Canal which are two waterways of navigational interest are also separately calculated. Further, dredging volumes are separated by 'native' and 'deposited' dredging volumes to highlight the fact that since dredging aims to deepen the existing deltaic channels that form the delta, most of the deposited material that forms the emerging land is actually not lost due to dredging. In fact, the dredged material which is considered lost in the current analysis may be used by CPRA in the future in other wetland restoration initiative (e.g., building Sediment Retention Devices, building or raising levees, terracing etc.). Land gained by such use of the dredged material is not considered in the land area estimates and therefore the estimates here can be considered slightly conservative.

The definition of what constitutes sub-aerial land, depends on the how land and water is separated for the calculation of land area built or sustained. The mean water level (MWL) predicted by the ESLR curve as in Figure 10.6 (red lines) is used to delineate which model cells are considered under water and which are above water (or sub-aerial land). The summation of the cell areas designated as sub-aerial land is the land area remaining at the end of the previous fact, cycle (year) for each year of the 50-year period. Since spatially variable subsidence (Figure 10.1) is modeled as linear change in a given year during the modeling process itself, the acceleration in ESLR hastens the 'sinking' and loss of land as time goes by, as will be seen in the figures of land/water later and is the primary reason for loss of land built by the diversion in the initial year as will be seen later. This definition of separation of land and water is similar in concept to what has been used in CPRA studies for the LA Coastal Master Plan (CPRA, 2017).

Figures 10.25 and 10.26 show the land and water distribution change, under without project (no action) scenarios for the Low SLR (USACE Intermediate, 0.5 m by 2100) and High SLR (USACE High, 1.5m by 2100) conditions. For these no action runs, for efficiency of computation not all the modules of the FTNOMLV-CONSOL model were run. This was because without the diversion, there are no significant sources of mineral sediment addition to the basin and it is not necessary to run detailed morphology models for 50 years. Also since there is no diversion operational to alter the existing water levels in the basin, the hydrodynamic module need not be run either. Instead, only the LAVEG (LV) module was run using mean water depths and existing averaged salinity conditions in the basin. Subsidence was included in the bathymetry change year to year similar to the with project conditions modeling and the annual mean water levels were adjusted based on ESLR. The averaged salinity distribution used in LAVEG module was obtained by averaging over the last 11 years (2008-2010) of salinity in the basin and therefore remains constant over the modeled 50 yrs. No consolidation was required to be modeled as there are no mineral sediment addition. Thus, for the No Action scenarios, the principal accretion source for the land was vegetation growth and senescence activity on the emergent wetlands only.

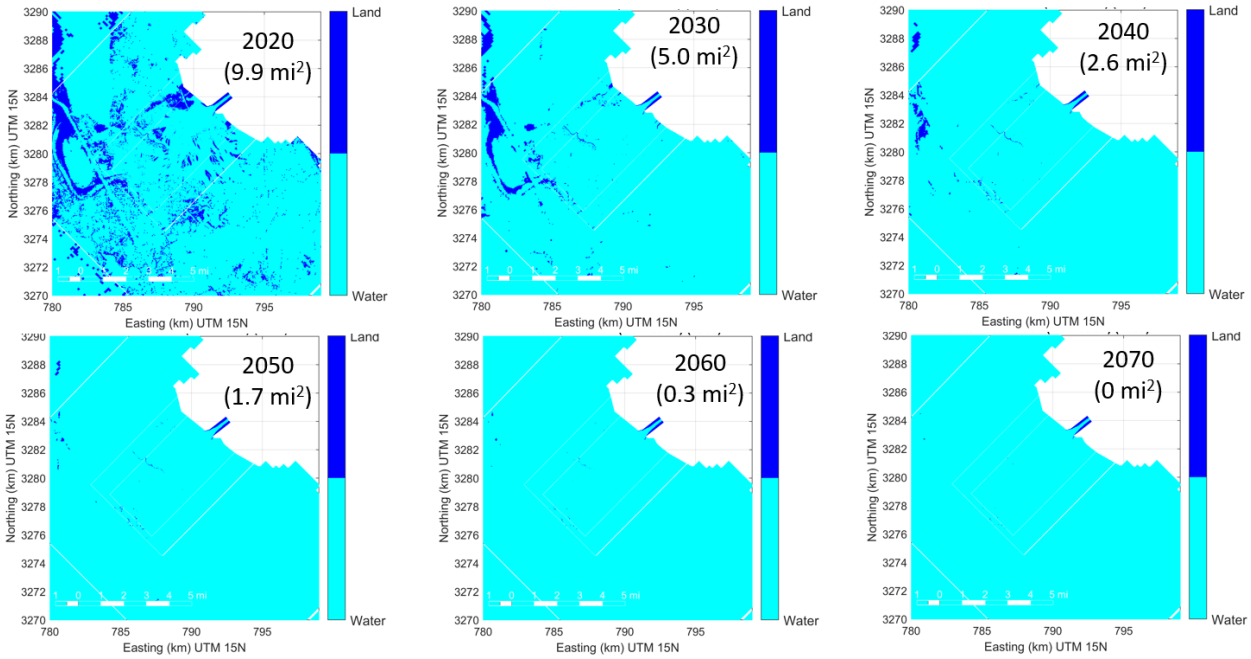

Figure 10.25. High SLR (USACE High, 1.5m by 2100) **Without Project** Scenario: Land Area.

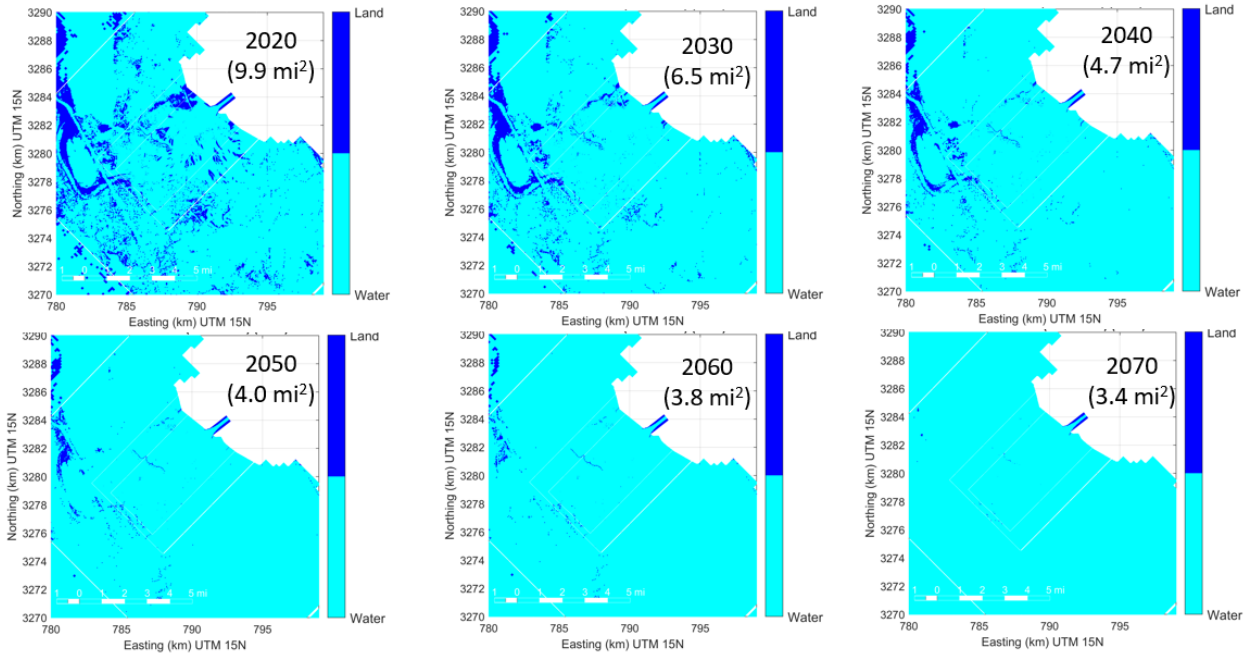

Figure 10.26. Low SLR (USACE Int., 0.5m by 2100) **Without Project** Scenario: Land Area.

Figures 10.27 to 10.30 show respectively the land-water distribution snapshots, every 10 years, from the 50-year modeling of the four scenarios: Low SLR (0.5m by 2100) with Base Flow and Dredging (Figure 10.27), High SLR (1.5m by 2100) with Base Flow and Dredging (Figure 10.28), High SLR (1.5m by 2100) with Base Flow and No Dredging (Figure 10.29), High SLR (1.5m by 2100) with No Base Flow but with Dredging (Figure 10.30). For all the scenarios modeled a common trend identified is that the delta extends out from the outfall in the first two decades (2020-2040). After that either the net land area becomes more almost constant (for the Low SLR case) or decreases (for the High SLR cases) over the last three decades. This shows that the benefits of land-building are most obvious during the first two decades of diversion operations after which the accretion (sum of mineral and vegetation) becomes almost equal to the sum of ESLR, subsidence and consolidation for the Low SLR (0.5m by 2100) scenario.

Among the High SLR scenarios, the role of base flow is the most important in sustaining the maximum amount of land after 50 years. This is demonstrated from Figures 10.28 and 10.29 where more or less the same amount of land is built in two decades (2020-2040), but after 50 years only 1.6 sq.mi. remains for the Without Base Flow case, whereas over 7 times that or 12.5 sq.mi. remains for the With Base Flow case. This demonstrates the importance of the role of the mineral sediment input of the diversion, during base flows, in decelerating the rate of land loss towards the later decades and the need to sustain base flow during the future years.

The effect of dredging is shown in 10.28 and 10.30, where under the High SLR scenario, dredging, which is conducted from 2040 onwards only improves the total land remaining at Year 50 by 5.2 sq. miles (=12.5-7.2). This is an important conclusion when examining the absolute dredging numbers shown later in Table 10.6, where even though a large amount of dredging (about 200 Mil Cubic Yards) is shown to be needed in the last two decades, it may not be cost beneficial when the SLR rise is high as the condition to maintain the target capacity and thereby sediment load input becomes less important when SLR floods most of the built land over time anyway. So even though the analysis for dredging is conducted, in reality dredging may only be done cost effectively for the third decade after which the diversion capacity can be allowed to degrade if SLR trends at that time (after 2-3 decades) still indicate similar to the High

SLR scenario modeled here. On the other hand, as shown in Figure 10.27, if SLR turns out to be lower and similar to the Low SLR scenario modeled here, dredging may be continued till 50 yrs and will remain lower than the High SLR scenarios anyway and benefit land building.

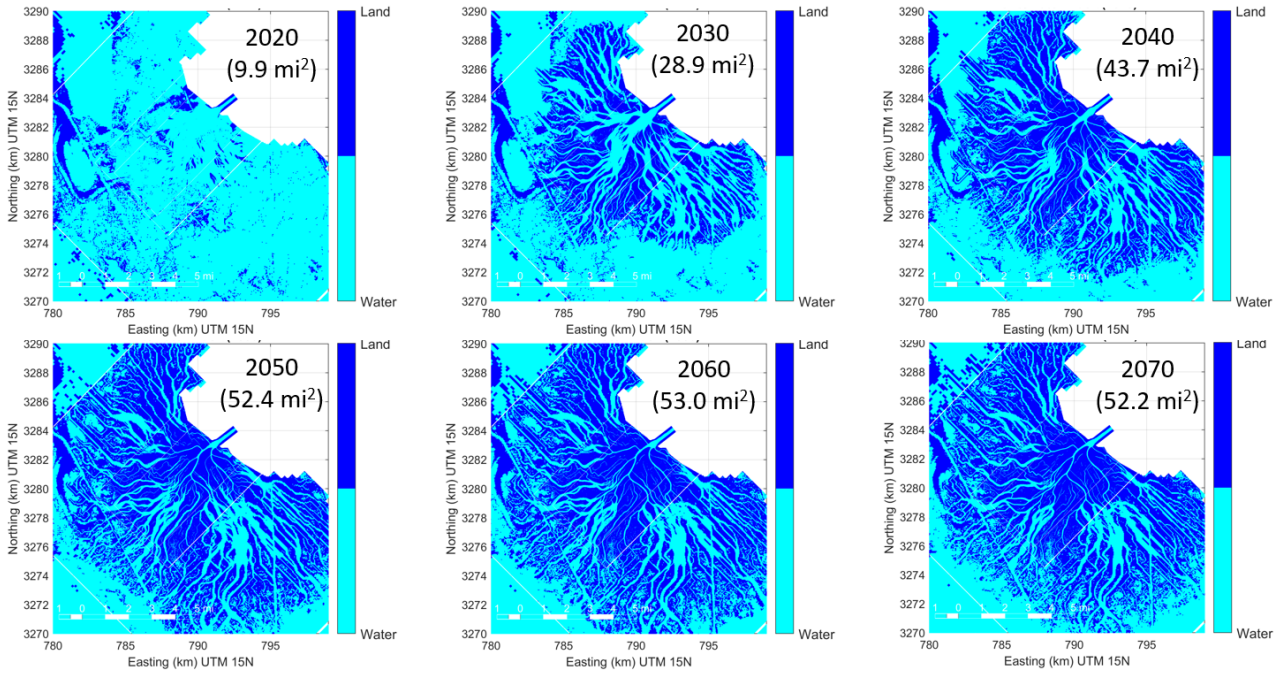

Figure 10.27. Low SLR (USACE Int., 0.5m by 2100) **With Project, With Base Flow, With Dredging** Scenario: Land Area.

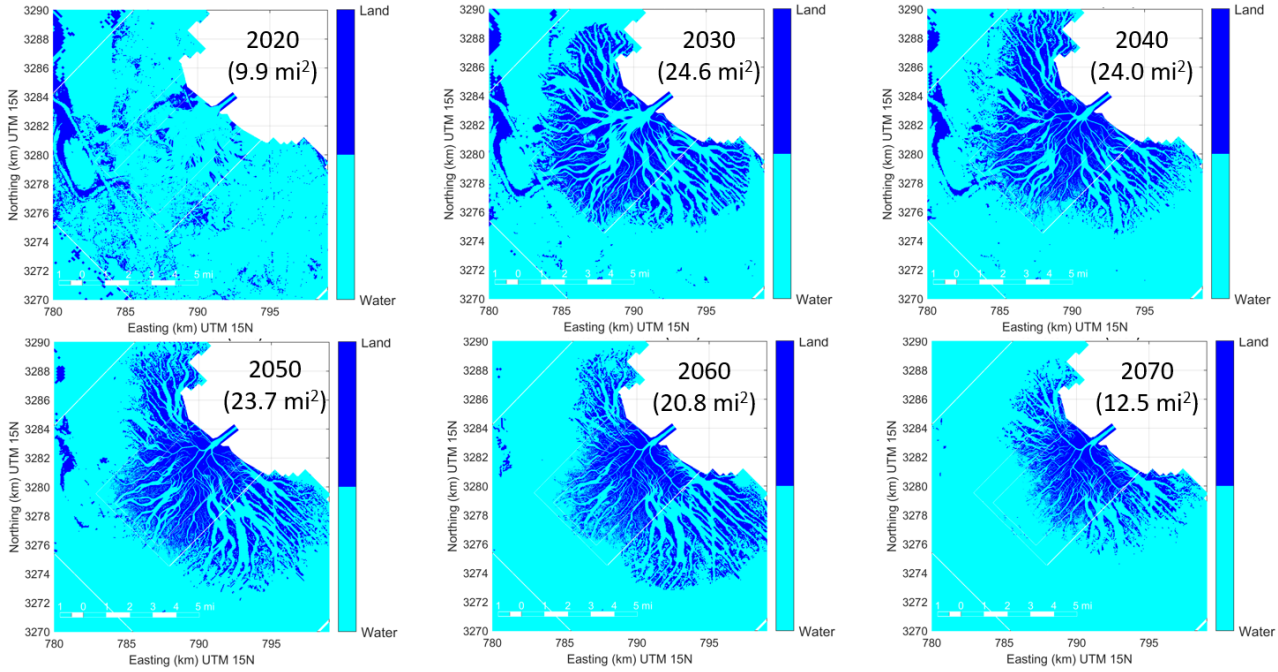

Figure 10.28. High SLR (USACE High, 1.5m by 2100*)* **With Project, With Base Flow, With Dredging** Scenario: Land Area.

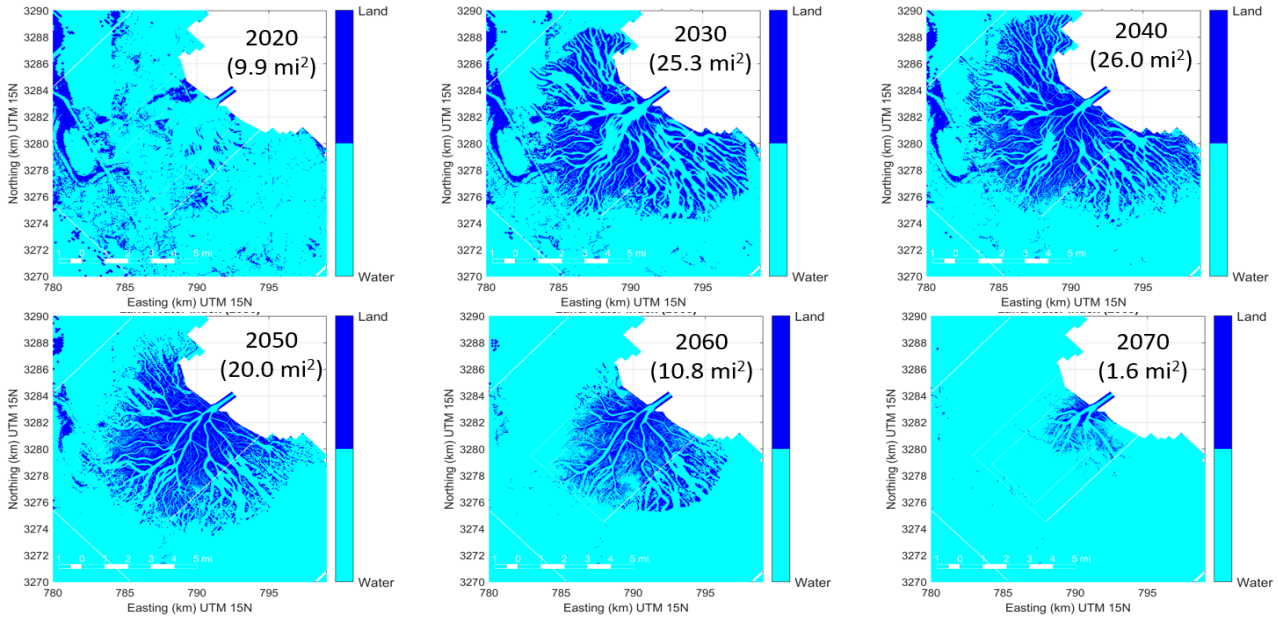

Figure 10.29. High SLR (USACE High, 1.5m by 2100) **With Project, No Base Flow, With Dredging** Scenario: Land Area.

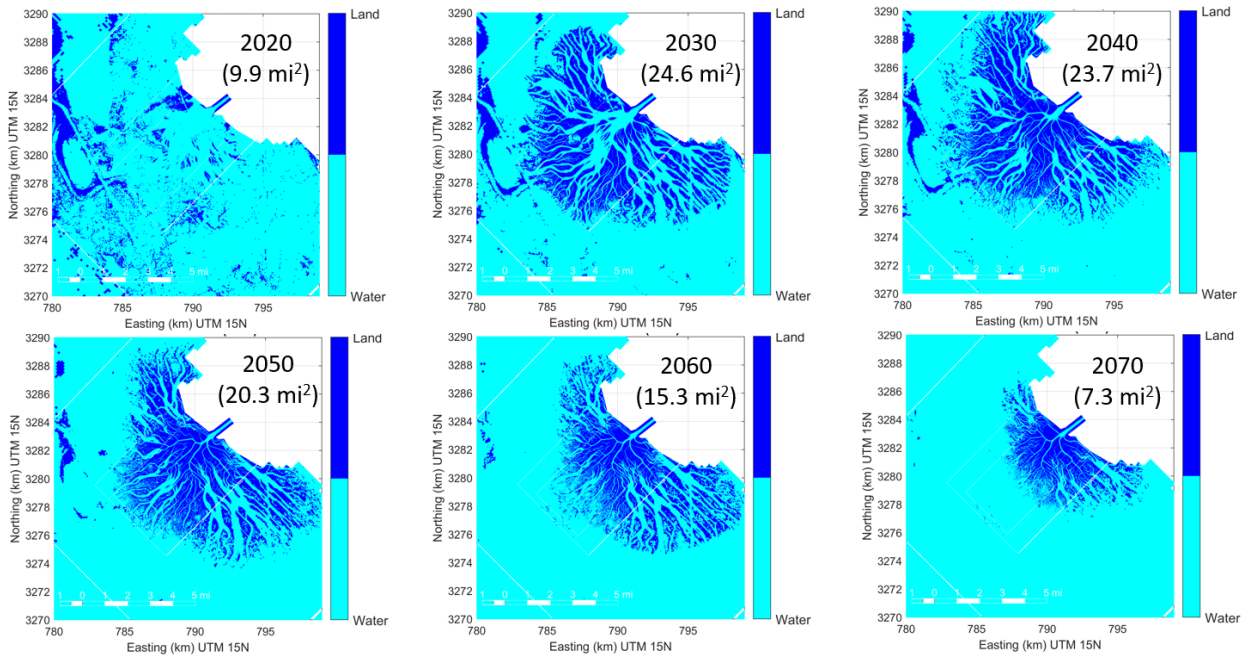

Figure 10.30. High SLR (USACE High, 1.5m by 2100) **With Project, With Base Flow, No Dredging** Scenario: Land Area.

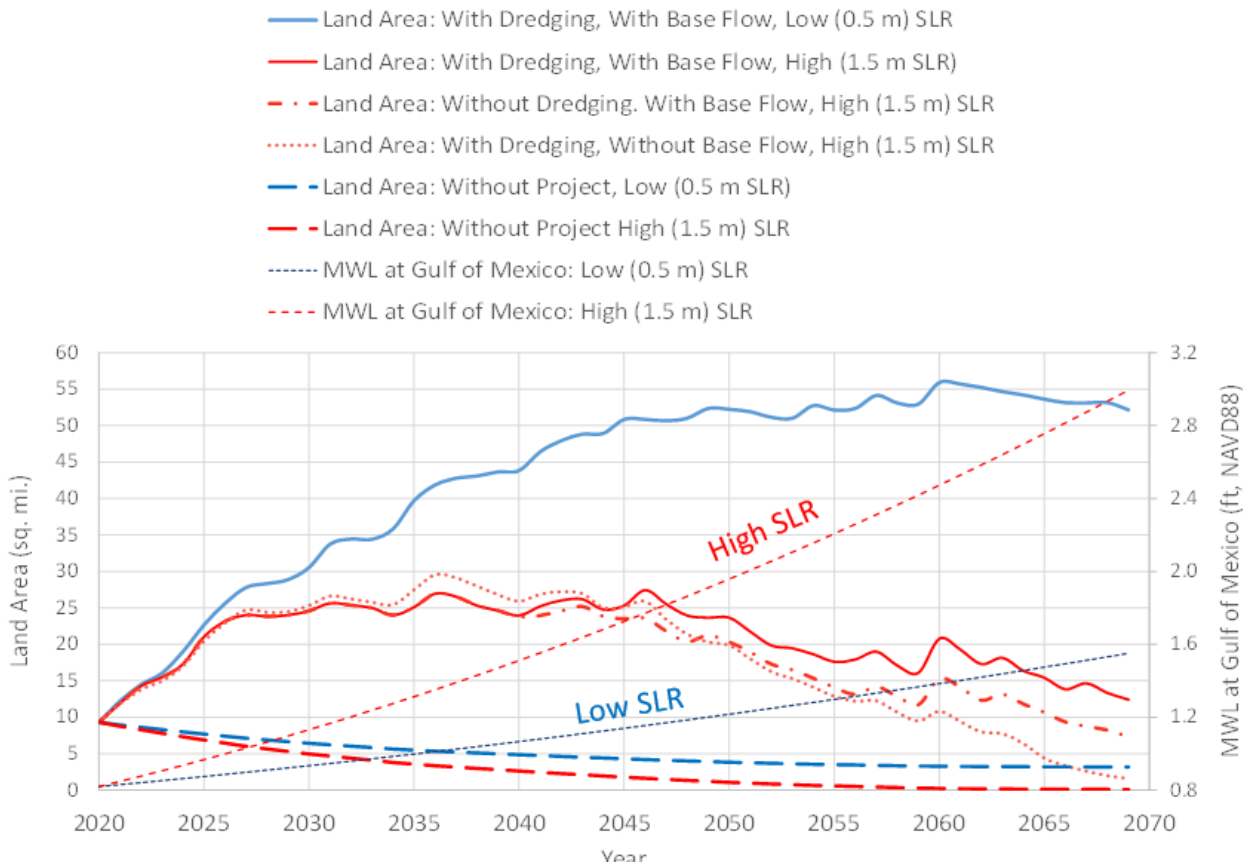

Figure 10.31. Comparison of Land Area Built or Sustained over 50 yrs (2020-2070) under the four scenarios modeled. The right vertical axis shows the annual mean water levels (MWL) rise at Gulf of Mexico based on the High and Low SLR trends.

Figure 10.31 shows the continuous trend of land building for the the four 50 year scenarios investigated here. The 10 year land areas shown in the inset of each snapshot corresponds to this plot. The secondary vertical axis on the right also shows the annual mean water level modeled and are the same as the mean water levels (red lines) shown before in Figure 10.6. As discussed before, the plots clearly show the land area attaining a plateau at around 2045 (Yr 25) for the Low SLR case indicating that the delta has reached an equilibrium where the net accretion balances almost the subsidence, ESLR and consolidation effects. For the High SLR cases a clear downward trend in land-building is seen after around 2040, with the no Base Flow with Dredging case showing the steepest decline. The reason for this declining trend can be traced to Figure 10.5 before which shows a rapid acceleration of SLR for the High SLR case

between 2040-2050 where a key ESLR acceleration (0.015 m/yr or 15 mm/yr) threshold is crossed. Figure 10.32 explains why most of the built land (over 50% from 2040 or about 11.5 sq. miles) near the distal part of the delta and away from the immediate mineral input source, ultimately goes under water during the last three decades. The spatially averaged values are shown here for a simple representation of this concept. It is seen that only about 4 mile radius of land remains above water as within this part the next accretion overcomes the effects of RSLR and consolidation. The major component of the accretion is by far the mineral component (24 mm/yr) which is almost 8 times the organic matter (OM) component (3 mm/yr) and is the principal factor that can overcome RSLR (which together is about 19.5mm/yr). This is also a validation of the basic premise of the need for the sediment diversion where consistent mineral input is a primary driver of vertical accretion of land. Note that the emergent land also provides a platform for the vegetation which builds a symbiotic relation with the delta by providing accreting organic matter that further builds the land.

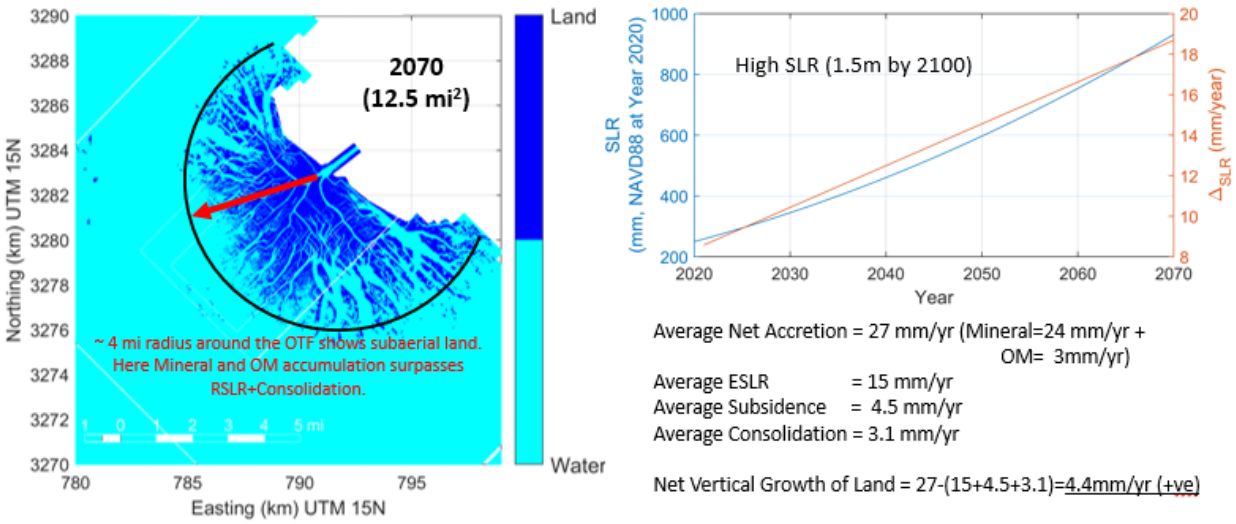

Figure 10.32. High SLR (1.5m by 2100) with Base Flow and With Dredging: Calculation showing that only land built within about 4 miles of the OTF remains sub-aerial due to net vertical accretion exceeding RSLR and consolidation effects within this area while land built in the distal part sinks below water.

The total self-weight consolidation settlement (cumulative settlement over each cycle) for the High SLR (1.5 m by 2100) with Base Flow and with Dredging scenario, after 50 years, is shown in Figure 10.33 left panel and an averaged per year settlement by simply dividing by 50 is shown in the right panel. Note that even though an average settlement is shown here as an example, the model calculates the full spatially and temporally variable settlement each year. The self-weight consolidation settlement in general is a smaller component of the total settlement (subsidence and consolidation) with most of the area other than the deep channels settling on an average about 0.15 ft (about 3.1 mm/yr) over 50 yrs within the active delta zone, which comprises of largely emergent or partially submerged deltaic islands, natural levees and vegetated platforms. As a reference, the subsidence in this area is about 0.8 ft (0.24 m) over 50 years as shown before in Figure 10.1 Self-weight consolidation settlement is the highest, about 0.5 ft or up to 5mm/yr within the deltaic channels which are actually the conduits of sand. The heavier sand (about 3 times heavier than silt) settles on the channel beds within a 2–4-mile distance from the outfall and provides a consistent overburden pressure compared to the lighter and more transient nature of fines deposits on the emergent wetland. The inset figure in left panel of Figure 10.33 shows the deposition zone for sand and indicates that most of the self-weight consolidation is likely to occur within the channels and due to sandy deposits. The major conclusion from this analysis is that given the future range of uncertainty in subsidence and sea-level rise, self-weight consolidation is a probably a small component when it comes to the question whether the delta will be able to remain sustainable over time.

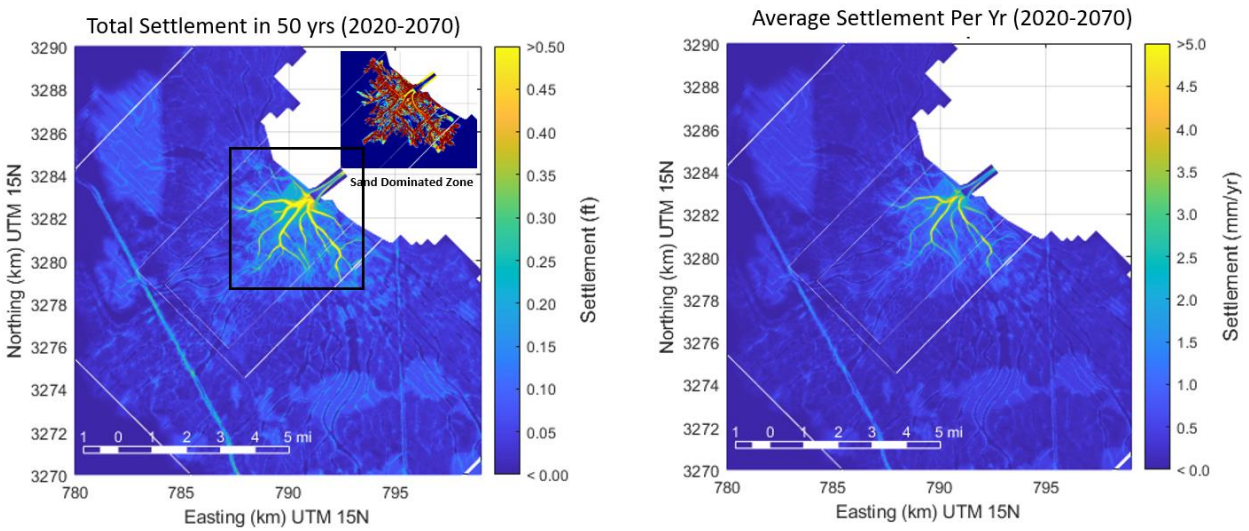

Figure 10.33. Self-weight consolidations settlement: High SLR (1.5 m by 2100) with Base Flow and Dredging shown here as an example. The other cases investigate show similar trends and consolidation settlement ranges.

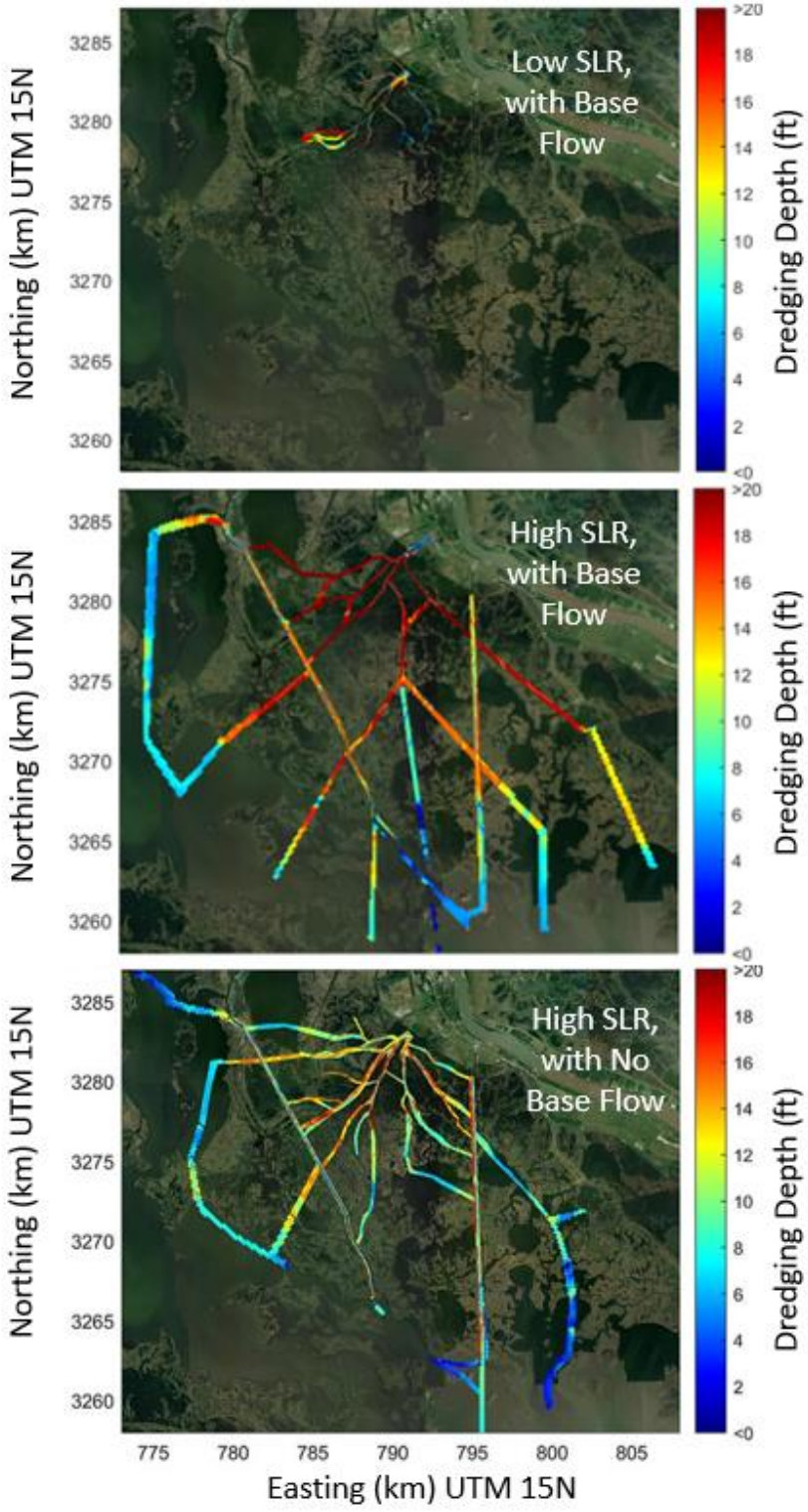

Figure 10.34. Dredging Templates showing total dredging over 50 years (2020-2070).

For the three With Dredging scenarios investigates, Figure 10.34 shows the investigate combined dredging template over 50 years (2020-2070). The dredging template is defined as depth below the Yr 50 (2070) mudline and spatial location of dredging, which is conducted mostly along the channel network of the delta built. Dredging only the channels was found to be the most efficient way to let water spread away from the immediate outfall area, thereby relieving backwater pressure buildup over time caused due to the rising far-filed sea level as well as macro-resistance of the delta which turns a primarily 2D sheet flow to a system of meandering radially progressing 1D channel system. The dredging usually is deeper near the outfall than away from the outfall. The maximum depths reach about 23 ft and the minimum about 2 ft. A trapezoidal cut with maximum side slopes of 1:5 was used for the dredging. While the layout of the dredging was chosen manually using a trial-and-error technique to achieve the most efficient flow path of the water, the depth was determined automatically by an algorithm that aimed to maintain similar cross-section along the pathway of a dredged channel to reduce blockage losses. There is some subjectivity involved in the manual process of dredged channel layout and alternative layouts could also provide as much performance improvements. The difference in dredging volumes due to varying dredging pathways was however less than 10% due to the fact that most of the dredging occurs below the existing 2020 mudline and very little of the deposited volume of the delta (which is only within the channels) is dredged out.

Table 10.4 shows the summary of land area built or sustained over 50 yrs along with dredging volume estimates every at 5 year interval from the 50 year model runs. Note that all these model results are with no MRSLR effects, as the FTNOMLV-CONSOL modeling was only conducted on the four scenarios as in Table 10.3 without MRSLR effects. The MRSLR results shown earlier in this section only are run with FTNOMBA (no morphology modeling) to estimate the possible capacity change and sediment load improvements without considering feedback from changing bathymetry or dredging due to MRSLR effects. The effect of MRSLR will reduce the dredging estimates, but have limited effect on the land-built as the target capacity remains the same with without MRSLR. The effect of MRSLR on dredging is discused later in this section. Table 10.4 shows that the difference in dredging estimate between the Low SLR and the High SLR scenario is about an order of magnitude (36.3 MCY for the Low SLR against

315-336 MCY for the High SLR), indicating that basin SLR is the most important future uncertainty in terms of dredging volume over time. As was shown before, dredging is required from the fourth decade (2050 or after Yr 30) for the Low SLR run and from the third decade (2040 or after Yr 20) for the High SLR runs. Another important insight from this analysis is that dredging volumes increase non-linearly over time and for the High SLR case almost triples in magnitude, increasing from 35-45 MCY in 2050 to 92-110 MCY in 2065, in just 15 years. An analysis of the dredging zone and source material reveals more than 95% of the dreding material is native, that is dredging cuts into the existing Yr 0 (2020) bathymetry to create accomodation space for the water volume.

Table 10.5 shows the dredging over 50 years required within Barataria Waterway and Wilkinson Canal. The total dredging is the same as shown before in Table 10.4. The dredging everywhere else if obtained by subtracting the sum of the dredging in the two channels from the total dredging. It is seen that the 7-13% of the total dredging occurs within any of these channels over 50 years. Note that the dredging volumes reported here are from consideration to maintain diversion capacity, no special consideration to maintain say a given navigable depth was given when dredging these two waterways.

An analysis into the source of dredged material reveals that over 90% of the dredging removes native material (material existing before 2020 or current conditions). This means that dredging depths mostly exceed below the existing 2020 mudline within the deltaic channels. This is shown in Table 10.6, which shows that dredging does not remove significantly the deposited material in the delta. The native material and the reworked deposited material dredged out can be utilized coastal managers in the future for other projects directly beneficial to land building (e.g., Sediment Retention Devices, terracing etc) or to improve existing back levees. The dredged material was mostly silt with some organic matter with those from near the outfall being sandy silt.

Table 10.4. Summary of Sub-aerial Land Area Built and Sustained along with required Dredging at every 5 year interval from the 50 year modeling of the four scenarios.

	Low SLR (0.5m by 2100), With Dredging, With Base Flow					High SLR (1.5m by 2100), With Dredging, With Base Flow					High SLR (1.5m by 2100), No Dredging, With Base Flow					High SLR (1.5m by 2100, With Dredging, No Base Flow				
Year	MWL at GoM (ft, NAVD88)	Dredging Volume (MCY)	Cumulative Dredging Volume (MCY)	Diversion Flow at MR 1,000,000 cfs (cfs)	Sub-aerial Land Area (sq.mi.)	MWL at GoM (ft, NAVD88)	Dredging Volume (MCY)	Cumulative Dredging Volume (MCY)	Diversion Flow at MR 1,000,000 cfs (cfs)	Sub-aerial Land Area (sq.mi.)	MWL at GoM (ft, NAVD88)	Dredging Volume (MCY)	Cumulative Dredging Volume (MCY)	Diversion Flow at MR 1,000,000 cfs (cfs)	Sub-aerial Land Area (sq.mi.)	MWL at GoM (ft, NAVD88)	Dredging Volume (MCY)	Cumulative Dredging Volume (MCY)	Diversion Flow at MR 1,000,000 cfs (cfs)	Sub-aerial Land Area (sq.mi.)
2020	0.82	0	0	86,000	9.9	0.8	0	0	82,000	9.9	0.8	N/A	N/A	82,000	9.9	0.8	0	0	86,000	10.0
2025	0.85	0	0	85,000	19.0	1.0	0	0	80,000	21.1	1.0	N/A	N/A	80,000	21.1	1.0	0	0	83,000	20.5
2030	0.92	0	0	82,000	28.9	1.2	0	0	78,000	24.6	1.2	N/A	N/A	78,000	24.6	1.2	0	0	81,000	25.3
2035	0.98	0	0	80,000	35.8	1.4	0	0	75,000	25.1	1.4	N/A	N/A	75,000	25.1	1.4	0	0	78,000	27.5
2040	1.05	0	0	78,000	43.7	1.6	7	7	75,000	24.0	1.6	N/A	N/A	66,000	23.7	1.6	3	3	75,000	26.0
2045	1.12	0	0	76,000	48.9	1.8	30	37	75,000	25.3	1.8	N/A	N/A	63,000	23.5	1.8	25	28	75,000	25.1
2050	1.22	1.8	1.8	75,000	52.4	2.1	45	82	75,000	23.7	2.1	N/A	N/A	57,000	20.3	2.1	35	63	75,000	20.0
2055	1.28	3.8	5.6	75,000	52.7	2.3	42	124	75,000	17.6	2.3	N/A	N/A	53,000	14.1	2.3	62	125	75,000	13.0
2060	1.47	3.2	8.8	75,000	53.0	2.6	102	226	75,000	20.8	2.6	N/A	N/A	49,000	15.3	2.6	92	217	75,000	10.8
2065	1.44	14.7	23.5	75,000	54.2	2.9	110	336	75,000	15.4	2.9	N/A	N/A	47,000	10.7	2.9	98	315	75,000	4.4
2070	1.55	12.8	36.3	75,000	52.2	3.1	N/A	N/A	70,000	12.5	3.1	N/A	N/A	45,000	7.3	3.1	N/A	N/A	72,000	1.6

Table 10.5. 50-Year Barataria Waterway a Wilkinson Canal Dredge volumes.

Scenario	Barataria Wwy Dredging (MCY)	Wilkinson Canal Dredging (MCY)	Dredging Everywhere Else (MCY)	Total Dredging (MCY)
Low SLR (0.5m by 2100), With Base Flow	0	0	36	36
High SLR (1.5m by 2100), With Base Flow	35	42	259	336
High SLR (1.5m by 2100), No Base Flow	23	33	259	315

Table 10.6. Source of dredged material.

Scenario	Native Material Dredged (MCY)	Deposited Material Dredged (MCY)	Total Dredging (MCY)
Low SLR (0.5m by 2100), With Base Flow	30	6	36
High SLR (1.5m by 2100), With Base Flow	298	38	336
High SLR (1.5m by 2100), No Base Flow	290	25	315

In order to understand the non-linear nature of dredging volume increase with time due to SLR and land-building effects as shown in Table 10.4, a series of steady state hydrodynamic runs were performed with the FTNOMBA model with the river domain (head driven system) and the basin-side bathymetries taken from the intermediate iterative dredging templates that were produced as part of the exercise to develop final dredging template shown in Figure 10.34. The goal of this exercise was to determine that if CPRA needs to limit dredging in the future, what target discharge may be a reliable estimate to set, e.g., say after 2060 dredging is suspended by a target discharge less than 75,000 cfs is still maintained. This is particularly more important for the High SLR cases where an order of magnitude higher dredging was obtained than the Low SLR case.

Figure 10.35 shows the influence of dredging on diversion flow. Each of the lines represent a given 5 yr sequence where a data point is the dredging volume computed from each iterative dredging template in between the year. As dredging increases, the diversion flow increases non-linearly with the return on dredging (say dredging needed per 1,000 cfs improvement in diversion capacity) decreasing as one reaches close to 75,000 cfs. For example, for the year 2060 (i.e., under constant SLR and land building), it takes a lot more dredging

(220-80=140 MCY) to improve capacity from 65,000 to 75,000 cfs versus say from 55,000 to 65,000 cfs (80-20=60 MCY). Also, as SLR increases over the years, it takes significantly more dredging to achieve the same diversion flow year to year. E.g., To achieve 65,000 cfs capacity in 2055 it takes only about 25 MCY of dredging, while to achieve the same in Yr 50 (2070) it takes about 160 MCY.

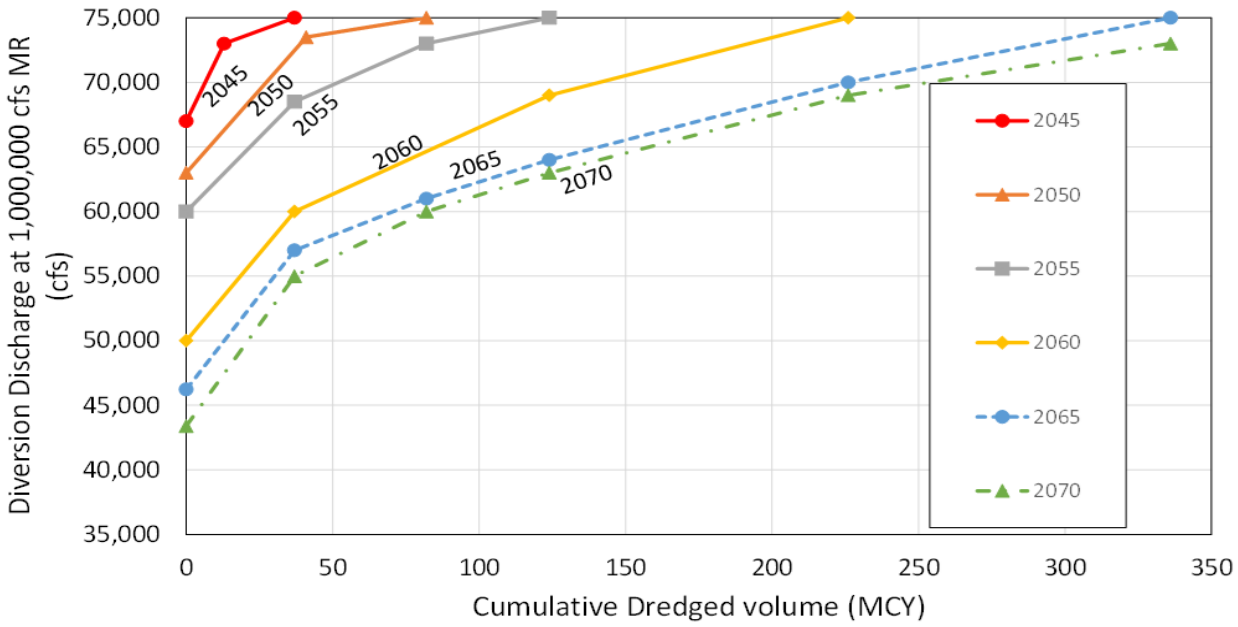

Figure 10.35. Influence of dredging on diversion discharge gain in performance. High SLR (1.5 m by 2100) with Base Flow case shown. No MRSLR effects considered.

10.5.2 Diversion Capacity Evolution including influence of MRSLR

In this section, the influence of Mississippi River Eustatic Sea Level Rise (MRSLR) on the diversion discharge and indirectly the sediment load diverted is analyzed. The MRSLR is known to be variable with river discharge and river mile from HOP (Karadogan et al., 2009, Nittrouer et al., 2011) primarily due to the backwater effect in a long (over 175 miles of) leveed channel as the Lower Mississippi River located below Baton Rouge (RM 228) and Bohemia (~RM 50), a section of the river which has little connection with the adjacent bays. The effect of

MRSLR induced water level rise at a given location reduces with increasing river flow and is negligible at the high flows (~1M cfs and above). This was the primary reason why MRSLR effects were considered absent in the modeling supporting the design of the dimensions of the structure (Chapter 8) which is aimed at meeting target diversion capacity of 75,000 cfs at 1,000,000 cfs MR flow. However, when discussing 50-year future effects in the basin, which depends on reasonable estimates of sediment load diverted, the effects of MRSLR cannot be neglected, as will be seen in figures below that show that at low to medium flows (200k-800k cfs) MRSLR effects affect diversion capacity. Figure 10.36, which shows the average number of days in a given month (averaged over 54 years, 1964-2018 period) that flow exceeds a certain threshold and indicates that between the months of Jan-July, which are the likely operational months of the diversion, the MR spends a majority (126 days or 60% of this period) of the time between 450,000-800,000 cfs range, which indicates the importance of considering MRSLR for continuous multi-decadal hydrograph analysis.

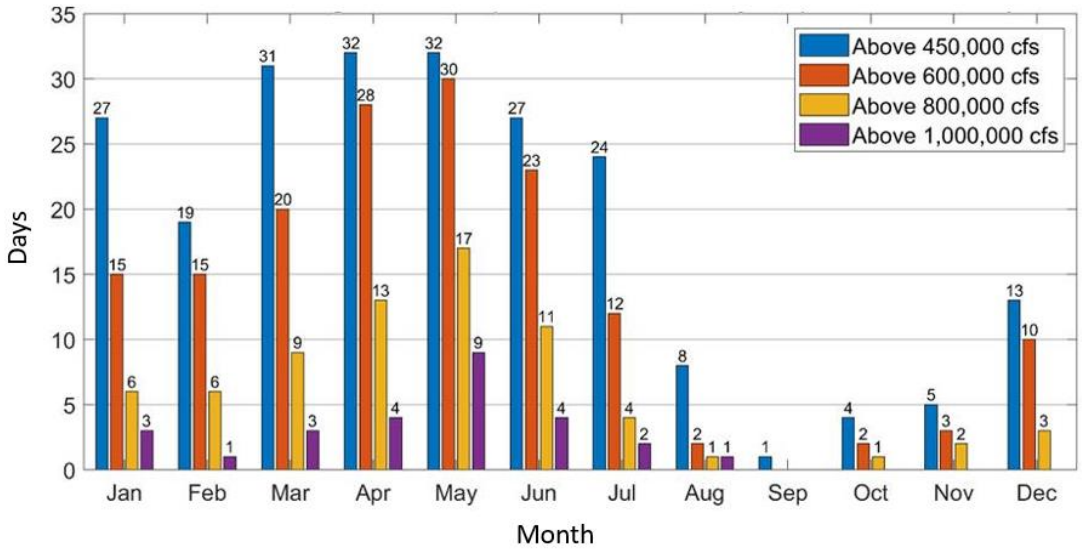

Figure 10.36. Number of days in a given month in an average representative year that flow in MR exceeds a certain threshold. Discharge data averaged over 1964-2018 period.

In order to quantify the flow varying MRSLR effects, the WI's Basin-wide model (PR4V3) results for water levels and discharges in the MR at RM 56 location were analyzed for the 50 year (1964-2013 MR hydrograph modeled as 2020-2070) model period. Since this model extends all the way upto the Gulf of Mexico in the MR, the effects of MRSLR are implictly captured within the model results and the access to the long dataset provides an oppurtunity to quantify this effect while remaining consistent with the LA Coastal Master Plan modeling framerwork. The model data was divided into current (2020-2030) and future (2060-2070) decadal periods and a pair of best fit lines drawn to define the envelope of this variation. The enveloped period was then divided into 10 year period in between based on the proportional change indicated within that period by the particular ESLR equation (eg, USACE High or USACE Intermediate). This approach produced a series of Q-H relations at RM 56 as shown in Figure 10.35 which shows the decadal variation of flow and water level in the MR for each ESLR scenario modeled. The relations indicate that MRSLR increases the mean water level in the river in 50 yrs from as much as 0.8 ft at the lowest flows (~200,000 cfs) to as little as 0.1 ft at the high flows (1,000,000 cfs) for the Low ESLR (0.5 m by 2100) scenario whereas for the High ESLR (1.5 m by 2100) scenario the same range is around 1.8 ft at the lowest flows (~200,000 cfs) to 0.6 ft at the high flows (1,000,000 cfs). These Q-H relations were then used as the downstream boundary in the FTNOMBA model (Table 1.1).

The FTNOMBA model, which is a 2D hydrodynamic only model connecting the river and basin was then run following the Monte Carlo type runs described before in Section 8.2.2. The basin bathymetry was based on the bathymetry predicted by the FTNOMLV-CONSOL modeling at the mid of the decade (eg., for 2030-2040 this was 2035), which means that the diversion discharge change over time reflects MRSLR effects, basin RSLR effects as well as land-building effects. The model results produced a series of decadal time series for each Q-H relation in the MR of diverted discharges. The results were then grouped into discrete MR flow ranges and is shown as a bar chart showing a discharge rating curve for the diversion and the MR in Figures 10.36 and 10.37. There are no MRSLR effects in the first decade, so it is not shown. Note that even though the diversion discharge is shown to exceed 75,000 cfs in order to show full maximum capacity, in reality the gate operations will limit flow to 75,000 cfs as in the WIBW-PR4V3 model.

Figure 10.38 which compares the MRSLR effects on the High SLR scenarios (dredged and undredged, both with base flow) only. Both for the dredged and undredged cases, it shows that MRSLR improves the diversion flow by as much as 20,000 cfs at the lowest operational flows (e.g., 40,000 cfs from 20,000 cfs at MR 500,000 cfs, a 100% increase) to as little as 5,000 cfs (80,000 cfs from 75,000 cfs at MR 1,000,000 cfs, a 7% increase) at the high flows. Note that dredging is not lowered here for the with MRSLR dredged case as the same dredged bathymetry is used for both with and without MRSR runs. Hence in reality, MRSLR will in fact reduce the need for dredging and as will be shown later this can be considerable, particularly in the later years. This is explained and quantified later in this section.

Figure 10.39 compares the MRSLR effects on the High SLR with no base flow with Low SLR with base flow scenario. Similar to the previous figure, this also shows that MRSLR improves diversion capacity and it is more pronounced at the low to medium MR discharge ranges. It is worth noting that the Low SLR scenario without MRSLR shows greater diversion capacity overall than the High SLR without MRSLR in the future. Also, the lower SLR scenario requires much lower dredging in the first place and the difference is about an order of magnitude, around 30MCY for the low SLR versus about 300 MCY for the high SLR as will be seen later. Therefore, impact of MRSLR is also important if different RSLR scenarios are compared and can help to reduce dredging more for the High SLR scenario.

Low

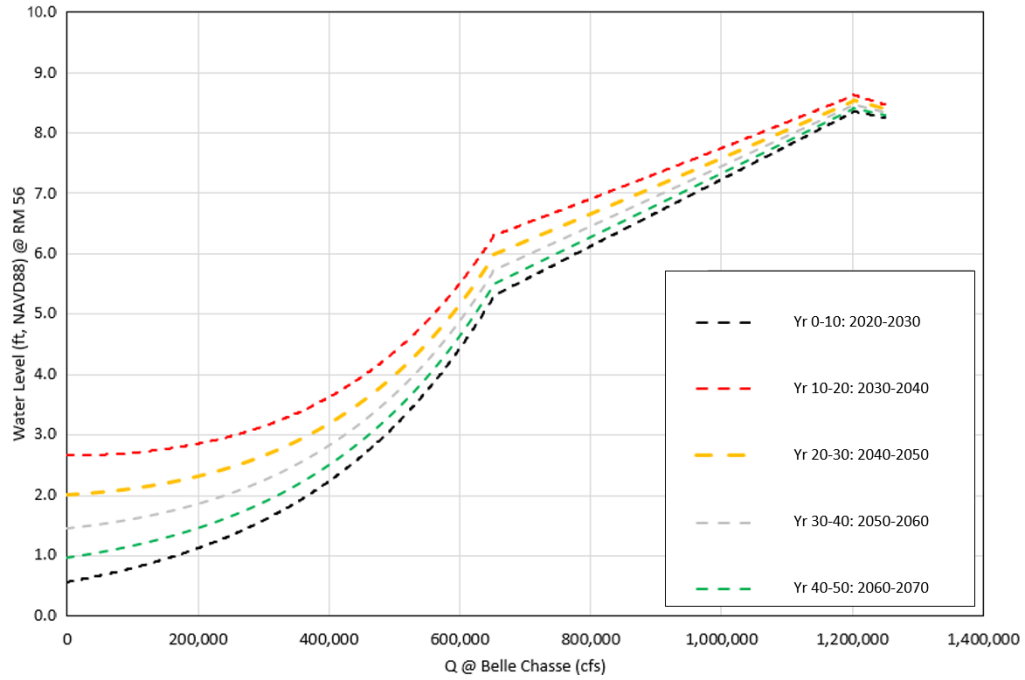

ESLR: USACE Intermediate (0.5m ESLR by 2100) MR Q-H

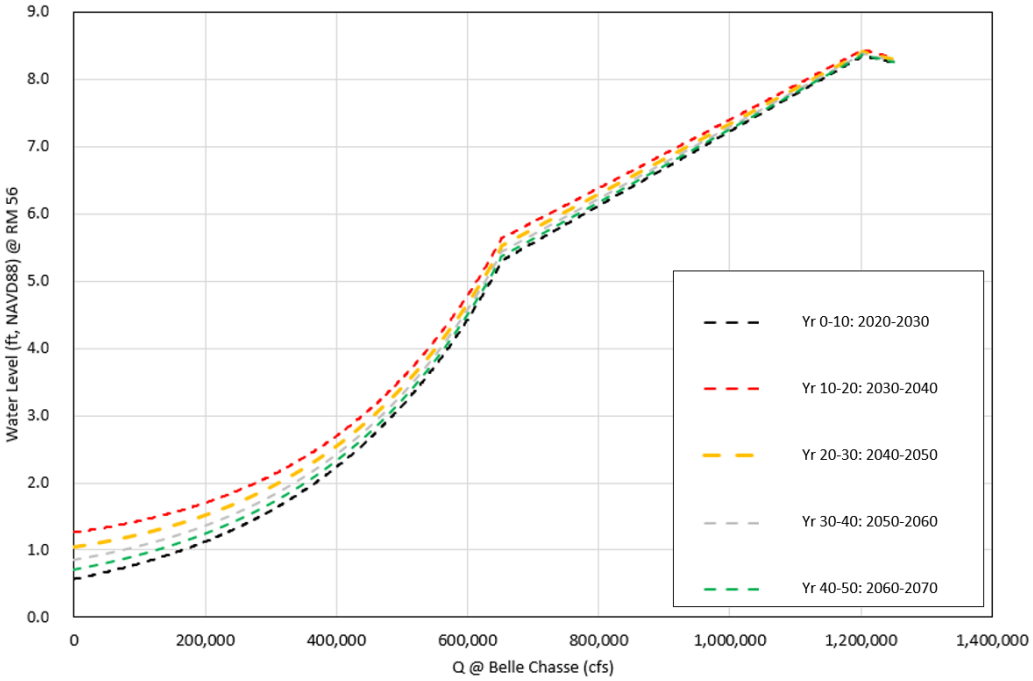

High ESLR: USACE High (1.5m ESLR by 2100) MR Q-H

Figure 10.37. Mississippi River (MR SLR) imposed as a series of decadal averaged stage discharge (Q-H) regression curves.

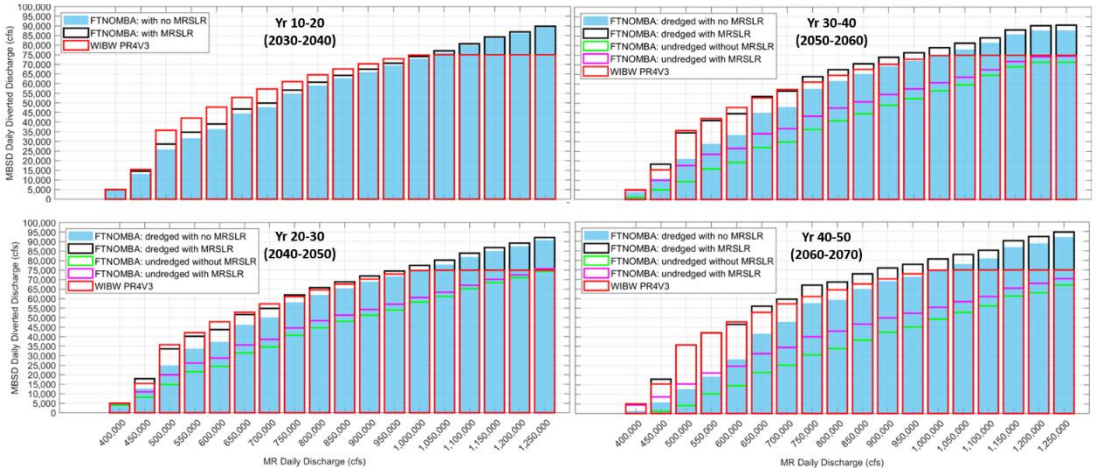

Figure 10.38. High SLR (1.5m by 2100), with and without dredging scenarios, both with base flow: Mississippi River (MR SLR) effects on diversion rating curve (Q_div vs Q_MR) shown. Even though the diversion discharge is shown to exceed 75,000 cfs in reality the gate operations will limit flow to 75,000 cfs as in the WIBW-PR4V3 model.

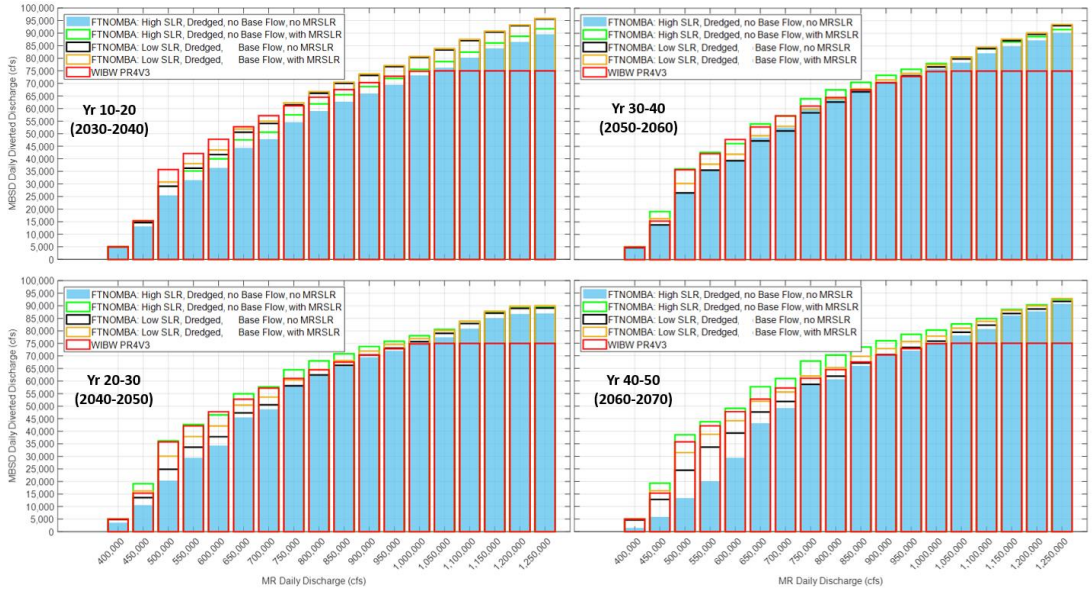

Figure 10.39. High (1.5m by 2100) with No Base Flow and Low SLR (0.5 m by 2100) with Base Flow: Mississippi River (MR SLR) effects on diversion rating curve (Q_div vs Q_MR) shown. Even though the diversion discharge is shown to exceed 75,000 cfs in reality the gate operations will limit flow to 75,000 cfs as in the WIBW-PR4V3 model.

Figure 10.40 shows the cumulative water volume diverted (left panel) and sediment load diverted (right panel) for the four scenarios investigated. Note that the 1:4 channel design was used for the High SLR with Dredging and Base Flow as well as the High SLR with no Dredging and Base Flow runs as the modeling was completed before the shift to 1:7 design. As was seen before in Chapter 6, the 1:7 channel improves the diversion capacity slightly. Therefore the later modeling with the High SLR witth Dredging and no Base Flow as well as the Low SLR with Dredging and Base Flow, conducted with the 1:7 channel shows slightly improved water and sediment load diversion estimates. For all the analysis with MRSLR since no additonal sediment model was run, the same concentration time series (as with the MRSLR) was assumed, the only change was the diversion discharge due to increased capacity. The water volume plot indicates that all the modeled scenarios divert less total water than the WIBW-PR4V3 which is largely because of the assumption in the WIBW-PR4V3 runs where it is assumed that the rating curve does not change in the future. The current modeling reflects the changing nature of the diversion rating curve. The range of total diverted water volume estimates are about 35-50 Trillion Cubic Feet, indicating the natural uncertainty in the future with SLR effects as well as how the diversion is managed (dredged or not dredged, base flow or no base flow). The water volume corresponds well with the total sediment diverted over 50 years, which varies between 210-290 Mil Tonnes. Since the aim should be to maximize as much as possible the sediment diverted to the basin, the lower SLR scenarios are likely to benefit the diversion by diverted more sediment. Among the High SLR scenarios, dredging the basin benefits in terms of sediment delivery the most. Similar to that seen in the water volume, the 1:7 design which delivers more sediment is a slight improvement over the 1:4 design. In terms of land-building the sediment load diverted however does not correspond linearly with land built or sustained. As was shown before in section 10.5.1, if the High SLR case is considered, dredging only improves the land building slightly even though as significant amount of additional sediment is diverted for the dredged scenario. This is because as was explained in Figure 10.32 before the rate of accumulation of sediment in the distal part of the delta cannot keep up with the rising sea level in this case and diverting more sediment by expensive dredging later on in the lifecycle of the diversion may not be cost beneficial in terms of per unit of land gained. It is also important to note that the out of the total sediment diverted, only about 60% is retained over 50 years while the remaining exits

the immediate 10 mile region of the delta and settles far below in the deeper portion of the bay or completely exits through the Grand Isle passes and is of no use to the delta building. Therefore while every possible effort should be made to improve the the cumulative sediment diverted, the actual land building will depend on factors which are depended on natural factors like ESLR, retention capacity of the basin and vegetation induced accumulation rates. An adaptive plan should be adopted where these factors are closely monitored and dredging plans adjusted based on how these trends take shape in the future. The WIBW-PR4V3 results for sediment were not available and is not included in the sediment volume plot.

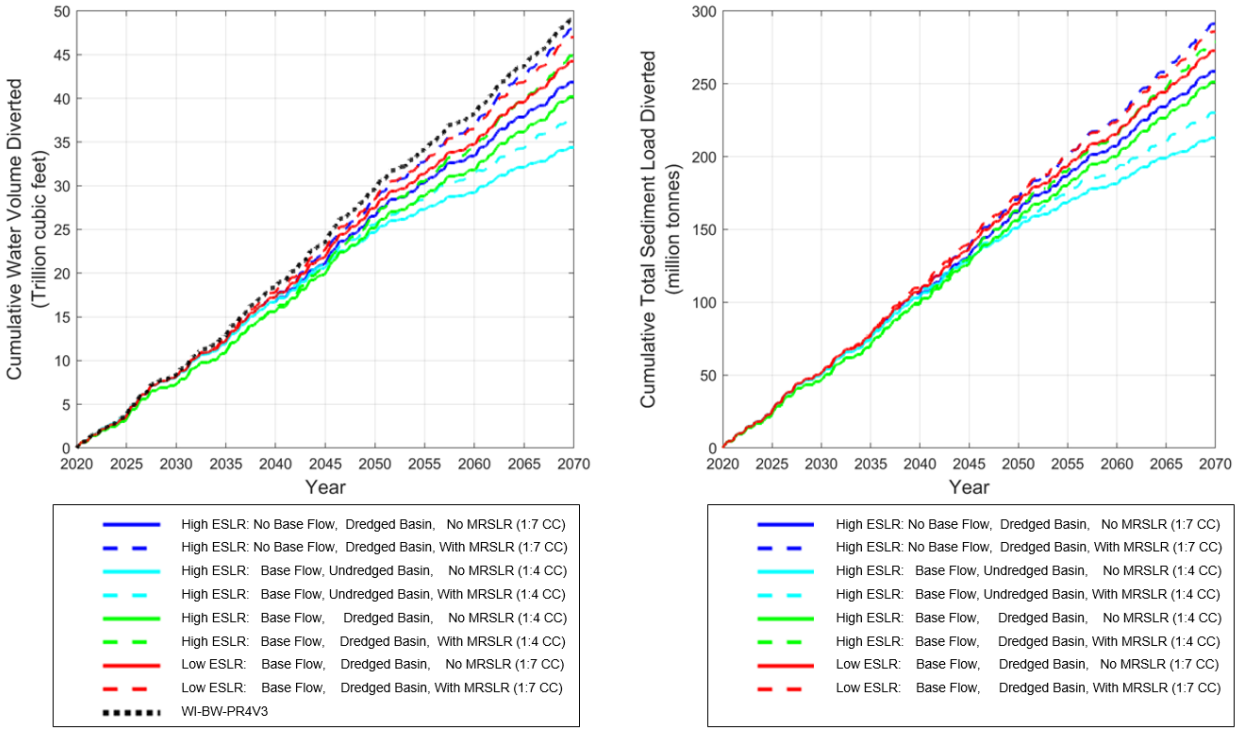

Figure 10.40. Cumulative Water (left panel) and Sediment (right panel) diverted in 50 Yrs.

The effect of MRSLR on dredging was similarly analyzes as shown in Figure 10.35 before. For the High SLR scenario, the total dredging in 50 years reduced to 210 when MRSLR was considered versus 336 MCY when no MR SLR was considered. It was also possible to achieve 75,000 cfs for the 50th year for the with SLR scenario. For the scenario without base flow the High SLR required about 190 MCY of dredging versus 315 MCY without MRSLR. On the other hand, separate model runs conducted to understand the dredging requirement if a

revision in the diversion target capacity in the future is considered indicated that revising the capacity to 75,000 cfs at 1,250,000 cfs from 75,000 cfs at 1,000,000 cfs MR flow, meant a reduction of the dredging to 110 MCY in 50 yrs without MRSLR from 336 MCY with MRSLR and only 65 MCY in 50 years from 315 MCY with MRSLR. For the Low SLR scenario, no dredging was found to be needed when MRSLR was considered over 50 years. This indicates that the dredging results may also be very sensitive to MRSLR effects and the current modeling done with no MRSLR effects are on the conservative side. Note that MRSLR is itself a highly uncertain factor due to possible change in downstream levee degradation, which can negate any positive MRSLR benefits by reducing the existing WL in the MR itself in the future.

10.6 Conclusions

In this section, the 50-year (2020-2070) model development and application of FTN's Outfall Model with Louisiana Vegetation and Consolidation Modeling (FTNOMLV-CONSOL) is presented. The diversion capacity is expected to decreases over time as sea level increases and land builds in the Barataria basin, primarily due to the increase of backwater pressure near the outfall in the future. Maintenance dredging is recommended in the future to overcome this effect and to maintain the target flow capacity of 75,000 cfs at 1,000,000 cfs MR flow. This modeling also quantifies the land-building due to regular diversion operations and the maintenance dredging volumes required to maintain the flow capacity in the future. In additional effect of MR sea level rise, which can potentially increase the net sediment load diverted to the basin is also presented and its impact on diversion capacity over various ranges of MR flows discussed. The specific conclusions from this study are as follows:

1. Water level and salinity calibration-validation was achieved mostly by varying Chezy coefficient in the basin, eddy viscosity and eddy diffusivity in the basin. Spatially varying coefficients were used in the production runs based on the calibration exercise.
2. In the calibration-validation modeling. open water stations (e.g., USGS and USACE) showed no significant water level bias, while the sheltered wetland stations (e.g., CRMS) showed a positive bias where the model is seen to overpredict the mean water level over the observed data by an average of 0.5 ft. This can be attributed to a variety of reasons and is treated as an uncertainty (stemming from both observed and modeling factors) for these stations.
3. Wind effects were neglected for the 50 yr modeling and was found to be as reasonable assumption based on the calibration-validation modeling.

4. For salinity, the model bias (<0.6 ppt) within the land-building zone was well within the minimum range (2 ppt) of variation between species. Since growth and death processes for each vegetation type (fresh, intermediate, brackish and saline) are influenced by salinity differences ranging between 2-10 ppt, the model bias can be considered much smaller than this. Therefore, the model when applied to determine establishment and mortality of species can be considered adequately calibrated for production runs under with project conditions.
5. Reduction in diversion capacity occurs from Yr 30 (2050) onwards for the Low SLR (0.5 m by 2100) and Yr 20 onwards (2040) for the High SLR (1.5 m by 2100) scenario. Dredging is expected to be required from this time onwards.
6. Without dredging diversion capacity reduces to 45,000 cfs at year 50 under High SLR.
7. Basin dredging volume estimates have a lot of uncertainty and is primarily a function of the Gulf MWL, cross-section of the deltaic channels emanating from the outfall and the connectivity of the deltaic network. The trends, particularly the influence of discharge with SLR and dredging found from this study are more reliable than the exact dredged volumes themselves, which may be influenced by the modeled channel formations and their depths, whose evolution can depend on grid size, cohesivity, sediment transport formulations, dry density of sediment, critical shear stress, erodibility, morphological acceleration factor etc. While every effort was made to choose reasonable estimates for input model parameters similar to those used in LA Coastal Master Plan models, modeling can be improved in the future with adaptive operations and model training with observed bathymetric and sediment data when the diversion starts operating.
8. Without dredging, the diversion capacity is reduced to 45,000 cfs at 1,000,000 cfs MR flow in 50 yrs (2070).
9. Without dredging, the total sediment (sand+fines) is reduced by about 48 Mil Tonnes (19%) over 50 yrs.
10. Relative sea level rise is the most important factor that determined amount of dredging required and land built/sustained over 50 years. The Low SLR scenario builds over 50 sq. miles of land with only 36 MCY of dredging requirement while the High SLR scenarios built 1.5-12.5 sq. miles of land with either no dredging or with as high as 336 MCY of dredging.
11. Even though without dredging the reduction in sediment delivered over 50 yrs is only 19%, the reduction in land area is 42% indicating that sediment load delivered is not proportional to land built/sustained. Fine sediment spreads further out and forms the principal marsh mineral base material of the delta on which vegetation thrives and sustains the wetland elevation. In particular the reduction in fines load (39 Mil Tonnes or 20%) is greater than reduction of sand load delivered (9 Mil Tonnes or 16%) and is a major factor for the reduction of delta planform area as the land reduction mostly happens further away from the outfall.

12. It is seen that once the diversion flow falls below target discharge, much more dredging is required to raise the capacity from 65,000 cfs to 75,000 cfs than up to 65,000 cfs and dredging required increases non-linearly with time as SLR increases.

13. Based on the results shown here, if ESLR in future approaches or excesses the High SLR case studied here, it may be possible to adopt a strategy where dredging costs may be lowered significantly by choosing a lower capacity as the target discharge in the last decade (2060-2070, Yrs 40-50). If say a target discharge of 60,000-65,000 cfs is adopted for the last decade, this would only require about 125 MCY of dredging over 50 yrs versus 336 MCY which is needed to bring capacity back to 75,000 cfs in the last decade.

14. Barataria Waterway and Wilkinson Canal dredged volumes are about 7-13% of the total dredging in the delta over 50 yrs that contributes to improvement of diversion performance.

15. MRSLR improves the net diverted sediment load by 12-19% depending upon whether base flow is allowed or dredging performed in the basin.

16. Basin dredging volume estimates depend primarily on the Gulf MWL (ESLR), cross-section of the deltaic channels emanating from the outfall and the connectivity of the deltaic network. The trends, particularly the influence of discharge with SLR and dredging found from this study are more reliable than the exact dredged volumes themselves, which may be influenced by the modeled channel formations and their depths, whose evolution can depend on grid size, cohesivity, sediment transport formulations, dry density of sediment, critical shear stress, erodibility, morphological acceleration factor etc. Modeling can be improved in the future with adaptive operations and model training with observed bathymetric and sediment data when the diversion starts operating.

11.0 DIVERSION OPERATIONS MODELING

11.1 Introduction

This chapter describes the results from diversion operations modeling, including gate operations during base flow conditions when the diversion flow is restricted to 5,000 cfs maximum at MR flow below 450,000 cfs as well near 1,000,000 cfs or above MR flow when the diversion flow is restricted to 75,000 cfs maximum. Apart from these two flow regimes, the diversion gates are expected to be fully open when diversion flows are expected to vary between 30,000 cfs to 75,000 cfs flows.

In addition to developing specific gate settings, this chapter also discusses the effect of channel flushing on salinity variations in the basin during base flow basin, typically from the months of June to December when the MR is most likely to be below 450,000 cfs. The channel flushing concept was introduced before in Chapter 6 and is meant to keep the channel clean of sediment during the base flow period. The effect of Davis Pond diversion on the background salinity in the Barataria basin without the MBSD project is also discussed. This chapter also discusses salinity modeling results from with and without base flow from the 50-year (2020-2070) future modeling of diversion as part of the land-building and dredging modeling done before using the FTNOMLV-CONSOL model in Chapter 10. The modeling results presented here are not meant to replace the EIS study conducted independently by CPRA where many other scenarios were discussed, but simply to provide insight into salinity effects in the basin as part of the modeling done that is included within the design team's scope, given the fact that the base flow modeling presented here offers more detailed insights into the possible diversion operations than what was presented before in CPRA's EIS modeling.

11.2 Base Flow (MR<450,000 cfs) Operations

In this section two main design issues are addressed, the gate positions that are most useful without frequent movement of the gates that can restrict base flow to 5,000 cfs or below and how to mitigate deposition within the U-Frame due to continuous base flow operation at that setting. The first topic is dealt with modeling of tidally influenced diversion base flow with

Delft3D FTNOMBA model with the FTNULMR river domain and thereby modeling various gate positions using the FTN2Comp FLOW-3D model based on typical flow regimes identified from that modeling. The second topic involved morphology modeling with Delft3D with select cases based on results from FLOW-3D modeling.

11.2.1 Delft3D modeling of Tidally Influenced Diversion Base Flow:

The FTNOMBA model was integrated with the FTNULMR model, which allowed full tidally dominated modeling within the river and the basin in one single model. The FTNULMR model was initially validated on its own against observed Belle Chasse hourly water level data before being implemented in the integrated model. This integration of the two models allowed for modeling of the complex tidal interaction between the basin and river, which is an important driver of discharge variation during low flows when the river and the basin can approach similar daily mean water levels and the phase variation between the hourly tidal water levels at the riverside and the basin side can drive the flow through the diversion. Further, this investigation also allowed for proper quantification a of daily mean discharge directly computed from the hourly tidal data and enabled identification of MR flow regimes when intra-daily (at least for one hour within a single day) or inter-daily (at least for one full day between two consecutive days) of reverse flows are possible between the river and the basin. Reverse flow indicates flow from the basin to the river and is generally undesirable from operations and water quality perspective.

The modeling for the January 2018 base flow period lasting for about 25 days is shown in Figure 11.1 which also demonstrates the effect of the attenuating tidal amplitude due to a set of Spring and Neap tides, an important driver of the bi-weekly variation of discharge and water levels. The top panel shows the water level at the MR near the diversion, at the outfall in the basin and the head-difference between the basin and the river. Only static head difference is reported here as the kinetic head is low due to the low discharge velocities at these flows. The bottom panel shows the corresponding diverted discharge in the right vertical axis and the MR discharge in the left vertical axis. The red solid lines indicate phases of the day when intra-daily reverse flow occurs due to negative head difference (river water level lower than basin). It is worth noting that as little as less than 0.5 ft of head difference can drive up to 20,000 cfs of

hourly flow. The hourly flow can fluctuate between as much as 20,000 cfs (e.g., January 11-12, 2018) or as little as 5,000 cfs (January 24-25, 2018) due to Spring and Neap tide influences. Indeed if 5,000 cfs average daily flow or less is set to be maintained, the hourly flows can still exceed that limit or even reverse (if allowed) with all gates open. Thus, a well-defined gate control is needed to limit the large tidal variability of discharge during the MR base flow regime (<450,000 cfs).

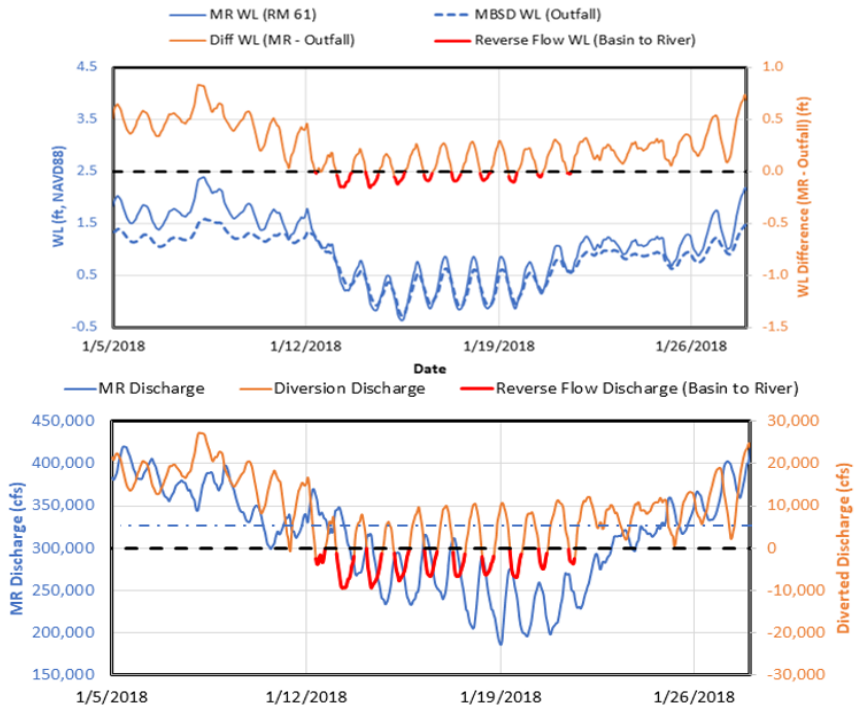

Figure 11.1. Tidal modeling of Diversion Flow during Base Flow (MR<450,000 cfs) period. The results are with no gate operations. Top panel shows the water levels and bottom panel the diversion and MR discharges.

Figure 11.2 shows the diversion discharge versus MR discharge scatter plot for the 2018 base flow model period. It is obvious that the tidal influence creates much more scatter in the diversion discharge at a given MR flow and can be highly variable day to day. For example, the same 15,000 cfs daily flow can occur anywhere between 325,000-400,000 cfs daily MR flow range. However, day to day adjustment of gate position is not feasible, nor desirable. Hence to

limit daily flow to 5,000 cfs the most restrictive setting may be desired at the higher end of the MR flow (say 400,000-450,000 cfs) so that once the gates are brough to this setting at MR 450,000 cfs during the last day of the falling limb of the previous year's hydrograph, it would not need to be operated other than due to emergency closure or full closure for the entire base flow period, that is till MR reaches 450,000 in the rising limb in the next year again. In order to search for the specific gate settings, first a certain MR flow (400,000 cfs) was selected and a range of diversion flows (5,000, 15,000 and 25,000 cfs) representative of the envelope of variation within the 300,000-400,000 cfs range selected as the diversion flow for further FLOW-3D modeling described in the next section.

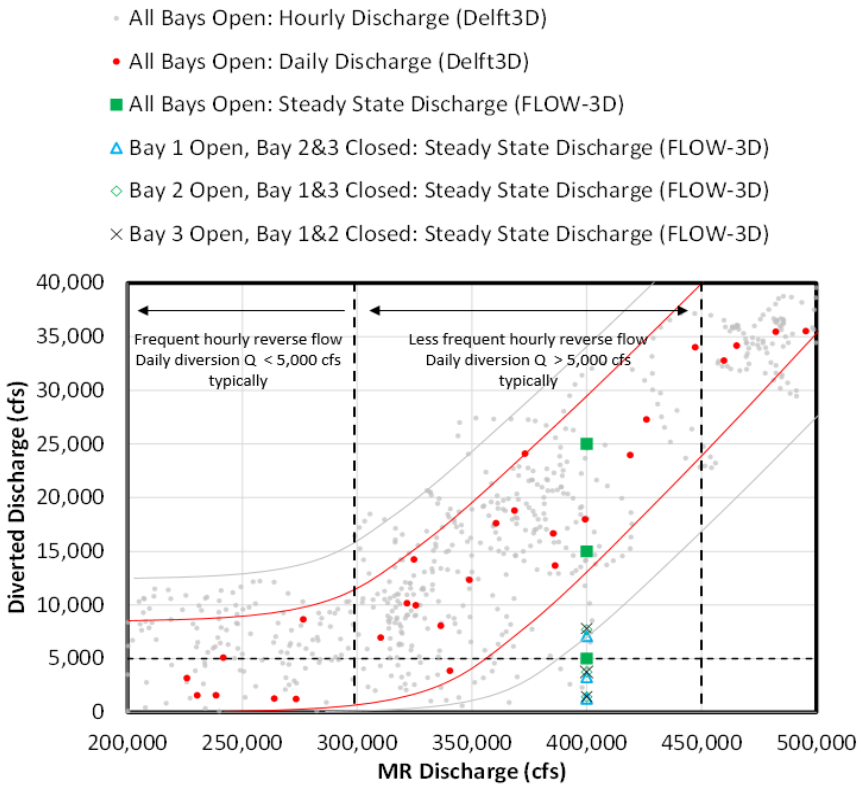

Figure 11.2. Diversion discharge versus MR discharge from tidal modeling of diversion flows during base flow period (MR<450,000 cfs). All gates open. Hourly data from Delft3D model is shown with grey solid circles and daily averaged data in red circles. The approximate envelopes of daily and hourly variation are also plotted. Also shown are FLOW-3D model results with only one gate open configurations as explained later.

11.2.2 FLOW-3D Modeling of Gate Positions and Diversion Flows

There are three bays in the diversion intake headworks as shown in Figure 11.3 with a stack of bulkhead gates in each bay, and the Gates are numbered in ascending order from upstream to downstream based on the MR flow direction. Assuming that gates can be opened at every 5 ft increments there can be 5x3 individual settings in each bay with the other bays closed for each setting. Further there are non-uniform head losses expected through each bay given the change in flow dynamics when one or more of the other bays are closed and the unique way the water enters the diversion for each configuration. In order to model the most likely configurations that will limit flow to 5,000 cfs, a two-step approach was followed. First the modeling investigated the cases where only one bay was closed at a time with the other two bays fully open. Table 11.1 shows the scenarios investigated with only one gate open. The FLOW-3D FTN2Comp steady state model was used where conveyance channel boundary was set at water levels based on the specified flow (25,000, 15,000 or 5,000 cfs) when all gates are open. Once those water levels were obtained, each gate closure scenario was run without changing the boundary conditions, with the assumption that the downstream boundary is far away from the gate to be affected by the discharge and is reasonable assumption given that basin conditions mostly dictate water level at these low flows (downstream control). This approach permitted the inclusion of the reduction in flow capacity as well as head loss effects due to the different gate closure scenarios modeled within the same consistent framework.

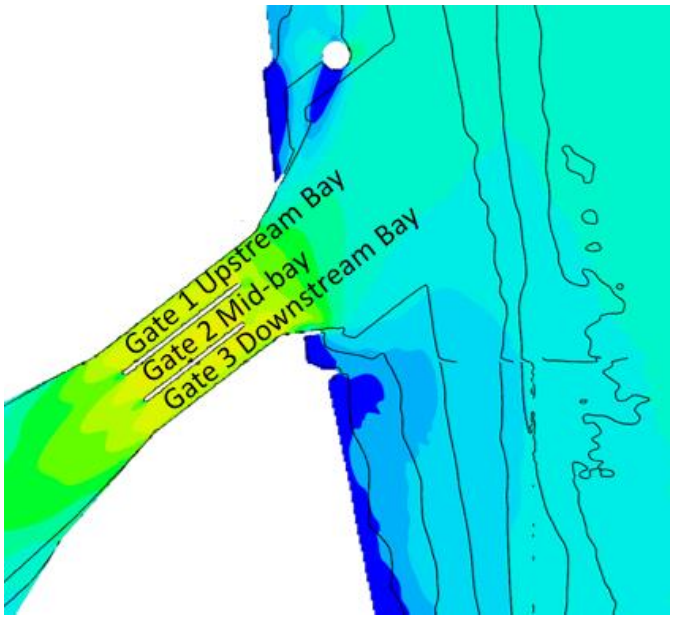

Figure 11.3. Naming convention of gate bays within the intake headworks.

Table 11.1 shows FLOW-3D model runs with only one gate fully open at a time and other two gates completely closed. Figures. 11.4 to 11.6 show the velocities under the 12 scenarios shown in Table 11.1. The table also provides the diversion discharge under each scenario and also the percentage of diversion discharge with respect to the fully open diversion flows. The velocities in each bay are also shown, except the 5,000 cfs case, all the velocities are above the 2 ft/s threshold. In general, the flow capacity of the Upstream most bay (Bay 1) is the lowest and that of the downstream most bay, the highest and the flow reduces by more than 2/3rd (66.7%) due to additional losses. Note that the flow percentages will not add up to 100% in one row because these are stand-alone cases and not simply a linear flow split between the bays. Based on this analysis it is seen that even with any one bay fully open with the others completely closed, the daily flow can be limited to 5,000 cfs except for the 25,000 cfs flow case.

Table 11.1. FLOW-3D model runs with only one gate fully open at a time and other two gates completely closed.

MR Discharge (cfs)	Diversion Discharge (cfs) (Percent discharge through open bay with respect to all open bay condition)			
	All Gates Open	Only Gate 1 Open	Only Gate 2 Open	Only Gate 3 Open
400,000	25,000	6,800 (27%)	7,300 (30%)	7,500 (30%)
400,000	15,000	3,400 (23%)	3,900 (26%)	3,900 (26%)
400,000	5,000	1,300 (26%)	1,400 (28%)	1,500 (30%)
Average Velocity in Open Bay (ft/s) (Percent velocity through open bay with respect to all open bay condition)				
400,000	4.7	3.8 (81%)	4.2 (89%)	4.2 (89%)
400,000	2.8	1.9 (68%)	2.2 (79%)	2.2 (79%)
400,000	0.9	0.7 (78%)	0.8 (89%)	0.8 (89%)

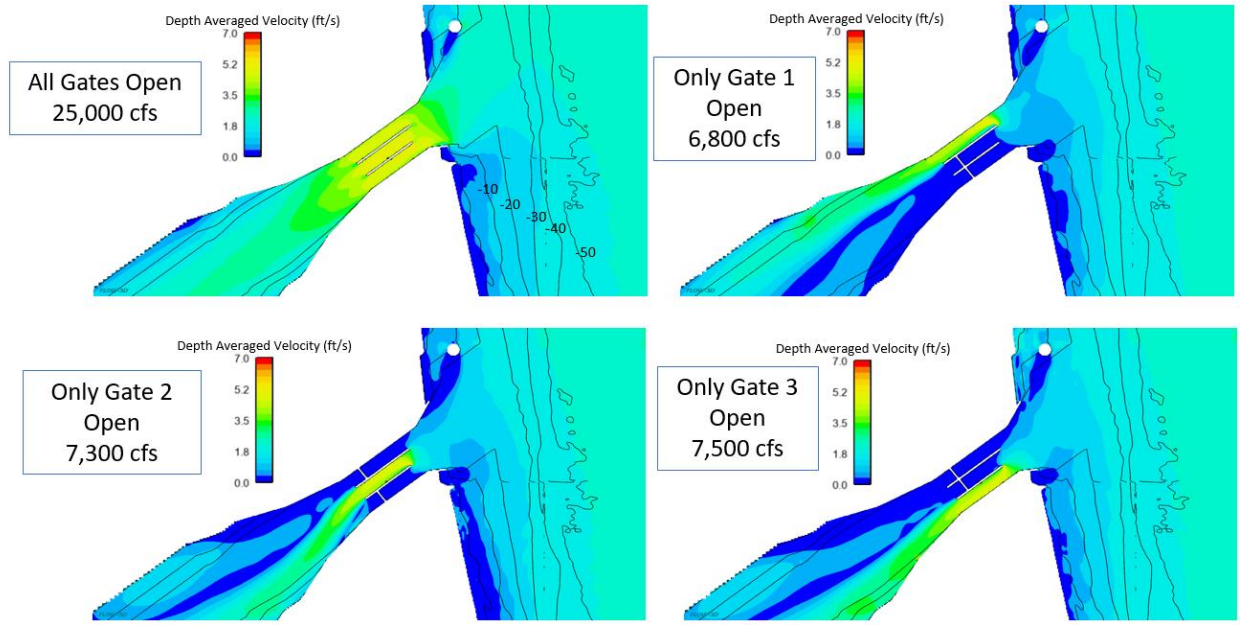

Figure 11.4. All Gates Open Diversion Flow 25,000 cfs (top left). Other panels show velocities when only one gate is fully open at a time and the others are fully closed.

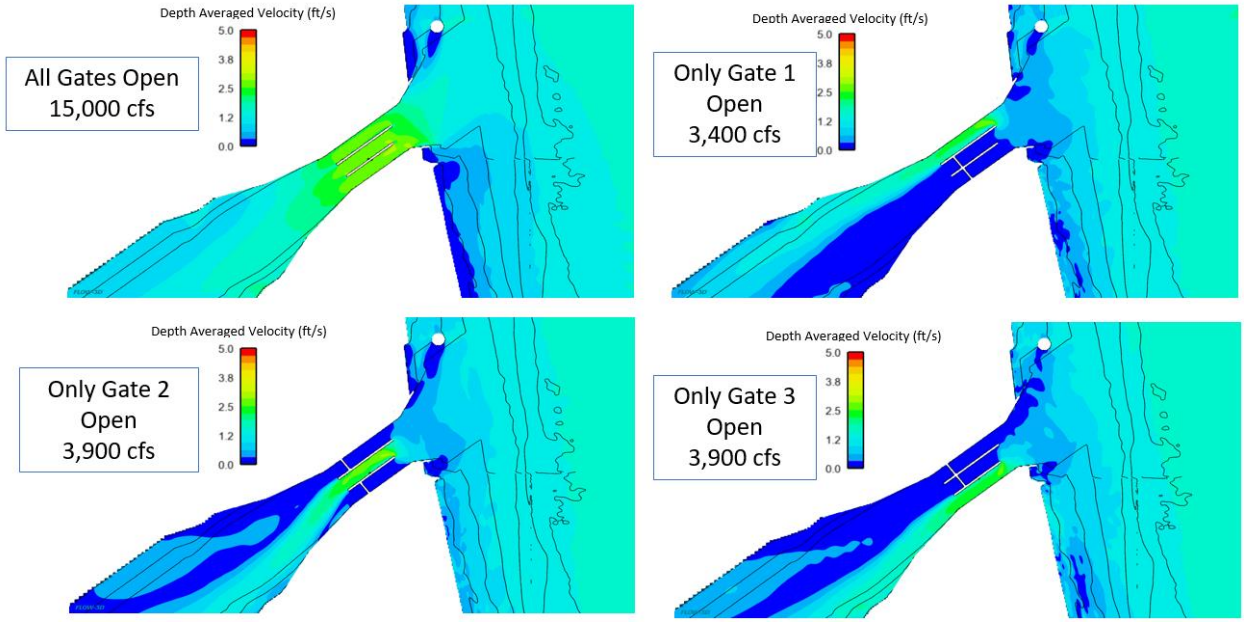

Figure 11.5. All Gates Open Diversion Flow 15,000 cfs (top left). Other panels show velocities when only one gate is fully open at a time and the others are fully closed.

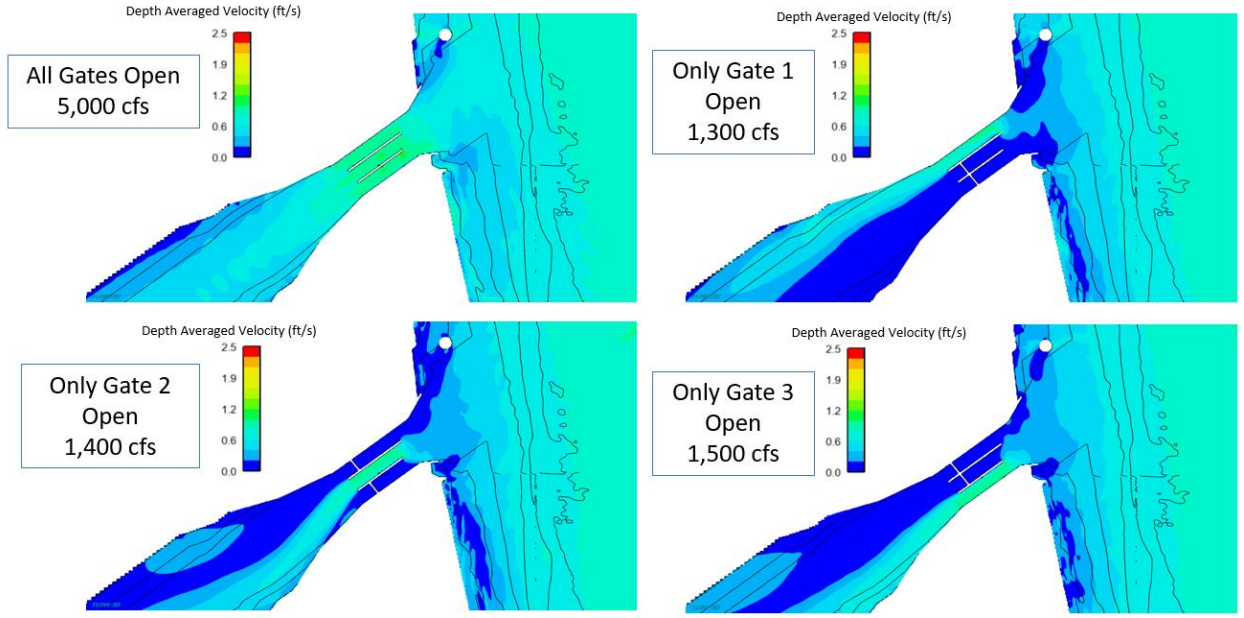

Figure 11.6. All Gates Open Diversion Flow 5,000 cfs (top left). Other panels show velocities when only one gate is fully open at a time and the others are fully closed.

This 25,000 cfs flow case therefore needs partial gate closure of the open bay as well. This test case along with two more flow scenarios 12,500 cfs (at 350,000 cfs MR) and 32,500 cfs (at 450,000 cfs MR, maximum flow) were next modeled as part of the partial gate closure modeling. Figure 11.7 shows an example of the model setup for the partial gate open model runs in FLOW-3D FTN2Comp model where Gate 1 is 15 ft open and the others completely closed. The figure also shows locations along the U-Frame at about 100 ft distances downstream where vertical profiles are later compared and Delft3D model calibrated before the latter is applied for U-Frame deposition modeling.

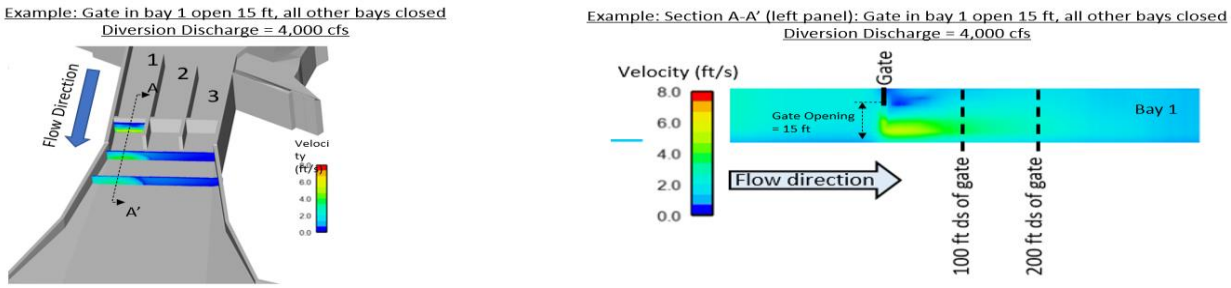

Figure 11.7. Model setup in FLOW-3D FTN2Comp model with partial gate closure. As an example, here Gate 1 is shown open 15 ft. with others closed completely at MR 400,000 cfs corresponding to the fully open discharge of 25,000 cfs. Gates are modeled as rectangular flat plates with similar thickness as the bulkhead gate and does not resolve the truss structure behind.

Table 11.2 shows the cases where only one bay was partially closed while the others are completely closed. In addition, a separate test case with all bays 5 ft open was also modeled and as will be explained later proved to be the best setting to reduce deposition concern within the U-Frame during low flows. The green highlighted cells within the Table indicate flows that are less than 5,000 cfs and therefore acceptable gate settings. If only one gate is planned to be operated it is suggested that the 10 ft open Gate 2 be the recommended setting as it is the most restrictive and will keep flow below 5,000 cfs threshold throughout the base flow period. However as will be discussed later keeping only one bay open causes deposition to build up in the other bays over long periods of base flow and gate cycling becomes necessary. The all gates 5 ft open is ultimately recommended based on results shown later.

Table 11.2. Partial gate closure modeling. Diversion flow at representative MR flows and gate settings. The 5 ft open for all gates is the recommended setting based on U-Frame deposition modeling shown later.

Daily MR Discharge (cfs)	Daily Diversion Discharge (cfs)															
	All Gates Fully Open	All Gates 5 ft open	Only Gate in Bay 1 Open					Only Gate in Bay 2 Open					Only Gate in Bay 3 Open				
Opening Height →	Full	5ft	Full	20 ft	15 ft	10 ft	5ft	Full	20 ft	15 ft	10 ft	5ft	Full	20 ft	15 ft	10 ft	5ft
350,000	12,500 (± 7,50)	2,300 (±200)	3,400 (±300)	2,900 (±200)	2,000 (±200)	1,400 (±100)	700 (±100)	3,900 (±300)	3,200 (±200)	2,100 (±200)	1,500 (±100)	700 (±100)	4,000 (±300)	3,100 (±200)	2,200 (±200)	1,500 (±100)	700 (±100)
400,000	25,000 (±1,500)	4,500 (±300)	6,800 (±500)	5,700 (±400)	4,000 (±300)	2,700 (±200)	1,300 (±200)	7,700 (±500)	6,400 (±400)	4,300 (±300)	3,000 (±200)	1,400 (±200)	7,800 (±500)	6,200 (±400)	4,400 (±300)	3,000 (±200)	1,400 (±200)
450,000	32,500 (±2,000)	4,900 (±400)	8,800 (±700)	7,400 (±500)	5,200 (±400)	3,500 (±300)	1,700 (±200)	10,000 (±700)	8,300 (±500)	5,600 (±400)	4,000 (±300)	1,800 (±200)	10,100 (±700)	8,100 (±500)	5,700 (±400)	3,900 (±300)	1,800 (±200)

Before the morphology modeling is presented in the next section, it is worth investigating the vertical profiles of velocity behind the gates for typical partially opened gate configuration. The near-bed velocities which are directly related to the sediment transport capacity of the jet flowing from under the gates is responsible for increasing the shear stress locally and cleaning any sediment downstream of the gate complex into the transition. Figure 11.8 shows the vertical profiles of velocity for a typical scenario where Gate 1 is partially closed at different heights, 20 ft open, 15 ft open, 10 ft open and 5 ft open. All the configurations showed high enough near bed velocities (>2 ft/s) to move silt at the low flows within the partially open bays. Therefore, any of these configurations can keep the bay clean. However, the closed bays where the velocities are almost zero (weak circulations are present) tend to accumulate sediment through advection in front and behind the closed gates. This is investigated through morphology modeling in the next section.

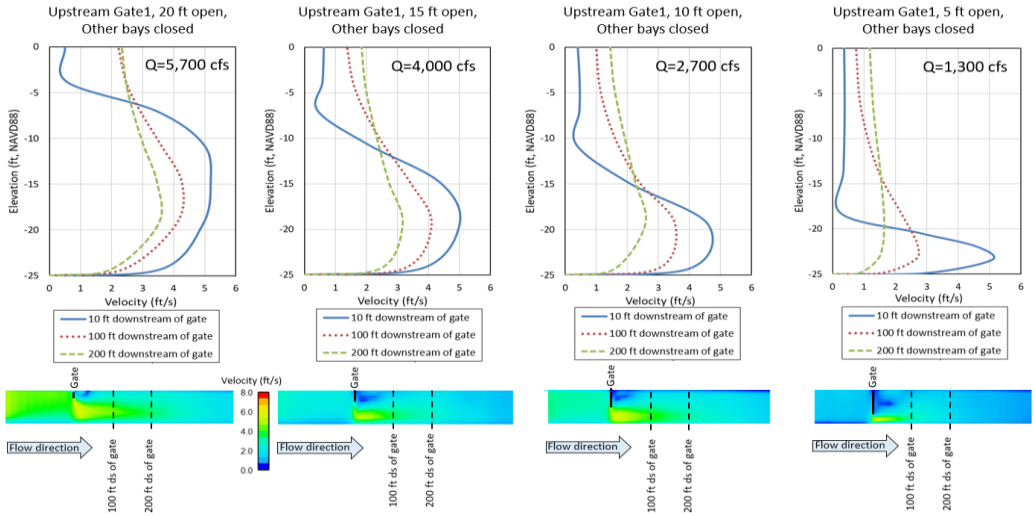

Figure 11.8. Vertical profiles of velocity magnitude modeled by FLOW-3D FTN2Comp model for various gate openings. Gate 1 operation at 400,000 cfs (25,000 cfs max flow when all bays open) shown as example.

11.2.3 Delft3D morphology modeling of Partial Gate Opening: U-Frame deposition concern

Deposition in front and behind the gates is a known concern at other lock and gate structures in the Lower Mississippi River and is usually caused by long periods of fine sediment laden flow at low velocities blocked by gate bays. When lifting the bulkheads when gates are planned to be open, after a period of base flow, if substantial amount of sediment deposits remain sitting on the gate members, this can lead to exceedance of crane capacity and costly dredging to remove the sediment. Therefore, the aim of the morphology modeling here is to investigate whether there is particular gate position or a method of operation that can minimize this deposition within the U-Frame. For this modeling three scenarios were modeled:

1. Gate 1 fully open 15 ft, with other gates closed, throughout the entire base flow period.
2. Gates 1 to 3 cycled every month with an opening of 15 ft for the partially open gate, with others closed.
3. All gates at 5 ft open for the entire base flow period.

The 3D FTN2Comp Delft3D model used a vertical barrier to block the flow through cells above the opening specified. The sigma-layer distribution was carefully adjusted to resolve the sharp feature at the gate bottom location. Before applying the model for the production runs, the Delft3D FTN2Comp 3D model was validated for vertical profiles of velocity magnitude behind the gate with the FLOW-3D FTN2Comp model as shown in Figure 11.9. The main parameter calibrated was the roughness in the U-Frame. After calibration the model was applied to the three runs mentioned above.

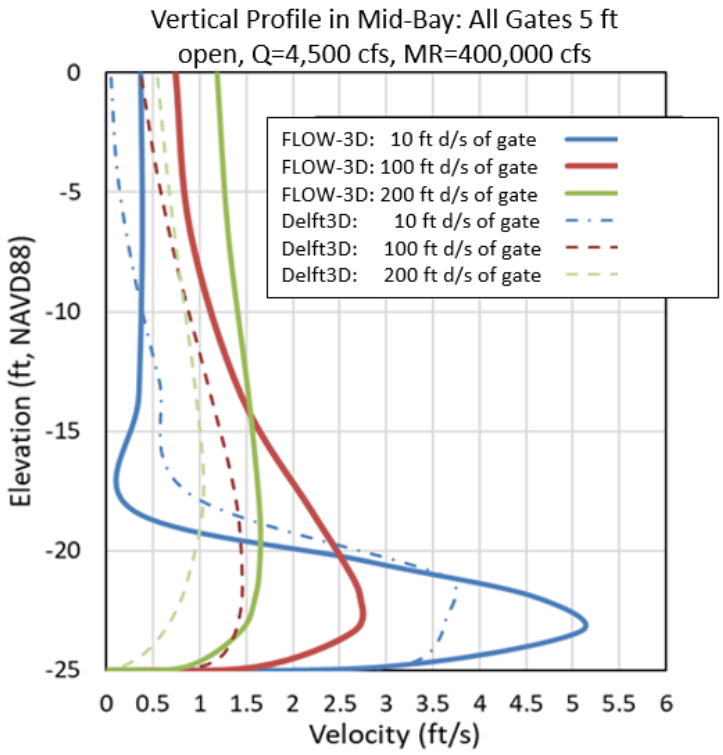

Figure 11.9. Calibration of the Delft3D model Vertical profiles of velocity magnitude FLOW-3D FTN2Comp model for various gate openings. Gate 1 operation at 400,000 cfs (25,000 cfs max flow when all bays open) shown as example.

The 1980 MR hydrograph which had one of the longest base flow periods in record from June 1980 to February 1981 (7.5 months) was selected for modeling. Initial testing with the 2018 hydrograph which had one of the shorted base flow periods no significant deposition. The boundary conditions for the 1980 hydrograph are discussed in the Channel Flushing section in Chapter 6. Figure 11.10 shows the model results of deposition at the end of the base flow period. The first run with Gate 1 open 15 ft throughout the hydrograph produced deposition of 4.5-6 ft in the closed bays in front and behind the gate, with the deposition in front of the gate being somewhat larger than behind. When the gates are cycled monthly the deposition is seen to reduce significantly to about 1-2.5 ft and can mean an alternative approach to minimize deposition within the U-Frame. The model run where all the gates were kept at 5 ft open shows no deposition within the intake and is therefore the recommended approach given that this only requires setting the gate once to this setting, until the gates are needed to be closed due to emergency or reverse flow prevention.

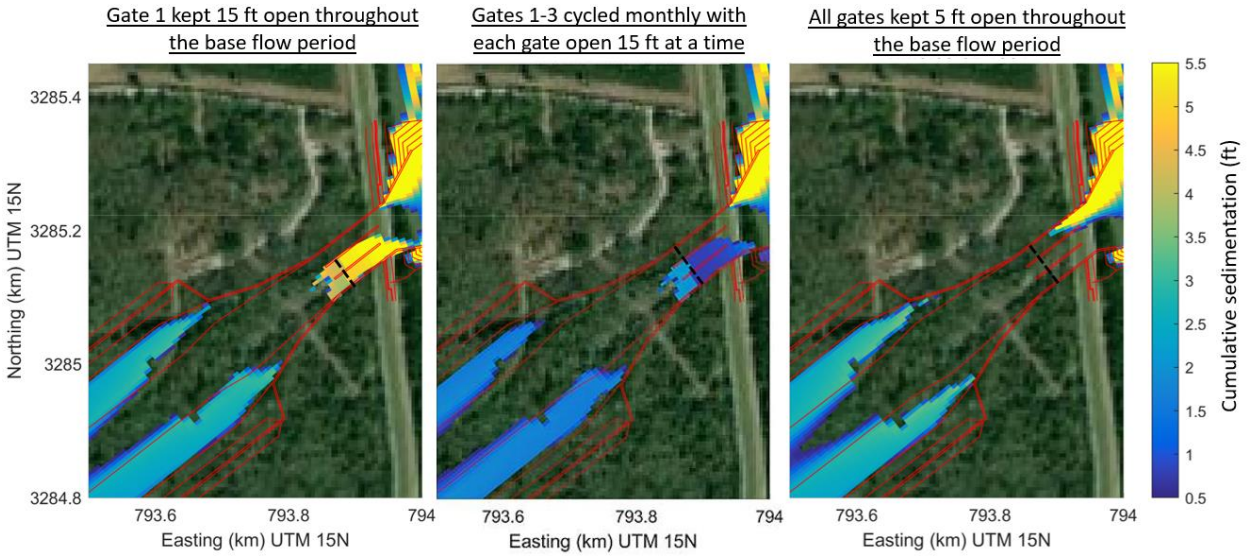

Figure 11.10. Deposition within the U-Frame during partial gate closure and base flow operations (MR<450,000 cfs).

11.3 High Flow (MR>900,000 cfs) Operations

Between 450,000 cfs MR flow and around 900,000 cfs, the diversion will remain fully open. Above 900,000 cfs the diversion flow is likely to exceed 75,000 cfs daily flows. Tidal

influences are not dominant at these flows and there is much less scatter in the diverted flow (less than 8,000 cfs) at these high flow ranges. One or more of the diversion gates will need to partially closed to restrict flow below 75,000 cfs. Gate 3 in the downstream bay, is the preferred gate for operation at high flow. This is because secondary currents at high flow bring in significant amount of sand and there is more concentration of sand in the upstream bay Gate 1 than the downstream bay. Impeding this sand flow into Gate 1 during high flows can reduce overall SWR. Tests performed to quantify efficiency of gate operations on SWR by closing the upstream or downstream bay partially (15 ft open) at 1.25M cfs, using the FLOW-3D FTNMSDI model revealed that sand SWR reduces by about 3-5% if the upstream bay is operated. On the other hand, there is a 2% increase in SWR if the downstream bay is operation. The partial blockage of the downstream bay actually strengthens the secondary current at the intake slightly and aid in sand intake within the diversion.

Table 11.3: High Flow (MR>1,000,000 cfs) Diversion Gate Model Tests.

Daily MR Flow (cfs)	**Daily Diversion Flow (1:7 Channel, 90% Design) (cfs)**							
	All Gates fully Open	**All Gates 25 ft Open**	**Gate 1 Partially open, all other bays fully open**			**Gate 3 Partially open, all other bays fully open**		
--	--	--	20 ft Open	15 ft Open	10 ft Open	20 ft Open	15 ft Open	10 ft Open
1,000,000	86,000	76,000	75,500	69,500	63,000	74,000	68,400	61,800
1,250,000	100,300	85,500	83,500	75,300	70,600	81,100	74,500	68,000

Table 11.3 shows the flow capacity at two steady state conditions, 1,000,000 cfs and 1,250,000 cfs MR daily flows with different partial gate closures. Gate 1 and Gate 3 closures were modeled and Gate 3 is preferred based on sediment modeling as described before. The green highlights indicate gate settings that restrict flow below 75,000 cfs. Based on the results it may be recommended to keep Gate 3 (downstream bay) at 20 ft open between say 900,000-1,100,000 cfs and at 15 ft between 1,100,000-1,250,000 cfs MR flow. The actual trigger of gate operations should always be based on real-time data during diversion operations. Note that there can be as much as 2,000-5,000 cfs of inter-daily flow variation due to tidal and wind effects in the basin and the river. As mentioned in the OMRRR manual it is recommended that

the above gate settings be only used as a preliminary guidance due and be verified by real-time data of water level, head difference and discharge readings from gages from the first few years of diversion operations. Further these settings may change in a decade or two as relative sea level rise occurs in the basin coupled with land building that may decrease the flow capacity.

11.4 Average number of days of gate operations at a specific setting

Using the MR hydrograph data from last 57 years (1964-2021), the average number of days each month of the year when the diversion is likely to spend in each gate setting is estimated. Figure 11.11 show the monthly distribution of the average number of days that the diversion is either likely to be closed (MR<300,000 cfs), all gates at 5 ft open (300,000 cfs < MR < 450,000 cfs), fully open (450,000 cfs < MR <900,000 cfs), Gate 3 twenty (20) ft open with other gates fully open (900,000 cfs < MR < 1,100,000 cfs) and Gate 3 fifteen (15) ft open with the other gates fully open (1,100,000 cfs < MR < 1,250,000 cfs). The number of days for each category separating among the operational months (typically January-July) and non-operational (base flow period, typically August-December) based on the bar chart is given below:

- Regular Operational Period (Typically January-July):
  Avg # Days All Gates Fully Open: 116 days (32% of year)
  Avg # Days Gate 3 Partially Closed: 42 days (12% of year)
  Avg # Days All Gates 5 ft Open = 38 days (10% of year)
  Avg # Days All Gates Fully Closed: 17 days (5% of year)
- Base Flow Operational Period (Typically August-December):
  Avg # Days All Gates Fully Open: 25 days (7% of year)
  Avg # Days All Gates 5 ft Open = 45 days (12% of year)
  Avg # Days All Gates Fully Closed= 80 (22% of year)

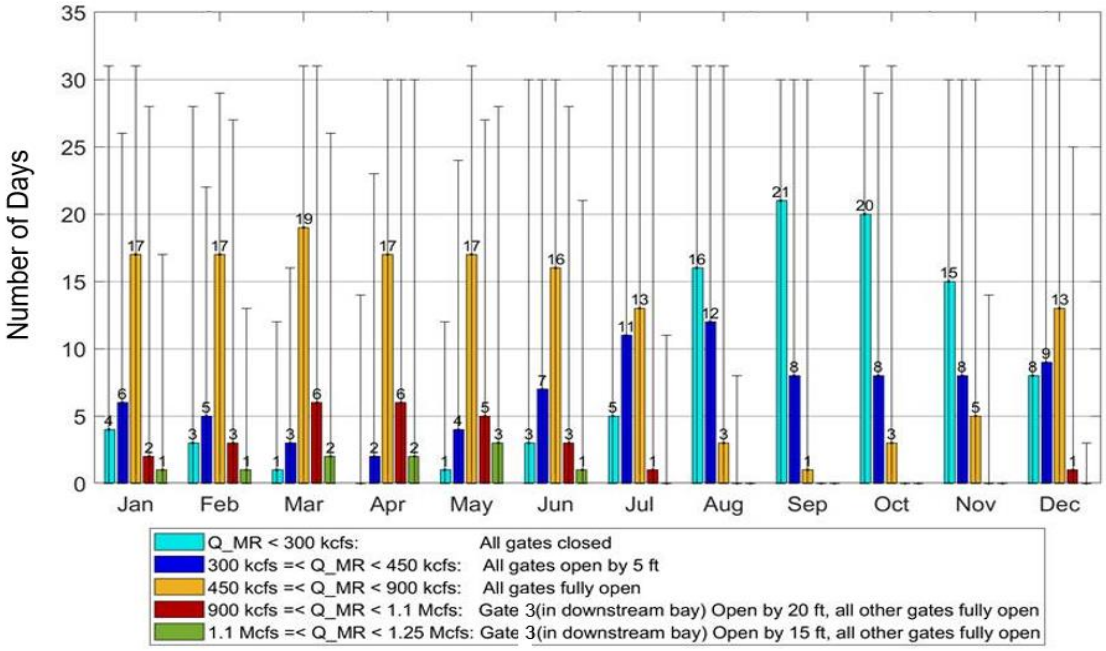

Figure 11.11. Distribution of the average number of days in a given month that the gates are likely to be in a particular position. Based on 57 years (1964-2021) MR hydrograph data and current (2020) conditions.

11.5 Comparison of Diversion Operational Rating Curve with Physical Model results

The physical modeling of the 60% diversion design indicated a higher headloss (about 2.2 ft) in the intake against the numerical model prediction of 1.4 ft at the highest diversion flow 75,000 cfs at 1,000,000 cfs MR flow. The numerical modeling is generally calibrated against FLOW-3D predicted head loss results. The headloss at the lower MR flows (<750,000 cfs) matched well in both physical and numerical models however. This section provides comparison of rating curves between the FLOW-3D and physical model calibrated diversion discharge rating curves as well as shows the updated 1:7 channel design (90%) which is only calibrated with FLOW-3D here. In addition, by extending the modeling to include the full MR hydrograph, these rating curves provide a more comprehensible understanding of the headloss which is not possible from the physical model which only includes the headworks and is not a head driven model but works by pumping a defined flow out which may or may not be in reality available at a particular river flow.

The main reason for the additional head loss at higher flows in the physical model was determined to be form drag from the headworks structures like the U-frame walls. In this numerical modeling exercise the FLOW-3D FTN2Comp and the Delf3D FTN2Comp models were recalibrated to the steady state headloss with and without partial gate closures with the physical model head loss and then run to provide updated estimates of diversion flow and MR flow rating curves.

The calibration for the additional drag at the headworks involved putting porous planes with a calibrated quadratic drag friction factor within the U-Frame wall portions for the case without gate structures. For the runs with gate structures, no additional porous planes were required and gates were added directly to the model with the porous planes. For the Delft3D model, similarly porous plates placed in the intake U-Frame simulated quadratic drag in the model. The quadratic coefficients were calibrated through a series of runs until the headloss within the intake matched the physical model results. The Delft3D FTN2Comp model was then extended to the FTNOMBA domain and the setup used to model a full hydrograph (2008) where flow varied from about 400,000 cfs to 1,250,000 cfs in the MR. Rating curves were generated by plotting daily diversion discharge and river discharge. Note that the physical model results are valid for the previous 1:4 intake as the update to 90% 1:7 channel was not made to the physical model. Hence the rating curves shown in Figure 11.12 use the 1:4 channel model for all runs except the latest 90% numerical model results (shown as solid circles) which is only calibrated with FLOW-3D. There were other gate models done in the physical model, like partially closing all gates keeping one gate closed at a time. However, the headloss from those models all exceeded the maximum head loss actually needed to reduce the no-gate diversion flows down to 75,000 cs and therefore those tests were not of important for comparison across models as far as operations modeling at high flows is concerned. In other words, even closing one gate fully even with other gates completely open was found to induce enough reduction in discharge (>25,000 cfs) so that only one partial gate closure was found to be sufficient at high flow operations as shown also before in tests shown in Section 11.3 before.

Figure 11.12 shows the comparison of diversion flow and MR flow (Q-Q) rating curves for the various model runs. As was mentioned before, the physical model calibrated numerical

model rating curve (dashed red line) diverges from the FLOW-3D calibrated numerical model rating curve (solid orange line) mostly above 750,000 cfs. At 1,000,000 cfs the predicted discharge from the numerical model that is calibrated with the physical model calibration is about 72,000 cfs while the same for FLOW-3D calibrated numerical model is about 80,000 cfs or a difference of about 11%. In terms of the trigger for gate operations at the high flows, this translates to the fact that while for the numerical model calibrated with FLOW-3D the diversion gates are required to be partially closed at about 920,000 cfs the same trigger for the model calibrated with the physical model is 1,080,000 cfs and means that for the latter case a lesser duration of operation of the gates may be necessary each year. For the model runs considering gate operations, only the 25 ft all gates open scenario is sufficient at high flow operations to limit the flow between 1,080,000-1,250,000 cfs MR flows.

The 1:7 channel design (90%) model results are also shown as solid grey circles and indicate the higher flow capacity available. Though no direct physical model was conducted using this updated design, considering the fact the 90% design has about 10% improved performance (88,000 cfs at 1,000,000 cfs against 80,000 cfs at 1,000,000 cfs) over the 60% design, primarily due to reduction in headloss in the channel and the transition, the 90% design may actually negate some of the reduction of performance perceived if the physical model results are deemed to be closer to the real-world performance. Thus the 90% design is an overall improvement and builds additional capacity over the 60% to reduce some of the discharge prediction uncertainty from different models.

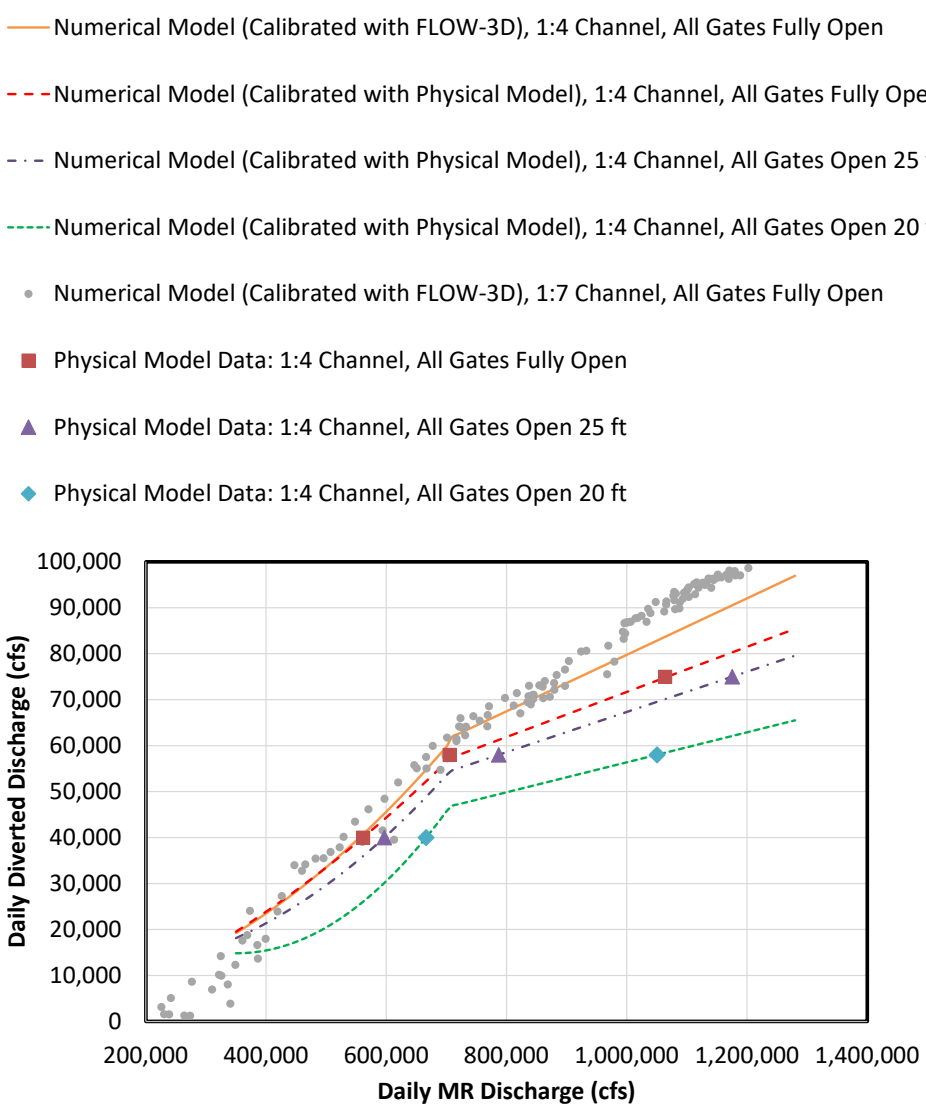

Figure 11.12. Distribution of the average number of days in a given month that the gates are likely to be in a particular position.

11.6 Channel Flushing Effects on Barataria Bay Salinity (MR<450,000 cfs)

Channel flushing was determined to be a necessary operational tool during the base flow period when MR<450,000 cfs as was described in detail in Chapter 6. Channel flushing may be defined as occasional periods, typically lasting a week or two when the average daily diverted discharge exceeds the maximum 5,000 cfs base flow during the period when MR<450,000 cfs. This may be affected by opening the gates fully when head difference is favorable to drive the necessary discharge. In this section the effects on Barataria Bay salinity due to channel flushing

are discussed through coupled flow and salinity modeling using the FTNOMBA model. The calibrated and validated model from the FTNOMLV-CONSOL salinity modeling (Chapter 10) is used for this task.

The modeling simulates about 6 months (June 25, 2020-December 24-2020) basin conditions (Gulf of Mexico water level and salinity boundaries). The MR hydrograph used is however the 1968 historical hydrograph from the Yr 1 (2020) FTNOMLV-CONSOL 50 yr run as in Chapter 10. The reason for selecting the 2020 basin condition is to retain current conditions in the modeling while the 1968 hydrograph simulated a representative historical hydrograph that shows the typical long non-operational periods during base flow months of September-November. Based on the river and basin condition, in reality two flushing periods were available during the modeled period:

Flushing 1: 10 days (08/14-08/24, all gates opened fully when >5,000 cfs diversion flow was expected to be available, max diversion flow reached ~7,200 cfs)

Flushing 2: 23 days (11/28-12/25), all gates opened fully when >5,0000 cfs diversion flow was expected to be available, max diversion flow reached 31,000 cfs. This period also contained a 7-day period (12/07-12/14) when the MR flow>450,000 cfs and the gates were fully opened for all the modeled scenarios except the no-diversion scenario.

The scenarios modeled were as follows:

i. Constant Diversion flow of 5,000 cfs when MR below 450,000 cfs with No Flushing (Not a Head-driven Model)

ii. Maximum Diversion flow of 5,000 cfs (gates remain partially closed to limit flow to 5,000 cfs) with the *diversion closed when MR below 300,000 cfs* (the typical threshold below which intra-daily reverse flow is possible) with No flushing. (A Head-driven Model).

iii. Maximum Diversion flow of 5,000 cfs (gates remain partially closed to limit flow to 5,000 cfs or below) with *diversion closed when MR below ~225,000 cfs* (the typical threshold below which the flow is predominantly from basin to river or inter-daily reverse flow is possible) with Flushing. (A Head-driven Model).

iv. No diversion scenario: There is no diversion flow.

Davis Pond and Gulf Intra-coastal Waterway (GIWW) are only two freshwater sources into the basin apart for the MBSD. The detailed boundary conditions for the two sources are

presented in Chapter 10. In addition to the above modeling another scenario with the no diversion scenario was conducted where no Davis Pond operations was modeled. This scenario investigated the effect of normal Davis Pond operations on the background salinity in the Barataria basin.

Figures 11.13 to 11.16 shows the change in salinity in the Barataria basin under the various operational scenarios at one CRMS and the three USGS stations. The figures show the general salinity ranges within the four principal areas in the basin, near the diversion delta building zone (CRMS 0225), border of the mid and lower basin (Barataria Wwy S Lafitte) and lower basin (Barataria N Grand Isle and Grand Isle). It is seen that the 5,000 cfs constant base flow scenario as assumed by the EIS modeling by CPRA significantly underestimates the salinity in the basin. In reality, since the river water levels actually regulate when diversion gates can be opened and even if opened how much flow can be diverted based on available head difference, the diversion remains closed for a fairly long period for all the model scenarios. Also, when open, the diversion reaches 5,000 cfs only for a few weeks within the 6-month period.

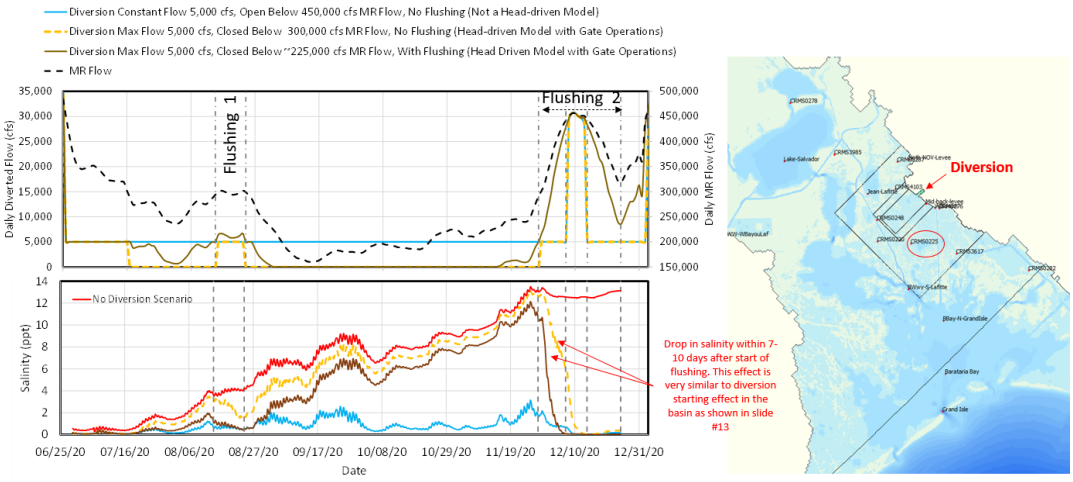

Figure 11.13. CRMS 0225: Top panel shows the diversion and MR flows, flushing periods and the three operational scenarios modeled. Bottom panel shows the salinity variation in the basin for the different scenarios. Map on the right shows the gage location.

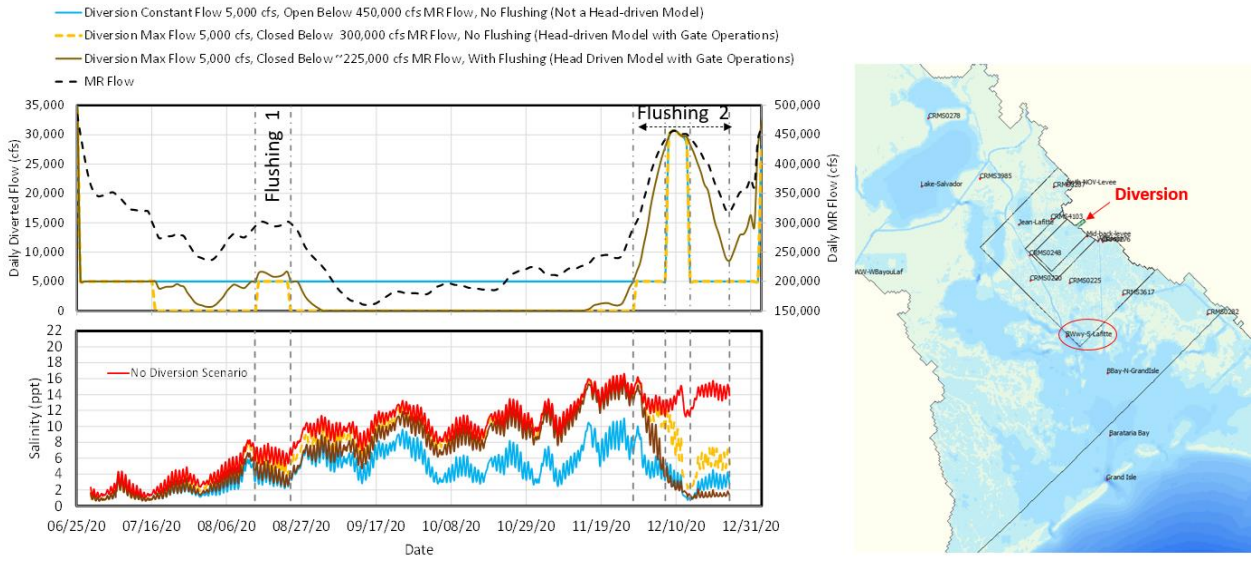

Figure 11.14. Barataria Wwy S Lafitte: Top panel shows the diversion and MR flows, flushing periods and the three operational scenarios modeled. Bottom panel shows the salinity variation in the basin for the different scenarios. Map on the right shows the gate location.

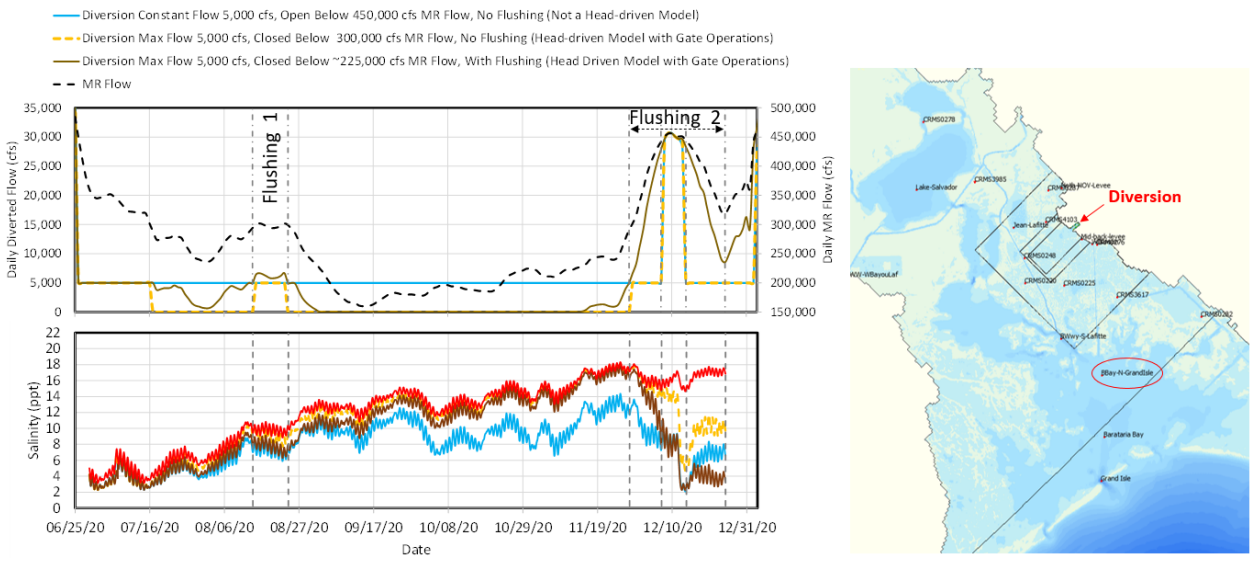

Figure 11.15. Barataria N of Grand Isle: Top panel shows the diversion and MR flows, flushing periods and the three operational scenarios modeled. Bottom panel shows the salinity variation in the basin for the different scenarios. Map on the right shows the gate location.

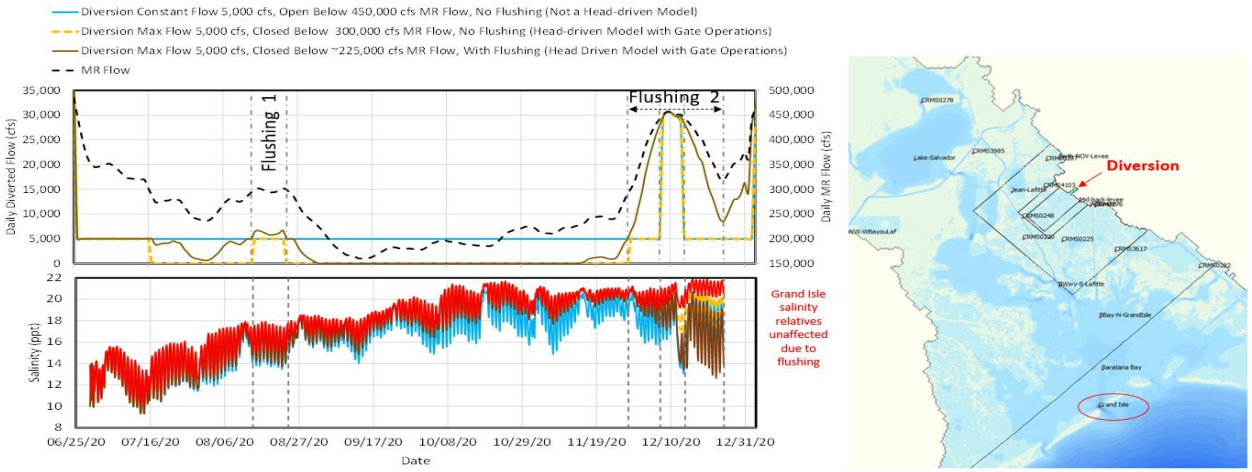

Figure 11.16. Grand Isle: Top panel shows the diversion and MR flows, flushing periods and the three operational scenarios modeled. Bottom panel shows the salinity variation in the basin for the different scenarios. Map on the right shows the gate location.

The channel flushing events are associated by quick drop in salinity with the rate and magnitude of decrease depending upon the peak flow and duration of flushing. For the first flushing event, which reached a peak of only 7,200 cfs and lasted for 10 days only, the salinity drop was insignificant due to flushing operations (<1 at most locations) compared to the regular base flow operations at 5,000 cfs max (head drive model). On the other hand, the second flushing event which reached a peak of over 30,000 cfs, lasted for about three weeks and also included a short full gate opening, the salinity dropped from 12 ppt to about 1 ppt (CRMS 0225) within 7-10 days, 13 to about 1 ppt (Barataria Wwy S Lafitte) within 12 days, 15 to 3 ppt (Barataria N of Grand Isle) in 13 days and 20 to 15 ppt in about 15 days (Grand Isle). The scenario with flushing and regular opening showed an even smaller duration of 5 days (CRMS 0225), 8 days (Barataria Wwy S Lafitte) and 10 days (Barataria N Grand Isle). There is relatively less effect at Grand Isle due to flushing for most of the scenarios. Further daily tidal fluctuations cause much more salinity differences at the Grand Isle location compared to the differences due to the diversion flushing operations. The steep decline in salinity and associated freshening of the middle and lower bay due to channel flushing, particularly when flows exceed 25,000 cfs represent very closely the regular diversion opening operations actually as is shown later in Figure 11.18. Since flushing flows above 25,000 cfs may not be always required, if such steep declines in salinity is undesired, the flushing could be limited to 25,000 cfs peak flows.

Figure 11.17 shows under no MBSD diversions scenario, the relative effect of Davis Pond operations on salinity variation within the basin, particularly near the diversion outfall and north near the Davis Pond outlet. This modeling demonstrates the relatively minor influence of Davis Pond freshwater benefits at the MBSD influence zone where land-building is most active. Davis Pond has a much greater effect on salinity in the upper basin on a percentage basis even though most of the upper basin remains relatively fresh most of the time.

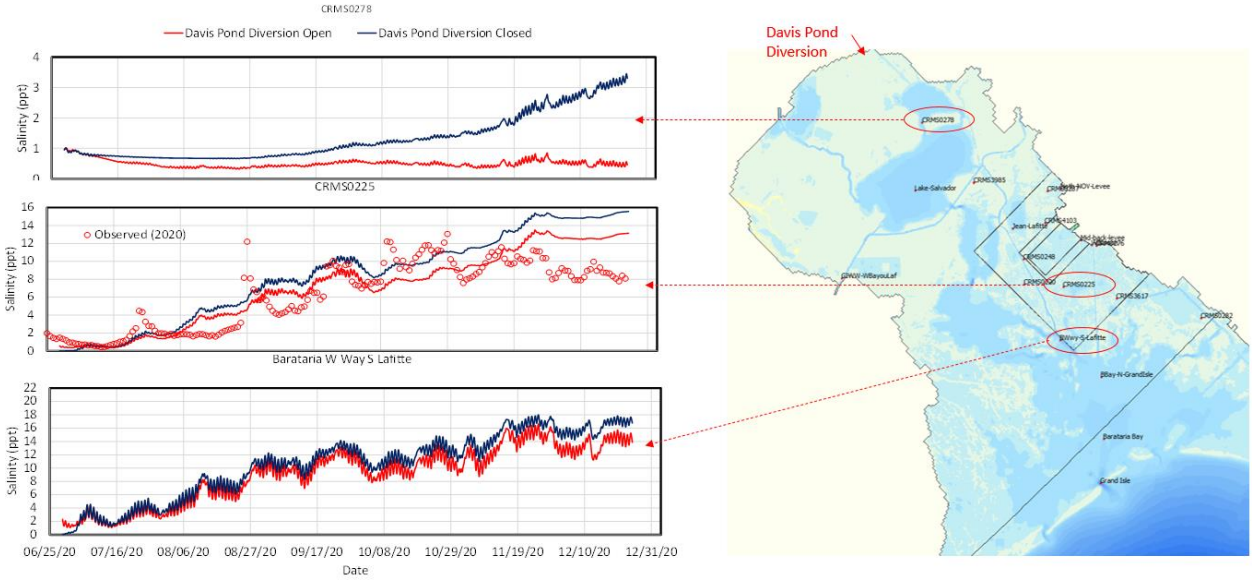

Figure 11.17. MBSD project scenario, effect of Davis Pond operations on Barataria Bay salinity. Top to bottom: CRMS 0278, CRMS 0225 and Barataria Wwy S Lafitte.

11.7 Salinity changes in the Barataria Basin at the start of yearly MBSD operations (MR>450,000cfs)

In this section, the salinity variation, particularly the typical time scales of sharp decline of salinity (freshening) of the mid and lower basin during regular MBSD operation initiation is presented. The model period shown is the Yr 0 (2020) opening of the diversion which simulates the 1968 MR historical hydrograph in the 50-year land building modeling as described in Chapter 10. The initial conditions are yearly averaged (2008-2018) conditions in the basin typical of March and beginning of the year. Figure 11.18 shows hydrograph and diversion flow in the top panel and the salinity change in the basin at the selected locations (shown in map to the right) in the bottom panel. The diversion is opened fully at 450,000 cfs MR flow and as the river

discharge rises to about 800,000 cfs in 5 days, the diversion discharge is seen to also rise quickly from 25,000 cfs to 63,000 cfs within about 5 days of opening. This type of quick rise is common for MR and usually reaches a peak of 900,000-1,000,000 cfs in about two weeks unless interrupted by a fall in between. As seen from model results, the salinity in the basin reduces quickly and most of the mid and lower basin becomes relative fresh (salinity reduces to 3 ppt or lower) in about 5-10 days with the gages near to the diversion outfall freshening quicker. Grand Isle salinity remains unaffected and remains around 7.5 ppt which is close to the mean monthly salinity during this period. Therefore, this exercise demonstrates that channel flushing effects simulated the previous section produces similar or sometimes smaller effects in terms of time to freshening that will happen eventually once the diversion is opened the next year.

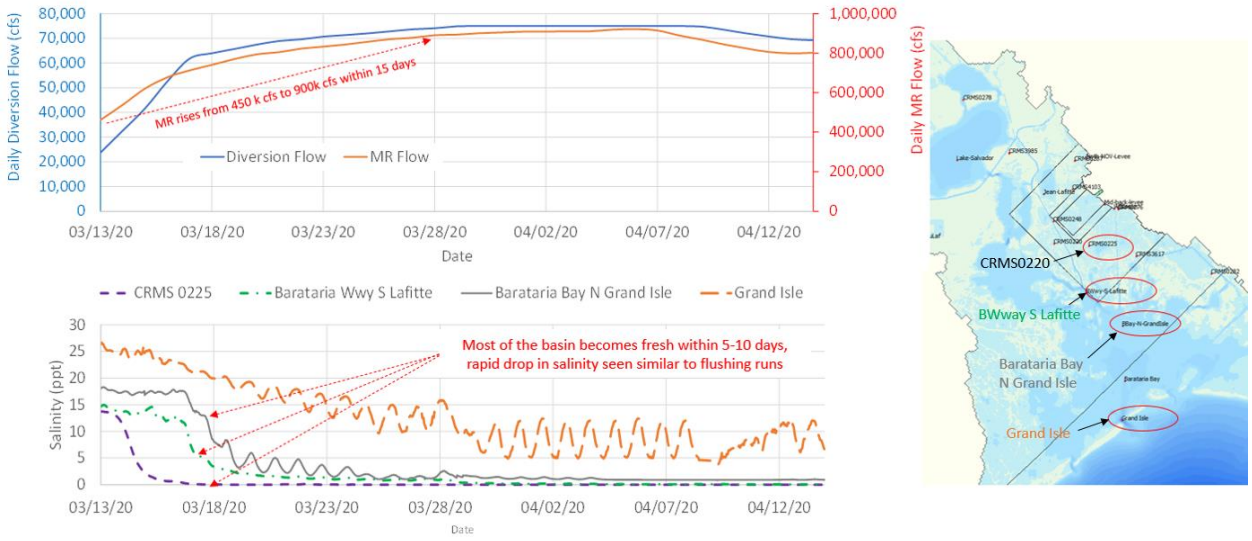

Figure 11.18. Salinity change in basin above MR 450,000 cfs after full diversion operations are initiated for the year. Figure shows typical freshening times and reduction in salinity at various locations north to south in the bay. Map to the right shows the gages.

11.8 With and Without Base Flow Monthly Mean Salinity Changes around MBSD outfall from 50 Yr Model Run

In this section, the monthly averaged salinity distribution in the Barataria basin is presented from the 50-year modeling results of the FTNOMLV-CONSOL modeling described in Chapter 10 and shows the expected change in the conditions with and without base flow assumptions. Figure 11.19 shows the monthly averaged salinity change in the basin due to base

flow operations and is concentrate within the mid-basin area where the diversion freshwater effects are most important for vegetation distribution and sustainability and directly aids in delta building by vegetation accretion. The model results indicate that in general while there is insignificant variation in January-June (period of regular diversion operations when MR>450,000 cfs typically) the base flow effects show a reduction of up to 3 ppt in salinity from without base flow conditions for the months of August-December. Generally, the salinity ranges from 3-10 ppt at the Barataria Wwy S of Lafitte while near the diversion outfall (CRMS stations) the salinity ranges from 1-7 ppt during the base flow period.

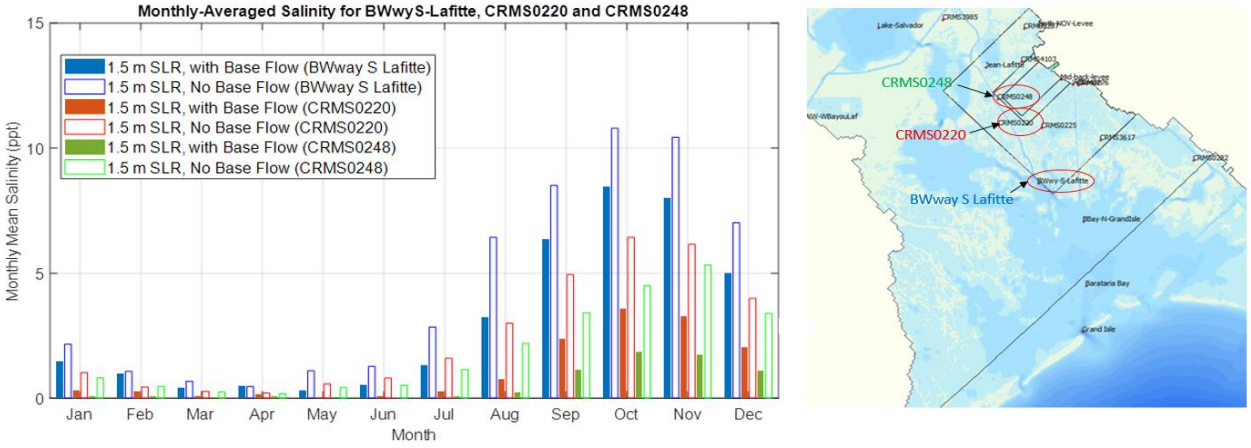

Figure 11.19. Comparison of average monthly salinity over 50 years with and without base flow modeling. All scenarios include MBSD diversion operations.

11.9 Conclusions

In this chapter, the base flow and regular diversion operational modeling design issues, particularly gate settings were discussed and presented. In addition, discharge rating curves from the physical model calibrated numerical models and the 1:7 side-sloped channel (90%) design numerical model were compared. Basin side effects of salinity change due to channel flushing operations, salinity change during the first few weeks of the diversion opening as well as difference in salinity in the basin with and without base flow operations were also quantified. The specific conclusions from this chapter area as follows:

1. Diversion flows during base flow period when MR<450,000 cfs shows significant tidal influence and resulting scatter in rating curve. Daily flows can vary from reverse flow conditions to up to 30,000 cfs in the 225,000<MR<450,000 cfs range.

2. Based on base flow modeling including tidal influence and gate openings tests, Table 11.4 summarizes the various regimes of diversion operations:

Table 11.4. Suggested diversion operation settings at different MR flow regimes.

Daily MR Flow (cfs)	Gate Opening Position			With Gate Operations, Daily Diversion Flow (cfs)	With Gate Operations Representative Daily River WL (at RM 60.7) (ft, NAVD88)	With Gate Operations Representative Daily Basin WL (at Outfall) (ft, NAVD88)
	Gate in Bay1	Gate in Bay2	Gate in Bay3			
< 300,000	Close	Close	Close	0*	< 1.7	N/A
300,000-450,000	5 ft Open	5 ft Open	5 ft Open	≤ 5,000	1.7-3.0	0.5-1.5
450,000-900,000	Open	Open	Open	35,000 - 75,000	3.0-6.5	1.5-3.5
900,000-1,100,000	Open	Open	20 ft Open	≤ 75,000	6.5-8.0	2.5-3.5
1,100,000-1,250,000	Open	Open	15 ft Open	≤ 75,000	8.0-9.5	2.5-3.5

*All Gates closed fully to prevent reverse flow from basin to river. Daily averaged discharges (+- 1,000 cfs) and water levels (+- 0.2 ft) are representative of current (2020) conditions only.

3. Since WL in the basin can vary over a wide range 0.5-3.5 ft due to basin conditions (tidal, meteorological, etc.) which are often independent of river conditions during the typical August-January low flow operations period, it is recommended to use river conditions as initial guide for low flow gate operations. During actual operations, when monitoring gage data will be available, the gate operations (openings and triggers) can be fine-tuned by including dynamic basin water level inputs into the gate operations trigger decision process. The diversion is expected to be closed completely during all hurricanes and tropical storms; this table does not apply for those conditions.
4. Even though other gate combinations can keep flow below 5,000 cfs during base flow periods, the all gates 5 ft open was recommended based on morphology modeling which showed no significant deposition in the U-Frame before and after the gates even after long base flow operations. The small opening creates high enough velocities near the bed to prevent deposition around the gates.
5. At high flows (MR>900,000 cfs), the Gate in Bay 3 (downstream bay) is recommended to be operated as it helps slightly in enhancing sand intake in the upstream-most bay by strengthening the secondary currents at the intake somewhat and does not impede sand delivery to the upstream most bay where generally sand concentrations are higher.
6. On an average, during the January-July operational period the diversion gates are likely to remain open either partially or fully for the majority of the time with only 17 days of full closure. During the August-December, base flow period, the

diversion is likely to remain closed most of the time or about 80 days with 25 days of full open and 45 days of partial opening. These are average based on 57 years of data but can show wide variability year to year based on the actual hydrograph. E.g., the 1980 year which had an extensive base flow period showed 7.5 months of flow less than 450,000 cfs while in a year like 2018-2019 less than 15 days of the year the diversion would have remained in base flow regime.

7. Salinity modeling of different realistic flushing scenarios with a head driven model indicate that the 5,000 cfs constant diversion flow condition modeled in CPRA EIS studies may significantly underpredict the salinity distribution in the basin.
8. Channel flushing operations for peak discharges less than 10,000 cfs and lasting a week or so do not show significant freshening of the basin with salinity reduction less than 1 ppt at most locations. For a higher peak flushing flow exceeding 25,000 cfs and lasting for three weeks, the freshening of the mid and lower basin up to north of Grand Isle occurs within 5-15 days typically with steep decline in salinity from 12-2 ppt. This effect is similar to the first time the diversion opened in any given year when MR reaches 450,000 cfs during January-June period.
9. Davis Pond diversion flow has relatively small impact (<2 ppt) at most locations near the MBSD outfall where the delta building is active.
10. Base flow reduces mean monthly salinity by 2-3 ppt in general across the mid and lower Barataria basin on an average based on 50 years future modeling.

12.0 REFERENCES

Alden. 2020. *Mid-Barataria State Project Number BA-153: Physical Modeling Report*. Technical report by Alden Research Labs to AECOM and CPRA.

Allison, M.A. 2011. *Water and Sediment Surveys of the Mississippi River Channel Conducted at Myrtle Grove and Magnolia in Support of Numerical Modeling (October 2008 to May 2011*. Technical Report to CPRA from WI.

Allison, M.A., Demas, C., Ebersole, B., Kleiss, B., Little, C., Meselhe, E., Powell, N., Pratt, T., Vosburg, B. 2012. *A Water and Sediment Budget for the Lower Mississippi-Atchafalaya River in Flood Years 2008-2010: Implications for Sediment Discharge to the Oceans and Coastal Restoration in Louisiana*. Journal of Hydrology 432-433 pp84-97.

Allison, M.A., Brendan, T. Y., Meselhe, E.A., Marsh, J.K., Kolker, A.S., Ameen, A.D. 2017. *Observational and numerical particle tracking to examine sediment dynamics in a Mississippi River delta diversion*. Est. Coast. Shelf Sc., 194, pp97-108

Allison, M.A., Di Leonardo D.R., Eckland, A.C., Ramatchandirane C., Weathers H.D. 2018. *Mid-Barataria Technical Team Field Data Support*. The Water Institute of the Gulf. Prepared for and funded by the Coastal Protection and Restoration Authority. Baton Rouge, LA.

ARCADIS & WI 2013. *Hydrodynamic and Sediment Transport Modeling using FLOW-3D for Siting and Optimization of the LCA Medium Diversion at White Ditch*. Technical Report to USACE by ARCADIS and The Water Institute at the Gulf.

Ayres, S.K. 2015. *Southwest Pass Outlets Bathymetry and Flow Distribution Assessment*. US Army Corps of Engineers, New Orleans District. MRG&P Report No. 5.

Banda, M.S., Dittrich, A., Pervez, J. 2017. *Morphodynamic modelling of a meandering sand bed river using Delft3D*. In River Sedimentation: Proceedings of the 13th International Symposium on River Sedimentation.

Biedenharn, D.S., Thorne, C.R., and Watson, C.C. 2000. *Recent morphological evolution of the Lower Mississippi River, USA*. Regul. Rivers: Res. Manage. 13, 517–536

Briaud, J.L., Govindasamy, A.V., and Shafii, I. 2017. *Erosion Charts for Selected Geomaterials*. J. of Geotech. and Geoenv. 143(10).

Brown, G. L., Letter, J. V., Heath, R. E., McAdory, R. T., Wehmeyer, L. L., and Gunkel, B. L. 2013. *A Simplified Analytical Investigation of the Riverside Effects of Sediment Diversions,* US Army Corps of Engineers Research and Development Center Coastal and Hydraulics Laboratory Technical Memorandum. ERDC/CHL CHETN-VII-13, Vicksburg, Mississippi.

Bulle, H. 1926. *Untersuchungen ber die Geschiebeableitung bei der Spaltung von Wasserlufen (in German)*. V.D.I Verlag, Berlin, Germany, Tech. Rep.

Chamberlain, E., Törnqvist, T.E., Shen, Z., Mauz, B. and Wallinga, J. (2018). *Anatomy of Mississippi Delta Growth and Its Implications for Coastal Restoration*. Sc. Advances, 4(4)

Coastal Protection and Restoration Authority. 2017. *Louisiana's 2012 Coastal Master Plan | Committed to our Coast*. Baton Rouge, La: Louisiana Legislature.

CPRA. 2020. *Davis Pond Operational Plan 2020.* Louisiana Coastal Protection and Restoration Authority. http://coastal.la.gov/diversion-operations/ Accessed May 20, 2020.

DT. 2018. *Mid-Barataria Sediment Diversion Basis of Design Report submitted to the Coastal Protection and Restoration Authority, Baton Rouge, LA*. AECOM Design Team.

Deltares. 2018. *Delft3D FLOW, User Manual: Simulation of multi-dimensional hydrodynamic flows and transport phenomena, including sediments*. Delft, The Netherlands.

Demissie, H. K., & Bacopoulos, P. 2017. *Parameter estimation of anisotropic Manning's n coefficient for advanced circulation (ADCIRC) modeling of estuarine river currents (lower St. Johns River)*. Journal of Marine Systems, 169, 1-10.

Dutta, S. and Garcia, M.H. 2018. *Nonlinear Distribution of Sediment at River Diversions: Brief History of the Bulle Effect and Its Implications*. J. Hyd. Engg., ASCE, 144 (5).

Engineering ToolBox. 2004. *Manning's Roughness Coefficients*. [online] Available at: https://www.engineeringtoolbox.com/mannings-roughness-d_799.html

Esposito, C., Liang, M., Meselhe, E. 2017. *TO5 Outfall Management Mid-Barataria and Mid-Breton Diversions*. Technical Memo by WI.

FlowScience. 2018. *FLOW-3D v11.2 User Manual*. FlowScience, New Mexico, USA.

Frölke, G. 2016. *Validate results of river bends modeled by Delft3D 4 Suite and D-Flow FM*. Master's Thesis, Faculty of Civil Engineering and Geo sciences Delft University of Technology, the Netherlands.

Gaweesh, A., Meselhe, E. 2016. *Evaluation of Sediment Diversion Design Attributes and Their Impact on the Capture Efficiency*. Journal of Hydraulic Engineering 142 Issue 5

GEC. 2021. *Environmental impact statement for the proposed Mid-Barataria Sediment Diversion project, Plaquemines parish, Louisiana.* Report to USACE.

HDR. 2014. *Mid-Barataria Sediment Diversion Alternative 1, Base Design Report 30% Basis of Design.* Technical Report to CPRA.

Integral. 2020. Mid-Barataria Sediment Diversion Barataria Basin SEDFLUME Interpretive Report. Technical Report by Integral Consulting submitted to AECOM and CPRA.

Jung, H., Messina, F., Moss, L., Baustian, M. Duke-Sylvester, S. and Roberts, H. 2019. *TO51 - Vegetation Model and Integration Framework for The Mid-Breton Outfall Management Model.* Technical Report by WI to CPRA.

Kalkwijk, J.P. Th. and Booij, R. 1986. *Adaptation of secondary flow in nearly-horizontal flow*. Journal of Hydraulic Research, 24:1, pp19-37.

Karadogan, E., Willson, C.S., Berger, C.R. 2009. *Numerical modeling of the Lower Mississippi River-influence of forcings on flow distribution and impact of sea level rise on the system.* In: OCEANS 2009, MTS/IEEE Biloxi-Marine Technology for Our Future: Global and Local Challenges, pp. 1–7.

Kombiadou, K., & Krestenitis, Y. N. 2012. *Fine sediment transport model for riverinfluenced microtidal shelf seas with application to the Thermaikos Gulf (NW Ae-gean Sea*). Continental Shelf Research, 36, 41-62

Kulp, M., Williams S.J., Kindinger, J. 2002. *Latest Quaternary Stratigraphic Framework of the Mississippi River Delta*. Gulf Coast Assoc. Geolog. Soc. Transactions. 52 (2)

Liang, M., Esposito, C., Meselhe E. 2017. *Technical Memorandum Mid-Barataria Invert Elevation and Outfall Channel Configuration.*

Lewis, J. W., G. L. Brown, and S. K. Ayres. 2017. *Investigation of Discharge Measurements of the Lower Mississippi River below Natchez, MS*. Technical Note #3 by USACE.

Lo, E.; Bentley, S.J.; Xu, K. 2014. *Experimental study of cohesive sediment consolidation and resuspension identifies approaches for coastal restoration: Lake Lery, Louisiana*. Geo Mar. Lett. 2014, 34, 499–509

Lopez, J., Henkel, T., Moshogianis, A., Baker, A., Boyd, E., and Hillmann, E.,Baker, D. 2014. *Evolution of Mardi Gras Pass within the Bohemia Spillway of the Mississippi Delta in Southeast Louisiana: March 2012 through December 2013*. Lake Pontchartrain Basin Foundation Technical Report.

Meselhe, E., Georgiou, I., Allison, M. and McCorquodale, J. 2012. *Numerical Modeling of Hydrodynamics and Sediment Transport in Lower Mississippi at a Proposed Delta Building Diversion. Journal of Hydrology*, 472-473, 340-354.

Meselhe, E., Pereira, J., Jung, H.S., Khadka, A., Kazi, S. 2014. *TO-21: Mid-Barataria Sediment Diversion Report.* Technical Report to CPRA.

Meselhe, E.A., Baustian, M.M., Allison, M.A. 2015. *Basin-wide model development for the Louisiana Coastal Area Mississippi River hydrodynamic and delta management study. The Water Institute of the Gulf*. Prepared for and funded by the Coastal Protection and Restoration Authority. Baton Rouge, Louisiana

Meselhe, E., Allison, M. A., Yuill, B., Pereira, J., & Khadka, A. 2015a. *Barataria sediment diversion* (Prepared for and funded by the Coastal Protection and Restoration Authority [CPRA]). Baton Rouge, LA: The Water Institute of the Gulf.

McCorquodale, A., Amini, S., Teran, G., Gurung, T., Kenny, S., Gaweesh, A., Pereira, J. and Meselhe, E. 2016. *Development of a Regional 3-D Model for the Lower Mississippi River*. Joint UNO –WI Technical Report to CPRA.

Meselhe, E.A., Sadid, K.M., Allison, M.A. 2016. *Riverside morphological response to pulsed sediment diversions*. Geomorphology. 270 184–202

Meselhe, E., Sadid, K., Xing, F., Jung, H., Baustian, M. (The Water Institute of the Gulf), Johannes, G.C., Smits, Bas D., Van Maren, S. (Deltares), Sylvester, S.M.D., Visser, J.M. (UL Lafayette). 2016. *Louisiana Coastal Area (LCA), Louisiana Ecosystem Restoration Study Mississippi River Hydrodynamics and Delta Management Study (MRHDMS): Assessment and Analysis of Alternative*. Final Report to the Louisiana Coastal Protection and Restoration Authority in Support of Task Order 36.1 and Task Order 5.

Meselhe, E., Sadid, F., Messina, F., Jung, H. 2017. *Technical Memorandum TO46: Basin-Wide Delft Evaluation of Diversion Operations (Production Runs 11-15)*. Technical memo for CPRA.

Mossa, J., 1996. *Sediment dynamics in the lowermost Mississippi River*. Eng. Geol. 45, 457–479.

Mitchener, H. and Torfs, H. 1996. *Erosion of mud/sand mixtures, Coastal Engineering*, 30 (3-4), pp 319.

Nienhuis, J., Törnqvist, T., Jankowski, K, Fernandes, A., and Keogh, M. 2017. *A new subsidence map for coastal Louisiana.* GSA Today. 27. 58-59. 10.1130/GSATG337GW.1.

Nittrouer, J. A., Allison, M. A., & Campanella, R. 2008. *Bedform Transport Rates for the Lowermost Mississippi River.* Journal of Geophysical Research: Earth Surface, 113(F3).

Nittrouer, J. A., Mohrig, D., Allison, M. A., and A. B. Peyret. 2011. *The Lowermost Mississippi River: A mixed bedrock-alluvial channel*, Sedimentology.

Partheniades, E. 1965. *Erosion and Deposition of Cohesive Soils*. Journal of the Hydraulics Division, ASCE 91 (HY 1): 105–139.

Ramirez, M. T., & Allison, M. A. 2013. S*uspension of Bed Material Over Sand Bars in The Lower Mississippi River and Its Implications for Mississippi Delta Environmental Restoration: Lower Miss River Bed Material Suspension*. Journal of Geophysical Research: Earth Surface, 118(2), 1085–1104.

Rodi, W. 1984. *Turbulence models and their application in Hydraulics, State-of-the-art paper article sur l'etat de connaissance.* IAHR Paper presented by the IAHR-Section on Fundamentals of Division II: Experimental and Mathematical Fluid Dynamics, The Netherlands.

Rijn, L. C. van. 1984a. *Sediment transport, Part I: bed load transport*. Journal of Hydraulic Engineering 110 (10): 1431–1456. 357

Rijn, L. C. van. 1984b. Journal of Hydraulic Engineering 110 (11): 1613–1640. 334, 357

Rijn, L. C. van. 1993. *Principles of Sediment Transport in Rivers, Estuaries and Coastal Seas.* Aqua Publications, The Netherlands.

Rijn, L. C. van. (2020). Literature review of critical bed shear stresses of mud-sand mixtures. Published in www.leovanrijn-sediment.com.

Rijn, L. C. van, D. R. Walstra and M. v. Ormondt. 2004. *Description of TRANSPOR2004 and implementation in Delft3D-ONLINE.* Tech. Rep. Z3748.10, WL | Delft Hydraulics, Delft, The Netherlands. 69, 85, 237, 239

Smagorinsky, J. 1963. *General Circulation Experiments with The Primitive Equations*. Monthly Weather Review, 91(3):99–164, March 1963.

Smerdon, E. T., and R. P. Beasley. (1959). *The Tractive Force Applied to Stability of Open Channels in Cohesive Soils*. Res. Bull. 715, Univ. of MO, Columbia.

TBS. 2019. *MBSD State Project No. BA-153: 2019 River Sediment Sampling Data Collection and Analysis Report*. Technical Report by T. Baker Smith LLC for AECOM and CPRA.

TBS. 2020. *MBSD State Project No. BA-153: 2020 River Sediment Sampling Data Collection and Analysis Report*. Technical Report by T. Baker Smith LLC for AECOM and CPRA.

Torrey, V.H. III, Dunbar, J.B. and Peterson, R. W. 1988. *Retrogressive Failures in Sand Deposits of the Mississippi River, Report 1: Field Investigations, Laboratory Studies and Analysis of the Hypothesized Failure Mechanism*. U.S. Waterways Experiment Station Technical Report GL-88-9 Report 1

Visser, J.M., Duke-Sylvester, S.M., Carter, J. and Broussard III, W.J. *A Computer Model to Forecast Wetland Vegetation Changes Resulting from Restoration and Protection in Coastal Louisiana.* Journal of Coastal Research 67(sp1), 51-59.

Wang, B., and Xu, Y. J. 2018. *Decadal-scale riverbed deformation and sand budget of the last 500 km of the Mississippi River: Insights into natural and river engineering effects on a large alluvial river.* Journal of Geophysical Research: Earth Surface, 123, 874– 890.

Winterwerp, J. C., and W. G. M. van Kesteren. 2004. *Introduction to the Physics of Cohesive Sediments in the Marine Environment*. Dev. Sedimentol., Vol. 56, Elsevier, New York

Winterwerp, J.C. and van Kerstern. 2012. *A Conceptual Framework for Shear Flow–Induced Erosion of Soft Cohesive Sediment Beds*. J. Geophy. Res., 117

Whitehouse, R.J.S., Soulsby, R., Roberts, W. and Mitchener, H.J. 2000. *Dynamics of Estuarine Muds*. Thomas Telford Publications, London, 232p

WI-SLR Memo. 2018. S*ea Level Rise Value Selection for the Mid-Barataria EIS Delft 3D Model Runs*. Technical memo to CPRA from WI.

Wu, C.-Y. and Mossa, J. 2019. *Decadal-Scale Variations of Thalweg Morphology and Riffle–Pool Sequences in Response to Flow Regulation in the Lowermost Mississippi River*. *Water, 11*, 1175

Yuill, B.T., Khadka, A.K., Pereira, J., Allison, M.A., Meselhe, E. 2016. *Morphodynamics of the Erosional Phase of Crevasse-Splay Evolution and Implications for River Sediment Diversion Function*. Geomorphology, 259 (12-69).

APPENDIX B1

West Bay Analogue Modeling as an Analogue for the Outfall Transition Feature of the Mid-Barataria Sediment Diversion

ftn Associates Ltd.
water resources / environmental consultants

APPENDIX B1

WEST BAY ANALOGUE MODELING AS AN ANALOGUE FOR THE OUTFALL TRANSITION FEATURE OF THE MID-BARATARIA SEDIMENT DIVERSION

JUNE 3, 2022

1.0 INTRODUCTION

The West Bay diversion, jointly constructed by the Louisiana Coastal Protection Restoration Authority (CPRA) and the US Army Corps of Engineers (USACE) in 2003 was designed as an uncontrolled lateral diversion channel at an intake invert of -25 ft, NAVD88 cut through the right descending bank of the Mississippi River (MR) at River Mile (RM) 4.7. While originally designed to divert 20,000 cfs at the 50^{th} percentile duration stage of the MR, the diversion intake widened and deepened itself within a period of 10 years. By 2014 the intake was over 650 ft wide with the highest depth being over 90 ft and a maximum diverted discharge reaching close to 60,000 cfs at the highest MR flow (Yuill et al., 2016). This fairly rapid evolution of the West Bay diversion intake and main channel is an expected behavior of the mouth of a crevasse splay and often a precursor to the subsequent delta formation. At the Mid-Barataria Sediment Diversion (MBSD) outfall the flow from the conveyance channel comes out of a non-erodible Outfall Transition Feature (OTF) and can be regarded as the initiation point of the crevasse splay. Therefore, the West Bay morphology evolution can serve as an important validation tool on which the MBSD Outfall Transition Feature morphology modeling methodology can be tested. The knowledge gained from this exercise and the modeling framework developed can be extended to design outfall features and predict crevasse induced morphological changes at other sediment diversion sites as well.

In Chapter 7, the MBSD OTF modeling was discussed in detail. In that section the role of the erosion characteristics of the soil (Critical Shear Stress and Erodibility) on the rate and depth of scour formation was discussed. However, since the MBSD is a proposed structure and no scour data exists at the MBSD side, the need was felt to validate methodology used in MBSD OTF modeling to hindcast the scour at the West Bay site as it was expected that soil properties will be similar.

FTN developed model based on the 2D Delft3D West Bay model grid and bathymetry provided by CPRA (Meselhe et al., 2015). In particular the goals of this work were:

- Review the CPRA provided West Bay model setup and adapt it for hindcasting the scour evolution within the initial (say 4-5 years) of the West Bay opening.

- Develop boundary conditions based on recent peer-reviewed research for continuous hydrograph and morphology runs.
- Validate the hydrodynamics of the model with available data from gages and ADCP backscatter measured velocity.
- Extend the validated hydrodynamic model to simulate the morphological evolution of the intake cut over the first 5 years (2004-2009) after opening and compare with the available data.
- Research any available geotechnical data collected pre-construction and develop erosional characteristics at the West Bay site based on the observed geotechnical data and knowledge gained from soil investigations, SEDflume study and empirical formulations used at the MBSD OTF site.
- Using the same morphology settings as at MBSD, model the cut evolution and compare against observations.

2.0 HYDRODYNAMIC MODEL SETUP

Figure 1 shows the domain extents of the West Bay 2D Delft3D model, henceforth called the FTNWB model. The MR upstream boundary is located just downstream of USACE Venice gage with the MR downstream at the Head of Passes (HOP). The southern boundary at the West Bay receiving area extends close to the NOAA Pilot Station on South West Pass of the MR Bird's Foot Delta. Two USACE gages, one on the MR and the other in the receiving basin are used for calibration/validation.

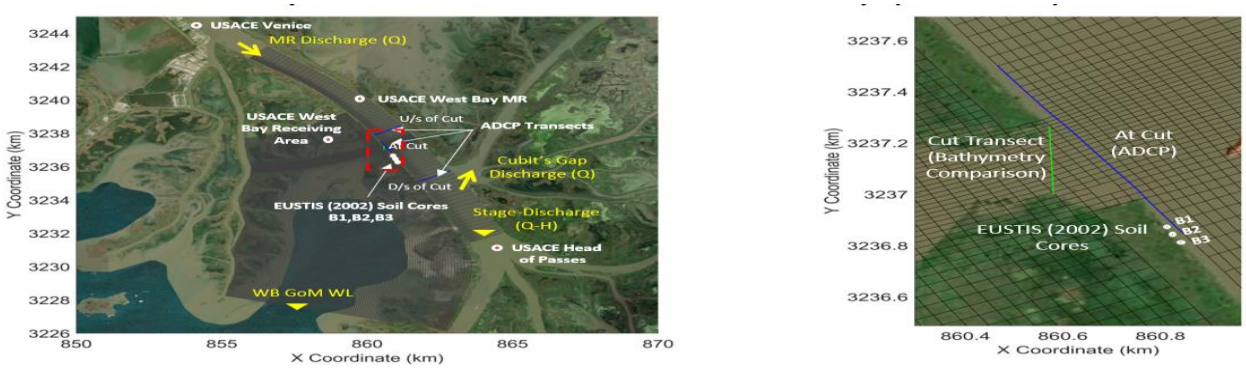

Figure 1. Left panel: West Bay model domain with boundary conditions, and location of USACE gages and pre-construction boring sites. Right panel: Zoomed in view near the intake cut showing the survey cut used for comparison, ADCP cross-section and B1, B2, B3 pre-construction borings from the EUSTIS (2002) geotechnical study used to estimate the erosional properties of the local soil.

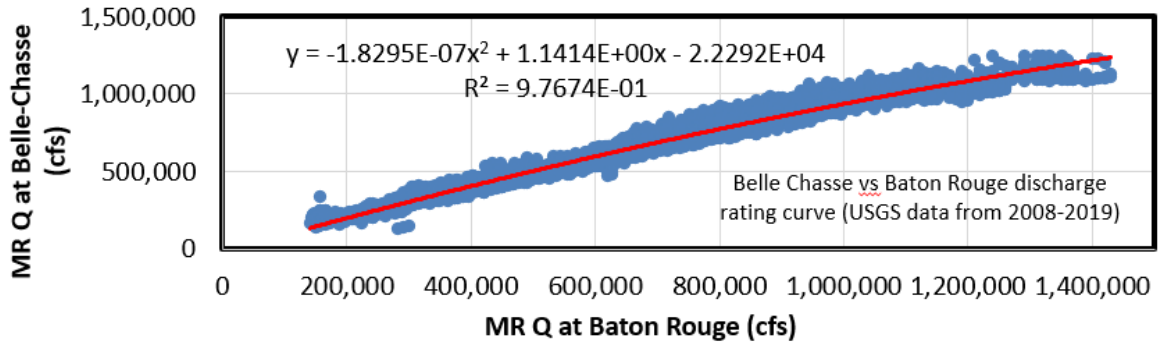

Figure 2. Discharge rating curve relating Baton Rouge (X axis) to Belle Chasse (Y axis) discharge. Best fit is based in 2008-2019 data from USGS gages at the two locations.

The upstream boundary at Venice was set as a discharge boundary specified by a discharge rating curve shown in Equation 1. The curve is based on Allison et al. (2012) corelating the Belle Chasse discharge to the ADCP measured discharge at Venice.

$$Q_{U/s\text{-}Venice}(cfs) = 0.5793*Q_{BelleChasse}(cfs)+38{,}930 \quad \ldots\ldots (1)$$

The Belle Chasse USGS station started reporting discharge data from October 2008 and since the model period (2004-2009) starts from 2004, the discharge prior to October 2008 at Belle chasse in Equation (1) was estimated from discharge at Baton Rouge using another rating curve developed (Figure 2) by correlating the USGS Belle Chasse to the USGS Baton Rouge discharge based on the data from the 2008-2019 period.

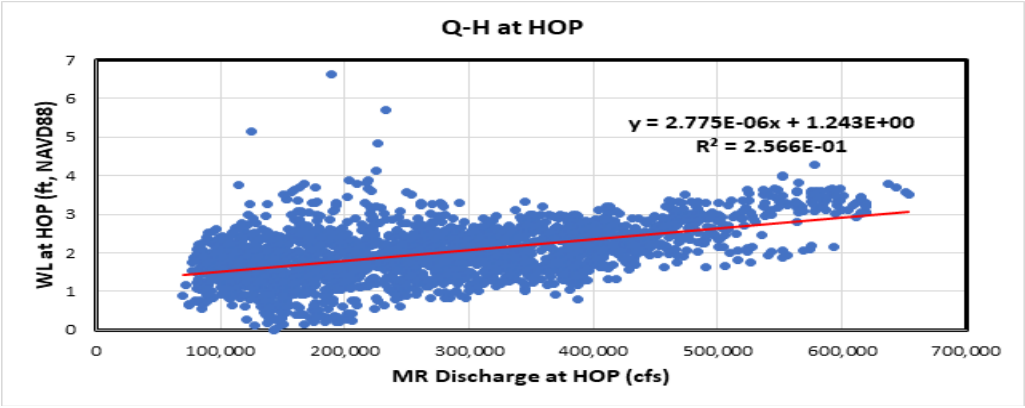

Figure 3. A State-discharge (Q-H) relation developed for the Head of Passes (HOP), the downstream boundary of the FTNWB model.

A stage-discharge (Q-H) relation was developed as shown in Figure 3 at the HOP using observed data from the USACE gage and discharge at HOP to use as a model downstream boundary. Note that using a Q-H boundary removes any tidal induced variation of WL and diversion discharge. This is reasonable for morphology models which are typically accelerated by morphological acceleration factors and devoid of tides. Moreover, this study does not take into account the complex tide driven morphology changes at the intake and instead assumes the changes in the intake morphology are driven by the tidally averaged mean diversion discharge. It is also worth noting that the tidal influence decreases with increasing flow. The range of water level variations at a given river discharge varies from 3 feet at about 100,000-200,000 cfs MR flow to about 1 ft between 500,000-600,000 cfs flows. Since most of the high discharge causing scour is expected to be at the higher MR flows, it is reasonable to assume that tidal flow influences on the diversion discharge for intake evolution is possibly small.

The discharge at HOP in Figure 3 is related to discharge at Belle Chasse using the discharge rating curve of Allison et al. (2012). For the period before October 2008, the Belle Chasse discharge was evaluated from the Baton Rouge discharge using the rating curve in Figure 1.

$$Q_{HoP}\,(cfs) = 0.5362*Q_{BelleChasse}(cfs) - 6{,}233 \quad \ldots\ldots\ldots\ldots\ldots\ldots\ldots\ldots\ldots\ldots \quad (2)$$

The Q-H relation developed and used (Figure 3) is as follows,

$$WL_{HoP}\,(ft) = 2.775\times10^{-6}*Q_{HoP}\,(cfs) + 1.243 \quad \ldots\ldots\ldots\ldots\ldots\ldots\ldots\ldots\ldots\ldots\ldots\ldots \quad (3)$$

The southern Gulf boundary was set from the NOAA Pilot Station daily levels after correcting for gage offset and removing daily and monthly tidal effects.

For the sediment boundary conditions, rating curves (Equations 4 to 6 below) were used based on the ADCP backscatter-based sediment surveys of Allison et al. (2012) and discharge measurements between RM 9.2 to 5.6 in the MR at the West Bay site,

At the upstream, the total load **(**Fines+Sand) is given as

$$\text{Total Load (tonnes/d)} = 0.9072*[-1.767*10^{4} + (7.826*10^{-7}*Q^{1.989}_{U/s\text{-}Venice}(cfs))] \quad \ldots. \quad (4)$$

And the sand load as,

Sand Load (tonnes/d) = $0.9072*[7*\exp[\ 1.433*10^{-5}\ *Q_{U/s\text{-}Venice}(cfs)]$ …… (5)

The 0.9072 factor above is a multiplier to convert US Short Tons (units in Allison et al., 2012) to Metric Tons (tonnes)

The fines load is computed as a difference of Equation (4) and (5),

Fines Load (tonnes/d) = Total Load (tonnes/d) – Sand Load (tonnes/d)

The Fines Load is divided into 75% silt and 25% clay similar to FTNOMBA model for MBSD and the Sand Load is assigned to a single median diameter (d50) of 100 microns in the model based on bed material surveys conducted at the site by Allison et al., (2012) and soil core data collected by EUSTIS (2002) which found bed material d50 to be 92-110 microns.

For the flow through Cubit's gap, discharge and sediment rating curves developed in Allison et al. (2012) were used as follows,

$Q_{Cubit'sGap}$ (cfs) = $0.1319*Q_{BelleChasse}(cfs) - 19{,}939$ ……. (6)

Total Load (tonnes/d) = $0.9072*[-1.434*10^{3} + (4.702*10^{-7}\ *Q^{\ 2.161}{}_{Cubit'sGap}(cfs))]$ …. (7)

Sand Load (tonnes/d) = $0.9072*\exp[\ 6.76*10^{-5}\ *Q_{Cubit'sGap}(cfs)]$ ….. (8)

Fines Load (tonnes/d) = Total Load (tonnes/d) – Sand Load (tonnes/d) … (9)

Sediment loads were converted to cross-sectionally uniform concentration by dividing by the corresponding MR discharge before specifying in the model.

3.0 MODEL CALIBRATION/VALIDATION

The hydrodynamic model calibration and validation periods were January to July 2009 and July to December 2009, respectively. The bathymetry was based on the USACE 2009 surveys. The Chezy roughness coefficient in the river, the intake, the diversion channel and the basin were the primary factors calibrated to improve correlations of water level, cross-sectional velocity distributions in the river and the intake and the discharge through the diversion. Close attention was paid to accurately model the intake velocity distributions and the diversion discharge, the two most important factors that govern the rate of scour and the channel evolution pattern.

Figure 4 shows the distribution of Chezy coefficients finally chosen for the production runs. The river had a spatially uniform constant C=65 $m^{1/2}$/s and the basin a spatially uniform constant C=40 $m^{1/2}$/s. The intake roughness distribution (right panel Figure 5) was further refined to match cross-sectional velocity distributions in the river and along the cut. Initially a uniform C=60 $m^{1/2}$/s was chosen at the intake (yellow region in Figure 5) which matched closely the observed diversion discharge. However, this yielded a more or less cross-sectionally uniform velocity magnitude and a (lower) intake scour depth when run later with the morphology run. Since a 2D model is used which is unable to capture the 3D secondary current effect at the intake, it was decided to vary the Chezy coefficient cross-sectionally across the cut to mimic the increased shear stress at the outer bed of the channel as flow turned into the diversion intake.

Yuill et al., (2016) described West Bay channel lateral migration within the first 5 years where the thalweg moved towards the left (looking downstream of the diversion cut) as shown in Figure 6. This was due to the concentration of the main high velocity core towards the outer bend and subsequent scouring and strong secondary current induced deposition along the inner bend. A 3D model subsequently run with the 2009 bathymetry proved the existence of the strong secondary currents at the intake. Figure 5 left panel shows the turning flow in the diversion intake and validated Yuill et al. (2016)’s findings of a reverse flow zone on the right of the channel cut (looking downstream) due to the curvature of the flow.

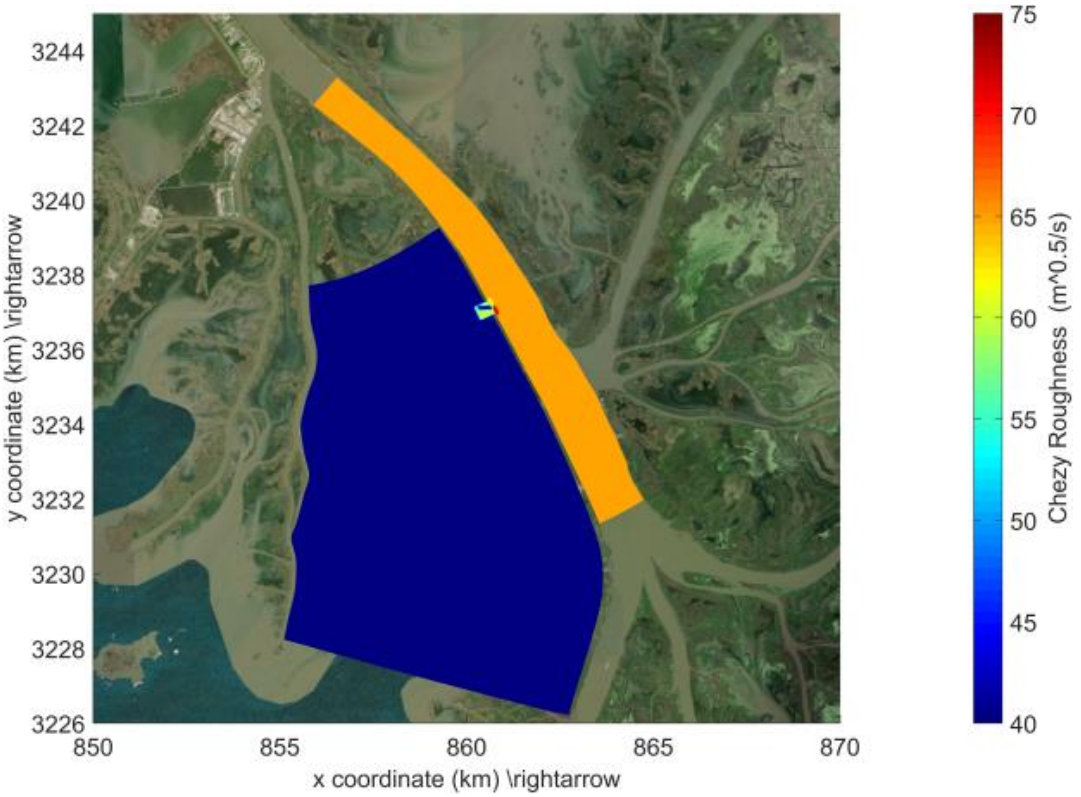

Figure 4. Chezy coefficient distribution used for the morphology production runs.

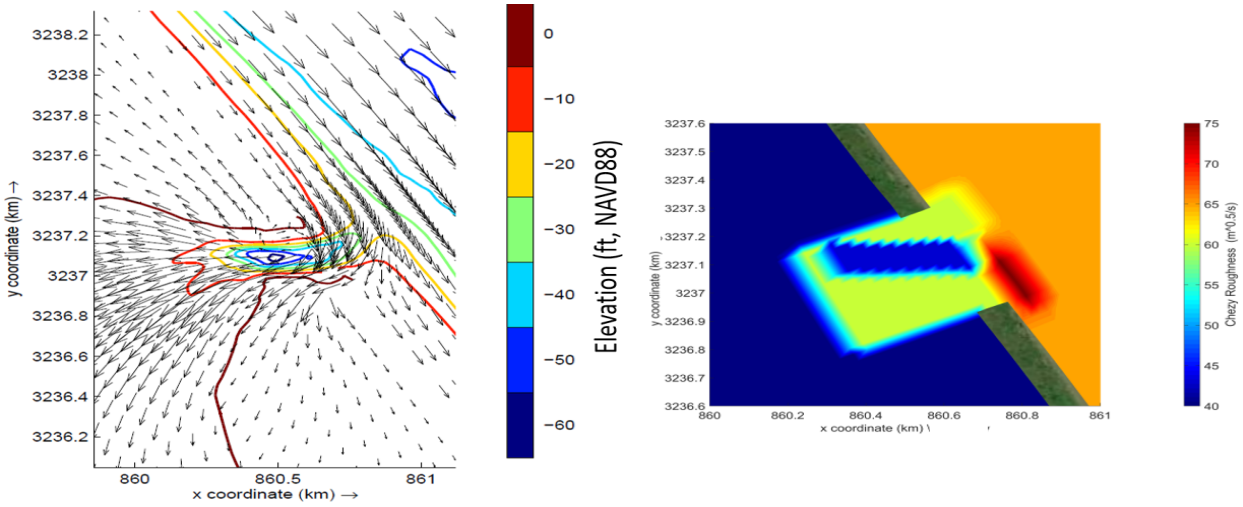

Figure 5. Left panel: Curving flow pattern from the river into the West Bay intake, at the point of highest river stage and flow in 2009, with diversion discharge at approximately 70,000 cfs from the Delft3D 3D model. Right panel: Zoomed in view near the intake in Figure 4 showing local modification of Chezy needed to match the cross-sectional velocity profiles near the intake. The deeper part of the cut is made rougher (C=43 $m^{1/2}/s$), while the intake is smoother (C=60 $m^{1/2}/s$).

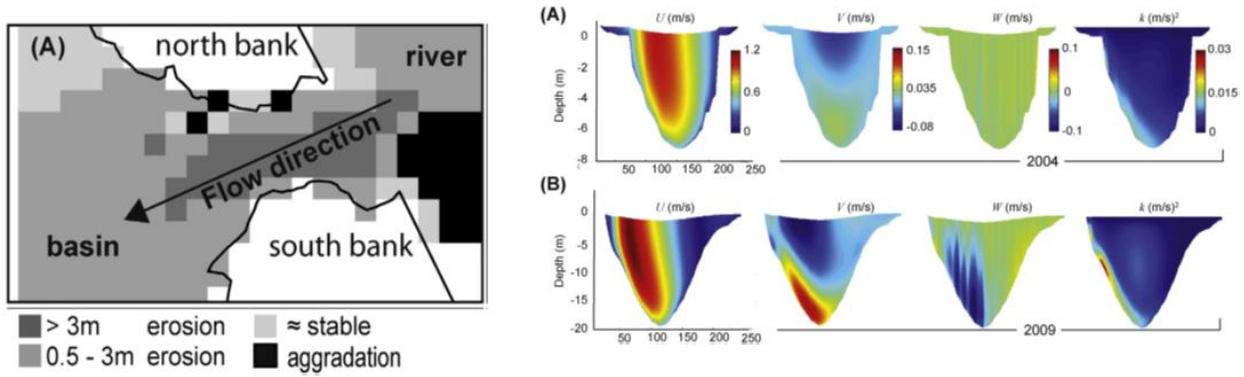

Figure 6. Excerpts from Yuill et al. (2016) showing lateral channel migration from 2004 (right panel (A)) to 2009 (right panel (B)). The figure also shows the evolution of the velocity distribution. Note the concentration of the high velocity core towards the deeper outer bend. The left panel shows the same phenomenon from the observed data in a plan view.

Since the goal of this hydrodynamic model is to drive the morphology runs with a morphological acceleration factor (MorFac), it was decided to calibrate the model with the MorFac factors. Various MorFac values (80, 60, 40, 20 and 10) were tested. It was found that MorFac greater than 20 was too fast for the river hydrograph change to be able to influence water level variations significantly in the basin. Since this is an entirely head driven system and the difference in water level (and hence the phase difference of the hydrograph with respect to the Gulf boundary) drives the diversion discharge, matching the diversion discharge was the key parameter necessary to match the scouring rates and therefore to attain the observed scour depths. Therefore, a MorFac was 20 was used for all hydrodynamic calibration/validation and morphology production runs. Note that the MorFac used for MBSD runs are 40-80 and higher than at West Bay. The higher MorFac is acceptable in case of MBSD as the Gulf boundary in that domain is sufficiently downstream (MBSD is at RM 60.7 vs WB at RM 4.7) that seasonal water level changes in the Gulf do not affect the diversion flow to that extent as at West Bay. Further the Barataria Bay has other intervening flow features, e.g., Barataria Waterway, Wilkinson canal as well as numerous marsh features which have secondary effects on the diversion flow in the nearfield resulting in relative insensitivity of MorFac itself to the diversion discharge.

Figure 7 shows the comparison of water levels observed in the MR (top panel) and at the WB receiving basin (bottom panel). The location of the gages is shown in Figure 1 (left panel).

The observed water levels show Spring and Neap tide signatures which is not reproduced in the model due to reasons stated before. Overall, the model does well in matching the observed water levels.

Figure 8 shows the comparison of the calibrated cross-sectional velocities across the MR and the intake. Two locations, at the diversion cut and immediately downstream are shown. Separately, the WI West Bay model results are also shown for reference. The calibrated FTNWB model results for velocity at the diversion intake and the river are in good agreement with the observed data. The FTNWB model performs better than the WIWB model results at times possibly due to local Chezy refinement which was not done in the WIWB model.

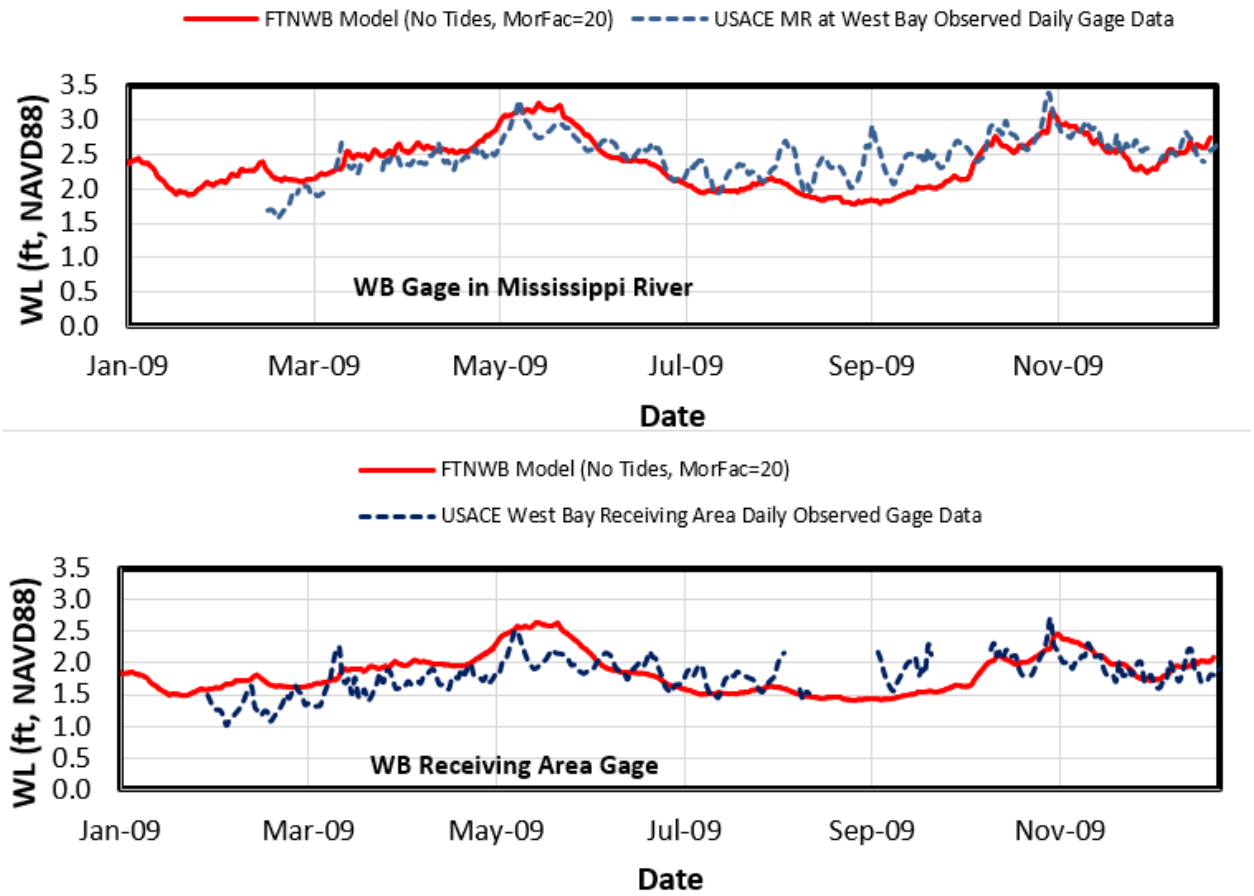

Figure 7. FTNWB 2D Delft3D modeled water level comparisons from the calibration/validation (shown together as continuous time series) for the 2009 year. The top panel shows comparisons in the river and the bottom panel.

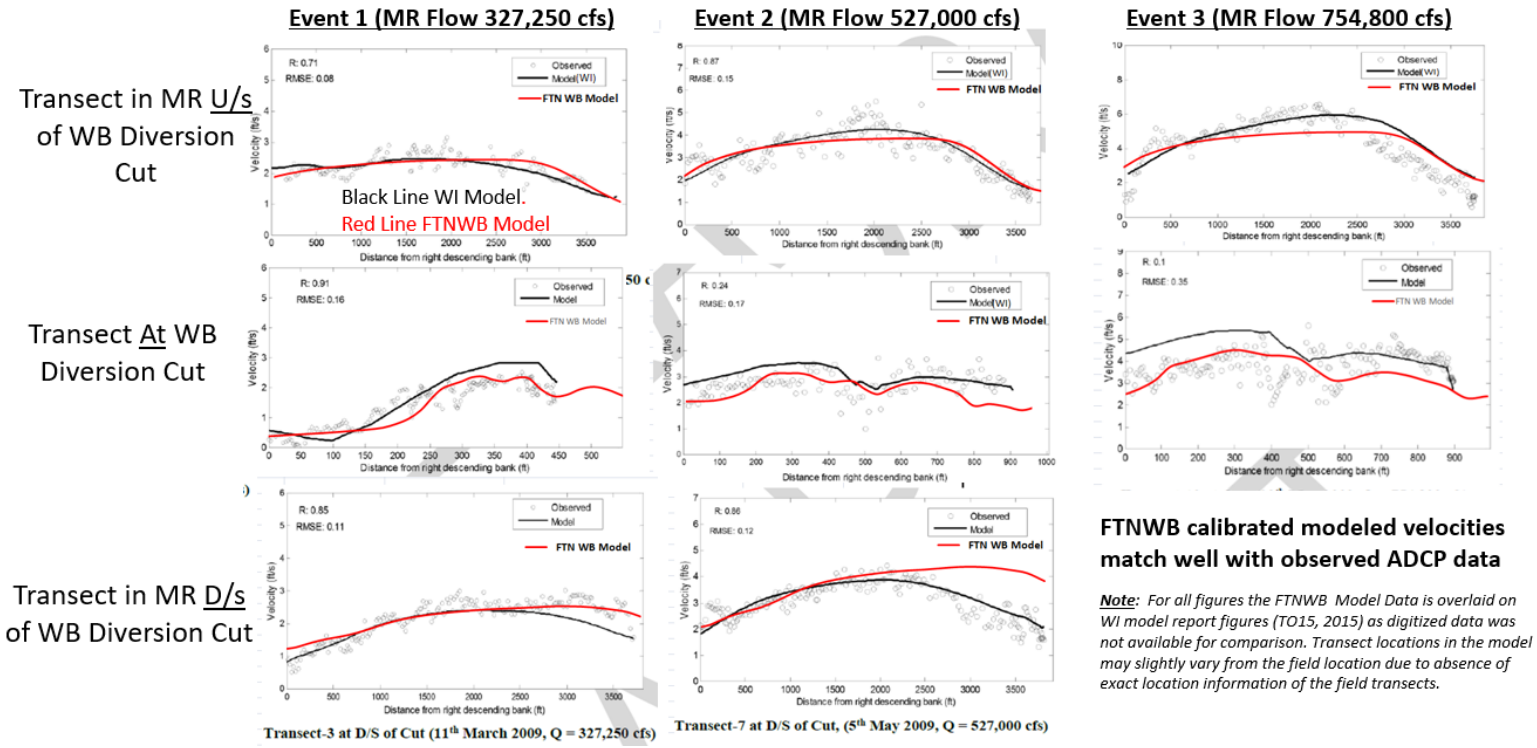

Figure 8. Comparison of cross-sectional profiles in the MR, the WB Diversion Intake and immediately downstream of the WB Diversion Intake. Positive velocities in the river are upstream to downstream while those in the diversion intake are right to left (i.e., upstream to downstream along the diversion flow). Background image with WI WB model data courtesy of Meselhe et al. (2015).

Once the rigid bed hydrodynamic model was calibrated and validated with the 2009 hydrograph, the model was extended to the morphology setup of the MBSD OTF model. The entire 2004-2009 duration was modeled, allowing the intake scour to evolve and modify the discharge through active hydrodynamic feedback. Figure 9 shows the comparison of the West Bay diversion discharge with the observed discharge in the initial period after diversion opening (2004-2006) based on the USACE ADCP based measurements as well as the later period (2009-2010) discharge predictions from Allison et al. (2012)'s rating curve. The model was able to predict fairly well the 2004-2009 period which is the period of interest in the morphology modeling presented in the next section. As will be discussed in the next section, the reason for the underprediction of the discharge in 2009 from that measured by Allison et al. (2012) rating curve is because of somewhat narrower prediction of the scour channel even though the simulated scour depths were in in good agreement with the observations.

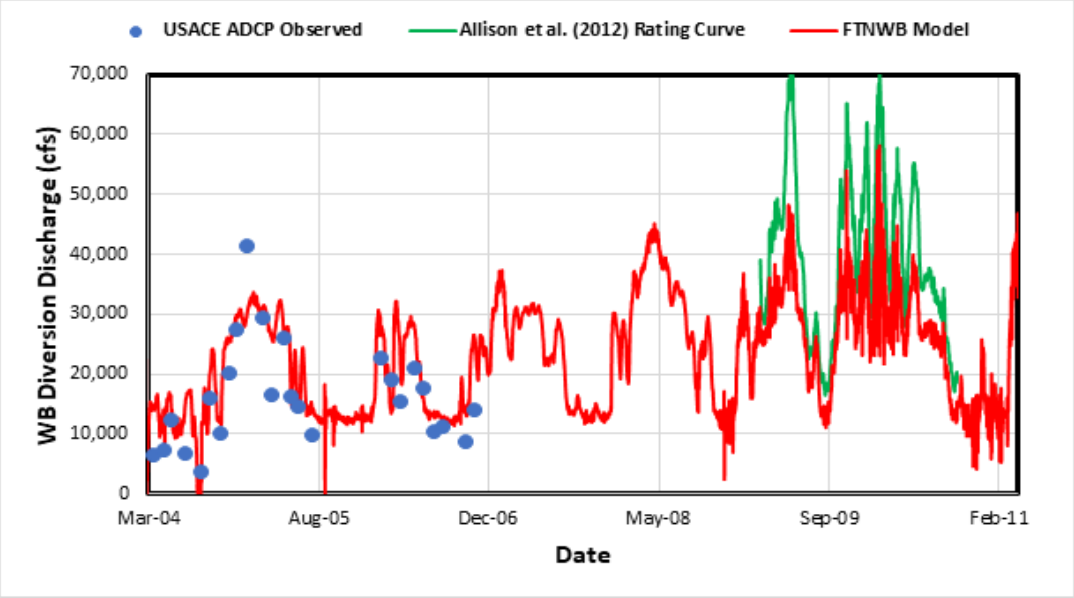

Figure. 9. Comparison of FTNWB modeled discharge with observed USACE (2004-2006) and Allison et al. (2012) rating curve-based data (2009-2010).

4.0 MORPHOLOGY MODEL SETUP

The morphology model was setup as a multi-layer stratigraphic model with spatially uniform thickness but different erosion properties for each layer. The number of pre-construction borings were insufficient to develop a reliable spatially variable stratigraphy. Figure 10 shows the geotechnical description of each layer and the grain size distribution of the constituent sand material from one of the samples. Table 1 shows the median grain size as derived from the Grain Size Distribution (GSD) curves. Based on this information a median grain size (d50) of 100 micron was assigned to the sand portion of the sediment.

Table 1. Median grain size of the collected cores.

Sample	Sample Depth (ft)	D50 (micron)
B1-24	103.5	80
B2-17	60.5	90
B2-34	129.5	94
B3-15	46.5	135
B3-18	59.5	107
B3-22	79.5	79
B3-26	99.5	103

Figure 11 shows the model stratigraphy chosen for the morphology runs. The proportion of silt and 'compact clay' were varied to obtain the desire erosion rate for each layer. This is reasonable because 'compact clay' is likely to be a mixture of fine to medium silt based on USGS classification as clay is often a loose terminology used in geotechnical analysis. The critical shear stress for silt was set as 0.092 Pa similar to that used in FTNOMBA modeling at MBSD outfall. For the compact clay, based on the large scatter in the critical shear was observed from the SEDflume analysis at the MBSD OTF site (Chapter 7) and literature survey of empirical relations, it was decided to test a series of critical shear stress values of 1.5 Pa, 2 Pa, 3 Pa and 4 Pa to examine its impact on the scour depths. The erodibility of both class of sediment was taken as $1x10^{-4}$ $kg/m^2/s$ based on the bulk of fine to medium silt data at MBSD outfall. Note that this value is an order of magnitude higher than the value used at MBSD OTF. This is because at MBSD OTF, only the information the OF samples were used which showed many

intervening layers of coarse to very coarse silt which mostly had erodibility greater than $1x10^{-4}$ kg/ m^2/s. However, at the West Bay site the soil was devoid of coarser silt sizes and a lower erodibility was appropriate.

A summary of the morphology settings used for each layer is presented below.

Silty Clay Layer (0-15 ft): Mixture of Silt (8%) and Compact Clay (92%)

Mixture Erodibility =1E-4 kg/sqm/s

Compact Clay Layer (16-70 ft): Compact Clay (100%)

Tau_cr =1.5, 2.0, 3.0 and 4.0 Pa (4 separate tests). 1.5Pa chosen for final production run.

Erodibility = 1E-4 kg/sqm/s

Sand Layer (71-135 ft):
d50=100 micron
Tau_cr=0.26 Pa (from Shields diagram, computed by Delft3D)
Erodibility = From VanRijn 1993 non-cohesive model, function of bed shear, variable.

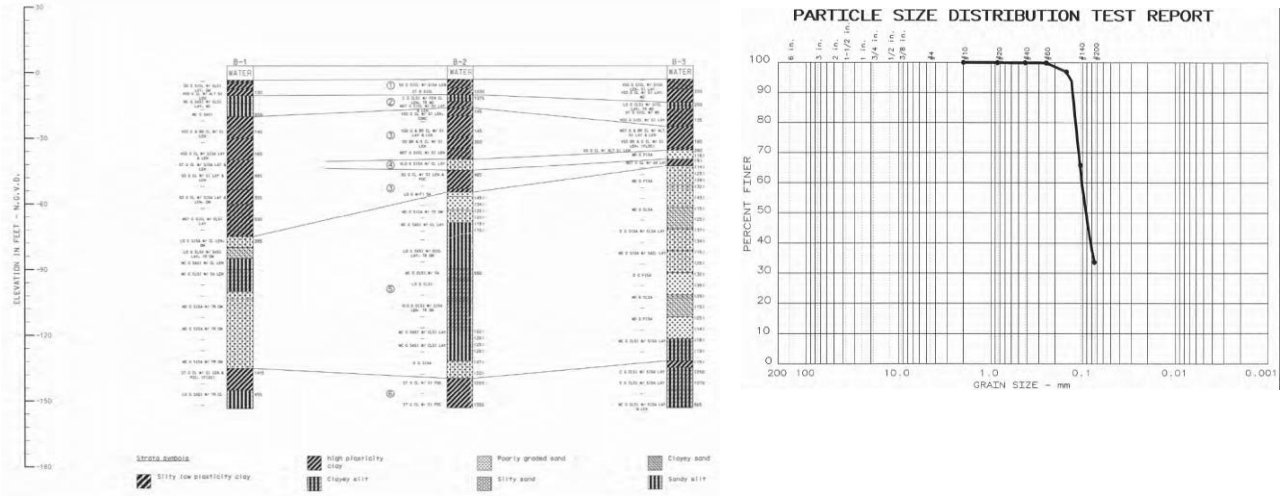

Figure 10. Left: Qualitative layer stratigraphy information from EUSTIS (2002) and Right: An example of grain size distribution of the sand constituents from a sample.

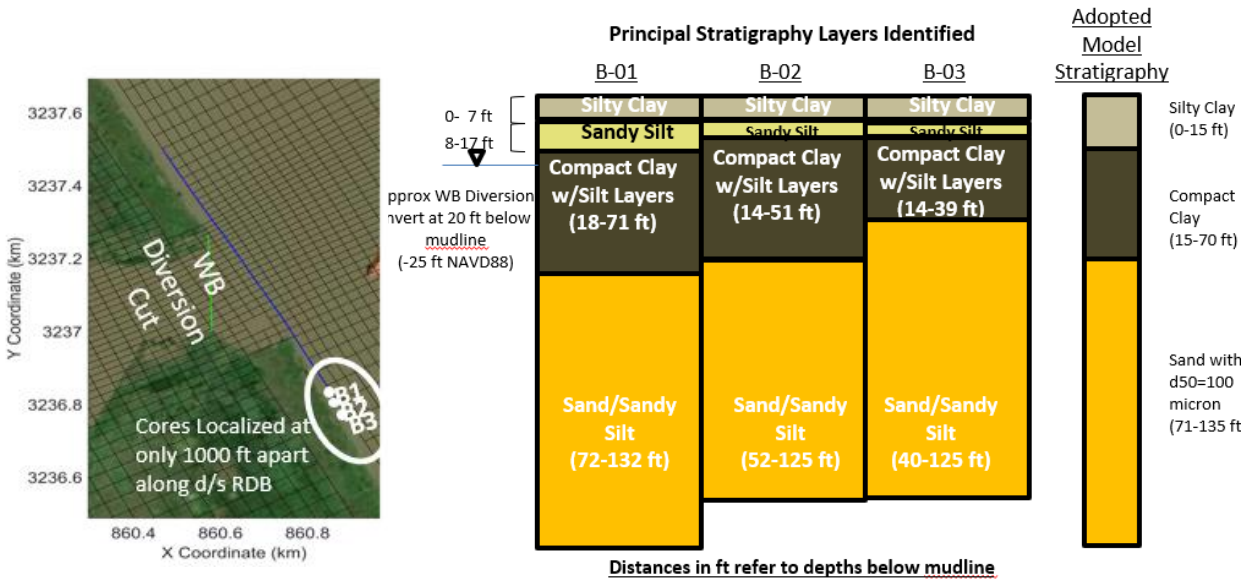

Figure 11. Left Panel: Locations of pre-construction boring sites in EUSTIS (2002) used for soil properties information. Right Panel: Final model stratigraphy adopted based on the layer distributions at the three sites.

5.0 MORPHOLOGY MODEL RESULTS

Figure 12 shows the comparison of modeled and observed scoured bathymetry profiles. Both 2004 (initial) and observed 2009 bathymetries are shown. The 2009 bathymetry results are compared for different choices of critical shear stress for compact clay and shows that scour is predicted only for critical shear stress of 2 Pa or less. For critical shear stress of 3- and 4 Pa results show negligible or no scour at all. The 1.5 Pa was adopted as the final critical shear as that is the same value used for the silty clay at MBSD OTF site.

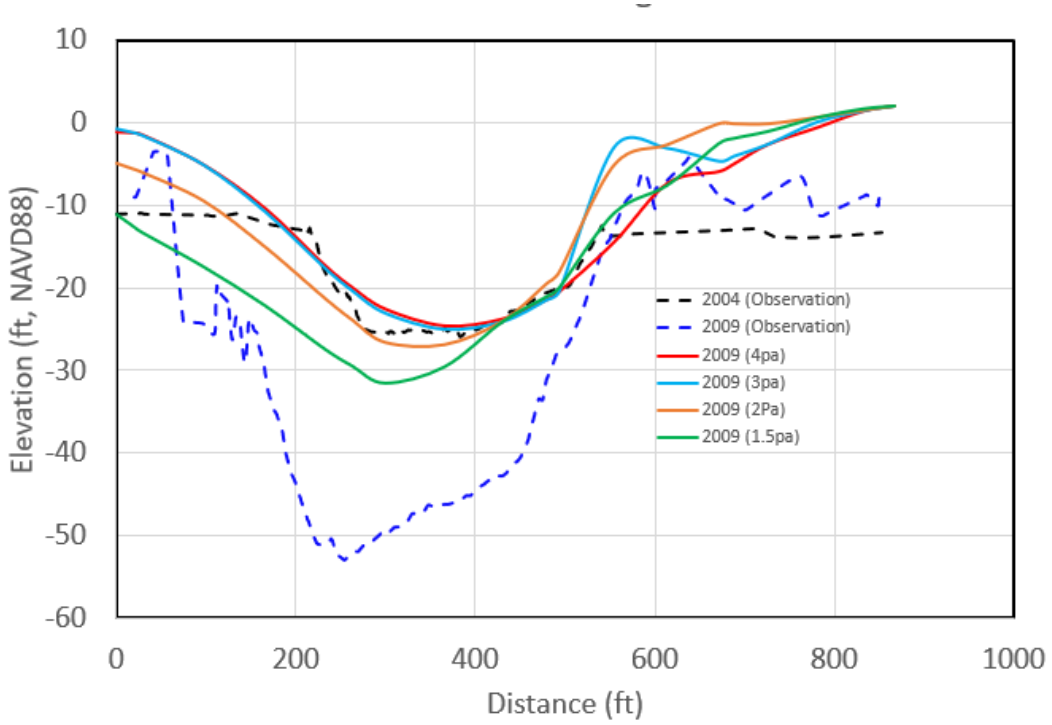

Figure 12. Sensitivity analysis of the model to the critical shear stress of erosion of the 'Compact Clay' layer. The channel cross-section is shown looking downstream. Location shown in Figure 1.

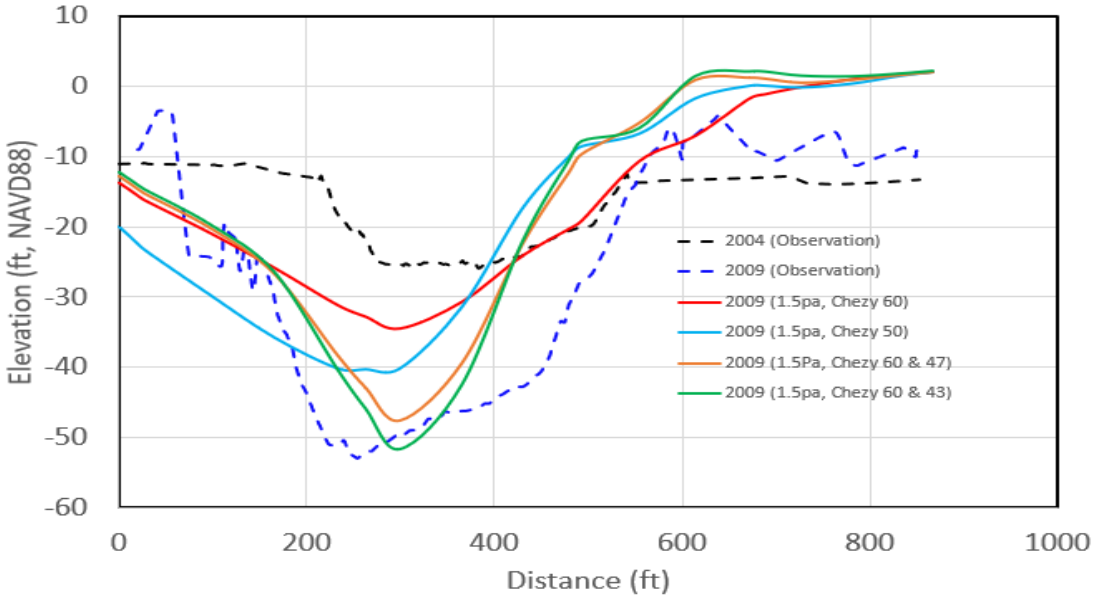

Figure 13. Sensitivity analysis of modeled roughness of the intake channel to the scour evolution. The results from C=60 $m^{1/2}/s$ (smoother shallower zones) and C=43 $m^{1/2}/s$ yielded the best comparison with observed 2009 profile.

As mentioned before in the hydrodynamic calibration/validation section, the initial choice of Chezy roughness of 60 $m^{1/2}/s$ uniform across the intake yielded lower scour depths in 2009 as seen in Figure 13. Since the complex 3D effects at the intake cannot be reproduced at the intake, a cross-sectionally varying Chezy distribution was created where the deeper portions of the cut were assigned a lower (rougher) value. A number of values were tested ranging from 40 to 60. Figure 13 shows that the scour depth is very sensitive to the choice of this coefficient. A value of C=43 $m^{1/2}/s$ for the deeper portion was ultimately found to produce the best match with the observed profile.

Figure 14 shows the comparison of the modeled and observed bathymetries at the cut from the final production run and shows that the model is able to match well the scour depths even though the predicted cut is somewhat narrower. This narrow cut is also the reason why the discharge is predicted somewhat lower in the 2009-2010 period shown previously in Figure 9. Figure 15 shows the plan view of the change in bathymetry from 2004-2009. Further refinement of the roughness in the cut geometry to improve the match with the shape of the cut was not performed to avoid the risk of 'overtuning' the model and deviate from the overall goal of the study of hindcasting the cut depth, which is the most important usually from a design standpoint and not the exact shape of the scour. Instead, this study aims to demonstrate that the scour depths at similar crevasse sites can be reasonably predicted within a possible range if sufficient local soil erosion characteristics can be estimated or available and the hydrodynamic flow effects can be modeled or parametrized relatively accurately through rigorous modeling.

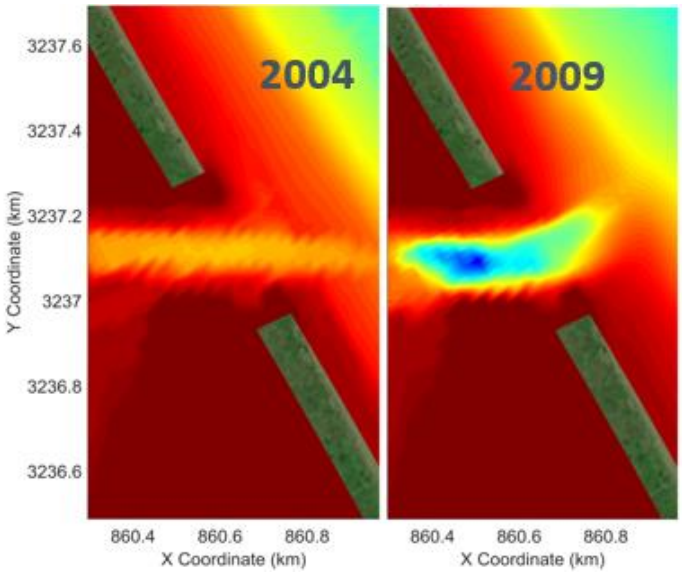

Figure 14. Comparison of modeled and observed scour profiles from the production run. The model reproduces the scour depths well but a slightly narrower profile.

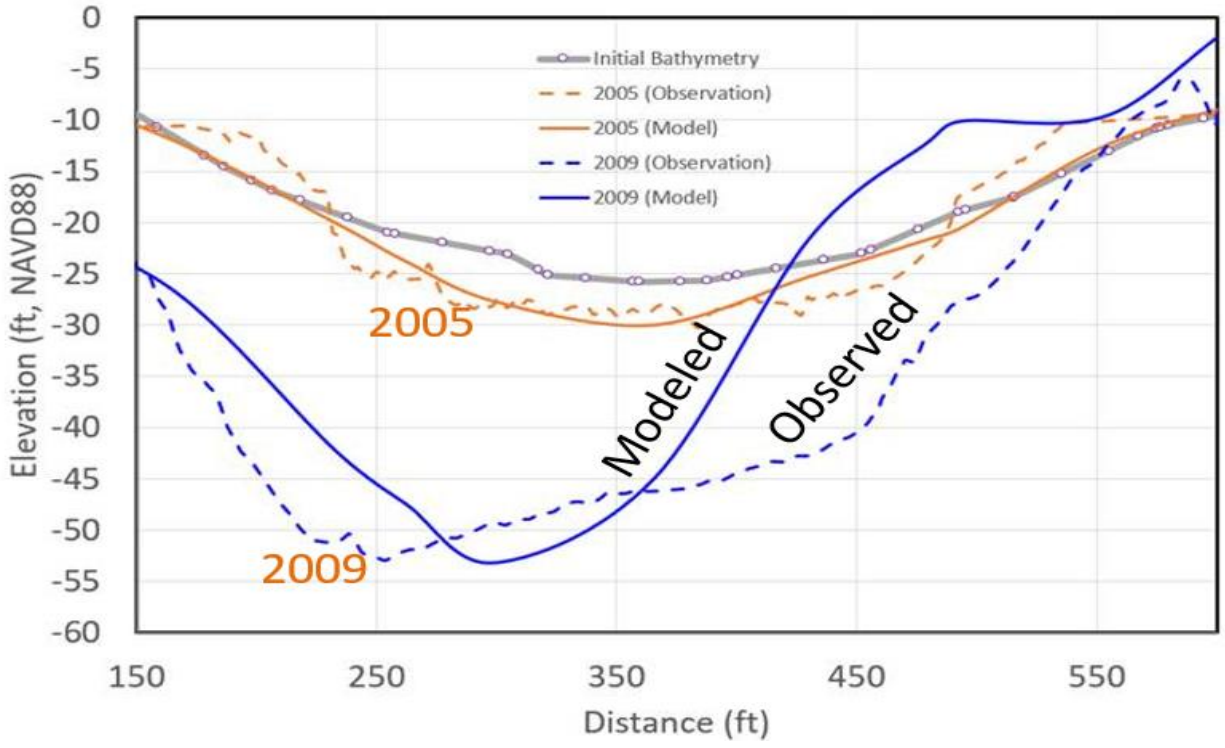

Figure 15. Evolution of West Bay crevasse splay induced intake scour from 2004-2009.

6.0 CONCLUSIONS

A Delft3D 2D Flow-Morphology model (FTNWB) was developed for the West Bay diversion to examine the evolution of the crevasse splay induced intake scour. The model uses similar methodology as the FTNOMBA model developed for the MBSD diversion Outfall modeling and the same morphology parameters. SEDflume studies at the MBSD Outfall were used to guide selection of critical shear stress and erodibility of the underlying stratigraphy layers. In the absence of detailed grain size data for the fine sediment (< 63 micron) at the West Bay site, determination of the critical shear stress was difficult and a sensitivity analysis was performed to choose the most likely shear stress at the West Bay site. Further refinement in the model included parametrization of the intake shear stress from insights gained from 3D rigid bed modeling as well as literature review of the West Bay intake evolution (Yuill et al. 2016). The model was calibrated and validated with the latest available boundary conditions. The specific differences between the WB and MBSD sites and the lessons that can be gained from this study that can benefit MBSD Outfall design and modeling are:

1. The West Bay intake was an uncontrolled, un-armored opening when built which was allowed to evolve both in depth and laterally in orientation and width. On the other hand, the MBSD diversion intake is a controlled gate opening which can be used to control the diversion flows. The intake, conveyance channel and the outfall transition feature are also fully armored. Therefore, the lateral evolution that occurred at West Bay will not happen at the MBSD intake but qualitatively similar scour phenomenon can happen at the MBSD outfall where the diversion flow first meets the unarmored wetland surface and mimics a crevasse mouth.
2. The morphology model settings, particularly the critical shear stress and erodibility developed for MBSD are reasonable approximations of the erosion characteristics of Louisiana wetland soils near the MR as validated by the good agreement of modeled and observed scour depths at the West Bay site.
3. While a cross-sectional variation of Chezy coefficient from 43 to 60 $m^{1/2}/s$ across the scoured intake channel was necessary at the West Bay to parametrize the complex 3D effects and secondary currents of the curving flow into the West Bay intake, no such modification is deemed necessary at the MBSD OTF because the OTF design is meant to specifically prevent such large change in cross-sectional flows and is expected to keep the flow relatively uniform across the exiting OTF edge at MBSD. The MBSD OTF area has a uniform Chezy of 50 $m^{1/2}/s$.
4. Large uncertainty exists in the ability of the model to predict the exact shape of the scour hole, which is also unnecessary from a design perspective.

7.0 REFERNCES

Allison, M.A., Demas, C., Ebersole, B., Kleiss, B., Little, C., Meselhe, E., Powell, N., Pratt, T., Vosburg, B. 2012. *A Water and Sediment Budget for the Lower Mississippi-Atchafalaya River in Flood Years 2008-2010: Implications for Sediment Discharge to the Oceans and Coastal Restoration in Louisiana*. Journal of Hydrology 432-433 pp84-97.

EUSTIS. 2002. *Chevron-Texaco directional drill site RM 4.7 Geotechnical Boring Logs and Field Report*. Technical report prepared by EUSTIS Engg. Company Inc.

Meselhe, E.A., Allison, M.A., Yuill, B, Pereira, J and Khadka, A.2015. *Lower Barataria Sediment Diversion Feasibility Modeling Report.* Technical report to CPRA under Task Order 15.

Yuill, B.T., Khadka, A.K., Pereira, J., Allison, M.A., Meselhe, E. (2016). *Morphodynamics of the Erosional Phase of Crevasse-Splay Evolution and Implications for River Sediment Diversion Function*. Geomorphology, 259 (12-69).

APPENDIX B2

Storm-based Wave Forces on Diversion System Components

Rev 1

AECOM

STATE OF LOUISIANA
COASTAL PROTECTION AND RESTORATION AUTHORITY

MID-BARATARIA SEDIMENT DIVERSION (MBSD) PROJECT
STATE PROJECT No. BA-0153
LaGOV NO. 4400020885

Preparation of Engineering and Design
DESIGN DOCUMENTATION REPORT (DDR)
60% DESIGN
STORM BASED WAVE FORCES

for

Prepared By:
AECOM Technical Services
7389 Florida Blvd.
Suite 300
Baton Rouge, LA 70806

August 8, 2021

Rev	Date	Description
0	07/02/2021	60% Draft Submittal
1	08/08/2021	Addressed CPRA 60% Comments

AECOM

AECOM Imagine it. Delivered.

AECOM Technical Services
7389 Florida Blvd.
Suite 300
Baton Rouge, LA 70806

Technical Memo

Project: BA-153 Mid-Barataria Sediment Diversion

Subject: Storm Based Wave Forces

Date: August 8, 2021

Introduction

The wave forces on 4 diversion components have been estimated for storm conditions. The components are the intake U-frame walls, the transition walls on the downstream side of the diversion gates, the abutments at the Hwy 23 bridge crossing, and T-walls located at the siphon crossing. The wave forces on the transition walls were evaluated for two water depths, representing the beginning and end of the transition.

The intake U-Frame walls are located along the banks of the Mississippi River, and subject to surge and waves generated in the river. The transition walls, bridge abutment, and siphon T-Walls are all located along the diversion conveyance channel and are subject to waves developed in the Barataria basin and then propagate into the channel.

The largest waves and water depths are associated with tropical storms and hurricanes, which are most likely to occur during the diversion non-operational period. The wave forces on each structure were evaluated using Goda's formulation for wave forces for three different design conditions, the 50year return period for both existing and future conditions, and the 100-year return period for future conditions. Existing conditions represent the current conditions in the basin and river and represent the conditions expected to occur during the first few years of diversion operations. Future conditions correspond to a 50-year horizon, after which land building and sea level rise will impact conditions in the basin and river. The 50-year return period design levels were finally selected considering the cost and feasibility of the project and 100-year return period design levels were not used in wave modeling and to calculate the wave forces. All of these design conditions are associated with tropical storm and hurricane events.

The analysis consists of three steps, summarized below:

1) Establish the surge and wave design conditions
2) Wave Modeling: Wave modeling was conducted to estimate the design wave conditions at the toe of each structure. The analysis accounted for wave transformation as they propagated into the basin and potential increases to wave energy due to wind generation.
3) Wave Forces. A wave force analysis was conducted for each structure for each surge/wave for each design condition.

Structure Details

The location of the structures within the diversion system is shown in **Figure 1**. The details of each structure are provided in the schematics in **Figures 2** through **Figure 5**. These design drawings were used to specify the parameter values for application in Goda's formula for wave forces. The siphon T-walls are approximately 2,250 feet from the conveyance channel outfall, the Hwy 23 Bridge flood walls are

approximately 7,250 feet from the channel outfall and the transition walls are approximately 10,000 feet from the channel outfall. The bottom elevation of the conveyance at the transitions walls ranges is -25 feet, NAVD88. . The intake U-frame walls are located along the Mississippi River west bank at approximately river mile 60.7.

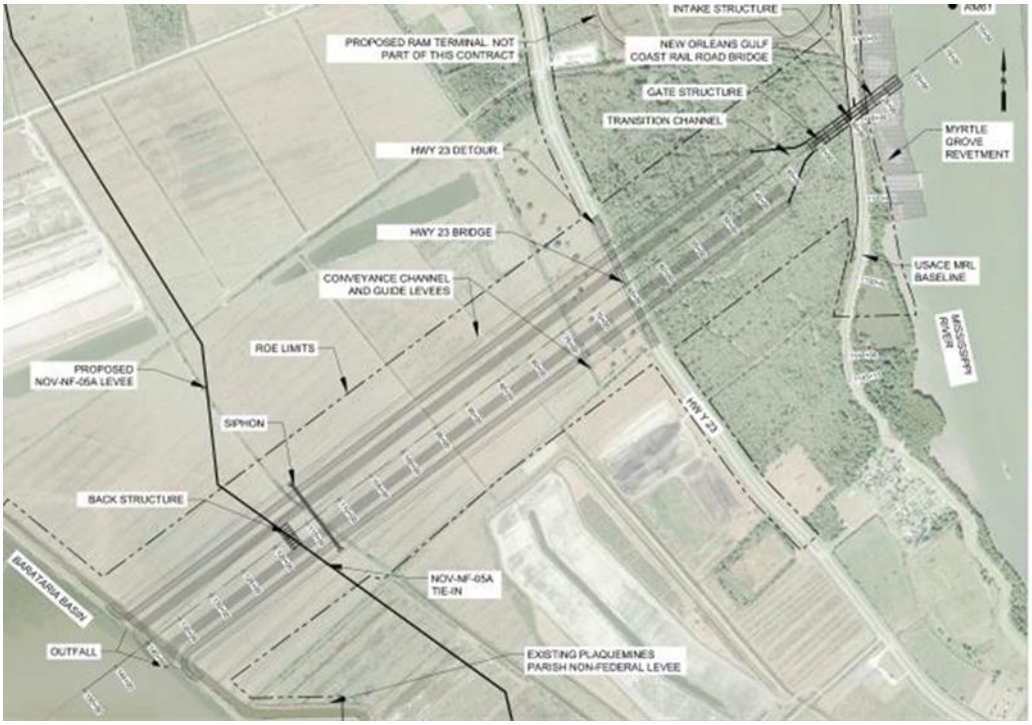

Figure 1: Structure Locations (Siphon, Hwy 23 Bridge Flood walls, Transition and Intake)

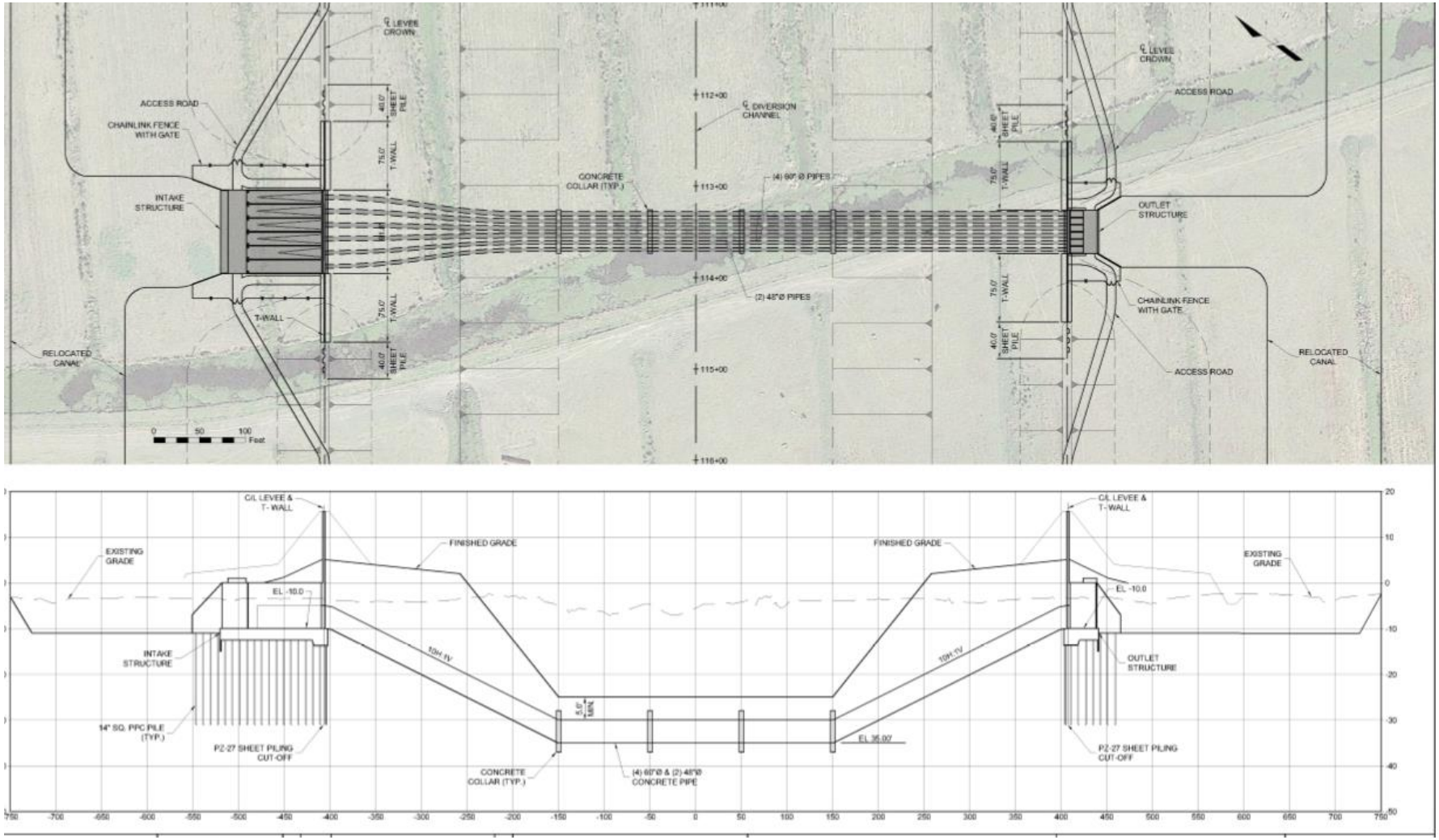

Figure 2: Siphon T-Walls

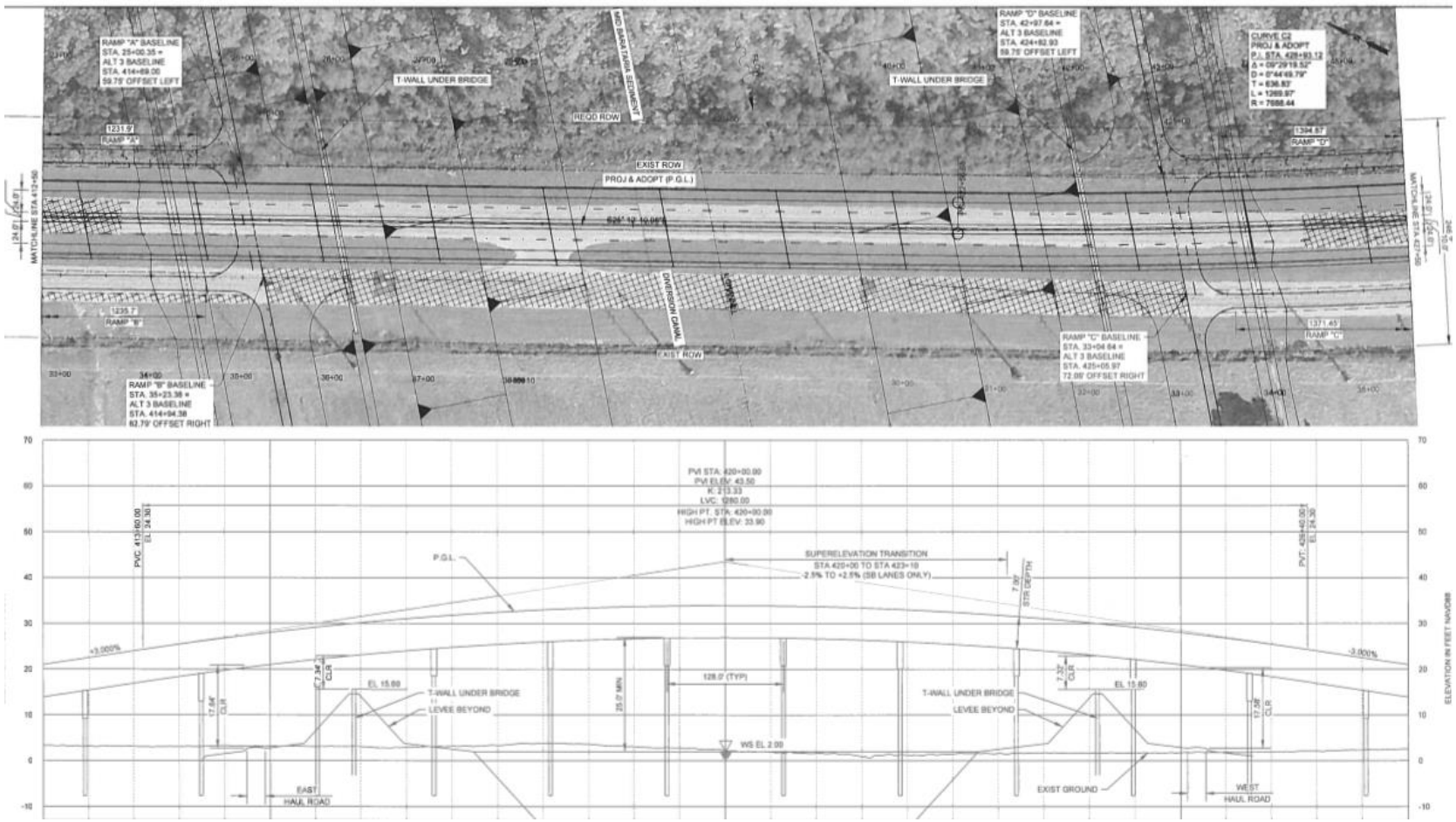

Figure 3: Hwy 23 Bridge Flood Walls

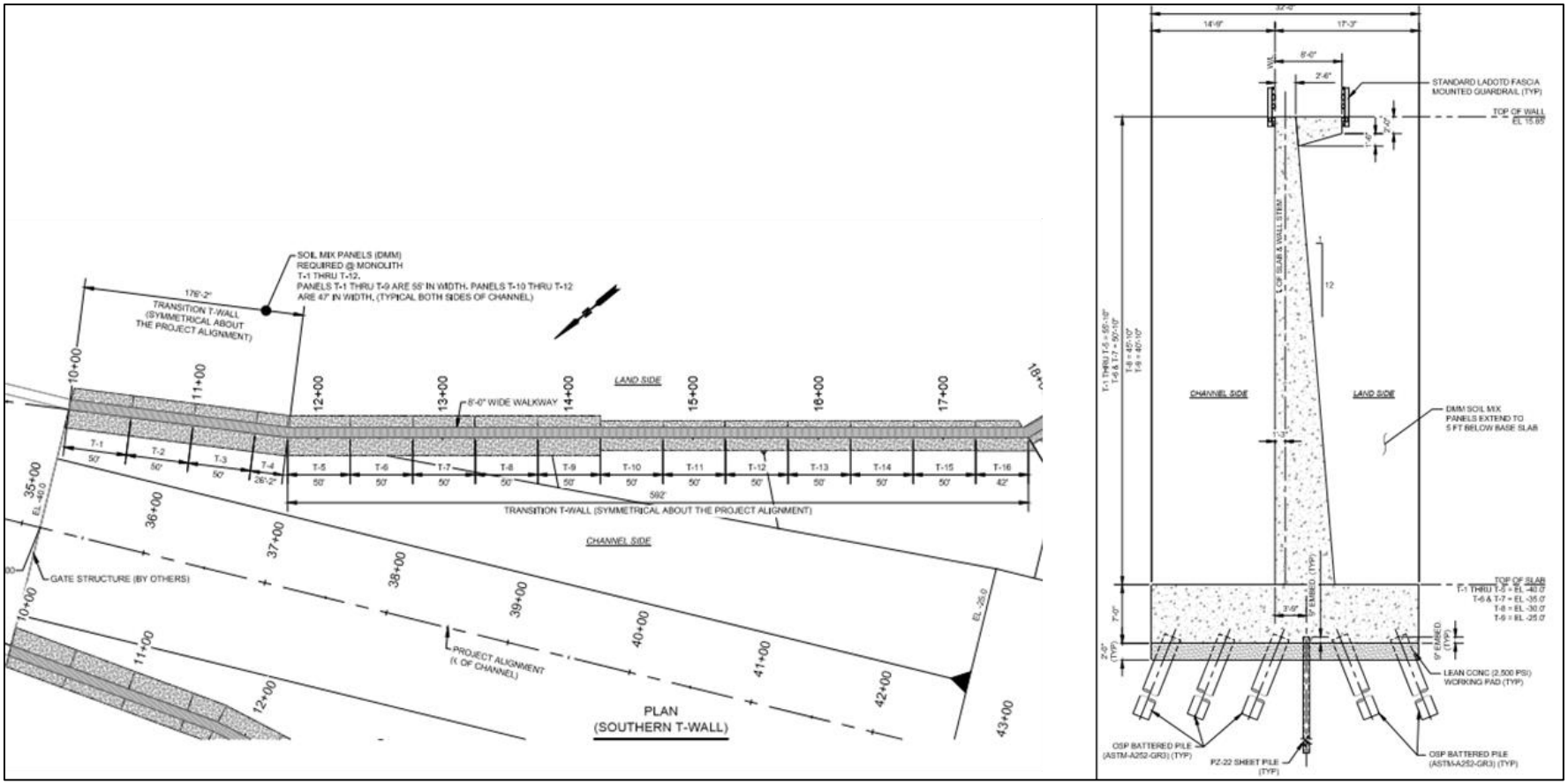

Figure 4: Transition T-Walls

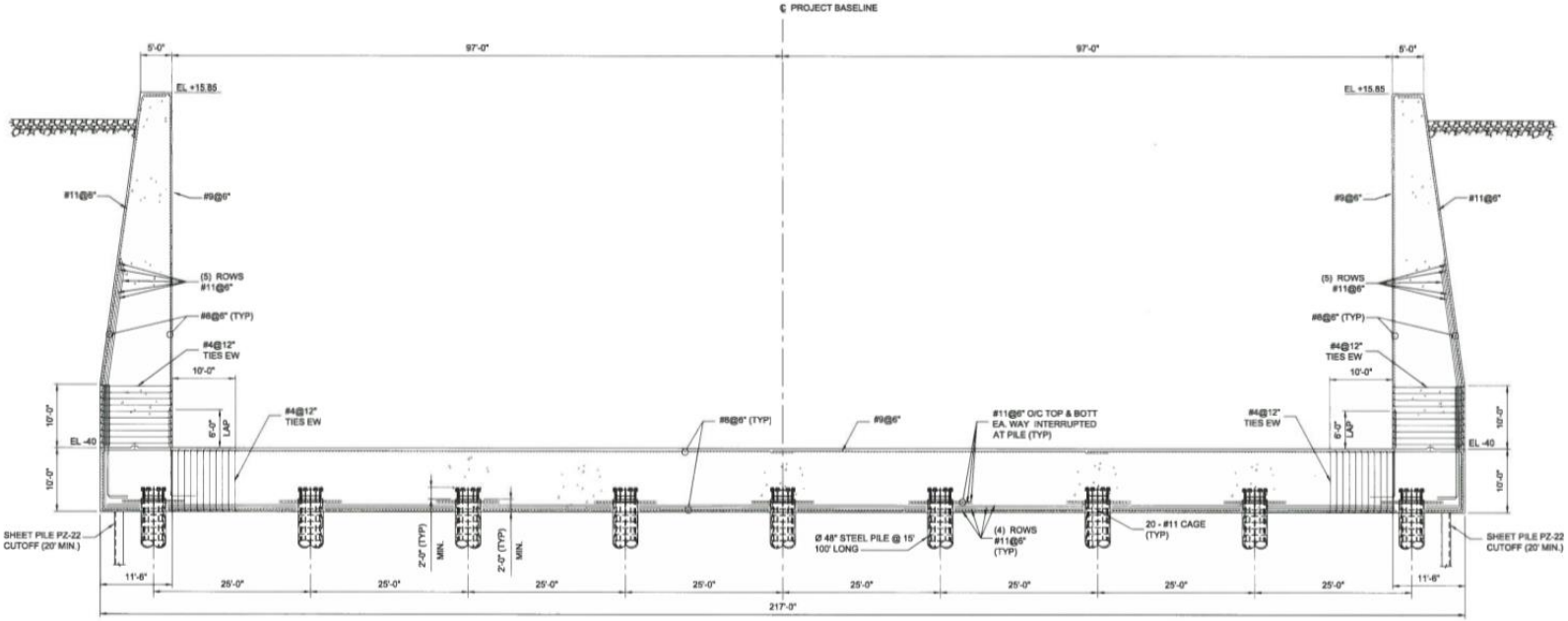

Figure 5: Intake U-Frame

Design Wave Conditions

Surge and wave conditions are needed for the Project components that provide flood protection in the MRL and NOV flood protection systems. Note that the reach of the MRL where the Project is located is only authorized for Riverine Flooding. CPRA has proactively added hurricane requirements to the MRL structures. The 50 yr (2% AEP) design grade is at El 20.35 compared to the authorized Mississippi River Project design grade of El 16.4. The selected 50 yr (2% AEP) agrees with the highest storm event used to design permanent structures in the NOV System in lower Plaquemines. The Project analysis was conducted for the 50-year surge and wave conditions for both existing and future conditions. The 100-year future design conditions were also considered. This was done to assess the relative force increase and the feasibility of designing the system to the 100-year level compared to the 50-year design level. Note that the Project design landbuilding life is also 50 years but there is no relationship between the two. The Project design landbuilding life starts at construction completion (estimated to be 2028) and ends 50 years later. The 50 yr (2% AEP) period replicates that used in the USACE 2017 Elevations for Design of Hurricane Protection Levees and Structures Report (DER), which is based on current year (start date) of 2013 with future ending in 2063. The USACE storm data did not include the MBSD Structure, since the design was not yet underway when the USACE DER modeling was performed. As such, the Design Team (DT) was required to develop its own wave conditions as described herein. The DT did use a similar suite of storms as used in the DER to develop wave pressures. The SWL and Design Grades were taken directly from the DER. Note that there is also a 100 yr Service Life mentioned throughout the DDR, in the Structures Section. The 100 year service life is a durability criteria added to assure structures will function for 100 years from the end of construction. This affects corrosion plans for steel structures and crack control for concrete structures. The 100 yr service life is unrelated to both future storm conditions and landbuilding goals.

The 50-year and 100-year design surge and wave conditions in the basin and in the Mississippi River were available from previous work documented in the 2017 update to the USACE report: Elevations for Design of Hurricane Protection Levees and Structures Report. The report provides data for sections along the non-Federal NOV levee as well as many other Levee systems. The 50 and 100 year surge and wave conditions for the levee section NOV-NF-W-05c, whose location coincides with the conveyance channel outfall, were obtained from the report. The basin data were located in Tables 6-2 and 6-3 of the report for existing and future conditions and are summarized below in **Table 1**. The River data are located in **Table 2** for future conditions. Hs is the significant wave height and Tp is the peak period.

Table 1: Summary of Surge and Wave Design Conditions adjacent to the Outfall

50 Year Return Period (yrs)	Existing Water Levels	Future Water Levels (includes 50 years SLR)
Surge(ft, NAVD88)	7.0	9.0
Hs(ft)	2.1	3.1
Tp(sec)	4.1	5.0

Table 2: Summary of Surge and Wave Design Conditions adjacent to the Intake

50 Year Return Period	Existing Water Levels	Future Water Levels

		(includes 50 years SLR)
Surge(ft,NAVD88)	12.7	14.5
Hs(ft)	2.3	3.8
Tp(sec)	2.5	3.8

The 3-scond gust wind speed of 145 mph was converted to a 30-minute wind speed for use in the wave modeling. The method of Siniu and Scanlan (1978) was used for the conversion. The method yields a wind a 30-minute wind speed of 93 mph.

Wave Modeling

The wave modeling was conducted using SWAN. A Cartesian grid with a cell size of 5 meters by 10 meters (16.4 by 32.8 feet) was configured to cover the conveyance channel and adjacent outfall area. The model bathymetry was adopted form The Water Institute Basin Wide Model and is shown in **Figure 6** after mapping it onto the model grid.

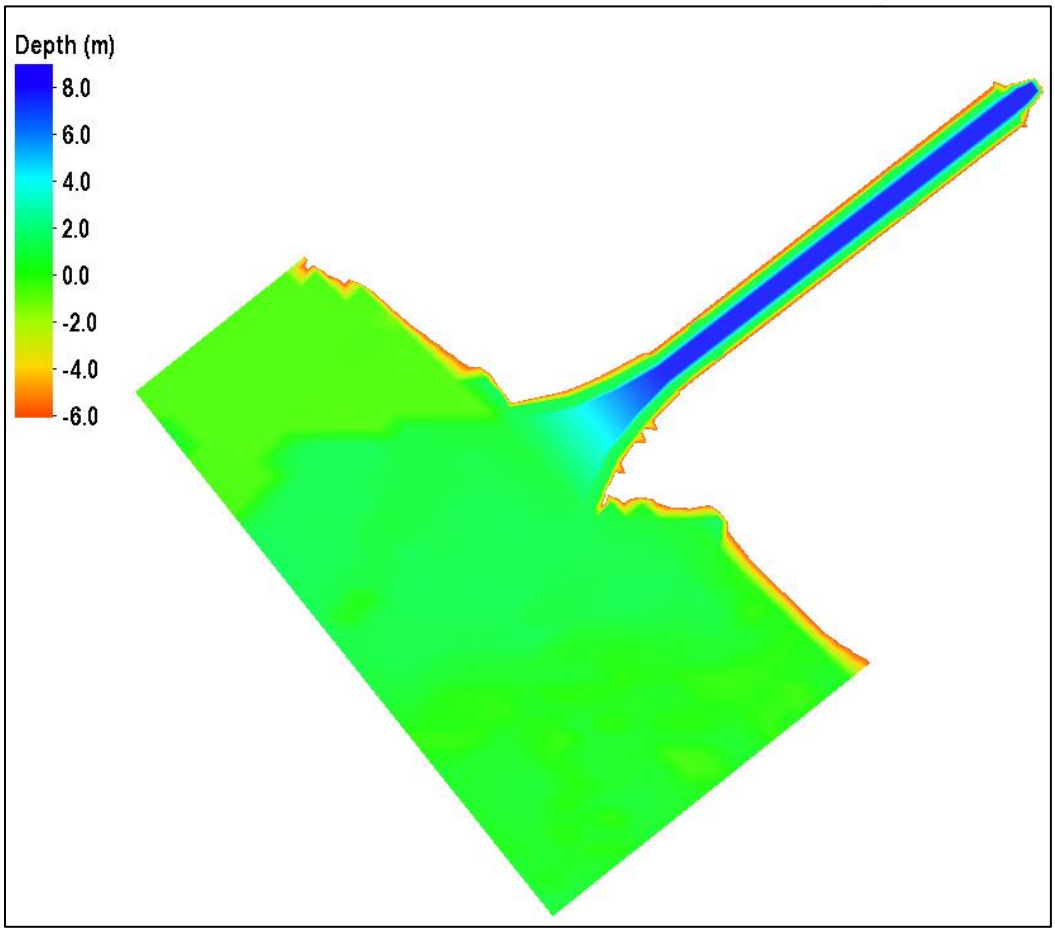

Figure 6: SWAN Wave Model Domain and Bathymetry

The design waves were applied at the western boundary and the model simulated the propagation of the waves across the basin and into the channel. The simulation included bottom friction, refraction, diffraction, reflection, shoaling and wave-breaking. The 50-year waves were applied at the boundary for both the existing and future conditions.

The model parameters include a manning's coefficient of 0.15, a reflection coefficient of 0.5 and a diffraction coefficient of 4.0. These values represent conservative estimates in that they will under-predict the wave attenuation mechanisms in the channel. The model default discrete frequency bins were modified to better represent the smaller wave periods. The bins were set to vary between 1 and 7 seconds.

The simulated wave height and wave direction vectors (scaled to the height) are shown in **Figures 7** and **8** for the exiting conditions scenario.

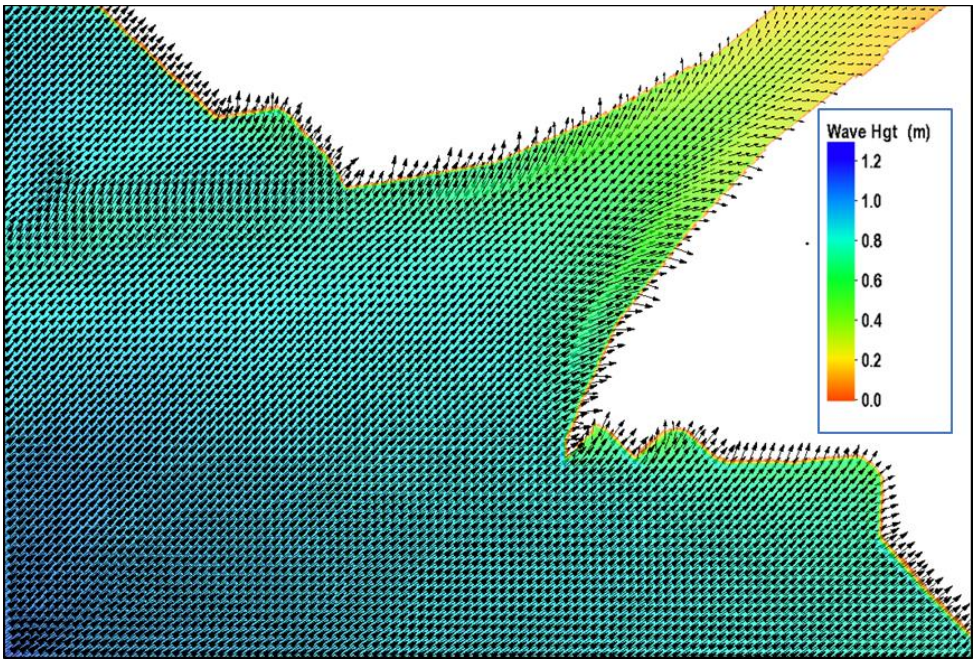

Figure 7: Simulated Waves propagating into the Channel

These results represent the application of the 50-year design wave height and period (Hs = 2.1 feet and T = 4.1 seconds, per Table 1 and the 93 mph wind). As the waves approach the channel entrance there is an inverse shoaling effect due to the presence of the outfall ramp feature. As the water depth increases, the wave length also increases, and as a result of the conservation of energy, the wave height decreases.

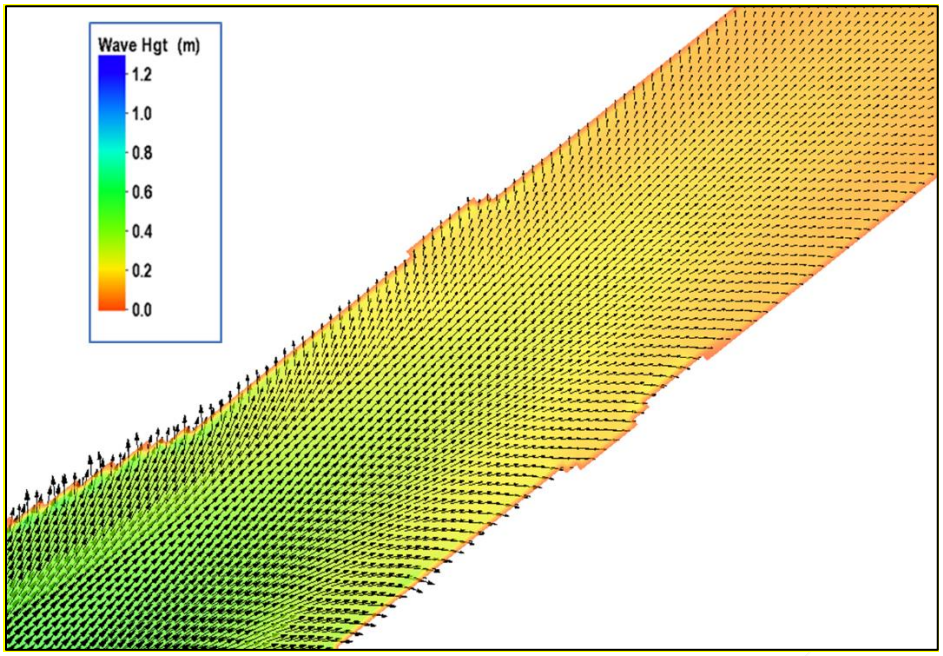

Figure 8: Simulated Waves refracting on Channel Berm

The results show that as the waves enter the channel, there is a refraction effect that causes the waves to turn toward the channel sides. The refraction is shown in more detail in Figure 8. This is due to the sloped channel sides (1:4). As these waves encounter the shallower berm, the frictional losses increase, wave breaking may occur and the impingement on the guide and hurricane levees will provide additional wave energy losses. This mechanism reduces the wave energy as the waves propagate into the channel.

The wave characteristics were extracted from the wave model simulations at the toe of each structure (approximately 10 feet from the toe) and are summarized in **Tables 3** and **4**. For the side slopes, the toe is the base of the slope, where it meets the channel bottom. For the siphon and bridge, it is the base of the T-wall and abutment where they meets the channel bottom. The tables show the significant wave height Hs, the mean period Tm and the wavelength L. The wavelength was also extracted from the model results. It is an input to the wave force calculations but was not provided with the design wave characteristics.

Table 3: Simulated wave conditions at structure toes in conveyance channel for existing conditions

Location	Hs (ft)	Tm (s)	L (ft)
Siphon	2.02	1.86	16.1
Hwy 23 Bridge	2.28	2.07	20.1
Transition	2.78	2.15	23.7

Table 4: Simulated wave conditions at structure toes in conveyance channel for future conditions (includes SLR 50 years out)

Location	Hs (ft)	Tm (s)	L (ft)
Siphon	2.43	2.07	21.3
Hwy 23 Bridge	2.81	2.29	25.3
Transition	2.85	2.39	29.3

The design wave height and period for the intake are provided at the Mississippi River west bank so no wave modeling is required for the Intake structure. However, the wavelength is required and was not provided with the design wave height and period. The wave length was estimated using the dispersion relationship assuming deep water conditions. The assumption of deep water dispersion relationship is valid because the waves are relatively small, and the water depth included the surge will exceed 50 feet at the Intake. The final design wave conditions use for the Intake structure on the west bank of the Mississippi River are summarized in **Table 5**.

Table 5: Wave conditions at Intake (west bank of MR)

Return Period (yrs)	50 (existing)	50 (future)
Surge(ft,NAVD88)	12.7	14.5
Hs(ft)	2.3	3.8
Tp(sec)	2.5	3.8
L(ft)	32	74

Wave Force Analysis

The wave forces were estimated using Goda's formula for vertical walls as presented in the Coastal-Engineering Manual (USACE, 2002). A depiction of the formulation is shown in **Figure 9**.

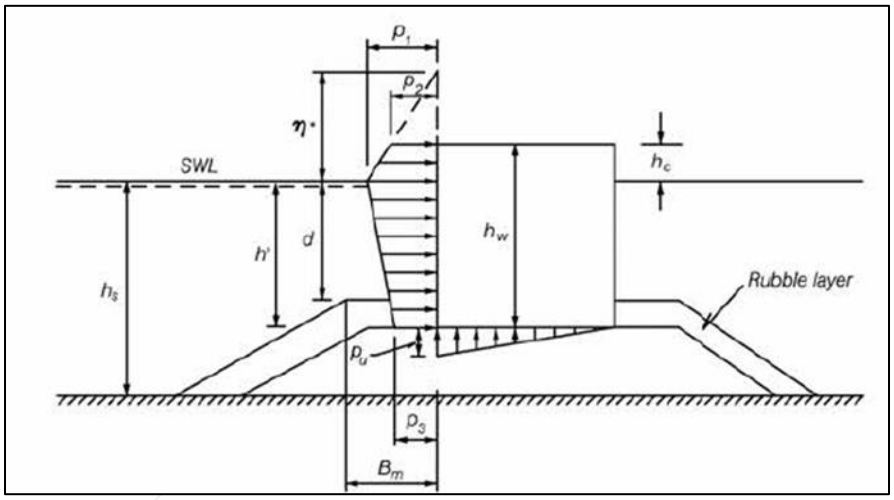

Figure 9: Structural and Hydrodynamic Parameters in Goda's Formula

The final design wave conditions for each structure have been entered into the Goda formulation and used to estimate the wave induced dynamic forces on the vertical wall of each structure (EM 1110-2-1100, VI - 5 – 139). The formula calculates the wave peak elevation η* and the three pressure p_1, p_2 and p_3. The loading is obtained by integrating the pressure profile over the vertical wall.

The remaining parameters in **Figure 9** represent the hydrodynamic and structure parameters and are specified by the design conditions and the structure geometry. The Goda equations are:

$$\eta^* = 0.75(1+\cos\beta)\,\lambda_1 H_{design}$$

$$p_1 = 0.5(1+\cos\beta)(\lambda_1\alpha_1 + \lambda_2\alpha_*\cos^2\beta)\,\rho_w\, g\, H_{design}$$

$$p_2 = \begin{cases} \left(1-\frac{h_c}{\eta^*}\right)p_1 & \text{for } \eta^* > h_c \\ 0 & \text{for } \eta^* \le h_c \end{cases}$$

$$p_3 = \alpha_3\, p_1$$

where β is the wave angle of incidence to the vertical wall and H_{design} is the $H_{1/250}$ wave height (approximated by 1.8*Hs). For all cases it is assumed that waves approach the wall head on and consequently β is set to zero. This represents a conservative assumption in estimating the wave loads. For all cases the structure parameters λ_1 and λ_2 were set to 1.0.

If the design conditions indicate no wave breaking, then the original Goda (Goda, 1974) formula is used. Wave breaking was determined to occur if the H_{design} was greater than 0.78*d. The intermediate parameter values in the Goda's equations for non-breaking conditions are:

$$\alpha_* = \alpha_2$$

$$\alpha_1 = 0.6 + 0.5\left[\frac{4\pi h_s/L}{sinh\ (4\pi h_s/L)}\right]^2$$

$$\alpha_2 = \text{the smallest of } \frac{h_b - d}{3h_b}\left(\frac{H_{design}}{d}\right)^2 \text{ and } \frac{2d}{H_{design}}$$

$$\alpha_3 = 1 - \frac{h_w - h_c}{h_s}\left[1 - \frac{1}{cosh\ (2\pi h_s/L)}\right]$$

where L is the wavelength and h_b is the water depth at a distance of 5*Hs seaward of wall.

If wave breaking occurs, then Goda's formula modified for impulsive forces due to head on wave breaking waves (Takahashi, Tanimoto, and Shimosako, 1994) is used. The intermediate parameter values in the modified Goda's equations for breaking conditions are:

$$\alpha_* = \text{largest of } \alpha_2 \text{ and } \alpha_I$$

$$\alpha_2 = \text{the smallest of } \frac{h_b - d}{3h_b}\left(\frac{H_{design}}{d}\right)^2 \text{ and } \frac{2d}{H_{design}}$$

$$\alpha_I = \alpha_{I0} \cdot \alpha_{I1}$$

$$\alpha_{I0} = \begin{cases} H_{design}/d & \text{for } H_{design}/d \le 2 \\ 2.0 & \text{for } H_{design}/d > 2 \end{cases}$$

$$\alpha_{I1} = \begin{cases} \frac{\cos\delta_2}{\cosh\delta_1} & \delta_2 \le 0 \\ \frac{1}{\cosh\delta_1 \cdot (\cosh\delta_2)^{\frac{1}{2}}} & \delta_2 > 0 \end{cases}$$

$$\delta_1 = \begin{cases} 20 \cdot \delta_{11} & \text{for } \delta_{11} \le 0 \\ 15 \cdot \delta_{11} & \text{for } \delta_{11} > 0 \end{cases}$$

$$\delta_{11} = 0.93\left(\frac{B_m}{L} - 0.12\right) + 0.36\left(\frac{h_s - d}{h_s} - 0.6\right)$$

$$\delta_2 = \begin{cases} 4.9 \cdot \delta_{22} & \text{for } \delta_{2\,2} \le 0 \\ 3 \cdot \delta_{22} & \text{for } \delta_{22} > 0 \end{cases}$$

$$\delta_{22} = -0.36\left(\frac{B_m}{L} - 0.12\right) + 0.93\left(\frac{h_s - d}{h_s} - 0.6\right)$$

Here, B_m is the berm width (in front of the wall). For the intake and transitions walls, there is no berm. For the siphon and the Hwy 23 bridge flood wall, the channel berm could be considered a berm. However,

the channel berm is approximately 97 feet wide and not explicitly a 'wave berm' intended to reduce wave impacts. Therefore, B_m was set to zero for all structures.

The input values, intermediate formula parameter calculations and final loadings are presented in **Tables 6** through **9** for existing conditions.

Table 6: Wave Loads for the Intake for Existing Conditions

Hydrodynamic Inputs	Value	Units
Water Elevation	12.7	feet, NAVD88
Wave Height	2.30	feet
Wave Period	2.5	seconds
Wave Angle β	0	degrees
Wave Length L	59.0	feet
Structure Inputs	**Value**	**Units**
Wall Top Elevation	22	feet, NAVD88
Wall Bottom Elevation	-20	feet, NAVD88
Sea Floor Elevation (at hs location)	-20	feet, NAVD89
Rubble Layer Thickness	0	feet
hw	42	feet
hc	9.3	feet
h_s	32.7	feet
d	32.7	feet
h_b	32.7	feet
B_m	0	feet
Physical Constants	**Value**	**Units**
Water Density ρ_w	1.94	sl/ft^3
Acceleration Due to Gravity g	32.2	ft/s^2
Derived and Intermediate Parameter Values	**Value**	**Units**
Design Wave Height H_{design}	4.14	feet
Breaking Wave	NO	-
η^*	6.21	ft
α_*	0	-
α_1	0.60008709	-
α_2'	0	-
α_2''	15.80	-
α_2	0	-
α_3	6.15E-02	-
p_1	155.2	psf
p_2	0.0	psf
p_3	9.5	psf
Physical Constants	**Value**	**Units**

Load	3175	lbs/ft

Table 7: Wave Loads for the Siphon for Existing Conditions

Hydrodynamic Inputs	Value	Units
Water Elevation	7	feet, NAVD88
Wave Height	2.02	feet
Wave Period	1.86	seconds
Wave Angle β	0	degrees
Wave Length L	11.8	feet
Structure Inputs	**Value**	**Units**
Wall Top Elevation	15.6	feet, NAVD88
Wall Bottom Elevation	4	feet, NAVD88
Sea Floor Elevation (at hs location)	2	feet, NAVD88
Rubble Layer Thickness	1.5	feet
hw	11.6	feet
hc	8.6	feet
h_s	5	feet
d	3	feet
h_b	2.1	feet
B_m	0	feet
Physical Constants	**Value**	**Units**
Water Density ρ_w	1.94	sl/ft^3
Acceleration Due to Gravity g	32.2	ft/s^2
Derived and Intermediate Parameter Values	**Value**	**Units**
Design Wave Height H_{design}	2.34	feet
Breaking Wave	YES	-
η^*	3.51	ft
α_*	0.030	-
α_1	0.601	-
α_2'	-0.087	-
α_2''	2.564	-
α_2	-0.087	-
α_3	0.483	-
α_{I0}	0.78	-
α_{I1}	0.039	-
α_I	0.030	-
δ_1	-3.672	-
δ_{11}	-0.184	-
δ_2	-0.700	-
δ_{22}	-0.143	-

p_1	92.3	psf
p_2	0.0	psf
p_3	44.6	psf
Physical Constants	**Value**	**Units**
Load	**470**	**lbs/ft**

Table 8: Wave Loads for the Hwy 23 Bridge Floodwall for Existing Conditions

Hydrodynamic Inputs	**Value**	**Units**
Water Elevation	7	feet, NAVD88
Significatn Wave Height	2.28	feet
Mean Wave Period	2.07	seconds
Wave Angle β	0	degrees
Wave Length L	15.1	feet
Structure Inputs	**Value**	**Units**
Wall Top Elevation	15.6	feet, NAVD88
Wall Bottom Elevation	4	feet, NAVD88
Sea Floor Elevation (at hs location)	2	feet, NAVD88
Rubble Layer Thickness	1.5	feet
hw	11.6	feet
hc	8.6	feet
h_s	5	feet
d	3	feet
h_b	2.1	feet
B_m	0	feet
Physical Constants	**Value**	**Units**
Water Density ρ_w	1.94	sl/ft^3
Acceleration Due to Gravity g	32.2	ft/s^2
Derived and Intermediate Parameter Values	**Value**	**Units**
Design Wave Height H_{design}	2.34	feet
Breaking Wave	YES	-
η^*	3.51	ft
α_*	0.030	-
α_1	0.608	-
α_2'	-0.087	-
α_2''	2.564	-
α_2	-0.087	-
α_3	0.547	-
α_{I0}	0.78	-
α_{I1}	0.039	-
α_I	0.030	-
δ_1	-3.672	-

δ_{11}	-0.184	-
δ_2	-0.700	-
δ_{22}	-0.143	-
p_1	93.4	psf
p_2	0.0	psf
p_3	51.1	psf
Physical Constants	**Value**	**Units**
Load	**489**	**lbs/ft**

Table 9: Wave Loads for the Transition Feature for Existing Conditions

Hydrodynamic Inputs	**Value**	**Units**
Water Elevation	7	feet, NAVD88
Wave Height	2.78	feet
Wave Period	2.15	seconds
Wave Angle β	0	degrees
Wave Length L	17.3	feet
Structure Inputs	**Value**	**Units**
Wall Top Elevation	15.6	feet, NAVD88
Wall Bottom Elevation	-20	feet, NAVD88
Sea Floor Elevation (at hs location)	-20	feet, NAVD89
Rubble Layer Thickness	0	feet
hw	35.6	feet
hc	8.6	feet
h_s	27	feet
d	27	feet
h_b	27	feet
B_m	0	feet
Physical Constants	**Value**	**Units**
Water Density ρ_w	1.94	sl/ft^3
Acceleration Due to Gravity g	32.2	ft/s^2
Derived and Intermediate Parameter Values	**Value**	**Units**
Design Wave Height H_{design}	5.00	feet
Breaking Wave	NO	-
η*	7.51	ft
α_*	0	-
α_1	0.6	-
α_2'	0	-
α_2''	10.79	-
α_2	0	-
α_3	1.13E-04	-
p_1	187.6	psf

p_2	0.0	psf
p_3	0.0	psf
Physical Constants	**Value**	**Units**
Load	**3236**	**lbs/ft**

Similar analysis has been completed for the Future conditions scenarios at each structure.

Summary

A wave force analysis has been competed for the vertical wall structures within the diversion system. Three structures, the Siphon, the Floodwalls at the Hwy 23 Bridge Crossing and the Transitions Walls are subject to storm waves generated in the basin and propagating into the conveyance channel. The fourth structure, the Intake, is located on the West Bank of the Mississippi River and is subject to storm waves generated in the river. Design wave conditions for the analysis were obtained from A USACE study of the storm impacts to federal and non-federal levee systems in Louisiana (USACE, 2017). Wave modeling using the SWAN model was implemented to propagate the waves in the basin adjacent to the channel outfall into the conveyance channel. The waves at the toe of each structure were extracted from the modeling analysis and used in Goda's formula to estimate the wave loads on the structures. When wave breaking was evident, the wave height was limited to 78% of the water depth and the modified Goda's formula was used to account for the impulse load. The results for existing and future conditions are summarized in **Tables 10** and **11.**

Table 10: Summary of Wave Loadings for Existing Conditions

Location	Surge (ft, NAVD88)	Water Depth (ft)	Hs (ft)	H_{design}(ft)	T (s)	Breaking Condition	p1 (lbs/ft²)	p2 (lbs/ft2)	p3 (lbs/ft2)	η* (ft)	Force (lbs/ft)
Diversion Intake	12.7	32.7	2.30	4.14	2.5	non-breaking	155.2	0.00	9.55	6.21	3175
Transition Walls	7.0	27.0	2.78	5.00	2.2	non-breaking	187.6	0.00	0.02	7.51	3236
Bridge Abutment	7.0	3.0	2.28	2.34	2.1	breaking	93.4	0.00	51.12	3.51	489
Siphon	7.0	3.0	2.02	2.34	1.9	breaking	92.3	0.00	44.64	3.51	470

Table 11: Summary of Wave Loadings for Future Conditions

Location	Surge (ft, NAVD88)	Water Depth (ft)	Hs (ft)	H_{design} (ft)	T (s)	Breaking Condition	p1 (lbs/ft²)	p2 (lbs/ft2)	p3 (lbs/ft2)	η* (ft)	Force (lbs/ft)
Diversion Intake	14.5	34.5	3.80	6.84	3.8	non-breaking	256.6	69.01	25.25	10.26	6082
Transition Walls (-20ft)	9.0	29.0	2.85	5.13	2.4	non-breaking	192.3	27.36	0.02	7.70	3513
Bridge Abutment	9.0	5.0	2.81	3.90	2.3	breaking	148.7	0.00	63.79	5.85	1126
Siphon	9.0	5.0	2.43	3.90	2.1	breaking	147.8	0.00	53.94	5.85	1088

References

EM 1110-2-1100, Engineering and Design COASTAL ENGINEERING MANUAL, U.S. Army Corps of Engineers , CECW-EW Washington, DC 20314-1000 30 April 2002

Simiu, E. and Scanlan, R. N., “Wind Effects on Structures: AN introduction to Wind Engineering”, New York, Wiley, p. 62, 1978.

APPENDIX B3

Water Quality in the Conveyance Channel
During Non-operational Periods

AECOM Technical Services
7389 Florida Blvd.
Suite 300
Baton Rouge, LA 70806

Technical Memo

Project: BA-0153 Mid-Barataria Sediment Diversion

Subject: Desktop Study – Mid Barataria Sediment Diversion and Nutrients

Date: August 9, 2021

Prepared by: AECOM Design Team

I. Introduction

A desktop water quality analysis has been conducted to address concerns of water quality in the conveyance channel during non-operational periods. During these periods, there may be stagnant or slow-moving water in the conveyance channel which coupled with warm temperatures and nutrient levels could lead to eutrophication. Overabundance of nutrients can cause adverse impacts such as excessive algal growth, reduced sunlight penetration, and decreased oxygen in the water. As oxygen concentrations fall below critical levels, organisms begin to die, and their decomposition can lead to a complete lack of oxygen. Consequently, public perceptions can be affected if green algal mats occur or foul odors emanate from the canal.

The analysis has been divided into two parts. In the first part, the potential for conditions in the diversion during non-operational periods conducive to eutrophication are evaluated. The factors include the residence time in the conveyance channel, water temperature and nutrient concentrations. These factors are evaluated to determine if there is a potential for eutrophication.

The second part is a review of available information and literature for two existing diversions, the Davis Pond Diversion and the Caernarvon Freshwater Diversion. These two freshwater diversions were reviewed to determine if eutrophication has been an issue during their operational life.

II. Expected Conditions in the Mid-Barataria Sediment Diversion

The non-operational period of the Mid-Barataria Sediment Diversion is currently defined by a flow rate (not an actual time period) during which the flow in the Mississippi River is above 450,000 cfs. Flow records have been reviewed to determine the typical time period for which flows are below this level and consequently the diversion will be closed, or a base flow will exist. A review of river flow data (Belle Chase and Talbot Landing) indicate that the daily average flows are below the 450,000 cfs threshold 50% of the time for the period April through September, with the exceedances being lowest for the period May through August. Consequently, we have defined the potential non-operational period from April through September for this analysis.

The growth of algae and potential for eutrophication require a combination of high nutrient levels, warm temperatures and slow moving or stagnant water conditions. The potential for each of these conditions to occur during the non-operational period has been evaluated.

River temperature data was obtained from the USGS station 07374525 located near Belle Chase (upstream of the proposed diversion intake location). The temperature data is plotted by month for two water years, 2010 and 2012 in Figure 1. The data indicate that temperatures during the non-operational period can exceed often 80 degrees and reach up to 90 degrees.

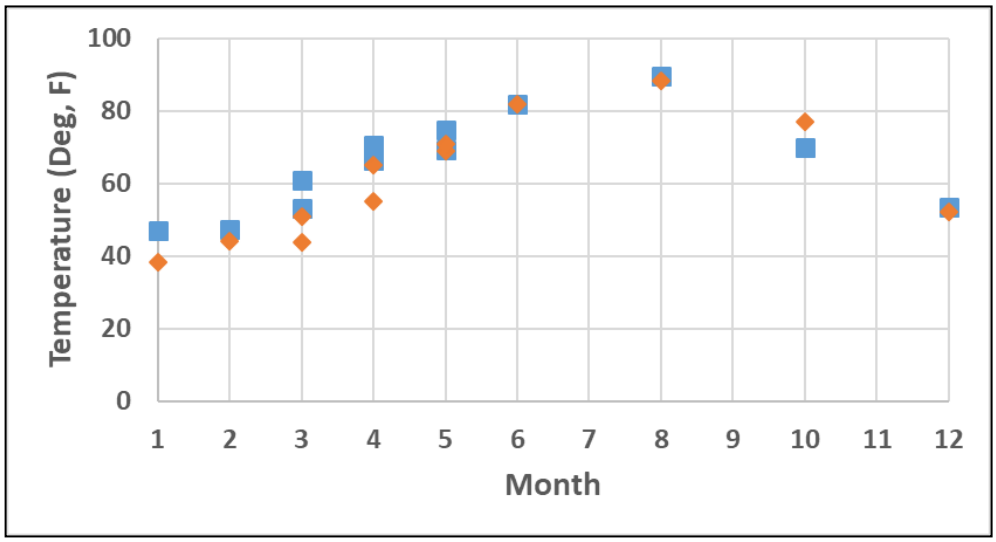

Figure 1 Monthly Variation in River Water Temperature Data

Water quality data has been obtained from the Belle Chase station for review. Up to 30 years (depending on availability) of nutrient data was downloaded from USGS Station 07374525 at Belle Chasse on the Mississippi River. The nutrient data downloaded includes:

- Ammonia & Ammonium
- Inorganic Nitrogen (Nitrate & Nitrite)
- Kjeldahl Nitrogen
- Organic Nitrogen
- Orthophosphate
- Phosphorus

Plots of the data are provided in Attachment A. A summary of the data for the non-operational period is provided in Table 1.

Table 1 Summary of Mississippi River Water Quality Data for the Non-Operational Period

Nutrient	Minimum Concentration	Maximum Concentration	Mean Concentration
Ammonia & Ammonium	0.006 mg/L as N	0.060 mg/L as N	0.022 mg/L as N
Inorganic Nitrogen	0.520 mg/L as N	3.03 mg/L as N	1.648 mg/L as N
Kjeldahl Nitrogen	0.150 mg/L as N	0.520 mg/L as N	0.341 mg/L as N
Total Phosphorus	0.040 mg/L as P	0.173 mg/L as P	0.101 mg/L as P
Orthophosphate	0.039 mg/L as P	0.155 mg/L as P	0.092 mg/L as P

To put these values in perspective, EPA and state water quality criteria were obtained for comparison. Unfortunately, the majority of criteria are written as cause and effect, or in other qualitative terms and not as numerical criteria. This reflects the high uncertainty in the impact of nutrients and other water quality components on algae growth and potential eutrophication. However, recently the EPA has approved numeric criteria for the state of Florida. Although these values are not derived from Louisiana lakes and streams, Florida ecosystems are reasonably similar, and the values derived from the Florida systems can be used as a surrogate. The values are provided for different sections of the state, again reflecting the uncertainty in the impacts, but at least provide some basis for comparison. For lakes, the ranges are 0.51 to 1.27 mg/L for Total Nitrogen, and 0.01 to 0.05 mg/L for Total Phosphorous. For streams, the ranges are 0.67 to 1.87 mg/L for Total Nitrogen, and 0.06 to 0.49 mg/L for Total Phosphorous. Note that the ranges reflect the best estimates of natural levels in the lakes and streams and vary by region within the state. They do not indicate levels at and below which eutrophication cannot occur, as eutrophication can occur naturally.

A comparison of the maximum and mean values listed in Table 1 to the Florida value for lakes and streams indicate that the river nutrient levels are generally higher than the criteria. For Total Nitrogen, the values can be as high as 6 times the criteria, and for Total Phosphorus, up to 127 times the criteria, although a value of 10 to 12 times the criteria is likely more reflective of the conditions. It is concluded that the nutrient and temperature data in the Mississippi River could potentially lead to water quality issues. Stated alternatively, potential impacts from nutrients cannot be ruled out based on concentration levels alone.

The flow rate in the conveyance channel during the non-operational period has not been determined by the AECOM Design Team (DT) at this time. The DT and Coastal Protection and Restoration Authority (CPRA) have discussed a range of possible flows, from zero, up to 5000 cfs base flow, or possibly a pulsed flow. The residence time of the water in the conveyance channel will depended on the base flow level. Another factor that has not been quantified at this time is the ability of the diversion to provide a base flow. The diversion flow is gravity driven and dependent on the water levels in the Mississippi River and the basin.

The residence time for a given base flow is equal to the volume of water in the conveyance channel divided by the base flow (flowrate). The residence time has been estimated for a range of flow conditions. The volume of water in the conveyance channel during the non-operational period is on the order of 116,000,000 ft^3. This volume is based on a channel length of approximately two miles, a trapezoidal cross-

section with a 300-foot bottom width, 4:1 side slopes up to an elevation of 2 feet, NAVD88 and an average water elevation in the channel of 2 feet, NAVD88.

A plot of the residence time for different base-flow flow rates through the channel is shown in Figure 2.

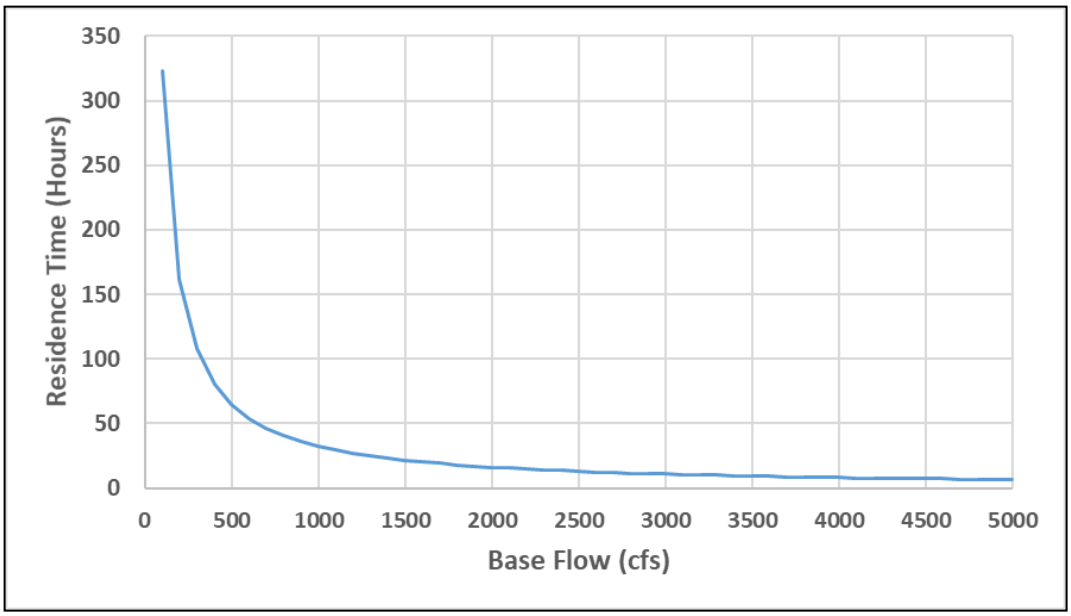

Figure 2 Residence Time Variation with Base Flow Rate

The analysis indicates that for base flow rates of 750 cfs and higher, the channel can be flushed within two days, and much faster for the higher flow rates (<7 hours at 5000 cfs). The ability of the diversion to yield a base flow will depend on the stage difference between the Mississippi River and the basin. At this time, the DT's analysis has been focused on the design flow rate (75,000 cfs) and associated sediment delivery and have not investigated the flow rates sustainable during the non-operational period.

An estimate of the range of water levels in both the river and the basin have been made for current conditions. A rating curve was developed by the water institute based on a HEC-RAS model of the lower Mississippi River. The curve indicates that the stage in the river near the proposed diversion intake for flow conditions below 450,000 cfs will range from approximately 0.75 feet, NAVD88 to 5 feet, NAVD88. This range is substantial and is due to tidal modulation and hysteresis effects.

Identifying the water elevation at the diversion outfall is more difficult because there are no nearby gauges. Data for the ten-year period from Oct. 2009 through Oct. 2019 was obtained for the USGS gauges 07380251 (Barataria Bay N of Grand Isle, LA) and USGS 073802512 (Hackberry Bay NW of Grand Isle, LA). The Grand Isle gage is approximately 26 miles south of the outfall and the Hackberry gage is approximately 18 miles south of the outfall. The 10-year water elevation at the two gages is 1.19 feet, NAVD88 and 0.65 feet NAVD88, respectively.

The monthly average water elevations at the Hackberry gage based on the 10-year period are shown in Figure 3. The average elevations are higher during the non-operational period and range from 0.75 feet, NAVD88 to 1.1 feet, NAVD88.

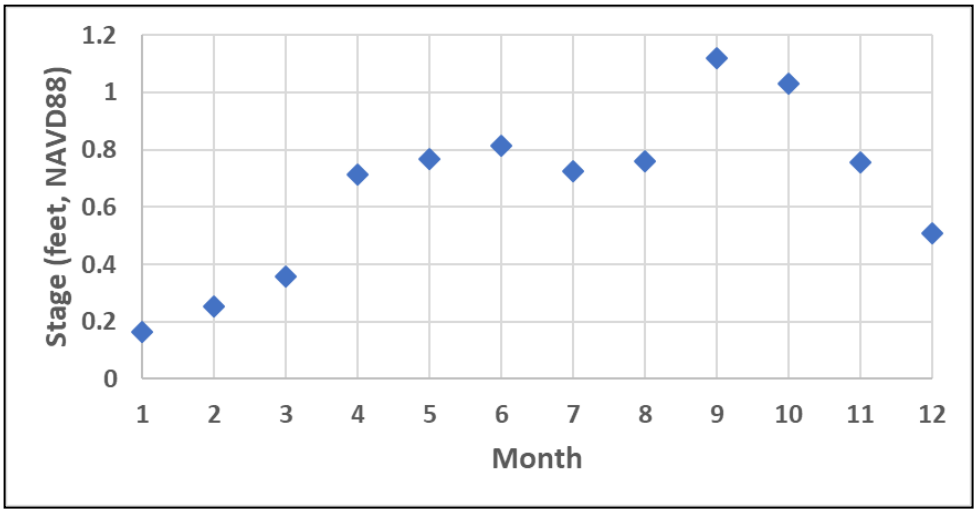

Figure 3 Water Elevations at the USGS Station 073802512 (Hackberry Bay NW of Grand Isle, LA)

A time series plot of stages for a two-year period (1/1/2010 – 12/31/2012) for the Hackberry gage is shown in Figure 4. Tide ranges are on the order of 1 to 2 feet.

Based on the available stage data for the Mississippi River and basin, it is not clear that a base flow can be supported during the entirety of the non-operational period. The higher stages in the available basin stage data exceed the lower range of river stages during the non-operational period. However, the ability of the diversion to provide a base flow will be sensitive to the timing of the relative stages in the basin and the Mississippi River. The available gage data is sufficiently far from the diversion outfall that it cannot be used in a direct comparison (time based) with the river stage data to determine if a sufficient stage difference exists to support a base flow.

It will be necessary to apply the DT models of the diversion and basin for non-operational periods to determine the potential for supporting a base flow.

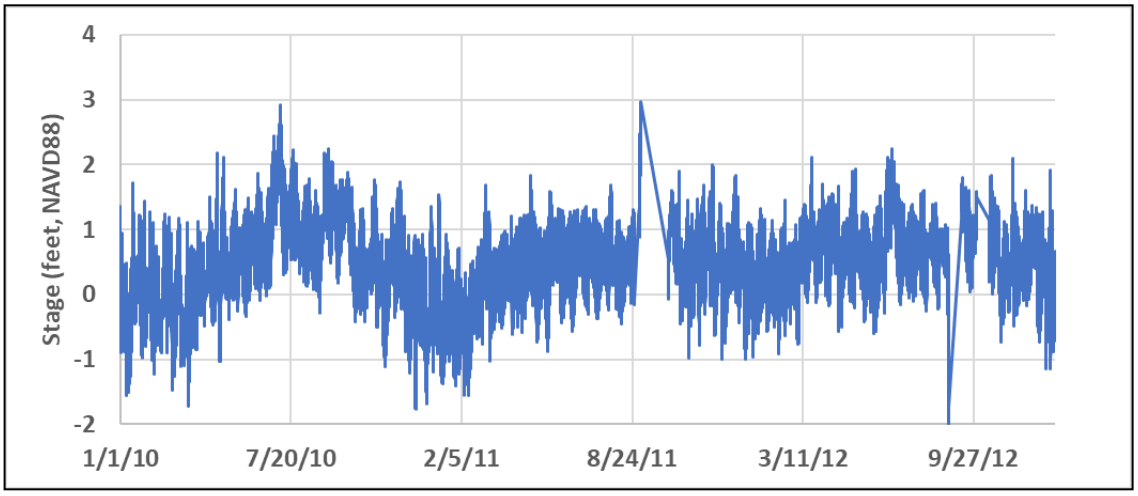

Figure 4 Stage Time Series at Hackberry Gage

III. Assessment of Existing Freshwater Diversions

The two existing diversions on the lower Mississippi River, in the general vicinity of the MBSD are known as the Davis Pond Freshwater Diversion and Caernarvon Freshwater Diversion. These diversions were reviewed with the intent of assessing whether there are any stagnant areas of open water associated with each diversion, and whether nutrients were ever an issue in these areas. The following subsections provide a brief overview of each diversion and their operations, as well as summarize some results of previous studies on nutrients and flows associated with each diversion.

Davis Pond Freshwater Diversion

Overview of Diversion

The Davis Pond Diversion is located on the west bank of the Mississippi River approximately 15 miles upstream of New Orleans, Louisiana. The project area is approximately 10,000 acres, with over 9,000 acres in the ponding area, and a maximum diversion flow of approximately 10,000 cfs. The diversion consists of a gated, four barrel, 14' x 14' concrete culvert with corresponding inflow and outflow channels, approximately 19 miles of guide levees, and 1.8 miles of rock weir. The diversion was fully operational in 2007.

The purpose of the Davis Pond project is to divert freshwater, along with its nutrients and sediments, from the Mississippi River to the Barataria Basin with the goals of reducing saltwater intrusion, establishing more favorable salinity conditions in the area, and combating land loss. Additional objectives of the Davis Pond Diversion include:

- Reduction of marsh loss and enhance marsh vegetation
- Improvements of fish and wildlife productivity
- Control of salinity intrusion
- Removal of nutrients and sediments

The Davis Pond diversion outflows into Lake Cataouatche, which then flows into Lake Salvador, Little Lake and then Barataria Bay.

Operations & Flow of Diversion

The Davis Pond Diversion is operated with the intent of maintaining a seasonal average salinity at designated target lines which range from 15 parts per thousand (ppt) from December to May, and 5 ppt from June through November. The 15 ppt line (or isohaline) is approximately 10 to 12 miles seaward (towards the Gulf of Mexico) from the 5 ppt line, which runs roughly east-west along the northern portion of Barataria Bay. The structure is operated when the 14-day moving average salinity is within or above the long-term data range for the gauges used to monitor the salinity. When the moving average drops below the trigger, which is the greater of the long-term average minus 1 SD or 5 ppt, the diversion operations will be maintained at a minimum flow of 1,000 cfs until the moving average re-enters the operational range. The operational settings are not to exceed 10,000 cfs.

Discharges may deviate from the operational plan for both projects as described in the three bullet points below:

- Emergency, maintenance and local parish situations are evaluated on a case-by-case basis to determine the needs of the operational plan [If operations outside the plan are required, the Davis Pond Advisory Committee shall be notified].
- Structure may be operated for public relations and/or educational purposes; however, output is not to exceed 5,000 cfs for a duration of no longer than 2 hours.
- Coordination with the Louisiana Department of Wildlife and Fisheries (LDWF) is required during the post-larval migration period for brown shrimp and the oyster reproductive seasons to maximize the system's benefit.

Caernarvon Freshwater Diversion

Overview of Diversion

The Caernarvon Diversion is located on the east bank of the Mississippi River, 15 miles downriver from New Orleans in Plaquemines Parish. It includes five, 15-ft gated box culverts and was designed to divert up to approximately 7,500 cfs of freshwater. The diversion began operating in 1991.

The purpose of the Caernarvon project is to re-introduce freshwater, sediments and nutrients into the marshes and bays of Breton Sound estuary, limiting the capture of sediment. Additional objectives of the Caernarvon Freshwater Diversion include:

- Enhancement of emergent marsh vegetation growth
- Reduction of marsh loss
- Improvements of fish and wildlife productivity

Operations & Flow of Diversion

Like the Davis Pond Diversion, the Caernarvon Diversion is operated with the intent of maintaining a seasonal average salinity at designated target lines which range from 15 parts per thousand (ppt) from December to May, and 5 ppt from June through November. The 15 ppt line is approximately 10 to 15 miles seaward (towards the Gulf of Mexico) from the 5 ppt line, which lies along the northwestern portion of Black Bay. The structure is operated when the 14-day moving average salinity is within or above the long-term data range for the gauges used to monitor the salinity. When the moving average drops below the trigger, which is the greater of the long-term average minus 1 SD or 5 ppt, the diversion operations will be maintained at a minimum flow of 500 cfs until the moving average re-enters the operational range. The operational settings are not to exceed 7,500 cfs.

Also, like Davis Pond, discharges may deviate from the operational plan for both projects as described in the three bullet points below:

- Emergency, maintenance and local parish situations are evaluated on a case-by-case basis to determine the needs of the operational plan [If operations outside the plan are required, the Caernarvon Advisory Committee shall be notified].
- Structure may be operated for public relations and/or educational purposes; however, output is not to exceed 5,000 cfs for a duration of no longer than 2 hours.
- Coordination with the LDWF is required during the post-larval migration period for brown shrimp and the oyster reproductive seasons to maximize the system's benefit.

Nutrients – Davis Pond & Caernarvon Diversions

As part of this desktop study, documents were reviewed on possible effects of freshwater diversions on nutrient loading in the Mississippi River and associated lakes and bays.

In an article written by Caffey, Coreil, and Demcheck in 2002, titled: *Mississippi River Quality: Implications for Coastal Restoration*, it mentions: "Overabundance of nutrients can cause adverse impacts such as eutrophication. To date, nutrients have not been a problem in river diversions used for coastal restoration." A 2105 report titled: *Davis Pond River Diversion Project: Pre and Post Diversion Trends for Salinity Intrusion and Nutrient Removal*, by the Coastal Protection and Restoration Authority (2015 CPRA Report) is quoted for saying: "In addition to improved management of nonpoint and point sources, river diversion projects have emerged as a key component of Louisiana's Nutrient Management Strategy to address the reduction of nutrient loading from the Mississippi River to mitigate hypoxia in the Gulf of Mexico." This 2015 CPRA Report compares pre and post diversion data for a variety of nutrients and mentions how the assessments of Davis Pond is consistent with results reported for studies on the Caernarvon Diversion, particularly regarding Nitrogen and Phosphorus. Some of these summary points include:

- "Consistent with other studies of the Davis Pond diversion and the Caernarvon diversion, almost all the nitrate load from the Mississippi River was seen to be rapidly removed from the freshwater wetlands and marshes of Davis Pond" (CPRA, 2015).
- Removal efficiency (45 – 50%) for Total Nitrogen and nitrate appear to be highest during low diversion discharge, and is about twice as high as the removal efficiency (20 – 27%) for high diversion discharges.
- Total Phosphorus has a removal of 10 – 43%, with a corresponding mass removal rate of 0.3 – 1.1 g P $m^{-2}yr^{-1}$ within the wetlands and marshes of Davis Pond. The highest removal efficiency of 43% was documented in this study for low river flow and low diversion discharges, whilst the lowest (at 10%) was seen for high river flow and high diversion discharges.

The 2015 CPRA Report also discusses the results of Chlorophyll-a sampling, before and after the Davis Pond Diversion as a means of assessing the diversion's effect on nutrients. According to the post-diversion analysis, the diversion has helped control the accumulation of excessive algal biomass, due to the increased flushing rate caused by the diversion. Apparently, excessive algal biomass was a common occurrence in the years before the Davis Pond Diversion became operational.

These statements and most of the research reviewed regarding the Davis Pond and Caernarvon diversions discuss how the freshwater diversions address nutrients on a larger scale (e.g., effects of the diversion on nutrient loading on the Mississippi River and its associated bays, and estuaries). However, specific discussions on nutrient-related issues within the boundaries of the diversions themselves was not encountered during the desktop study.

IV. Summary

A review of potential water quality issues in the conveyance channel during non-operational periods has been conducted. The following conclusions can be drawn from this review.

- The primary water quality issue is potential algae growth and eutrophication due to a combination of high nutrient levels, low flow or stagnant flow conditions and warm temperatures.
- The available measured nutrient and temperature data are sufficiently high enough, that their potential impact cannot be ruled out, but the potential is also not overwhelming.
- A review of adjacent existing diversions did not indicate negative impacts in the diversion channels. However, the Davis Pond diversion does maintain a base flow of 500 cfs and the Caernarvon Diversion has a minimum flow of 1000 cfs.
- The most feasible means to prevent potential negative impacts is to maintain a base flow or intermittently provide pulsed flow to flush the conveyance channel.
- Since the system is gravity driven, the ability to maintain a base flow or provide pulsed flow during non-operational periods is dependent on basin and river stages. Measured data is not currently available to provide a means to establish the head difference. However, the data reviewed does indicate the potential for some periods when the gradient may not be enough to support a base flow.
- The ability to evaluate stage differences for future conditions cannot be determined using measured data (since do data is available to represent future conditions).

It is recommended that in the next design phase the DT conduct modeling analyses to assess the proposed design's ability provide base flow. The ability to provide base flow is the most viable means to cure any nutrient based negative impacts on water quality in the conveyance channel during non-operation periods. Note that the stage gradient is not the only factor to consider, and other processes such as shoaling in front of the diversion gates may impact the ability to provide base flow for flushing the conveyance channel.

In summary, the potential for negative water quality impacts is considered minor but possible. The most feasible way to eliminate the potential is to provide capability for base flow. However, the potential to provide base flow cannot be demonstrated without additional modeling analysis, which is recommended for the next design phase.

Fortunately, there are other methods that can be used to mitigate potential negative water quality impacts if a base flow cannot be maintained. For instance, auxiliary pumps may be installed to provide the base flow (i.e. gates closed and pumping from the river into the diversion). Since boat access will be provided at the outfall, vessel-based reaeration is another possibility. Either of these options can be developed after the diversion is constructed and operated, and only considered if water quality issues do occur. Thus, not addressing nutrient-based water quality impacts is a viable approach for the diversion design.

V. References

State of Louisiana – Coastal Protection and Restoration Authority (CPRA), 2015, Davis Pond River Diversion Project: Pre and Post Diversion Trends for Salinity Intrusion and Nutrient Removal

Coastal Protection & Restoration Authority (CPRA) on Caernarvon & Davis Pond Diversions (http://coastal.la.gov/diversion-operations/)

Caernarvon Freshwater Diversion and Delta; LPBF, website: https://saveourlake.org/lpbf-programs/coastal/coastal-projects/caernarvon-freshwater-diversion-and-delta/

Environmental Assessment – Mississippi Delta Region – Caernarvon Freshwater Diversion Structure – Change in Structure Operation – Plaquemines and St. Bernard Parishes, Louisiana (EA # 32), website: https://saveourlake.org/wp-content/uploads/PDF-Documents/our-coast/CaernarvonEA392Final.pdf

Caffey, R. H., P. Coreil, and D. Demcheck (2002); Mississippi River Water Quality: Implications for Coastal Restoration, website: https://www.lacoast.gov/new/Data/Reports/ITS/MRWQ.pdf

ATTACHMENT A

PLOTS OF NUTRIENT DATA

:

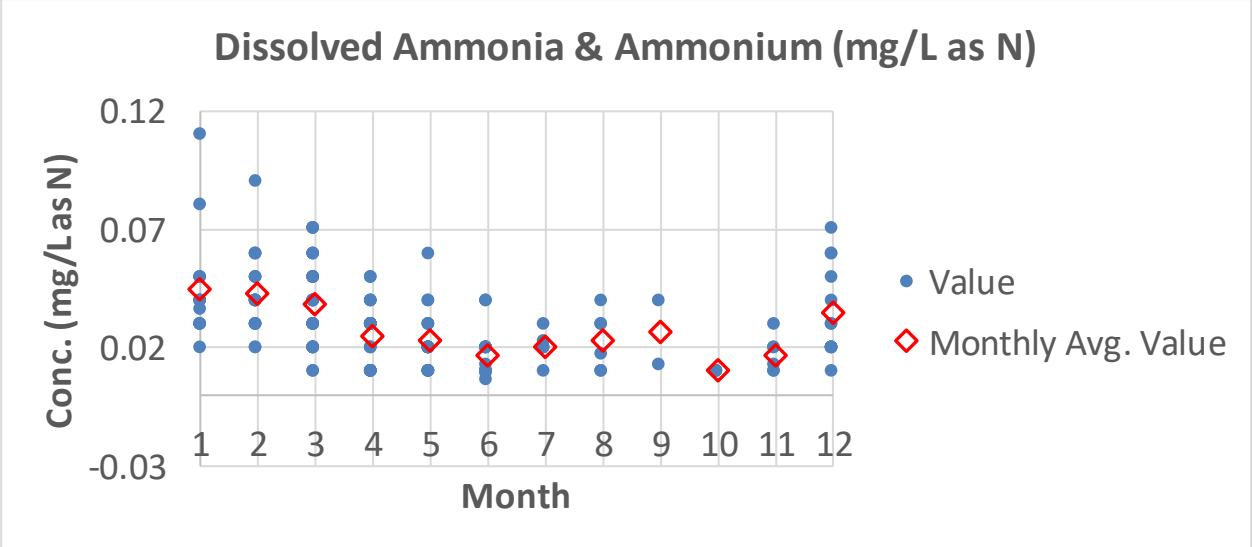

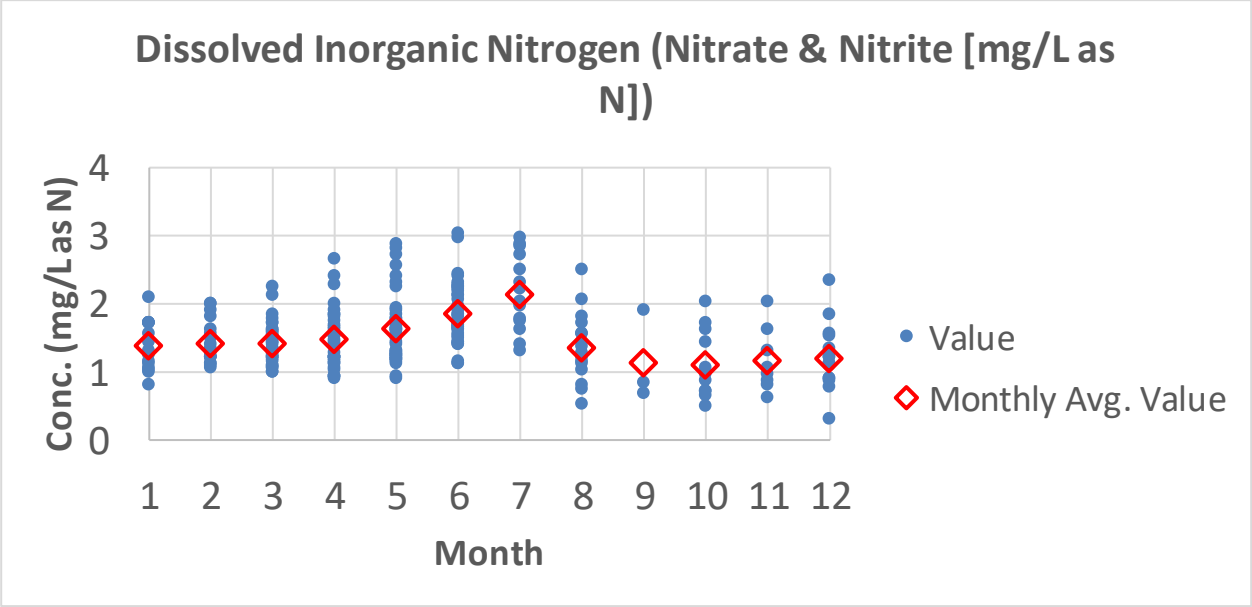

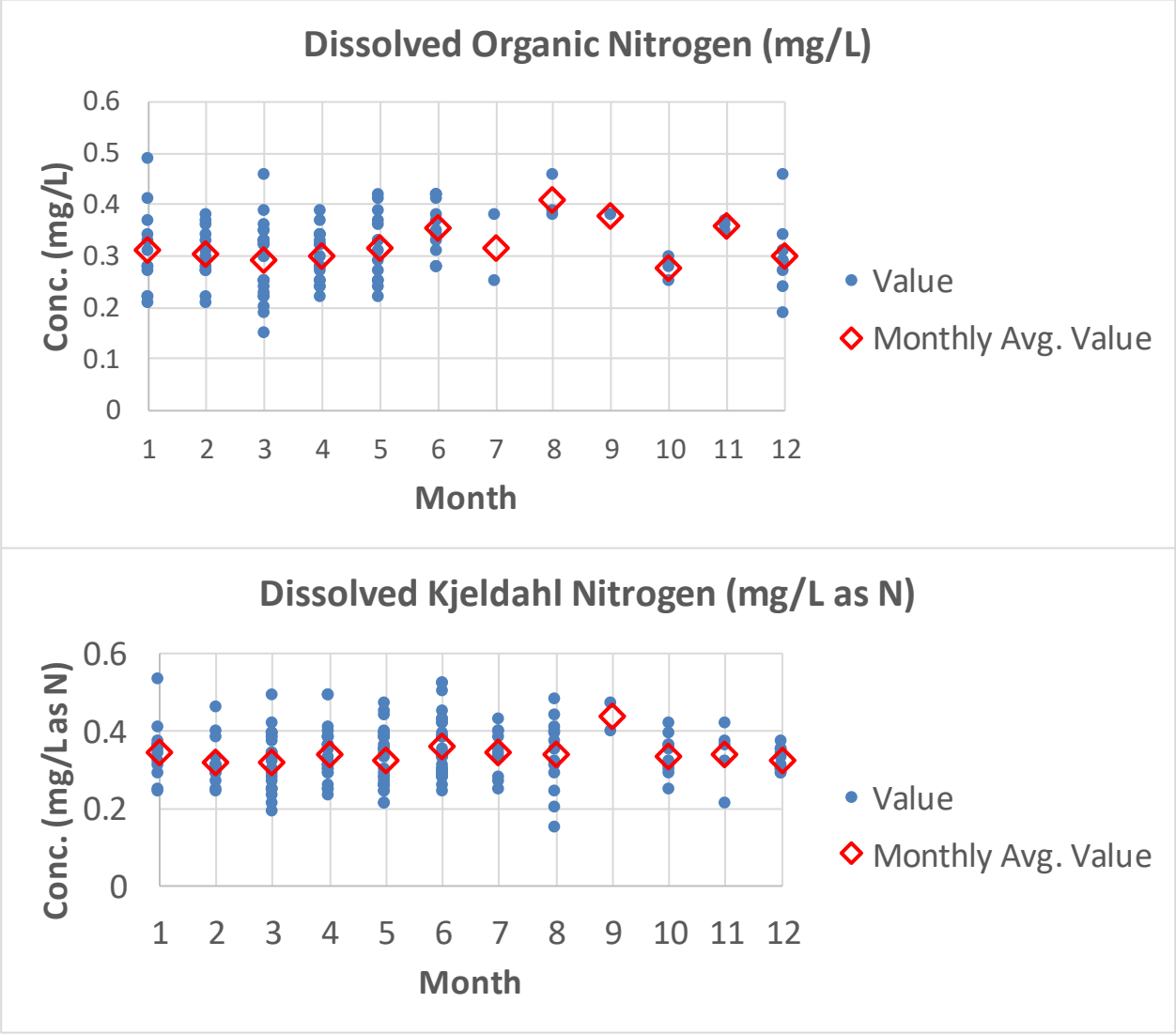
Dissolved Organic Nitrogen (mg/L)
Conc. (mg/L)
0.6
0.5
0.4
0.3
0.2
0.1
0
1 2 3 4 5 6 7 8 9 10 11 12
Month
Value
Monthly Avg. Value
Dissolved Kjeldahl Nitrogen (mg/L as N)
Conc. (mg/L as N)
0.6
0.4
0.2
0
1 2 3 4 5 6 7 8 9 10 11 12
Month
Value
Monthly Avg. Value

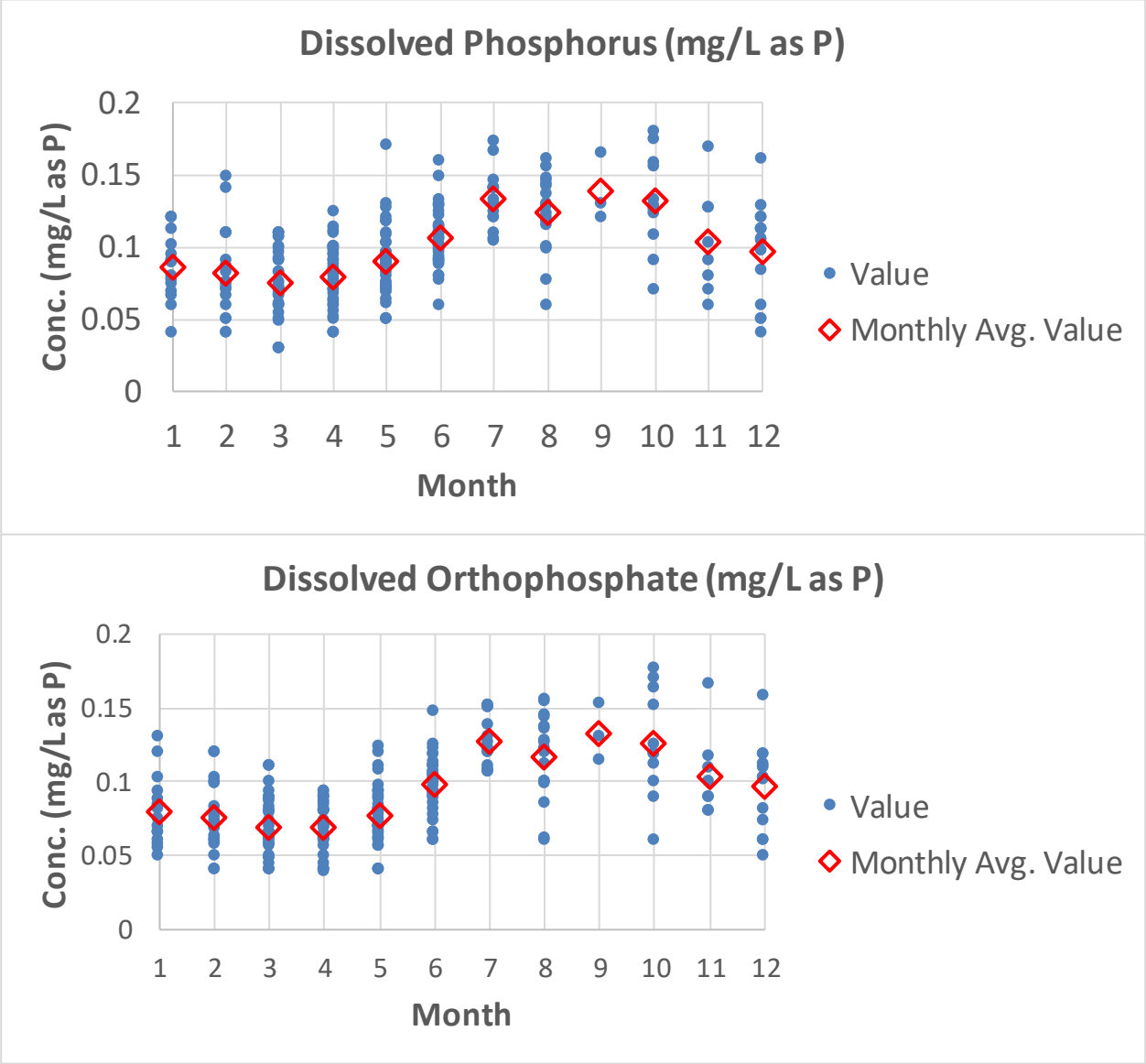
Dissolved Phosphorus (mg/L as P)
Conc. (mg/L as P)
0.2
0.15
0.1
0.05
0
1 2 3 4 5 6 7 8 9 10 11 12
Month
Value
Monthly Avg. Value
Dissolved Orthophosphate (mg/L as P)
Conc. (mg/L as P)
0.2
0.15
0.1
0.05
0
1 2 3 4 5 6 7 8 9 10 11 12
Month
Value
Monthly Avg. Value

APPENDIX B4

Louisiana Highway 23 Bridge Scour Evaluation

Final Deliverable Release

Final Deliverable Release

Task or Service: BA-0153 MBSD

Deliverable: Revised Hwy. 23 Bridge Scour Report

Technical Lead: Mark Gonski, PE

Date: 4/24/2020

Part 1-Quality Review Certification

As AECOM's Technical Lead for this project, I hereby release this deliverable in its final form consistent with the associated Quality Management Plan. Outstanding quality issues that must be deferred for resolution in a subsequently work phase, if any, have been discussed with the PMT Technical Lead, and have been placed in the Issue Tracking System.

Items added to Issue Tracking System: Yes [X] No

Mark Gonski, PE

Signature

Mark Gonski, PE

AECOM Technical Lead (print)

4/24/2020

Date

AECOM

Date: April 2018
Rev. 0

Technical Quality Review Record

Project #	60591673	Delivery Date	04/14/2020
Project Name	BA-153 MBSD	Originator	Sarah McEwen
Client/Client POC	CPRA	Comments Due By	04/20/2020
PM Name	Bruce Lelong, PE	Assigned Individual(s):	Jennifer Duhe
Title of Work Product	Revised Hwy. 23 Bridge Scour Report		

Type

☐ Calculation Check ☐ Independent Review (IR) ☐ Interdisciplinary Coordination Review ☐ Specification Package Review
☐ Discipline Review ☐ Verification ☐ Technical Approach/Solution ☐ Bidability Review
☐ Subconsultant, Client, or Third-Party Information Review ☐ Constructability Review
☑ Other Specify (e.g. Construction Services documentation): Backcheck

Review Scope

☐ Technical edit for elements such as grammar, punctuation and formatting
☐ Detail check of calculations and graphics
☑ Organization, clarity and completeness
☐ Soundness of approach/design
☐ Conformance with standards
☑ Completion of check
☐ Technical Approach/Solution
☐ Application of Statements of Limitations
☑ Basis and validity of conclusion/recommendation
☐ Completion of review of client and third-party information
☑ Other Specify: Backcheck

Quality Control (QC) Checking

For comments column, select N (None), HC (Hard Copy), EF (Electronic File – add network link), or (Review Comment Form)

Discipline	*Description (Calc/Rpt/Dwg/Specs)*	*Comments*	*Network Link*	*Originator Initials*	*Date*	*Reviewer Initials*	*Date*
Hydraulics	Report	None	n/a	SM	04/14/2020	JD	04/21/2020

Independent Review (ITR) Verification

(Note: Technical Quality Reviews are often iterative, requiring multiple rounds to verify accuracy and completeness of the work product. This section is to be completed by the Lead Verifier after verification of comment incorporation to include subsequent or new comments.)

Select:

☑ Lead Verifier has verified that comments have been adequately addressed. There are no outstanding issues.

or

☐ Lead Verifier has verified that comments have been adequately addressed, except for unresolved issues. Any unresolved issues have been submitted to the Project Manager or Designee for final resolution.

and

☑ Lead Verifier confirms that the work product is complete and in accordance with the technical approach/solution.

Duhe, Jennifer Digitally signed by Duhe, Jennifer
DN: cn=Duhe, Jennifer, ou=USNOL1
Date: 2020.04.23 22:30:27 -05'00'

Lead Verifier Signature — Date

Lead Verifier Signature — Date

Independent Reviewer Signature (If Delegated by Lead Verifier**)** — Date

FOR USE BA-153 MBSD PROJECT ONLY

AECOM	Date: April 2018 Rev. 0

Technical Quality Review Record

Quality Assurance (QA) Approval

☑ Confirmation that the deliverable has been reviewed for overall completeness, compatibility and conformance with scope and other contract requirements; all applicable reviews have been completed and deliverable is ready for submission to the client.

Bruce Lelong, PE — Digitally signed by Bruce Lelong, PE Date: 2020.04.24 09:07:20 -05'00'

Project Manager (or Designee) Signature — Date

Jeff Decoteau — Digitally signed by Jeff Decoteau Date: 2020.04.24 09:09:06 -05'00'

Project Quality Manager Signature (as applicable) — Date

DISTRIBUTION	Project Central File – Quality File Folder	Other Specify:

FOR USE BA-153 MBSD PROJECT ONLY

LA 23 Bridge Scour Evaluation Report

Mid-Barataria Sediment Diversion
Route LA 23

Coastal Restoration and Protection Authority

CPRA No. 4400013603
AECOM Project No. 60591673

April 2020

150 Terrace Ave
Baton Rouge, LA 70802

AECOM Imagine it. Delivered.

Table of Contents

List of Appendices

List of Tables

List of Figures

Preface

The Coastal Protection and Restoration Authority (CPRA) has located the Mid-Barataria Sediment Diversion (MBSD) on the West Bank of the Mississippi River (MR) in Plaquemines Parish, Louisiana, at River Mile 60.7 Above Head of Passes (AHP), between the Phillips 66 Alliance Refinery upriver and the Town of Ironton downriver. The diversion will reconnect the MR to the Barataria Basin, delivering sediment to rebuild the delta marshes with the ultimate goal of improving coastal protection against the effects of sea level rise, subsidence, and storm events. The diversion intake is sited at a point bar to facilitate the capture of sand. As part of this project, a new Hwy 23 Bridge will be constructed along the current alignment of Hwy 23. This report includes a summary of the hydraulic modeling and scour analysis used as the basis of design for the proposed bridge at the intersection of Hwy 23 and the Mid-Barataria Sediment Diversion.

I. Summary

Hwy 23 is a north-to-south state highway that serves both Plaquemines and Jefferson Parishes. It is also known as Belle Chasse Highway, Lafayette Street, and the West Bank Expressway at different locations along its length. Hwy 23 connects Gretna and Venice. Between Belle Chasse and Venice, the highway is the main thoroughfare along the western bank of the Mississippi River. This route provides the only access in and out of Plaquemines and lower Jefferson Parishes and is a State of Louisiana evacuation route during hurricane season. Hwy 23 is approximately 74 miles long. Within the area of the project, the roadway is a four-lane rural arterial asphalt composite roadway with 4 feet wide inside and 10 feet wide outside shoulders and a 42 feet wide depressed grass median.

The Hwy 23 Bridge will begin approximately 4,300 feet downstream of the confluence of the conveyance channel with the Mississippi River. The bridge will span the guide levees and Conveyance Channel. Currently 16 bents spaced on 128-foot centers are proposed for support of the bridge. There are 4 bents located in the conveyance channel and 2 on the adjacent berms. Design and construction of the bridge will conform to standard requirements of the Louisiana Department of Transportation and Development (LADOTD). Scour protection will be provided throughout the Conveyance Channel, between the top of the channel, the levee toe, and up the levee slope.

II. General Description of the Area

The Mid-Barataria Sediment Diversion (MBSD) will span from the Mississippi River to Barataria Bay, intersecting the Mississippi River Levee (MRL), a railroad crossing, Hwy 23, an existing back levee, drainage ditches, and two drainage canals, the Timber Canal and Back Levee Canal. The site location along the Mississippi River is shown in Figure II-I and a schematic of the diversion structure, including the intake, conveyance channel and outfall is shown in Figure II-II. A river barge fleeting area, with mooring monopoles, is located along the river's right, descending bank, where the Intake Structure will be located. The barge fleeting area extends both upriver and downriver of the Intake location. The existing MRL crown elevation is approximately EL 15.5, but is authorized to EL 16.4. An existing railroad track, operated by NOGC Railway, is located at grade, on the protected side of the MRL, and terminates just south of the MBSD site. The wooded fastlands reach stretches from the MRL to Hwy 23, which is an at-grade 4-lane divided highway running in a north-south direction.

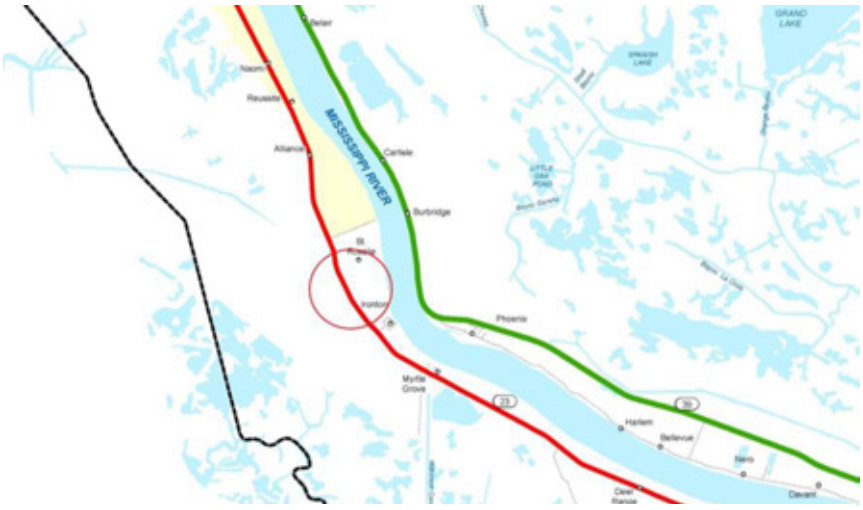

Figure II-I: Project Location

Between Hwy 23 and the back levee, the existing site is mostly comprised of borrow pits and drainage ditches. The downstream end of the proposed Conveyance Channel will intersect the existing back levee, for which the United States Army Corps of Engineers (USACE) is planning to construct improvements.

This project, titled NOV-NF-W-05a.1 LaReussite to Myrtle Grove, originally called for the enlargement of the existing levee near its existing alignment. However, USACE is currently considering shifting this alignment close towards Hwy 23. After USACE announces their final alignment decision, the MBSD Conveyance Channel Levees will be designed to tie-in to the chosen levee alignment.

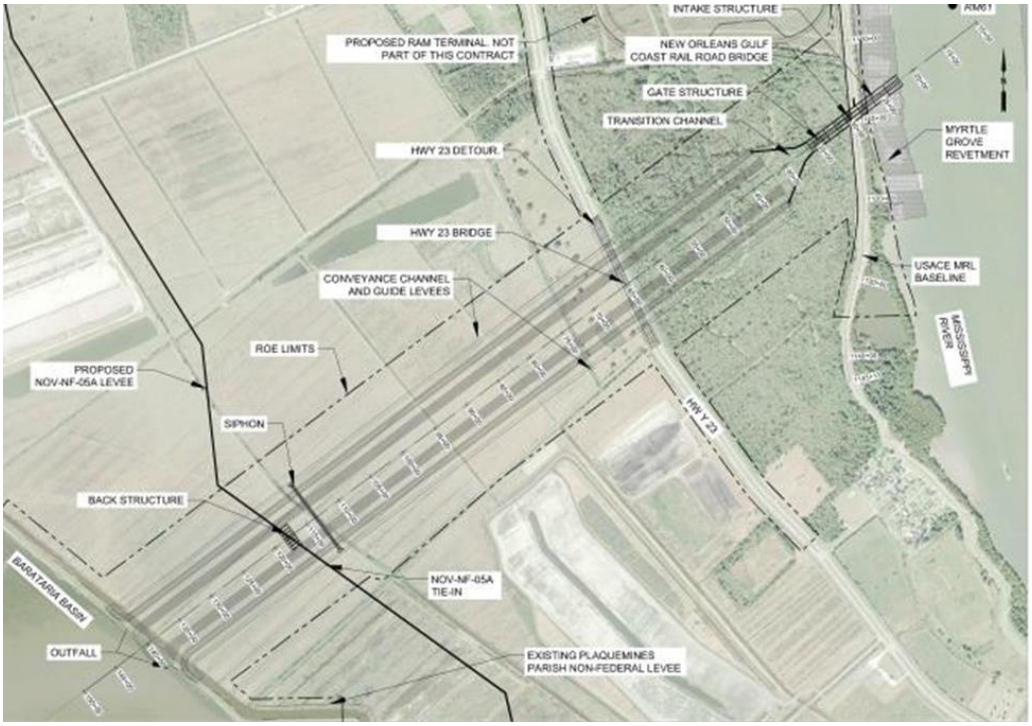

Figure II-II: Diversion Structure

III. Existing Data Sources

Hwy 23 is classified as a Rural Minor Arterial. The Design Team (DT) conducted a field visit on June 1, 2018 to visually inspect the corridor. Within the project area, road and pavement markings including outside lane edge rumble strips were in good condition. During the visit, the DT reviewed the two main intersections along the corridor. A visual review at the intersection of Hwy 23 and Ravenna Road did not indicate any issues with line of sight or signs and pavement markings. W. Ravenna Road is a gravel road with no surface markings or signs while E. Ravenna Road is an asphalt paved roadway with signs and pavement markings. During the visit, East Ravenna Road was observed to have several commercial trucks making a left turn from Hwy 23. A visual review at the Intersection of Hwy 23 and Ironton Road also did not indicate any issues with line of sight, signage and marking, or artificial lighting. No queueing was observed at any of the intersections. While efforts to obtain current data are ongoing, existing data was used to initiate conceptual designs and perform alternatives screening. Examples of existing data include the following:

- Results from previous geotechnical borings and testing
- Hydraulic models performed by TWIG (The Water Institute of the Gulf) and CPRA
- Aerial imagery
- Light Detection and Ranging (LIDAR) data
- 2013 River Bathymetry
- 2017 USACE Revetment Surveys
- TWIG's Mississippi River Sediment Data at the MBSD site

For the purpose of developing the hydraulic model, current 60% design phase plans were used to set the sediment diversion channel shape and elevations. The conveyance channel as modeled in the 2D FTNOMBA model was used to calibrate the hydraulic model for the diversion discharge.

IV. Interagency Coordination

CPRA is executing the E&D services for the MBSD project in two phases: a BOD Phase, in which the DT performs 15%-level alternatives analyses, and Phase 2, which will include detailed E&D of the diversion, permitting support, and coordination with the Construction Manager at Risk (CMAR). The Basis Of Design Report (BODR) documents the work performed in the BOD Phase. The bridge scour and hydraulic evaluation is also being completed as part of the BODR. This report will be submitted separately to LADOTD to meet agency requirements for bridge hydraulic reporting.

V. Design Analysis

The evaluation of scour has been conducted for the proposed bridge piers. The analysis follows the LADOT design guidance and includes analysis methods provided in both the HEC-18 and Florida Department of Transportation (FDOT) scour manuals. The analysis requires the description of the

A. Pier and cannel cross-section geometry,

B. Specification of the design flow conditions and

C. Soil characteristics

Each of these is summarized below, followed by a flow analysis to determine the flow velocities associated with the design flows and then the scour estimates.

A. Proposed Bridge Layout and Pier Geometry

The superstructure would consist of an 8-inch concrete bridge deck with a 4-inch haunch and ten lines of 63-inch tall LG prestressed concrete girders. Concrete barrier rails will be the current standard 36-inch MASH compliant straight sloped barriers.

The substructure would consist of two controlling bent types. Outside the levee sections of the Conveyance Channel, the bents would be 24” Prestressed, Precast Concrete (PPC) piles extending up to the pile cap. Most bents would be supported on a single row of vertical piles, 10 piles per bent. Intermittent bents would have 2 rows of PPC piles extended to the cap, the piles will be battered in the direction of the bridge access. There are 10 PPC piles in each of the 2 rows. The 6 bents located in the channel and adjacent berms, bents 7 thru 12, would consist of 60-inch diameter columns, a continuous pile cap 10.5 feet width with a rounded head, and a pile group consisting of 2 rows of 24”x24” PPC piles with 10 piles per row battered in the direction of the channel flow. The cap was placed 5 ft below the channel armoring. Bents are skewed to the flow in the channel.

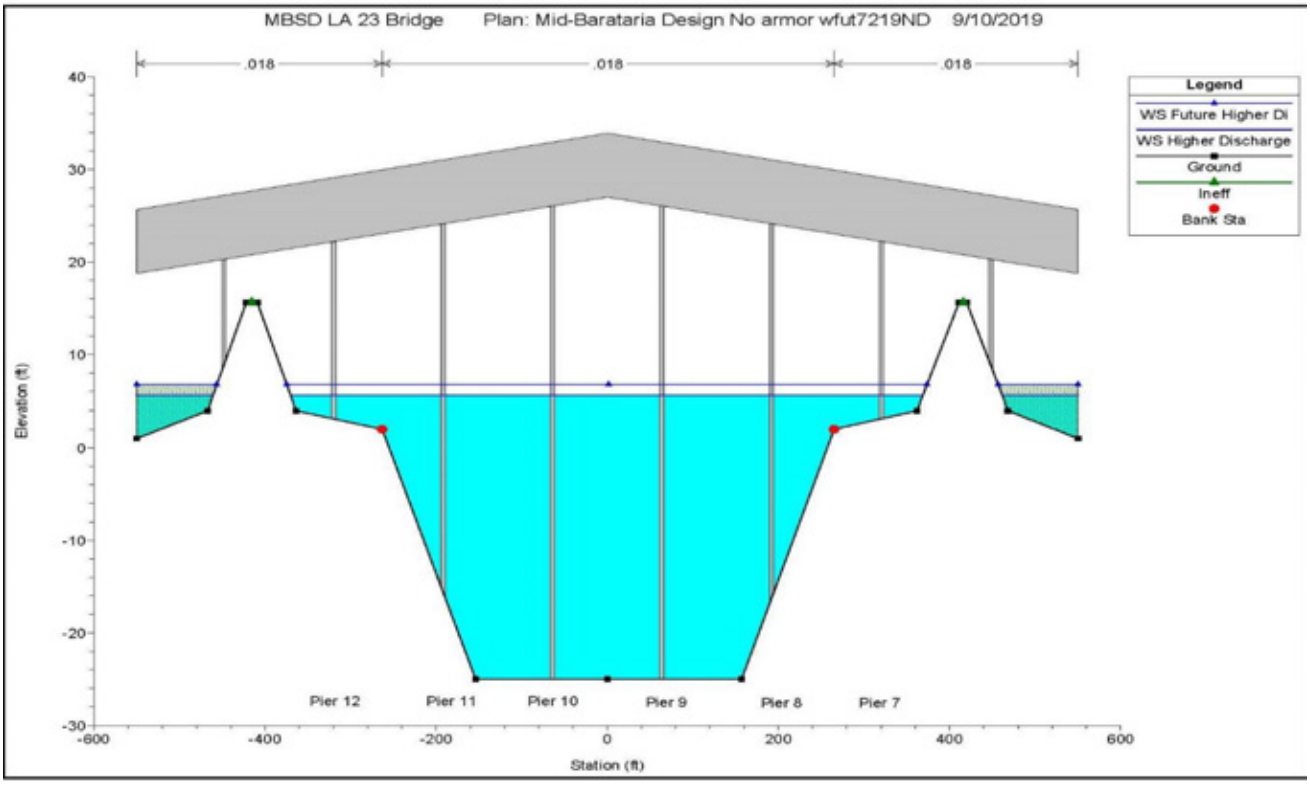

Figure V-I: Proposed Option 1 (60" Columns)

At grade abutments and approach slabs would be constructed to LADOTD standard details. All bridge plan and foundation information was taken from the 60% Preliminary Bridge plans. Figure V-I shows the proposed option internal bridge cross section looking downstream.

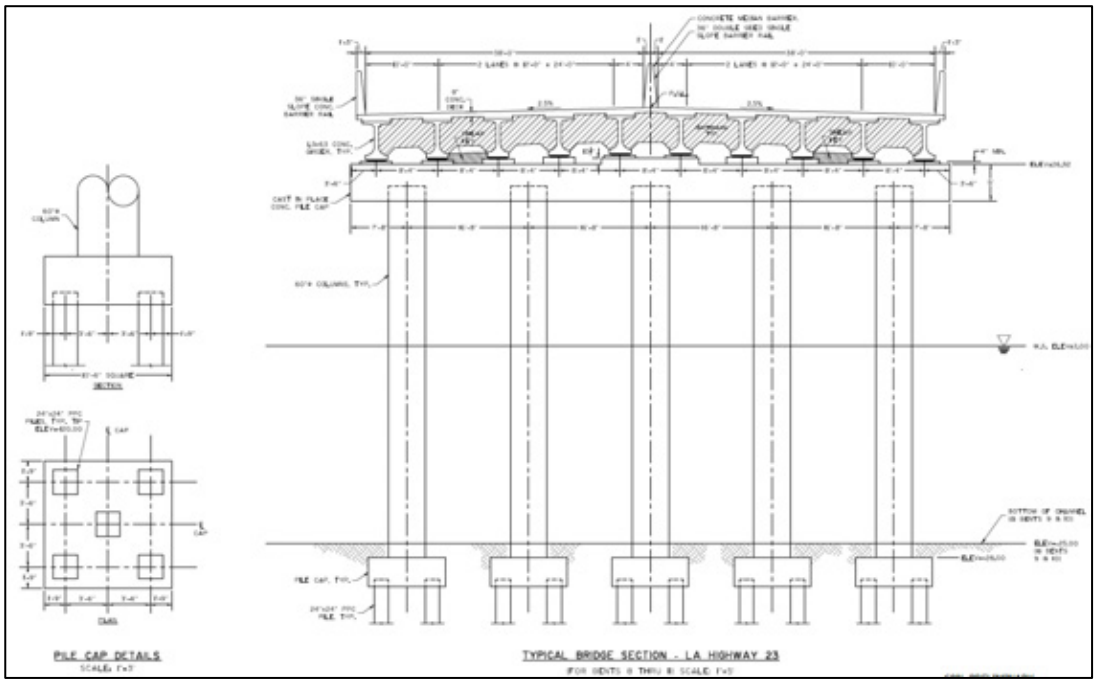

Figure V-II: Proposed Bridge Typical Section for Bents 8-11

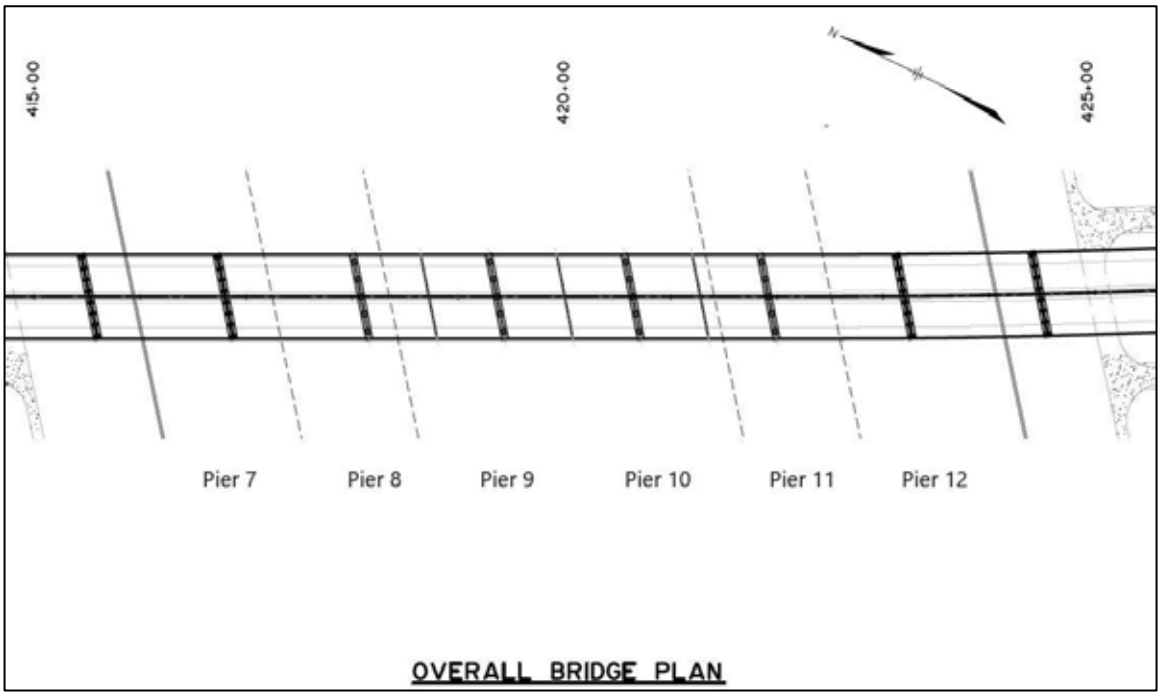

Figure V-III: Proposed Bridge Plan View from 60% Bridge Plans

The proposed bridge structure begins at Roadway Station 409+03 and ends at Station 430+79, and overall length of 2,176 feet. It will consist of 17 spans that are 128 feet long each. The bridge clearance over the levee roads will be at least 16 feet, 6 inches at the high point of the roadway. The controlling clearance is 25 feet above a Water Elevation of 2 (NGVD 88) which is centered at Roadway Station 420+00 seen in Figure V-III above and HEC-RAS cross section station 0+00 in Figure V-I on the previous page. There is at least 7 feet of clearance above top of the Conveyance Channel floodwalls of 15.6 feet NGVD.

B. Hydrodynamics

The hydrologic and hydraulic analyses of the diversion structure and the numerical and physical modeling to support the E&D are described in the BODR. CPRA has a parallel, ongoing modeling effort with TWIG on MBSD. The DT's modeling is expected to be consistent with those efforts. The analysis performed leverages work already completed by CPRA/TWIG including the model setup (e.g. model geometry, boundary conditions) and findings. The primary modeling analysis is based on a DELFT3D model of the river, diversion and basin called 2D-FTN Outfall Management Model (OMBA).

The overall goal of the numerical modeling is to develop the design of an Intake Structure that can divert a maximum flow of 75,000 cfs flow when the Mississippi River reaches 1,000,000 cfs at the Belle Chasse gage with as high Sediment-to-Water (SWR) ratio as achievable; approaching 1.0. Physical models at 1/65th scale, that include a portion of the conveyance channel, have been built and the results are being used to verify the numerical model.

The DT is recommending the governing design condition to be 96k cfs. The 96k cfs exceeds the project design requirement of 75k cfs. The higher flows are possible at a maximum river discharge of 1.25 Mil cfs if gates are improperly operated. This same higher flow was adopted for the design of the conveyance channel and outfall armoring. The 96,000 cfs peak flow will be reduced in the future due to a loss of head across the diversion structure. This is due to sea level rise and land building expected to occur in the basin. At the 50 year horizon, based on the results of the 2D-FTN OMBA model, the peak flow under the same operational scenario as for the 96,000 cfs flow is excepted to be reduced to 87,000 cfs.

For the purpose of the pier scour analysis, both the 96,000 cfs (existing conditions scour design flow) and 87,000 cfs (future conditions scour design flow) were used to evaluate the bridge hydraulic capacity and associated scour within the conveyance channel.

The flow conditions chosen for the scour analysis model are adopted from the 2D FTN Outfall Management Model (OMBA) model results and are summarized in Table V-I.:

Table V-I: Calibration Point Conditions

Diversion Discharge (CFS)	WSEL at Bridge (ft, NAVD88)
96,000 (Current Conditions)	5.7±0.2
87,000 (Future Conditions)	6.8±0.2

The variability of the WSEL at the bridge is with respect to the FTN OMBA model, this is the variability in tolerance shared for that model. When calibrating to the model this was used as the allowable tolerance to match with WSEL from HEC-RAS.

Channel roughness factors (Manning's n) values used in the hydraulic computations for both channel and overbank areas were based on values provided by Chow Manning's values (Chow, 1959 (Edition January 1, 2009)). See the table below of the summary of manning's values.

Table V-II: Manning's "n" Values

Model Landuse	Typical Value
Armored Channel	0.033
Unprotected Channel	0.018

The downstream boundary condition was set to normal depth and varies for each design flow. The boundary condition along with the manning's n was used to calibrate and match the elevation at the bridge produced by the design flow in the 2D FTN OMBA model.

Armored channel values were used throughout the diversion structure within the levees except in the vicinity of the internal bridge. No armoring was assumed in the vicinity of the bridge to represent natural channel sediment conditions. This was done at the request of LADOTD in order to evaluate the unprotected channel conditions at the bridge should the design armoring move during the design life.

C. Sediment Characteristics

Soil borings were located throughout the proposed channel and roadway location. Three borings were selected for review and applicability in determining soil parameters. The borings used are HB-3U, HB-4, and HB-5. The samples from the borings at a depth range of 20-40 were used to develop the soil parameters. There were three types of soil found in the substrate. They are classified within this depth range as sand, silt, and clay.

In order to evaluate the scour susceptibility at this location each soil type was reviewed independently with respect to scour. Although it should be noted that the realistic composition of the soil could be a mix of soil classifications and vary throughout the site. The sand analysis was generally assumed with a D50 particle size of 0.063 mm (0.0002 ft) in absence of more detailed information. The silt analysis used the

samples from the borings that were classified as silt and had additional hydrostatic testing associated. This analysis used average silt D50 of 0.0387 mm. The clay analysis used the samples from the boring that had associated plasticity index values. These values were averages and applied to equations relating plasticity index to critical shear. A more detailed review and explanation of the associated procedures is included in Appendix B.

VI. Design Velocities

The U.S. Army Corps of Engineers Hydrologic Engineering Center, River Analysis System (HEC-RAS) software, Version 5.0.3 was used to perform a one-dimensional steady flow analysis of MBSD within the study area. The layout of the HEC-RAS cross-section are shown in Figure VI-I.

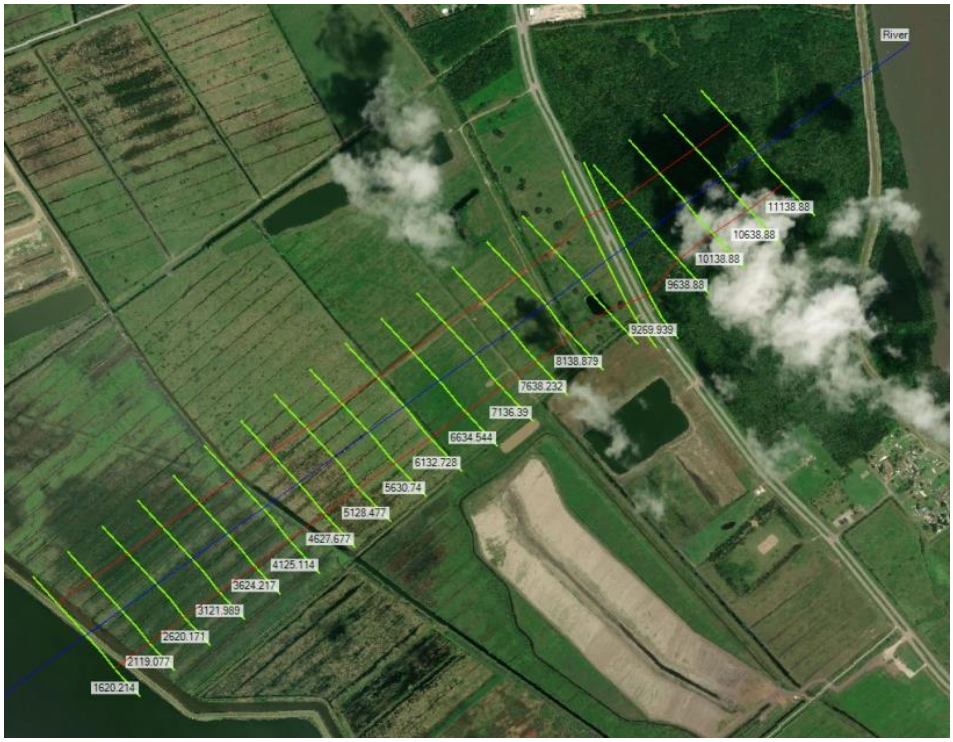

Figure VI-I: Geometric Data HEC-RAS

The HEC-RAS model was calibrated to the results of the 2D-FTN OMBA model. The design flows were applied at the upstream end of the HEC_RAS model and the water surface elevation obtained at the Hwy 23 bridge crossing were compared to the 2D-FTN OMBA model results. The manning's values were adjusted to reflect the roughness of the channel but also calibrate the water surface elevations. The table below summarizes the water surface elevations at the Hwy 23 Bridge for the calibration of the HEC-RAS model to the 2D FTN OMBA model.

Table VI-I: Proposed Condition WSELs

	Water Surface Elevations (ft. NAVD88)			
	2D FTNOMBA Current	96,000 Current	2D FTNOMBA Future	87,000 Future
XS 9177 U/S of Bridge	5.70	5.68	6.80	6.80

The output from the HEC-RAS model for the two scenarios (96K Existing Conditions and 84K Future Conditions) are shown in Table VI-II and VI-III. The results are shown at channel sections 10638 and 9176 as the model results at these sections are used in the subsequent scour calculations.

Table VI-II: Current 96k Scour Inputs

Plan: No Armor fut 7219ND River 1 RS: 10638.88 Profile: Higher Discharge			
Element	Left OB	Channel	Right OB
Max Channel Depth (ft)		31.18	
Top Width (ft)		928.94	
Q Total (cfs)		96000.00	
E.G. Slope (ft/ft)		0.000346	
Flow (cfs)	553.94	94892.12	553.94
Top Width (ft)	206.47	516.00	206.47
Avg. Vel. (ft/s)	1.74	7.20	1.74
Hydraulic. Depth (ft)	3.01	25.53	3.01
Plan: No Armor fut 7219ND River 1 RS: 9176.787BR U Profile: Higher Discharge			
Element	Left OB	Channel	Right OB
Max Channel Depth (ft)		30.60	
Top Width (ft)		886.74	
Q Total (cfs)		96000.00	
E.G. Slope (ft/ft)		0.000179	
Flow (cfs)	518.59	94984.54	496.86
Top Width (ft)	191.39	508.00	187.35
Avg. Vel. (ft/s)	2.03	7.48	2.03
Hydraulic. Depth (ft)	2.49	25.01	2.48

Table VI-III: Future 87K Scour Inputs

Plan: No Armor fut 7219ND River 1 RS: 10638.88 Profile: Future Higher Di			
Element	Left OB	Channel	Right OB
Max Channel Depth (ft)		32.14	
Top Width (ft)		944.32	
Q Total (cfs)		87000.00	
E.G. Slope (ft/ft)		0.000249	
Flow (cfs)	732.19	85535.63	732.19
Top Width (ft)	214.16	516.00	214.16
Avg. Vel. (ft/s)	1.74	6.26	1.74
Hydraulic Depth (ft)	3.84	26.49	3.84
Plan: No Armor fut 7219ND River 1 RS: 9176.787BR U Profile: Future Higher Di			
Element	Left OB	Channel	Right OB
Max Channel Depth (ft)		31.74	
Top Width (ft)		905.10	
Q Total (cfs)		87000.00	
E.G. Slope (ft/ft)		0.000127	
Flow (cfs)	785.59	85461.15	753.26
Top Width (ft)	200.22	508.00	196.88
Avg. Vel. (ft/s)	2.10	6.43	2.09
Hydraulic Depth (ft)	3.51	26.15	3.48

VII. Scour Analysis

The scour analysis was performed using FHWA's Hydraulic Toolbox version 4.4 and the FDOT spreadsheet available from FDOT's Roadway Drainage Manuals and Handbook webpage (FDOT Drainage Manual, January 2019). Guidance in the Federal Highway Administration (FHWA) Hydraulic Engineering Circular Number 18 (L.A. Arneson, April 2013)) Evaluating Scour at Bridges 5th Edition, and FHWA Hydraulic Engineering Circular Number 23 (P.F. Lagasse, September 2009) Bridge Scour and Stream Instability Countermeasures were used to prepare the inputs to both the Hydraulic Toolbox the FDOT spreadsheet.

Total scour includes (1) long-term degradation, (2) contraction scour, and (3) local scour. Long-term degradation is the long-term streambed elevation change. For this site long-term degradation was not evaluated, Conditions in the conveyance channel will be continually monitored, and if the channel armoring was to fail, which is be required for long-term degradation to commence, the diversion would be immediately shut down, preventing degradation scour from occurring.

The diversion flow is entirely confined within the channel levees, and as the bridge abutments are outside the levees, abutment scour was not conducted since no flow will occur adjacent to the abutments.

Two flow conditions and three soil conditions were considered for a total of six scour scenarios. For the local scour, the HEC-18 scour equations are not directly applicable to piers with fully buried pile caps (only partially buried caps in which the scour is not expected to extend below the cap base). Due to this limitation, the FDOT Complex Pier Case 3 equations were applied for the piers. FDOT pier equations are based on research by Sheppard and Miller (HEC-18 5th Edition page 7.5). They are noted as generally performing better for both laboratory and field data. However, the FDOT methods are only applicable to sand substrates, and therefore the HEC-18 methods for cohesive materials were used to estimate the local scour. This HEC-18 method represents the maximum potential scour for the hydraulic conditions over a sustained period. This means a singular event may not create the maximum scour but it may be reached over the life of the bridge. The approach for each sediment type and scour component (local and contraction) are summarized in Table VII-I below.

Table VII-I: Scour Equation Methods

Sand	Silt	Clay
Pier Equation		
FDOT Complex Case 3*	HEC-18 Cohesive Pier	HEC-18 Cohesive Pier
Contraction Equation		
HEC 18 Equation 6.2 and 6.3	HEC 18 Equation 6.6	HEC 18 Equation 6.6

Note*: Used for Pier Scour Depths

All scour was calculated using flow and geometry conditions at cross section 10638388 and upstream internal bridge cross section 9176.787. Cross section 10638.88 was selected to represent the channel and overbank cross section at full flow un-constricted by the LA 23 Bridge and piers. Internal bridge cross section 9176.787 was chosen as it models conditions at the upstream section of the proposed bridge. Flow at cross section 106383.88 is entirely within the banks of the levee; and the piers are closely set next to the channel, all data derived from the internal bridge cross section is taken from the entire bridge opening within the levee. In some cases, channel and overbank values were used for piers 7 and 12. Upstream contraction data (results of HEC-RAS flow modeling) from cross section 10638.88 indicates contraction scour at the bridge to be under live-bed scour conditions.

The contraction scour calculations for the sand substrate scenario were developed based on the HEC-18 guidance and HEC-RAS results and are summarized in Tables VII-II. These results are combined with the FDOT Complex Pier Case 3 local scour estimates which are summarized later in this section. The complete inputs and results of the HEC-18 scour calculations for sand are described in Appendix B.

Table VII-II: Sand Condition Input Variables

Sand					
Variable		Current 96K	Future 87K	Units	Source
Contraction Scour					
Flow in the upstream channel transporting sediment	Q_1	94892.12	85535.63	cfs	HEC-RAS
Average velocity in upstream channel	V_1	7.20	6.26	ft/s	HEC-RAS
Width of upstream channel	W_1	516.00	516.00	ft	HEC-RAS
Average depth in upstream channel	Y_1	25.53	26.49	ft	HEC-RAS
Flow in the contracted section	Q_2	94984.54	85461.15	cfs	HEC-RAS
Width of contracted section	W_2	488.00	488.00	ft	HEC-RAS
Existing depth in contracted section before scour	Y_0	25.01	26.15	ft	HEC-RAS
Slope of energy grade line	S_1	0.000346	0.000249	ft/ft	HEC-RAS
Particle size of which 50% are smaller	D_{50}	0.063	0.063	mm	Typical Sand
		0.000207	0.000207	ft	Typical Sand
Critical Velocity	V_C	1.14	1.14	ft/s	Eq HEC-18

The general inputs needed for the scour scenarios for cohesive substrates with respect to the flow and soil condition were developed based on the HEC-18 guidance and HEC-RAS results and are summarized in Tables VII-III and VII-IV. The complete inputs and results of the HEC-18 scour calculations are in Appendix B.

Table VII-III: Silt Condition Input Variables

Silt					
Variable		Current 96K	Future 87K	Units	Source
Contraction Scour					
Average velocity in contracted section	V_2	7.48	6.43	ft/s	HEC-RAS
Average depth in upstream channel	Y_1	25.53	26.49	ft	HEC-RAS
Critical shear stress	T_C	0.084	0.084	lb/ft^2	HEC-18 Fig 6.9
Manning's n	n	0.02	0.02		HEC-RAS
Correction factor	K_u	1.49	1.49	ft	HEC-18
Gravity	g	32.20	32.20	ft/s^2	
Density of water	ρ	1.94	1.94	sl/ft^3	
Particle size of which 50% are smaller		0.0387	0.0387	mm	Gradation Chart
	D_{50}	0.000114	0.000114	ft	Gradation Chart
Pier Scour					
Average channel velocity	V_1 Channel	7.2	6.26	ft/s	HEC-RAS
Average overbank velocity	V_1 Overbank	1.74	1.74	ft/s	HEC-RAS
Critical Velocity for Soil	V_C	5.25	5.25	ft/s	HEC-18 Fig 4.7
Pier length	L	78	78	ft	Bridge Plan
Gravity	g	32.2	32.2	ft/s^2	
Shape of pier	Pier Type	Round Nose	Round Nose		Bridge Plan
Correction factor for pier nose shape	$K_{1\ (drilled\ shaft)}$	1	1		HEC-18
Correction factor for angle of flow	K_2	1	1		HEC-18
Angle of attack (degrees)	Θ	0	0		HEC-18
Effective pier width	a (drilled shaft)	5	5	ft	Bridge Plan

For silt, the D50 determined from the grain analysis for the silt layers were averaged. This value was placed in the critical shear stress equation from Figure 4.6 in HEC-18. The critical shear stress is then converted into English units. This, along with values from the approach cross section and bridge cross section in HEC-RAS, is applied to the ultimate contraction scour Equation 6.6. For pier scour the critical shear stress derived from HEC-18 was reviewed along with information provided from the numerical modeling to inform our assumed critical velocity. This critical velocity along with the average velocity upstream were applied to Equation 7.35 to develop the pier scour calculations. More information on how the critical velocities were developed can be found in Appendix B.

Table VII-IV: Clay Condition Input Variables

Clay					
Variable		Current 96K	Future 87K	Units	Source
Contraction Scour					
Average velocity in contracted section	V_2	7.48	6.43	ft/s	HEC-RAS
Average depth in upstream channel	Y_1	25.53	26.49	ft	HEC-RAS
Critical shear stress	T_C	0.060	0.060	lb/ft^2	Eq Jacob 2009
Manning's n	n	0.02	0.02		HEC-RAS
Correction factor	K_u	1.49	1.49	ft	HEC-18
Gravity	g	32.20	32.20	ft/s^2	
Density of water	ρ	1.94	1.94	sl/ft^3	
Pier Scour					
Average channel velocity	V_1 Channel	7.2	6.26	ft	HEC-RAS
Average overbank velocity	V1 Overbank	1.74	1.74		HEC-RAS
Critical Velocity for Soil	V_C	4.92	4.92	ft/s	HEC-18 Fig 4.7
Pier length	L	78	78	ft	Bridge Plan
Correction factor for pier nose shape	K_1 (drilled shaft)	1	1		HEC-18
Correction factor for angle of flow	K_2	1	1		HEC-18
Angle of attack (degrees)	Θ	0	0		HEC-18
Effective pier width	a (drilled shaft)	5	5	ft	Bridge Plan

For Clay, the critical shear stress was found by averaging the Tc from a Plasticity Index conversion developed by Smerdon and Beasley (1959) using boring log data in the depth range between 20 and 40 feet deep. The critical shear stress is then converted into English units. This along with values from the approach cross section and bridge cross section in HEC-RAS is applied to the ultimate contraction scour Equation 6.6. For pier scour the critical shear stress derived from HEC-18 was reviewed along with information provided from the numerical modeling to inform our assumed critical velocity. This critical velocity along with the average velocity upstream were applied to Equation 7.35 to develop the pier scour calculations. More information on how the critical velocities were developed can be found in Appendix B.

An example of the input values used for the FDOT Complex Pier Case 3 is demonstrated in the snapshot of the spreadsheet input menus show in Figure VII-I.

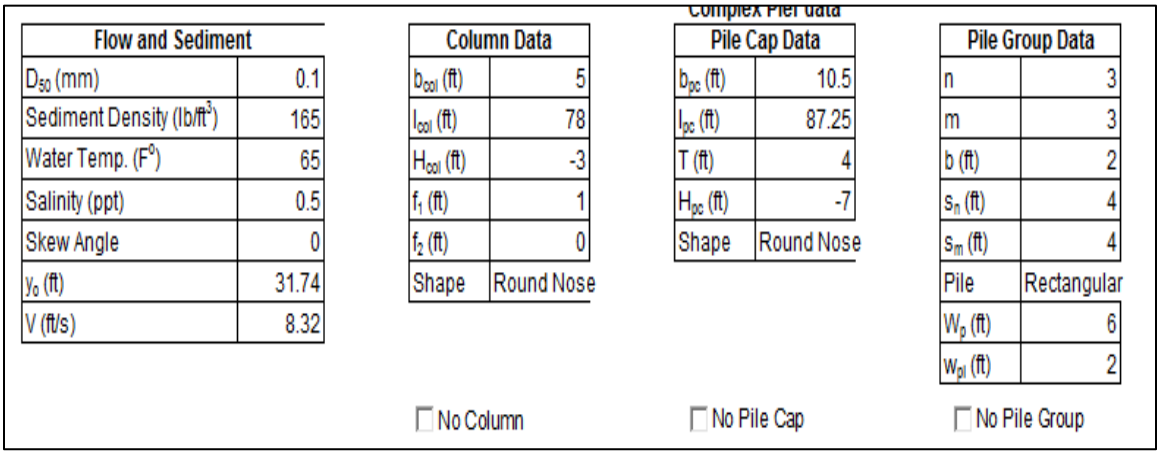

Figure VII-I: Example of Input Required for FDOT Complex Pier

The following tables provide a summary of the scour depths for the design event for the LA23 Bridge over Mid-Barataria Sediment Diversion Channel.

Table VII-V: Current 96,000 Design Storm Scour Results for Sand Condition Column Bents

Scour Depths Sand Condition Column Bents				
As-Built Bent	Contraction Scour. (ft)	Pier (ft)	Degradation Scour (ft)	Total Scour (ft)
12	1.54	4.64	0.00	6.19
11	1.54	8.77	0.00	10.31
10	1.54	8.77	0.00	10.31
9	1.54	8.77	0.00	10.31
8	1.54	8.77	0.00	10.31
7	1.54	4.67	0.00	6.19

Table VII-VI: Future 87,000 Design Storm Scour Results for Sand Condition Column Bents

Scour Depths Sand Condition Column Bents				
As-Built Bent	Contraction Scour. (ft)	Pier (ft)	Degradation Scour (ft)	Total Scour (ft)
12	1.36	4.82	0.00	6.18
11	1.36	7.83	0.00	9.19
10	1.36	7.83	0.00	9.19
9	1.36	7.83	0.00	9.19
8	1.36	7.83	0.00	9.19
7	1.36	4.82	0.00	6.18

Table VII-VII: Current 96,000 Design Storm Scour Results for Silt Condition Column Bents

Scour Depths Silt Condition Column Bents				
As-Built Bent	Contraction Scour. (ft)	Pier (ft)	Degradation Scour (ft)	Total Scour (ft)
12	7.21	0.00	0.00	7.21
11	7.21	11.47	0.00	18.68
10	7.21	11.47	0.00	18.68
9	7.21	11.47	0.00	18.68
8	7.21	11.47	0.00	18.68
7	7.21	0.00	0.00	7.21

Table VII-VIII: Future 87,000 Design Storm Scour Results for Silt Condition Column Bents

Scour Depths Silt Condition Column Bents				
As-Built Bent	Contraction Scour. (ft)	Pier (ft)	Degradation Scour (ft)	Total Scour (ft)
12	5.68	0.00	0.00	5.68
11	5.68	9.97	0.00	15.65
10	5.68	9.97	0.00	15.65
9	5.68	9.97	0.00	15.65
8	5.68	9.97	0.00	15.65
7	5.68	0.00	0.00	5.68

Table VII-IX: Current 96,000 Design Storm Scour Results for Clay Condition Column Bents

Scour Depths Clay Condition Column Bents				
As-Built Bent	Contraction Scour. (ft)	Pier (ft)	Degradation Scour (ft)	Total Scour (ft)
12	7.78	0.00	0.00	7.78
11	7.78	11.67	0.00	19.45
10	7.78	11.67	0.00	19.45
9	7.78	11.67	0.00	19.45
8	7.78	11.67	0.00	19.45
7	7.78	0.00	0.00	7.78

Table VII-X: Future 87,000 Design Storm Scour Results for Clay Condition Column Bents

Scour Depths Clay Condition Column Bents				
As-Built Bent	Contraction Scour. (ft)	Pier (ft)	Degradation Scour (ft)	Total Scour (ft)
12	6.27	0.00	0.00	6.27
11	6.27	10.18	0.00	16.44
10	6.27	10.18	0.00	16.44
9	6.27	10.18	0.00	16.44
8	6.27	10.18	0.00	16.44
7	6.27	0.00	0.00	6.27

The recommended design scour depths for the unarmored condition can be seen below:

Table VII-XI: Scour Depth Summary

Scour Depths Column Bents		
As-Built Bent	Total Scour Min (ft)	Total Scour Max (ft)
12	5.68	7.78
11	9.19	19.45
10	9.19	19.45
9	9.19	19.45
8	9.19	19.45
7	5.68	7.78

VIII. RipRap Design

As covers in the Design Criteria, Basis of Design Report (BODR), and the Conveyance Channel Revetment Study appended to the BODR, all submitted to CPRA, the most feasible revetment material selected to protect the wetted earthen surface of the diversion is rock riprap. Rip rap design was performed for the design of the Conveyance Channel, the Transition section, and the Outfall all further developed during the 30% Design phase report submitted to CPRA. This report is only to evaluate the required riprap for the channel and the piers with respect to the HEC-RAS model developed for bridge scour evaluation and to serve as an additional check on the both numerical modeling of the hydraulics as well as scaled physical modeling of the diversion features to determine the stability of various riprap sizes under select scenarios run for the 30% design report.

The 96,000 cfs event was used in the sizing of this riprap with respect to the HEC-RAS Bridge Modeling. The cross-sectional depth and velocity were the primary parameters taken from the model.

Riprap can reduce the frequency and volume of scour, but it does not reduce the potential scour depths that have been estimated.

FHWA HEC-23, Design Guide 4 and 11, was used to size riprap for the channel and piers and it was determined that riprap should be installed around roadway embankments and sloped abutments. This installation will provide protection from:

- Erosion due to localized runoff during heavy rainfall events
- Localized high velocities that may occur due to debris in the channel during large flow events
- Initially higher channel velocities where sufficient backwater has not yet developed to suppress the channel velocities

As previously stated, the channel will have 10# rip-rap armoring layer, based on the diversion channel 30% design (reference). Guidance for channel armoring suggests that the placed channel riprap should have a minimum thickness of D_{100} or $1.5*D_{50}$, whichever is larger, and should include a base of granular or geosynthetic filter material. In addition, the depth below ambient bed elevation should be evaluated to tie the toe of the bank riprap with respect to the maximum contraction scour depth, which ranges from 1.36 feet to 7.78 feet. This is suggesting that the depth of the toe of the embankment protection and depth of riprap in the main channel be either 7.78 feet thick or the minimum thickness of 1 feet put placed below the ambient grade to the elevation of maximum contraction scour.

Placed channel pier riprap thickness should be the greatest of maximum total channel scour (contraction plus long term aggradation) depth or three times the median diameter, whichever is larger, and should include a base of granular or geosynthetic filter material per FHWA HEC-23 DG 11. Minimum riprap pier extent is 10 feet. Detailed design calculations are included in Appendix B. The 2D FTNOMBA model has been verified with results from the 1/65 scale model. It is noted that the models were run at design conditions, and there was no evidence of scouring to the proposed 10# stone armoring. For comparison the 10# stone has a spherical diameter of approximately 6 inches which exceeds the requirement of the D50 for channel bank protection.

Table VIII-I: Channel and Pier Riprap Sizing

Riprap Design					
Application	Riprap Depth (ft)	Riprap Extents (ft)	D50 (in)	D100 (in)	Min Thickness (ft)
Channel Bank	1.36-7.78*	2' above Design High Water Elevation 26.15= 28.15'	5.05	9.20	1'
Pier	1.36-7.78*	10' around pier	18.50	36.00	5'

*range represents results for assumption of sand, silt and clay substrate

IX. Recommendations

AECOM developed a one-dimensional hydraulic model for the LA-23 Bridge over Mid-Barataria Sediment Diversion Channel utilizing HEC-RAS. Topographic data for the 1D model was developed from proposed diversion plan view and typical sections. All of the LA-23 bridge geometry and related information was obtained from proposed bridge plans and related BODR (Basis of Design Report) information. The information contained in the advanced numerical and physical modeling done as part of the BODR was utilized to calibrate the model. The model runs indicated that the Proposed Condition will experience maximum of 20 feet total scour. The site does not currently have an existing bridge, the proposed bridge and proposed channel would be new constructed features to the site. This means there are no unintended impacts to any existing bridge structures from this design. All scour considerations would be incorporated into the proposed design.

A scour analysis was performed for the proposed bridge to determine scour depths used for substructure design. The conveyance armoring was excluded in this analysis, yielding a conservative estimate of scour. The soil is made up of a variety of soil types, and therefore by assuming the worst-case all-clay stratum scour depth at all bents, an additional level of conservatism is provided. Additionally, calculations will be performed to determine the need for any additional scour countermeasures at the site. Rip rap design was performed for the design of the Conveyance Channel, the Transition section, and the Outfall all further developed during the 30% Design phase report submitted to CPRA. This report is only to evaluate the required riprap for the channel and the piers with respect to the HEC-RAS model developed for bridge scour evaluation and to serve as an additional check on the both numerical modeling of the hydraulics as well as scaled physical modeling of the diversion features to determine the stability of various riprap sizes under select scenarios run for the 30% design report. The recommended design scour depths for the unarmored condition can be seen in Table VII-XI.

X. References

Chow, V. T. (1959 (Edition January 1, 2009)). Open Channel Hydraulics. The Blackburn Press; 30057th edition .

E.T. Smerdon, R. B. (1959). The Tractive Force Theory Applied to Stability of Open Channels in Cohesive Soils" Research Bulletin 715. Columbia, Missouri: University of Missouri Agricultural Expereiment Station.

FDOT Drainage Manual. (January 2019). Florida Department of Transportation.

L.A. Arneson, L. Z. (April 2013). Hydraulic Engineering Circular Evaluating Scour at Bridges FIfth Edition. Federal Highway Administration.

P.F. Lagasse, P. C.-O. (September 2009). HEC-23 Bridge Scour and Stream Instability Countermeasures Third Edition. Federal Highway Administration .

Walter Jacobs, P. L. (July 2011 Vol 31 Issue 10 Suppl 1 pp S14-S25). Erosion threshold of sand-mud mixtures- Continental Shelf Research . Elsevier Ltd.

Van Rijn, Leo.(1990). Principles of Sediment Transport in Rivers, Estuaries and Coastal Seas. Aqua Publications, Amsterdam.

APPENDIX A

APPENDIX B

Sarah S McEwen, PE
111 E. Capitol Street, Suite 400
Jackson, MS 39201
601-352-2701

About AECOM

AECOM is built to deliver a better world. We design, build, finance and operate infrastructure assets for governments, businesses and organizations. As a fully integrated firm, we connect knowledge and experience across our global network of experts to help clients solve their most complex challenges. From high-performance buildings and infrastructure, to resilient communities and environments, to stable and secure nations, our work is transformative, differentiated and vital. A Fortune 500 firm, AECOM had revenue of approximately $20.2 billion during fiscal year 2018. See how we deliver what others can only imagine at aecom.com and @AECOM.